SUPRAMOLECULAR MODIFICATION OF SELECTED ANTITUBERCULAR DRUGS

By: Jinjing Li B.Sc.

Thesis Presented for the Degree of

DOCTOR OF PHILOSOPHY

in the Department of Chemistry

UNIVERSITY OF CAPE TOWN

August 2010

ACKNOWLEDGEMENTS

I would like to thank:

My supervisors, Professors Mino R Caira and Susan A Bourne, for their excellent supervision, guidance, support and encouragement. Words cannot express my feelings, nor my thanks for all your help.

Professor Luigi R Nassimbeni, for his knowledge, kindness and inspiration.

All the members of the Centre for Supramolecular Chemistry Research, UCT, for their friendship, entertainment and conversation during the course of this project, especially Dyanne Cruickshank, Lee Trollope and Kate Davies.

Dr Vincent J. Smith for his assistance, friendship and sense of humour.

The University of Cape Town for financial support.

Professor Melgardt M. de Villiers at the University of Wisconsin (USA) for recording solubility data for Isoxyl samples.

Professor Graham E. Jackson and Dr Melinda Duer (Cambridge University) for helping to interpret the ^{13}C Solid-state NMR Spectra of Isoxyl.

My parents and my friend for their love, support and encouragement.

Journal Articles and Conference Presentations:

Nicoli, S., Bilzi, S., Santi, P., Caira, M. R., Li, J. and Bettini, R. *Ethyl-paraben and nicotinamide mixtures: apparent solubility, thermal behaviour and X-ray structure of the 1:1 co-crystal*. *J. Pharm. Sci.*, 2008, 97, 4830-4839.

de Villiers, M. M., Caira, M. R., Strydom, S. J., Bourne, S. A, Li, J. and Liebenberg, W. *Crystallization of toxic glycol solvates of rifampin from glycerin and propylene glycol contaminated with ethylene glycol or diethylene glycol*. *Pharm. Res*., for submission, August 2010.

Carman National Physical Chemistry Symposium, Cape Town, 23 – 27 September 2007.

Poster presentation: Polymorphs of the Thiourea Drug Isoxyl.

Li, J., Caira, M. R. and Bourne, S. A.

Fifth Conference: Isotopic and Molecular Processes, Cluj-Napoca, Romania, 20 – 22 September 2007.

Invited lecture: Structural elucidation of chemically modified cyclodextrins and their inclusion complexes for medicinal applications.

Caira, M. R., Mhlongo, W. T. and Li, J.

International Seminar on Inclusion Compounds, Stellenbosch, South Africa, 4 – 9 April 2009.

Poster presentation: Thermal and X-Ray Structural Characterization of Solvates of rifaximin and rifampicin.

Li, J., Caira, M. R. and Bourne, S. A.

South African Chemical Institute Young Chemists' Mini Symposium, Stellenbosch, South Africa, 25 November 2009.

Oral Presentation: Supramolecular modification of the antitubercular drug isoxyl.

Li, J., Caira, M. R. and Bourne, S. A.

ABSTRACT

Jinjing Li

SUPRAMOLECULAR MODIFICATION OF SELECTED ANTITUBERCULAR DRUGS

August 2010

The author's objective was to prepare new solid phases of the antitubercular drug isoxyl [specifically polymorphs, solvates, cyclodextrin (CD) inclusion complexes and cocrystals] and to isolate and characterise a range of solvated forms of the rifamycin antibiotics rifampicin and rifaximin.

Two polymorphic phases and a solvated phase of isoxyl were successfully isolated by the recrystallisation method. β- and γ-CD inclusion complexes with isoxyl as guest were prepared by the kneading technique. No cocrystal of isoxyl was isolated in reactions between the drug and potential co-formers; instead, serendipitous precipitation of new polymorphs of two widely used co-formers, namely isonicotinamide and nicotinamide, occurred. These were isolated and studied in depth. Eleven novel crystalline solvated forms of the rifamycin antibiotic rifampicin were prepared, as were two crystalline solvated forms of rifaximin.

In this study, polymorphs and solvate crystals were analysed using thermal analysis methods (differential scanning calorimetry, thermogravimetric analysis and hot stage microscopy) and X-ray diffraction methods (on monocrystals and powders). The CD complexes were analysed using powder X-ray diffraction.

For the polymorphic systems (comprising two isoxyl polymorphs, three isonicotinamide polymorphs and two nicotinamide polymorphs), the differences in their molecular conformations, crystal packing features and thermal properties were determined. For each system, schematic Energy-Temperature diagrams showing the relative thermodynamic stabilities of the polymorphs were subsequently derived. In addition, for the two isoxyl polymorphs, spectroscopic studies (FTIR, ^{13}C SSNMR) and solubility data were recorded, enabling a comprehensive characterisation of this dimorphic system.

Solvated forms were investigated using a combination of thermal analysis and single crystal X-ray structural analysis, the latter revealing new isostructural solvate series and unusual molecular conformations. The invariant occurrence of the zwitterionic forms of the rifampicin and rifaximin molecules in the solid state was also established and the role of different solvent molecules in the solvate crystal structures was determined.

Complexation between native CDs and isoxyl was established using powder X-ray diffraction and data from known isostructural CD inclusion complexes. This procedure also enabled deduction of approximate unit cell dimensions for each complex, crystal space groups and the structures of the host frameworks in the crystals. In addition, solubility enhancement measurements using β- and γ-CDs with isoxyl indicated that the aqueous solubility of the drug in β-CD and γ-CD solutions increased by factors of 2-3 relative to its concentration in pure water.

The new supramolecular phases that were prepared and characterised are significant in the context of the solid-state chemistry of active pharmaceutical ingredients.

TABLE OF CONTENTS

Chapter 1

Introduction

In this chapter, we briefly introduce and discuss four different supramolecular modification methods: polymorph generation, solvate formation, cyclodextrin inclusion and co-crystal formation. We also introduce the antitubercular drugs selected for study, namely isoxyl, rifampicin and rifaximin, and list the objectives of their investigation *via* supramolecular modification.

Supramolecular Chemistry

In 1987, the Nobel Prize in chemistry was awarded to Cram, Lehn and Pedersen for their respective work in the field of supramolecular chemistry whose importance had been established by that time. In 1988, the definition of 'supramolecular chemistry as chemistry beyond the molecule' was introduced by Lehn in his Nobel lecture.[1] In brief, non-bonded interactions play a crucial role in supramolecular chemistry. These interactions include hydrogen bonding, π-π, C-H···π, van der Waals and hydrophobic interactions.

Davy[2] had discovered the chlorine clathrate hydrate [$Cl_2 \cdot 6H_2O$] in 1811; this is considered to have initiated the concept of guest entrapment by a host. The discovery of X-rays in 1895 and X-ray crystal structure analysis introduced in 1912 enhanced the growth of the field of structural chemistry. In 1936, the field of supramolecular chemistry started developing with the application of crystallographic techniques by Kratky and Giacomello[3] to elucidate the crystal structure of cholanic acid. The formation of a crystal is a process of self-assembly of molecules. This is regarded as a crucial concept of supramolecular chemistry. Therefore, crystallography plays a key role in this field for the understanding of crystal structures, crystal growth and molecular interactions.

The principles of supramolecular chemistry have been applied in a large variety of areas, as described in the monograph by Steed and Atwood.[4] In this thesis, the focus is on supramolecular modification of selected drug molecules, through their conversion into different polymorphic forms, new solvated forms, cyclodextrin inclusion compounds and co-crystals. The general aim of such transformation is to expand the solid-state chemistry landscape of these drugs by providing a variety of solid forms with different properties and possible applications. The crucial feature of this approach is that on generating any 'supramolecular derivative' of a drug, no covalent bonds are created or destroyed, and so the pharmacological activity of the drug is not compromised.

Polymorphism

Polymorphism occurs when a single chemical compound crystallises in different molecular arrangements.[5] Different polymorphs can display significant differences in their physical properties, such as density, hardness, melting points, solubility, dissolution rate, stabilities and even colour.[6] A well-known example is graphite and diamond. Both of them consist of the element carbon only but their vastly different structural arrangements lead to significantly different physical properties.

Applications

Polymorphism is very common in the pharmaceutical area.[7] The production of most active pharmaceutical ingredients requires a crystallisation stage in the manufacturing process.[8] However, drugs can exist in a number of polymorphic forms, each having different properties that may affect their pharmaceutical performance. Furthermore, the various forms of the drug may interconvert under various conditions.

Preparative Methods

Theoretically, a given compound may adopt several different crystalline forms. However, there is no certainty in our ability to predict the occurrence or the properties of a new polymorph. The onus is on the individual pharmaceutical scientist to apply due diligence in isolating and characterising the various solid-state forms of a new chemical entity.[9] The most common method of isolating polymorphs is crystallisation from a large variety of single solvents; this has been successful in many cases. The other methods normally employed to obtain different polymorphic forms are crystallisation by evaporation from a binary mixture of solvents, precipitation using anti-solvents, sublimation, vapour diffusion, thermal treatment, crystallisation from the melt, grinding and thermal desolvation of crystalline solvates. In some cases, the formation of different polymorphic crystals is very sensitive to subtle differences in the crystallisation conditions. For instance, crystallisation of the α-polymorph of mannitol is favoured by a slow freezing rate, whereas the δ-polymorph is favoured by a fast freezing rate.[9]

Analytical Tools

There is no strict limit for the range of analytical tools applicable to the study of polymorphs. The range should be as broad as possible.[10] Commonly used methods include X-ray diffraction, thermal and spectroscopic techniques. These range from molecular to particulate and bulk techniques.[11] For instance, X-ray diffraction methods can provide complete structural information at the molecular level. Thermal analysis can help to establish the thermodynamic relationship between polymorphs, which is a critical step in selecting the appropriate form for development.[12] Spectroscopic studies are normally applied to fully characterise polymorphs by probing solid-state properties at the spectral energy level in conjunction with X-ray diffraction analyses.[13]

Structural Features

Structural features are the ultimate criteria for distinguishing different polymorphs.[14] One type of polymorphism is called 'conformational polymorphism'. Here, the molecule adopts significantly different conformations in its various crystal forms.[15] The other type of polymorphism is termed 'packing polymorphism' and represents instances where conformationally rigid molecules can be assembled into different three-dimensional structures through the employment of different intermolecular interactions.[16] Figure 1 illustrates these types. However, the overlaps between the two definitions are somewhat blurred since different packing arrangements can induce conformational differences in the molecules while the conformationally different molecules will inevitably packing in different arrangements.[16]

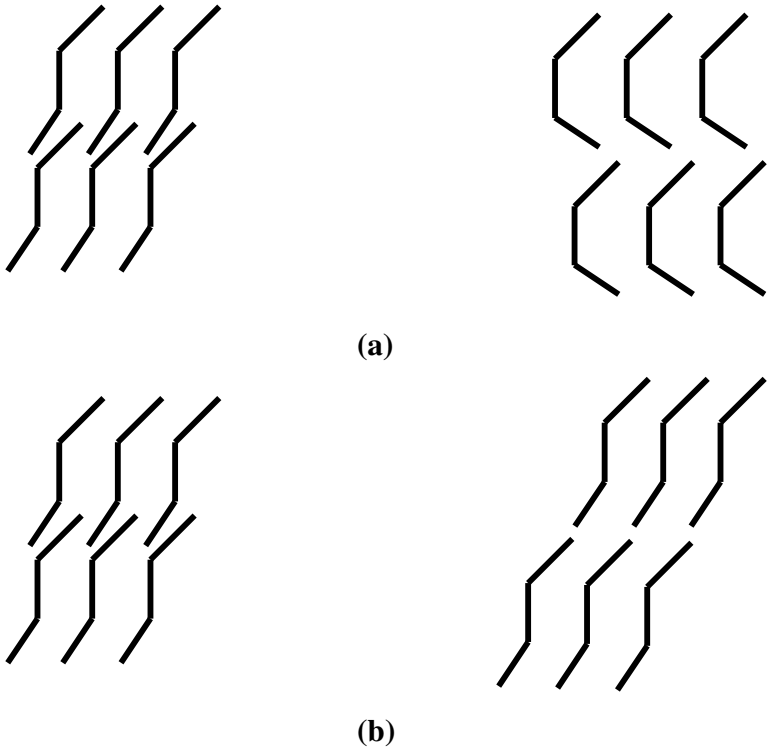

Figure 1 Schematic diagrams illustrating the definitions of (a) conformational polymorphism and (b) packing polymorphism.

Thermodynamic Relationships

The transformation process from one polymorph into another polymorph is considered as a phase transition.[17] The two forms are related enantiotropically if an endothermic transition is observed at some temperature, while the two forms are related monotropically if an exothermic transition occurs.[18] In the enantiotropic system, the stability order of two polymorphs is reversible before and after the transition point. In the monotropic system, the stability order of two polymorphs would remain the same at all temperatures. The Gibbs free-energy of a phase is defined by

$$G = H - TS \qquad (1)$$

In this expression, H is the enthalpy, T the absolute temperature and S the entropy of the phase in question.[19] The thermodynamic behaviour of the polymorphs may be summarised by constructing their qualitative energy *vs* temperature diagram,[19, 20] as

shown in Figure 2. At the absolute zero of temperature, G is equal to H. Also, at the given temperature, the thermodynamically stable modification has the lowest value of G.[20]

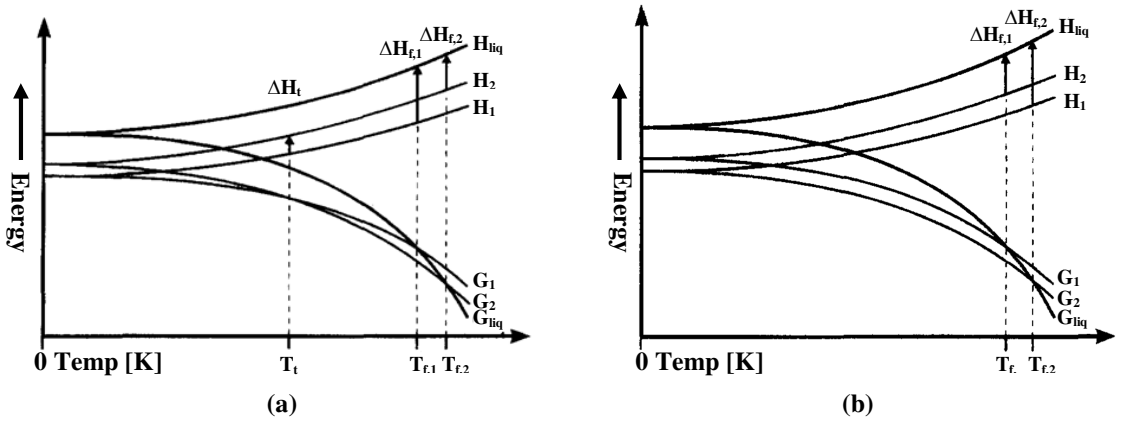

Figure 2 Semi-schematic E/T diagrams for (a) an enantiotropic and (b) a monotropic dimorphic system (adapted from reference 19). The subscripts 'f', 't' and 'liq' refer to 'fusion', 'transition' and 'supercooled liquid', respectively, whilst the subscripts '1' and '2' stand for the two polymorphs (the higher melting polymorph is indicated by '2').

Noticeably, the H isobars will always have a positive slope and never intersect while the G isobars will always have a negative slope and intersect at most once (only in the enantiotropic system).[10] Accordingly, Burger and Ramberger developed four useful rules that enable distinction between enantiotropy and monotropy and these are adapted as follows:[18, 21]

Heat-of-Transition Rule: (a) If an endothermic transition is observed at some temperature, it may be assumed that there is a transition point below it, i.e. the two forms are related enantiotropically.

(b) If an exothermic transition is observed at some temperature, it may be assumed that there is no transition point below it, i.e. the two forms are either related monotropically or the transition temperature is higher.

Heat-of–Fusion rule: If the higher melting form has the lower heat of fusion the two forms are usually enantiotropic, otherwise they are monotropic.

Density rule: If one modification of a molecular crystal has a lower density than the other, it may be assumed to be less stable at absolute zero.

Infrared Rule: For polymorphs with strong hydrogen bonds, the one with the larger frequency for the highest frequency infrared absorption band will have the larger entropy.

Interestingly, the heat of transition rule and the heat of fusion rule have rare exceptions while the density rule has many exceptions.[22] There are a few pharmaceutical examples where actual experimental results violate the density rule, for instance: Neotame andydrate,[22] Ribavirin,[23, 24] chloropeocaine[25] and resorcinol.[26] Therefore, the density rule can only be employed as a rough guide, whilst the heat of transition rule and the heat of fusion rule are the crucially reliable principles during the examination of thermodynamically related polymorphs.[22]

Dissolution Rate Measurement

As stated previously, the different polymorphic forms of drugs give rise to variations in solubility.[27] Due to the poor solubility of a compound as well as the lack of awareness of the implications, or time constraints, a solubility measurement may often not be performed; instead, an effective dissolution rate measurement is employed.[14] The dissolution rate measurement has often been studied in pure solvent; however, solvent mixtures may be used in cases of very poor solubility of some drugs.[28] Among the polymorphs, any metastable form should display higher dissolution rate than a more stable form.[29, 30]

Solvatomorphism

Bernstein[31] defined polymorphism as follows: 'classification of a system as polymorphic would be if the crystal structures are different but lead to identical liquid and vapour states.' This statement implies that solvates (including hydrates as a special type) belong to the category of polymorphs. Solvates, therefore, have been described using the term 'pseudopolymorph' which invoked continuing debate and discussion in the recent

literature[32-34] on its use. The origin of the ongoing dispute is the existence of polymorphs of solvates. Specifically, solvates can adopt the same chemical composition (identical numbers of host and guest molecules) but crystallise in different structures. For instance, the monohydrates of nitrofurantoin (an antibacterial compound) crystallise in two forms (Form 1: monoclinic $P2_1/n$ and Form 2: orthorhombic Pbca).[35] Therefore, the term 'pseudopolymorph' may not be appropriate to describe solvates of this type. They are, in fact, polymorphic solvates. Also, solvates can exist in different packing arrangements with different elemental compositions[36] (identical host but different number or species of solvent molecules). An example of this is a monohydrate and a 2.5-hydrate modification of terbutaline sulfate. These species have been characterised by single crystal X-ray diffraction methods and shown to have significantly different crystal structures.[37] Hence, a new term 'solvatomorphism' has been introduced. It is stated by Brittain[38] that 'solvatomorphism is used to denote other crystal variations where the crystal structure of the substance is defined by other unit cells and where these unit cells differ in their elemental composition through the inclusion of one or more molecules of solvent.'

Preparative Methods and General Structural Features

Generally, solvates are obtained by recrystallising the parent substance from single solvents or from solvent mixtures. In some instances, more than one type of solvent molecule may be incorporated in the crystal of the solvates. Sometimes, it is possible to exchange one solvent within the crystal structure for another[9] from the vapour phase or liquor which contains another kind of solvent (guest exchange). In other words, guests may be free to diffuse into or out of solvated crystals since there is no covalent bond to bind the solvent molecules to the host assemblies.[39] This can sometimes even lead to a structural change in the crystal during the guest exchange process [Figure 3 (a)]. An example of this is the dramatic structural change occurring between the solvate of cholic acid with 2-fluorobenzyl alcohol (space group $P2_1$) and that with water (space group $P6_522$) when the single crystal of the former was soaked in aqueous solution.[40] However, most commonly, guest exchange leads to the production of solvates that are isomorphous with the parent solvate. More specifically, organic crystalline solvates may show a tendency to exchange the solvation solvent with water or another solvent when exposed

to ambient air or if left to equilibrate in another solution, without the host structures converting to a different crystalline form, thus maintaining the same packing arrangement as the original crystal[41, 42] [Figure 3 (b)]. Generally, permanent channels or tunnels are formed in the solvate crystal structure and the solvent molecules may move freely through them.[43] Furthermore, the channel can expand slightly or more extensively to take up additional moisture when solvate crystals are exposed to high humidity. This may even lead to changes in the dimensions of the unit cells[16] [Figure 3 (c)]. Due to the small size of water molecules, they can easily fill structural voids in crystals. A known case is cromolyn sodium (disodium cromoglycate) hydrate crystals which can rapidly absorb (or lose) water as a continuous series of interstitial solid solutions, causing the lattice to expand reversibly, especially in the crystallographic *b*-direction.[44] In addition, the guest molecules should have similar structural features, e.g. hydrogen bond donor or acceptor functionalities, to allow them to form similar interactions and they also should possess similar sizes to allow their facile movement through the channel.

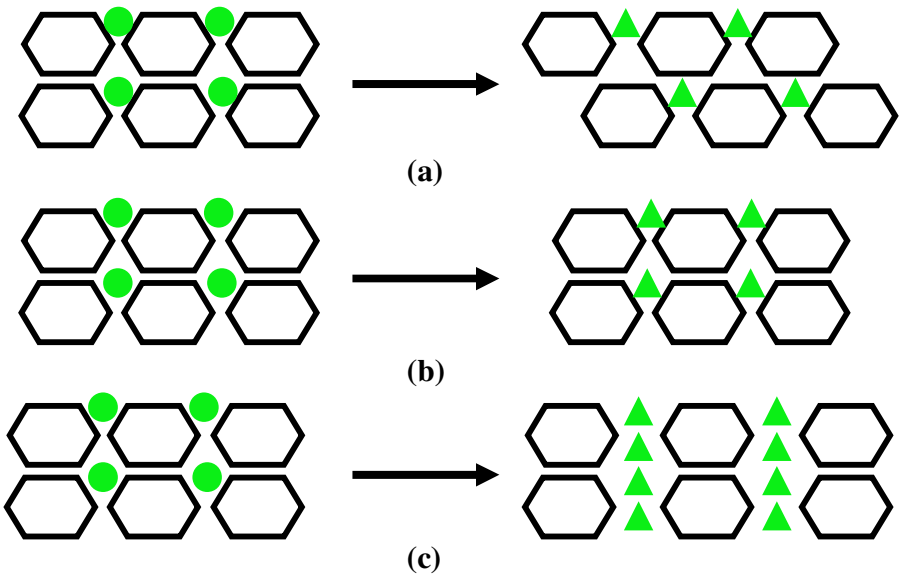

Figure 3 Schematic diagrams illustrating (a) a structural change in the crystal of a solvate during the guest exchange process, (b) isomorphic guest change and (c) expanded channel. Solvent molecules are shown in green. Different solvent molecules are indicated by different geometrical figures (circles and triangles).

Isostructurality

As mentioned above, isostructurality or isomorphism often occurs among two or even more solvates where the included solvent varies but the host framework is retained in each case. A case in point is the compound *o*-acetamidobenzamide, which forms five isostructural solvates with 1-propanol, 1-butanol, 2-butanol, 1, 2-dichloroethane and 1,4-dioxane.[45] Furthermore, isostructurality not only occurs in solvates, but is a common phenomenon in other areas, e.g. cyclodextrin inclusion and co-crystal formation. Caira's[46] description of isostructurality states that 'crystal isostructurality refers to identical or nearly identical packing arrays of chemically distinct compounds and is inversely related to the phenomenon of polymorphism, which instead, refers to the ability of a single compound to crystallise in different packing arrays.' Therefore, the packing diagrams, until cell parameters and atomic coordinates would be similar in the crystal structures of isostructural compounds.[47] The identification of isostructural compounds is readily achieved by recognising similarities in their respective powder X-ray diffraction patterns.[48]

Further Structural Features of Solvates

Bingham et al.[49] classified the solvates of organic compounds into two broad categories as 'cocrystals' and 'inclusion phases'. In the former, the solvent molecules are essential components of the crystal by forming intermolecular interactions, e.g. strong hydrogen bonds with the host molecules.[50, 51] In the latter, solvent molecules function as space fillers in the crystal and there are few or no significant intermolecular interactions between solvent and host molecules.[50] The solvent molecules can fill the space in different ways; for instance, they may be entrapped within the lattice, forming clathrates[52] or they may locate along channels in the lattice, forming layers. Furthermore, the solvates of clathrate structures are found to be more stable than those of layer structures.[50] In addition, solvates are stabilised when the incorporated solvent molecules strengthen the intermolecular interactions in the crystal.[50]

Sometimes, incorporation of different solvent molecules can disturb the host molecules, forcing them to adjust their conformations, or even adopt unfavourable conformations.[53-55] Furthermore, the same solvent molecules can also alter the host conformation depending on the different crystallisation conditions. As an example, we cite the case of the three solvates (hemihydrate, dihydrate and formamide solvate) of 5-(morpholinemethyl)-3-[(4-chlorobenzylidene)amino]-2-oxazolidinone.[56] The host adopts an extended conformation in the hemihydrate while a bent conformation occurs in the dihydrate and formamide solvate. Noticeably, water is the common solvent in the hemihydrate and dihydrate; however, the host molecules nevertheless adopt different conformations in the two cases. In addition, host molecules with different conformations may be present in the same solvate structure.

Characterisation Methods

The common methods for the characterisation of solvates include thermal analysis, spectroscopic and X-ray diffraction methods[57] which are often used in combination. For thermal analysis techniques, DSC (differential scanning calorimety) is the basic thermal technique. TGA (thermogravimetric analysis) plays an important role in characterising solvates since the mass change evaluation allows quantitative determinations of stoichiometry.[58] In the situation of solvates which contain mixed solvents, combined techniques such as TG-IR or TG-MS (TGA with the aid of an evolved gas analyser e.g. infrared spectroscopy and mass spectrometry) are particularly helpful. These methods can be used to identify each component of the solvent mixture incorporated in the crystal,[16] since the identity of the volatile component is determined *in situ*.[59-61] In the case of hydrates, Karl Fischer titration is an unequivocal method for quantifying water contents.[60, 63] For spectroscopic techniques, ^{13}C SSNMR (^{13}C Solid-state Nuclear Magnetic Resonance spectroscopy) can usually be employed to detect organic solvents in solvates.[60] However, the solvent molecules trapped in open cavities or located in layers may be highly mobile or even resemble liquid phase.[63] This can lead to non-stoichiometric solvates in which solvent molecules may not be observed by SSNMR. Noticeably, the high solvent mobility may give rise to disorder of the solvent molecules,

which introduces great difficulty in modelling them from single crystal X-ray diffraction data. Therefore, X-ray analysis may not be able to ascertain that the systems are stoichiometric with respect to solvent molecules.[64] Despite these difficulties, the identity of included solvent molecules is normally known from the preparation of the solvate, or can be confirmed spectroscopically. Furthermore, the respective amounts of mixed solvents may also be determined with the combined use of thermogravimetric analysis.

Applications

Solvates exhibit different physical properties such as density, stability, dissolution rate or bioavailability[47, 65] and different mechanical behaviours during processing (e.g. tableting, grinding) and product performance.[66] In addition, solvates containing pharmaceutically acceptable solvents (e.g. water, ethanol) may have advantageous properties (e.g. favourable crystal morphology). Hence, the formation of solvates is not only of extreme importance to experimental and theoretical structural chemists, but is also of crucial importance in the pharmaceutical industry.[67, 68]

Desolvation and its Applications

Solvates may desolvate under ambient conditions or require thermal activation for this process to occur.[69] Furthermore, the desolvation process may proceed *via* two mechanisms: one-step desolvation (simultaneous release of all the guest molecules) and multi-step desolvation (step-wise release of the guest molecules giving rise to intermediate phases).[69] In addition, the desolvation process provides an opportunity to draw meaningful comparisons of thermal quantities for a series of isostructural compounds since the host molecular framework is constant in these compounds.

The desolvation process can lead to several types of solid forms. Examples include isomorphic desolvates which retain the same overall molecular packing as the parent solvate,[60, 61] the same polymorph from which the solvate was prepared but one having a different texture, which may give rise to the improvement of certain properties (such as flowability and uniformity of particle size),[70] amorphous material with higher free-energy

and solubility,[71] or even an entirely new polymorph of the host. If spontaneous desolvation were to go undetected, the resulting form might present undesirable properties.[72] Eventually, these could influence the manufacturing process, dissolution rate, storage stability and bioavailability of pharmaceuticals.[73]

The desolvation/desorption and resolvation/resorption processes that occur in molecular crystals may also allow the storage or transportation of guest molecules, for instance, organic compounds, gas and water.[74]

Cyclodextrin Inclusion

Cyclodextrins [hereinafter CDs] are macrocyclic oligosugars composed of glucopyranose units varying in number due to the unspecificity of the enzyme action involved in their production from starch.[75, 76] The CDs have significance in both pure and applied research due to their ability to selectively form inclusion complexes with other molecules, ions or even radicals.[77] The simplest CDs consist of 6, 7 or 8 glucosidic units and bear the names α-, β- and γ-CD, respectively (Figure 4). Numerous CD derivatives have been synthesised in order to improve their complexing properties and to make them suitable for various applications, especially to increase the bioavailability of drugs which may be included in the CDs.[77]

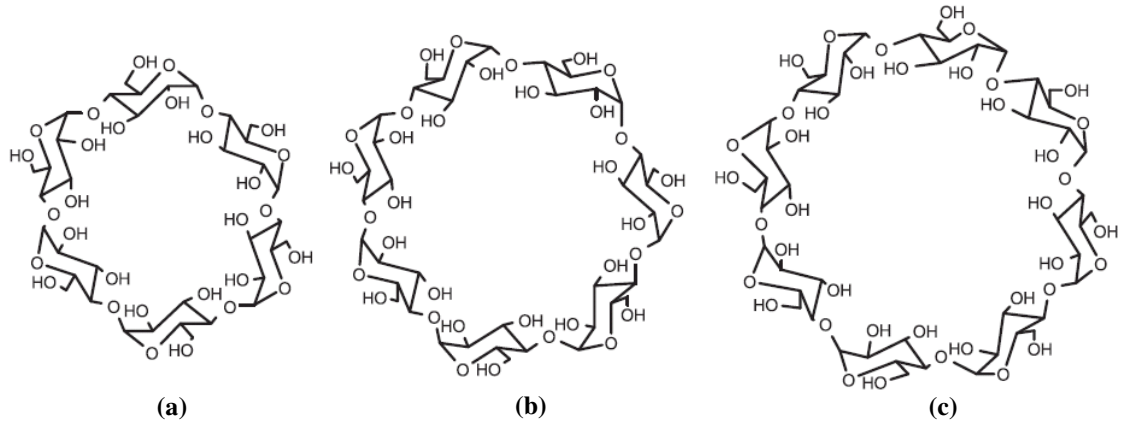

Figure 4 Schematic diagrams of (a) α-, (b) β- and (c) γ-CD

Structural Features

Figure 5 (a) includes a schematic diagram of the glucopyranose unit atom labelling. The glucopyranose unit adopts a $^4C_1$-chair conformation and can be considered as fairly rigid.[78-80] The structure of the CD molecule is also reasonably rigid due to the presence of such chair conformations and the intramolecular ring of hydrogen bonds formed between the secondary hydroxyl groups of adjacent glucopyranose units. However, there is conformational flexibility in the structures of CDs, reflected in the rotational freedom of the O6-H hydroxyl groups around the C5-C6 bond and the limited rotational movement around the C1-O4′-C4′ glycosidic link (the primed numbers refer to the adjacent glucose unit).

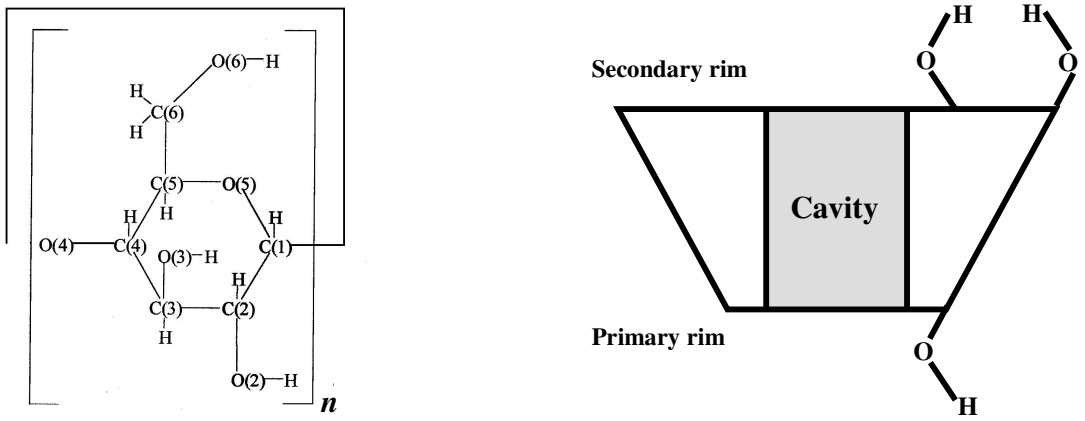

Figure 5 Schematic diagrams of (a) glucopyranose unit labelling and (b) CD molecule showing the cavity, primary and secondary faces.

The entire structure of the CD molecule adopts the shape of a hollow, truncated cone with the wide side being the secondary rim (O2-H and O3-H secondary hydroxyl groups) and the narrow side being the primary rim (O6-H primary hydroxyl groups), as shown in Figure 5 (b). These hydroxyl groups render CDs soluble in aqueous solution while the internal wall of the cavity, which is lined with methine hydrogen atoms (C3-H and C5-H), methylene (C6-H_2), and the glycosidic O4 atoms, possesses a hydrophobic character. The important feature of CD molecules is their ability to encapsulate parts of, or entire, hydrophobic guest molecules within the cavity, thus forming CD inclusion complexes. In

solution, the complex dissociates leading to an equilibrium between complexed and free guest.

Guest Inclusion

A guest molecule with lower polarity than water has the potential to be included in the CD due to the hydrophobic property of the cavity, as shown in Figure 6. However, the affinity of a guest towards a CD depends on various factors. For instance, the guest molecule must be of the appropriate shape and size to fit into the cavity, sometimes even only partially. Also, the guest will be favoured if it is able to hydrogen bond with the CD since no covalent bonds are formed or broken during the formation of a guest-CD complex. One of the main driving forces of the complexation is the release of the higher enthalpy water molecules from the CD cavity. The reason for this is that the replacement of enthalpy-rich water molecules by a suitable guest molecule in the cavity will result in lowering the energy of the system. Several factors aimed at elucidating the driving forces for complexation have been considered, including van der Waals forces, hydrophobic interactions and hydrogen bonding. However, the nature of the guest decides the extent to which each of these factors contributes to host-guest binding.[78]

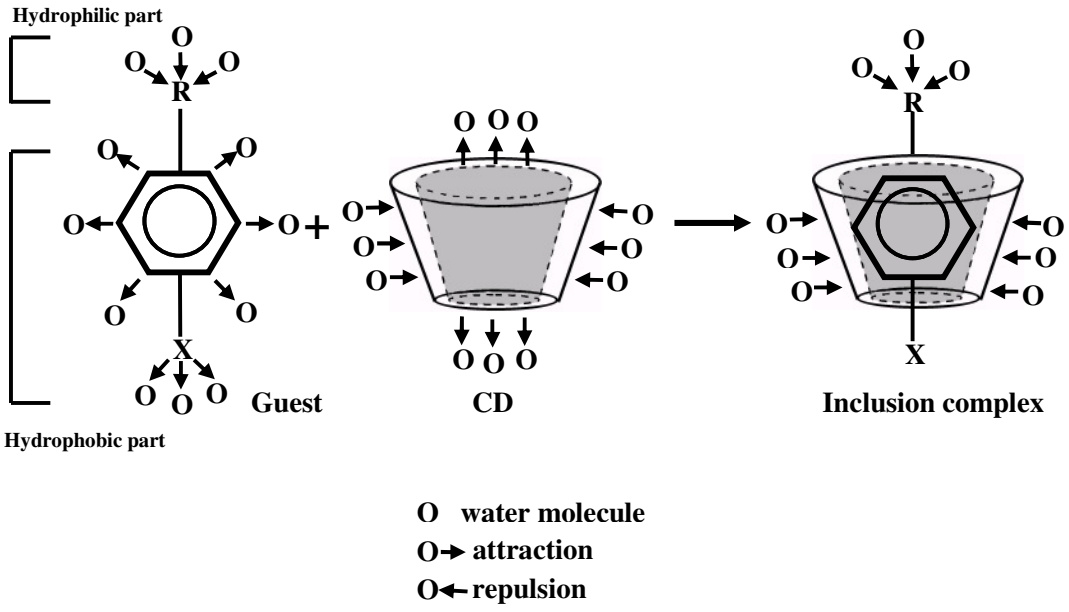

Figure 6 Schematic diagram of guest inclusion by CD and the expulsion of water from CD cavity

Isostructurality

Isostructurality, as mentioned earlier, refers to two or more crystalline phases having similar unit cell dimensions, the same space group and common moieties having almost identical atomic co-ordinates.[81] Thus, isostructural compounds would adopt nearly identical packing arrangements and display nearly superimposable Powder X-ray diffraction (PXRD) patterns. Because CD inclusion complexes tend to crystallise in various isostructural series, the use of PXRD for their definitive characterisation has become possible.[81, 82] PXRD is therefore a crucial tool in confirming the successful complexation between a CD and a guest and identification of complex phases in the absence of single crystal X-ray data.

Applications

Over the past twenty years, CDs have been applied in a variety of areas, such as the pharmaceutical, food, pesticide, biomedical and analytical industries.[88] However, since the aim of this study was supramolecular modification of different drugs, the pharmaceutical applications of CDs are most relevant to the present discussion.

The most frequent use of CDs in the pharmaceutical area includes (i) improvement of certain properties of water-insoluble drugs, such as their solubility, dissolution rate, stability and bioavailability,[84] (ii) control of the rate of drug release when the CD functions as drug carrier, thus increasing the duration of effectiveness,[85] (iii) improvement in the stability of several labile drugs against hydrolysis, oxidation and photodecomposition,[86] and (iiii) stabilisation of volatile drugs, suppression of unpleasant odours or tastes of certain drugs, and reduction of some adverse side effects (e.g. gastrointestinal ulceration).

An example of a drug to which CD technology has been applied is praziquantel (PZQ), the drug of choice for the treatment of schistosomiasis. Due to its low aqueous solubility, large doses are required to achieve adequate concentrations at the target sites. However, the aqueous solubility of PZQ was significantly improved by forming inclusion complexes with α-, β- and γ-CDs. Specifically, the dissolution rate of PZQ from α-, β-

and γ-CD complexes was 2.6-, 5- and 8-fold greater, respectively, than that of the pure drug.[87]

Cocrystals

The term 'cocrystals' has been widely used in the last twenty years. However, the definition of a 'cocrystal' is still under discussion and remains a matter of topical debate.[88] A so-called 'cocrystal', which might be obtained by experiment, contains at least two distinct species connected by intermolecular forces.[89] The nature of this force is the major difference between the formation of cocrystals and salts. In a salt, proton transfer from one molecule to the partner molecule occurs, yielding ions that are held together by electrostatic interactions. Instead, in a cocrystal, the individual components retain their electrical neutrality and are typically associated *via* hydrogen bonding.[88] It should be noted that the term 'cocrystal' as defined here is quite different from that used by Bingham et al.[49] to describe a particular category of solvates, as mentioned in the earlier section on Solvatomorphism. In the case of solvates, one component is a solvent at room temperature whereas in the case of the cocrystals described here, molecules involved in their formation are both solid at room temperature and atmospheric pressure.[88]

Pharmaceutical Application

Co-crystals exhibit different physicochemical properties from those of the free component. Properties affected include solubility, dissolution rate, chemical stability, meting point and hygroscopicity. Many active pharmaceutical ingredients (APIs)[90] can form molecular complexes ('cocrystals') with other more soluble and pharmaceutically acceptable molecules[91] (co-crystal formers), of which there are over a hundred solid materials classified as 'generally regarded as safe' (GRAS).[88] This presents an opportunity to tailor the properties of a solid-state dosage form at the molecular level.[90] Also, during the co-crystal preparation, it is a common to employ so-called 'green' methods, i.e. co-grinding of the solid API and the co-crystal former. Therefore, the pharmaceutical co-crystals offer enormous potential to provide new, stable structures of

novel API forms. This introduces a significant opportunity for improving the diversity and performance of drug compounds without breaking or making covalent bonds.[88, 90] Figure 7 illustrates the formation of a so-called 'pharmaceutical cocrystal'.

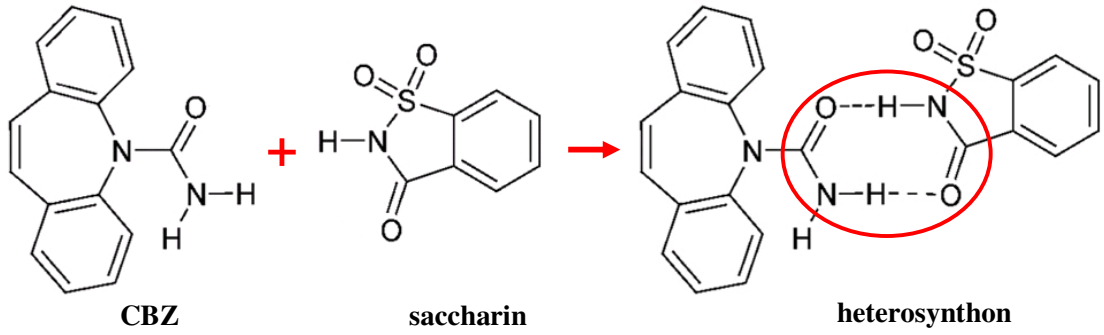

Figure 7 Schematic diagram of the formation of a cocrystal compound in the pharmaceutical area

In this example, the anticonvulsant carbamazepine (CBZ) reacts with a GRAS co-former, namely saccharin, to form a co-crystal. Here, the hydrogen bonding between the partner molecules is complementary and produces a motif called a 'synthon' in this case a 'heterosynthon', since the H-bonding functionalities of the partners are different.

Sometimes, a new polymorph of either or both of the cocrystal partners results during the attempted preparation of a cocrystal since one of the components may act to enhance or inhibit the nucleation and/or growth of a particular form of the other component rather than act to form a co-crystal.[92] A case of this is the isolation by Rafilovich et al.[93] of four polymorphs of benzidine (a compound to treat bladder and pancreatic cancer) during their attempts to prepare co-crystals of benzidine with triphenylphosphine oxide .

Antitubercular Drugs Selected for Study

Tuberculosis (TB) is a disease caused by *Mycobacterium tuberculosis* which is a bacterium that can be spread through the air. The World Health Organization (WHO) estimates that there are nearly 2 million deaths from tuberculosis annually.[94] The disease ranks second as an infectious cause of human death (the first one is AIDS, caused by the human immunodeficiency virus),[94] and occurs primarily in developing countries, especially Asian and African countries. Although several drugs [e.g. isoxyl, isoniazid

(INH), ethionamide (ETH) and rifamycins] have been employed to successfully cure the disease, the problem of drug resistance and the continuing rise in disease incidence have promoted research on the modification of the existing drugs.[95] In this study, supramolecular modification was carried out on the antitubercular drugs isoxyl, rifampicin and rifaximin.

Isoxyl

Isoxyl (Thiocarlide; N, N′-[4-(3-Methylbutoxy)phenyl]thiourea; 4, 4′-bis(isopentyloxy) thiocarbanilide; 4, 4′-di(isoamyloxy)thiocarbanilide; 1, 3-bis(*p*-isoamyloxyphenyl)-2-thiourea; thiocarlide; DATC; Datanil (Wander); Disocarban) is a poorly water soluble (dissolution rate-limiting) thiourea derivative that was used in the 1960s to successfully treat tuberculosis.[96] Figure 8 shows the chemical structure of the compound.

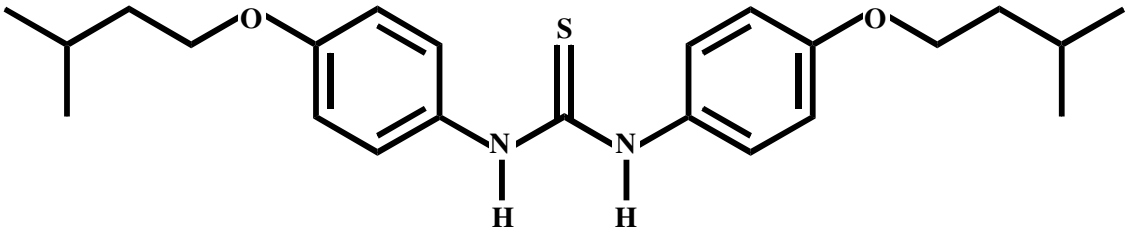

Figure 8 Chemical structure of isoxyl

Isoxyl has considerable anti-mycobacterial activity *in vitro* and is effective against multi-drug resistant strains of *Mycobacterium tuberculosis* in the range of 1-10 µg/ml.[95] Specifically, isoxyl strongly inhibits the mycolic acid synthesis of *Mycobacterium bovis* during six hours of exposure which is similar to INH and ETH, two other prominent anti-TB drugs.[95, 96] However, unlike INH and ETH, isoxyl also partially inhibits the synthesis of fatty acids of free lipid, which are stimulated by INH and ETH.[95] Furthermore, isoxyl shows no acute toxicity against primary macrophage cell cultures as demonstrated by diminution of redox activity.[95]

Recently, there has been renewed interest in isoxyl. In 2003, its activity against a range of multidrug-resistant strains of TB was demonstrated.[97] In 2007, the mode of action of

isoxyl was finally elucidated.[98] Also, new derivatives of isoxyl were synthesised in 2006[99] and 2008.[100] These developments motivated our revisiting isoxyl in this study.

Another cogent reason for a re-investigation of the polymorphism of isoxyl is as follows. The crystal polymorphism of isoxyl was investigated by Csonka-Horvai et al. in 1971.[101] Two polymorphic phases α and β were isolated. Their unit cell dimensions were determined from X-ray diffraction photographs and crude structural arrangements were postulated on the basis of these unit cell data. However, no attempts to obtain accurate crystal and molecular structures for these phases followed. These authors also investigated a thermal transformation between the two phases and determined the melting point of the stable form as ~140 ^{o}C. This temperature is consistent with the melting point of isoxyl measured by Hearn et al.[102] (141.5 ^{o}C) in 2006. However, Buu-Hoi et al.[103] reported the melting point of isoxyl as 148-149^{o}C in 1953. These conflicting results give rise to the possible suspicion of the existence of another polymorphic phase of isoxyl which may melt in the range 148-149^{o}C. Such inconsistencies arising in previous studies of isoxyl polymorphs therefore also motivated the more detailed investigation presented in this thesis.

Rifampicin and Rifaximin

Rifamycins belong to the family of naphthalenic ansamycins and they display a broad spectrum of antibiotic activity against a large variety of organisms.[104] The structural studies on rifamycins are of great interest to researchers and to the pharmaceutical industry. A great number of chemical modifications to the structure of rifamycin have been made.[105] These derivatives share a common structural feature comprising a naphthoquinonic chromophore and a 17-membered ansa chain and differ in the type of substituents R1 and R2 attached to the chromophore at C3/C4,[105] as shown in Figure 9. Currently-marketed rifamycins include rifampicin, rifaximin, rifapentine and rifabutin.[104] Rifampicin and rifaximin are used to treat tuberculosis and diarrhoea caused by *E. coli*. Isolation and unequivocal characterisation of new solid forms of these drugs provides physicochemical data that are relevant in the context of their processing, formulation and performance.

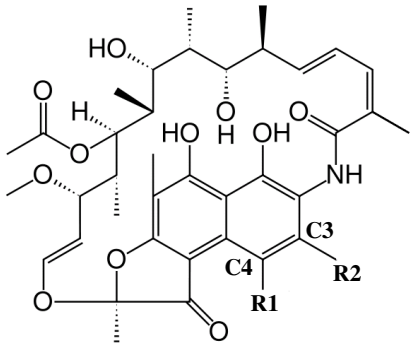

Figure 9 Chemical structure of rifamycin derivatives.

Rifampicin

Rifampicin (rifampin, rifaldazine, R/AMP, Rofact and 5,6,9,17,19,21-Hexahydroxy-23-methoxy-2,4,12,16,18,20,22-heptamethyl-8-[*N*-(4-methyl-1-piperazinyl)formimidoyl]-2,7-(epoxypentadeca[1,11,13]trienimino)-naphtho[2,1-*b*]furan-1,11(2*H*)-dione21-acetate) is a semisynthetic derivative of rifamycin. Figure 10 shows the chemical structure of rifampicin.

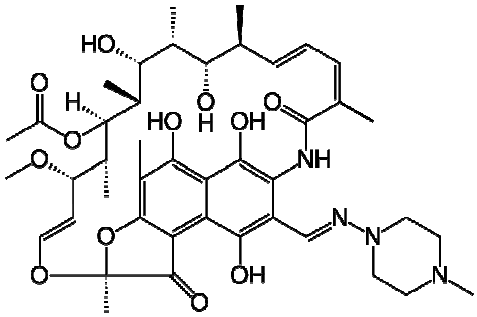

Figure 10 Chemical structure of rifampicin

The drug was introduced in 1967 and since then it has functioned as part of the standard therapy and an essential component to treat TB.[106] It has also shown excellent oral bioavailability since its therapeutic concentrations can be achieved 2 to 4 hours after oral administration and it is well distributed throughout body tissue.[107] However, spontaneous resistance against rifampicin from TB strains develops quite rapidly.[108]

The polymorphism of rifampicin had been investigated in 1977 by Pelizza et al.[109] who reported the isolation of two polymorphic forms and their characterisation by thermal

analysis, IR spectroscopy and PXRD. In 2000, Henwood et al.[110] confirmed the existence of two forms which normally co-exist in the commercial sample powder. In 2001, Santos et al.[111] reported the NMR spectrum of rifampicin in $CDCl_3$ solution. This served as the reference for peak assignments by Agrawal et al.[112] when they employed solid-state NMR spectroscopy for the investigation of two polymorphic forms in 2004. Furthermore, they determined the thermal relationship of these forms as monotropy and identified the possible intramolecular hydrogen bonds in the two forms by interpreting both NMR and IR spectra. However, due to the fact that rifampicin predominantly crystallises as a hydrate with different numbers of water molecules incorporated in the crystal,[109, 110] a water-free crystalline modification of rifampicin has not been structurally elucidated by X-ray analysis.

The solvatomorphism of rifampicin is also of great interest since the physicochemical properties of rifampicin when recrystallised from various solvent systems may vary quite significantly. In 1975, Gadret et al.[113] reported the single crystal structure of rifampicin pentahydrate. In 1977, Pelizza et al.[109] reported the isolation of four distinct rifampicin solvates which were prepared respectively by heating an absolute ethanol suspension of an amorphous form and by crystallisation from a mixture of ethanol and water (1:1 v/v), THF (tetrahydrofuran) and CCl_4. The latter two solvents yielded a 1:9 THF solvate and a 1:1 CCl_4 solvate. In 2001, Henwood et al.[114] reported the isolation of a monohydrate and a dihydrate of rifampicin and a 1:1 rifampicin • acetone solvate and a 1:2 rifampicin • 2-pyrrolidone solvate. To date, although nine rifampicin solvates have been isolated, the crystal structure of only one of these, namely rifampicin • $5H_2O$, has been reported.[113]

Rifaximin

Rifaximin (4-deoxy-4'-methylpyrido[1',2'-1,2]imidazo [5,4-c]rifamycin SV, Xifaxan, Normix, Flonorm, Redactiv, Zaxine, Rifacol and Spiraxin) belongs to a new generation of semi-synthetic derivatives of rifamycin with improved pharmaceutical properties. The drug was first described in 1982 and was introduced onto the Italian market five years later, then subsequently introduced into other European countries and licensed in some northern African and Asian areas as well as in Mexico.[115] The use of the compound for

the treatment of infectious diarrhoea in the traveller was approved by the U.S. Food and Drug Administration in 2004.[115] It is a promising new oral drug in the treatment of TB and it is characterised by a wide spectrum of antibacterial action with a good record of safety and efficacy.[116] A unique property of rifaximin is its lack of systemic absorption. This is different from other derivatives of rifamycin which are orally administered antibiotics. The poorly absorbable nature of rifaximin is due to an additional pyridoimidazole ring at C3 and C4, as shown in Figure 11.[117] This ring also gives rise to the good safety profile of rifaximin and reduction of unwanted side effects.

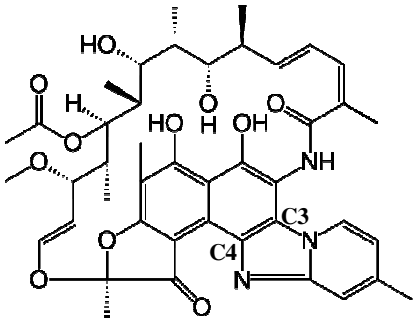

Figure 11 Chemical structure of rifaximin

Five distinct hydrates of rifaximin were prepared by Visocomi et al.[118] *via* modification of the drying conditions. These five hydrates were identified on the basis of their PXRD patterns and they were characterised by solid-state ^{13}C NMR and IR spectroscopy. Furthermore, these distinct crystalline forms of rifaximin displayed very different bioavailabilities which promoted the need for putting appropriate manufacturing and analytical procedures in place to consistently yield rifaximin of the required crystalline structure.[118] In addition, single-crystal X-ray diffraction characterisation was carried out on one of the hydrates (rifaximin tetrahydrate) by Bacchi et al.[119] in 2008.

Objectives of the Study

The first aim of this study was to attempt preparation of polymorphs, solvates, cyclodextrin complexes and cocrystals of isoxyl. The proposed investigation of the solid-state features of the modified phases included determination of differences in the structural features among different polymorphs, establishment of the thermal

relationships among polymorphs and confirmation of successful isolation of cyclodextrin complexes and cocrystals.

The other important objective of the present study was to isolate and characterise a range of solvated forms of rifampicin and rifaximin in order to systematise their solid-state chemistry. Specific objectives included identification of novel crystalline forms of rifampicin and rifaximin, establishment of the nature of the molecules in the solid state (neutral/zwitterionic character) and determination of the role of different solvent molecules in the solvate crystal structures.

References:

1. Lehn, J-M., *Angew. Chem., Int. Ed. Engl.* (Nobel lecture), **1988**, 27, 89.
2. Davy, H., *Trans. R. Soc. London*., **1811**, 1, 101.
3. Kratky, O. and Giacomello, G., *Monatsh. Chem*., **1936**, 69, 427.
4. Steed J. W. and Atwood, J. L., *Supramolecular Chemistry*, John Wiley & Sons. Ltd., **2009**.
5. Clas, S-D., Dalton, C. R., Hancock, B.C., *Pharm. Sci. Technol. Today*, **1999**, 2, 311-320.
6. Grant, D. J. W., In: *Theory and origin of polymorphism*, Brittain, H. G. (eds.), Marcel Dekker, New York, **1999,** 1–33.
7. Morissette, S. L., Soukasene, S., Levinson, D., Cima, M. J. and Almarsson, O., *PNAS*, **2003**, 100, 2180-2184.
8. Howard, K. S., Nagy, Z. K., Saha, B., Robertson, A. L., Steele, G., and Martin, D., *Cryst. Growth Des*., **2009**, 9, 3964-3975.
9. Guillory, J. K., In: *Polymorphism in Pharmaceutical Solids*, Brittain, H. G. (eds.): Marcel Dekker, New York, **1999**, 183-226.
10. Bernstein, J., *Polymorphism in Molecular Crystals*, Oxford University Press: Oxford, **2002**, 94-149.
11. Tian, F., Zhang, F., Sandler, N., Gordon, K. C., Mcgoverin, C. M., Strachan, C. J., Saville, D. J. and Rades, T., *Eur. J. Pharm. Biopharm*., **2007**, 66, 466-474.
12. Katrincic, L. M., Sun, Y. T., Carlton, R. A., Diederich, A. M., Mueller, R. L. and Vogt, F. G., *Int. J. Pharm.*, **2009**, 366, 1-13.
13. Gubica, T., Temeriusz, A., Paradowska, K., Ostrowski, A., Klimentowska, P. and Cyrański**,** M. K., *Carbohydr. Res*., **2009**, 344, 1734-1744.
14. Threlfall, T., *The Analyst*, **1995**, 120, 2435-2460.
15. Corradini, P., *Chim. Ind. (Milan)*, **1973**, 55, 122-129.
16. Vippagunta, S. R., Brittain, H. G. and Grant, D. J. W., *Adv. Drug Delivery Rev.,* **2001**, 48, 3-26.
17. Giron, D., *Pharm. Sci. Technol. Today*, **1998**, 1, 191-199.
18. Burger, A., Ramberger, R., *Mikrochim. Acta*, **1979**, *II*, 259-271.
19. Grunenberg, A., Henck, J-O., Siesler, H. W., *Int. J. Pharm*., **1996**, 129, 147-158.
20. Barsky, I., Bernstein, J., Stephens, P. W., Stone, K. H., *New J. Chem*., **2008**, 32, 1747-1753.
21. Burger, A., Ramberger, R., *Mikrochim. Acta*, **1979**, *II*, 273-316.
22. Dong, Z., Munson, E. J., Schroeder, S. A., Prakash, I., and Grant, D. J. W., *Pharmacol. Res*., **2002**, 19, 1259-1264.
23. Tong, H. H. Y., Shekunov, B. Y., Chan, J. P., Mok, C. K. F., Hung, H. C. M. and Chow, A. H. L., *Int. J. Pharm.*, **2005**, 295, 191-199.
24. Prusiner, P., and Sundaralingam, M., *Nat. New Biol.*, **1973**, 244, 116–117.

25. Naoki, M., Yoshizawa, T., Fukushima, N., Ogiso, M., and Yoshino, M., *J. Phys. Chem. B*, **1999**, 103, 6309-6313.
26. Yoshino, M., Takahashi, K., Okuda, Y., Yoshizawa, T., Fukushima, N., and Naoki, M., *J. Phys. Chem. A*, **1999**, 103, 2775-2783.
27. Shefter, E. and Higuchi, T., *J. Pharm. Sci.*, **1963**, 52, 781–791.
28. Romero, S., Escalera, B., Bustamante, P., *Int. J. Pharm.*, **1999**, 178, 193–202.
29. Yoshihashi, Y., Kitano, H., Yonemochi, E., Terada, K., *Int. J. Pharm.*, **2000**, 204, 1-6.
30. Shah, J. C., Chen, J. R. and Chow, D., *Drug Dev. Ind. Pharm.*, **1999**, 25, 63-37.
31. Bernstein, J., *Polymorphism in Molecular Crystals*, Oxford University Press: Oxford, **2002**, 4-8.
32. Seddon, K. R., *Cryst. Growth Des*., **2004**, 4, 1087-1087.
33. Bernstein, J., *Cryst. Growth Des*., **2005**, *5*, 661.
34. Nangia, A., *Cryst. Growth Des*., **2006**, 6, 2-4.
35. Pienaar, E. W., Caira, M. R., Lötter, A. P., *J. Crystallogr. Spectr. Res.,* **1993**, 23, 739-744.
36. Bari, S. B., Kadam, B. R., Jaiswal, Y. S. and Shirkhedkar, A. A., *Eurasian J. Anal. Chem.*, **2007**, 2, 32-53.
37. Harris, R. K., Hodgkinson, P., Larsson, T., Muruganantham, A., Ymén, I., Yufit D. S. and Zorin, V., *Cryst. Growth Des*., **2008**, 8, 80-90.
38. Brittain, H. G., *J. Pharm. Sci.*, **2009**, 1-22.
39. Pluth, M. D. and Raymond, K. N., *Chem. Soc. Rev*., **2007**, 36, 161-171.
40. Shibakami, M., Tamura, M., and Sekiya, A., *J. Am. Chem. Soc*., **1995**, 117, 4499-4505.
41. Bettinetti, G. P., Caira, M. R., Sorrenti, M., Catenacci, L., Ghirardi, M. and Fábián, L., *J. Therm. Anal. Calorim.*, **2004**, 77, 695-708.
42. Fábián, L. and Kálmán, A., *Acta Crystallogr., Sect. B*, **1999**, 55, 1099-1108.
43. Caira, M. R., Bettinetti, G., Sorrenti, M. and Catenacci, L., *J. Pharm. Sci*., **2003**, 92, 2164-2176.
44. Cox , J. S. G., Woodard, G. D. and McCrone, W. C., *J. Pharm. Sci*., **1971**, 60, 1458-1465.
45. Barnett, S. A., Tocher, D. A. and Vickers, M., *CrystEngComm*, **2006**, 8, 313-319.
46. Caira, M. R., In: *Encyclopaedia of Supramolecular Chemistry* (Vol. 1), Atwood, J. L. and Steed, J. W. (eds.): Marcel Dekker, Inc., **2004**, 767.
47. Kálmán, A., Párkányi, L. and Argay, G., *Acta Crystallogr., Sect. B*, **1993**, 49, 1039-1049.
48. Stephenson, G. A., Groleau, E. G., Kleemann, R. L., Xu, W. and Rigsbee, D. R., *J. Pharm. Sci*., **1998**, 87, 536-541
49. Bingham, A. L., Hughes, D. S., Hursthouse, M. B., Lancaster, R. W., Tavener S. and Threlfall, T. L., *Chem. Commun.*, **2001**, 7, 603-604.
50. Hosokawa, T., Datta, S., Sheth, A. R., Brooks, N. R., Young, V. G., Jr. and Grant, D. J. W., *Cryst. Growth Des.*, **2004**, 4, 1195-1201.
51. Jetti, R. K. R., Boese, R., Thallapally, P. K. and Desiraju, G. R., *Cryst. Growth Des.*, **2003**, 3, 1033-1040.

52. Lipkowski, J., *Crystallography of Supramolecular Compounds*, NATO ASI Ser. C, Boston, **1996**, 480, 265-283.
53. Yamato, K., Yuan, L., Feng, W., Helsel, A. J., Sanford, A. R., Zhu, J., Deng, J., Zeng, X. C. and Gong, B., *Org. Biomol. Chem*., **2009**, 7, 3643-3467.
54. Rychlewska, U. and Warżajtis, B., *J. Mol. Struct*., **2003**, 647, 141-150.
55. Bryan, J. C. and Levitskaia, T. G., *Acta Crystallogr., Sect. C: Cryst. Struct. Commun*., **2001**, 57, 1457-1459.
56. Mazur, L., Koziol, A. E., Krzywda, J., Glice, M., and Cybulski, J., *J. Mol. Struct*., 647, **2003**, 151-158.
57. Brittain, H. G., In: *Polymorphism in Pharmaceutical Solids*, Brittain, H. G. (eds.): Marcel Dekker, New York, **1999**, 95, 227-278.
58. Giron, D., *J. Therm. Anal. Calorim.*, **2002**, 68, 335-357.
59. Giron, D., *J. Therm. Anal. Calorim.*, **2001**, 64, 37-60.
60. Yu, L., Reutzel, S. M. and Stephenson G. A., *Pharm. Sci. Technol. Today*, **1998**, 1, 118-126.
61. Byrn, S., Pfeiffer, R., Ganey, M., Hoiberg, C. and Poochikian, G*., Pharm. Res*., **1995**, 12, 945-954.
62. Gergen, I., Radu, F., Bordean, D. and Isengard, H-D., *Food Control*, **2006**, 17, 176-179.
63. Morris, K. R. and Rodriguez-Hornedo, N., In: *Encyclopedia of Pharmaceutical Technology*, Swarbrick, J. and Boylan, J. C. (eds.): Marcel Dekker, **1993**, 7, 393-440.
64. Othman, A., Evans, J. S. O., Evans, I. R., Harris, R. K., Hodgkinson, P., *J. Pharm. Sci*., **2007**, 96, 1380-1397.
65. Bechtloff, B., Nordhoff, S. and Ulrich, J., *Cryst. Res. Technol*., **2001**, 36, 1315-1328.
66. Khankari, R. K. and Grant, D. J. W., *Thermochim. Acta*, **1995**, 248, 61-79.
67. Das, D. and Barbour, L. J., *Cryst. Growth Des*., **2009**, 9, 1599-1604.
68. Nangia, A. and Desiraju, G. R., *Chem. Commun*., **1999**, 7, 605-606.
69. Beketov, K., Weber, E., Ibragimov, B. T., Seidel, J. and Köhnke, K., *Adv. Mater*., **2002**, 12, 664-667.
70. Caira, M. R., In: *Topics in Current Chemistry*, Springer-Verlag, Berlin, Berlin, Heidelberg, **1998**, 198, 164-208.
71. Guo, Y., Byrn, S. R. and Zografi, G., *J. Pharm. Sci*., **2000**, 89, 128-143.
72. Schultheiss, N., Smit, J. P. and Hanko, J. A., *Eur. J. Pharm. Sci*., **2009**, 38, 498-503.
73. Mirza, S., Miroshnyk, I., Heinämäki, J., Christiansen, L., Karjalainen, M. and Yliruusi, J., *AAPS PharmSci*, **2003**, 5, 1-9.
74. Dobrzyńska, D., Litwin, M., Jerzykiewicz, L. B. and Matraszek, A., *J. Hazard. Mater*., **2009**, 169, 1040-1044.
75. Szejtli, J., In: *Topics in Inclusion Science – Cyclodextrin Technology*, Davies, J. E. D. (eds.), Kluwer Academic Publishers, Dordrecht, The Netherlands, **1998**.

76. Cramer, F., *Einschlussverbindungen (Inclusion Compounds)*, Springer Verlag, Berlin, **1954**.
77. Dodziuk, H., *Cyclodextrins and Their Complexes, Chemistry, Analytical Methods, Applications*, Weinheim:Wiley-VHC Verl., **2006**, Ch 1.
78. Saenger, W., *Angew. Chem., Int. Ed. Engl*., **1980**, 19, 344.
79. Saenger, W., In: *Inclusion Compounds*, (Vol. 2), Atwood L. J., Davies E. D. J. and MacNicol D. D. (eds.), Oxford Universty Press, London, **1984**, Ch 8.
80. Harata, K., In: *Inclusion Compounds*, (Vol. 5), Atwood L. J., Davies E. D. J. and MacNicol D. D. (eds.), Oxford Universty Press, London, **1984**, Ch 9.
81. Caira, M. R., *Rev. Roum. Chim*., **2001**, 46, 371-386.
82. Nakanishi, I., Arai, M., Fujiwara, T. and Tomita, K-I., *J. Incl. Phenom.,* **1984**, 2, 689-699.
83. Szejtli, J., *Chem. Rev.*, **1998**, 98, 1743-1753.
84. Irie, T. and Uekama, K., *J. Pharm. Sci*., **1997**, 86, 147-162.
85. Uekama, K., *J. Inclusion Phenom. Macrocyclic Chem*., **2002**, 44, 3-7.
86. Challa, R., Ahuja, A., Ali, J. and Khar, R. K., *AAPS PharmSciTech*, **2005**, 6, 329-357.
87. Becket, G., Schep, L. J. and Tan M. Y., *Int. J. Pharm*., **1999**, 179, 65-71.
88. Vishweshwar, P., McMahon, J. A., Bis, J. A. and Zaworotko, M. J., *J. Pharm. Sci*., **2006**, 95, 499-516.
89. Zukerman-Schpector, J. and Tiekink, E. R. T., *Z. Kristallogr*., **2008**, 223, 233-234.
90. Childs, S. L., Chyall, L. J., Dunlap, J. T., Smolenskaya, V. N., Stahly, B. C. and Stahly, P. G., *J. Am. Chem. Soc.*, **2004**, 126, 13335-13342.
91. McNamara, D. P., Childs, S. L., Giordano, J., Iarriccio, A., Cassidy, J., Shet, M. S., Mannion, R., O'Donnell, E. and Park, A., *Pharm. Res*., **2006**, 23, 1888-1897.
92. Bernstein, J., *Chem. Commun*., **2005**, 40, 5007-5012.
93. Rafilovich, M. and Bernstein, J., *J. Am. Chem. Soc*., **2006**, 128, 12185-12191.
94. Jasmer, R. M., Nahid, P. and Hopewell, P. C., *N. Engl. J. Med*., **2005**, 347, 1860-1866.
95. Phetsuksiri, B., Baulard, A. R., Cooper, A. M., Minnikin, D. E., Douglas, J. D., Besra, G. S. and Brennan, P. J., *Antimicrob. Agents Chemother*., **1999**, 43, 1042-1051.
96. Winder, F. G., Collins, P. B. and Whelan, D., *J. Gen. Microbiol*., **1971**, 66, 379-380.
97. Phetsuksiri, B., Jackson, M., Scherman, H., McNeil, M., Besra, G. S., Baulard, A. R., Slayden, R. A., DeBarber, A. E., Barry, C. E., Baird, M. S., Crick, D. C. and Brennan, P. J., *J. Biol. Chem*., **2003**, 278, 53123-53130.
98. Korduláková, J., Janin, Y. L., Liav, A., Barilone, N., Dos, V. T., Rauzier, J., Brennan, P. J., Gicquel, B. and Jackson, M., *Antimicrob. Agents Chemother*., **2007**, 51, 3824-3829.
99. Bhowruth, V., Brown, A. K., Reynolds, R. C., Coxon, G. D., Mackay, S. P., Minnikin, D. E. and Besra, G. S., *Bioorg. Med. Chem. Lett*., **2006**, 16, 4743-4747.
100. Liav, A., Angala, S. K., Brennan, P. J. and Jackson, M., *Bioorg. Med. Chem. Lett*., **2008**, 18, 2649-2651.

101. Csonka-Horvai, J., David, A., Horvath, G. and Naray-Szabo, G., *Z. Naturforsch., B: Chem. Sci*., **1971**, 26, 21-23.

102. Hearn, M., Chen, M., Cynamon, M., Wang'ondu, R. and Webster, E., *J. Sulfur Chem*., **2006**, 27, 149-164.

103. Buu-Hoi, N. P. and Xuong, N. D., *C.R. Hebd. Seances Acad. Sci*., **1953**, 237, 498-500.

104. Bacchi, A., Carcelli, M., and Pelizzi, G., *New J. Chem*., **2008**, 32, 1725-1735

105. Arora, S. K. and Arjunan, P. *J. Antibiot*., **1992**, 45, 428-431.

106. Xu, M., Zhou, Y. N., Goldstein, B. P. and Jin, D. J., *J. Bacteriol*., **2005**, 187, 2783-2792.

107. Douglas, M. J. and Mcleod, M-J, *Clin. Pharmacokinet*., **1999**, 37, 127-146.

108. Hugo, D. L., *Appl. Microbiol*., **1970**, 20, 810-814.

109. Pelizza, G., Nebuloni, M., Ferrari, P. and Gallo, G. G., *Farmaco Sci*., **1977**, 32, 471-81.

110. Henwood, S. Q., de Villiers, M. M., Liebenberg, W. and Lötter, A. P., *Drug Dev. Ind. Pharm*., **2000**, 26, 403-408.

111. Santos, L., Medeiros, M. A., Santos, S., Costa, M. C., Tavares, R. and Curto, M. J. M., *J. Mol. Struct.*, **2001**, 563-564, 61-78.

112. Agrawal, S., Ashokraj, Y., Bharatam, P. V., Pillai, O. and Panchagnula, R., *Eur. J. Pharm. Sci*., **2004**, 22, 127-114.

113. Gadret, M., Goursolle, M., Leger, J. M. and Colleter, J. C., *Acta Crystallogr., Sect. B: Struct. Sci*, **1975**, 31, 1454-1462.

114. Henwood, S. Q., Liebenberg, W., Tiedt, L. R., Lötter, A. P. and de Villiers, M. M., *Drug Dev. Ind. Pharm.*, **2001**, 27, 1017-1030.

115. Scarpignato, C. and Pelosini, L., *Digestion*, **2006**, 73, 13-27.

116. Ochoa, T. J., Chen, J., Walker, C. M., Gonzales, E. and Cleary, T. G., *Antimicrob. Agents Chemother*., **2007**, 51, 2837-2841.

117. Huang, D. B. and DuPont, H. L., *J. Infection*, **2005**, 50, 97-106**.**

118. Viscomi, G. C., Campana, M., Barbanti, M., Grepioni, F., Polito, M., Confortini, D., Rosini, G., Righi, P., Cannata, V. and Braga, D., *CrystEngComm*, **2008**, 10, 1074-1081.

119. Bacchi, A., Carcelli, M. and Pelizzi G., *New J. Chem*., 32, **2008**, 1725-1735.

Chapter 2

Materials and Experimental Methods

Materials

Isoxyl (formula: $C_{23}H_{32}N_2O_2S$, Mol. Mass: 400.58 g/mol) was purchased from Sapphire (Redfern NSM, Australia) and rifamycin compounds rifampicin (formula: $C_{43}H_{58}N_4O_{12}$, Mol. Mass: 822.94 g/mol) and rifaximin (formula: $C_{43}H_{51}N_3O_{11}$, Mol. Mass: 785.88 g/mol) were purchased from Lanospharma Laboratories Company (Chongqing, China).

Methanol and ethanol were supplied by Sigma-Aldrich Chemie Gmbh (Steinheim, Germany). 1-propanol, iso-propanol, 1-butanol, ethylene glycol and 1,4-dioxane were obtained from Merck (Modderfontein, South Africa).

β-cyclodextrin (formula: $(C_6H_{10}O_5)_7$, Mol. Mass: 1135.00 g/mol) and γ-cyclodextrin (formula: $(C_6H_{10}O_5)_8$, Mol. Mass: 1297.00 g/mol) were obtained from Cyclolab (Budapest, Hungary) and used as received.

Cocrystal formers isonicotinamide (formula: $C_6H_6N_2O$, Mol. Mass: 122.12 g/mol) and nicotinamide (formula: $C_6H_6N_2O$, Mol. Mass: 122.12 g/mol) were purchased from Sigma-Aldrich Chemie Gmbh (Steinheim, Germany) and used as received.

Preparation Methods

Recrystallisation of raw materials from a large range of single solvent systems and binary solvent systems at different temperatures was the primary method for polymorph and solvate preparation. Three different methods of crystal growth were carried out, namely slow cooling, slow evaporation and crystal growth at variable temperature.

The kneading method was applied in attempts to prepare CD inclusion complexes and co-crystals. The co-precipitation method was also employed. This involved addition

of the guest compound to a saturated solution of the CD with stirring at elevated temperature, filtration and crystallisation.

Full details of the preparation of individual species are given in the appropriate chapters.

Thermal Analysis

Thermal analysis methods, which measure the change in physical properties of a compound as a function of temperature, play a pivotal role in the investigation of polymorphism, solvatomorphism and inclusion complex chemistry. In this study, thermal analysis methods included differential scanning calorimetry (DSC), thermogravimetric analysis (TGA) and hot stage microscopy (HSM). All three methods were used in combination to investigate the complex behaviour of the compounds.

DSC

In power-compensated DSC, both the sample and a reference material are maintained at the same temperature throughout the controlled program. DSC detects the energy difference between the actual sample and the reference sample by showing either an endothermic or an exothermic deviation from the baseline. These endothermic and exothermic peaks are associated with a series of thermal events, such as guest release, phase transformation, recrystallisation, melting and decomposition. Thus, the onset temperatures and enthalpy changes (area under the peak $\propto \Delta H$) of these thermal events can be determined.

In this study, DSC measurements were performed on a Perkin-Elmer PC7-series instrument at scanning rate of 10 K/min (unless otherwise stated) under N_2 as purge gas with a flow rate of 30 cm^3/min. A sealed and empty pan was used as a reference. The apparatus was calibrated against the melting points and fusion enthalpy of

standard materials, namely Indium (ΔH = 28.5 J/g, m.p. = 156.6 ^{o}C) and Zinc (ΔH = 102.1 J/g, m.p. = 419.5 ^{o}C). Prior to the analyses, 0.3 - 3.0 mg of samples were placed in a crimped and vented aluminum sample pan after surface-drying on filter paper. Guest release from a solvate and some phase changes (e.g. fusion) are usually indicated by endothermic peaks while decomposition and recrystallisation processes appear as exothermic peaks.

TGA

TGA measures the changes in the sample mass with temperature recorded by a thermobalance. In case of solvates and inclusion compounds containing volatile solvents, sample mass loss usually occurs before decomposition; this is generally due to the guest release. Thus, TGA can be employed to determine the ratio of guest and host molecules in the original sample.

In this work, TGA analysis was performed on a Mettler Toledo TGA/SDTA851^{e} instrument using the STAR^{e} software (version 6.10). The sample was heated at a scanning rate of 10 K/min under N_2 as purge gas with a flow rate of 30 cm^3/min. Sample masses were between 0.8 and 3 mg. The samples were gently crushed and thoroughly dried on a filter paper as rapidly as possible. The weighed samples were placed in open aluminium oxide crucibles. The temperature range over which mass loss occurred was determined based on the first derivative of the TGA trace.

HSM

HSM is a technique used to investigate visually the thermal behaviour of chemical compounds. It usually serves as a complementary tool to TGA and DSC by visually recording the thermal events during the heating and cooling process. For instance, guest loss is usually indicated by the appearance of bubbles when the sample is immersed in an inert medium (e.g. silicone oil), and polymorphic transition is usually shown by colour or opacity changes in crystals.

In this study, a Linkam TP92 manual temperature controller was linked to a Linkam THMS600 hot stage apparatus in order to perform the heating process at a controlled rate, whilst images of thermal events were captured by a real-time Sony Digital Hyper HAD colour video camera fitted to a Nikon SMZ-10 stereo-microscope and analysed by the Soft Imaging System program, analySIS.[1] The temperature of a given event obtained from HSM is often slightly different from that obtained by DSC and TGA analysis. This is due to the different heating environments of the various instruments, but it is also affected by differences in the particle sizes in the samples (single crystals in the case of HSM and powder samples in case of DSC and TGA).

Spectroscopic Studies

Infrared Spectroscopy (FTIR)

FTIR is a very sensitive technique that finds multiple uses in solid-state chemistry. In the present study, it was used to probe the N-H stretching region for polymorphs of the antitubercular isoxyl. Spectra were recorded using a Perkin Elmer 983 IR spectrophotometer and samples were run as Nujol mulls.

^{13}C Solid-state Nuclear Magnetic Resonance Spectroscopy (SSNMR)

Solid-state NMR spectroscopy is gaining increasing importance in the determination of the structure, conformation and crystallographic features of polymorphs since different hydrogen bond motifs and variations in packing can introduce changes in the spatial relations of nuclei, leading to the differences in their resonance frequencies.[2] In the present study, the ^{13}C solid state NMR spectra were acquired on a Varian VNMRS 500 MHz two-channel spectrometer using 4 mm zirconia rotors and a 4 mm Chemagnetics™ T3 HX MAS probe. All cross-polarization (CP) spectra were recorded at ambient temperature with proton decoupling, a 4 μs 90° pulse, and a recycle delay of 10 s. The acquisition time was 20ms and contact time for cross-polarization was 2.5 ms. The free induction decay had 1667 complex points, Fourier

transformed with 10 Hz line broadening. Magic-angle-spinning (MAS) was performed at 14 kHz and Adamantane was used as an external chemical shift standard where the downfield peak was referenced to 38.3 ppm.

X-ray Diffraction Analysis

Powder X-ray Diffraction (PXRD)

The unique 'fingerprint' traces of each crystalline material can be recorded by PXRD, which is normally employed for the identification of new species of polymorphs, cyclodextrin inclusion complexes and cocrystals. Variable temperature PXRD, used frequently in this study, enables processes such as desolvation of solvates and solid-solid transformations to be detected during programmed heating of the sample. Such information complements data from other techniques such TGA and DSC.

In this study, powder X-ray diffraction patterns of samples were measured using a Philips PW1120/00 X-ray generator with nickel-filtered CuKα_1 radiation (λ = 1.5418 Å). The generator, which was fitted with a Huber long fine-focus tube PW2273/20 and a Huber Guinier Monochromator Series 611/15, produced X-ray at 20 mA and 40 kV. The PXRD patterns were then recorded using a Huber Imaging Plate Guinier Camera 670. In case of variable temperature PXRD, the Huber High Temperature controller HTC 9634 unit was used with the capillary rotation device 670.2. Samples were manually ground and packed into Markröhrchen non-diffracting glass capillaries supplied by Hilgenberg (Germany). In this study, samples were exposed to radiation for 30 – 120 min depending on the quantity and quality of the sample. A 2θ range of 4 to 100.0^o was used with a step size of 0.005^o 2θ.

Single Crystal X-ray Diffraction

Single crystals of good quality (as indicated by their ability to extinguish plane-polarized light uniformly) and suitable size were selected for intensity data

collections. Two single crystal X-ray diffractometers were employed in this study: a Nonius Kappa CCD (Charge Coupled Device) Single Crystal X-ray Diffractometer and a Bruker KAPPA APEX II DUO diffractometer.

The Nonius Kappa CCD four-circle diffractometer used graphite-monochromated MoKα radiation (λ = 0.71069 Å) produced at 50 kV and 30 mA with a Nonius FR590 generator. For polymorphic crystals, unit cell determinations were carried out both at ambient temperature (294 ± 2 K) as well as low temperature (173 ± 2 K) in order to test whether there were any phase changes during the cooling process. Solvated crystals were quickly removed from mother liquor and coated with paratone N oil. Unit cell determinations were carried out directly at low temperature without delay, so as to avoid solvent loss. The low temperatures were maintained by using a constant stream of nitrogen vapour produced by a Cryostream cooler (Oxford Cryosystems UK) at a flow rate of 20 cm^3 /min. The strategies for data collections were evaluated by using COLLECT[3] software. Intensity data were collected by the standard φ- and ω-scan techniques and they were scaled and reduced using DENZO-SMN[4] software. For the isoxyl crystals, containing sulfur atoms, the data were subjected to absorption correction using the multi-scan program SADABS[5].

The Bruker KAPPA APEX II DUO diffractometer used graphite-monochromated Mo-Kα radiation (λ = 0.71069 Å). The unit cells of the solvated crystals were determined at low temperature (100 ± 2 K) after their removal from the mother liquor. The data collections were carried out in the above temperature range using Cryostream coolers (Oxford Cryosystems UK). Data reduction was performed using the program SAINT.[6]

For the intensity data obtained from both instruments, the space group symmetry was determined by examining systematic absences in the data. The program XPREP[7] was employed to facilitate this process. Examination of the mean $|E^2-1|$ values (E is the

normalised structure factor) enabled centrosymmetric ($|E^2-1| = 0.968$) and non-centrosymmetric ($|E^2-1| = 0.736$) space groups to be distinguished.

Crystal structures that contained relatively small molecules (e.g. isoxyl, isonicotinamide and nicotinamide) were solved by direct methods using SHELXS-97[8] and those containing large molecules (e.g. rifampicin and rifaximin) were solved with program SHELXD[9]. All structures were refined by full-matrix least-squares techniques using SHELXH-97[10] and the graphic interface program X-Seed[11]. More detail concerning programs SHELXD[9] and SHELXH-97[10] follows below.

SHELXD

SHELXD[9] is a program especially designed for *ab initio* solution of larger structural problems. The solution strategy of this program is based on the dual-space iteration strategy, called '*shake and bake*',[12] which has solved structures of up to 1000 independent atoms with native data to least 1.2 Å resolution.[13]

SHELXH-97

Model refinement was performed with program SHELXH-97[10] which employs full-matrix least-squares minimisation of the sum of the squares of the differences between observed and calculated intensities ($\sum w\left(F_o^2 - F_c^2\right)^2$). The accuracy of the model being refined is expressed by the residual index, R, defined by R_1 and wR_2. The residue index R_1 (see expression 1) represents the agreement between the observed (F_o) and the calculated (F_c) structure factor amplitudes for the refinement against F, whereas the residual index wR_2 (see expression 2) gives the agreement between intensities for the refinement against F^2, which is the base of the goodness-of-fit parameter, S (defined later).

$$R_1 = \left(\sum \| F_o | - | F_c \|\right) / \sum |F_o| \qquad (1)$$

$$wR_2 = \left[\left(\sum w\left(F_o^2 - F_c^2\right)^2\right) / \left(\sum w\left(F_o^2\right)^2\right)\right]^{1/2} \qquad (2)$$

The default weighting scheme w employed had the form:

$$w = 1/\left[\sigma^2\left(F_o^2\right) + (aP)^2 + bP\right]$$

where $P = \left[\max\left(0, F_o^2\right) + 2F_c^2\right]/3$ and the terms a and b were refined to produce constant distributions of $\left[w\left(F_o^2 - F_c^2\right)^2\right]$ with sinθ and $(F_o/F_{max})^{½}$.

S (Goodness-of-Fit) was also quoted for each structure and is defined as $S = \left[\sum\left(w\left(F_o^2 - F_c^2\right)^2\right)/(n-p)\right]^{½}$, where n is the number of reflections and p is the total number of parameters refined. For a well-behaved model, S should be close to unity while the over-determination ratio (n/p) should be ~ 10.

Structure solution and refinement details for the individual structures will be described in the relevant chapters.

Computer Packages

The following computer packages were employed for the analysis of crystal structures.

LAYER[14] displays the intensity data as simulated precession photographs, which can be employed to determine the space group symmetry from systematic absences.

POV-RAY[15] was used to create all molecular packing diagrams.

LAZY PULVERIX[16] was employed to generate idealised PXRD patterns which were usually compared with the corresponding experimental PXRD traces to confirm the homogeneity of bulk materials and to prove the accuracy of the crystallographic models. Input to this program included atomic fractional coordinates, thermal parameters and space group data.

Program **SECTION**[17] was used to establish the topologies of voids in the host molecule frameworks that contained solvent molecules. The host molecules were represented with their van der Waals radii after the guest molecules were artificially removed from the structural models. The program then allowed one to plot sections through the unit cell along a selected axis at pre-determined intervals.

X-Seed[11] was employed as a graphical interface for SHELXH-97[10], LAYER[14], POV-RAY[15], LAZY PULVERIX[16] and SECTION[17].

PLATON[18] was used to calculate geometrical parameters (bond distances, bond angles and torsion angles) and the non-covalent interaction parameters (e.g. for hydrogen bonding, π···π-ring and C-H···π-ring interactions) as well as their associated standard deviations, for each structure.

WINGX[19] was used as an interface for PLATON[18].

The Cambridge Structural Database (CSD)[20] was used to access the published crystal data for comparison with experimental data for the polymorphs and solvatomorphs presented in this study.

Additional Resources

Table 1 lists the final crystallographic data files of the compounds in this thesis.

Table 1 File types contained in Appendix 3.

File extensions/formats	Contents
.HKL	Reflection data
.RES	SHELX co-ordinate data
.CIF	Crystallographic information file
.FCF	Structure factor tables
.LIS	Platon output
.XL	SHELX output file
.SUP	Tabulated supplementary data

References:

1. Soft Imaging System GmbH, *Digital Solutions for Imaging and Microscopy*, Version 3.1 for Windows © **1987-2000**.
2. Tishmack, P. A., Bugay, D. E., Byrn, S. R., *J. Pharm. Sci*., **2003**, 92, 441-474.
3. COLLECT, data collection software, Nonius, **1998**.
4. Otwinowski, Z., Minor, W., *Processing of X-ray Diffraction Data in Oscillation Mode in Methods in Enzymology*, Vol. 276, Carter, C.W., Sweet, R.M., (eds.), Academic Press, New York, **1996**, 307-326.
5. Sheldrick, G. M., *SADABS*. University of Göttingen, Germany., **1996.**
6. SAINT Version 7.60a, Bruker AXS Inc., Madison, WI, USA, **2006**.
7. XPREP, *Data Preparation and Reciprocal Space Exploration*, Version 5.1, © Bruker Analytical X-ray Systems, **1997**.
8. Sheldrick, G. M., *SHELXS-97*, *Program for Crystal Structure Solution*, Institüt für Anorganische Chemie der Universität, Tammanstrasse 4, D-3400 Göttingen, Germany, **1997**.
9. Sheldrick, G. M., In: *Direct Methods for Solving Macromolecular Structures*, Fortier, S. (eds.), Kluwer Academic Publishers: Dordrecht, **1998**, 401-411.
10. Sheldrick, G. M. SHELXH, *Acta Crystallogr.,* **2008**, A64, 112-122.
11. Barbour, L. J. *X-Seed*, *A software tool for Supramolecular Crystallography*, *Supramol. Chem*., **2001**, 1, 189-191.
12. Miller, R., Gallo, S. M., Khalak, H. G. and Weeks, C. M., *J. Appl. Cryst.,* **1994**, 27, 613-621.
13. Usón, I., Sheldrick, G. M., *Curr. Op. Struct. Biol*., **1999**, 9, 643-648.
14. Barbour, L. J., Layer - A computer program for the graphic display of intensity data as simulated precession photographs., *J. Appl. Cryst.* **1999**, 32, 351-352.
15. Pov-Ray for Windows Version 3.1e.watcom.win32, The persistence of vision development team, © **1991-1999**.
16. Yvon, K., Jeitschko, W. and Parthé, E., *J. Appl. Cryst.,* **1977**, 10, 73-74.
17. Barbour, L. J., SECTION - a computer program for the graphic display of cross sections through a unit cell, *J. Appl. Cryst.* **1999**, 32, 353.

18. Spek, A. L. PLATON, *A multipurpose crystallographic tool*, Version 10500 © **1980-2000**.
19. Farrugia, L. J. WinGX, An integrated system of windows programs for the solution, refinement and analysis of single crystal X-ray diffraction data, Version 1.63, *J. Appl.Cryst*., **1999**, 32, 837-838.
20. Cambridge Structural Database and Cambridge Structural Database System, Version 5.31, February **2010**, Cambridge Crystallographic Data Centre, University Chemical Laboratory, Cambridge England.

Chapter 3

Supramolecular Modification of Compound Isoxyl

Attempts to isolate different polymorphic and solvatomorphic phases as well as cyclodextrin inclusion complexes and cocrystals for the compound isoxyl were carried out. Based on the results achieved, this chapter is divided into four parts:

Part One: Two polymorphic phases of isoxyl (**Form 1** and **Form 2**).
Part Two: A solvatomorphic phase of isoxyl (S1).
Part Three: β- and γ-cyclodextrin complexes of isoxyl.
Part Four: Attempts to form cocrystals with isoxyl were not successful. However, a new polymorphic phase of a cocrystal former, isonicotinamide, and that of a second cocrystal former, nicotinamide, were successfully isolated.

We describe here the investigation of the solid-state features of these new phases using single crystal and powder X-ray diffraction as well as thermal analysis methods.

Part One

Polymorph Preparation

The experimental methods comprised mainly recrystallisation of the raw material from a wide range of single solvents and binary solvent systems at different temperatures, sublimation of the raw material at different temperatures, and solid-state grinding. Table 1 lists the outcomes of recrystallisation from a range of randomly selected solvents/solvent mixtures, as well as the results from other methods of polymorph preparation. A full listing appears in Appendix 1.

Table 1 Selected results of polymorph preparation using various methods

Method	Concentration (mg/ml)	Crystallising form
Crystallisation of raw material from single solvent systems*		
Acetonitrile	**1**	**Form 1**
Methanol	**2**	**Form 1**
Formamide	**1**	**Form 1**
Sec-butyl acetate	**2**	**Form 1**
1,3-dioxolane	**1**	**Form 1**
Ethyl isobutyrate	**2**	**Form1**
Propyl chloride	**2**	**Form 1**
n-propyl acetate	**1**	**Form 1**
Ethyl propionate	**2**	**Form 1**
Diacetamide	**2**	**Form 1**
m-cresol	**2**	**Form 1**
3-methyl-1-butanol	**2**	**Form 2**
3-pentanone	**2**	**Form 2**
3,3-dimethyl-2-butanone	**1**	**Form 2**
Crystallisation from binary solvent systems*		
Water:Ethanol (1:9 v/v)	**1**	**Form 1**
Water:Ethanol (2:8 v/v)	**0.5**	**Form 2**
Vapor diffusion		
formamide[a]:2-propanol[b]	**1**	**Form 1**
formamide[a]: cyclohexanol[b]	**1**	**Form 1**
formamide[a]: ethanol 90%[b]	**1**	**Form 1**
Solid-state grinding of either Form 1 or Form 2		No effect
Sublimation		**Form 1 + Form 2**

* Each solution was prepared at 10 ^{o}C lower than the boiling point of the solvent and filtered. The solution was then allowed to cool to room temperature spontaneously for recystallisation to occur.
[a] solvent, [b] precipitant

As is evident from Table 1, only two distinct crystalline forms of isoxyl were isolated. These were initially distinguished from significant differences in their PXRD patterns and they were consequently named **Form 1** and **Form 2**.

Thermal Analysis

Hot Stage Microscopy

HSM was used to analyse the thermal behaviour of the two isoxyl polymorphs [**Form1** (needle) and **Form 2** (plate)] at a constant heating rate of 10 K/min. Single crystals of the two polymorphs were immersed in silicone oil, placed side by side on a glass slide and photographs were taken in the temperature range 30 ^{o}C to 160 ^{o}C. These HSM pictures are presented in Figure 1. The **Form 1** crystal became opaque at ~93 ^{o}C, indicating a possible phase change. At the same time, the **Form 2** crystal remained unchanged during the entire heating process before melting. Both crystals melted at the same temperature, indicating that **Form 1** had possibly transformed into **Form 2** during the heating process.

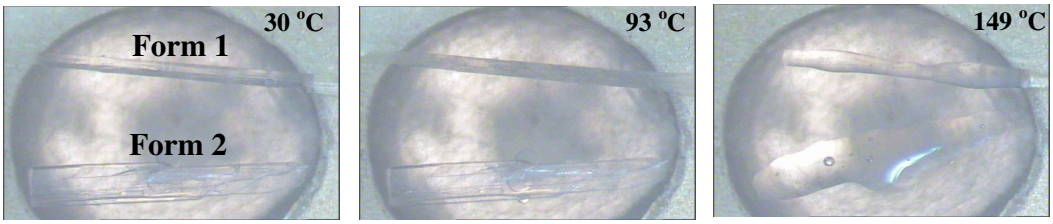

Figure 1 HSM photographs at various temperatures of the crystals of **Form 1** and **Form 2**

Differential Scanning Calorimetry and Thermogravimetric Analysis

TGA analysis (not shown) indicated negligible mass loss for both **Form 1** and **Form 2** before the decomposition event occurs, thus confirming that they are not solvates. The DSC results for the two polymorphs are shown in Figure 2. The accurate heats of transition (ΔH_t) and fusion (ΔH_f) as well as their extrapolated onset temperatures (T_t and T_f respectively) for **Form 1** and **Form 2** are presented in Table 2. The DSC trace for **Form 1** exhibited two endotherms, namely A and B. The first endotherm A corresponds to a phase change, since no mass loss was observed in the TGA curve. It also coincides with the observation from HSM of a change in the **Form 1** crystal from colourless to

opaque (Figure 1). The second endotherm B results from the melting of the resulting modification. The DSC trace for **Form 2** exhibited one endotherm B, which represents the melting of **Form 2**. The fact that the T_f value of the endotherm B in **Form 1** is very close to that in **Form 2** provides evidence of a complete phase transformation from **Form 1** to **Form 2** on heating. In addition, the onset melting point of **Form 2** can be determined as 142.7 ^oC.

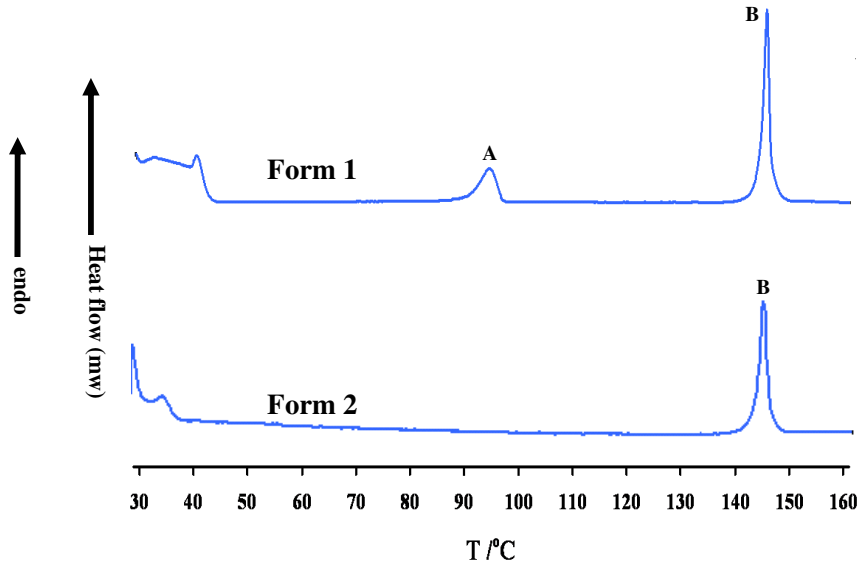

Figure 2 DSC traces for **Form 1** and **Form 2**

Table 2 DSC results for **Form 1** and **Form 2**

Polymorph	onset T_t (^oC)	ΔH_t (J g^{-1})	onset T_f (^oC)	ΔH_f (J g^{-1})
Form 1 Peak A	91.7 ± 0.4 (n=2)	34.7 ± 1 (n=2)	----------	----------
Peak B	----------	----------	142.7 ± 0.2 (n=2)	96.2 ± 2 (n=2)
Form 2 Peak B	----------	----------	142.1 ± 0.3 (n=2)	95.2 ± 2 (n=2)

Variable Temperature Powder X-ray Diffraction

It was first established by PXRD at ambient temperature (25^oC) that the raw material corresponded to **Form 1**. The PXRD patterns of **Form 1** and **Form 2** were then characterised as a function of temperature as shown in Figure 3.

In the case of **Form 1**, the PXRD pattern was first recorded at temperature intervals of 10 ^oC between 30 and 90 ^oC. In this range, no evidence of phase transition was observed. At ~90 ^oC, the PXRD pattern changed very significantly, indicating complete

transformation of **Form 1** to a new phase, later identified as **Form 2** by PXRD analysis. This new phase persisted as **Form 2** during the rest of the heating process.

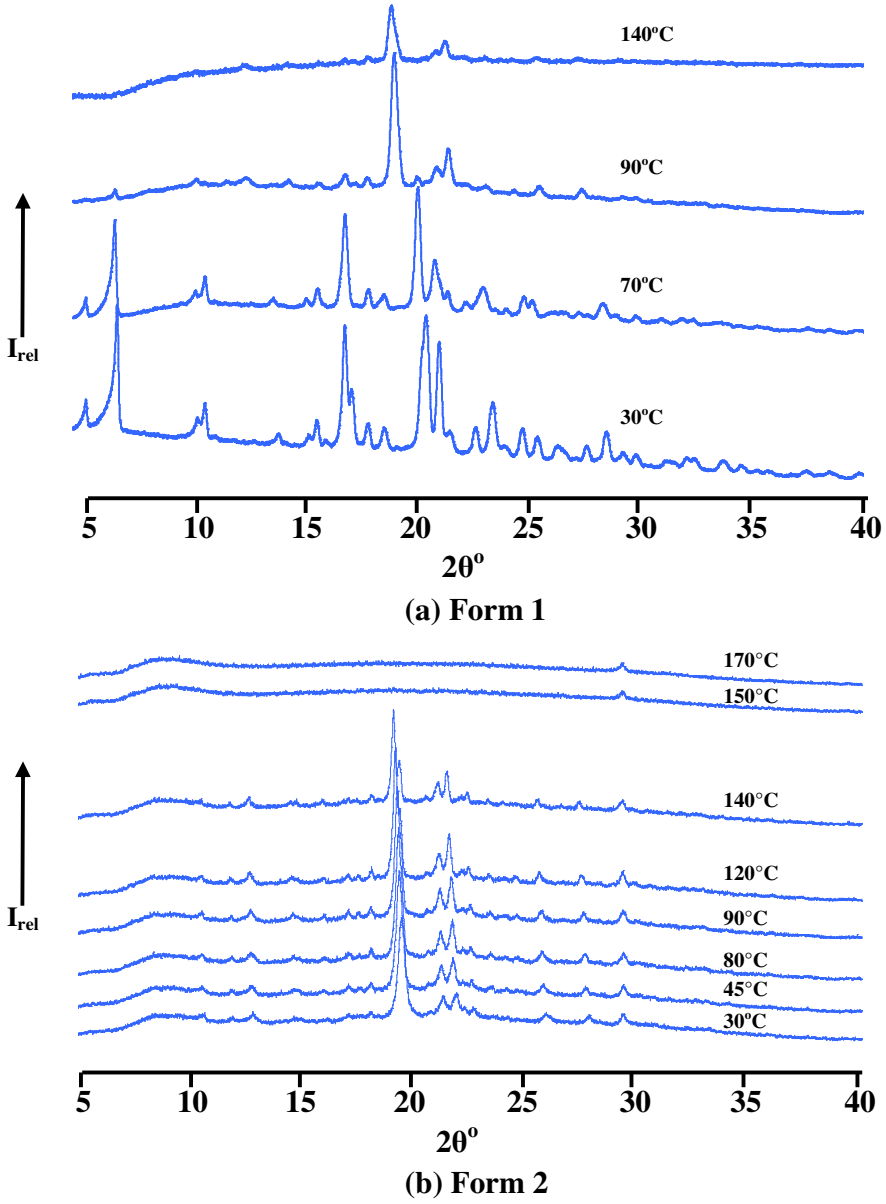

Figure 3 Variable temperature PXRD patterns of (a) **Form 1** and (b) **Form 2**.

In the case of **Form 2**, the PXRD pattern was recorded in steps of 10 K over the temperature range 30-170 °C. No phase change was evident during this heating process. **Form 2** melted at ~150 °C. This temperature was different from the melting point of **Form 2** determined by DSC (142.1 °C). (The difference can be attributed to the closed and open samples used in DSC and variable-temperature PXRD, respectively).

Attempted Measurement of the Melting Point of Form 1

The attempt to measure the melting point of **Form 1** by DSC is shown in Figure 4. A sample of **Form 1** was heated from 30 °C to 160 °C at 10 K/min (run 1) while a second sample of **Form 1** was heated from 30 °C to 180 °C at 50 K/min (run 2) in order to remove the endothermic peak A in run 1 which indicates the phase change from **Form 1** to **Form 2**. The results for run 1 and run 2 are listed in Table 3.

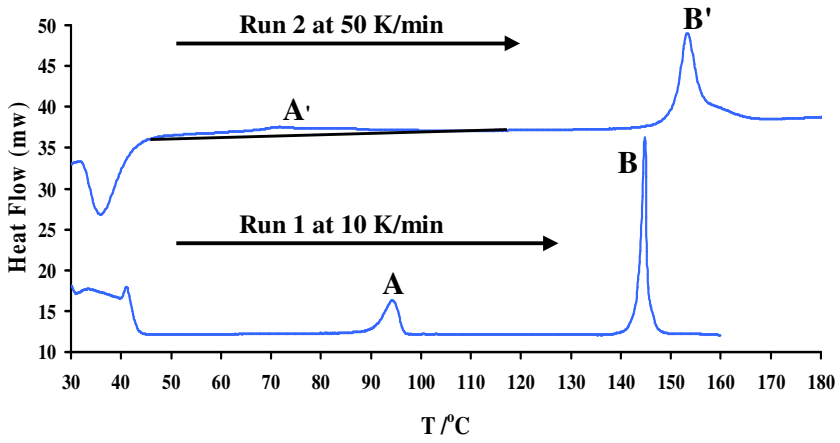

Figure 4 DSC curves for **Form 1** at different heating rates of 10 (run 1, bottom) and 50 (run 2, top) K/min

Table 3 DSC results of **Form 1** at different heating rates of 10 and 50 K/min

Run	T_t (°C)	T_f (°C)
Run 1 Peak A	91.7 ± 0.4 (n=2)	----------
Peak B	----------	142.7 ± 0.2 (n=2)
Run 2 Peak A'	39.0 ± 6 (n=2)	----------
Peak B'	----------	150.6 ± 1 (n=2)

Although the sample was heated at a relatively high scanning rate in run 2, a broad endothermic peak A' can be observed. This indicates that the phase change from **Form 1** to **Form 2** still occurs during the heating process at high scanning rate.

A notable observation was the significant broadening of the peaks in the DSC trace recorded at high scanning rate. Also, T_f of peak B shifted to a higher temperature. A possible explanation is that the high heating rate, which can involve higher temperature gradients within the sample, increased the size of the power signals due to an alteration in heat capacity since DSC output is measured in mW (mJ/s).[1, 2]

Consequently, it was concluded that the melting point of **Form 1** cannot be measured by the experimental methods used in this study.

Stability Relationship between Form 1 and Form 2

The stability relationship between the polymorphs is discussed in this section as DSC analyses, variable temperature PXRD analysis and hot stage microscopy were the main tools used for this investigation.

Figure 2 and Table 2 show that an endothermic phase change occurred at 91.7 ^{o}C. According to the Burger and Ramberger Heat of Transition Rule,[3] this would establish the stability relationship between **Form 1** and **Form 2** as enantiotropy with **Form 1** being the stable form below 91.7 ^{o}C.

In Figure 5, a single crystal of **Form 2** and crystals of **Form 1** were immersed in solvent mixture (water/ethanol 2:8 v/v) saturated with isoxyl at 25 ^{o}C. **Form 1** crystals gradually assembled on the surface of the **Form 2** crystal; the latter was entirely covered by the former after 3 hours. The single crystal of **Form 2** completely changed into crystals of **Form 1** after 4 hours. These HSM photographs provide complementary evidence that **Form 2** is the metastable modification at 25 ^{o}C.

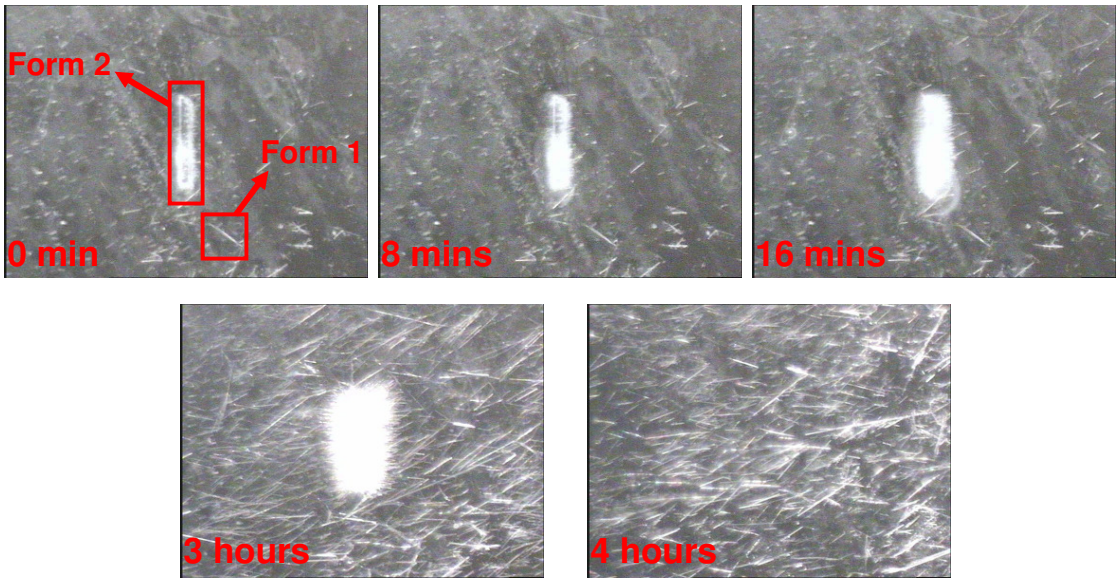

Figure 5 HSM photographs of a crystal of **Form 2** and crystals of **Form 1** immersed in the mother liquor at 25°C for 4 hours. The single crystals of both **Form 1** and **Form 2** are highlighted in red.

Since an enantiotropic relationship between the two forms was determined, the G isobars of the two modifications would intersect and this specific intersection point would be defined as the thermodynamic transition point (91.7 °C). Based on this, the order of stability of the two forms should differ between absolute zero and the melting point. In addition, the variable temperature PXRD patterns illustrate that **Form 2** is the stable modification after 91.7 °C (Figure 3). Therefore, it can be assumed that **Form 1** is the thermodynamically stable form from the absolute zero to the transition temperature. The observation from Figure 5 gives experimental evidence to support this conclusion. Consequently, the relative positions of the G isobars of each form at absolute zero can be determined.

Given the result that **Form 2** is the thermodynamically stable form between the thermodynamic transition point and its melting point, **Form 2** must have a higher melting point than **Form 1**. Therefore, it can be predicted that **Form 1** will melt in the temperature range 91.0 °C – 142.3 °C. Based on the course of the G isobar of the liquid, the melting points of the modifications are indicated by the points of intersection of the G isobars of each form (G_1 and G_2) with that of the liquid (G_{liq}).[4]

An E/T diagram for the dimorphic system comprising **Form 1** and **Form 2** can therefore be constructed, as shown in Figure 6. According to the Heat of Fusion Rule, the enthalpy of fusion of **Form 1** corresponds approximately to the sum of that of **Form 2** and the heat of transition. Based on the values in Table 2, the enthalpy of fusion of **Form 1** may thus be estimated as ~130 J g^{-1}.

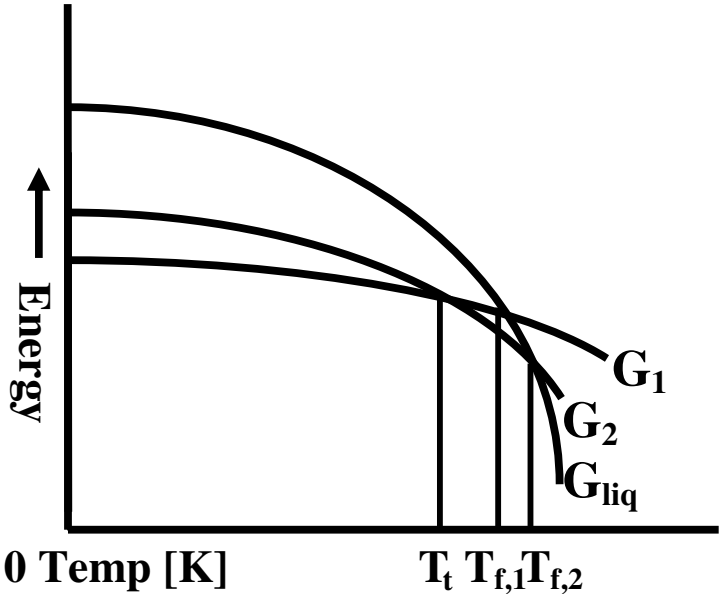

Figure 6 An E/T diagram for the two polymorphs of isoxyl

In conclusion, although the melting point of **Form 1** cannot be measured directly, it can be predicted that it is lower than that of **Form 2** by interpreting the E/T diagram. Furthermore, **Form 1** can be confirmed as the thermodynamically stable form between absolute zero and 91.7 ^{o}C while **Form 2** is the stable form between 91.7 ^{o}C and its melting point.

X-Ray Crystallographic Analysis of Forms 1 and 2

Single Crystal X-Ray Diffraction

Data-collection and Space Group Determination

A Nonius Kappa CCD four-circle diffractometer was employed to collect the intensity data for **Form 1** and **Form 2** at low temperature (LT, 173 K). In both cases, the measurement of the unit cell dimensions was first performed at room temperature (RT, 294 K) and then compared with those at LT to establish that no phase change occurred during the cooling process. In both cases, the unit cell dimensions generally decreased slightly as expected but no phase changes were evident. **Form 1** was found to belong to the triclinic crystal system and therefore, the two possible space groups are P1 and P $\bar{1}$. The latter was chosen on the basis of the intensity statistics $|E^2-1| = 0.966$ provided by XPREP.[5] The X-ray diffraction pattern of **Form 2** possesses *2/m* Laue symmetry and therefore it was assigned to the monoclinic crystal system. The following reflection conditions were observed on inspection of X-ray intensity data: *hkl*: *none*; *h0l*: $l = 2n$ and *0k0*: $k = 2n$. These conditions indicate the space group $P2_1/c$, which is thus uniquely determined. Successful refinements of the structures subsequently confirmed the correct choices of the space groups.

Structure Solution and Refinement

SHELXS-97[6] was used for the structure solution of **Form 1** and **Form 2**. Direct methods yielded the positions of all non-hydrogen atoms in the respective asymmetric units (a single molecule in each case). All the non-hydrogen atoms were then refined isotropically on F^2 with SHELXH-97.[7]

All hydrogen atoms were located in difference Fourier syntheses. The hydrogen atoms of the N-H functions were found in trigonal planar geometry. Subsequently, all H atoms were added in idealised positions in a riding model with isotropic thermal parameters in

the range 1.2 – 1.5 times those of the parent atoms. The latter were all refined anisotropically. The crystal and refinement data are presented in Table 4.

Table 4 Crystal and refinement data for **Form 1** and **Form 2**

Parameter	**Form 1**	**Form 2**
Formula unit	$C_{23}H_{32}N_2O_2S$	$C_{23}H_{32}N_2O_2S$
Formula Weight / g mol^{-1}	400.58	400.58
Crystal system	triclinic	monoclinic
Space group	$P\bar{1}$	$P2_1/c$
a / Å	5.5321(2)	19.269(5)
b / Å	13.7052(6)	8.981(2)
c / Å	16.7032(7)	13.360(4)
α / °	67.987(2)	90
β / °	87.272(2)	95.912(9)
γ / °	78.724(2)	90
Volume / Å^3	1150.96(8)	2299.72(1)
Z	2	4
Density$_{calc}$/g cm^{-3}	1.1557	1.1568
μ (MoK$_\alpha$) /mm^{-1}	0.160	0.160
F (000)	432	864
Crystal size /mm^3	0.10x0.10x0.20	0.04x0.20x0.42
Temperature / K	173(2)	173(2)
Range scanned θ / °	$1.02 \leq \theta \leq 25.03$	$1.00 \leq \theta \leq 25.35$
Index ranges	h: -6, 6	h: -23, 22
	k: -16, 16	k: -10, 10
	l: -19, 19	l: -15, 16
φ scan angle / °, frames	302 / 151	352 / 1112
ω scan angle / °, frames	160 / 80	182.7 / 574
Dx / mm	30	40
No. of measured reflections	17188	17028
No. of unique reflections	3907	3954
No. of reflections with I > 2σ(I)	2524	2186
No. of L.S. parameters	262	257
R$_{int}$, R$_\sigma$	0.0819, 0.0821	0.0675, 0.0880
S	1.052	1.016
R$_1$ (F$_o$ > 4σ(F$_o$))	0.0553	0.0665
No. of reflections omitted	17	34
wR2 (all reflections)	0.1221	0.1482
Weighting scheme	a = 0.0420	a = 0.0840
	b = 0.3974	b = 1.0553
(Δ / σ)$_{mean}$	< 0.001	< 0.001
Δρ excursions / eÅ^{-3}	-0.17, 0.04	-0.21, 0.05

Structural Description

Conformation of the Isoxyl Molecules

The numbering scheme for isoxyl used in this study is given in Figure 7.

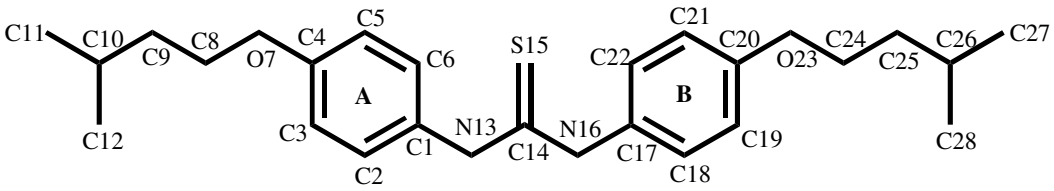

Figure 7 The numbering scheme for isoxyl

Figure 8 shows the structures of the isoxyl molecules in **Form 1** (top) and **Form 2** (bottom) and the principal torsion angle labels. Significant conformational differences are evident from Figure 8.

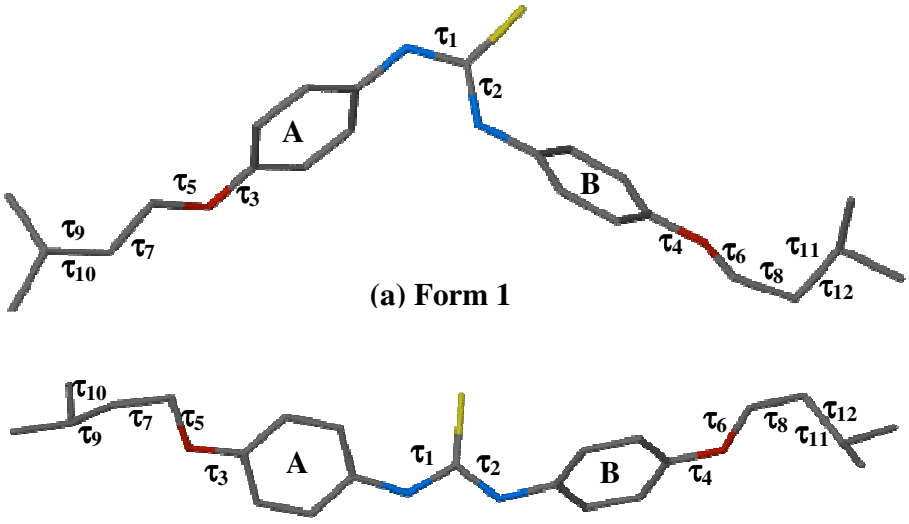

Figure 8 The molecular structures in **Form 1** (top) and **Form 2** (bottom)

Table 5 lists all the torsion angles of the isoxyl molecule in **Form 1** and **Form 2.** Twelve principal torsion angles are identified as defining the conformation of the molecule. The major conformational difference between the two molecules is reflected in the torsion angle τ_1. In **Form 1**, the atom S15 and the aromatic ring plane A are in a *trans*-configuration with respect to the linking bond C14-N13 while the aromatic ring plane B

is *cis* with respect to atom S15. Instead, in **Form 2**, both aromatic planes A and B are in a *cis* configuration with respect to S15.

Table 5 Torsion angles for **Form 1** and **Form 2**

Torsion angle (°)	**Form 1**	**Form 2**
S15-C14-N13-C1 **(τ_1)**	165.1(2) --- *trans*	-8.0(5) --- *cis*
S15-C14-N16-C17 **(τ_2)**	-8.1(4) --- *cis*	6.7(5) --- *cis*
C3-C4-O7-C8 **(τ_3)**	-171.1(3) --- *trans*	-177.8(3) --- *trans*
C21-C20-O23-C24 **(τ_4)**	176.1(2) --- *trans*	169.4(3) --- *trans*
C4-O7-C8-C9 **(τ_5)**	-179.4(2) --- *trans*	-171.8(3) --- *trans*
C20-O23-C24-C25 **(τ_6)**	-177.2(2) --- *trans*	-168.5(3) --- *trans*
O7-C8-C9-C10 **(τ_7)**	-174.0(3) --- *trans*	-54.0(5) --- *gauche*
O23-C24-C25-C26 **(τ_8)**	57.7(4) --- *gauche*	-58.3(4) --- *gauche*
C8-C9-C10-C11 **(τ_9)**	70.4(3) --- *gauche*	176.0(4) --- *trans*
C8-C9-C10-C12 **(τ_{10})**	-165.6(3) --- *trans*	-57.0(6) --- *gauche*
C24-C25-C26-C27 **(τ_{11})**	54.1(5) --- *gauche*	-61.5(5) --- *gauche*
C24-C25-C26-C28 **(τ_{12})**	178.9(3) --- *trans*	176.1(4) --- *trans*
C5-C4-O7-C8	8.6(4)	3.8(5)
C19-C20-O23-C24	-3.0(4)	-10.0(5)
C14-N13-C1-C6	131.7(3)	-22.5(5)
C1-N13-C14-N16	-15.8(4)	175.9(3)
C14-N13-C1-C2	-51.1(4)	163.4(3)
C14-N16-C17-C22	-58.6(4)	-134.4(4)
C17-N16-C14-N13	172.8(3)	-177.1(3)
C14-N16-C17-C18	125.4(3)	49.1(5)
C2-C1-C6-C5	0.3(4)	-2.2(5)
N13-C1-C6-C5	177.5(3)	-176.1(3)
N13-C1-C2-C3	-179.0(3)	175.8(3)
C6-C1-C2-C3	-1.7(4)	1.3(5)
C1-C2-C3-C4	1.3(5)	0.3(6)
C2-C3-C4-C5	0.6(5)	-1.0(6)
C3-C4-C5-C6	-2.0(4)	0.1(6)
O7-C4-C5-C6	178.3(3)	178.4(4)
C4-C5-C6-C1	1.6(4)	1.5(6)
N16-C17-C18-C19	177.2(3)	178.7(3)
N16-C17-C22-C21	-177.3(3)	-177.6(3)
C22- C17-C18-C19	1.2(4)	2.2(6)
C18- C17-C22-C21	-1.3(4)	-1.0(6)
C17-C18-C19-C20	-0.1(4)	-0.8(6)
C18-C19-C20-C21	-0.9(4)	-1.9(6)
C19-C20-C21-C22	0.7(4)	3.2(6)
O23-C20-C21-C22	-178.5(2)	-176.2(3)
C20-C21-C22-C17	0.3(4)	-1.8(6)
C2-C3-C4-O7	-179.8(3)	-179.5(3)
C18-C19-C20-O23	178.3(2)	177.4(3)

This significant difference is emphasised in the overlay of the isoxyl molecules present in the two polymorphs in Figure 9. The **Form 1** molecule adopts a '*trans-cis*' conformation while that of **Form 2** adopts a 'both-*cis*' conformation. Although the absolute values of torsion angles τ_2 are very similar, the planes of the aromatic rings B are significantly inclined to one another [angle of intersection = 70.1(2)^o].

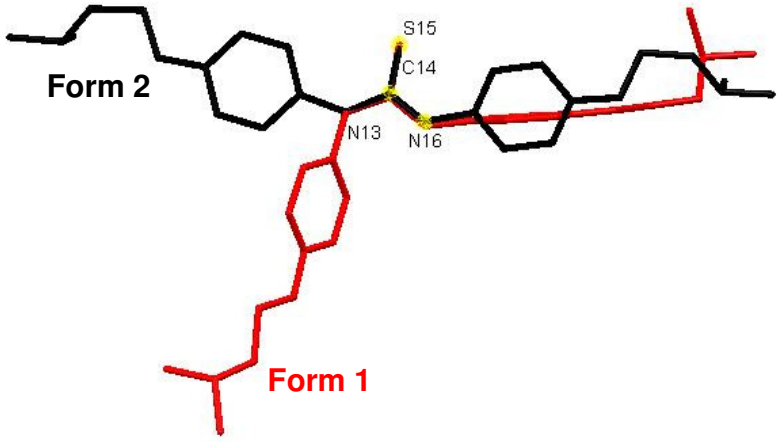

Figure 9 An overlay of the central moiety N_2CS of the isoxyl molecules in **Form 1** (red) and **Form 2** (black).

Hydrogen Bond Interactions

Table 6 lists all the hydrogen bond interactions for both polymorphs. An intermolecular hydrogen bond N13-H13···S15 and an intramolecular hydrogen bond C26-H26···O23 are found in the structures of both **Form 1** and **Form 2**. Two other intramolecular hydrogen bonds C6-H6···S15 and C10-H10···O7 are found only in the structure of **Form 2**.

Table 6 Hydrogen bonding interactions for **Form 1** and **Form 2**[a]

Hydrogen bond	N···S, C···S or C···O Distance (Å)	Angle (°)	Symmetry operator[b]
Form 1			
N13-H13···S15	3.364(2)	165.0	2-x,1-y,-z
C26-H26···O23	2.926(5)	97.3	x, y, z
Form 2			
N13-H13···S15	3.354(3)	137.0	1-x,-1/2+y,1/2-z
N16-H16···S15	3.311(3)	135.0	1-x,-1/2+y,1/2-z
C6-H6···S15	3.240(4)	122.0	x, y, z
C26-H26···O23	2.928(5)	100.0	x, y, z
C10-H10···O7	2.878(5)	99.0	x, y, z

[a] Where no e.s.d. is reported for the angle, H atoms involved were added in idealised positions in a riding model.
[b] Symmetry operator applies to hydrogen bonding acceptors.

Figure 10 illustrates the hydrogen bond interactions in the structures of **Form 1** and **Form 2.** In the structure of **Form 1,** the isoxyl molecules associate as centrosymmetric, hydrogen bonded dimers, the unique H-bond being N13-H13···S15^{i} (i = 2-x, 1-y, -z). The cyclic H-bonded pattern contains a total of eight atoms, two of them being donors and two being acceptors, and is hence designated as $R_2^2(8)$.[8, 9] Furthermore, the weak hydrogen bond C26-H26···O23 generates a ring that has a graph set analysis descriptor $R_1^1(5)$.[8, 9]

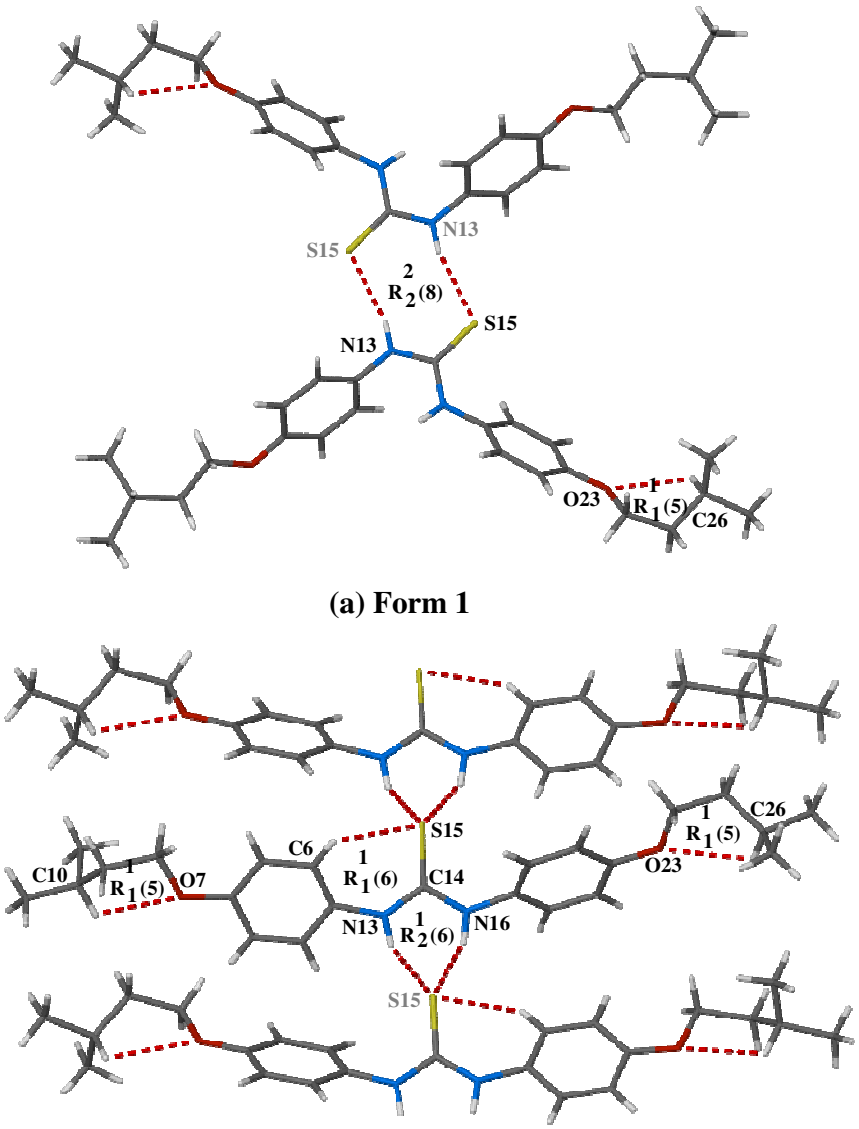

Figure 10 Hydrogen bond interactions in (a) **Form 1** and (b) **Form 2.** Atoms with gray labels have been symmetry-generated from their asymmetric unit counterparts.

In the structure of **Form 2**, the hydrogen bonding motif is of the α-network 'tape' variety,[10] occurring in N, N'-diarylureas. In the case of isoxyl, a chain results from bifurcated N-H···S (rather than N-H···O) hydrogen bonds between the NH donors and the C=S acceptors of successive screw-related molecules. The graph set analysis descriptors $R_1^1(6)$, $R_2^1(6)$ and $R_1^1(5)$, involving C-H donors in weak hydrogen bonds, are shown in their respective hydrogen bonded rings.[8, 9] These hydrogen bonds stabilise the molecular conformation.

The *trans-cis* conformation adopted by the molecule of **Form 1** is associated with formation of only one chemically unique N-H···S hydrogen bond (involving N13 only). Instead, in **Form 2**, the both-*cis* conformation allows generation of the tape motif in which both N13 and N16 engage in intermolecular N-H···S hydrogen bonds. Notably, in the **Form 1** molecule, the two N-H functions are distinctly different, one engaging in H-bonding and the other not, whereas in the **Form 2** molecule, the two N-H functions are chemically equivalent, forming symmetrical N-H···S hydrogen bonds.

Also noteworthy is the fact that the additional intramolecular C-H···S and C-H···O hydrogen bonds in **Form 2** render the molecule more rigid. The effects are respectively to reduce the rotational flexibility of one aromatic ring and to stabilise a folded conformation of the isoamyloxy moiety.

Crystal Packing

The packing diagrams of **Form 1** are shown in Figure 11. The centrosymmetric dimers pack with interdigitation of the isoamyloxy residues [Figure 11(a)]. All the molecules in Figure 11 (a) define a layer, as evident in the alternative view of Figure 11 (b) (layer labelled B). Furthermore, no hydrogen bond interactions are observed between the layers shown in Figure 11 (b).

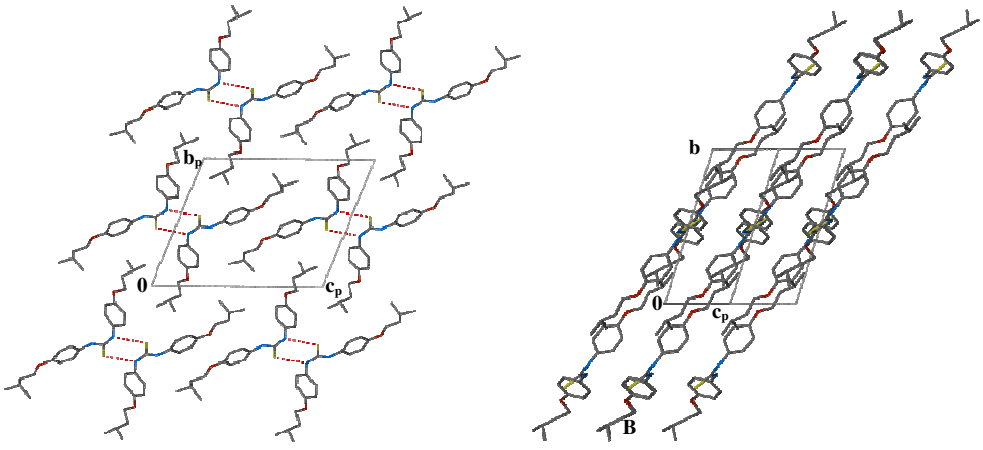

(a) [100] **(b) [10-1]**

Figure 11 Crystal packing diagrams for **Form 1** viewed along (a) [100] and (b) [10-1]. Hydrogen bonds are shown as red dotted lines. Hydrogen atoms are omitted for clarity.

Figure 12 illustrates a partial packing diagram for **Form 2.** The N-H···S hydrogen bonds generate a 'tape' motif adopting a zigzag shape along the *b*-axis.

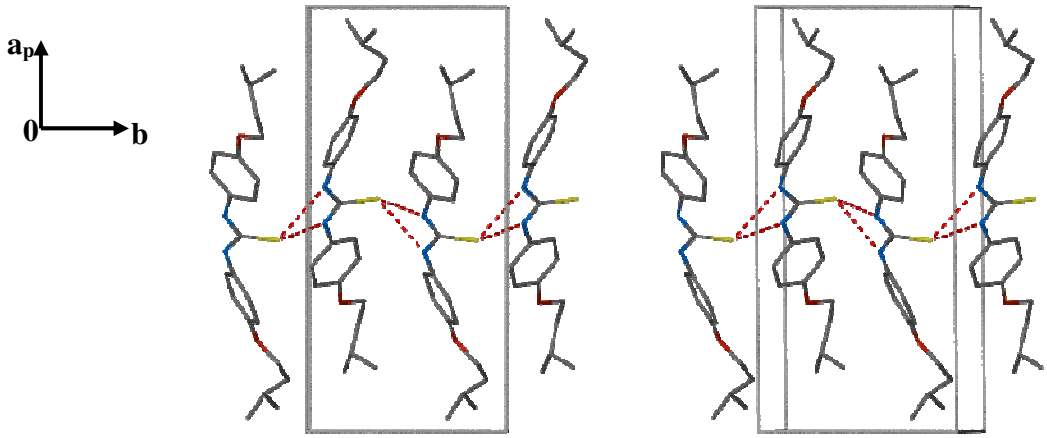

Figure 12 Stereoview of crystal packing diagram for **Form 2** viewed along [001]. Hydrogen bonds are shown as red dotted lines. Hydrogen atoms have been omitted for clarity.

Other than the hydrogen bonds described above, no other significant intermolecular interactions, such as π-π stacking, were found in the crystals of **Forms 1** and **2**.

Comparative PXRD

Figure 13 presents comparisons between the experimental PXRD patterns and those calculated from the single crystal X-ray structures (program Lazy Pulverix[11]) for both **Form 1** and **Form 2** of isoxyl.

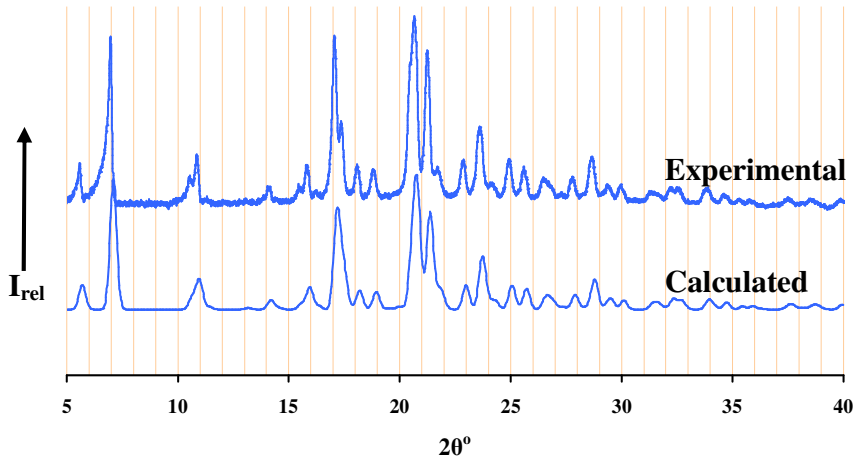

(a) Form 1

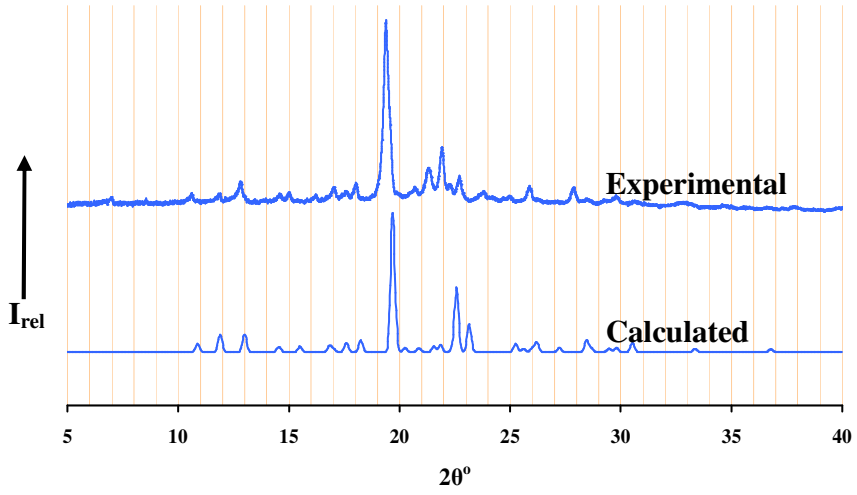

(b) Form 2

Figure 13 Calculated and experimental PXRD traces for (a) **Form 1** and (b) **Form 2**.

In both cases, the match between the experimental and calculated patterns is convincing. Specifically, the relative intensity distributions, numbers and 2θ-values of the peaks in these two patterns are in general agreement. The slight shifts of the peaks in the computed PXRD patterns to higher 2θ-values are due to shrinkage of the crystal unit cells on cooling to 173 K, the temperature of X-ray intensity data collections. The close agreement of experimental and computed patterns in both cases is an indication of the correctness of the respective single crystal X-ray structural models. Also, these matches prove that the single crystals are representative of the respective bulk polymorphs.

Fourier-transform Infrared Spectroscopy

Two new torsion angles τ_A and τ_B are introduced in this section. τ_A describes the rotation of atom H13 relative to atom S15 around the C14-N13 bond while τ_B describes the rotation of atom H16 relative to atom S15 around the C14-N16 bond (Figure 14).

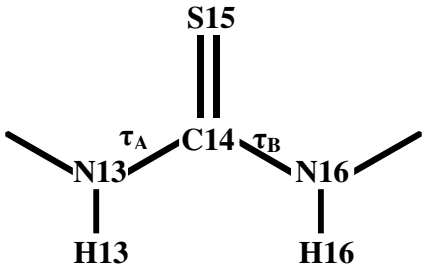

Figure 14 The numbering scheme of the central moiety in the isoxyl molecule and torsion angles τ_A and τ_B.

Table 7 lists torsion angles τ_A and τ_B in the structures of **Form 1** and **Form 2**. The two S/NH configurations for the isoxyl molecule in **Form 1** are *cis*- and *trans*-, and the configuration would be named *cis-trans* on this basis. Instead, in **Form 2**, the configuration is both-*trans*.

Table 7 Torsion angles τ_A and τ_B for **Form 1** and **Form 2**[a]

Torsion angle (°)	**Form 1**	**Form 2**
S15-C14-N13-H13 (τ_A)	-14.9	172.0
S15-C14-N16-H16 (τ_B)	157.8	-173.3

[a] The average e.s.d. value is 0.4°

FTIR spectra for **Form 1** and **Form 2** as Nujol mulls are presented in Figure 15. The investigation is focused on N-H stretching bands in the spectral range 3000 - 3450 cm^{-1}. Both the traces of **Form 1** and **Form 2** present sharp bands at around 2825 and 2925 cm^{-1}, which are due to the Nujol mull. Hearn et al.[12] reported that isoxyl displays an IR N-H stretching band at 3270 cm^{-1}. The presence of a strong band at 3271 cm^{-1} in the spectrum of **Form 2** therefore suggests that this phase corresponds to that reported by Hearn et al. This identity is further supported by the similar melting points for these phases (142.1°C for **Form 2**, 140.5°C reported by Hearn et al.). The presence of only one sharp band at 3271 cm^{-1} can be explained on the basis of the two equivalent N-H bonds

associated with the both-*trans* conformation in the **Form 2** molecule, and their engagement in symmetrical intermolecular N-H···S hydrogen bonds (Figure 10).

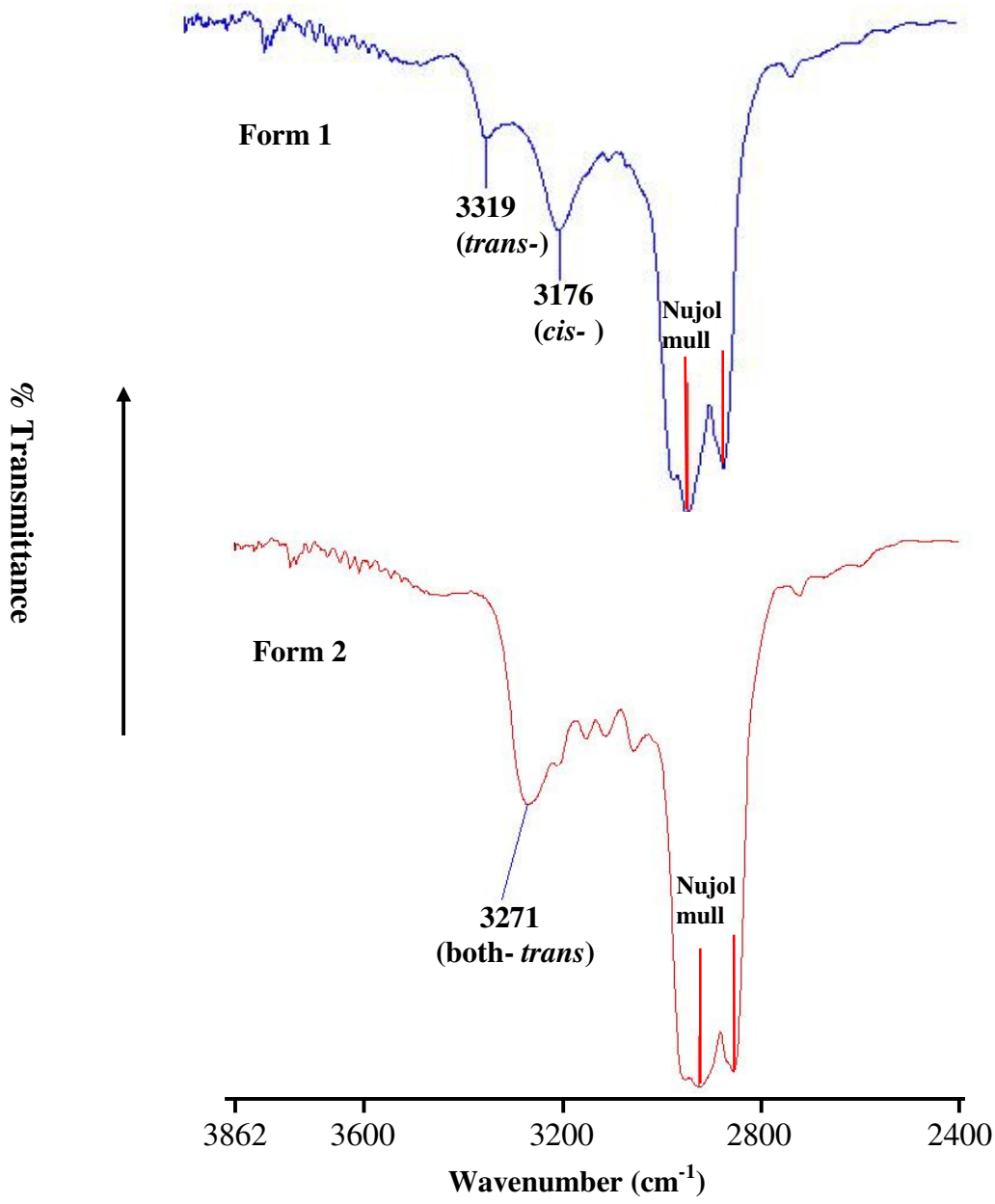

Figure 15 FTIR spectra for **Form 1** (top) and **Form 2** (bottom) in the N-H stretching region.

In the IR spectrum of **Form 1**, there are two N-H stretching bands, one at ~3176 cm^{-1} and one at ~3319 cm^{-1}. Since the lower frequency corresponds to the *cis* configuration,[13] the former band can be associated with the N13-H13 bond in the **Form 1** molecule (Figure 10). It follows that the band at 3319 cm^{-1} can be assigned to the stretching of the

N16-H16 bond. These assignments are consistent with the X-ray structural results that revealed strong hydrogen bonding involving N13-H13 (expected at lower frequency) and no hydrogen bonding in the case of N16-H16.

Based on the above analysis, **Form 1** and **Form 2** show distinctly different numbers and frequencies of peaks in the spectral range 3000-3450 cm^{-1}, that both correlate with the X-ray structural data and allow them to be distinguished by FTIR spectroscopy.

^{13}C Solid-state Nuclear Magnetic Resonance Spectroscopy

The purpose of recording the ^{13}C SSNMR spectra of the polymorphic **Forms 1** and **2** of the drug isoxyl was to establish whether they might differ sufficiently to allow this technique to be used for their identification. In addition, it was desirable to reconcile the spectra with the single crystal X-ray structures determined in this study.

^{13}C SSNMR assignments were based on the solution NMR peak assignments and the corresponding shifts for polymorphs **1** and **2** are listed in Table 8. The atom numbering scheme is shown in Figure 16 and the ^{13}C SSNMR spectra in Figure 17.

Table 8 Peak assignments for isoxyl ^{13}C NMR and ^{13}C SSNMR spectra

Atoms	Chemically equivalent Atoms	Solution NMR / ppm	**Form 1** SSNMR / ppm	**Form 2** SSNMR / ppm
C1	C17	129.58	132.57, 130.47	132.25
C2, C6	C18, C22	127.42	126.58	126.58
C3, C5	C19, C21	115.17	115.13	114.27
C4	C20	158.16	157.14	156.05
C8	C24	66.634	63.84, 66.06	66.23, 65.74
C9	C25	37.85	39.02, 38.22	39.51, 38.21
C10	C26	24.98	25.06	25.46
C11,C12	C27, C28	22.49	21.12,22.79, 23.76, 24.57	23.68, 22.99
C14		180.89	180.58	174.39

The first two columns of Table 8 indicate the sets of chemically equivalent carbon atoms, from which it is evident that in the solution ^{13}C NMR spectrum, as many as nine distinct peaks can be expected, as was the case (third column). A gross count of the number of resonances in the ^{13}C SSNMR spectra (last two columns) reveals a similar number for

each of the polymorphs, closer inspection showing, however, that in each case, the resonances consist of a mixture of single and double peaks for the most part. In a situation where there are e.g. two crystallographically independent molecules in the asymmetric unit, one would expect two closely spaced peaks for all resonances. Since this is clearly not the case for either **Form 1** or **Form 2** one concludes that there is only one molecule in each of the respective asymmetric units. This conclusion is consistent with the single crystal X-ray results for these polymorphs, which yielded $Z' = 1$ molecule per asymmetric unit in both cases (**Form 1**, space group $P\bar{1}$, $Z = 2$; **Form 2**, space group $P2_1/c$, $Z = 4$).

One further concludes that since the peak doubling does not arise from crystallographically distinct molecules in either polymorph, they must originate from conformational and environmental differences only. One of the primary results of the X-ray diffraction analyses was the classification of **Forms 1** and **2** as conformational polymorphs, the molecule in **Form 1** adopting the unsymmetrical *trans-cis* conformation while that of **Form 2** adopts the both-*cis* conformation (Figure 16). It turns out that practically all of the features of the resonances in Figure 17 can be reconciled with significant features of the accurately known solid-state molecular conformations.

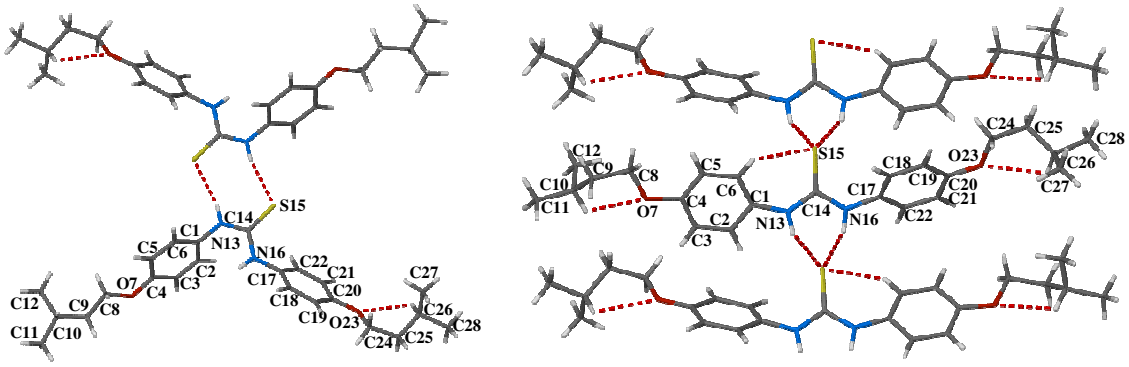

(a) Form 1 **(b) Form 2**

Figure 16 Hydrogen bond interactions and the atom numbering scheme in (a) **Form 1** and (b) **Form 2**.

Starting from the centre of the molecule (C14), we note from Table 8 that the magnitude of the difference in the shifts for this atom in the two polymorphs is the largest of all such differences ($|\Delta\delta| \sim 6.19$ ppm). This is readily explained, as the gross conformational

difference described above affects C14 most severely. Considering now the pair C1, C17 appearing as two separate peaks in **Form 1** and a single peak in **Form 2**, this again is consistent with the respective asymmetric *trans-cis* conformation and the symmetrical both-*cis* conformation.

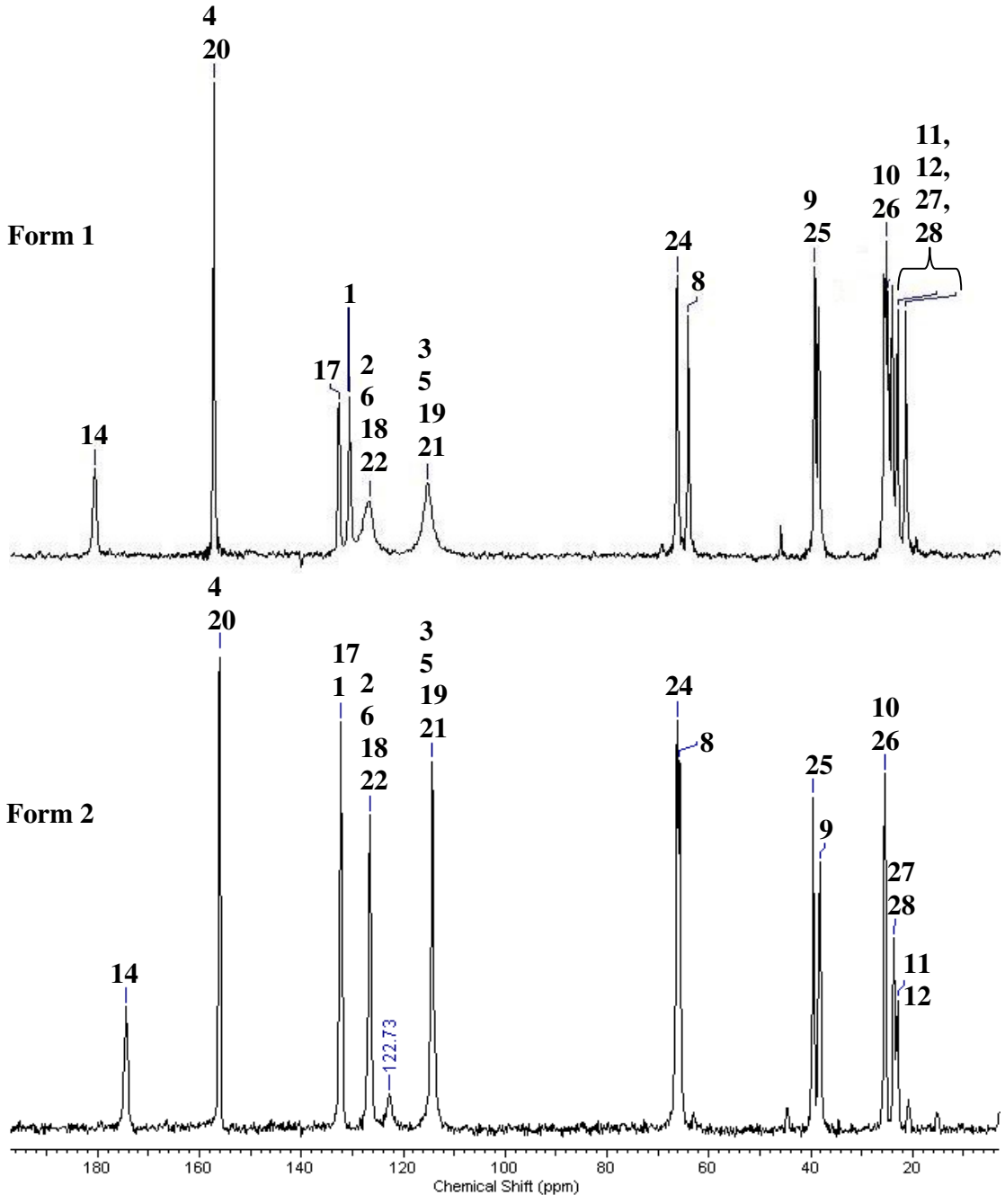

Figure 17 ^{13}**C SSNMR** spectra of **Form 1** and **Form 2**. (The chemical shift at 122.73 ppm is due to an impurity)

For each of the two sets of aromatic carbon atoms C2, C6, C18, C22 and C3, C5, C19, C21, virtually parallel behaviour of the resonances is observed in both **Forms 1** and **Form 2** as far as frequency is concerned. Interestingly, however, both resonances are significantly broader in **Form 1**. These features can be attributed to some degree of phenyl ring vibration around the C1····C4 axis, which is partially hindered in the **Form 2** crystal by the intramolecular C-H···S hydrogen bond, which tethers one of the phenyl rings of the isoxyl molecule to the sulfur atom.

Resonances associated with the isoamyl moieties are divided into four sets in Table 8. Considering the first entry, for the pair C8, C24, we note that their resonances are split in both **Forms 1** and **2**, but that in the former $|\Delta\delta|$~2.20 ppm while in the latter $|\Delta\delta|$~0.49 ppm only. The smaller difference can be reconciled with the two analogously folded chain conformations established in the **Form 2** molecule by equivalent intramolecular C-H···O hydrogen bonds that produce the two $R_1^1(5)$ rings. Instead, in **Form 1**, one isoamyloxy chain is folded but the other is extended. Features of the resonances for the pairs C9, C25 and C10, C26 are very similar and unremarkable in both polymorphs.

Finally, we note that each of the four terminal C atoms in the isoxyl molecule C11, C12 C27, C28 in the **Form 1** crystal produces a separate resonance while only two peaks appear for the **Form 2** crystal. Again, the higher multiplicity is associated with the asymmetry of the conformations of the two isoamyloxy residues in **Form 1**, while the lower multiplicity is consistent with the symmetrical, folded conformation of these chains in **Form 2**.

Interestingly, the signal for the central atom C14 in **Form 1** appears at virtually the same frequency as its counterpart in chloroform solution (180.58 vs 180.89 ppm) whereas in **Form 2**, the resonance for C14 is shifted to 174.39 ppm. This presumably indicates that in chloroform solutions the preferred molecular conformation is the *trans-cis* conformation.

In summarising the results of this section, we note that the ^{13}C SSNMR spectra of the two polymorphs are significantly different and that this technique is therefore capable of distinguishing these two crystalline forms. Furthermore, while local environmental effects also play a role in determining the ^{13}C resonance frequencies for this dimorphic system, practically all of the observed spectral differences can be reconciled with the accurately known conformational differences revealed by the X-ray crystal structures determined in this study.

Solubility Determination

The aqueous solubilities of **Form 1** and **Form 2** were determined by accurately weighing 5-10 mg of each crystalline solid in a 4 ml amber HPLC vial with a screw cap. Three milliliters of milli-Q water was subsequently added. Three samples were prepared for each analysis. The samples were rotated at 15 rpm in a VWR hybridization oven (West Chester, PA) which was previously equilibrated at 30 °C. After the predetermined time, the liquid in each vial was extracted using a sterile 5 ml luer-lok tip syringe fitted with a 0.45 μm syringe filter and an 18 gauge needle. The solutions were then analysed by determining the UV absorbance for each sample (in triplicate) at a wavelength 272 nm using a Cary UV-Vis Spectrophotometer (Palo Alto, CA). The concentration of isoxyl in each solution was subsequently determined from the calibration curve described by $y = 0.0448x - 0.1666$ ($R^2 = 0.9997$). Due to the very limited solubility of isoxyl in water, a solvent ethanol/water (4:1 v/v) mixture was used for setting up this calibration curve. The solubilities of **Form 1** and **Form 2** were calculated by determining the averages of the concentrations of the three samples, and are summarised in Table 9.

Table 9 The solubility results obtained for **Form 1** and **Form 2**.

Polymorph	Sample 1	Sample 2	Sample 3	Average solubility (μg/ml)
Form 1	3.47	3.89	3.26	3.5(3)
Form 2	3.06	3.86	3.20	3.4(4)

The results listed in Table 9 show that the equilibrium solubilities of the two polymorphs are not significantly different. PXRD analysis was carried out to identify the undissolved powder before and after the dissolution analysis. A noteworthy observation is that the

pattern of the undissolved sample of **Form 2** is identical to the pattern of **Form 1** while the pattern of the undissolved sample of **Form 1** remains the same as the pattern of **Form 1**. This suggests that a significant portion of **Form 2** transformed into **Form 1** during the solubility analysis. This corresponds to a solvent-mediated transformation from the metastable form at 25°C to the stable phase at that temperature.

To explore the possible polymorphic transformation during the solubility analysis, a series of solubility measurements were made after 6, 12, 24 and 48 h. These results are shown in Figure 18.

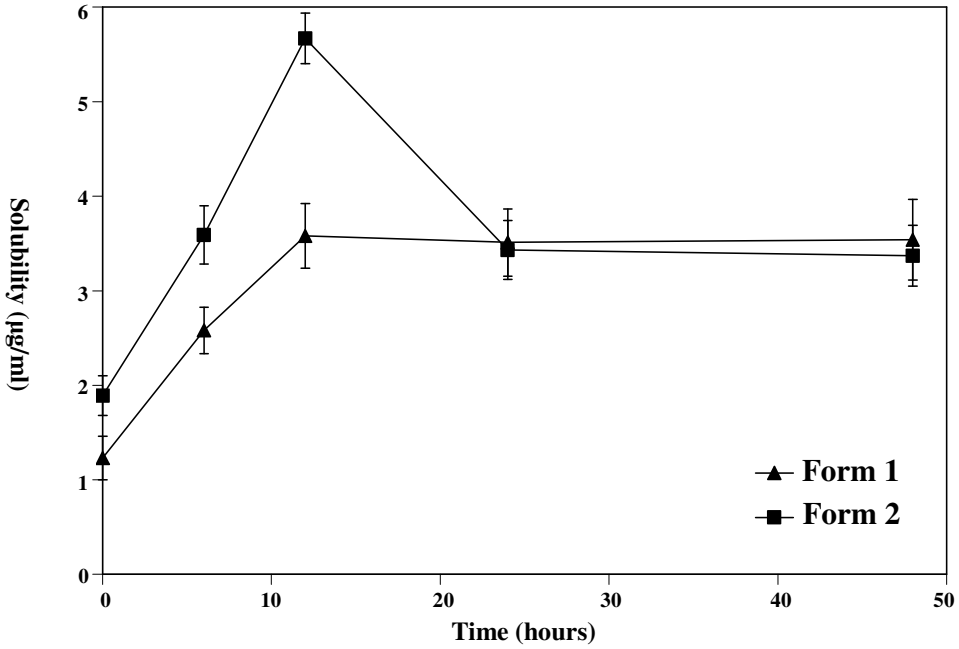

Figure 18 Solubility as a function of time for **Form 1** and **Form 2**

The solubility of **Form 2** increases at a faster rate than that of **Form 1** within the initial 12 h period. This is the expected behaviour since **Form 2** is the metastable form. At ~12 h, the solubility of **Form 2** reaches its maximum value (~ 5.8 µg/ml) which is approximately double that of **Form 1.** At the same time, **Form 1** also reaches its maximum solubility. During the period from 12 h to ~25 h, the solubility of **Form 2** gradually drops and that of **Form 1** remains constant. After ~25 h, the solubility of **Form 1** and that of **Form 2** reach the same level. This is due to the fact that a significant portion of **Form 2** transformed into **Form 1** during the solubility analysis.

Conclusion

Two polymorphs, **Form 1** and **Form 2**, of the compound isoxyl were isolated and characterised by thermal, X-ray diffraction and spectroscopic methods.

The melting point of **Form 1** cannot be determined by the experimental methods employed in this study. However, DSC results indicate that **Form 1,** which has been identified as the commercial material, transforms into **Form 2** at 91.7 ^{o}C in the solid state, the latter melting at 142.7 ^{o}C. In addition, **Form 2** was found to undergo a solvent-mediated transformation into **Form 1** at 25 ^{o}C. Therefore, the thermodynamic relationship between **Form 1** and **Form 2** can be defined as enantiotropy. Based on this, a schematic energy-temperature diagram was constructed. From the E/T diagram, it can be predicted that the melting point of **Form 1** will occur in the range of 91.7 ^{o}C to 142.7 ^{o}C and its enthalpy of fusion will be ~130 J g^{-1}. Furthermore, **Form 1** is the thermodynamically stable form from absolute zero to 91.7 ^{o}C while **Form 2** is the stable form between 91.7 and 142.7 ^{o}C.

Csonka-Horvai et al.[14] had isolated two polymorphic phases (α and β) of isoxyl in 1971. They reported that phase α crystallises in P $\bar{1}$ with a = 5.52, b = 13.80, c = 16.82 Å, α = 66.9, β = 92.7, γ = 100.6º and Z = 2 while phase β crystallises in the space group P2$_1$/a with a = 13.08, b = 9.02, c = 20.31 Å, β = 94.0º and Z = 4. The unit cell parameters, of relatively low precision, were obtained from precession and Weissenberg techniques.[14] In the present study, full three-dimensional X-ray intensity data were employed to determine the structures of **Form 1** and **Form 2**. **Form 1** crystallises in the triclinic space group P $\bar{1}$ with a = 5.5321(2), b = 13.7052(6), c = 16.7032(7) Å, α = 67.987(2), β = 87.272(2), γ = 78.724(2)º and 2 molecules per unit cell, whilst **Form 2** crystallises in the space group P2$_1$/c with a = 19.076(3), b = 8.952(1), c = 13.342(1) Å, β = 96.234(4)º and 4 molecules per unit cell.* We note that the unit cell parameters of **Form 1** and **Form 2** are sufficiently similar to those of the phases α and β respectively to assume that the same two polymorphs were investigated earlier.

*The space group P2$_1$/a is physically identical to space group P2$_1$/c. They differ only by interchange of axial labels a and c.

For interest, an attempt has been made to reconcile the accurate molecular structure in **Forms 1** and **2** [Figure 19 (a) and (c), respectively] and their placement within the accurate unit cells with those postulated in the phases α and β [Figure 19 (b) and (d)] by Csonka-Horvai et al.[14] The latter based their crude models on consideration of the unit cell dimensions and the probable existence of *cis-trans* rotational isomerism for isoxyl, gleaned from IR spectra. The necessarily crude models of the α and β phases are incorrect in detail, but remarkably do bear some resemblance to the accurate structures determined in the present study.

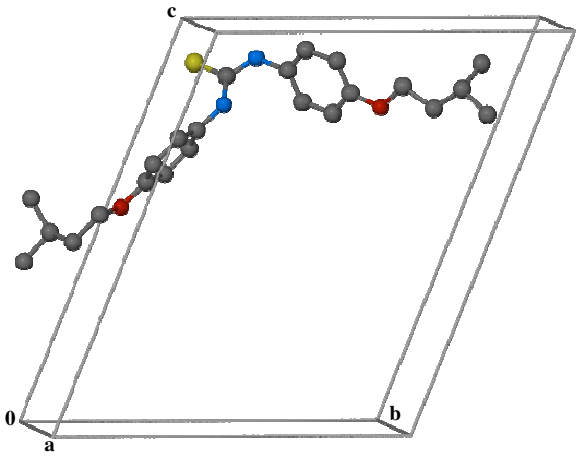

(a) Form 1

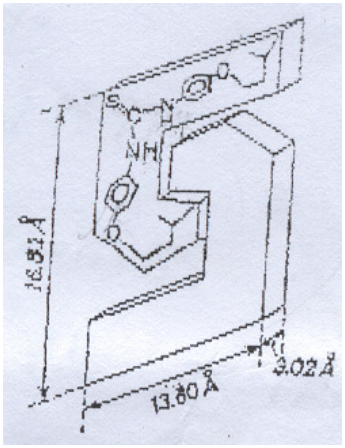

(b) Phase α

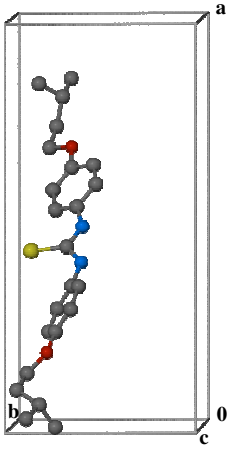

(c) Form 2

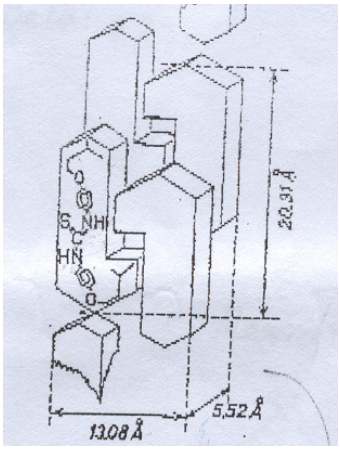

(d) Phase β

Figure 19 A representative molecule of isoxyl in the unit cell of (a) **Form 1**, (b) Phase α (postulated)[14], (c) **Form 2** and (d) Phase β (postulated)[14].

The molecule of **Form 1** adopts a *trans-cis* conformation [S-C-N-C torsion angles 165.1(2), -8.1(4)º] and that of **Form 2** adopts a both-*cis* conformation [S-C-N-C torsion angles -8.0(5), 6.7(5)º]. Different hydrogen bond patterns occur in the two crystal structures, designated as $R_2^2(8)$ and $R_1^1(5)$ in **Form 1**, but as a combination of $R_1^1(6)$, $R_2^1(6)$, $R_1^1(5)$ and $R_1^1(5)$ in **Form 2**. Consequently, in **Form 1**, centrosymmetric hydrogen bonded dimers of molecules of isoxyl assemble in layers, with the isoamyloxy residues of neighbouring dimers interdigitated. In **Form 2**, isoxyl molecules assemble *via* the α-network tape motif, with the tapes extending infinitely along the *b*-axis.

In both cases, the experimental PXRD traces were found to match the calculated patterns, allowing the latter to serve as references for polymorphic identification as well as proving that the experimental batches were polymorphically pure.

Both the FTIR spectra and solid-state NMR spectra highlighted differences between the polymorphs that allow these techniques to be used for diagnostic purposes. The observed spectral similarities and differences could be correlated with the crystal structures as established by X-ray diffraction.

Solubility measurements were carried out on **Form 1** and **Form 2** at 30°C in a solvent mixture (ethanol/water 4:1 v/v). In both cases, the solubility increased during the initial 12 h period. However, the solubility of **Form 2** increased at a faster rate, reaching a maximum value which is about twice that of **Form 1.** The sample of **Form 2** transformed into **Form 1** during the solubility test, evidenced by PXRD analysis of the undissolved sample of **Form 2**. This solvent-mediated transformation proceeded from the metastable polymorph to the stable polymorph i.e. in the expected direction based on DSC data from which the thermodynamic stability order was originally determined.

Evidence for a third polymorph of isoxyl, melting at 148 - 149 °C, has been published.[15] During the present study, much effort was invested into isolating this form in order to characterise it completely. However, it has to date remained elusive.

Part Two

Solvate Preparation

A crystalline solvate of isoxyl and 1,4-dioxane (designated S1) was successfully isolated. Suitable crystals were obtained by dissolving 0.020 g (0.050 mmol) of the isoxyl raw material (host) in 2 ml of 1,4-dioxane (guest) with stirring at 54 ^{o}C. The solution was then filtered (0.45 µm nylon filter) and allowed to cool spontaneously. Crystals of suitable quality appeared by slow evaporation at 25 ^{o}C over a period of one week.

The guest numbering scheme is given in Figure 20.

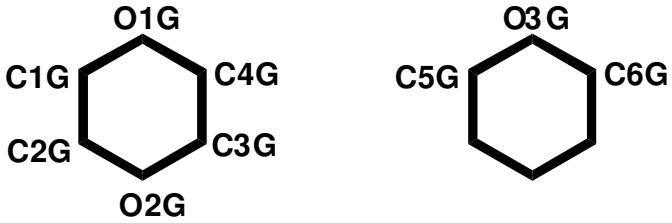

Figure 20 Guest numbering scheme for 1,4-dioxane molecules. Hydrogen atoms have been omitted for clarity. (The molecule on the left occupies a general position in the crystal while that on the right is located on a centre of inversion.)

Multiple TGA measurements revealed a mass loss of 14.8 ± 1.0% (n=3) for S1. This is equivalent to ~0.75 1,4-dioxane molecules per solvate unit. The stoichiometric formula of S1 based on X-ray analysis was calculated and found to be consistent with the formula calculated from the experimental results.

X-Ray Crystallographic Analysis of S1

Single Crystal X-Ray Diffraction

Data-Collection and Space Group Determination

A crystal of S1, extracted from the mother liquor, was covered in paratone N oil without delay in order to prevent the loss of solvent molecules. A Nonius Kappa CCD four-circle diffractometer was employed to collect reflection intensity data for S1 at 98 K.

The unit cell parameters, crystal system and space group were determined from the X-ray diffraction data which revealed Laue *2/m* symmetry for S1 indicating the monoclinic system. It was found to belong to the space group $P2_1/c$, from the following reflection conditions: *hkl: none*; *h0l: l = 2n* and *0k0: k = 2n*.

Structure Solution and Refinement

SHELXS-97[6] was used for the structure solution of S1. Direct methods yielded the positions of all non-hydrogen atoms in the asymmetric unit, which consisted of two independent molecules of isoxyl (A and B), one molecule of 1,4-dioxane in a general position, and one half of a 1,4-dioxane molecule located near a centre of inversion. All the non-hydrogen atoms were then refined isotropically on F^2 with SHELXH-97.[7] Atom C28B in the host molecule B was found to be disordered over two positions (C28B and C28C). C28B, the major component, was assigned a value of x for its s.o.f. while the minor component C28C was allocated the value 1-x. The s.o.f.s refined to 0.77(5) and 0.23(4) respectively while their U_{iso} values refined to 0.06(Å^2) and 0.05(Å^2), respectively. Distance restraints were employed to ensure reasonable molecular geometries of bonds C26B-C28B and C26B-C28C. The C-O bond length was set at 1.52 Å with a standard deviation σ = 0.002 Å.

Attempts to locate all the hydrogen atoms in S1 from difference Fourier maps were successfully carried out. Based on the positions of the peaks found, a riding model was employed to place hydrogen atoms for host molecules with idealised stereochemistry.

All the methyl hydrogen atoms were refined with isotropic temperature factors 1.5 times those of their parent atoms while all the other hydrogen atoms were assigned temperature factors 1.2 times those of their parent atoms. Crystal and refinement parameters for solvate S1 are presented in Table 10.

Table 10 Crystal and refinement data for S1

Parameter	**S1**
Formula unit	2(isoxyl) • 1.5(1,4-dioxane)
Formula Weight / g mol^{-1}	933.36
Crystal system	monoclinic
Space group	$P2_1/c$
a / Å	23.8995(6)
b / Å	9.1639(3)
c / Å	24.2628(7)
α / °	90.000
β / °	103.062(1)
γ / °	90.000
Volume / Å^3	5176.4(3)
Z	4
Density$_{calc}$ / g cm^{-3}	1.198
μ (MoK$_α$) /mm^{-1}	0.156
F (000)	2016
Crystal size /mm^3	0.06x0.12x0.44
Temperature / K	98(2)
Range scanned θ / °	1.00≤ θ ≤ 25.68
Index ranges	h: -28, 28
	k: -11, 10
	l: -29, 29
φ scan angle / °	0.9
ω scan angle / °	0.9
Dx / mm	40
No. of measured reflections	17143
No. of unique reflections	9571
No. of reflections with I > 2σ(I)	5257
No. of L.S. parameters	596
R$_{int}$, R$_σ$	0.0599, 0.1126
S	0.998
R$_1$ (F$_o$ > 4σ(F$_o$))	0.0505
No. of reflections omitted	32
wR2 (all reflections)	0.1223
Weighting scheme	a = 0.0500
	b = 0.0000
(Δ / σ)$_{mean}$	< 0.001
Δρ excursions / eÅ^{-3}	-0.41, 0.40

Conformation of the Isoxyl Molecules

There are two crystallographically independent isoxyl host molecules (A and B) in the asymmetric unit of solvate S1 as shown in Figure 21. Table 11 lists all the principal torsion angles of the molecules A and B. Those of the isoxyl molecule in polymorphic **Form 2** are also shown for comparison. In the molecules A and B in S1 as well as the molecule in **Form 2**, the aromatic planes A and B adopt the both-*cis* conformation relative to atom S15 around the N13-C14 and N16-C14 bonds.

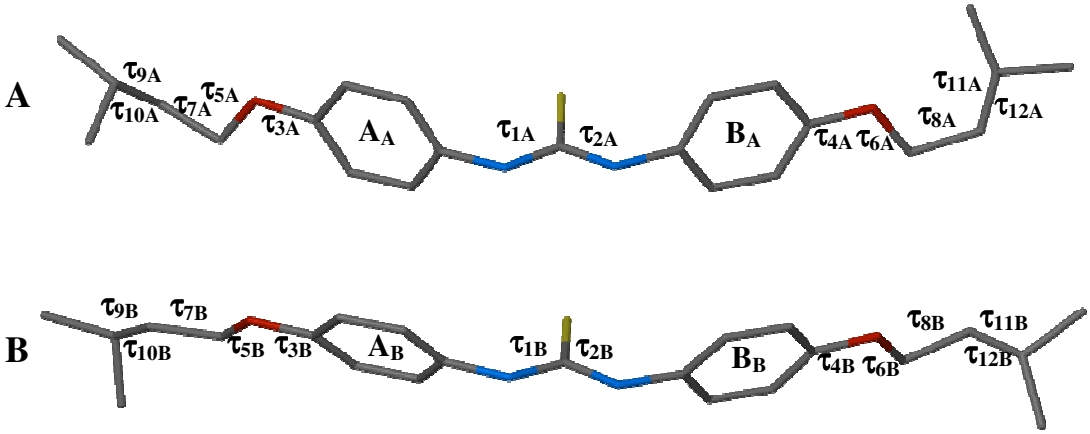

Figure 21 The structures and the principal torsion angles of the molecules A and B in S1.

Table 11 Principal torsion angles for the molecules A and B in S1 as well as the isoxyl molecule in **Form 2**[a]

Torsion angle (°)	**A** in S1	**B** in S1	**Form 2**
S15-C14-N13-C1 (τ_1)	0.3(3) --- *cis*	0.3(3) --- *cis*	-8.0(5) --- *cis*
S15-C14-N16-C17 (τ_2)	-1.0(3) --- *cis*	3.4(3) --- *cis*	6.7(5) --- *cis*
C3-C4-O7-C8 (τ_3)	9.4(3) --- *cis*	-1.2(3) --- *cis*	-177.8(3) --- *trans*
C21-C20-O23-C24 (τ_4)	-7.2(3) --- *cis*	-0.3(3) --- *cis*	169.4(3) --- *trans*
C4-O7-C8-C9 (τ_5)	-173.4(2) --- *trans*	170.6(2) --- *trans*	-171.8(3) --- *trans*
C20-O23-C24-C25 (τ_6)	-174.9(2) --- *trans*	172.6(2) --- *trans*	-168.5(3) --- *trans*
O7-C8-C9-C10 (τ_7)	-56.6(3) --- *gauche*	174.9(2) --- *trans*	-54.0(5) --- *gauche*
O23-C24-C25-C26 (τ_8)	-76.1(3) --- *gauche*	71.7(3) --- *gauche*	-58.3(4) --- *gauche*
C8-C9-C10-C11 (τ_9)	172.8(2) --- *trans*	-171.7(2) --- *trans*	176.0(4) --- *trans*
C8-C9-C10-C12 (τ_{10})	-62.4(3) --- *gacuhe*	63.7(3) --- *gauche*	-57.0(6) --- *gauche*
C24-C25-C26-C27 (τ_{11})	70.4(3) --- *gauche*	-166.7(2) --- *trans*	-61.5(5) --- *gauche*
C24-C25-C26-C28 (τ_{12})	-166.3(2) --- *trans*	74.1(4) --- *gauche*	176.1(4) --- *trans*

[a] See Figure 7, Part One for the isoxyl numbering scheme.

The isoxyl molecules A and B in solvate S1 as well as the molecule in **Form 2** are overlayed in Figure 22. With the central N_2CS moieties overlayed, a distribution of

aromatic ring orientations is evident, as is a range of conformations for the isoamyloxy chains. The symmetry-independence of molecules A and B in S1 is clear.

Figure 22 An overlay of the structures of the molecules A (gray) and B (pink) in S1 as well as the molecule in **Form 2** (black). Hydrogen atoms are omitted for clarity.

Hydrogen Bond Interactions

Table 12 lists all the hydrogen bond interactions for S1. Two host-host intermolecular N-H···S hydrogen bonds can be found between the host molecule A and a symmetry-generated molecule A. This motif is identical to the hydrogen bond motif of **Form 2**. Two host-guest N-H···O hydrogen bonds can be found between a host molecule B and a 1,4-dioxane guest molecule. The average N···S distance and N-H···S angle are 3.40 Å and 157°, while the average N···O distance and N-H···O angle are 3.05 Å and 160°.

Table 12 Hydrogen bonding interactions for S1[a]

Hydrogen bond	N···S or N···O Distance (Å)	Angle (°)	Symmetry operator[b]
N13A-H13A···S15A	3.456(2)	154.0	1-x,1/2+y,1/2-z
N16A-H16A···S15A	3.337(2)	160.0	1-x,1/2+y,1/2-z
N13B-H13B···O3G	3.134(2)	155.0	x, y, z,
N16B-H16B···O3G	2.966(2)	164.0	x, y, z,

[a] Where no e.s.d. is reported for the angle, H atoms involved were added in idealised positions in a riding model.
[b] Symmetry operator applies to hydrogen bond acceptor atoms.

Figure 23 illustrates the hydrogen bond interactions for the solvate S1. Bifurcated N-H···S hydrogen bonds link successive A molecules in the crystal. The graph set analysis descriptor $R_2^1(6)$ is shown in its hydrogen bonded ring.[8, 9] Again, this is identical to the hydrogen bond motif of **Form 2**. The host molecule B is hydrogen bonded to the guest molecule located on a centre of inversion, forming a hydrogen bonded ring which can be described as $R_2^1(6)$ [8, 9] as shown in Figure 23.

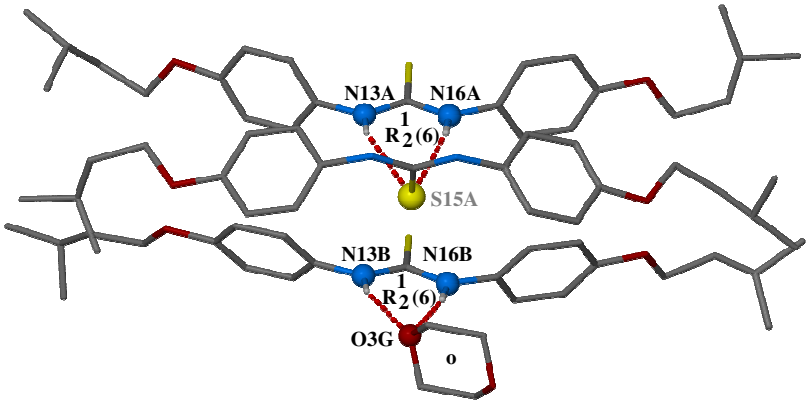

Figure 23 Hydrogen bonds N-H···S and N-H···O for S1. Atoms with gray labels have been symmetry-generated from their asymmetric unit counterparts. The relevant N, S and O atoms are shown as spheres.

Several C-H···O interactions (Table 13) were found in the structure of S1. Specifically, the host intramolecular interactions C10A-H10A···O7A and C27A-H27A···O23A stabilise the conformation of the host molecule A. The host-host interaction C19B-H19B···O7A associates the host molecules A and B. The host-guest intermolecular interactions C3B-H3B···O2G and C24B-H24C···O1G associate the host molecule B with the guest molecule located in a general position.

Table 13 C-H···O interactions of solvate S1[a]

Hydrogen bond	C···O Distance (Å)	Angle (°)	Symmetry operator[b]
C10A-H10A···O7A	2.899(3)	102.0	x, y, z,
C27A-H27A···O23A	3.101(3)	117.0	x, y, z,
C19B-H19B···O7A	3.439(3)	154.0	1-x,1/2+y,1/2-z
C3B-H3B···O2G	3.395(3)	164.0	x, y, z,
C24B-H24C···O1G	3.283(3)	127.0	1-x,-y,1-z

[a] Where no e.s.d. is reported for the angle, H atoms involved were added in idealised positions in a riding model.
[b] Symmetry operator applies to hydrogen bond acceptor atoms.

In summary, no N-H···S or N-H···O hydrogen bond interactions occur between the host molecules A and B. Intermolecular hydrogen bond interactions can be found between the host molecules A which adopt a very similar hydrogen bond motif to that in polymorphic **Form 2**. However, the host molecule A is not hydrogen bonded to any solvent molecule. The host molecule B is associated with both the fully-occupied and the half-occupied

1,4-dioxane molecules through C-H···O interactions and N-H···O hydrogen bonds, respectively, as shown in more detail below.

Crystal Packing

The symmetry-independent host molecules A and B in the asymmetric unit of solvate S1 are shown in Figure 24.

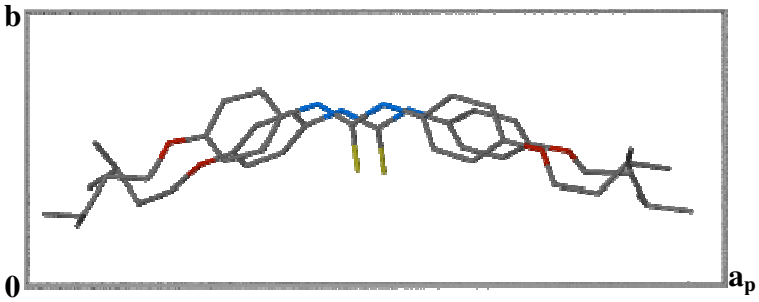

Figure 24 Two symmetry-independent host molecules A and B in the asymmetric unit of S1.

Figure 25 illustrates the packing diagram of S1**.** As mentioned above, host molecules A are linked to each other *via* bifurcated N-H···S hydrogen bonds, as in polymorphic **Form 2** of isoxyl. In an analogous way, a continuous 'tape' is generated along the crystal *y*-direction.

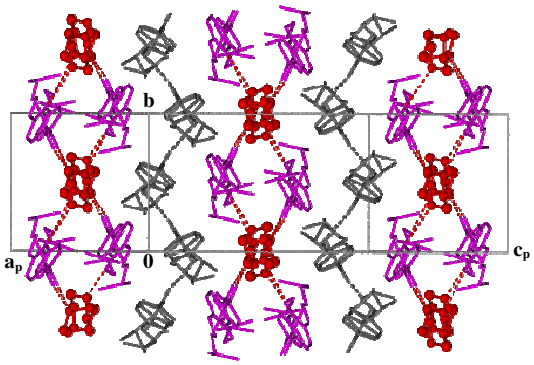

Figure 25 Crystal packing diagram for S1. The atoms of the solvent molecules are shown as red spheres for clarity. The molecules A and B are shown in gray and pink, respectively. The host-host and guest-host intermolecular hydrogen bonds are shown in gray and red dashed lines, respectively.

The layers which consist of the host molecules B and guest molecules are interleaved by the layers of the host molecules A. However, the former actually consist of two inverted, interpenetrating assemblies which are not hydrogen bonded to each other, as shown in

Figure 26. Furthermore, the guest molecules serve as bridges, connecting the host molecules B.

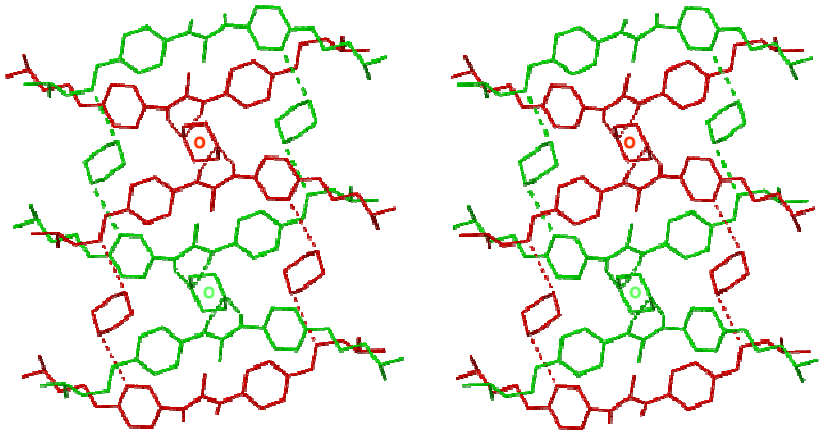

Figure 26 Stereoview showing two interpenetrating host B-guest hydrogen bonded assemblies, represented in red and green. The two assemblies are not hydrogen bonded to one another.

Guest 1,4-dioxane molecules are located between the assemblies of the host molecules B as shown in Figure 27. No guest-guest interactions are observed, but the three guest molecules shown in Figure 27 are in contact, forming an isolated solvent motif roughly parallel to the unit cell *ac*-diagonal. The guest molecules are intimately associated with the host molecules B.

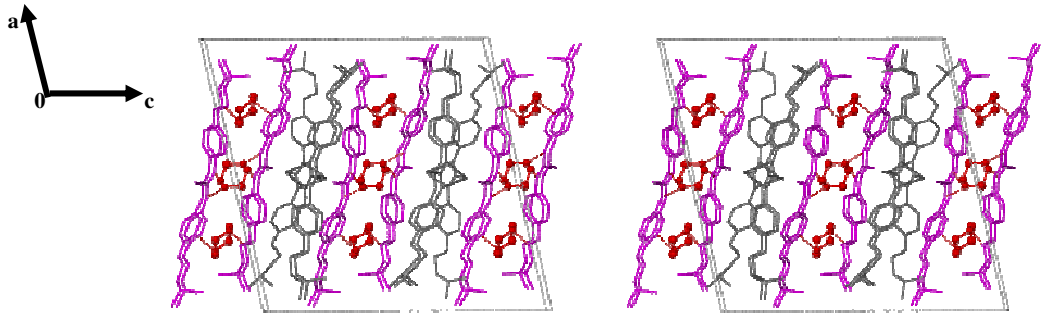

Figure 27 Stereoview showing crystal packing for S1 viewed along [010]; atoms of the solvent molecules are shown as red spheres for clarity. Molecules A and B are shown in gray and pink, respectively. The host-host and guest-host intermolecular hydrogen bonds are shown in gray and red dashed lines, respectively.

The program SECTION[16] was used to view planes at y = 0 and y = 0.5 through the unit cell along the *b*-axis (Figure 28). The isolated sets of three 1,4-dioxane molecules are evident.

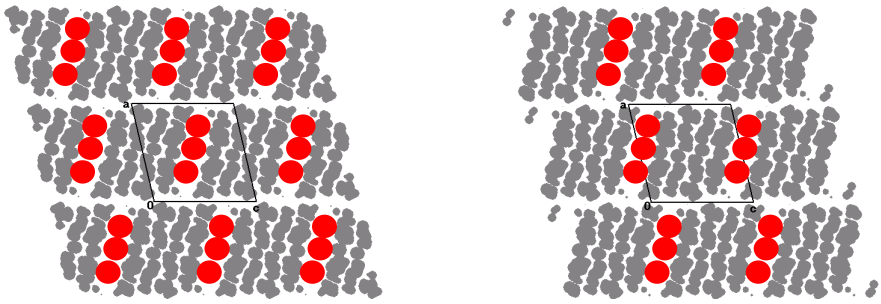

(a) 0 Å **(b) 4.5 Å**

Figure 28 Sections through S1 with guest molecules represented schematically by three red circles and host molecules represented by gray areas, viewed along [010] with the unit cell sectioned at (a) 0 Å and (b) 4.5 Å from 0,0,0.

Comparative PXRD

The calculated and experimental PXRD traces for solvate S1 are shown in Figure 29. The experimental PXRD trace is in reasonable agreement with the calculated one, based on the single crystal X-ray data, confirming that the prepared sample was homogeneous. The low temperature X-ray analysis results in calculated peaks appearing at slightly higher 2θ-values. Differences in the relative intensities of peaks in the two traces are attributed to residual preferred orientation, the small amount of material available, and possible desolvation of the solvate crystals during the sample preparation.

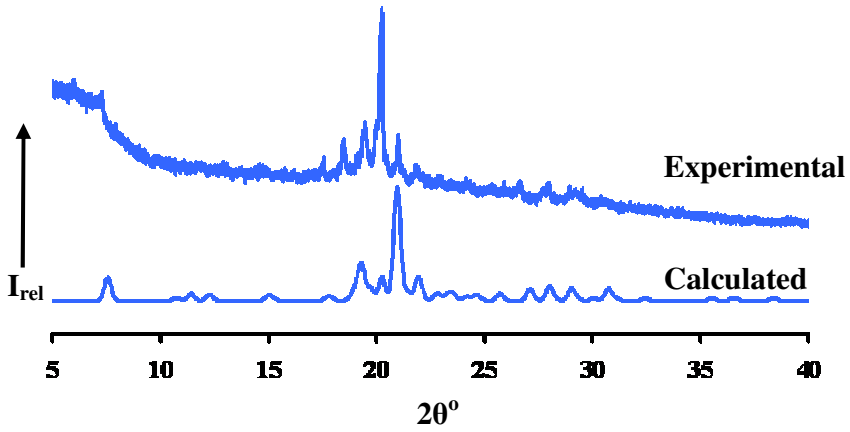

Figure 29 Calculated and experimental PXRD traces for S1.

Thermal Analysis

Hot Stage Microscopy

The crystal of S1 was placed under silicone oil and was heated at a constant rate of 10 K/min (Figure 30). No bubbling associated with desolvation or other obvious optical change was observed during the heating process. The crystal melted at ~148 ^{o}C.

(a) 25 ^{o}C **(b) 120 ^{o}C** **(c) 148 ^{o}C**

Figure 30 HSM photographs of a crystal of S1 at various temperatures

Differential Scanning Calorimetry and Thermogravimetric Analysis

The TGA and DSC traces for S1 are shown in Figure 31. The DSC results are summarised in Table 14. The DSC trace showed two thermal events which are indicated by peaks C and D. The endothermic event C represents the solvent loss which corresponds to the mass loss indicated by A in the TGA trace. Notably, the event C occurred over a wide temperature range. The end point of this range was indicated by D in the figure, evidenced by the fact the DSC trace returned to the baseline at this point. Correspondingly, point B was placed in the TGA trace based on the position of D in the DSC trace, representing the complete solvent release. Therefore, the TGA result showed an apparent two-step mass loss over the wide temperature range 35 – 119 ^{o}C with a value of 14.8 ± 1.0 % (n=3). The calculated mass loss is 14.1% which agrees reasonably well with the experimental mass loss. Event E indicates the melting of the desolvated phase. The fact that the melting point of the desolvated phase is very similar to that of **Form 2** [142.1 ± 0.3^{o} (n=2)] implies that the solvate S1 possibly transformed into **Form 2** after losing the solvent molecules.

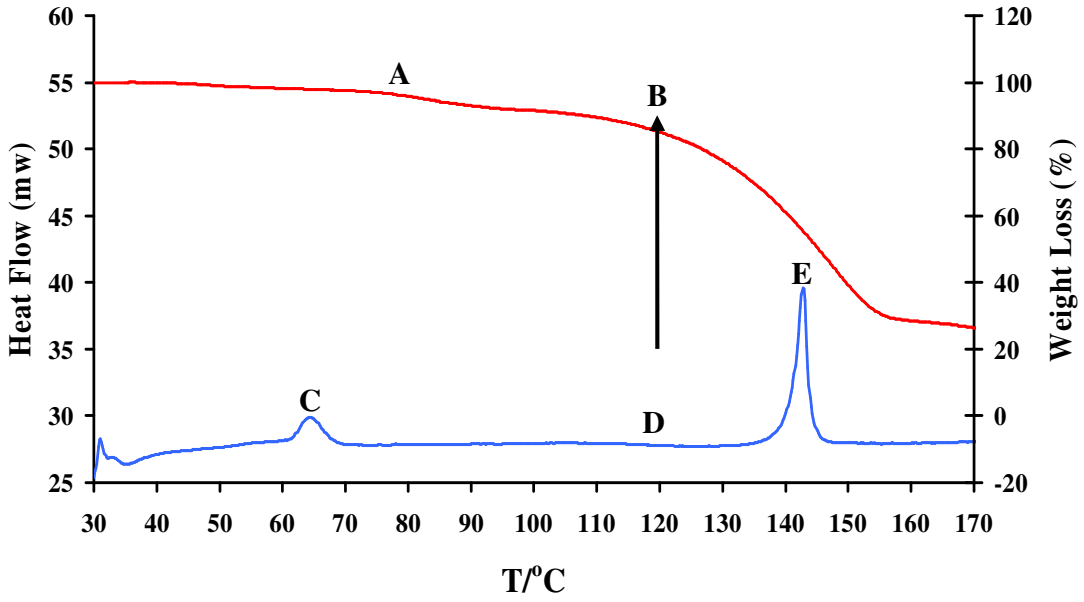

Figure 31 TGA (red) and DSC (blue) traces for S1.

Table 14 DSC results for solvate S1

S1	Onset Temperature (°C)
Peak C (desolvation)	61.6 ± 1.0 (n=2)
Peak E (fusion)	141.7 ± 1.0 (n=2)

Furthermore, in the TGA trace, the appearance of a two-step mass loss A instead of a single-step mass loss may be related to the fact that the two crystallographically distinct 1,4-dioxane molecules are involved in different hydrogen bond environments in the structure of S1, as noted earlier from the X-ray structural analysis.

Variable Temperature Powder X-ray Diffraction

The PXRD patterns of the crystals of S1 were characterised as a function of temperature (Figure 32). At approximately 70 °C, the crystals of solvate S1 transformed to another phase. This was readily confirmed by PXRD analysis to be the isoxyl polymorphic **Form 2**. The appearance of **Form 2** was assumed to be associated with the fact that it becomes the thermodynamically stable form of isoxyl at elevated temperature. Furthermore, the melting point of the desolvated phase of S1 was earlier shown by DSC to be very similar to that of **Form 2**.

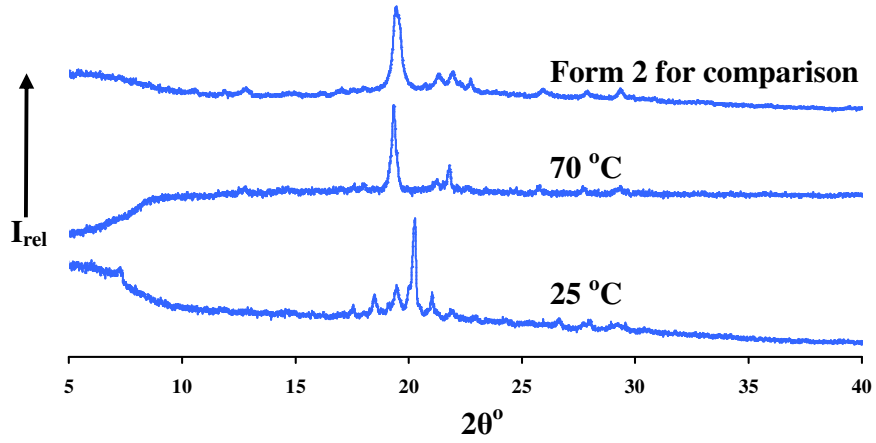

Figure 32 Variable temperature PXRD patterns for S1. The pattern of **Form 2** at 25 °C is added for comparison.

A noteworthy observation is that the crystals of S1 desolvated also when they were exposed to the atmosphere at 25 °C. After equilibrating with the atmosphere for a period of 2 days, the desolvated phase was again identified as **Form 2** by PXRD.

Thus, the solvate S1 desolvates to yield the metastable polymorphic **Form 2** of isoxyl, either during controlled heating or by spontaneous loss of included solvent at ambient temperature during exposure to the atmosphere. We assume that this transformation to **Form 2** (rather than **Form 1**) is facilitated by the presence of similar structural features in the crystals of S1 and **Form 2**, namely the common 'both-*cis*' conformation of all of the isoxyl molecules, and the existence of a common 'tape' motif mediated by bifurcated N-H···S hydrogen bonds.

Conclusion

Concluding remarks interrelate various aspects of both the polymorphic species (**Form 1** and **Form 2**) as well those of the solvate S1.

Powder X-ray Diffraction

The experimental PXRD traces for isoxyl polymorphs (**Form 1** and **Form 2**) and solvate (S1) were in reasonable agreement with their respective calculated traces based on single crystal X-ray data. The calculated traces are presented here in a stacked format for

comparison, Figure 33. In general, the dissimilarity among these traces is remarkable enough to identify and distinguish these three different phases of isoxyl.

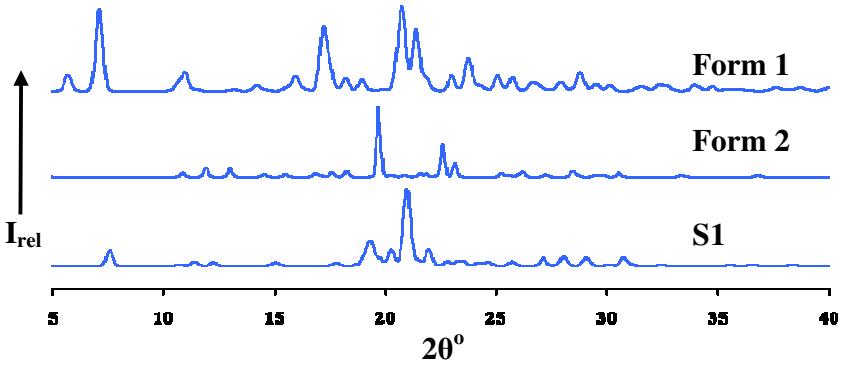

Figure 33 Calculated PXRD traces of isoxyl polymorphs (**Form 1** and **Form 2)** and solvate S1.

Conformation of Isoxyl Molecules

The conformational difference among the isoxyl molecules (**Form 1**, **Form 2**, host molecules A and B in S1) is mainly reflected in the conformations of their thiourea moieties. The isoxyl molecule in **Form 1** adopts a *trans-cis* conformation while those of **Form 2** and S1 all adopt both-*cis* conformations. Among the isoxyl molecules in **Form 2** and S1, the isoamyloxy chains adopt a range of conformations.

Hydrogen Bond Interactions

Form 1 contains a unique hydrogen bond motif comprising two isoxyl molecules related by a crystallographic inversion centre, associated by two identical N-H···S hydrogen bonds. **Form 2** and the molecule A in S1 contain identical hydrogen bonded motifs in which isoxyl molecules link to form infinite 'tapes' *via* bifurcated N-H···S hydrogen bonds N13-H13···S15 and N16-H16···S15. In the isoxyl molecule B in solvate S1, the N13B and N16B atoms function as hydrogen bond donors to the same acceptor atom O3G of the 1,4-dioxane molecule located on a centre of inversion.

Crystal Packing

Given that isoxyl molecules in **Form 2** and those of type A in the solvate S1 associate in a very similar motif, it is useful to compare partial packing diagrams that highlight this finding. Both the set of four isoxyl molecules in the **Form 2** unit cell [Figure 34 (a)] and

that in the S1 unit cell [Figure 34(c)] occur as separate, inversion-related pairs, each of which displays the common 'tape' motif. The latter is evident in the Figure 34 (b) and (d).

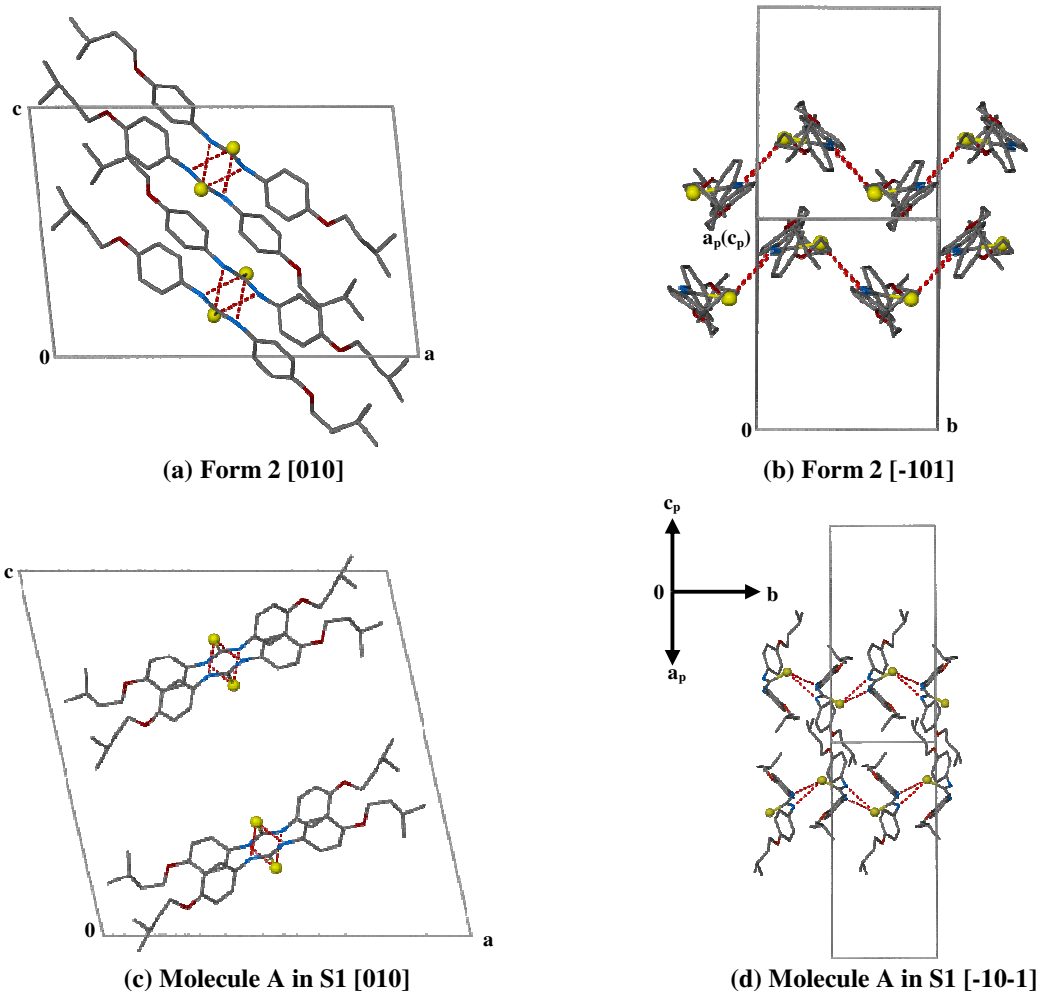

Figure 34 The packing diagrams for **Form 2** along (a) [010] and (b) [-101] as well as the packing diagrams of the molecules A in S1 along (c) [010] and (d) [-10-1]. The S atoms are shown as spheres and the H atoms are omitted for clarity. In the diagrams of S1, the host molecules B and the solvent molecules are omitted for clarity.

Part Three

The third method of attempted supramolecular modification of isoxyl is described here, namely its inclusion in cyclodextrin molecules.

Cyclodextrin (CD) Inclusion Complex Preparation

The hosts which were investigated for the isoxyl inclusion are α-CD, β-CD, γ-CD, heptakis(2,6-di-*O*-methyl)-β-CD, heptakis(2,3,6-tri-*O*-methyl)-β-CD, hexakis(2,3,6-tri-*O*-methyl)-α-CD, heptakis(2,3,6-tri-*O*-acetyl)-β-CD, heptakis(2,3,6-tri-*O*-benzoyl)-β-CD, heptakis(2,3,6-tri-*O*-ethyl)-β-CD, and octakis(2,3,6-tri-*O*-acetyl)-γ-CD (all obtained from Cyclolab, Budapest, Hungary). The experimental methods were kneading, recrystallisation of kneaded product and co-precipitation. The first method yielded microcrystalline complexes of β-CD and γ-CD. However, the latter two methods did not result in the expected formation of inclusion complexes in the form of single crystals. For all other CD s tested, crystallisation of the pure (uncomplexed) host occurred.

Equimolar amounts of host and guest were used in the preparation of the inclusion complexes of β- and γ-CD with isoxyl. The amount of isoxyl used was 20 mg. Thus, the amounts of β- and γ-CD were 56.74 and 64.85 mg respectively.

In each experiment, the CDs were placed in the mortar with a few drops of water and ground to a paste. The guest (isoxyl) was slowly added with simultaneous gentle manual trituration. After all the guest had been added, the paste was triturated for 45 minutes with dropwise additions of water to keep it moist.

Confirmation of Complexation

Powder X-ray diffraction was employed to confirm complexation. The resultant PXRD traces were compared with reference traces.[17, 18] The latter were originally obtained[19] by averaging computed PXRD traces for a number of isostructural series of CD inclusion complexes using the single crystal XRD data available in the Cambridge Crystallographic

Database. Such traces have thus been used routinely both to obtain confirmation of complex formation and to deduce structural information for new CD inclusion complexes prepared in the laboratory. In the present study, experimental PXRD traces of putative CD inclusion complexes were compared with reference PXRD patterns to find matches that would confirm genuine complex formation (Figure 35).

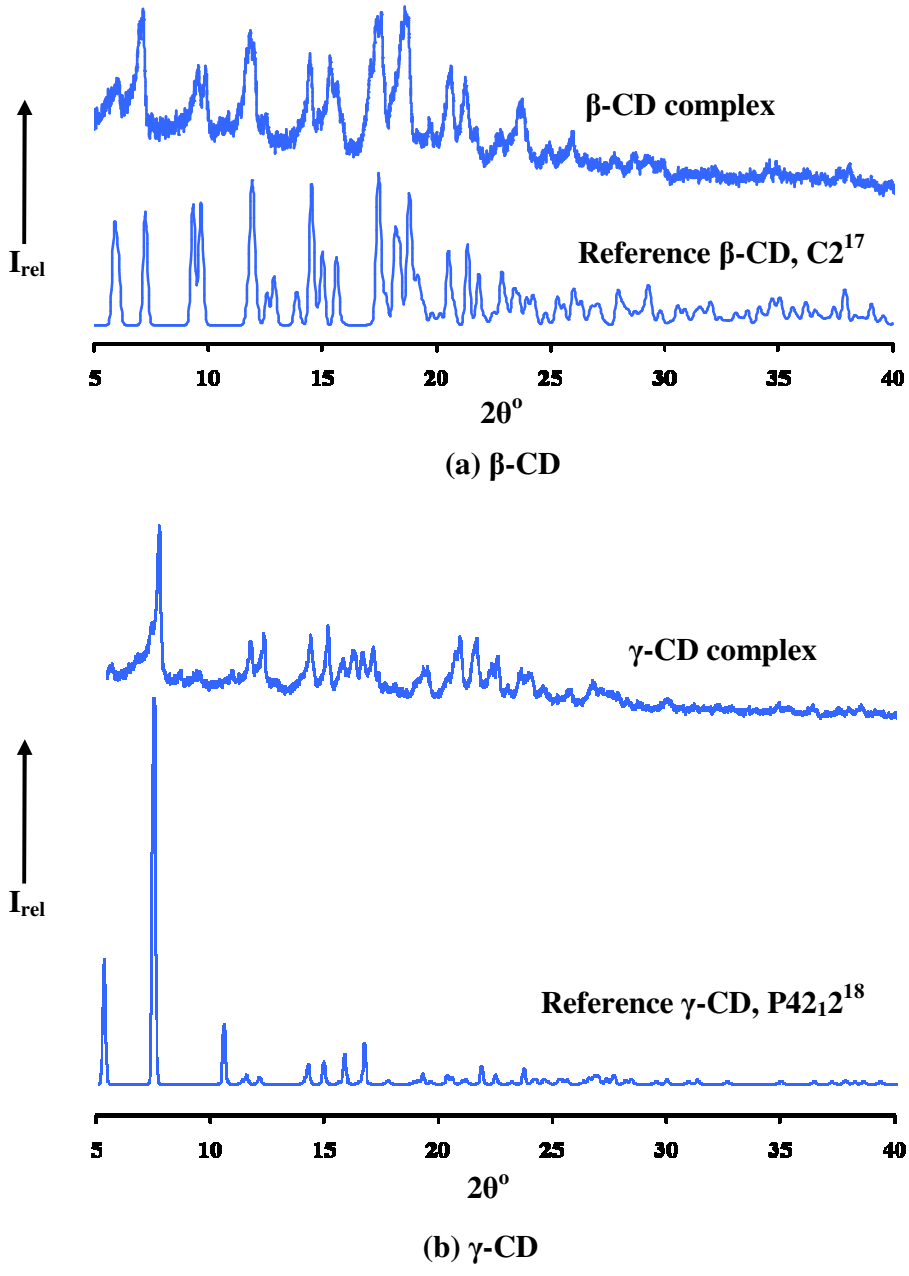

Figure 35 (a) The PXRD pattern for a β-CD-isoxyl complex and the reference pattern for β-CD complexes of a specific isostructural series crystallising in space group C2. (b) The PXRD pattern for the γ-CD-isoxyl complex and the reference pattern for γ-CD complexes.

As explained in detail in the original reference,[19] this simple procedure relies primarily on finding reasonably good peak angular matches. (Complex isostructurality can still be reliably deduced even when there are significant differences in the experimental and reference PXRD peak intensities). In Figure 35 (a), there is a very convincing match between the angular positions of the experimental PXRD peaks of the putative β-CD-isoxyl inclusion complex and those of the reference trace for a specific isostructural series of known β-CD inclusion complexes crystallising in the space group C2. (There is, in fact, also a fair match in the relative intensities of the two PXRD traces in this case). Most of the peaks in the PXRD pattern of the putative γ-CD-isoxyl inclusion complex similarly have counterparts in the reference pattern for all known γ-CD inclusion complexes [Figure 35 (b)]. In both cases, we can thus deduce from these results, formation of genuine CD inclusion complexes. Furthermore, through isostructurality, this identification yields space group information for each complex and allows deduction of approximate unit cell dimensions as well as the CD frameworks in the respective inclusion complexes.

Host Frameworks in the Complexes

In the case of the β-CD inclusion complex of isoxyl [Figure 36 (a)], its isostructurality with a known complex series crystallising in space group C2 informs us that dimers of the host molecules are stacked in a 'head-to-head' (and 'tail-to-tail') arrangement parallel to the *c*-axis, along which infinite channels are formed. The gray column [Figure 36 (a)] is generated by the symmetry operator 1/2+x, 1/2+y, z (corresponding to the *C*-centering). For the γ-CD complex of isoxyl [Figure 36 (b)], the host molecules are stacked on top of each other along the fourfold axes parallel to the *c*-axis of the tetragonal unit cell. Specifically, molecules A and C have the same orientation (with respect to their primary and secondary sides) while molecule B is of opposite orientation. The host molecules are thus arranged in three possible ways: tail-to-tail (A and B), head-to-head (B and C) and tail-to-head (C and A′). [20]

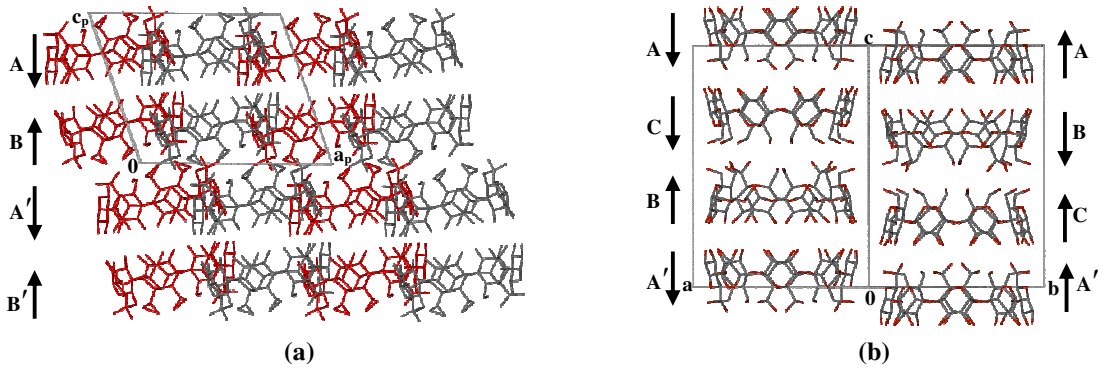

(a) (b)

Figure 36 The packing motif of dimeric β-CD complexes (space group C2) viewed along [010] (a) and γ-CD complexes viewed along [-1-10][20] (b).

Furthermore, based on the known isostructurality between the prepared complexes and those of the reference series, the approximate unit cell parameters for the β- and γ-CD complexes of isoxyl can be predicted as listed in Table 15.

Table 15 Predicted space groups and approximate unit cell parameters for the β- and γ-CD complexes of isoxyl

Complexes	Space group	*a* (Å)	*b* (Å)	*c* (Å)	(°)	(°)	(°)	Vol. (Å^3)
β-	C2	19.3	24.5	15.9	90	109	90	7109
γ-	$P42_12$	23.8	23.8	23.2	90	90	90	13158

Attempts to form complexes of isoxyl with derivatised CDs were not successful.

Solubility Enhancement Measurement

Isoxyl is known to be practically insoluble in water. The approximate aqueous solubility of isoxyl was determined as 1.6 μg/ml (25°C) by Nestler et al.[21] In the present study, the aqueous solubility enhancement measurement using β- and γ-CDs was carried out.

Isoxyl, in successive very accurately weighed amounts, was added to fixed, measured volumes of aqueous solutions of β-CD (3% w/w) and γ-CD (17% w/w) at 30 ± 2 °C over a period of 3 days. Due to paucity of the raw drug, attaining saturation was not the objective of the experiment. Instead, some notion of the solubility enhancement in these solutions of arbitrary CD-concentration[22] was sought. Based on the measured masses of drug and the solution volumes employed, it could be concluded that the aqueous

solubility of isoxyl in the β-CD and γ-CD solutions had increased by at least a factor of two in the former case, and three in the latter case, relative to its concentration in pure water. To put this into perspective, a similar experiment with the anti-inflammatory drug ibuprofen dissolved in a 1.8% solution of β-CD at 25 ^{o}C led to a solubility enhancement factor of 2.1.[22]

Part Four

The rationale for our pursuing cocrystal formation as a supramolecular modification of the drug isoxyl was based on observations from our investigation of its polymorphism. There, it was noted that the thiourea moiety -HN-C(S)-NH- is able to adopt different configurations (*cis*-*trans*, both-*cis*, leading to different modes of supramolecular association *via* N-H···S hydrogen bonds in the solid state. Cocrystal formation involving reaction between isoxyl and cocrystal formers containing amide and carboxylic acid functions was considered to have potential for producing novel solid phases, since these latter functions present possibilities for synthon formation with the thiourea moiety, at least in principle.

In the attempts to form such cocrystals, a variety of cocrystal formers was investigated. These included isonicotinamide, nicotinamide, saccharin, L-(+)-tartaric acid, D-(+)-tartaric acid, citric acid, succinic acid, maleic acid, salicylic acid and oxalic acid. Methods of preparation included dry co-grinding, liquid-assisted co-grinding and co-precipitation with different molar ratios of isoxyl : cocrystal former and different solvents. A list of several such experiments and their outcomes is provided in Appendix 2. The fact is, however, that none of the products of these reactions turned out to be a cocrystal. This was the outcome gauged from examination of PXRD patterns of the products, which revealed primarily unreacted mixtures of the original phases. However, during the screening of the products by PXRD, in a few instances, new peaks appeared that strongly suggested the appearance of new solid phases. The experiments in question were those involving attempted cocrystallisation of isoxyl with the widely employed cocrystal formers isonicotinamide and nicotinamide (Figure 37).

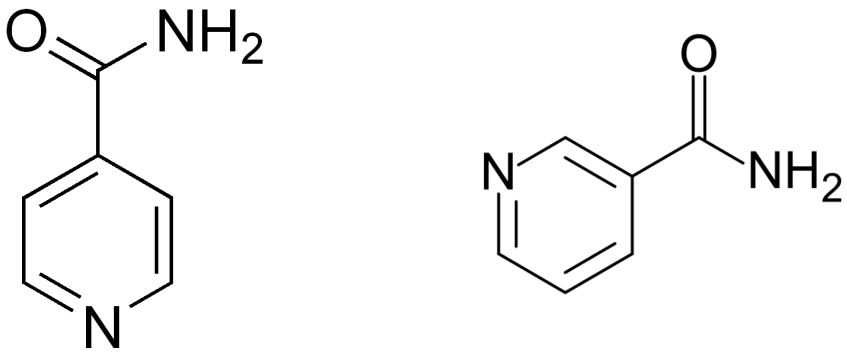

(a) isonicotinamide **(b) nicotinamide**

Figure 37 Chemical structures of (a) isonicotinamide and (b) nicotinamide

Further careful investigation revealed that the new solid phases were, in fact, polymorphs of the cocrystal formers that had not hitherto been structurally characterised. Given the widespread current interest in pharmaceutical cocrystals and the frequent use of isonicotinamide and nicotinamide as cocrystal formers, the unexpected appearance of new polymorphs of the latter molecules in this study was recognised as providing an opportunity for contributing to the knowledge base of organic crystal polymorphism.

In addition, though the pursuit of new polymorphs of the cocrystal formers isonicotinamide and nicotinamide was not an original objective of this study, it was nevertheless considered a sufficiently interesting and important outcome to warrant bringing it to the attention of others working in the field of pharmaceutical cocrystals. Specifically, it was decided to determine the molecular conformations and crystal structures of these new isonicotinamide and nicotinamide crystal modifications and to relate them structurally and thermodynamically to the known polymorphs.

Isonicotinamide

In an early attempt to form a cocrystal between isoxyl and the co-former isonicotinamide by co-precipitation from chloroform solution, different polymorphic forms of isonicotinamide crystallised simultaneously, among these one whose measured unit cell dimensions suggested a new phase. To establish whether this outcome depended on the presence of isoxyl, isonicotinamide alone was dissolved in chloroform and the products of crystallisation were identified. Again an apparently new phase of isonicotinamide was present in the mixture of crystal forms. Details of this procedure are reported below. In addition to an apparently new polymorph of isonicotinamide, this preparative procedure yielded also crystals of two polymorphs, referred to here as **Forms 1** and **2**, whose structures had both been reported in 2003 (CSD refcode EHOWIH02,[23] CSD refcode EHOWIH01[24]). The new polymorph was accordingly named **Form 3**.

Polymorph Preparation

In a typical experiment, 38 mg of isonicotinamide was dissolved in 2 ml chloroform at 45 ^{o}C. The solution was stirred for 10 minutes and filtered (0.45 μm nylon filter) while hot. It was then placed in a Dewar flask containing water at ~45 $^{\circ}$C. The Dewar flask was covered with an insulating material to allow slow cooling. The water in the Dewar flask returned to ambient temperature over a period of one and a half days.

Visual inspection of the batch of precipitated material indicated the possible presence of crystals of different morphologies and thus of possibly different polymorphs (i.e. concomitant polymorphism). However, morphological differences were not reliable in allowing definitive separation into different crystal polymorphic forms. The very tedious, but reliable, procedure of determining crystal unit cells for each specimen in the batch using single crystal X-ray diffraction followed. This revealed three distinct polymorphs of isonicotinamide, namely two monoclinic forms, **Forms 1** and **2**, that were described previously,[23, 24] and a third modification of orthorhombic crystal symmetry, not hitherto described, and assigned as **Form 3**. No crystallisation procedure yielding **Form 3** exclusively could be devised. Only in this way, was it possible to obtain **Form 3** in a

sufficiently large sample to carry out all of the structural and thermal analyses described below.

Thermal Analysis

Differential Scanning Calorimetry and Thermogravimetric Analysis

TGA analyses (not shown) indicated negligible mass loss for all three forms in the temperature range 30-180 ^{o}C, indicating that **Forms 1**, **2** and **3** are not solvates.

Preliminary DSC runs indicated possible phase transitions on heating these crystals, though the enthalpies of transition appeared to be very small.

Figure 38 shows the DSC results of the three forms heated at 10 K/min. In order to enhance the appearance of peaks representing phase transitions, traces for both **Forms 1** and **2** were recorded using a large amount (10 mg) of each sample. However, due to the difficulty in obtaining large amounts of **Form 3**, only 0.3 mg of this species was used in DSC measurement.

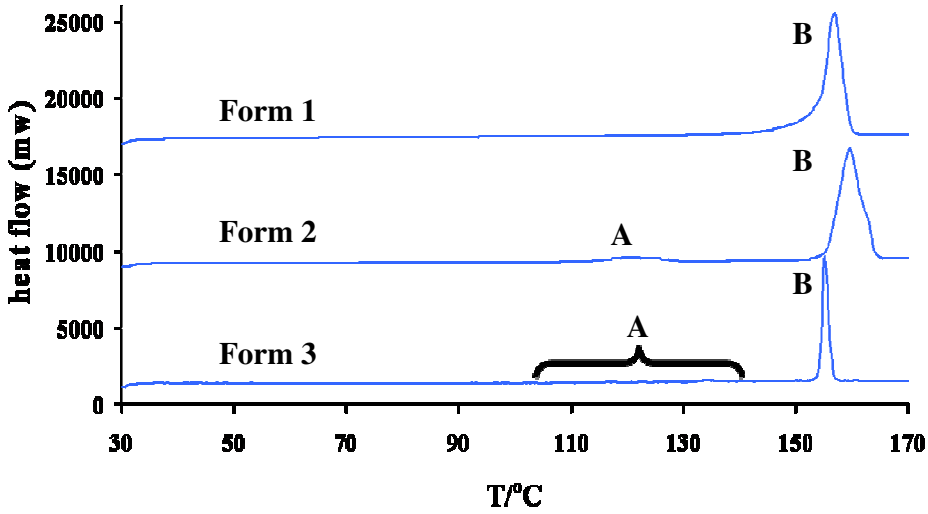

Figure 38 DSC traces of **Form 1**, **Form 2** and **Form 3** of isonicotinamide (heating at 10 K/min)

The DSC trace for **Form 1** exhibited one endotherm B, which represents the melting of **Form 1**. The DSC trace for **Form 2** exhibited two endotherms, namely A and B. The

first endotherm A corresponds to a phase change, since no mass loss was observed in the TGA curve. The second endotherm B results from the melting of the resulting modification. Similar results were obtained for **Form 3**, with however a very small, barely discernible, endotherm A. The fact that the T_f value (Table 16) of the endotherm B in **Form 1** is very close to those in **Form 2** and **Form 3** provides evidence of a complete phase transformation from **Form 2/Form 3** to **Form 1** on heating. The observation that both the melting peaks B in the DSC traces for **Forms 1** and **2** were broader than that in the trace for **Form 3** is attributed to the very small sample of the latter form used in the measurement. This possibly also accounted for the difficulty in identifying the peak A and determining the T_t value associated with **Form 3**.

Table 16 Thermo-analytical data obtained from DSC for the **Forms 1**, **2** and **3** at 10 K/min

Form	Phase change onset temperature T_t (^oC)	Melting onset temperature T_f (^oC)
1	none	153.9 ± 2 (n=2)
2	114.9 ± 0.4 (n=2)	155.9 ±2 (n=2)
3	inconclusive	154.1

Separate DSC experiments were performed to enhance the appearance of the phase transition endotherm for **Form 3**. Figure 39 shows the DSC results for the three forms heated at 70 K/min.

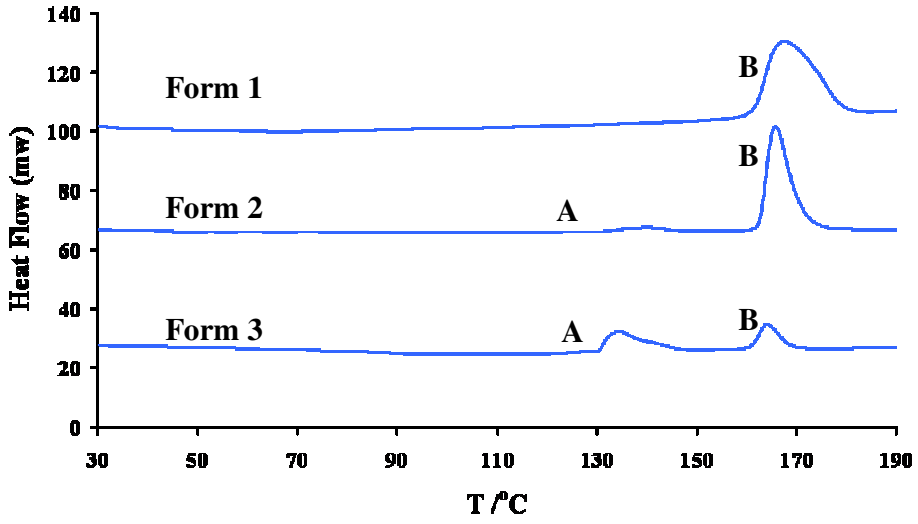

Figure 39 DSC traces of **Form 1**, **Form 2** and **Form 3** of isonicotinamide (heating at 70 K/min)

The DSC trace for **Form 1** obtained at 70 K/min exhibited a single endothermic peak B representing fusion, this behaviour being consistent with that of **Form 1** heated at 10 K/min. The DSC trace for **Form 2** obtained at 70 K/min exhibited an initial endothermic peak A, followed by a second endothermic peak B. These possibly represent the phase change of **Form 2** and the melting of the modified form, respectively. Again, the DSC trace for **Form 2** obtained at 70 K/min is consistent with that obtained at 10 K/min. The trace for **Form 3** obtained at 70 K/min showed a more convincing endothermic peak A compared to that obtained at 10 K/min. This peak A indicated that **Form 3** underwent a phase change into a modified form (peak A) which then melted (peak B). Also, the DSC trace for **Form 3** obtained at 70 K/min is consistent with that obtained at 10 K/min. However, the onset temperature for each endothermic peak in all three DSC traces at 70 K/min (Table 17) is higher than those for the corresponding peaks at 10 K/min (Table 16). A possible explanation is that the higher heating rate introduces higher temperature gradients of the endothermic peak, leading to the delay in the onset temperatures.[1, 2] In addition, since the instrument was calibrated for a 10 K/min heating rate, temperatures measured at higher heating rates may not be very reliable.

Table 17 Thermo-analytical data obtained from DSC for the **Forms 1**, **2** and **3** at 70 K/min

Form	Phase change onset temperature T_t(^{o}C)	Melting onset temperature T_f (^{o}C)
1	none	161.5 ± 1 (n=2)
2	131.7 ± 1 (n=2)	162.6 ±2 (n=2)
3	130.5	161.0

Based on the above DSC data obtained at 10 and 70 K/min, it can be assumed that both **Forms 2** and **3** experienced a phase change into **Form 1**, the latter then melting at 153.9 ^{o}C. The phase change of **Form 2** occurs at 114.9 ^{o}C (Table 16) while an accurate temperature for the phase transition of **Form 3** cannot be determined. However, based on the onset temperatures of **Forms 2** and **3** heated at 70 K/min, the phase change temperature of **Form 3** can be determined as being slightly lower than that of **Form 2** (Table 17).

Variable Temperature Powder X-ray Diffraction

In order to confirm the conclusions drawn from the DSC analyses, variable temperature powder X-ray diffraction was introduced.

Figure 40 firstly presents the comparison of the measured PXRD pattern of **Form 1** at 25 °C with the calculated pattern derived from the single crystal structure of **Form 1** using program LAZY PULVERIX.[11] Crystals of **Form 1** were then characterised by PXRD as a function of temperature. The PXRD pattern was recorded at temperature intervals of 10 K between 30 and 180 °C.

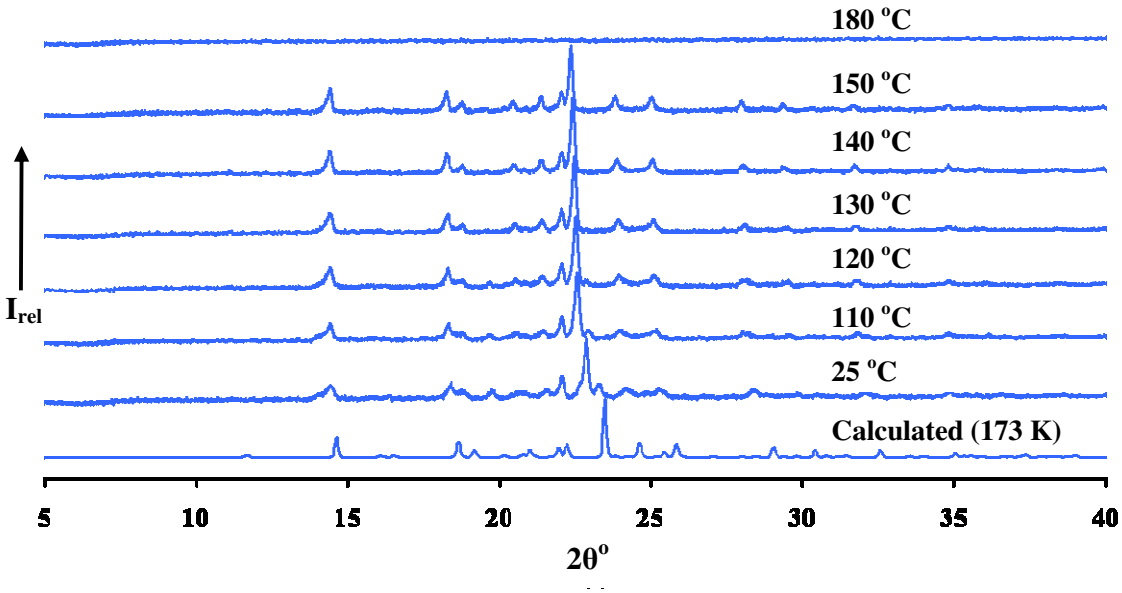

Figure 40 Variable temperature PXRD patterns of **Form 1**

The peak positions in the calculated trace (173 K) are displaced to higher 2θ-angle compared to those of the experimental trace (25 °C), as expected. However, the match between the two traces is convincing, proving that the bulk sample is homogeneous and has the same crystal structure as **Form 1** described by Aakeröy et al.[23]

No evidence of phase change was observed when **Form 1** was heated to the melting temperature. This is consistent with the fact that only a single endothermic peak B was observed in the DSC trace of **Form 1** (Figure 38).

Figure 41 firstly shows the comparison between the measured PXRD pattern of **Form 2** at 25 °C and the calculated pattern derived from the single crystal structure of **Form 2** using program LAZY PULVERIX.[11] Crystals of **Form 2** were then characterised by PXRD as a function of temperature. The PXRD pattern was recorded at temperature intervals of 10 K between 30 and 180 °C.

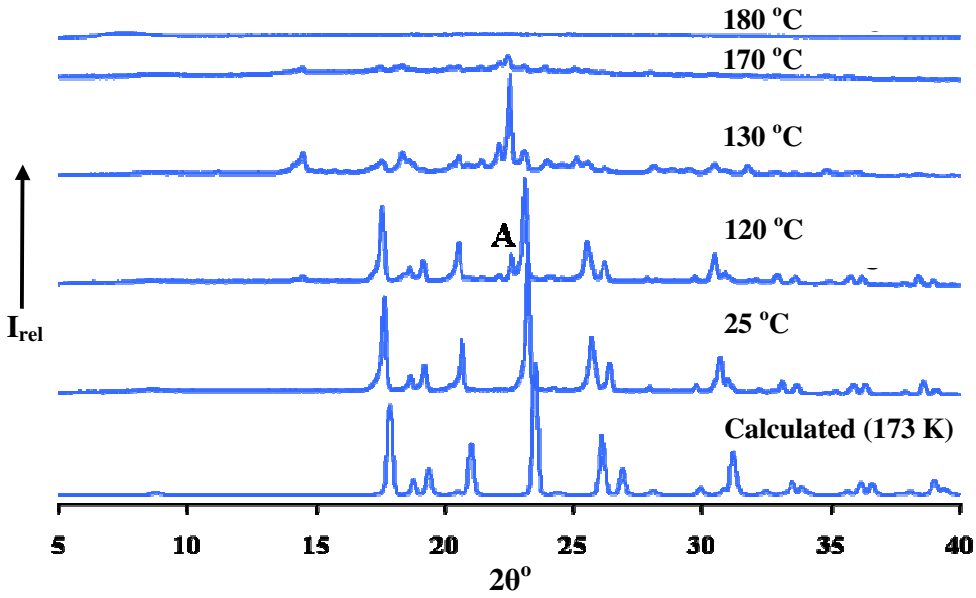

Figure 41 Variable temperature PXRD patterns of **Form 2**

In Figure 41, the calculated PXRD trace (173 K) is in a good agreement with the experimental trace (25 °C). This confirms that the bulk sample is homogeneous and has the same crystal structure as **Form 2** described by Vishweshwar et al.[24]

When crystals of **Form 2** were heated, no evidence of phase change was observed until 120 °C at which a new peak A appeared in the trace. **Form 2** produced a totally different trace at 130 °C from that at 25 °C. The PXRD traces indicate the start of the phase transition of **Form 2** at ~120 °C and its completion by ~130 °C. This provides proof that the endothermic peak A, present in the DSC trace of **Form 2** in Figure 38, represents a phase transition.

Figure 42 firstly presents the comparison of the measured PXRD pattern of **Form 3** at 25 °C with the calculated pattern derived from the single crystal structure of **Form 3**

(determined in the present study and described later) using program LAZY PULVERIX.[11] Crystals of **Form 3** were then characterised by PXRD as a function of temperature. The PXRD pattern was recorded at temperature intervals of 10 K between 30 and 180 °C.

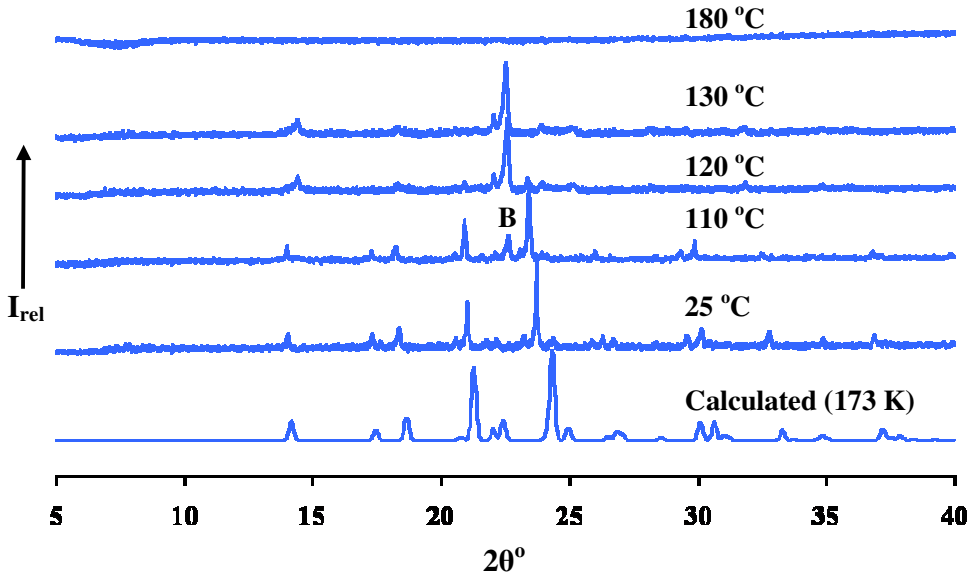

Figure 42 Variable temperature PXRD patterns of **Form 3**

The match between the calculated PXRD pattern (173 K) and the experimental pattern (25 °C) confirms the polymorphic purity of the experimental sample of **Form 3**.

When the crystals of **Form 3** were heated, they remained the same phase until ~110 °C. A distinct peak B was observed in the trace at ~110 °C. The PXRD trace of **Form 3** was found to be completely different at ~120 °C compared to that determined at 25 °C. This indicates that **Form 3** experienced a phase transition which started at ~110 °C and ended at ~120 °C. Based on these results, the endothermic peak B in the DSC trace of **Form 3** in Figure 39, is confirmed as an indication of a phase change.

We note that, **Form 2** shows an indication of phase change at ~120 °C (Figure 41) while **Form 3** shows the indication at ~110 °C (Figure 42). This confirms the conclusion from DSC that the phase change temperature of **Form 3** is lower than that of **Form 2**.

Although it was proved that both **Forms 2** and **3** underwent a phase change when heated, these modified phases still needed to be identified unambiguously. Therefore, the PXRD patterns of all three forms at 130 °C are compared in Figure 43. The calculated trace of **Form 1** at 173 K is shown for comparison. The reason for choosing to display the traces at 130 °C is that both **Forms 2** and **3** have completed the phase transition at this particular temperature.

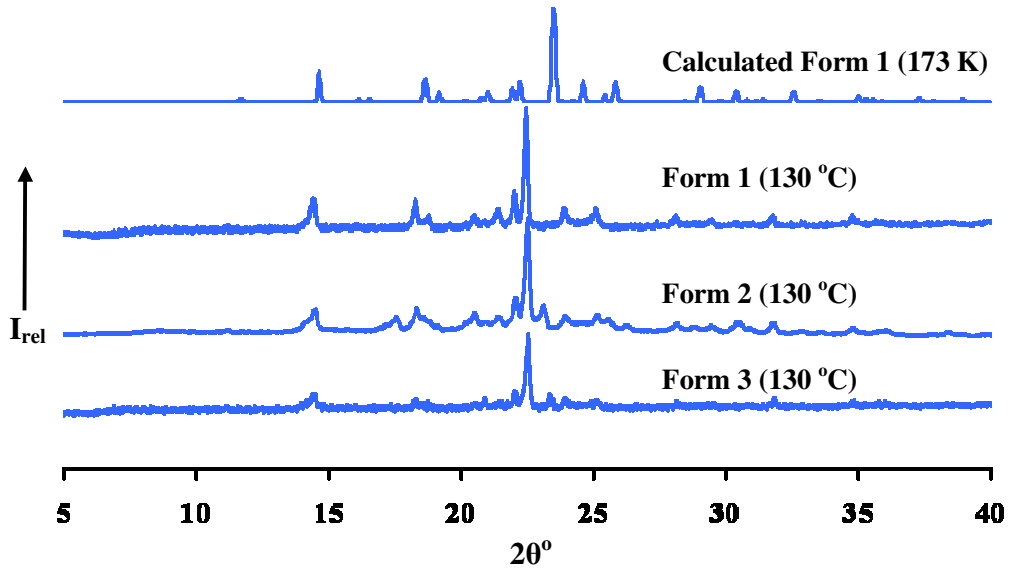

Figure 43 PXRD patterns of **Form 1** (calculated at 173 K) and **Forms 1**, **2**, **3** at 130 °C.

The PXRD patterns of all three forms at 130 °C appear to represent the same phase. Although the peak positions in the experimental traces are significantly displaced to lower 2θ-angle owing to the different temperature conditions (a difference of 230 K), there is good agreement between all the experimental traces and the calculated PXRD pattern of **Form 1** at 173 K. This gives strong evidence that both **Forms 2** and **3** experienced phase transitions into **Form 1**. In other words, both **Forms 2** and **3** are enantiotropically related to **Form 1**.

However, it was also necessary to establish in this study, the thermal relationship between **Form 2** and **Form 3**. Considering the fact that **Form 2** underwent a phase change commencing at ~120 °C, it seemed useful to compare the PXRD patterns of

Form 2 at 120 °C, **Form 2** at 110 °C, **Form 1** at 110 °C and **Form 3** at 110 °C (Figure 44).

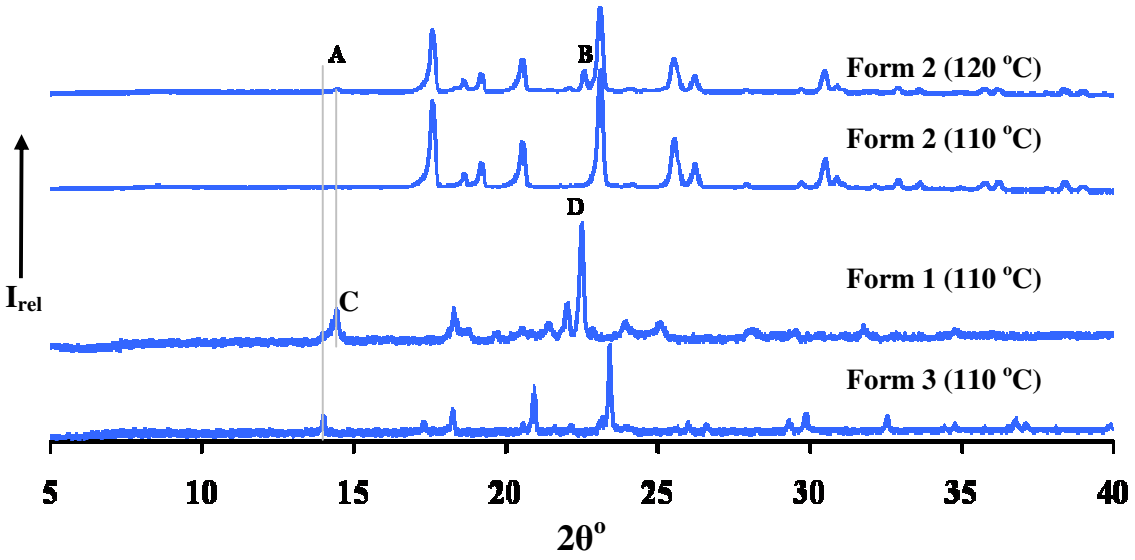

Figure 44 PXRD patterns used to establish direct transition of **Form 2** into **Form 1** upon heating.

Two extra peaks A and B are observed in the PXRD pattern of **Form 2** at ~120 °C compared to that at ~110 °C. These two peaks are due to the phase change. In other words, **Form 2** at ~120 °C is a mixture of **Form 2** and the modified phase. The trace of **Form 2** at ~120 °C was then compared with those of **Forms 1** and **3** at ~110 °C. Peaks A and B in the trace of **Form 2** at ~120 °C are found to be consistent with peaks C and D in the trace of **Form 1** at ~110 °C, respectively. No peaks in the trace of **Form 3** at ~110 °C are located in the same 2θ positions as peaks A and B in the trace of **Form 2** at ~120 °C. Therefore, no evidence of **Form 3** was found in the phase of **Form 2** at ~120 °C. In other words, the mixed phase of **Form 2** at ~120 °C consists of the phases of **Form 2** and **Form 1**. Consequently, **Form 2** did not convert into **Form 3** first; instead, it experienced a phase change into **Form 1** directly.

A similar comparison was carried out to investigate **Form 3** at ~110 °C at which temperature **Form 3** starts to show indications of phase change. The PXRD patterns of **Form 3** at ~110 °C, **Form 3** at ~100 °C, **Form 1** at ~110 °C and **Form 2** at ~110 °C were compared in Figure 45.

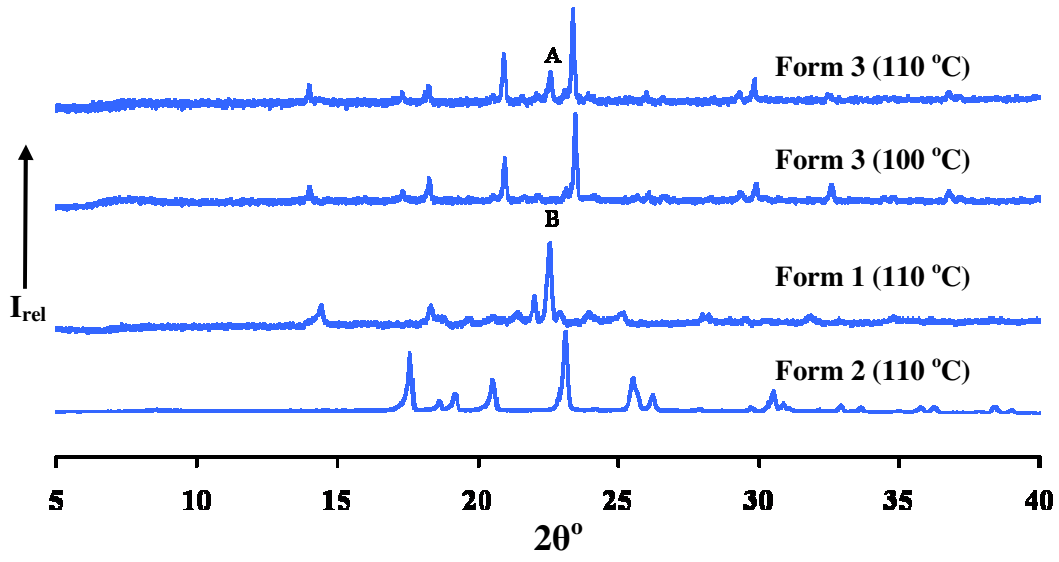

Figure 45 PXRD patterns employed to establish direct transformation of **Form 3** into **Form 1** upon heating.

An extra peak A was observed in the PXRD trace of **Form 3** at ~110 °C compared to that of **Form 3** at ~100 °C. Therefore, **Form 3** started to show an indication of phase change at ~110 °C and this particular peak A is due to the new phase. The trace of **Form 3** at ~110 °C was then compared with those of **Forms 1** and **2** at ~110 °C. The 2θ value of the peak A in the trace of **Form 3** at ~110 °C and that of the peak B in the trace of **Form 1** at ~110 °C were found to be in close correspondence. Also, the peak A was not consistent with any peak in the trace of **Form 2** at ~110 °C. Consequently, the phase of **Form 3** at ~110 °C is a mixed phase containing the phases of **Form 3** and **Form 1**. In other words, **Form 3** did not transform into **Form 2** first; instead, it experienced a phase change into **Form 1** directly.

From all of the above results, it is concluded that **Forms 2** and **3** are both enantiotropically related to **Form 1**, and furthermore that **Form 2** and **Form 3** are monotropically related.

Hot Stage Microscopy

In order to provide visual evidence for the above conclusions, HSM analysis was introduced. Crystals of **Forms 1**, **2** and **3** were placed between cover slips and immersed in silicone oil. Photographs were taken in the temperature range 30-170 ^{o}C at a heating rate of 10 K/min (Figure 46). (It should be noted that the single crystals chosen for HSM were identified unambiguously from measurement of their unit cell dimensions at room temperature on a four-circle single crystal X-ray diffractometer).

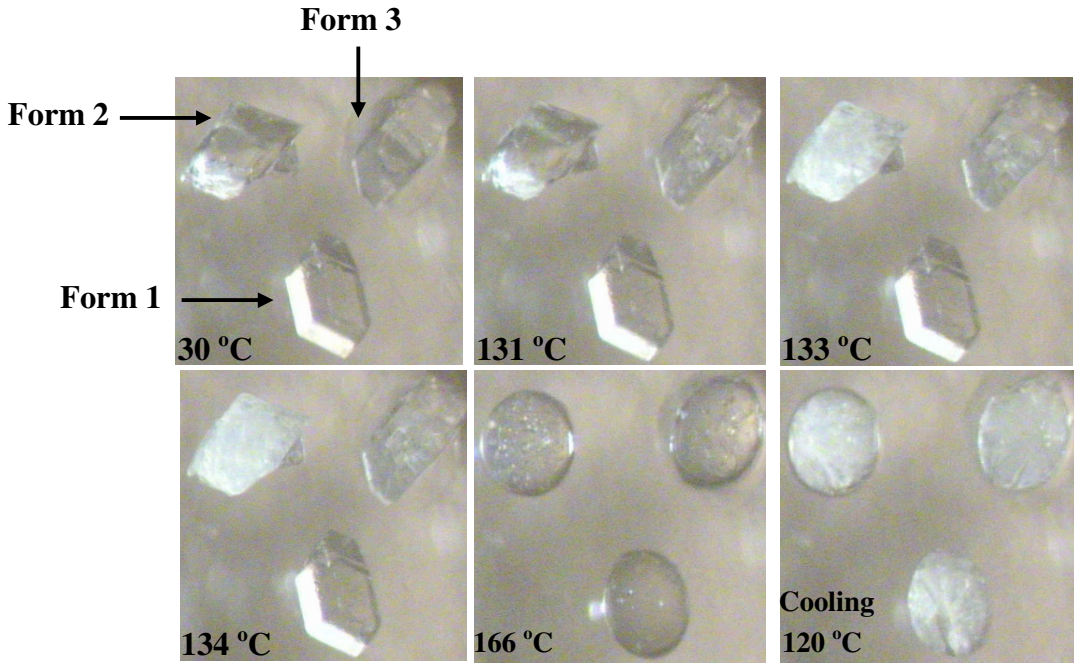

Figure 46 HSM photographs taken at various temperatures of crystals of **Forms 1**, **2** and **3** of isonicotinamide heated at 10 K/min

The crystals of **Forms 1**, **2** and **3** were clear and transparent at 25 ^{o}C. The crystals of **Forms 2** and **3** appeared to become opaque at 133 ^{o}C and 131 ^{o}C, respectively. These events represent the previously established phase changes of **Forms 2** and **3**, respectively. Furthermore, these observations confirm the conclusion that the phase change temperature of **Form 3** is slightly lower than that of **Form 2**. The crystal of **Form 1** remained clear during heating, indicating that no phase transition had occurred. The three crystals melted simultaneously at ~166 ^{o}C and the melts all recrystallised on cooling to ~120 ^{o}C. These observations are consistent with the conclusions drawn from DSC analysis and variable temperature PXRD.

In order to further explore distinction of the phase change temperatures of **Form 2** and **Form 3**, separate HSM experiments were performed at a much lower heating rate (1 K/min). The results are shown in Figure 47.

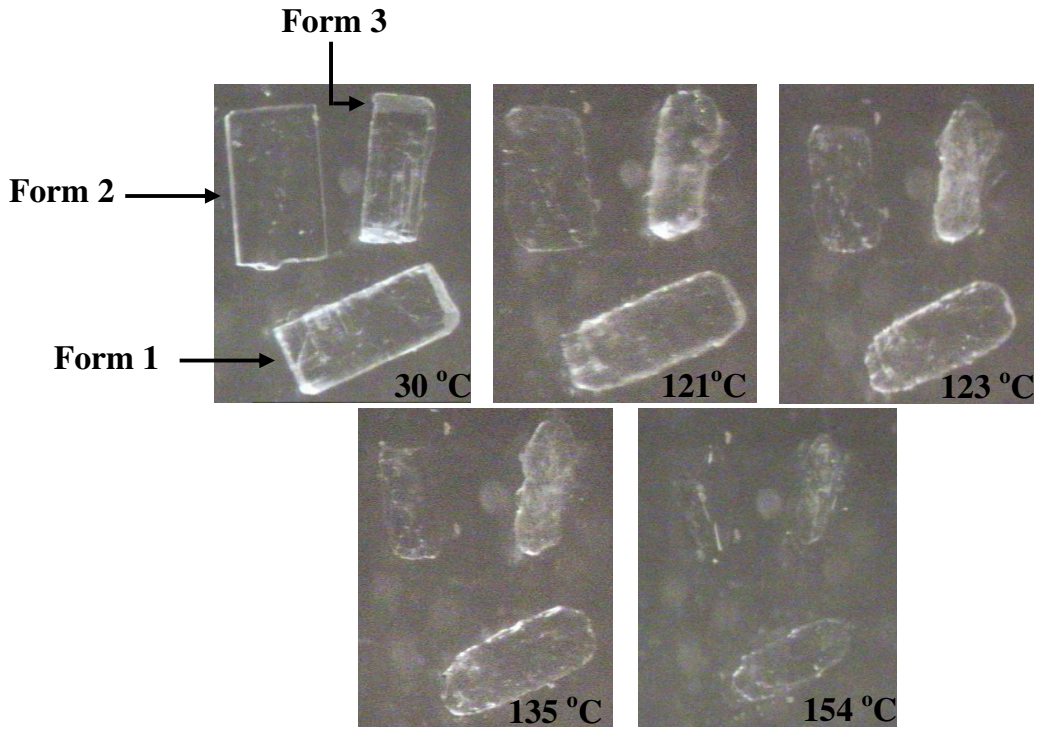

Figure 47 HSM photographs at various temperatures of crystals of **Forms 1**, **2** and **3** heated at 1 K/min

Crystals of **Forms 1**, **2** and **3** were heated at 1 K/min from 30 °C. At ~121 °C, the crystal of **Form 3** gradually became opaque, indicating the occurrence of the phase change to **Form 1**. However, the crystal of **Form 2** remained clear throughout the heating process. The three crystals eventually melted simultaneously at ~154 °C, strongly suggesting that **Form 2** nevertheless experienced a phase change to **Form 1**.

DSC and PXRD were introduced to confirm this assumption. Crystals of **Form 2** were placed in the open furnace of the DSC apparatus, and heated at 1 K/min. The heating process was stopped at 130 °C. The sample was then analysed by PXRD and the trace compared with the calculated pattern of **Form 1** (Figure 48).

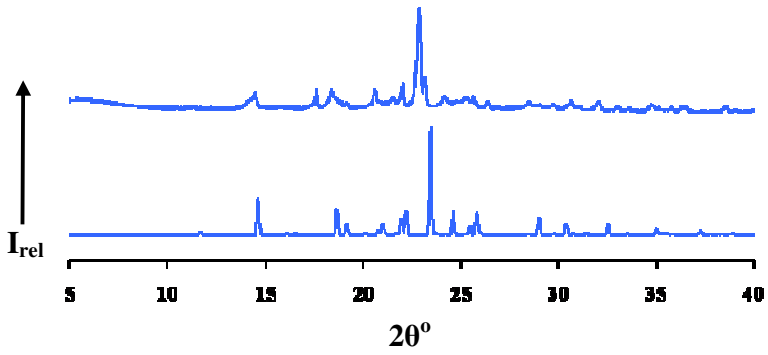

Figure 48 From top to bottom: PXRD patterns of **Form 2** heated until 130 °C at 1 K/min; the calculated PXRD pattern of **Form 1**.

The match between the two PXRD traces is very convincing, indicating that **Form 2** did experience a phase change to **Form 1** when heated at 1 K/min. Consequently, it can be concluded that there is no visual phase change when **Form 2** is heated at low heating rate; nevertheless, the phase change still occurs. On the other hand, the phase change when **Form 3** is heated is visible at both high and low heating rates.

Construction of the Energy – Temperature Diagram

As concluded earlier, **Forms 2** and **3** are enantiotropically related to **Form 1**. Also, the phase transition temperature of **Form 2** is slightly higher than that of **Form 3**. Furthermore, **Form 2** and **Form 3** are monotropically related. Based on these data, a schematic Energy–Temperature diagram for the three polymorphs of isonicotinamide can therefore be constructed, as described below and shown in Figure 49.

Since **Form 1** is enantiotropically related to **Form 2**, the G isobars of the two modifications should intersect and this specific intersection point (114.9 °C) would be defined as the thermodynamic transition point T_{t2}. Similarly, the G isobars of **Form 1** and **Form 3** should intersect at a specific point which is defined as T_{t3}. In addition, the variable temperature PXRD patterns illustrate that **Form 1** is the stable modification after T_{t2} (Figure 43). This requires the G isobar of **Form 1** to be located below that of **Form 2** after the point T_{t2}. Considering the fact that the G-T curve of **Form 1** should intersect with that of **Form 2**, the former would be located above the latter below the temperature T_{t2}. In addition, the variable temperature PXRD patterns indicate that **Form 1** is more

stable than **Form 3** above T_{t3}. This requires the G-isobar of **Form 1** to be located below that of **Form 3** above point T_{t3}. Considering that the G-isobar of **Form 1** must intersect that of **Form 3** also, the former must be located above the latter below T_{t3}. Based on the course of the G isobar of the liquid, the melting point of **Form 1** is indicated by the point of intersection of its G isobar ($G_{Form\ 1}$) with that of the liquid (G_{liq}). This corresponds to the temperature T_{f1} ~154 ^{o}C, the melting point of **Form 1**.

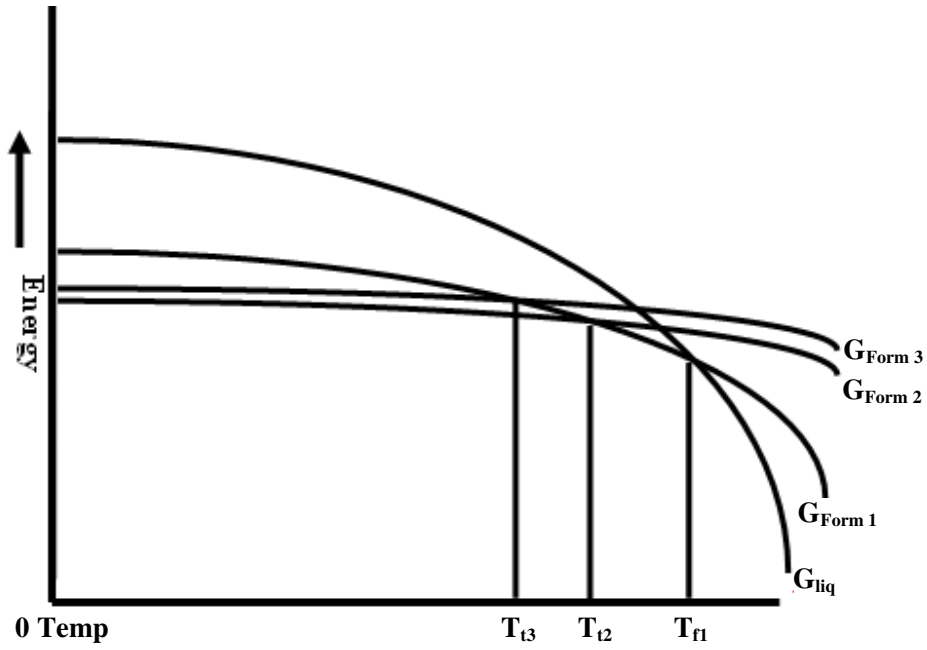

Figure 49 A schematic E/T diagram for the three polymorphs of isonicotinamide. (Note that the interval $T_{t3} \rightarrow T_{t2}$ is highly exaggerated).

Since **Form 2** is monotropically related to **Form 3**, their G isobars would not intersect. Therefore, the two G-T curves will be parallel to each other. Although the exact value of T_{t3} cannot be determined, it can be confirmed that T_{t3} locates slightly ahead of T_{t2} in the E/T diagram. Based on this, the G-isobar of **Form 3** must lie above that for **Form 2**.

According to the density rule, the thermodynamically stable form at 0 Kelvin has the highest density.[4] From the E/T diagram for isonicotinamide polymorphs, it can be predicted that the order of density at room temperature is: **Form 2 > Form 3 > Form 1**. It can also be predicted from the E/T diagram that these polymorphs would have a solubility order at room temperature: **Form 2 < Form 3 < Form 1**. Furthermore, the

density order and the solubility order can be applied from 0 Kelvin to the phase transition temperatures. We revisit the density order in the following section.

X-Ray Crystallographic Analysis of Isonicotinamide, Form 3

Single Crystal X-Ray Diffraction

Data-collection and Space Group Determination

Structural information for **Forms 1** and **2** was obtained from Aakeröy et al.[23] and Vishweshwar et al.,[24] respectively. The crystal data for **Forms 1** (CSD refcode EHOWIH02[23]) and **2** (CSD refcode EHOWIH01[24]) were obtained from the CSD[25].

Intensity data for **Form 3** were collected on a Nonius Kappa CCD four-circle diffractometer. It was confirmed that cooling the crystal of **Form 3** from 294 K to 173 K, the temperature of the data-collection, did not result in a phase transformation.

Program LAYER[26] was used to determine the crystal system and space group of **Form 3**. The crystal system was found to be orthorhombic since the Laue symmetry was *mmm* and the reflection conditions were *hkl: none; 0kl: k = 2n; h0l: l = 2n; hk0: h = 2n*, indicating the space group Pbca. This assignment was confirmed using program XPREP.[5]

Structure Solution and Refinement

SHELXS-97[6] was used for the structure solution of **Form 3.** The positions of all non-hydrogen atoms in the asymmetric unit (one molecule of isonicotinamide) were determined by direct methods. The atoms were placed and refined isotropically on F^2 in SHELXH-97[7]. All the non-hydrogen atoms were then refined anisotropically based on well-behaved isotropic temperature factors. Attempts to locate the hydrogen atoms from difference Fourier maps followed and were successful. Based on the positions of the peaks, a riding model was subsequently used to place all the hydrogen atoms in idealised positions. These hydrogen atoms were assigned isotropic temperature factors 1.2 times

those of their parent atoms. Table 18 contains relevant crystal data for **Forms 1** and **2** taken from the CSD[25] as well as the crystal and refinement data for **Form 3**.

Table 18 Crystal and refinement data for **Forms 1**, **2** and **3**

Parameter	Form 1*	Form 2**	Form 3
Formula unit	$C_6H_6N_2O$	$C_6H_6N_2O$	$C_6H_6N_2O$
Formula Weight / g mol^{-1}	122.13	122.13	122.13
Temperature / K	173 (2)	173 (2)	173 (2)
Crystal system	monoclinic	monoclinic	orthorhombic
Space group	$P2_1/c$	$P2_1/c$	Pbca
a / Å	15.735(3)	10.176(1)	10.1603(7)
b / Å	7.998(1)	5.732(1)	7.3231(5)
c / Å	9.885(3)	10.034(1)	15.8720(6)
α / °	90.00	90.00	90.00
β / °	105.59(1)	98.04(1)	90.00
γ / °	90.00	90.00	90.00
Volume / Å^3	1198.21(5)	579.48(1)	1180.95(1)
Z	8	4	8
Density$_{calc}$/g cm^{-3}	1.3538	1.3997	1.3736
μ (MoK$_α$) /mm^{-1}	----------	----------	0.098
F (000)	----------	----------	512
Crystal size /mm^3	----------	----------	0.32x0.32x0.46
Range scanned θ / °	----------	----------	1.00≤ θ ≤ 26.37
Index ranges	----------	----------	h: -12,12
	----------	----------	k: -9,9
	----------	----------	l: -19,19
φ scan angle / °	----------	----------	1.0
ω scan angle / °	----------	----------	1.0
Dx / mm	----------	----------	34
No. of measured reflections	----------	----------	2126
No. of unique reflections	----------	----------	1188
No. of reflections with I > 2σ(I)	----------	----------	896
No. of L.S. parameters	----------	----------	82
R_{int}, $R_σ$	----------	----------	0.0286, 0.0307
S	----------	----------	1.120
R_1 (F_o > 4σ(F_o))	----------	----------	0.0453
No. of reflections omitted	----------	----------	6
wR2 (all reflections)	----------	----------	0.0960
Weighting scheme	----------	----------	a = 0.0367
	----------	----------	b = 0.6587
(Δ / σ)$_{mean}$	----------	----------	< 0.001
Δρ excursions / eÅ^{-3}	----------	----------	-0.19, 0.22

* Data taken from the CSD, refcode EHOWIH02.[23]

** Data taken from the CSD, refcode EHOWIH01.[24]

A noteworthy observation is that the calculated densities above are in the order deduced earlier from the E/T diagram, namely **Form 2** > **Form 3** > **Form 1**.

In the following section, detailed structural comparisons of **Forms 1**, **2** and **3** of isonicotinamide are presented at both the molecular and crystal structural levels.

Molecular Structure

The numbering scheme of the isonicotinamide molecule used in this study is presented in Figure 50 (left). There are two crystallographically independent molecules (A and B) in the asymmetric unit of **Form 1** as shown in Figure 50 (right).

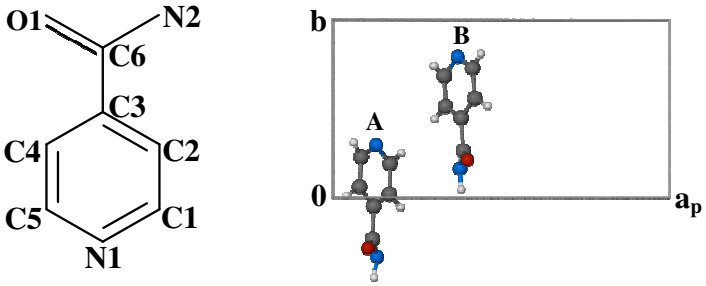

Figure 50 The numbering scheme of the isonicotinamide molecule (left); two crystallographically independent isonicotinamide molecules (A and B) in the asymmetric unit of **Form 1**.

Essentially, the main conformational degree of freedom is rotation around the C3-C6 bond (expressed in e.g. the dihedral angle O1-C6-C3-C4). The value of this torsion angle is listed in **Forms 1**, **2**, and **3** in Table 19. It is evident that molecules A and B of **Form 1** adopt very similar conformations, but that these differ significantly (but not remarkably) from the nearly identical conformations observed in **Forms 2** and **3**.

Table 19 The torsion angle O1-C6-C3-C4 of isonicotinamide molecules in **Forms 1, 2** and **3***

Torsion angle (°)	**Form 1** (A and B）	**Form 2**	**Form 3**
O1-C6-C3-C4	25.4(4), -24.0(3)	30.5(2)	30.9(3)

*Note that since the crystals are all centrosymmetric, for any torsion angle listed, there is a corresponding parameter with the same magnitude but opposite sign.

Figure 51 shows the overlay diagrams of the molecules in **Forms 1, 2** and **3** from different orientations. Only the molecule A in **Form 1** is shown for comparison because

of its very similar conformation to that of molecule B' (where B' is the inverse of molecule B).

Figure 51 An overlay of the molecules in **Form 1** (green), **Form 2** (red) and **Form 3** (gray). Hydrogen atoms are omitted for clarity.

Hydrogen Bond Interactions

Analogous intermolecular hydrogen bonds N2-H6···O1 are found in the structures of **Forms 1**, **2** and **3.** A common hydrogen bond N2-H5···N1 is found in the structures of **Forms 1** and **3**. A unique hydrogen bond N2-H5···O1 is found only in the structure of **Form 2**. The geometrical details of these hydrogen bonds are listed in Table 20.

Table 20 Intermolecular hydrogen bond interactions for **Forms 1**, **2** and **3**[a]

Hydrogen bond	N···N or N···O Distance (Å)	Angle (°)	Symmetry operator[b]
Form 1			
N2A-H5A···N1A	2.982(2)	171.0	x, -1+y, z
N2A-H6A···O1A	2.935(3)	170.0	x, 1/2-y, -1/2+z
N2B-H5B···N1B	2.974(2)	169.0	x, -1+y, z
N2B-H6B···O1B	2.947(3)	174.0	x, 1/2-y, -1/2+z
Form 2			
N2-H6···O1	2.935(2)	158.0	x, 1/2-y, 1/2+z
N2-H5···O1	2.937(2)	173.0	-x, 1-y, -z
Form 3			
N2-H5···N1	2.982(2)	178.0	x, 1/2-y, 1/2+z
N2-H6···O1	3.015(2)	173.0	1/2+x, 1/2-y, 2-z

[a] Where no e.s.d. is reported for the angle, H atoms involved were added in idealised positions in a riding model.
[b] Symmetry operator applies to hydrogen bond acceptor atoms.

Figure 52 illustrates the hydrogen bond interactions for each form. In the crystal of **Form 1**, the molecule A is hydrogen bonded to other symmetry-generated molecules A only. Molecule B is likewise hydrogen bonded to symmetry-generated B molecules only. Since the hydrogen bond motifs are analogous, only that of the molecule A is shown as a representative in the figure. A graph set analysis descriptor $R_3^4(20)$ [8, 9] can be assigned to the hydrogen bond motif of **Form 1**. In **Form 2**, two isonicotinamide molecules

associate as centrosymmetric, hydrogen bonded dimers, the unique H-bond being N2-H5···O1^{i} (i = -x, 1-y, -z). The cyclic H-bonded pattern contains a total of eight atoms, two of them being donors and two being acceptors, and is hence designated as $R_2^2(8)$.[8, 9] Furthermore, a second hydrogen bond N2-H6···O1^{ii} (ii = x, 1/2-y, 1/2+z) also associates two isonicotinamide molecules, and has a graph set analysis descriptor $C_1^1(4)$.[8, 9] A noteworthy observation is that pyridine atom N1 in **Form 2** is not hydrogen bonded to other atoms, which is not common in the hydrogen bond motifs of isonicotinamide molecules. **Form 3** adopts a similar hydrogen bonded framework as that in **Form 1**.

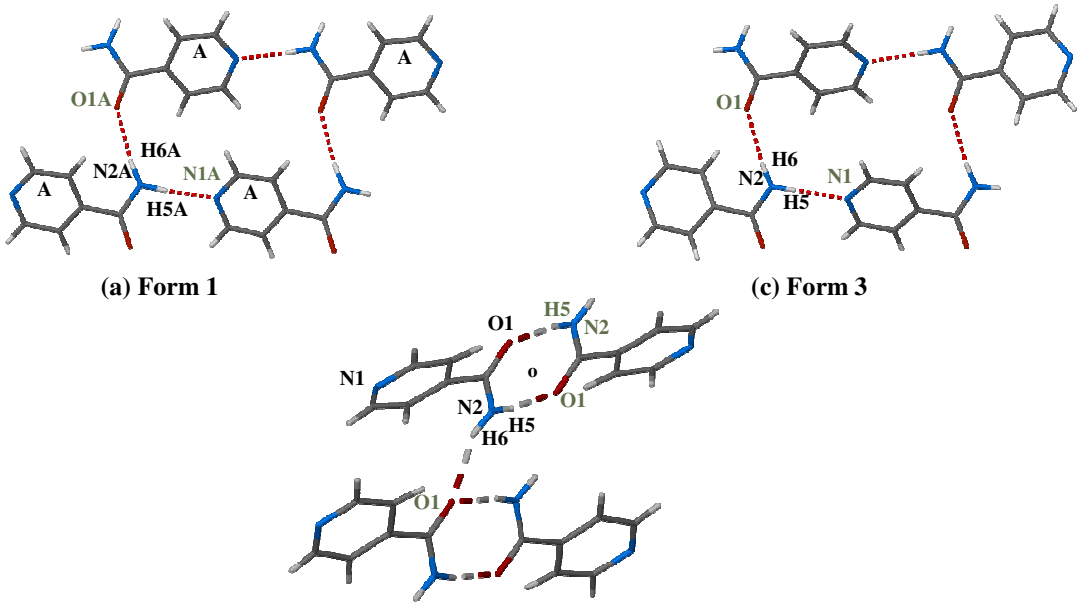

Figure 52 Hydrogen bonded motifs in (a) **Form 1**, (b) **Form 2** and (c) **Form 3**. Atoms with gray labels have been symmetry-generated from their asymmetric unit counterparts.

The hydrogen bond motifs of **Forms 1** and **3** are overlayed in Figure 53. Although the framework is similar in these two cases, the pyridine rings A1 and A2 of the two structures cannot be superimposed simultaneously. This indicates the primary difference between the hydrogen bond motifs of **Form 1** and **Form 3**.

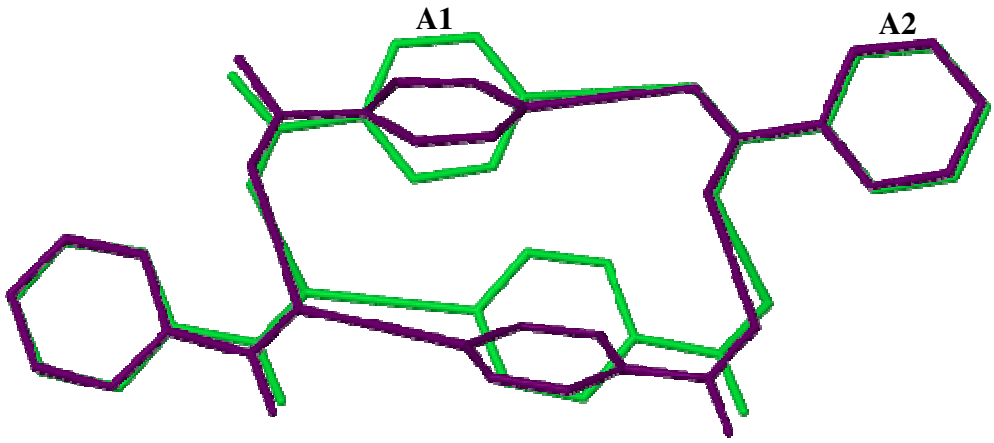

Figure 53 An overlay of hydrogen bond motifs of **Form 1** (green) and **Form 3** (purple). Hydrogen atoms are omitted for clarity.

A unique weak intermolecular hydrogen bond C2-H2···O1 is found in the structure of **Form 3** (Figure 54). This is associated with the different pyridine ring orientations in the hydrogen bond motifs of **Forms 1** and **3.** The geometrical details of this hydrogen bond are listed in Table 21. Therefore, **Form 3** contains hydrogen bonded rings with graph set analysis descriptors $R_2^1(7)$ and $R_3^4(17)$,[8, 9] as indicated in Figure 54.

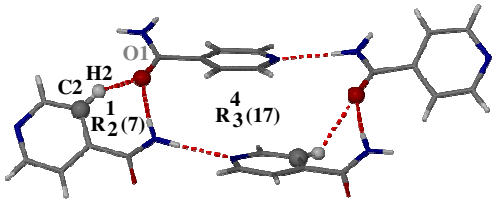

Figure 54 The detailed hydrogen bond motif of **Form 3.** Atoms forming hydrogen bond C2-H2···O1 are shown as spheres for clarity. Atom O1 with the gray label has been symmetry-generated from its asymmetric unit counterpart.

Table 21 The geometrical detail of hydrogen bond C2-H2···O1 in **Form 3**[a]

C2···O1 Distance (Å)	C2-H2···O1 Angle (°)	Symmetry operator for O1
3.205(2)	127.0	1/2+x, 1/2-y, 2-z

[a] No e.s.d. is reported for the angle since the atom H2 was added in an idealised position in a riding model.

The hydrogen bond motifs of **Form 1** and **Form 3** are also investigated here on a larger scale. Figure 55 illustrates the motif for the molecule A in **Form 1** from different

perspectives. In Figure 55(b), all of the pyridine rings (A1, A2, A3, A4, A5 and A6) are parallel to each other.

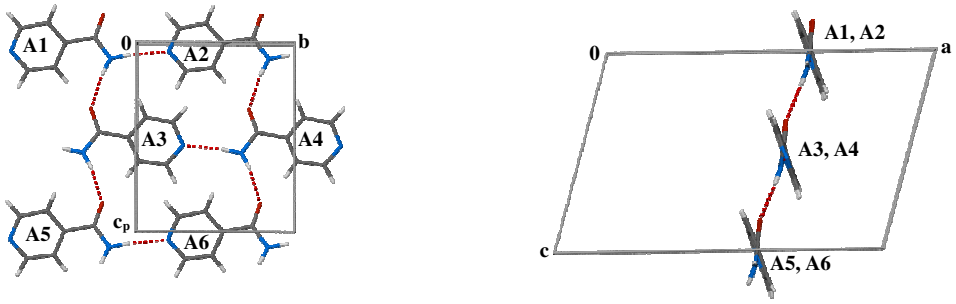

Figure 55 The hydrogen bond motif for the molecule A in **Form 1** viewed along (a) [100] and (b) [010].

Figure 56 illustrates the hydrogen bond motif for the molecule in **Form 3** from different orientations. Although the motif in Figure 56 (a) shows significant similarity with that in Figure 55 (a), the rings A1-A6 are not all parallel to one another. The set of parallel planes A1, A4 and A5 is related to the parallel set A2, A3 and A4 by the *c*-glide plane perpendicular to the *b*-axis at *b* = 1/4.

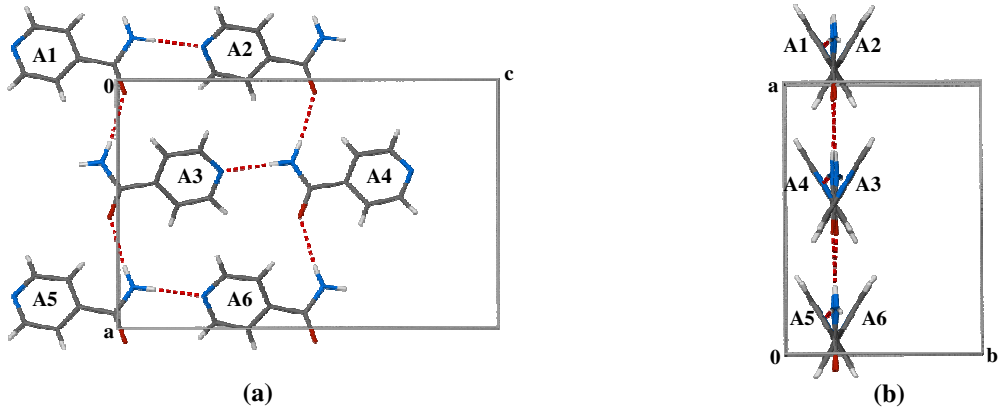

Figure 56 The hydrogen bond motif for the molecule in **Form 3** viewed along (a) [010] and (b) [001].

The detailed comparisons above serve to highlight the different hydrogen bond motifs that distinguish **Forms 1**, **2** and **3** of isonicotinamide.

Crystal Packing

For **Form 1**, (CSD refcode EHOWIH02[23]), the asymmetric unit contains two symmetry-independent molecules (A and B) which form two independent hydrogen bonded layers A and B, Figure 57 (a). The unit cell contains eight symmetry related molecules arranged in four layers (A, B, A′ and B′) which extend infinitely parallel to the *c*-axis. For **Form 3** (this study), there are eight symmetry related molecules in the unit cell; they arrange in two layers which extend infinitely parallel to the *a*- axis, Figure 57 (b). Furthermore, in both **Forms 1** and **3**, there is no hydrogen bond interaction between the layers. Layers A and B of **Form 1** differ in the relative inclinations of the pyridine rings, whereas layers A and A′ in **Form 3** are related to one another by a centre of inversion.

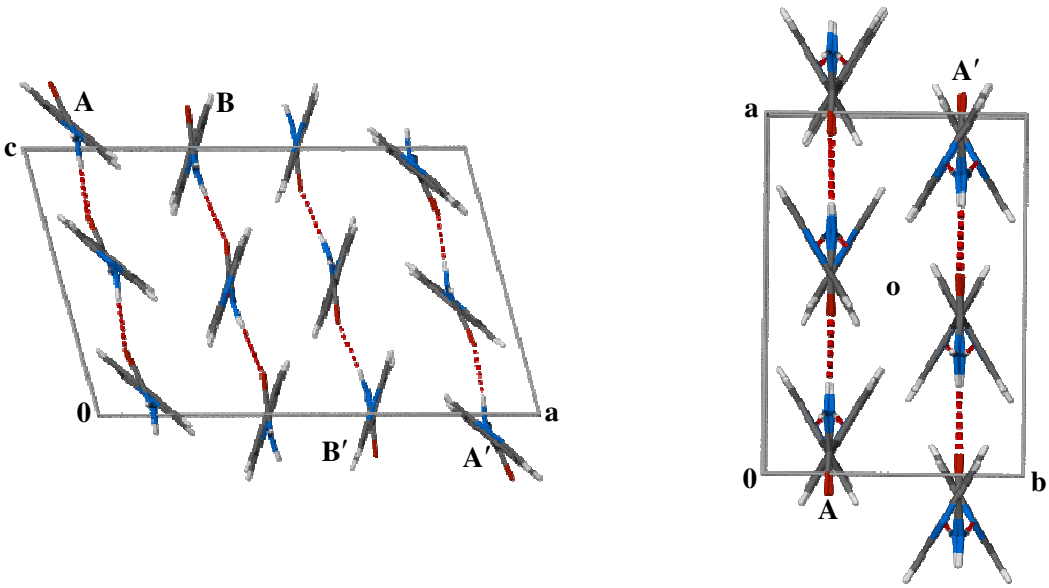

(a) Form 1 [010] **(b) Form 3 [001]**

Figure 57 Crystal packing diagrams for (a) **Form 1** viewed along [010] and (b) **Form 3** viewed along [001]

The layers A and B in **Form 1** and the layers A and A′ in **Form 3** are shown in Figure 58 from a different perspective.

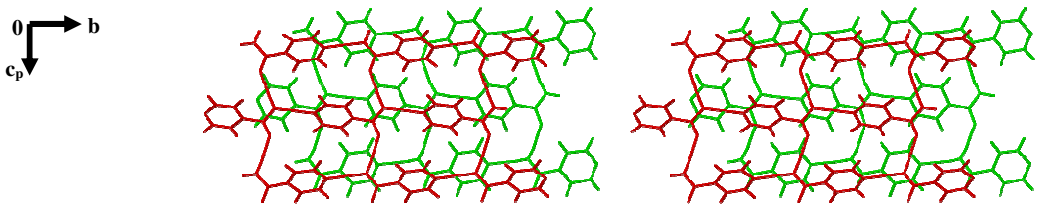

(a) Form 1

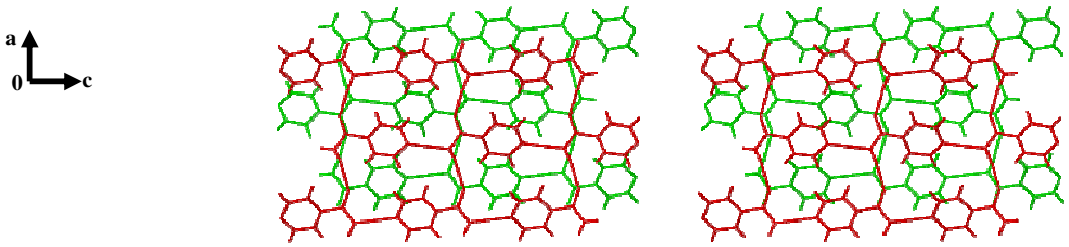

(b) Form 3

Figure 58 (a) The hydrogen bonded layers A (red) and B (green) in **Form 1** viewed along [100]. (b) The hydrogen bonded layers A (red) and A′ (green) in **Form 3** viewed along [010].

The unique feature of the crystal packing in **Form 2** (CSD, refcode EHOWIH01[24]) is the formation of centrosymmetric hydrogen-bonded isonicotinamide dimers. The second hydrogen atom of the amide group is used to link the dimers in infinite chains parallel to the *c*-axis, Figure 59.

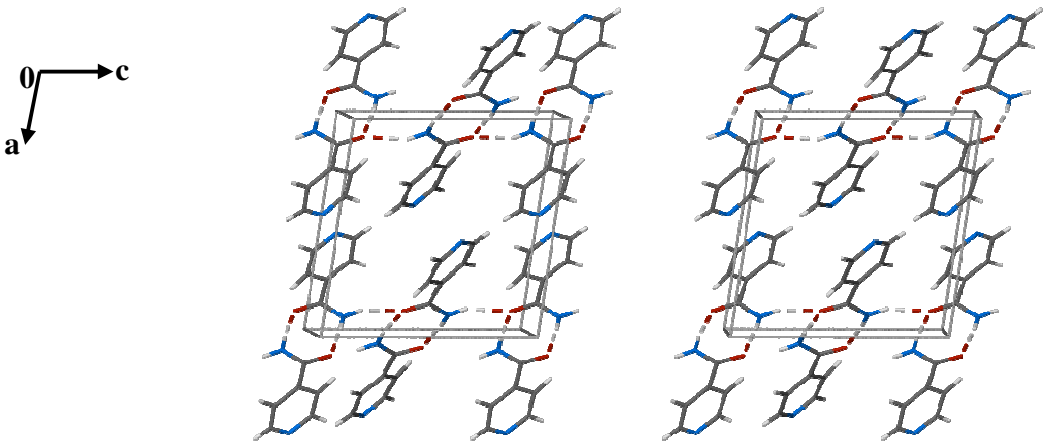

Figure 59 Stereoview of crystal packing diagram for **Form 2** viewed along [010].

Conclusion

Two polymorphs of isonicotinamide, namely **Forms 1** and **2,** had been isolated in 2003.[23, 24] However, their thermal relationship had not been determined. A new form (**Form 3**) was isolated and characterised in this study. The thermal relationship among all three polymorphs was determined by thermal methods coupled with variable temperature PXRD data. In order to isolate **Form 3**, it was not necessary for isoxyl to be present in the crystallising medium employed.

Form 1 experienced no phase change during the heating process and it melted at ~154 ^{o}C. **Form 2** underwent a phase change into **Form 1** at ~114 ^{o}C. Similarly, **Form 3** transformed into **Form 1** upon heating. Therefore, **Form 1** is enantiotropically related to **Form 2** and **Form 3**. In addition, the fact that the changing phase of **Form 2** during the heating process contains both **Forms 1** and **2** while the changing phase of **Form 3** upon heating contains both **Forms 1** and **3** leads to the conclusion that both **Forms 2** and **3** convert to **Form 1** directly. In other words, the G isobars of **Forms 2** and **3** do not intersect and so these polymorphs are monotropically related.

Although the exact transition temperature of **Form 3** could not be determined, evidence from variable temperature PXRD and HSM confirmed that the transition temperature of **Form 3** is slightly lower than that of **Form 2**.

Based on the above conclusions, a schematic Energy-Temperature diagram of the three forms of isonicotinamide was constructed. Calculated crystal densities of the three polymorphs, based on their respective crystal data, were found to be in the order predicted from the Energy-Temperature diagram.

Form 1 crystallises in the monoclinic space group $P2_1/c$ with a = 15.735(3), b = 7.998(1), c = 9.885(3) Å, β = 105.59(1)º and 8 molecules per unit cell. This requires that there are two symmetry-independent molecules in the asymmetric unit (namely molecules A and B).[23] **Form 2** crystallises in the space group $P2_1/c$ with a = 10.176(1), b = 5.732(1), c = 10.034(3) Å, β = 98.04(1)º and 4 molecules per unit cell.[24] **Form 3**, isolated and fully

characterised in this study, crystallises in the orthorhombic space group Pbca with a = 10.1603(7), b = 7.3231(5), c = 15.8720(6) Å and 8 molecules per unit cell.

Form 1 and **Form 3** adopt very similar hydrogen bonding motifs; however, these are not identical. Analogous intermolecular hydrogen bonds (N2-H5···N1 and N2-H6···O1) can be observed in the structures of **Forms 1** and **3**. However, an additional hydrogen bond C2-H2···O1 is observed only in **Form 3**. **Form 2** contains a very different hydrogen bonding motif from those of **Forms 1** and **3**. A noteworthy observation is that the pyridine nitrogen atom (N1) is not hydrogen bonded to any atoms in **Form 2**. In other words, only one nitrogen atom (N2 of the amide function) is involved in the hydrogen bond motif of **Form 2**. Consequently, **Forms 1**, **2** and **3** contain hydrogen bond motifs that are distinct and that may be described using graph set analysis descriptors as $R_3^4(20)$, $C_1^1(4)R_2^2(8)$ and $R_2^1(7)R_3^4(17)$,[8, 9] respectively.

Infinite hydrogen-bonded layers are found in the structures of both **Forms 1** and **3**. In **Form 1**, the molecules A assemble to form layer A while the crystallographically distinct molecules B assemble to form a distinct layer B. These layers individually contain coplanar pyridine rings, but the layers are not superimposable because of the different inclinations of the rings in layers A and B. For **Form 3**, the molecules assemble as two layers (A and A') in the unit cell and these two layers are related by a crystallographic inversion centre. Molecules of isonicotinamide in **Form 2** form centrosymmetric hydrogen bonded dimers, linked to forms chains parallel to the c-axis. Thus, **Forms 1**, **2** and **3** are different polymorphs with different hydrogen bond motifs and crystal packing arrangements.

As is evident from the variable temperature PXRD Figures 40, 41 and 42, experimental PXRD traces of the three polymorphs are found to be consistent with their respective calculated patterns, allowing the latter to serve as reliable references for polymorphic identification.

Nicotinamide

In an early attempt to form a cocrystal between isoxyl and nicotinamide by co-precipitation from ethyl acetate solution, the products of crystallisation were identified as a mixture of a known polymorphic form of nicotinamide and a new phase of nicotinamide by measuring the unit cell dimensions of the respective crystals. To establish whether this outcome depended on the presence of isoxyl, nicotinamide alone was dissolved in ethyl acetate and the products of crystallisation were found to be a known polymorphic form of nicotinamide only. Thus, through the preparative method used in this study, the appearance of the new polymorphic phase of nicotinamide requires the participation of the compound isoxyl. Specifically, isoxyl evidently acts to enhance the nucleation and growth of this particular new phase of nicotinamide rather than acting to form a co-crystal. Details of this new phase are reported below. In addition to producing an apparently new polymorph of nicotinamide, this preparative procedure also yielded crystals of one other polymorph, referred to here as **Form 1**, whose structure was first reported in 1953[27] and for which a more accurate crystal and molecular structure was determined in 1999 (CSD refcode NICOAM01).[28] The polymorphism of nicotinamide was subsequently first discussed by Hino et al.[29] based on evidence obtained by DSC analysis. However, no crystal structure of a second nicotinamide polymorph has hitherto been determined. In this study, the new polymorph was accordingly named **Form 2** and its structure was determined, as was its polymorphic relationship to **Form 1**. As with the new isonicotinamide polymorph described previously, the widespread use of nicotinamide as a co-former in cocrystallisation is a strong motivation for clarifying its solid-state chemistry.

Polymorph Preparation

In a typical experiment, a physical mixture of nicotinamide (19 mg) and isoxyl (9 mg) was dissolved in 2 ml ethyl acetate at 54 ^{o}C. The solution was stirred for 10 minutes and filtered (0.45 μm nylon filter) while hot. It was then placed in a Dewar flask

containing water at ~54 ^{o}C. Rapid cooling was prevented by using an insulating material to cover the flask. It took two days for the water in the Dewar flask to cool to ambient temperature. The solution was then allowed to evaporate slowly and crystallise under ambient conditions. Crystallisation occurred within two weeks of standing. It should be noted that using this procedure repeatedly resulted in random outcomes as far as the precipitation of **Form 2** is concerned.

Similarly to isonicotinamide, visual comparison of the batch of precipitated material indicated the possible presence of crystals of different morphologies and thus of possibly different polymorphs (i.e. concomitant polymorphism). After that, the very thorough, but reliable procedure of determining crystal unit cells for each specimen in the batch using single crystal X-ray diffraction was employed in order to guarantee definite separation of each polymorphic species. This revealed two distinct polymorphs of nicotinamide, namely **Form 1**, described previously,[27, 28] and a second modification, not hitherto reported, and assigned as **Form 2**. No crystallisation procedure yielding **Form 2** exclusively could be devised. Only by following the procedure above was it possible to obtain **Form 2** in a sufficiently large sample to carry out all of the structural and thermal analyses described below.

Thermal Analysis

Differential Scanning Calorimetry and Thermogravimetric Analysis

TGA analyses (not shown) indicated negligible weight loss for **Forms 1** and **2** of nicotinamide in the temperature range 30-180 ^{o}C, indicating that they are not solvates. DSC analysis was performed on **Form 1** and **Form 2** at 10 K/min as shown in Figure 60. Both DSC traces exhibited a single melt endotherm, labelled A1 and A2, respectively. Peak A2 displays a shoulder and a peak respectively, the shoulder possibly functioning as a lead into the melt. This is probably due to the fact that an intact crystal (1.03 mg) of **Form 2** was used for this analysis (the operation of

grinding was not performed to avoid the possibility of phase transformation). Therefore, the thickness of the specimen possibly led to non-uniform heat transport through the crystal.

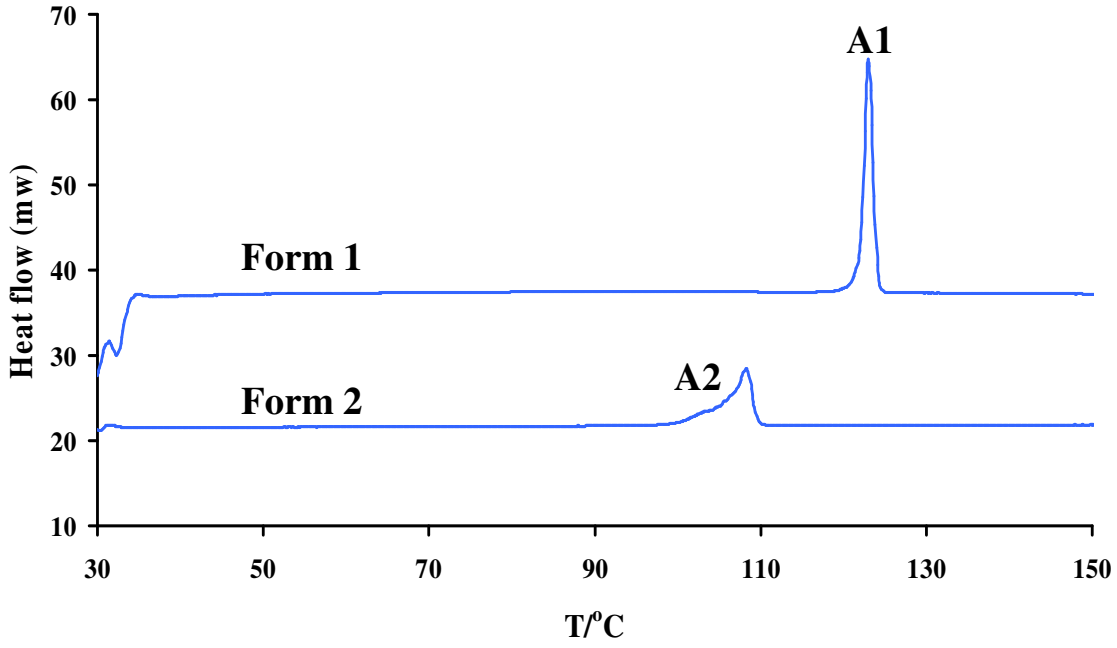

Figure 60 DSC traces of **Form 1** and **Form 2** of nicotinamide (heating at 10 K/min)

The thermal data of **Forms 1** and **2** obtained by DSC analyses are listed in Table 22. The onset temperature (T_f) for the melt of **Form 2** is very significantly lower than that of **Form 1**. Also, **Form 2** has the lower heat of fusion. Based on the Burger and Ramberger Heat of Fusion rule,[3] **Form 1** is monotropically related to **Form 2**.

Table 22 Thermo-analytical data obtained from DSC for the **Forms 1** and **2** at 10 K/min

Polymorph	T_f (°C) – onset temperature	ΔH_f (J g^{-1}) – heat of fusion
Form 1	121.9 ± 0.8 (n=2)	262.0 ± 5 (n=2)
Form 2	105.8 ± 0.4 (n=2)	165.0 ± 4 (n=2)

Variable Temperature Powder X-ray Diffraction

Figure 61 firstly shows the comparison between the measured PXRD pattern of **Form 1** at 25 °C and the calculated pattern derived from the single crystal structure of **Form 1** (CSD refcode NICOAM01[28]) using program LAZY PULVERIX.[11] Crystals of

Form 1 were then characterised by PXRD as a function of temperature. The PXRD pattern was recorded at temperature intervals of 10 K between 25 and 160 °C.

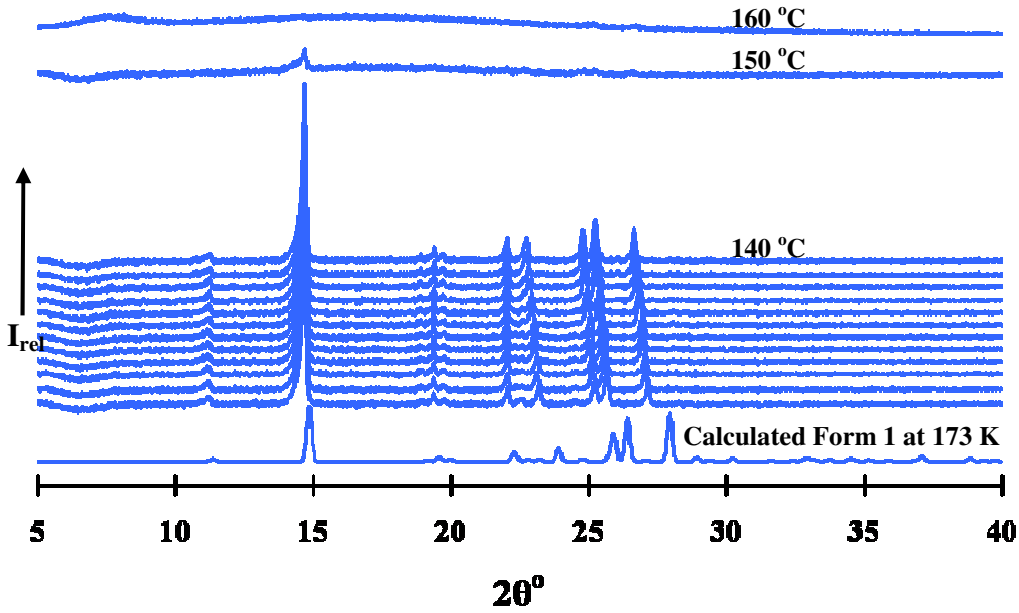

Figure 61 Variable temperature PXRD patterns of **Form 1** [From bottom to top: calculated (173 K), experimental at 25, 40, 50, 60, 70, 80, 90, 100, 110, 120, 130, 140, 150 and 160 °C]

The peak positions in the calculated trace (173 K) are displaced to higher 2θ-angles relative to those of the experimental trace (25 °C), as expected. However, the match between the two traces is convincing, proving that the bulk sample is homogeneous and has the same crystal structure as **Form 1**(CSD refcode NICOAM01[28]).

No evidence of phase change was observed when **Form 1** was heated to the melting temperature. This is consistent with the fact that only a single endothermic peak A1 was observed in the DSC trace of **Form 1** (Figure 60).

Figure 62 firstly shows the comparison between the measured PXRD pattern of **Form 2** at 25 °C and the calculated pattern derived from the single crystal structure of **Form 2** (described later in this study) using program LAZY PULVERIX.[11] Crystals of **Form 2** were then characterised by PXRD as a function of temperature. The PXRD pattern was recorded at temperature intervals of 10 K between 25 and 140 °C.

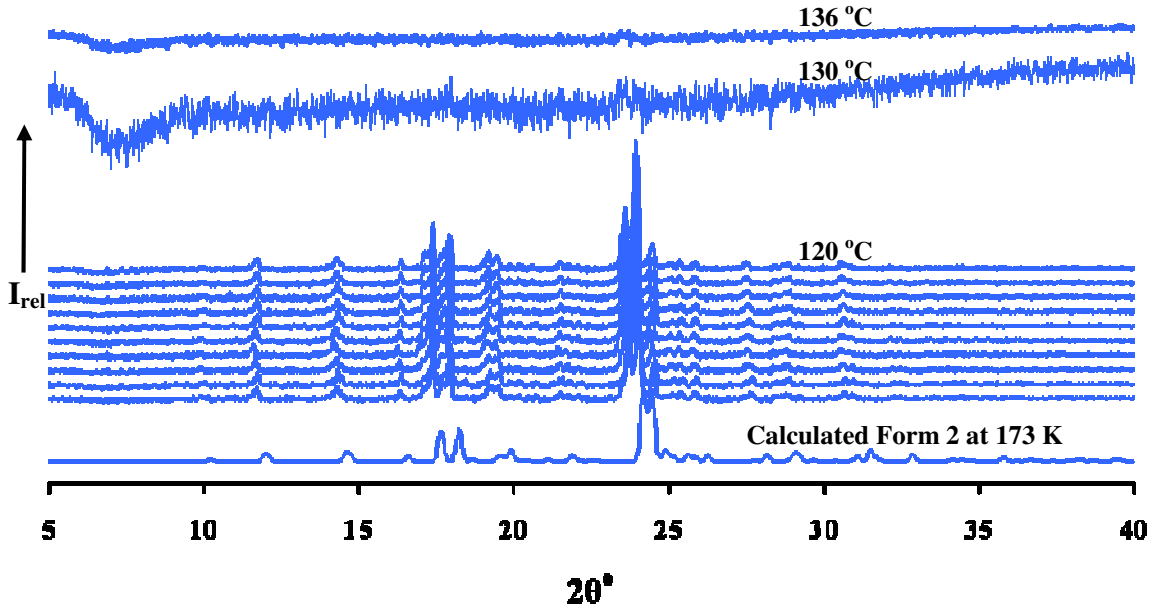

Figure 62 Variable temperature PXRD patterns of **Form 2** [From bottom to top: calculated (173 K), experimental at 30, 40, 50, 60, 70, 80, 90, 100, 110, 120, 130 and 136 °C]

The match between the calculated PXRD pattern (173 K) and the experimental pattern (25 °C) confirms the polymorphic purity of the experimental sample of **Form 2**.

No phase change of **Form 2** was evidenced during this heating since the PXRD patterns remained the same. At ~120 °C, the crystals of **Form 2** started to lose their crystallinity. However, the main peaks still remained, providing strong evidence that **Form 2** melted as the original phase. Consequently, **Form 2** experienced no phase transition until melting. Again, this corresponds to the observation from DSC analysis.

A relatively large temperature difference in melting shown by DSC compared with PXRD can be attributed to the closed and open samples used in the respective methods.

Hot Stage Microscopy

The single crystals of **Form 1** and **Form 2** were examined by HSM. The crystals were placed side by side between cover slips and immersed in silicone oil. Photographs were recorded in the temperature range 30-140 ^{o}C at a heating rate of 10 K/min, Figure 63.

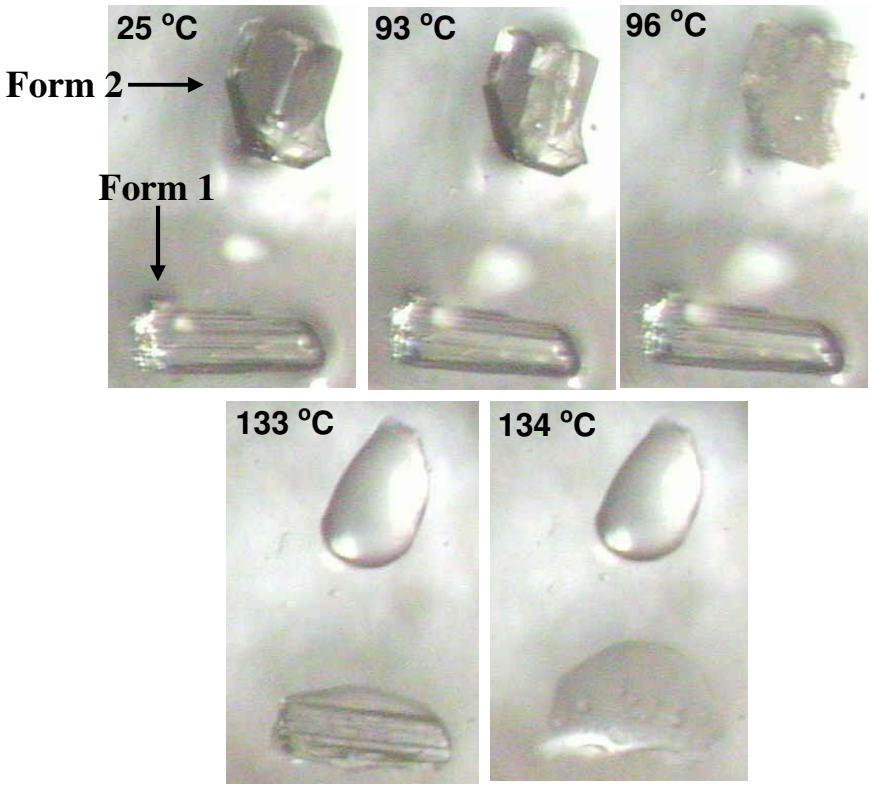

Figure 63 HSM photographs taken at various temperatures of crystals of **Forms 1** and **2** heating at 10 K/min

The crystals were clear and transparent at 25 ^{o}C. The crystal of **Form 2** started to become opaque at ~93 ^{o}C and its shape started to round at ~96 ^{o}C. This shape change indicates that it is melting slowly during heating rather than undergoing a phase change. Meanwhile, the crystal of **Form 1** remained clear and maintained a rigid shape upon heating. Finally, the crystal of **Form 2** completely melted at ~133 ^{o}C when the crystal of **Form 1** only started to melt; the latter then completely melted at ~134 ^{o}C. This HSM experiment was repeated successfully, confirming the existence of this small temperature difference (~1 ^{o}C). This strongly indicates that the crystals of **Form 1** and **Form 2** melt at different temperatures.

The fact that the crystal of **Form 2** melts over a very wide temperature range (90–133 ^{o}C) is possibly due to its thickness. Also, this is consistent with the fact that the melting peak of **Form 2** in the DSC trace is composed of two parts.

Construction of the Energy – Temperature Diagram

Based on the thermal data of **Form 1** and **Form 2**, an E/T diagram was constructed in Figure 64. As concluded earlier, **Form 1** is monotropically related to **Form 2**. Hence, the G-isobars of **Form 1** and **Form 2** do not intersect before the melting points. The G isobar of the liquid intersects that of **Form 1** at a specific point T_{f1} [121.9 ± 0.8 ^{o}C(n=2)] which represents the melting of **Form 1** (Table 22). Similarly, the G-T curve of the liquid intersects that of **Form 2** at the point T_{f2} [105.8 ± 0.4 ^{o}C (n=2)] which indicates the melt of **Form 2**. The fact that T_{f2} is lower than T_{f1} allows the G-T curve of **Form 2** to be located above that of **Form 1**.

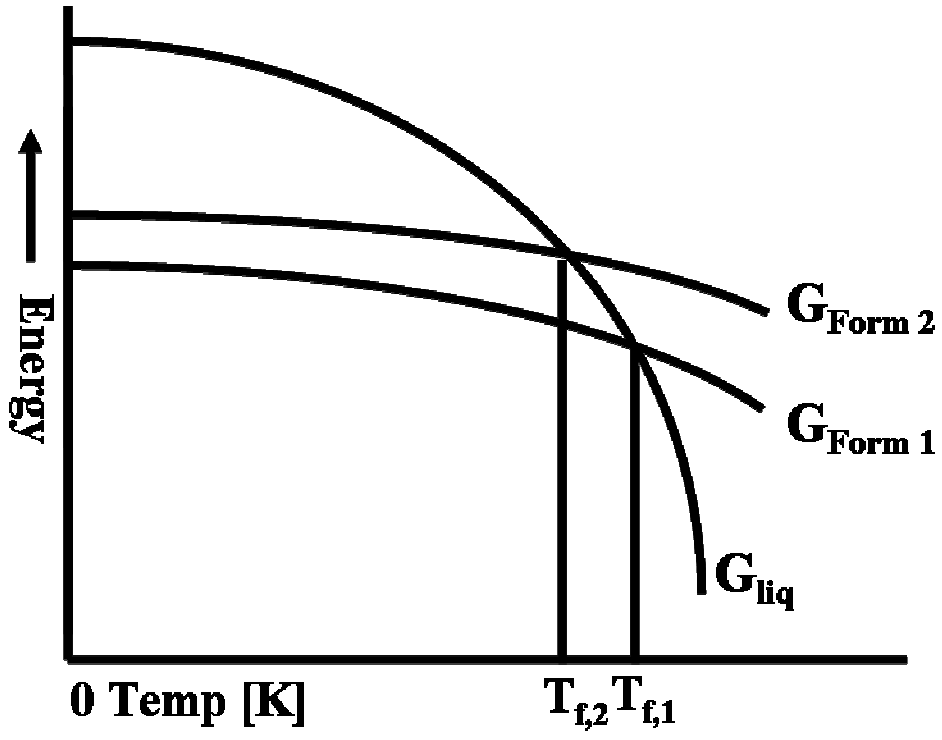

Figure 64 A schematic E/T diagram for the two polymorphs of nicotinamide

From the E/T diagram, it can be predicted that **Form 1** is the thermodynamically stable form between absolute zero and its melting point while **Form 2** is the

thermodynamically metastable form between absolute zero and its melting point. Also, in this temperature range, the densities of the two polymorphs would be in the order: **Form 1 > Form 2** while the solubilities of two forms would be in the order: **Form 1 < Form 2**. The point is addressed again later.

X-Ray Crystallographic Analysis of Nicotinamide, Form 2

Single Crystal X-Ray Diffraction

Data-collection and Space Group Determination

Structural information for **Form 1** was obtained from Miwa et al.[28] The crystal data for **Form 1** (CSD refcode NICOAM01[28]) were obtained from the CSD.[25]

A Nonius Kappa CCD four-circle diffractometer was employed to collect the data for **Form 2** at 173 K. The X-ray diffraction pattern of **Form 2** displayed 2/*m* Laue symmetry, which indicated that the compound crystallises in the monoclinic crystal system. The conditions limiting reflections were: *hkl*: *none*; *h0l*: $h+l = 2n$; *0k0*: *none*. This indicates either the space group P2/n or Pn. The centrosymmetric space group P2/n was indicated by the value of the intensity statistic $|E^2-1| = 1.017$, and the structure was successfully solved and refined in this space group. A preliminary calculation based on the estimated density indicated the unusually high value of $Z = 16$ molecules per unit cell.

Unit-cell dimension measurement for **Form 2** was carried out at both ambient temperature and low temperature (173 K). No significant change was observed, indicating that there is no phase transition of **Form 2** during cooling.

Structure Solution and Refinement

The structure solution of **Form 2** was performed using SHELXS-97.[6] Direct methods yielded the positions of all the non-hydrogen atoms in the asymmetric unit, which contains four crystallographically independent molecules. SHELXH-97[7] was used to place the atoms which were initially refined isotropically and subsequently anisotropically. Attempts to locate the hydrogen atoms from difference Fourier maps followed and were successful. Based on the positions of the peaks, a riding model was subsequently employed to place the hydrogen atoms. They were assigned isotropic temperature factors 1.2 times those of their parent atoms. Table 23 lists relevant crystal data for **Form 1** (CSD refcode NICOAM01[28]) taken from the CSD,[25] as well as the crystal and refinement parameters for **Form 2**.

Table 23 Crystal and refinement parameters for **Form 1** and **Form 2**

Parameter	**Form 1***	**Form 2**
Formula unit	$C_6H_6N_2O$	$C_6H_6N_2O$
Formula Weight / g mol^{-1}	122.13	122.13
Crystal system	monoclinic	monoclinic
Space group	$P2_1/c$	P2/n
a / Å	3.877(4)	15.0634(5)
b / Å	15.60(1)	10.6976(4)
c / Å	9.375(6)	15.2067(5)
α / °	90.00	90.00
β / °	98.45(7)	102.188(2)
γ / °	90.00	90.00
Volume / Å^3	560.9(8)	2395.21(14)
Z	4	16
Density$_{calc}$ /g cm^{-3}	1.4463	1.3545
μ (MoK$_α$) /mm^{-1}	0.103	0.096
F (000)	256	1024
Crystal size /mm^3	0.7x0.7x0.6	0.28x0.4x0.52
Temperature / K	150	173(2)
Range scanned θ / °	----------	1.02≤ θ ≤ 25.03
Index ranges	----------	h: -18,18
	----------	k: -13,13
	----------	l: -19,19
φ scan angle / °	----------	1.0
ω scan angle / °	----------	1.5
Dx / mm	----------	40
No. of measured reflections	----------	88974
No. of unique reflections	----------	4881
No. of reflections with I > 2σ(I)	----------	3492
No. of L.S. parameters	----------	325
R$_{int}$, R$_σ$	----------	0.1173, 0.0536
S	----------	1.101
R$_1$ (F$_o$ > 4σ(F$_o$))	----------	0.0499
No. of reflections omitted	----------	13
wR2 (all reflections)	----------	0.1241
Weighting scheme	----------	a = 0.0489
	----------	b = 0.7737
(Δ / σ)$_{mean}$	----------	<0.001
Δρ excursions / eÅ^{-3}	----------	-0.27, 0.19

* Data taken from the CSD, refcode NICOAM01.[28]

We note that the calculated density order of the polymorphs, namely **Form 1** > **Form 2**, agrees with the density order deduced from the E/T diagram in the temperature range of absolute zero to the melting point of **Form 2**.

In the following section, detailed structural comparisons of **Forms 1** and **2** of nicotinamide are presented at both the molecular and crystal structural levels.

Molecular Structure

The numbering scheme of the nicotinamide molecule is shown in Figure 65 (left). There are four crystallographically independent molecules (A, B, C and D) in the asymmetric unit of **Form 2,** as shown in Figure 65 (right).

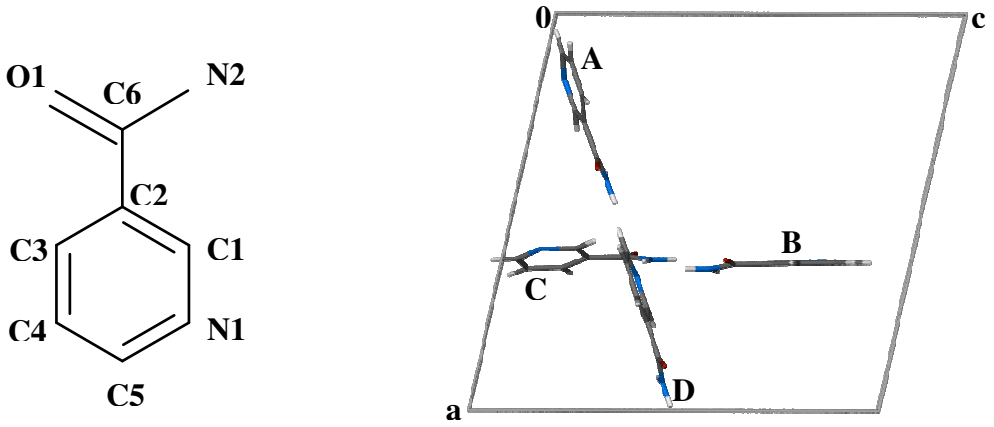

Figure 65 The numbering scheme of the nicotinamide molecule (left) and four crystallographically independent nicotinamide molecules (A, B, C and D) in the asymmetric unit of **Form 2** (right).

The conformations of the molecules in **Forms 1** and **2** are compared in Figure 66.

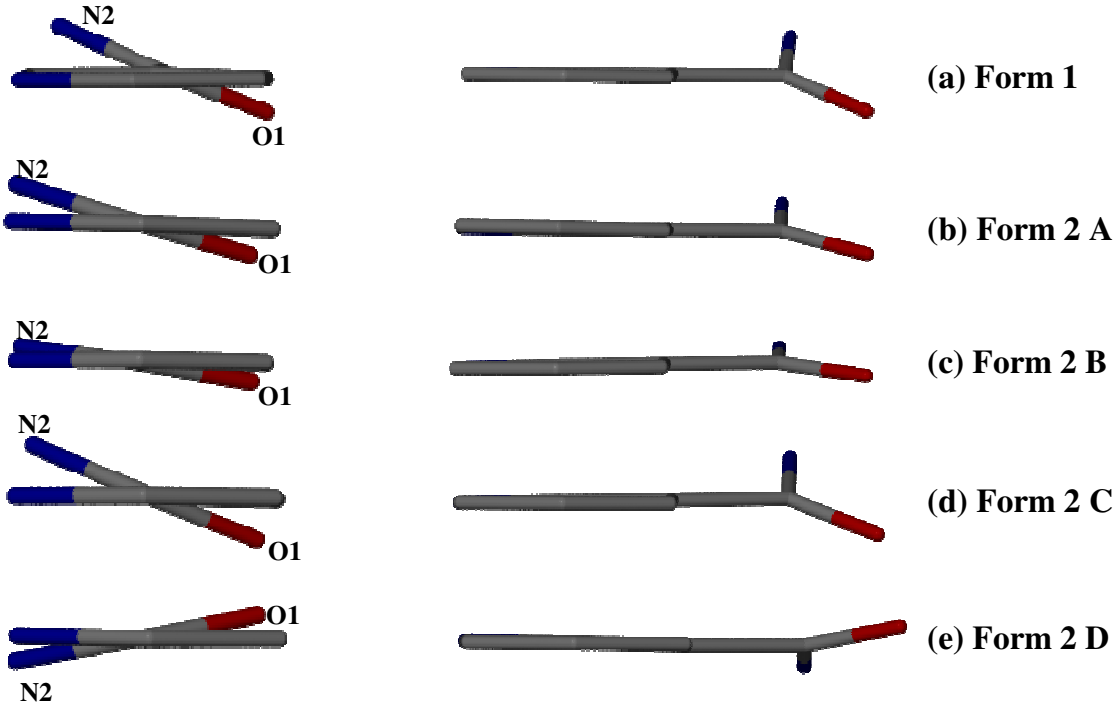

Figure 66 The conformational comparison among the molecules in **Form 1** and **Form 2**. From top to bottom: (a) the molecule in **Form 1**; (b) Molecule A in **Form 2**; (c) Molecule B in **Form 2**; (d) Molecule C in **Form 2**; (e) Molecule D in **Form 2**.

Variable conformations can be observed among these molecules. Essentially, the main conformational degree of freedom is rotation around the C2-C6 bond (expressed e.g. in the dihedral angle O1-C6-C2-C3). In Table 24, the value of this torsion angle is quoted as representative. We note that molecule Form 2D has opposite handedness from the other three in the asymmetric unit. In order to make a valid comparison of the various conformations, the torsion angle O1-C6-C2-C3 for the inverted image of Form 2D (D′) was calculated and included in Table 24.

Table 24 The torsion angle τ for nicotinamide molecules in **Form 1 and Form 2**

Torsion angle (°)	**Form 1**	**Form 2**			
		A	B	C	D′
O1-C6-C2-C3 (τ)	20.8(1)	14.2(3)	7.3(3)	21.3(3)	10.6(3)

D′ is the inverse of molecule D shown in Figure 66.

From Table 24, τ spans a significant range [7.3(3)-21.3(3)°] and the significant differences among the four values of τ confirm that these four molecules are symmetry-independent.

Hydrogen Bonding Interactions

The hydrogen bond motif of **Form 1** is shown in Figure 67 and the details of these interactions are listed in Table 25. The atom N2 simultaneously serves as a hydrogen bond donor to atoms O1 and N1 through different hydrogen bonds. In other words, all the N and O atoms are involved in the hydrogen bond interactions in **Form 1**. The graph set analysis descriptors[8, 9] for two rings formed by the three different hydrogen bonds are shown in Figure 67.

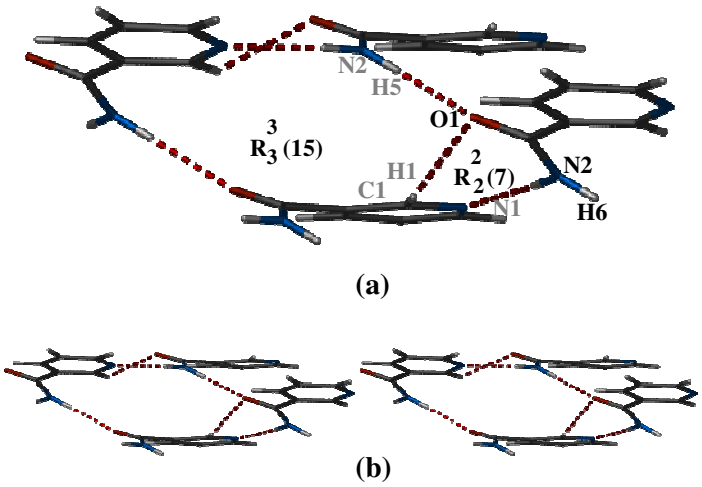

Figure 67 (a) The hydrogen bond motif for **Form 1** (b) The stereoview illustrating the hydrogen bond motif for **Form 1.**

Table 25 The hydrogen bond interactions in **Form 1**

Hydrogen bond	N···O, N···N or C···O Distance (Å)	Angle (°)	Symmetry operator[a]
N2-H5···O1	2.964(3)	178.4(9)	x, 1/2-y, -1/2+z
N2-H6···N1	3.076(3)	169.7(9)	1+x, 1/2-y, 1/2+z
C1-H1···O1	3.304(4)	138.9(9)	-1+x, 1/2-y, -1/2+z

[a] Symmetry operator applies to hydrogen bond acceptor atoms.

Molecules of nicotinamide in **Form 1** form infinite ribbons by hydrogen bonding, the unit cell containing two such parallel ribbons that are not hydrogen bonded to one another, Figure 68.

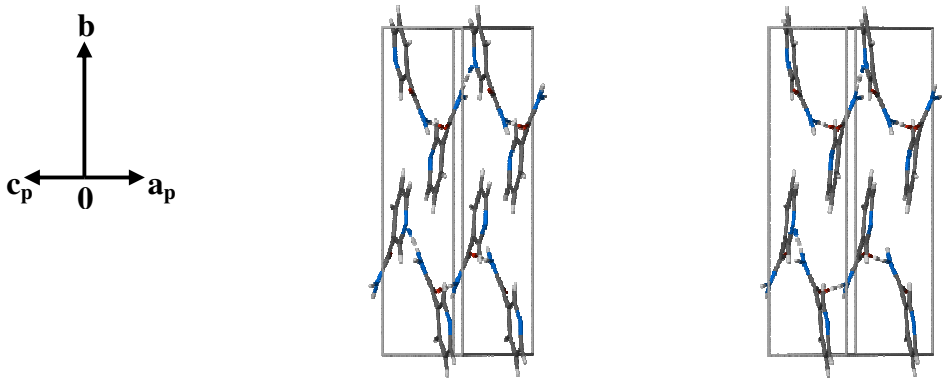

Figure 68 Stereoview of the hydrogen bond motif of **Form 1** viewed along [101]

Figure 69 shows the hydrogen bond interactions in **Form 2**. In **Form 2**, a noteworthy observation is that the atom O1A in the molecule A is not involved in any hydrogen bonds while all the O and N atoms in molecules B, C and D are involved in hydrogen bonding. Also, the molecule D is related to a symmetry-generated molecule D' by a crystallographic inversion center.

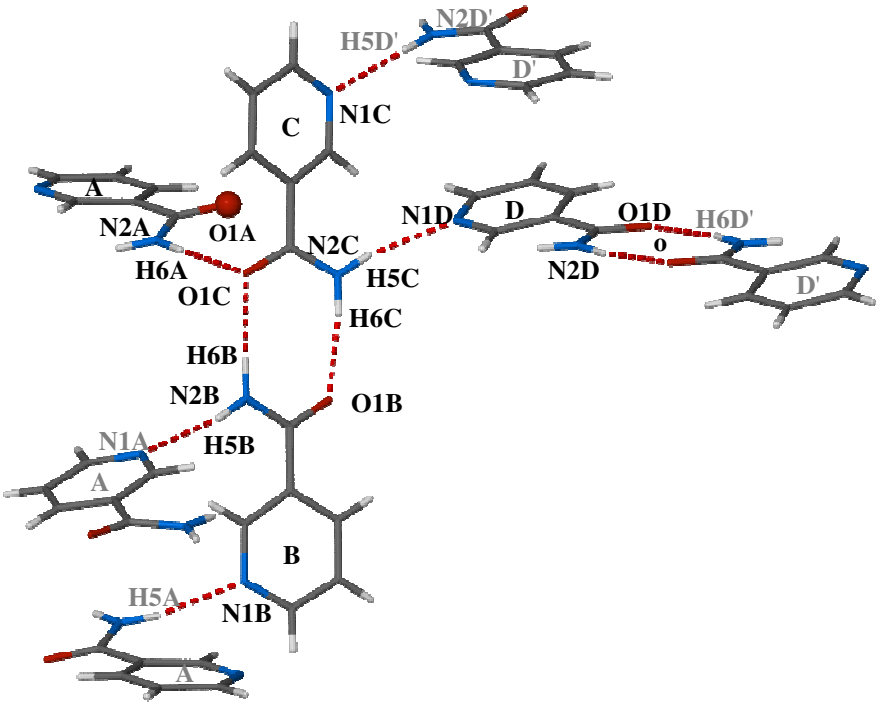

Figure 69 The hydrogen bond interactions in **Form 2**. Atom O1A is shown as a sphere for clarity. Atoms with gray labels have been symmetry-generated from their asymmetric unit counterparts.

Since there are four crystallographically independent molecules in the asymmetric unit of **Form 2**, the detailed hydrogen bond motifs of each independent molecule are investigated separately in Figure 70.

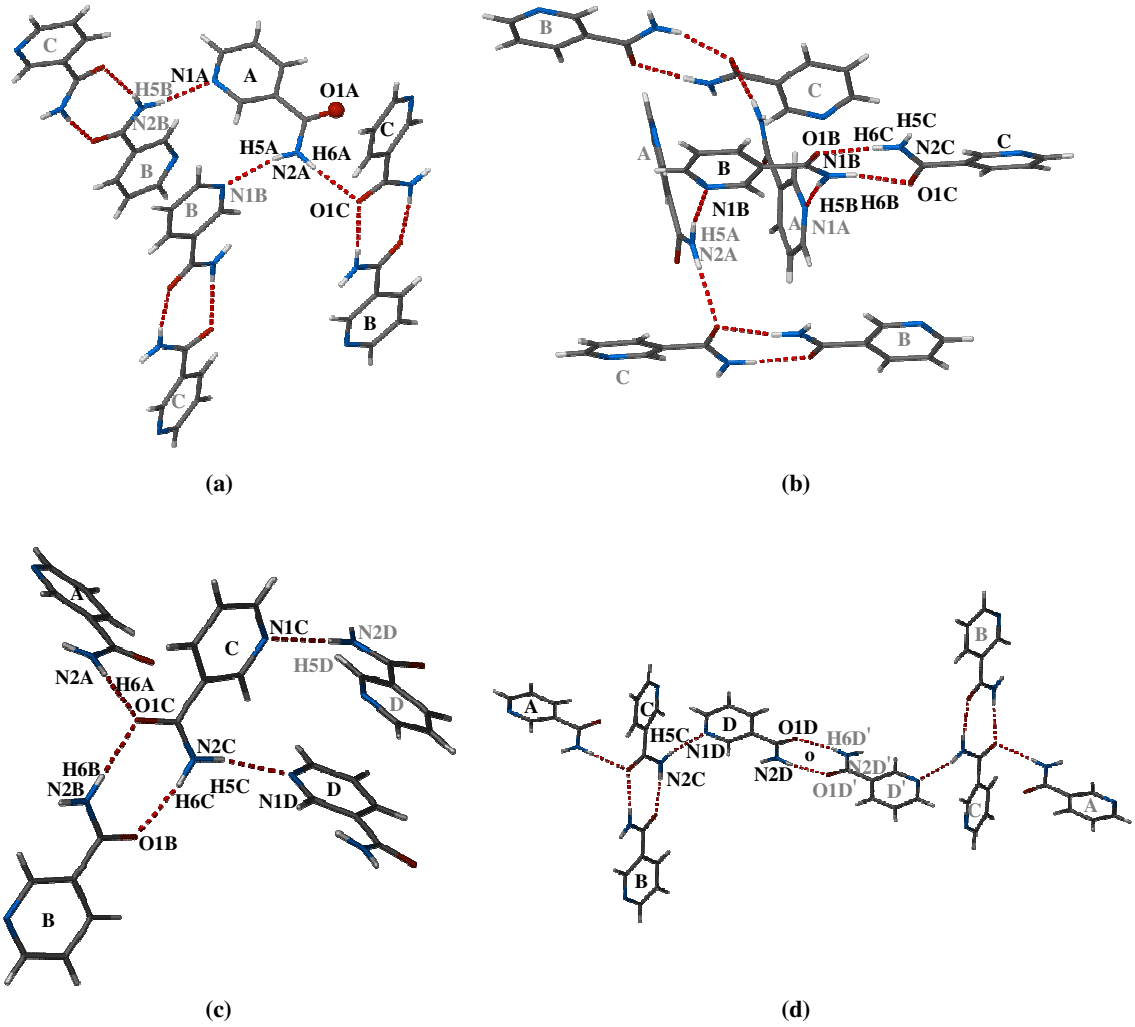

Figure 70 (a) The hydrogen bond motif of the molecule A in **Form 2**; atom O1A is shown as a sphere for clarity; (b) The hydrogen bond motif of the molecule B; (c) The hydrogen bond motif of the molecule C; (d) The hydrogen bond motif of the molecule D. Atoms with gray labels have been symmetry-generated from their asymmetric unit counterparts.

The geometrical details of the hydrogen bonds in **Form 2** are listed in Table 26. The hydrogen bonds N2-H···O1 and N2-H···N1 can be found in both **Form 1** and **Form 2**. The mean distance for the N-H···N interactions in **Form 2** is 3.10 Å while the mean angle is 168°. The average distance for the N-H···O interactions is 2.98 Å while the average angle is 169.5°.

Table 26 The hydrogen bond interactions for **Form 2**[a]

Hydrogen bond	N···N or N···O Distance (Å)	Angle (°)	Symmetry operator[b]
N2A-H5A···N1B	3.089(2)	167.0	1-x, 2-y, 1-z
N2B-H5B···N1A	3.118(2)	170.0	1/2+x, 2-y, 1/2+z
N2C-H5C···N1D	3.067(2)	166.0	x, y, z
N2D-H5D···N1C	3.111(2)	169.0	3/2-x, y, 1/2-z
N2A-H6A···O1C	3.053(2)	173.0	x, y, z
N2B-H6B···O1C	2.975(2)	163.0	x, y, z
N2C-H6C···O1B	2.917(2)	171.0	x, y, z
N2D-H6D···O1D	2.957(2)	171.0	2-x, -y, 1-z

[a] Where no e.s.d. is reported for the angle, H atoms involved were added in idealised positions in a riding model.

[b] Symmetry operator applies to hydrogen bond acceptor atoms.

Several C-H···N and C-H···O hydrogen bond interactions are observed in **Form 2**, as listed in Table 27. The mean C···N distance in C-H···N interactions is 3.15 Å with a mean angle of 134°. The average C···O distance in C-H···O interactions is 3.27 Å with a mean angle of 137°.

Table 27 The C-H···N and C-H···O interactions for **Form 2**[a]

Hydrogen bond	C···N or C···O Distance (Å)	Angle (°)	Symmetry operator[b]
C1A-H1A···N1B	3.336(2)	149.0	1-x, 2-y, 1-z
C1B-H1B···N2B	2.907(2)	100.0	x, y, z
C1B-H1B···N1A	3.294(2)	167.0	1/2+x, 2-y, 1/2+z
C1D-H1D···N2D	2.908(2)	100.0	x, y, z
C1D-H1D···N1C	3.311(2)	154.0	3/2-x, y, 1/2-z
C3B-H2B···O1A	3.174(2)	123.0	1-x, 1-y, 1-z
C4B-H3B···O1A	3.184(2)	122.0	1-x, 1-y, 1-z
C5B-H4B···O1D	3.466(2)	166.0	3/2-x, 1+y, 3/2-z

[a] Where no e.s.d. is reported for the angle, H atoms involved were added in idealised positions in a riding model.

[b] Symmetry operator applies to hydrogen bond acceptor atoms.

Crystal Packing

Form 1 contains infinite hydrogen bonded parallel ribbons which are not hydrogen bonded to one another (Figure 71).

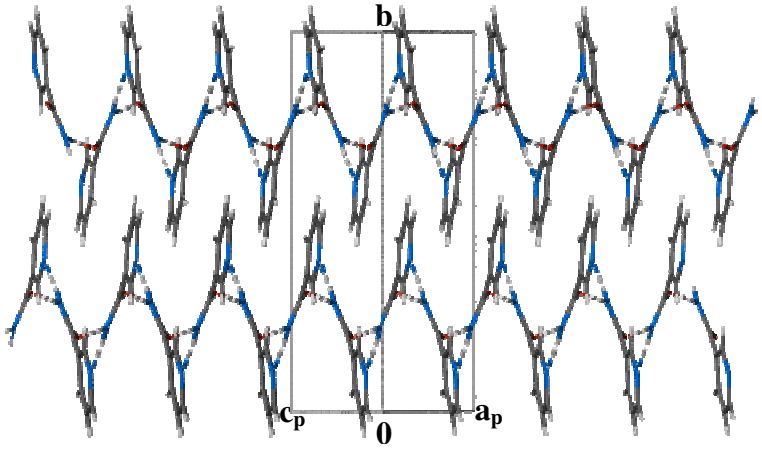

Figure 71 Crystal packing diagram for **Form 1** viewed along [101]

The packing arrangement for **Form 2** is shown in Figure 72.

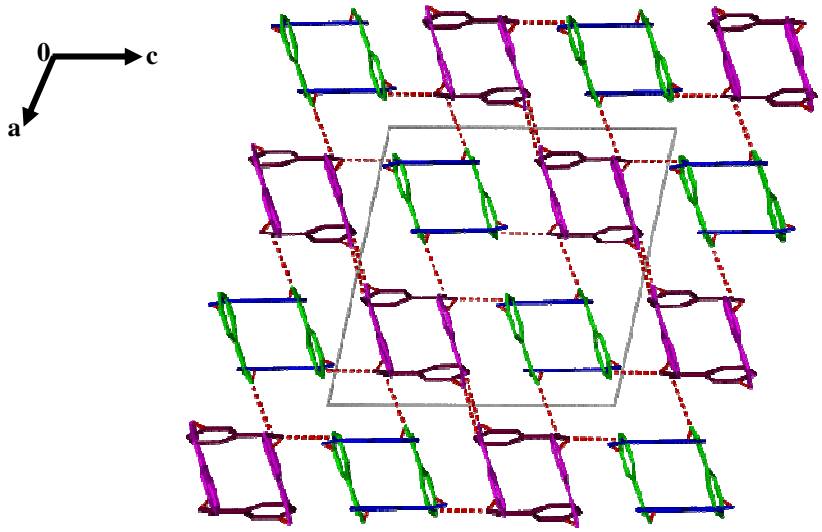

Figure 72 Crystal packing diagram for **Form 2** viewed along [010]. Molecules A, B, C and D are shown in green, blue, brown and pink, respectively. Hydrogen atoms are omitted for clarity.

The molecules A (green) and B (blue) and their respective diad-related molecules form a parallelogram in projection (parallelogram AB) and they are associated by hydrogen bonds. Similarly, the molecules C (brown) and D (pink) and their respective diad-related molecules assemble as a parallelogram pattern (parallelogram CD) and they are associated by hydrogen bonds. The parallelogram AB is connected to the parallelogram CD through the hydrogen bonds N2A-H6A···O1C and N2C-H6C···O1B and the former is not associated with another symmetry-generated

parallelogram AB. However, the parallelogram CD is associated with another symmetry-generated parallelogram CD through the hydrogen bond N2D-H6D···O1D.

Stacked networks of the type shown above along the *y*-direction are shown in Figure 73. Successive networks have alternating colours (red, green). Within each network (red or green in Figure 73), molecules are hydrogen bonded to one another, but there are no hydrogen bonds linking a red and green network.

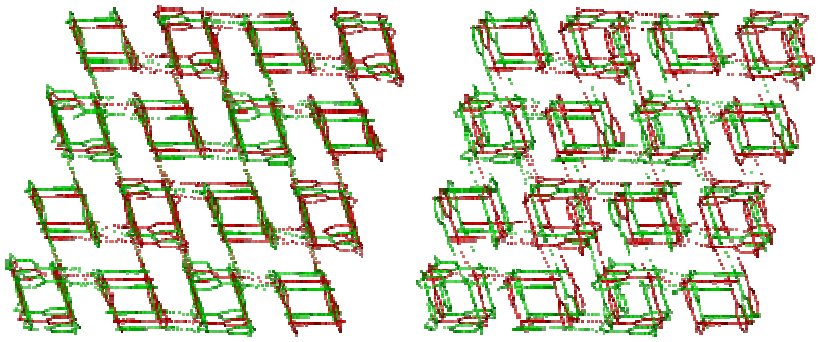

Figure 73 A stereoview of the crystal packing for **Form 2** viewed along [010]. Alternating networks are shown in red and green. Hydrogen atoms and the unit cell are omitted for clarity.

Conclusion

The structure of nicotinamide was determined in 1953.[27] After that, no re-examination was carried out until 1999, when Miwa et al.[28] improved the accuracy of the first structure, namely **Form 1** (CSD, refcode NICOAM01). The indication of the existence of other polymorphic forms was reported by Hino et al.[29] in 2001. However, no structural information for other forms of nicotinamide was reported. In this study, a new form, namely **Form 2**, was isolated successfully. It is noteworthy that production of **Form 2** crystals required the participation of the compound isoxyl when the preparative procedure used in this study was employed. The thermodynamic relationship between the two polymorphs was determined by thermal methods coupled with variable temperature PXRD data.

Neither **Form 1** nor **Form 2** experienced a phase change during the heating process until melting. This was confirmed from DSC, HSM and variable temperature PXRD data. Therefore, the two forms are monotropically related. Furthermore, the melting points of **Form 1** and **Form 2** were determined as 121.9 ± 0.8 ^{o}C (n=2) and 105.8 ± 0.4 ^{o}C (n=2), respectively. Based on these data, a schematic Energy-Temperature diagram of the two polymorphic forms of nicotinamide was constructed. From the E/T diagram, it can be predicted that the densities of the two polymorphs should be in the order: **Form 1** > **Form 2** while the solubilities of two forms would be in the order: **Form 1** < **Form 2**. Notably, the density order deduced from the E/T diagram is in accord with the calculated densities of the two polymorphs based on their respective crystal data.

Form 1 crystallises in the monoclinic space group $P2_1/c$ with a = 3.877(4), b = 15.60(1), c = 9.375(6) Å, β = 98.45(7)º and 4 molecules per unit cell. **Form 2** crystallises in the space group P2/n with a = 15.063(4), b = 10.697(6), c = 15.206(7) Å, β = 102.18(8)º and 16 molecules per unit cell. The latter requires the existence of four symmetry-independent molecules in the asymmetric unit, namely molecules A,

B, C and D. These four molecules adopt significantly different conformations. Molecule C does, however, closely resemble the molecule present in **Form 1** (respective torsion angles O1-C6-C2-C3: 21.3(3)^{o}, 20.8 (1)^{o}].

All the N and O atoms in the molecule in **Form 1** and those in the molecules B, C and D in **Form 2** are involved in hydrogen bond motifs. However, the atom O1A in the molecule A is isolated from the hydrogen bonding environment. The hydrogen bond motifs of **Form 1** and **Form 2** are very different. Hydrogen-bonded ribbons and hydrogen-bonded nets are found in **Form 1** and **Form 2**, respectively. Ribbons in **Form 1** extend infinitely and are isolated from one another. This also applies to nets in **Form 2**.

As is evident from the variable temperature PXRD Figures 61 and 62, the experimental PXRD traces of the two polymorphs were found to be consistent with their respective computed patterns, allowing the latter to serve as reliable references for polymorphic identification.

References:

1. Gramaglia, D., Conway, B. R., Kett, V. L., Malcolm, R. K. and Batchelor, H. K., *Int. J. Pharm*., **2005**, 301, 1-5.
2. Kamasa, P., Varga, L. K., Myslinski, P., Rassolov, S. G., Maksimov, V. and Idzikowski, B., *Mater. Sci.*, **2008**, 26, 947-952.
3. Burger, A. and Ramberger, R., *Mikrochim. Acta*, **1979**, II, 259-271.
4. Grunenberg, A., Henck, J. O. and Siesler, H. W., *Int. J. Pharm,*, **1996**, 129, 147-158.
5. XPREP, *Data Preparation and Reciprocal Space Exploration*, Version 5.1, © Bruker Analytical X-ray Systems, **1997**.
6. Schneider, T. R. and Sheldrick, G. M., *Acta Crystallogr.,* **2002**, D58, 1772-1779.
7. Sheldrick, G. M. SHELXH, *Acta Crystallogr.*, **2008**, A64, 112-122.
8. Etter, M. C., Macdonald, J. C. and Bernstein, J., *Acta Crystallogr., Sect. B: Struct. Sci*., **1990**, B46, 256-262.
9. Bernstein, J., Davis R. E., Shimoni, L. and Chang, N-L., *Angew. Chem. Int. Ed.*, **1995**, 34, 1555-1573.
10. Reddy, L. S.; Basavoju, S.; Vangala, V. R.; Nangia, A., *Cryst. Growth Des.*, **2006**, 6, 161-173.
11. Yvon, K., Jeitschko, W. and Parthé, E., *J. Appl. Crystallogr.*, **1977**, 10, 73-74.
12. Hearn, M. J., Chen, M. F., Cynamon, M. H., Wang'ondu, R. and Webster, E. R., *J. Sulfur Chem*., **2006**, 27, 149-164.
13. Gosavi, R. K., Agarwala, U., and Rao, C. N. R., *J. Am. Chem. Soc.,* **1967**, 89, 235-239.
14. Csonka-Horvai, J., David, A., Horvath, G. and Naray-Szabo, G., *Z. Naturforsch., B: Chem. Sci*., **1971**, 26 (1), 21-23.
15. Buu-Höi, N. P. and Xuong, N. D., *C. R. Hebd. Seances Acad. Sci*., **1953,** 273 (9), 498-500**.**
16. Barbour, L. J., SECTION, A computer program for the graphic display of cross sections through a unit cell, *J. Appl. Crystallogr.*, **1999**, 32, 353.
17. Udachin, K. A. and Ripmeester, J. A., *J. Am. Chem. Soc.,* **1998**, 120, 1080-1081.
18. Steiner, T. and Saenger, W., *Acta Crystallogr., Sect. B: Struct. Sci*, **1998**, 54, 450-455.
19. Caira, M. R, *Rev. Roum. Chim.,* **2001**, 46, 371-386.
20. Ding, J., Steiner, T. and Saenger, W., *Acta Crystallogr*., **1991**, B47, 731-738.

21. Nestler, H. J., Seydel, J. K., *Arzneim.-Forsch*., **1966**, 16, 1494-1500.

22. Frömming, K. H. and Szejtli, J., *Cyclodextrins in Pharmacy*, Kluwer: Dordrecht, **1994**, 22-23.

23. Aakeröy, C. B., Beatty, A. M., Helfrich, B. A. and Nieuwenhuyzen M., *Cryst. Growth Des.*, **2003**, 3, 159-165.

24. Vishweshwar, P., Nangia, A. and Lynch, V. M., *Cryst. Growth Des.*, **2003**, 3, 783-790.

25. Cambridge Structural Database and Cambridge Structural Database system, Version 5.31, November **2009** (updates Feb 2010), Cambridge Crystallographic Data Centre, University Chemical Laboratory, Cambridge, England.

26. Barbour, L. J., LAYER, a computer program for the graphic display of intensity data as simulated precession photographs., *J. Appl. Cryst.,* **1999**, 32, 351-352.

27. Wright, W. B. and King, G. S. D., *Acta Crystallogr*., **1954**, 7, 283-288.

28. Miwa Y., Mizuno T., Tsuchida K., Taga T. and Iwata Y., *Acta Crystallogr*., **1999**, B55, 78-84.

29. Hino, T., Ford, J. L. and Powell, M. W., *Thermochim. Acta*, **2001**, 374, 85-92.

Chapter 4

Rifampicin Solvates

This chapter is divided into three parts:

Part One: Isostructural Rifampicin solvates containing methanol/ethanol/water molecules.
Part Two: Isostructural Rifampicin solvates containing 1-propanol/iso-propanol/water molecules.
Part Three: Four distinct Rifampicin solvates containing iso-propanol/1-butanol/ethylene glycol/1,4-dioxane and water molecules.

We report the isolation of these solvates and we investigate the solid-state features of these solvates using single crystal and powder X-ray diffraction.

Part One

Isostructural Rifampicin Solvates Containing Methanol/Ethanol and Water Molecules

Crystal Preparation

The abbreviations for the discrete rifampicin solvates in this chapter are as follows:

Rifampicin • 1.57methanol • 3H_2O: P1

Rifampicin • 0.39methanol • 4.17H_2O: P2

Rifampicin • 2ethanol • 2H_2O: P3

Rifampicin • 0.54ethanol • 3.92H_2O: P4

Suitable crystals of P1 and P3 were obtained by dissolving 0.020 g (0.024 mmol) of the host drug (rifampicin) in 2 ml of methanol-water mixture (1:1 v/v) and ethanol-water mixture (1:1 v/v) at 25 ^oC, respectively. Crystals of suitable quality appeared by slow evaporation at 4 ^oC over a period of two weeks.

Crystals of P1 and P3 were allowed to stand on an open bench at 25 ^oC. After equilibrating with the atmosphere for a period of 10 h, crystals of P1 and P3 were found to have transformed to phases P2 and P4, respectively, with different solvent compositions from those of the original phases.

The host and guest numbering schemes are given in Figure 1.

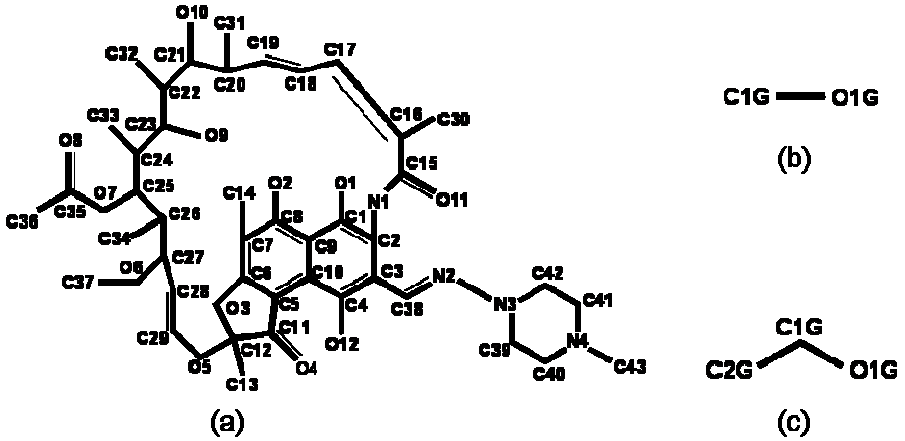

Figure 1 Host and guest numbering schemes: (a) rifampicin, (b) methanol, (c) ethanol. Hydrogen atoms have been omitted for clarity.

TGA and XRD Characterisation

Multiple TGA measurements were firstly employed to optimise the values of total mass loss for all the solvates described in this chapter. The X-ray analyses were then used to reveal the nature of included solvents, either singly, or as mixtures in the solvates. Careful analysis of the thermal parameters and the site-occupancy factors of the solvent molecules eventually gave rise to reasonable crystallographic modelling of solvent contents consistent with the experimental TGA data. Therefore, the derivation of molecular formulae for the solvates was achieved by combining the TGA data with data from X-ray structural refinements. More details of this procedure are given in Chapter 6, dealing with the thermal analysis of these solvates.

Single Crystal X-Ray Diffraction

Data-collection and Space Group Determination

A crystal of P1 from mother liquor was covered in paratone N oil without delay in order to prevent the loss of solvent molecules. The crystals of P2, P3 and P4 were handled in the same way. A Nonius Kappa CCD four-circle diffractometer was employed to collect the data for P1, P2 and P3 at 173 K. However, the data for P4 were collected on a Bruker Apex Duo diffractometer at 100 K. The unit cell parameters, crystal systems and space groups were determined from the X-ray diffraction data which revealed Laue *mmm* symmetry for all four solvates. Therefore, these solvates belong to the orthorhombic system. The space group $P2_12_12_1$ was deduced from the systematic absences: *hkl*: none; *h00*: $h = 2n+1$; *0k0*: $k = 2n+1$; *00l*: $l = 2n+1$.

Structure Solution and Refinement

For all four solvates, program SHELXD[1] was used to solve the structures by *ab initio* methods, which revealed the positions of all the non-hydrogen atoms of the rifampicin molecule (host) in each structure. Full-matrix least-squares refinements were performed with SHELXH-97.[2] Difference Fourier maps exhibited the positions of primary oxygen and carbon atoms of the water and solvent molecules (guest). Some of these atoms were

found to have full site-occupancy while the others were generally disordered over two or even three positions. The host and guest molecules having full s.o.f. were then refined isotropically. However, atom C41 in phase P3 is disordered over two positions (C41A and C41B). C41A, the major component, was assigned a value of x for its s.o.f. while the minor component C41B was allocated the value 1-x. The s.o.f.s refined to 0.54(3) and 0.46(3) respectively while their U_{iso} values refined to 0.033(3) $Å^2$ and 0.035(4) $Å^2$, respectively.

For the disordered solvent molecules, a fixed U_{iso} (the mean of U_{eq} for the chemically equivalent ordered atoms) was assigned to each molecule and these atoms were allowed to refine with s.o.f.s x and 1-x, with x variable. For some molecules, the s.o.f.s were then assigned as a fixed value, allowing the U_{iso} to refine freely. The details of the U_{iso} values and s.o.f.s of the guest molecules in each solvate are listed in Table 1.

Table 1 Isotropic thermal parameters and site-occupancy factors for the guest molecules of the four solvates

Solvate	Guest molecule	U_{iso} ($Å^2$)	s.o.f
P1	O1W	0.07	1.00
	O2W	0.05	1.00
	O3WA	0.05	0.57
	O3WB	0.06	0.43
	O1G-C1G	0.09-0.09	1.00
	O2G-C2G	0.04-0.07	0.57
P2	O1W	0.07	1.00
	O2W	0.05	1.00
	O3W	0.06	1.00
	O4W	0.07	0.70
	O5W	0.07	0.47
	O1GB-C1GB	0.09 (global U_{iso})	0.39
P3	O1W	0.08	1.00
	O2W	0.06	1.00
	O1G-C1G-C2G	0.08-0.06-0.07	1.00
	O2GA-C3GA-C4GA	0.07 (global U_{iso})	0.30
	O2GB-C3GB-C4GB	0.06 (global U_{iso})	0.36
	O2GC-C3GC-C4GC	0.07 (global U_{iso})	0.34
P4	O1WA	0.03	0.54
	O1WB	0.05	0.46
	O2W	0.03	1.00
	O3W	0.09	1.00
	O4WB	0.06	0.46
	O5WB	0.04	0.46
	O1GA-C1GA-C2GA	0.02-0.08-0.08	0.54

In general, attempts to locate all the hydrogen atoms in each solvate from difference Fourier maps were made. Special attention was given to establishing the nature of the rifampicin molecules (neutral/zwitterionic) in each solvate by careful inspection of the difference electron density maps for the relevant hydrogen atom candidates. Based on the positions of the peaks found, a riding model was employed to place hydrogen atoms for rifampicin and solvent molecules in idealised positions except for the water hydrogen atoms which were positioned based on reasonable locations of suitable electron density peaks and their possible hydrogen bond geometry. All the methyl hydrogen atoms were refined with isotropic temperature factors 1.5 times those of their parent atoms while all the other hydrogen atoms were assigned temperature factors 1.2 times those of their parent atoms.

For the methanol and ethanol molecules as well as the hydrogen atoms of water molecules, distance restraints were employed to ensure reasonable molecular geometries. The C-O bond length in the methanol molecule was set at 1.41 Å with a standard deviation σ = 0.001 Å. The C-O and C-C bond lengths in the ethanol molecule were set at 1.43 and 1.51 Å, respectively. The standard deviation σ for these was set between 0.001 and 0.008 Å. The O-H bond length of water molecules was fixed at 0.84 Å with the H-O-H angle setting as 104.5^{o}. The standard deviations σ were set between 0.001 and 0.008 Å.

Crystal and refinement parameters for each solvate are presented in Tables 2 and 3.

Table 2 Crystal and refinement data for P1 and P2

Parameter	P1	P2
Formula unit	Rifampicin · 1.57 methanol · $3H_2O$	Rifampicin · 0.39 methanol · 4.17 H_2O
Formula Weight / g mol^{-1}	927.29	910.39
Crystal system	orthorhombic	orthorhombic
Space group	$P2_12_12_1$	$P2_12_12_1$
a / Å	13.8750(3)	13.8697(3)
b / Å	17.5152(2)	17.4494(5)
c / Å	20.1133(4)	19.8807(5)
α / °	90.000	90.000
β / °	90.000	90.000
γ / °	90.000	90.000
Volume / Å^3	4888.0(2)	4811.5(2)
Z	4	4
Density$_{calc}$ / g cm^{-3}	1.260	1.260
μ (MoK$_α$) /mm^{-1}	0.096	0.096
F (000)	1993	1955
Crystal size /mm^3	0.12x0.14x0.14	0.23x0.40x0.42
Temperature / K	173(2)	173(2)
Range scanned θ / °	1.00≤ θ ≤ 25.35	1.00 ≤ θ ≤ 26.37
Index ranges	h: -16, 16	h: -17, 17
	k: -21, 21	k: -21, 21
	l: -24, 24	l: -24, 24
φ scan angle / °	1.0	1.0
ω scan angle / °	1.0	1.0
Dx / mm	32	40
No. of measured reflections	69973	9796
No. of unique reflections	8888	5457
No. of reflections with I > 2σ(I)	7132	4539
No. of L.S. parameters	625	619
R$_{int}$, R$_σ$	0.0632, 0.0407	0.0243, 0.0334
S	1.051	1.027
R$_1$ (F$_o$ > 4σ(F$_o$))	0.0464	0.0407
No. of reflections omitted	85	26
wR2 (all reflections)	0.1215	0.1030
Weighting scheme	a = 0.0575	a = 0.0557
	b = 1.8841	b = 1.1459
(Δ / σ)$_{mean}$	< 0.001	< 0.001
Δρ excursions / eÅ^{-3}	-0.232, 0.697	-0.317, 0.267

Table 3 Crystal and refinement data for P3 and P4

Parameter	P3	P4
Formula unit	Rifampicin · 2ethanol · $2H_2O$	Rifampicin · 0.54 ethanol · 3.92 H_2O
Formula Weight / g mol^{-1}	951.10	918.43
Crystal system	orthorhombic	Orthorhombic
Space group	$P2_12_12_1$	$P2_12_12_1$
a / Å	13.9546(4)	13.8297(2)
b / Å	17.9092(6)	17.3984(2)
c / Å	20.1400(4)	19.7789(2)
α / ^{o}	90.000	90.000
β / ^{o}	90.000	90.000
γ / ^{o}	90.000	90.000
Volume / Å^3	5033.3(2)	4759.1(9)
Z	4	4
Density$_{calc}$ /g cm^{-3}	1.2550	1.2817
μ (MoK$_α$) /mm^{-1}	0.094	0.098
F (000)	2048	1973
Crystal size /mm^3	0.08x0.11x0.22	0.20x0.26x0.27
Temperature / K	173(2)	100(2)
Range scanned θ / ^{o}	$1.00 \leq \theta \leq 25.35$	$2.14 \leq \theta \leq 28.35$
Index ranges	h: -14, 16	h: -18, 17
	k: -21, 21	k: -23, 19
	l: -24, 22	l: -26, 23
φ scan angle / ^{o}	1.0	0.5
ω scan angle / ^{o}	----	0.5
Dx / mm	33	50
No. of measured reflections	23585	38713
No. of unique reflections	9150	6516
No. of reflections with I > 2σ(I)	6165	6209
No. of L.S. parameters	629	629
R$_{int}$, R$_σ$	0.0658, 0.0922	0.0272, 0.0189
S	1.029	1.185
R$_1$ (F$_o$ > 4σ(F$_o$))	0.0698	0.0542
No. of reflections omitted	45	1
wR2 (all reflections)	0.1616	0.1387
Weighting scheme	a = 0.0734	a = 0.0426
	b = 2.0293	b = 5.4773
(Δ / σ)$_{mean}$	< 0.001	< 0.001
Δρ excursions / eÅ^{-3}	-0.365, 0.526	-0.408, 0.437

Structural Description

Rifampicin Molecule Conformation and Antibiotic Activity

As described in the introductory section, rifampicin belongs to the rifamycin family whose antibiotic activity (via inhibition of DNA-dependent RNA polymerase) has been under extensive investigation. However, not all the rifamycin derivatives show antibiotic properties. Much attention has been given to the relation between the structures and activities of rifamycin derivatives. In particular, conformational parameters determined from single crystal X-ray diffraction have been correlated with antibiotic activity.[3.4] In this study, the rifampicin host molecules are also investigated with regard to their solid-state conformations.

As shown in Figure 1, the rifampicin molecule can be described in terms of the ansa chain, involving atoms from C15 to C29, N1 and O5; the chromophore system comprising atoms from C1 to C12, from O1 to O4, and O12; and finally the piperazinyl substituent at C3, formed by carbon atoms from C38 to C43, and nitrogen atoms from N2 to N4.[4] Based on this structure, planes A, B, C are introduced to describe the average planes of the ansa chain backbone, the chromophore, and the piperazinyl subsitituent respectively.

The rifampicin host molecule skeletons in the four solvates are overlaid in Figure 2. A remarkable similarity is found in the conformations of these host molecules. However, the dihedral angles between planes A and B as well as those between planes B and C are slightly different in each case. Table 4 gives the relevant data for each solvate. The fact that the dihedral angles between planes A and B are similar in the four cases while the angles between planes B and C are also similar represents quantitative evidence for the overall similarity of the host conformations in the four solvates. Furthermore, since the A and B dihedral angles lie within the range 64 to 124^{o} (established as critical for antibiotic activity),[4, 5, 6, 7] we conclude that the crystals contain the rifampicin molecule in biologically relevant conformations.

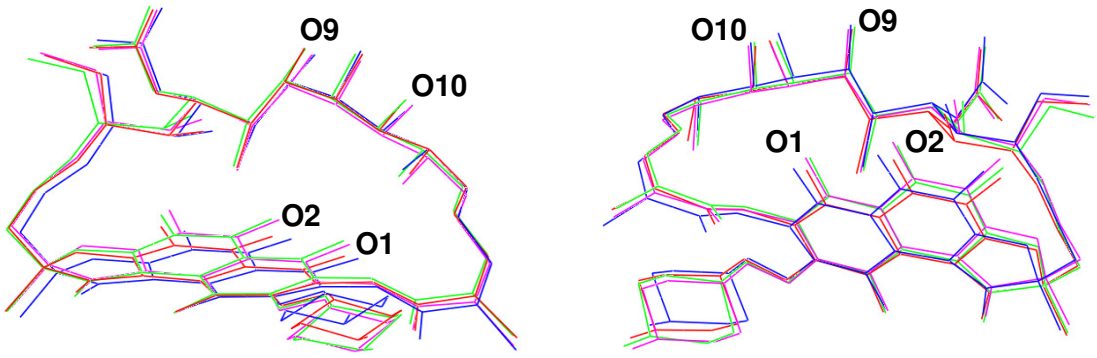

Figure 2 An overlay of the host molecules in solvates P1 (green), P2 (pink), P3 (red) and P4 (blue). Guest molecules and hydrogen atoms are omitted for clarity. Left: view normal to the ansa chain backbone; right: view roughly perpendicular to the plane of the chromophore.

Table 4 The dihedral angles between planes A and B as well as those between planes B and C of the host molecule in each solvate.

solvates	**P1**	**P2**	**P3**	**P4**
Angle between A and B (°)	83.04(2)	82.74(2)	76.63(3)	81.44(3)
Angle between B and C (°)	10.19(9)	10.69(8)	10.7(1)	12.22(9)

Figure 3 shows the structure of the rifampicin molecule in solvate P1 and the torsion angle labelling along the ansa chain backbone.

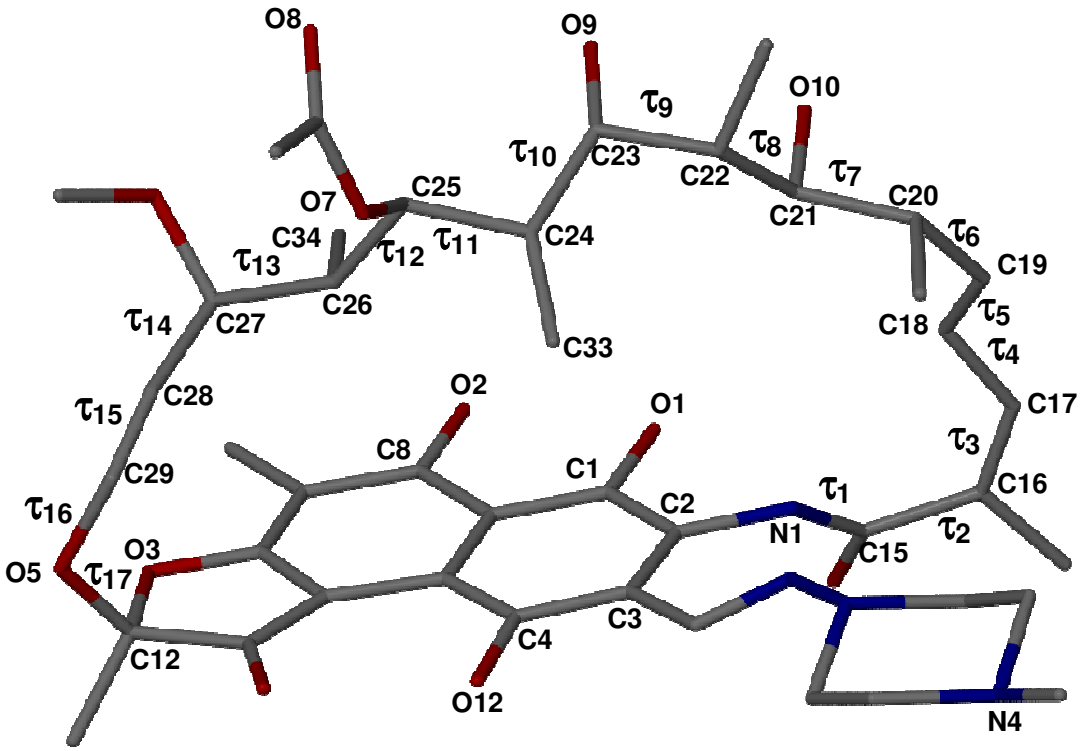

Figure 3 The molecular structure and torsion angle scheme along the ansa chain.

Table 5 lists the torsion angles τ_1-τ_{17} along the ansa chain backbone of the rifampicin host. Among these angles, τ_1 defines the junction between the chromophore and the ansa chain. It is evident that the chromophore plane and the major plane of the ansa chain adopt a *trans* conformation in the rifampicin molecules of all four solvates (Table 5). The torsion angle τ_{17} indicates a *gauche* conformation of the etheric junction in the rifampicin molecule in each case.

Table 5 The torsion angles along the ansa chain in the rifampicin host molecule of each solvate

Torsion angles (°)	**P1**	**P2**	**P3**	**P4**
C2-N1-C15-C16 (τ_1)	176.8(2)	177.7(3)	178.1(3)	178.3(3)
N1-C15-C16-C17 (τ_2)	-27.1(4)	-29.6(4)	-24.5(6)	-30.3(5)
C15-C16-C17-C18 (τ_3)	-0.3(5)	2.1(5)	0.2(7)	3.2(6)
C16-C17-C18-C19 (τ_4)	152.2(3)	152.5(3)	159.1(4)	153.6(4)
C17-C18-C19-C20 (τ_5)	-164.9(3)	-164.2(3)	-166.0(4)	-164.4(3)
C18-C19-C20-C21 (τ_6)	-17.5(4)	-17.9(4)	-18.0(5)	-16.7(5)
C19-C20-C21-C22 (τ_7)	170.6(2)	170.0(2)	171.2(3)	168.9(3)
C20-C21-C22-C23 (τ_8)	-176.9(2)	-176.7(2)	-179.2(3)	-178.0(3)
C21-C22-C23-C24 (τ_9)	62.6(3)	62.2(3)	56.4(4)	62.0(4)
C22-C23-C24-C25 (τ_{10})	163.8(2)	165.1(2)	171.0(3)	166.3(3)
C23-C24-C25-C26 (τ_{11})	160.7(2)	159.3(2)	162.8(3)	159.9(3)
C24-C25-C26-C27 (τ_{12})	148.3(2)	151.5(2)	156.9(3)	154.9(3)
C25-C26-C27-C28 (τ_{13})	-172.2(2)	-170.6(2)	-173.8(3)	-172.7(3)
C26-C27-C28-C29 (τ_{14})	121.0(3)	119.5(3)	118.5(4)	118.3(3)
C27-C28-C29-O5 (τ_{15})	-175.1(2)	-175.1(2)	-175.2(3)	-174.9(3)
C12-O5-C29-C28 (τ_{16})	66.1(3)	63.3(3)	61.1(5)	61.6(4)
C29-O5-C12-O3 (τ_{17})	-78.0(3)	-77.0(3)	-80.3(4)	-77.4(3)

Figure 4 shows the diagram of the rifampicin host molecule in P1 viewed side-on to the ansa chain backbone. The methyl group C26-C34 is on the same side as O1 and O2 with respect to the ansa chain, pushing the acetyl group (C25-O7-C35-O8-C36) backwards over the chromophore.[3] The bonds C21-O10 and C23-O9 are parallel to the chromophore plane. Four oxygen atoms (O9, O10, O1 and O2) protrude from the cavity of the ansa chain and the chromophore face while their C-O vectors are perpendicular to the ansa chain. Furthermore, all four oxygen atoms are disposed in the opposite direction from the piperazinyl subsitituent. Based on these structural features, again the rifampicin host molecules in each solvate are seen to retain the characteristic arrangement of the four

oxygen atoms necessary for antibiotic action through the postulated drug-enzyme interaction.[8 - 10]

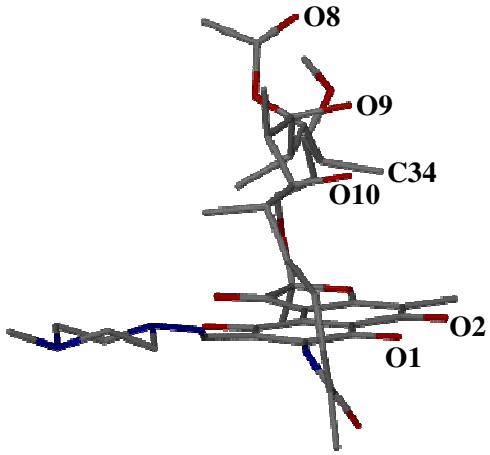

Figure 4 Diagram of the rifampicin host molecule in P1 viewed side-on with respect to the ansa chain.

Furthermore, it is known that the intramolecular distances between O1 and O9, O1 and O10, O2 and O9 as well as O2 and O10 fall in the range between ~5.41 and 9.58 Å in the active rifamycin derivatives.[4] As listed in Table 6 which summarises the above distances in the rifampicin host molecules in all four solvates, all the distances fall within the relevant range. Therefore, considering the geometrical location of the O9 and O10 atoms (see Figure 4) as well as the distances listed in Table 6, the rifampicin host molecule in each solvate can be characterized as having an open conformation, which once more gives rise to the conclusion that the host molecules adopt the antibiotically active conformation in the solid state.

Table 6 Interatomic distances involving O1, O2, O9 and O10 atoms in the host molecules in the four solvates[a]

Distance (Å)	**P1**	**P2**	**P3**	**P4**
O1···O9	6.102	6.086	6.687	6.208
O1···O10	5.339	5.349	5.688	5.405
O2···O9	6.773	6.738	7.393	6.840
O2···O10	6.908	6.895	7.197	6.907

[a] Average e.s.d. 0.003 Å.

In conclusion, the conformational parameters for the rifampicin molecules in the four solvated crystals generally span quite narrow ranges. Furthermore, the values of these

parameters (dihedral angles-planes A and B, planes B and C, τ_1 - τ_{17}, spatial arrangement of O1, O2, O9 and O10 and their interatomic distances) fall within the ranges previously established as prerequisites for rifamycin antibiotic activity.[4]

Intra- and Intermolecular Interactions

Host Intramolecular Interactions

Four analogous intramolecular O-H···O and one N-H···N hydrogen bond (H-bond) interactions were found in the host molecules of P1, P2, P3 and P4 as listed in Table 7.

Table 7 Intramolecular O1-H1···O2, O10-H10···O9, O12-H12···O4 and N1-H1N···N2 H-bond interactions in the host molecules of four solvates[a]

Hydrogen bond	O···O or N···N Distance (Å)	Angle (°)
P1		
O1-H1···O2	2.500(3)	148
O10-H10···O9	2.742(3)	144
O12-H12···O4	2.558(3)	168
N1-H1N···N2	2.710(3)	112
P2		
O1-H1···O2	2.500(3)	148
O10-H10···O9	2.720(3)	147
O12-H12···O4	2.545(2)	167
N1-H1N···N2	2.712(3)	113
P3		
O1-H1···O2	2.484(4)	149
O10-H10···O9	2.708(4)	149
O12-H12···O4	2.558(4)	164
N1-H1N···N2	2.707(4)	113
P4		
O1-H1···O2	2.498(3)	148
O10-H10···O9	2.694(3)	147
O12-H12···O4	2.537(3)	167
N1-H1N···N2	2.704(4)	113

[a] Where no e.s.d. is reported for the angle, H atoms involved were added in idealised positions in a riding model.

The distance between the hydrogen bond acceptor and donor, the hydrogen bond angles, the distance ranges and the angle ranges for the O-H···O interactions in the host molecules of each solvate are summarised in Table 8. The average distance for the O-H···O interactions is very close in all cases.

Table 8 The mean distances and angles as well as their ranges for the O-H···O interactions in the host molecules of each solvate

O···O	**P1**	**P2**	**P3**	**P4**
Average distance (Å)	2.60	2.59	2.58	2.58
Distance range (Å)	2.50 – 2.74	2.50-2.77	2.48 – 2.71	2.50 – 2.69
Average angle (^{o})	153	154	154	154
angle range (^{o})	144 – 168	147 – 167	149-164	147 – 167

A noteworthy observation is that the bond length between atoms C8 and O2 is significantly shorter than those of the other C-O bonds which are in a similar chemical environment, as listed in Table 9. Based on the data listed in International Tables for Crystallography[11], the typical distance for the C-O bond in the above environment is 1.333 Å. Therefore, although bonds C4-O12, C1-O1 and C8-O2 are all represented as single bonds in Figure 1, the former two bonds can be confirmed as being single whilst C8-O2 has significant double bond character. (In P1, the bond lengths C8-O2 and e.g. C1-O1 differ by 16.5 σ_c, where σ_c is the combined standard derivation. For P2-P4, the corresponding values are 15.8σ_c, 7.1σ_c and 10.4σ_c respectively).

Table 9 Bond lengths C4-O12, C1-O1 and C8-O2 in the host molecule of each solvate.

Bond length (Å)	**P1**	**P2**	**P3**	**P4**
C4-O12	1.372(3)	1.373(3)	1.369(4)	1.371(4)
C1-O1	1.361(3)	1.348(3)	1.340(5)	1.344(4)
C8-O2	1.291(3)	1.281(3)	1.290(5)	1.285(4)

Moreover, during the structural refinements of all four solvates, geometrically sensible electron density peaks, that qualified as potential H atoms, were found associated with all the hydroxyl oxygen atoms (O1, O9, O10, O12) except the O2 atom. At the same time, an extra peak was found at ~ 1 Å from the N4 atom having an electron density value similar to the other peaks which had been assigned as hydrogen atoms. Also, between N4 and an oxygen atom of a solvent (methanol/ethanol/water) molecule, this specific peak was ideally located, accounting for the formation of a N^+-H···O hydrogen bond with very favourable geometry. Therefore, it can be assumed that the proton transferred from the hydroxyl group on C8 to the nitrogen atom N4, forming a zwitterion. This conclusion is in accord with an early statement that rifampicin exists as a zwitterion in the solid state,[12] although the present study is the first to prove this zwitterionic character in the case of solvates P1-P4 using X-ray diffraction. Figure 5 shows the zwitterionic structure

and the intramolecular O-H···O and N-H···N interactions for each rifampicin host molecule. The host molecules in each solvate adopt the same motif of intramolecular O-H···O and N-H···N hydrogen bond interactions.

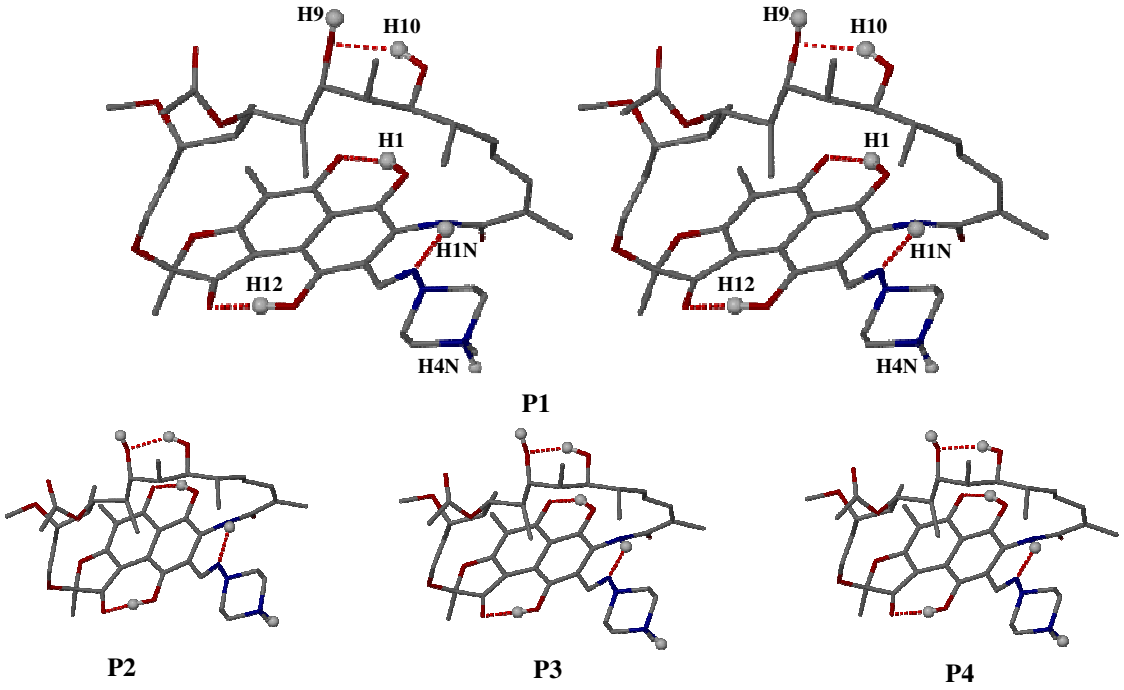

Figure 5 The zwitterionic structures and the intramolecular O-H···O and N-H···N interactions for each rifampicin host molecule. The relevant hydrogen atoms are shown as spheres. The other hydrogen atoms and the guest molecules are omitted for clarity. The host molecule in P1 is shown as a stereoview.

Several intramolecular C-H···O and C-H···N interactions (Table 10) were found to be associated with the rifampicin conformations in P1, P2, P3 and P4. The hydrogen bonds C14-H···O3, C18-H18···N1, C25-H···O8, C25-H···O9, C27-H···O7 and C18-H18···N1 are found to exist in the host molecule for each solvate.

Table 10 Intramolecular C-H···O and C-H···N interactions in the host molecules of the four solvates[a]

Hydrogen bond	C···O or C···N Distance (Å)	Angle (°)
P1		
C14-H14C···O3	2.906(3)	107
C18-H18···N1	2.892(4)	104
C25-H25···O8	2.746(4)	106
C25-H25···O9	2.948(3)	105
C27-H27···O7	2.739(3)	102
P2		
C14-H14A···O2	2.842(3)	107
C14-H14D···O3	2.901(4)	107
C18-H18···N1	2.885(4)	105
C25-H25···O8	2.736(4)	106
C25-H25···O9	2.938(3)	105
C27-H27···O7	2.758(3)	103
C28-H28···O3	3.073(3)	112
P3		
C14-H14A···O3	2.897(3)	107
C18-H18···N1	2.884(3)	105
C25-H25···O8	2.733(4)	106
C25-H25···O9	2.943(3)	106
C27-H27···O7	2.759(3)	103
C28-H28···O3	3.067(3)	113
C30-H30A···O11	2.818(3)	107
P4		
C14-H14A···O3	2.898(4)	106
C18-H18···N1	2.894(4)	106
C25-H25···O8	2.718(5)	106
C25-H25···O9	2.911(4)	105
C27-H27···O7	2.757(4)	102
C28-H28···O3	3.060(4)	113
C38-H38···O12	2.671(4)	100
C34-H34C···O6	2.896(5)	100

[a] Where no e.s.d. is reported for the angle, H atoms involved were added in idealised positions in a riding model.

The average distances, angles and their ranges for the intramolecular C-H···O interactions of each solvate are summarised in Table 11. The average distances are very close in each host molecule, as are the average angles. This is consistent with the previous observations that indicated a high level of conformational similarity among the four independent rifampicin molecules.

Table 11 The average distances and angles as well as their ranges for the intramolecular C-H···O interactions in the host molecules of each solvate

C···O	**P1**	**P2**	**P3**	**P4**
Average distance (Å)	2.83	2.87	2.87	2.85
Distance range (Å)	2.74 – 2.95	2.74 – 3.07	2.73 – 3.07	2.72 – 3.06
Average angle (°)	105	107	107	105
angle range (°)	102 – 107	103 – 112	103 – 113	102 – 113

Furthermore, the intramolecular hydrogen bonds O-H···O, N-H···N, C-H···O and C-H···N stabilise the conformation of the host molecules in P1, P2, P3 and P4.[13]

Host-host Interactions

A common host-host intermolecular H-bond interaction O9-H9···O12 is observed between the host molecules in each solvate. Table 12 lists the distances between O9 and O12, and the angles of this interaction in each solvate. The four solvates adopt similar distances and angles for this interaction.

Table 12 Host-host intermolecular O9-H9···O12 interactions for the host molecules in each solvate.[a]

O9···O12	Distance (Å)	Angle (°)	Symmetry operator for O12
P1	2.848(3)	168	1/2-x, 1-y, 1/2+z
P2	2.811(3)	169	1/2-x, 1-y, 1/2+z
P3	2.910(4)	171	1/2-x, 1-y, 1/2+z
P4	2.792(3)	169	1/2-x, 1-y, 1/2+z

[a] Where no e.s.d. is reported for the angle, H atoms involved were added in idealised positions in a riding model.

Figure 6 shows the above interaction as well as the neighbouring host intramolecular O12-H12···O4 and O10-H10···O9 interactions occurring in the host molecules in each solvate. Similar interactions occur in all four solvates. For example, in P1, the O9 and O12 atoms serve both as hydrogen bond acceptor and donor while O4 and O10 atoms act only as acceptor and donor, respectively.

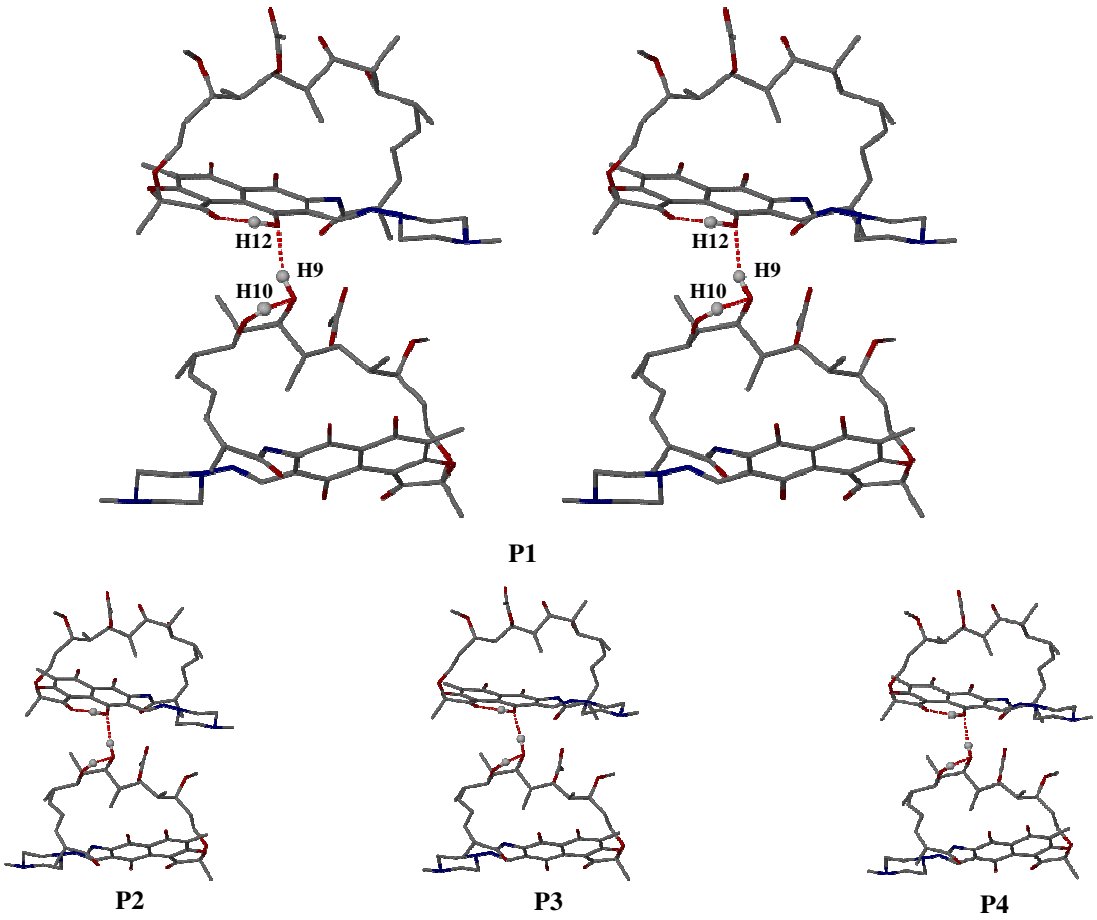

Figure 6 The host-host intermolecular O-H···O interactions in each solvate. The relevant hydrogen atoms are shown as spheres, while the remaining H atoms and the guest molecules are omitted for clarity. The host molecule in P1 is presented in stereoview.

Several common host-host intermolecular C-H···O interactions are found in solvates P1, P2, P3 and P4 as well. These include C29-H···O2, C32-H···O4 and C40-H···O1. The details of all C-H···O interactions are listed in Table 13.

Table 13 Intermolecular C-H···O interactions between the rifampicin molecules[a]

Hydrogen bond	C···O Distance (Å)	Angle (°)	Symmetry operator[b]
P1			
C29-H29···O2	3.466(3)	169	1-x, 1/2+y, 3/2-z
C31-H31B···O11	3.268(4)	142	-x, 1/2+y, 3/2-z
C32-H32A···O4	3.449(4)	151	1/2-x, 1-y, 1/2+z
C40-H40B···O1	3.323(4)	143	-x, 1/2+y, 3/2-z
C43-H43C···O1	3.371(4)	138	-x, 1/2+y, 3/2-z
P2			
C29-H29···O2	3.397(3)	168	1-x, 1/2+y, 3/2-z
C31-H31B···O11	3.325(4)	150	-x, 1/2+y, 3/2-z
C32-H32A···O4	3.450(4)	153	1/2-x, 1-y, 1/2+z
C36-H36A···O11	3.492(4)	158	1/2-x, 1-y, 1/2+z
C40-H40B···O1	3.406(4)	146	-x, 1/2+y, 3/2-z
P3			
C29-H29···O2	3.496(4)	171	1-x, 1/2+y, 3/2-z
C32-H32A···O4	3.371(5)	141	1/2-x, 1-y, 1/2+z
C40-H40B···O1	3.369(5)	139	-x, 1/2+y, 3/2-z
C43-H43A···O10	3.451(5)	152	-x, 1/2+y, 3/2-z
C43-H43C···O1	3.247(5)	144	-x, 1/2+y, 3/2-z
P4			
C29-H29···O2	3.335(4)	169	1-x, 1/2+y, 3/2-z
C31-H31B···O11	3.375(4)	153	-x, 1/2+y, 3/2-z
C32-H32C···O4	3.399(4)	149	1/2-x, 1-y, 1/2+z
C36-H36C···O11	3.426(5)	154	1/2-x, 1-y, 1/2+z
C40-H40B···O1	3.401(4)	146	-x, 1/2+y, 3/2-z
C43-H43A···O1	3.402(7)	140	-x, 1/2+y, 3/2-z

[a] Where no e.s.d. is reported for the angle, H atoms involved were added in idealised positions in a riding model.
[b] Symmetry operator applies to hydrogen bond acceptor atoms.

The mean distances and angles, and their ranges for the host-host intermolecular C-H···O interactions in each solvate are summarised in Table 14. The average C···O distances are very close in each solvate.

Table 14 The average distances and angles as well as their ranges for the host-host intermolecular C-H···O interactions in the host molecules of each solvate

C···O	**P1**	**P2**	**P3**	**P4**
Average distance (Å)	3.38	3.41	3.39	3.39
Distance range (Å)	3.27 – 3.47	3.33 – 3.49	3.24 – 3.50	3.34 – 3.43
Average angle (°)	149	155	150	152
angle range (°)	138 – 169	146 – 168	139-171	140 – 169

Host-guest Interactions

The host-guest intermolecular O-H···O and N-H···O interactions in solvates P1, P2, P3 and P4 are shown in Figure 7. Analogous interactions are found in each solvate.

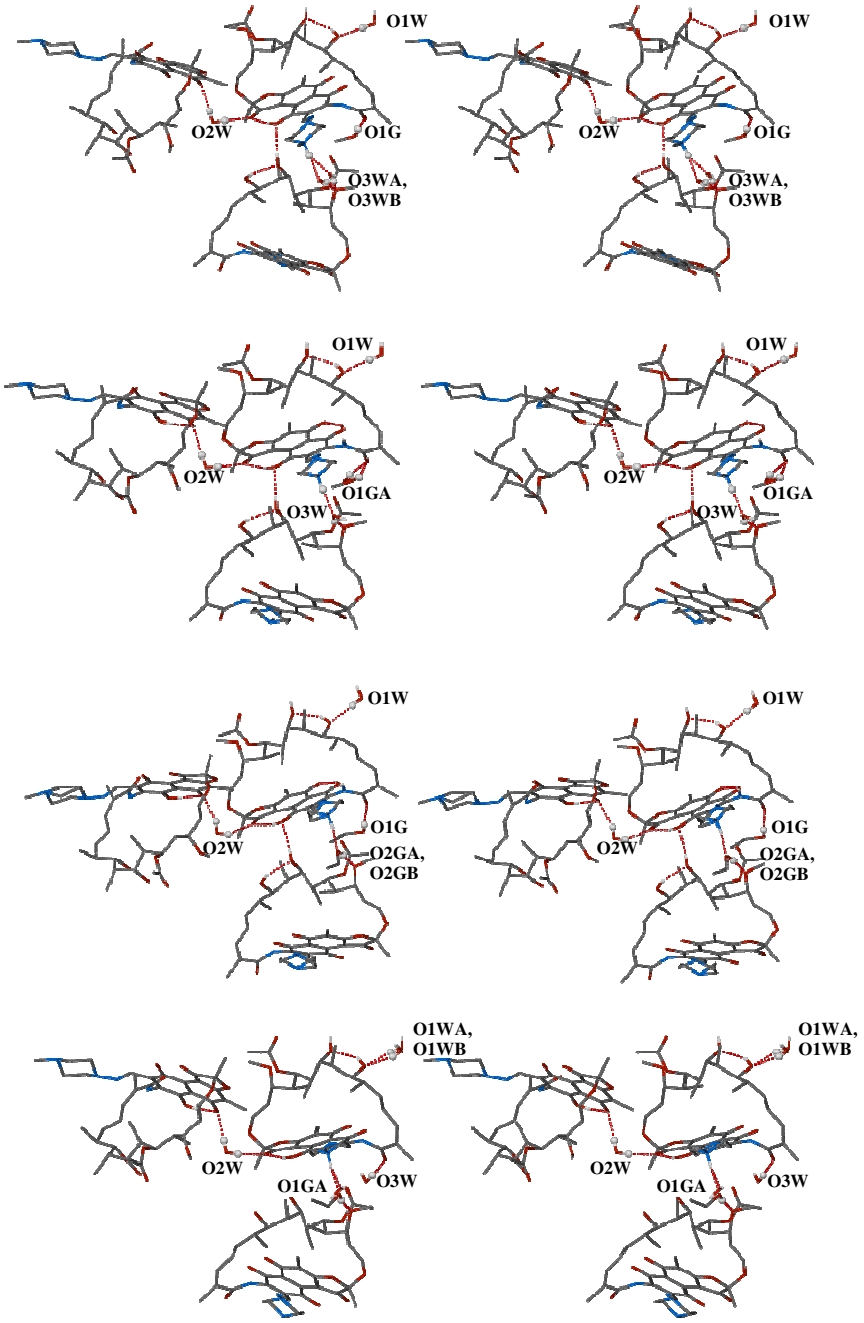

Figure 7 Stereoviews of the intermolecular O-H···O and N-H···O hydrogen bonds between the host and guest molecules in the solvates P1, P2, P3 and P4. The relevant hydrogen atoms are shown as spheres. The other hydrogen atoms and guest molecules are omitted for clarity.

In the cases of P1, P2 and P3, O1W atoms serve as hydrogen bond donors to O10 atoms, thus linking the water molecule O1W to the ansa bridge of each rifampicin host molecule via the hydrogen bond O1W-H1W1···O10. In the case of P4, atom O1W is disordered over two positions (O1WA and O1WB) while the hydrogen atom H1W1 is also disordered over two positions namely H1W1 and H1W3. In addition, both H1W1 and H1W3 atoms form hydrogen bonds to the O10 atom in the host molecule. Table 15 lists the distances between hydrogen bond donor (O1W) and acceptor (O10) as well as the angles in the four solvates. The distances O1W···O10 in the four solvates span a narrow range.

Table 15 Intermolecular O1W-H1W···O10 interactions in the four solvates

Solvate	**P1**	**P2**	**P3**	**P4**	
	O1W···O10	O1W···O10	O1W···O10	O1WA···O10	O1WB···O10
Distance (Å)	2.796(3)	2.807(3)	2.800(5)	2.809(6)	2.789(9)
Angle (^{o})	173(2)	170(2)	161(2)	160(5)	166(5)

For all the solvates, the O2W atoms serve as hydrogen bond donors and function as bridges which stabilise the chromophore in one host molecule and that of the adjacent host molecule. Considering the intramolecular and intermolecular interactions occurring around the O2W atoms, three adjacent rifampicin host molecules are held together by a long hydrogen bonded 'chain', namely O1···O2···H2W2-O2W-H2W1···O4···O12···O9···O10. In more detail, the chromophore in one rifampicin molecule interacts with the chromophore in a second host molecule through the host-guest interactions; this second chromophore also interacts with the ansa chain in a third host molecule through a host-host interaction.

Table 16 lists the distances and angles for hydrogen bonds O2W···O4 and O2W···O2 in the solvates. In four cases, the distances between the hydrogen bond donor (O2W) and the acceptor (O4) are very close while the distances between O2W (donor) and O2 (acceptor) are also very close, implying the presence of strong hydrogen bonding. On average, the former represent stronger hydrogen bonds than the latter due to their shorter O···O distance.

Table 16 Host-guest intermolecular O2W-H2W1···O4 and O2W-H2W2···O2 interactions in four solvates

Hydrogen bond	O···O Distance (Å)	Angle (°)	Symmetry operator[a]
P1			
O2W-H2W1···O4	2.688(3)	176(3)	x, y, z
O2W-H2W2···O2	2.800(3)	163(2)	1-x, 1/2+y, 3/2-z
P2			
O2W-H2W1···O4	2.684(3)	171(2)	x, y, z
O2W-H2W2···O2	2.790(3)	168(4)	1-x, 1/2+y, 3/2-z
P3			
O2W-H2W1···O4	2.742(4)	153(1)	x, y, z
O2W-H2W2···O2	2.847(4)	156(3)	1-x, 1/2+y, 3/2-z
P4			
O2W-H2W1···O4	2.682(3)	173(4)	x, y, z
O2W-H2W2···O2	2.789(4)	176(5)	1-x, 1/2+y, 3/2-z

[a] Symmetry operator applies to hydrogen bond acceptor atoms.

Two other analogous hydrogen bond interactions are also found between the host and guest molecules in all four solvates: the hydrogen bond chain $(N4)^{+}$-HN4···O_{guest}–H_{guest}···O6 connects the piperazinyl atom N4 in one host molecule with the ansa bridge (O6) in the symmetry-generated host molecule. The solvent molecules serve as hydrogen bond acceptors and donors at the same time. The hydrogen bond interaction O_{guest}–H_{guest}···O11 links one water or solvent alcohol molecule with one host molecule (O11). However, the alcohol or water molecules which are involved in the above two hydrogen bonds are different in each solvate. Table 17 lists the details of these hydrogen bonds.

Table 17 Intermolecular $(N4)^{+}$-HN4···O_{guest}-H_{guest}···O6 and O_{guest}-H_{guest}···O11 interactions in the four solvates[a]

Hydrogen bond	N^{+}···O or O···O Distance (Å)	Angle (°)	Symmetry operator[b]
P1			
N4-H4N···O3WA	2.690(5)	158	x, y, z
N4-H4N···O3WB	2.760(8)	169	x, y, z
O3WA-H3W1···O6	2.753(5)	147(2)	1/2-x, 1-y, -1/2+z
O3WB-H3W3···O6	2.844(7)	165(3)	1/2-x, 1-y, -1/2+z
O1G-H1G···O11	2.763(4)	163	x, y, z
P2			
N4-H4N···O3W	2.761(4)	170	x, y, z
O3W-H3W1···O6	2.810(3)	157(2)	1/2-x, 1-y, -1/2+z
O1GA-H1GA···O11	2.723(11)	157	x, y, z
O5W-H5W1···O11	2.887(7)	168(6)	x, y, z
P3			
N4-H4N···O2GA	2.604(1)	171	x, y, z
N4-H4N···O2GB	2.869(8)	137	x, y, z
O2GA-H2GA···O6	2.557(12)	173	1/2-x, 1-y, -1/2+z
O1G-H1G···O11	2.768(5)	169	x, y, z
P4			
N4-H4N···O1GA	2.851(7)	175	x, y, z
N4-H4N···O4WB	2.594(10)	154	x, y, z
O1GA-H1GA···O6	2.751(6)	170	1/2-x, 1-y, -1/2+z
O3W-H3W1···O11	2.850(6)	175(3)	x, y, z

[a] Where no e.s.d. is reported for the angle, H atoms involved were added in idealised positions in a riding model.
[b] Symmetry operator applies to hydrogen bond acceptor atoms.

The mean distances and angles as well as ranges for the host-guest intermolecular O-H···O interactions for all four solvates molecules are summarised in Table 18. The mean distances are very close in each solvate.

Table 18 The average distances and angles as well as their ranges for the host-guest intermolecular O-H···O interactions in all four solvates.

O···O	**P1**	**P2**	**P3**	**P4**
Average distance (Å)	2.77	2.78	2.74	2.78
Distance range (Å)	2.69 – 2.84	2.68-2.89	2.56 – 2.85	2.68 – 2.85
Average angle (°)	164.5	165.1	162.4	170.0
angle range (°)	147 – 176	157 – 171	145-175	160 – 176

Several host-guest intermolecular C-H···O interactions are found in the structures of P1, P2, P3 and P4 as well. The intermolecular C43-H···O2W interaction is common for all four solvate structures. Geometrical details are listed in Table 19.

Table 19 Intermolecular C-H···O interactions between the rifampicin and guest molecules[a]

Hydrogen bond	C···O Distance (Å)	Angle (°)	Symmetry operator[b]
P1			
C43-H43A···O2W	3.481(4)	159	-1+x, y, z
C43-H43B···O2G	3.282(4)	139	x, y, z
P2			
C43-H43B···O2W	3.432(4)	157	-1+x, y, z
C43-H43C···O4W	3.271(5)	136	x, y, z
P3			
C13-H13B···O1G	3.459(6)	155	1/2+x,1/2-y,1-z
C40-H40A···O2W	3.473(5)	148	-1+x, y, z
C43-H43B···O2W	3.444(5)	147	-1+x, y, z
P4			
C40-H40A···O2W	3.468(4)	146	-1+x, y, z
C43-H43B···O2W	3.390(5)	154	-1+x, y, z

[a] Where no e.s.d. is reported for the angle, H atoms involved were added in idealised positions in a riding model.
[b] Symmetry operator applies to hydrogen bond acceptor atoms.

The average distances and angles for the host-guest intermolecular C-H···O interactions for the four solvates are summarised in Table 20. The mean distances are very close (~ 3.4 Å) in all cases.

Table 20 The average distances and angles for the host-guest intermolecular C-H···O interactions in solvate crystals P1-P4.

C-H···O	**P1**	**P2**	**P3**	**P4**
Average distance (Å)	3.38	3.35	3.46	3.43
Average angle (°)	149	147	150	150

Guest-guest Interactions

In the structures of P1, P2, P3 and P4, isolated guest clusters are formed by the alcohol and water molecules (but not including the molecule which is involved in the guest-host intermolecular interaction O_{guest}-H_{guest}···O11) as shown in Figure 8.

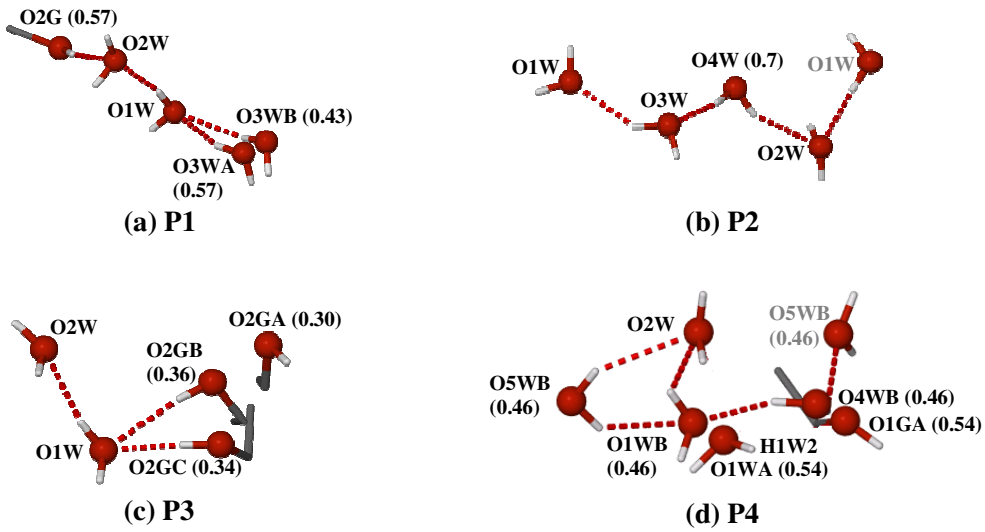

Figure 8 The guest-guest intermolecular O-H···O interactions among the water and alcohol molecules in (a) P1, (b) P2, (c) P3 and (d) P4. Atoms with gray labels have been symmetry-generated from their asymmetric unit counterparts. The disordered atoms are labelled with their site-occupancies.

In P1, water molecule O3W is disordered over two positions O3WA and O3WB, both of which are hydrogen bonded to O1W. Similarly, ethanol molecule O2G-C3G-C4G in P3 is disordered over three positions (O2GA-C3GA-C4GA, O2GB-C3GB-C4GB and O2GC-C3GC-C4GC). O2GA is hydrogen bonded to the host molecule directly while both O2GB and O2GC serve as hydrogen bond donors to O1W. In P4, O1W is disordered over two positions, O1WA and O1WB, both of which are hydrogen bonded to O2W. In particular, the hydrogen H1W2 of O1WA forms two hydrogen bonds with two distinct acceptors simultaneously, forming a (bifurcated) hydrogen bond with O2W and O1GA. Furthermore, ethanol molecule O1GA-C1GA-C2GA and water molecules O4WB and O5WB are two disordered components which will not be present at the same time (i.e. the site-occupancy of atom O1GA is 54% while that of atoms O4WB and O5WB is 46%). In addition, both the distances between O1WA···O2W and O1WA···O1GA fall within the hydrogen bonding distance range. However, no peak was found at ~ 1 Å from the O1WA atom having an electron density value similar to the other peaks which had been assigned as hydrogen atoms. Therefore, an artificial hydrogen atom H1W2 was generated and placed so as to maintain a reasonable molecular geometry for water molecule O1WA, being directed towards the midpoint of the line joining O2W

and O1GA. This indicates the simultaneous O···O interactions between O1WA···O2W and O1WA···O1GA.

The solvent clusters in P1 and P3 are completely isolated whilst those in P2 and P4 extend infinitely. All these clusters and the molecules which are involved in the guest-host intermolecular interaction including O_{guest}-H_{guest}···O11 in each solvate are overlayed in Figure 9. The included alcohol and water molecules in all four solvates are distributed in a similar pattern in their respective crystals. The oxygen atom in each alcohol and water molecule occupies analogous positions in every solvate. However, O2GA in P3 is located in a unique position. Furthermore, O2W is involved in only one guest-guest hydrogen bond in P3 instead of two guest-guest hydrogen bonds as in the other solvates.

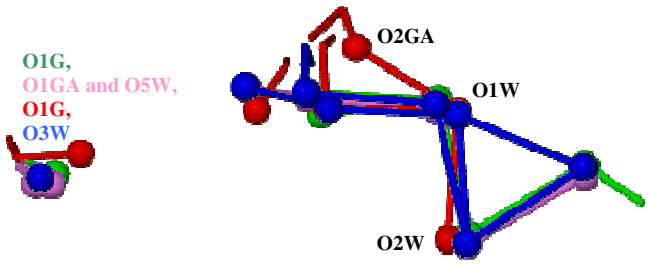

Figure 9 An overlay diagram of the guest-guest intermolecular O-H···O interactions in P1 (green), P2 (pink), P3 (red) and P4 (blue). The molecules which are involved in the guest-host intermolecular interaction O_{guest}-H_{guest}···O11 are also shown and labelled.

Details of guest-guest intermolecular O-H···O hydrogen bond interactions are listed in Table 21. The average distances, average angles, the distance ranges and the angle ranges for the guest-guest intermolecular O-H···O interactions for all four solvates are summarised in Table 22 (bifurcated hydrogen bonds O1WA-H1W2···O2W and O1WA-H1W2···O1GA in P4 are not considered). The mean distances for the intermolecular guest-guest O···O interactions in P1, P2, P3 and P4 are very close (~ 2.8 Å) in the four solvates.

Table 21 The details of guest-guest intermolecular hydrogen bond interactions in solvates P1, P2, P3 and P4[a]

Hydrogen bond	O···O Distance (Å)	Angle (°)	Symmetry operator[b]
P1			
O2G-H2G···O2W	2.909(4)	167	-1/2+x, 3/2-y, 1-z
O1W-H1W2···O2W	2.908(3)	166(2)	1/2-x, 1-y, 1/2+z
O3WA-H3W2···O1W	2.662(5)	162(5)	-1/2-x, 1-y, -1/2+z
O3WB-H3W4···O1W	2.785(7)	148(4)	1/2-x, 1-y, -1/2+z
P2			
O3W-H3W2···O1W	2.690(4)	143(3)	-1/2-x, 1-y, -1/2+z
O4W-H4W1···O3W	2.867(5)	171(4)	x, y, z
O4W-H4W2···O2W	2.895(5)	154(3)	-1/2+x, 3/2-y, 1-z
O1W-H1W2···O2W	2.863(4)	157(3)	1/2-x, 1-y, 1/2+z
P3			
O1W-H1W2···O2W	2.817(5)	168(5)	1/2-x, 1-y, 1/2+z
O2GB-H2GB···O1W	2.827(11)	148	-1/2-x, 1-y, -1/2+z
O2GC-H2GC···O1W	2.556(12)	170	-1/2-x, 1-y, -1/2+z
P4			
O5WB-H5W2···O2W	2.941(8)	144(3)	-1/2+x, 3/2-y, 1-z
O5WB-H5W1···O1WB	2.831(2)	139(5)	-x, 1/2+y, 3/2-z
O1WB-H1W4···O2W	2.640(8)	129(7)	1/2-x, 1-y, -1/2+z
O1WA-H1W2···O2W	2.926(7)	85(2)	1/2-x, 1-y, -1/2+z
O1WA-H1W2···O1GA	2.684(8)	89(2)	-1/2-x, 1-y, -1/2+z
O4WB-H4W1···O1WB	2.664(14)	147(2)	-1/2-x, 1-y, -1/2+z
O4WB-H4W2···O5WB	2.813(11)	126.8(8)	x, y, z

[a] Where no e.s.d. is reported for the angle, H atoms involved were added in idealised positions in a riding model.
[b] Symmetry operator applies to hydrogen bond acceptor atoms.

Table 22 The average distances and angles as well as their ranges for the guest-guest intermolecular O-H···O interactions in all four solvates.

O-H···O	**P1**	**P2**	**P3**	**P4**
Average distance (Å)	2.84	2.83	2.74	2.78
Distance range (Å)	2.75 – 2.91	2.69 – 2.90	2.57 – 2.83	2.64 – 2.94
Average angle (°)	157	156	162	134
angle range (°)	148 – 167	143 – 171	148 –168	129 – 147

Overall Intramolecular and Intermolecular Interactions in P1, P2, P3 and P4

Figure 10 shows the overall hydrogen bond interactions in solvates P1, P2, P3 and P4. A similar assembly of five rifampicin molecules around the solvent cluster is observed in each solvate structure.

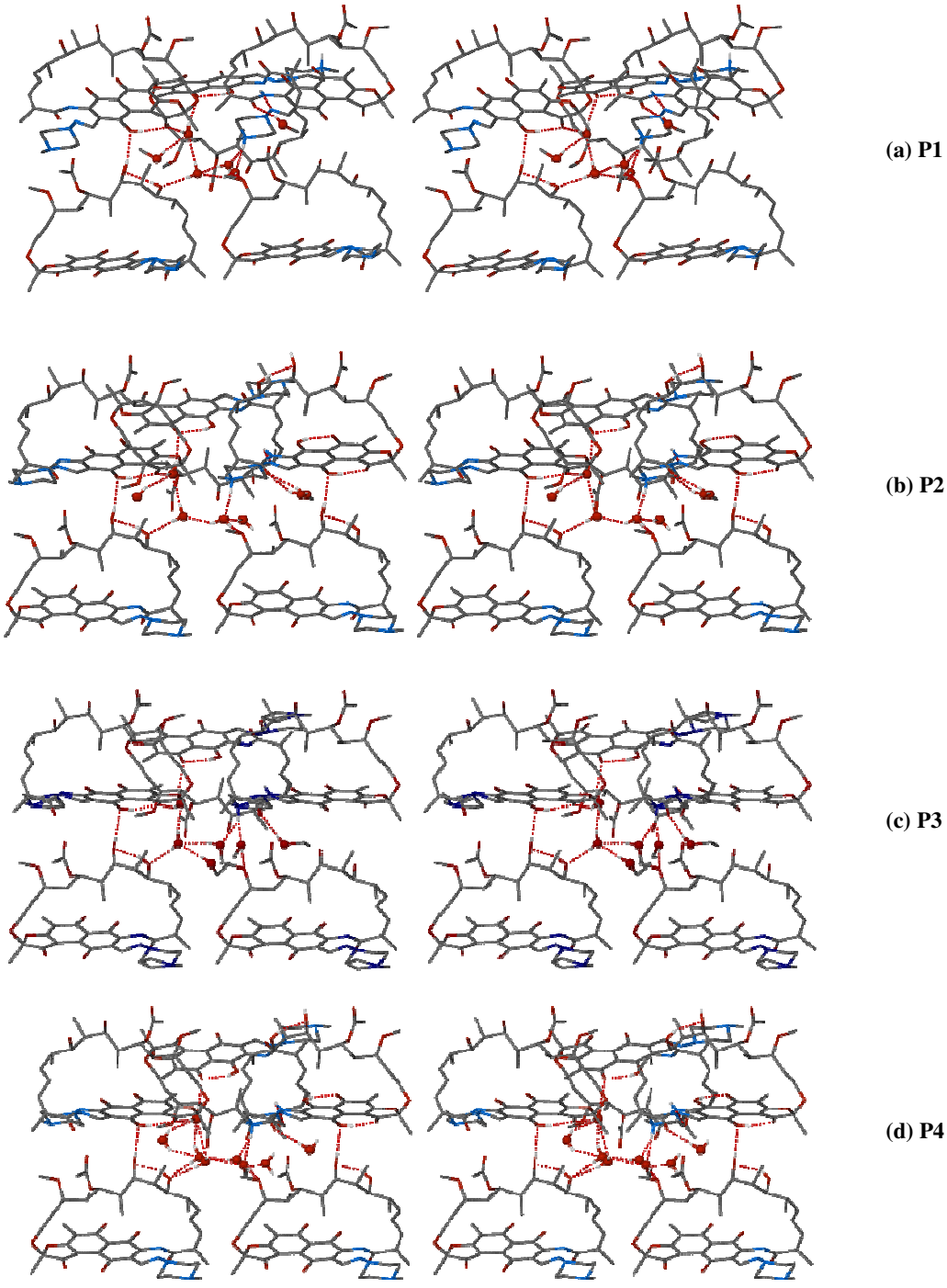

Figure 10 Stereoviews of the overall hydrogen bond interactions in (a) P1, (b) P2, (c) P3 and (d) P4. The oxygen atoms of alcohol and water molecules are shown as spheres.

For the independent rifampicin molecules, the same set of oxygen and nitrogen atoms in the four independent rifampicin molecules of solvates P1 – P4 is involved in hydrogen

bonding with guest molecules. In other words, although the content of the solvent cluster is different in each solvate, the hydrogen bonding environments provided by the rifampicin molecules are identical in P1, P2, P3 and P4.

In solvate P4, there is only one oxygen atom within hydrogen bonding distance of water oxygen O3W. This implies that the latter forms only one H-bond in the crystal, namely O3W-H3W1···O11 (as listed in Table 17).

The schematic diagrams illustrating the overall hydrogen bond interactions for rifampicin solvates P1, P2, P3 and P4 are presented in Figure 11. The solvent clusters in the fresh solvates P1 and P3 (which were rapidly removed from the mother liquor for X-ray analysis) are found to be intimately associated with the rifampicin molecules. However, the clusters in the solvates P2 and P4 (which resulted from exposure of P1 and P3 respectively to the atmosphere) form a more continuous solvent distribution, extending indefinitely along the channels parallel to the *a*-axis. This is described in detail in the next section and illustrated in Figure 12.

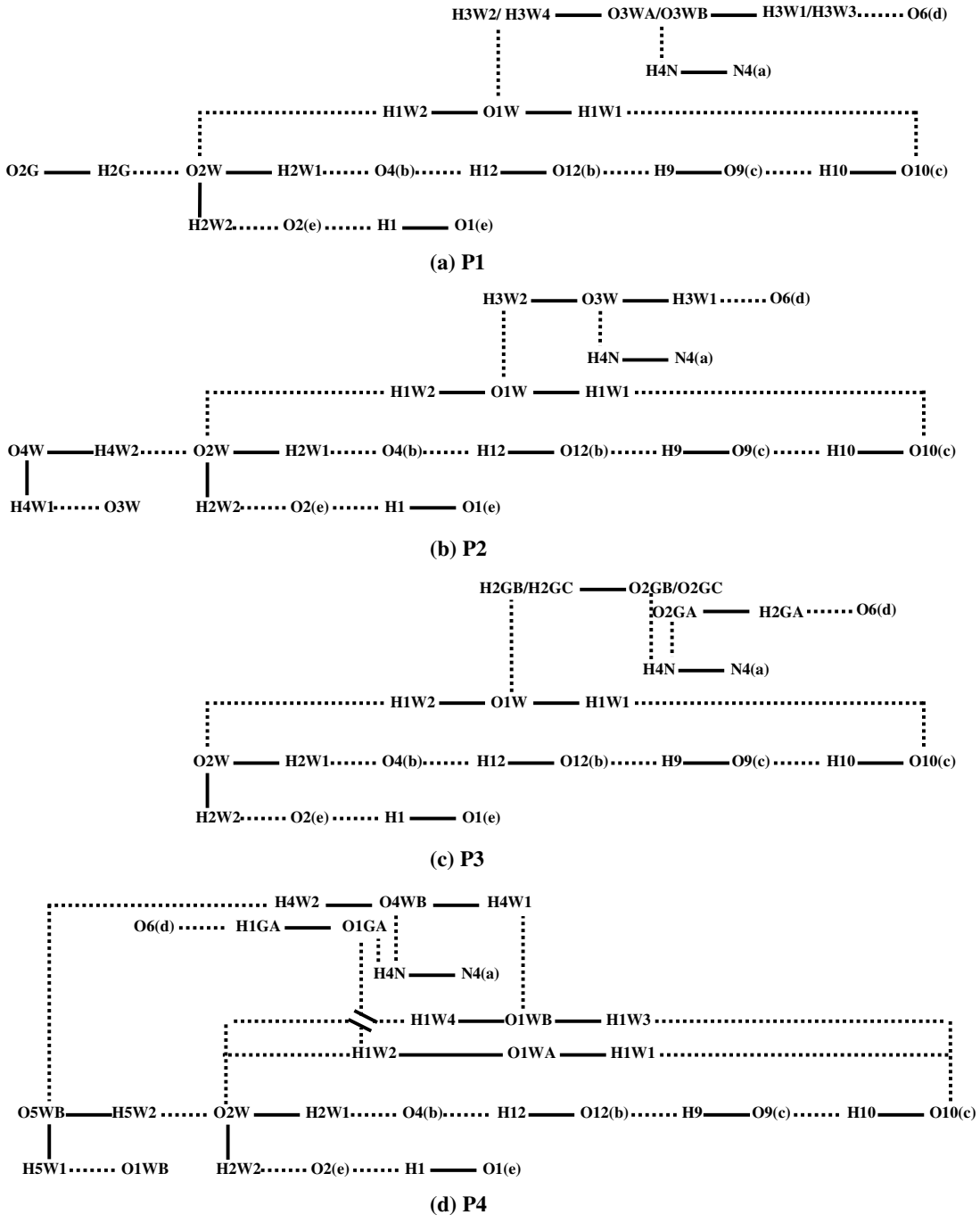

Figure 11 Schematic diagrams for the overall hydrogen bond interactions in (a) P1, (b) P2, (c) P3 and (d) P4. The code letter for the symmetry operator of each rifampicin molecule is given as a suffix in the atom label. (a = x, y, z; b = x-1, y, z; c = -x-1/2, 1-y, z-1/2; d = 1/2-x, 1-y, z-1/2; e = -x, 1/2+y, 3/2-z).

Crystal Packing

For all four solvates, the rifampicin, solvent and water molecules shown in the packing diagrams are held together by hydrogen bonds whose details were discussed earlier.

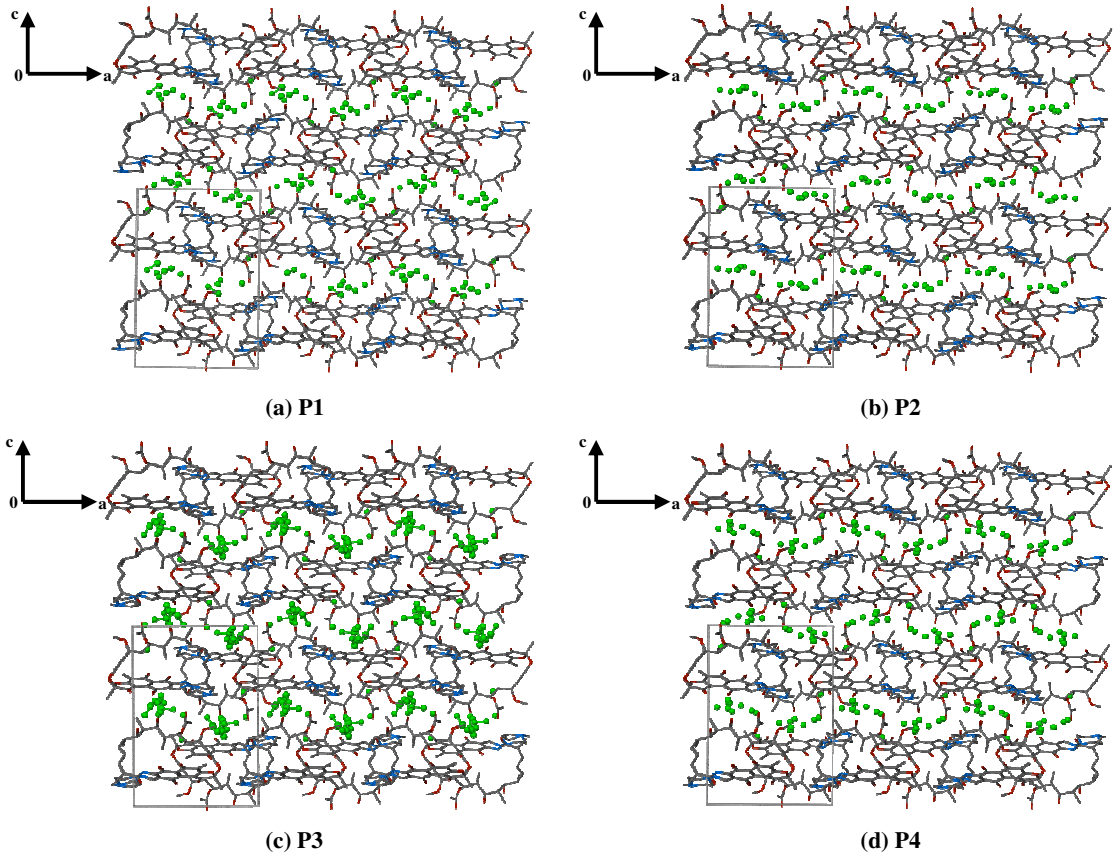

Figure 12 Crystal packing diagrams for (a) P1, (b) P2, (c) P3 and (d) P4 viewed along [010]; solvent molecules are shown as green spheres for clarity.

The host rifampicin packing arrangements in solvates P1, P2, P3 and P4 are identical. For all the solvates, rifampicin molecules pack in a head-to-tail mode parallel to the *c*-axis and form layers parallel to the *a*-axis between which the guest molecules are located. This arrangement gives rise to a solvent tunnel which provides the possibility of easy exchange of solvent molecules in the solvates and water molecules in the atmosphere.

The solvent channels in P1, P2, P3 and P4 were examined using the program SECTION,[14] which was used to view parallel sections through the unit cell along the *a*-

axis. Selected sections for P1 are shown in Figure 13 as representative for the isostructural series. A series of views taken at regular intervals along the *a*-axis clearly illustrates the 'endless' channels in which the guest molecules are accommodated. Figure 13 shows representative sections as examples.

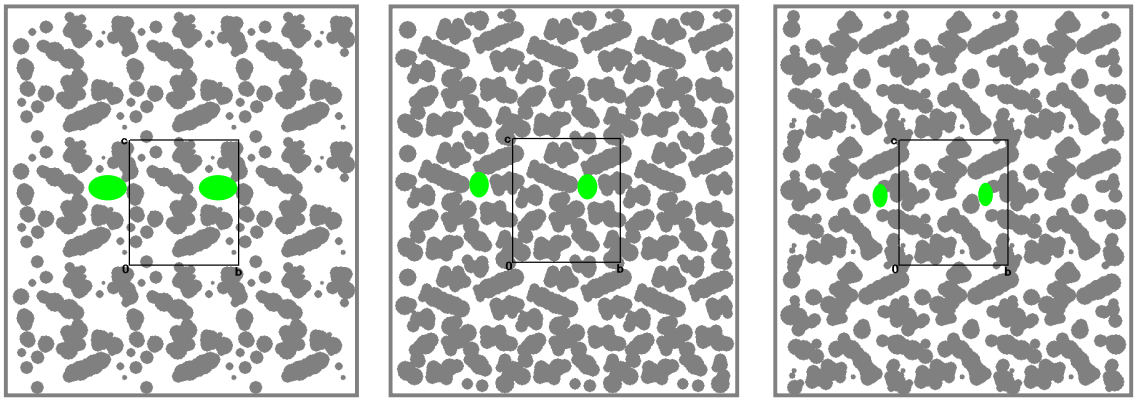

(a) 4 Å **(b) 7 Å** **(c) 9 Å**

Figure 13 Section of P1 with guest molecules omitted and host molecules represented by gray areas, viewed along [100] with the unit cell sectioned at (a) 4 Å (b) 7 Å (c) 9 Å from 0,0,0. The channel locations are shown in green. Host atoms are drawn with their van der Waals radii.

Comparative PXRD

The calculated and experimental PXRD traces for solvates P1, P2, P3 and P4 are shown in Figure 14. For all four solvates, the experimental PXRD traces are in reasonable agreement with the calculated ones, confirming that each prepared sample was homogeneous. Differences in the relative intensities of peaks in the traces of the four solvates are attributed to residual preferred orientation and differences in the respective solvent contents.

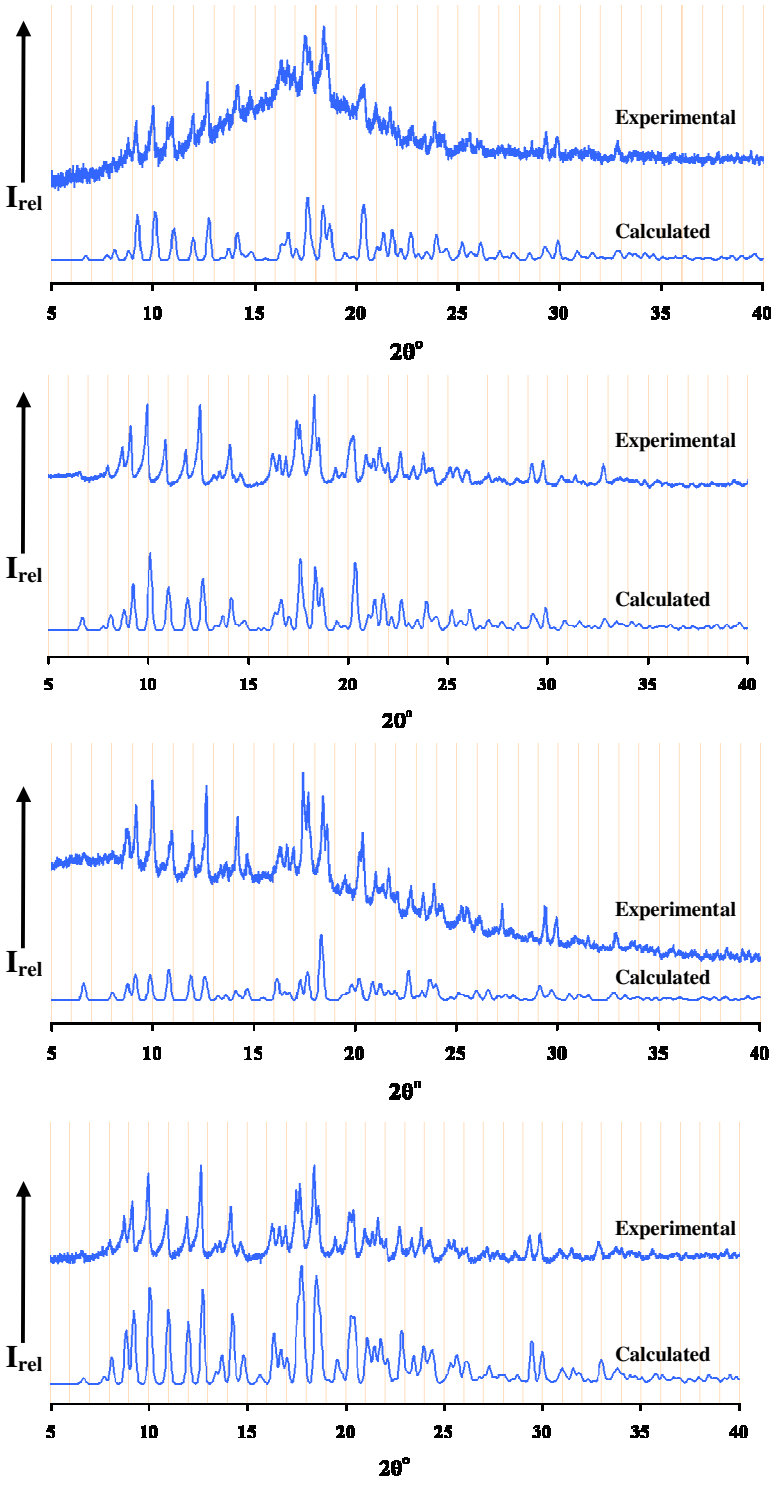

Figure 14 Calculated and experimental PXRD traces for (a) P1, (b) P2, (c) P3 and (d) P4.

Conclusion

Isostructurality

The solvates P1, P2, P3 and P4 display similar unit cell dimensions (a = ~14, b = ~17, c = ~20 Å, $\alpha = \beta = \gamma = 90°$), crystallise in the same space group $P2_12_12_1$, and they have similar PXRD patterns (Figure 15). Furthermore, the atomic co-ordinates of the host molecules in each solvate are similar, evidenced by their similar packing arrangements (Figure 12). In addition, the host molecules in the four solvates are in close superposition (Figure 2), confirming that they adopt similar conformations. Therefore, P1, P2, P3 and P4 are identified as isostructural compounds primarily with respect to the common host rifampicin molecular framework but also extending to some degree to include particular solvent atoms. In addition, any of the calculated PXRD patterns in Figure 15 could serve as a reference for the identification of future crystalline forms belonging to this isostructural series.[15]

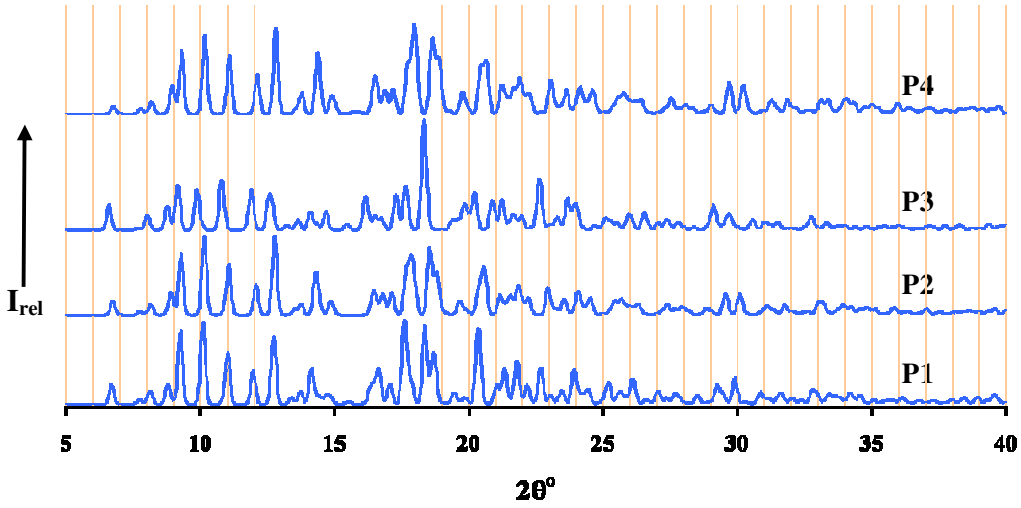

Figure 15 Calculated PXRD traces of solvates P1, P2, P3 and P4.

It is relevant to mention that the X-ray structure of a phase described as rifampicin pentahydrate was reported by Gadret et al. in 1975.[16] The structures of P1, P2, P3, P4 and the pentahydrate are superimposed in Figure 16. As shown there, the host molecule in the pentahydrate adopts a similar conformation to those in the four solvates. In addition, the atomic co-ordinates of the water molecules in the pentahydrate are found to correspond to the co-ordinates of the oxygen atoms in the guest molecules in each

solvate. Also, the pentahydrate crystallises in the same space group $P2_12_12_1$ and has similar unit cell dimensions [a = 17.50(8), b = 19.94(3), c = 13.86(9) Å, $\alpha = \beta = \gamma = 90°$]. Therefore, rifampicin pentahydrate belongs to the series of isostructural solvates of mixed solvents discovered and described in the present study.

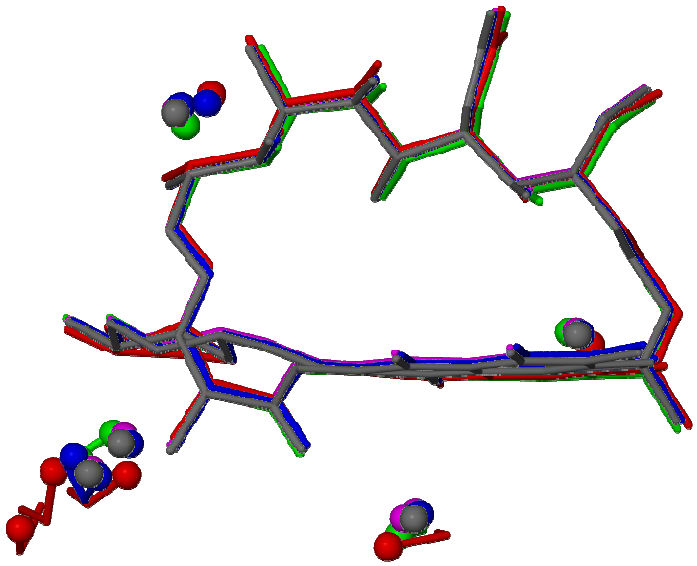

Figure 16 An overlay diagram of the asymmetric units in P1 (green), P2 (pink), P3 (red), P4 (blue) and the rifampicin pentahydrate (grey). The oxygen atoms of the solvent molecules are drawn as spheres

There are, however, shortcomings in the structural report for the pentahydrate, namely the omission of H atoms on the water molecules and no definitive statement as regards the possibility of a zwitterionic structure for the rifampicin molecules.[16] In Figure 17, the published structure of the pentahydrate is compared with that of solvate P1. The bond lengths C1-O1, C8-O2 and C4-O12 in the pentahydrate are 1.340(7), 1.273(3), 1.374(7) Å, respectively. The relatively short length of C8-O2 strongly suggests significant double bond character and thus unwarranted modeling as C-OH. Furthermore, the H atoms of assumed -OH groups (H1, H9, H10 and H12) in the pentahydrate are located in unfavourable positions, having no acceptor atoms in their vicinity.

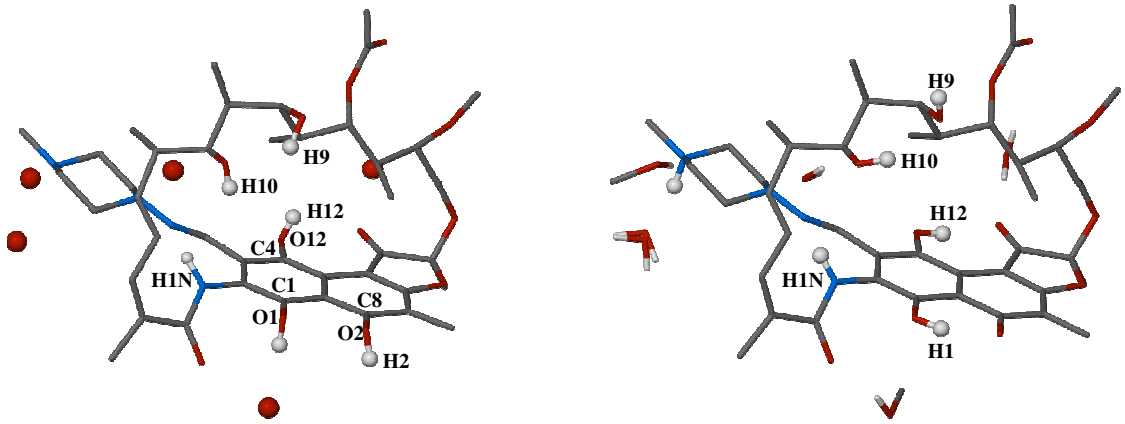

(a) Pentahydrate **(b) P1**

Figure 17 The molecular structures of (a) rifampicin pentahydrate[16] and (b) P1. The hydroxyl hydrogen atoms in the host molecules are shown as spheres and the hydrogen atoms on carbon atoms are omitted for clarity.

A noteworthy observation is that the crystals of both P1 and P3 were converted to a common phase after equilibrating with the atmosphere for a period of ~1 week. X-ray structural analysis and TGA analysis revealed that this phase is rifampicin pentahydrate. Therefore, solvates P1 and P3 undergo guest exchange when equilibrated with the water in the atmosphere for a sufficiently long period, resulting in complete displacement of alcohol molecules by water molecules while maintaining a high level of crystallinity and the same host framework in the crystal structure.

Conformation of the Rifampicin Host Molecules

The similarity of the rifampicin host molecules in P1, P2, P3 and P4 has been demonstrated in the overlay diagram (Figure 2). Furthermore, corresponding dihedral angles among the three principal planes (Table 4) are very similar in the host molecules in all four solvates. This also applies to the torsion angles along the ansa chain (Table 5). However, the conformations of the host molecules in the four solvates are not identical; subtle differences can be found among these molecules. In particular, a short intermolecular C38···O8 contact between host molecules (shown in Figure 18) was observed in each solvate when the crystal assembles. The distances between C38 and O8 in P1, P2, P3 and P4 are 3.11(4), 3.06(3), 3.07(4) and 2.98(4) Å, respectively. Therefore, when rifampicin molecules pack, repulsive interaction occurs between the ansa chain of

one molecule and the piperazinyl subsitituent in another host molecule (at position 1/2-x, 1-y, 1/2+z). Specifically, O8 in one molecule pushes plane C (the piperazinyl ring) away from plane B (the chromophore) in the symmetry related host molecule. Since the distance between C38 and O8 in P4 is shortest while that in P1 is the longest among those in the four solvates, the host molecule in P4 adopts the biggest dihedral angle between planes B and C in the four solvates while the host molecule in P1 adopts the smallest angle (as listed in Table 4).

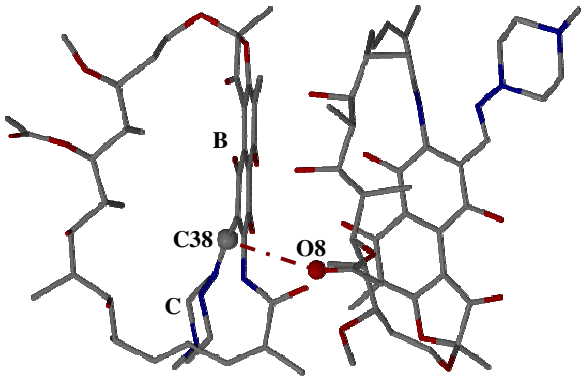

Figure 18 Representative figure showing the short contact C38···O8 between the host molecules

Host-host Intramolecular and Intermolecular Hydrogen Bond Interactions

In all of the solvates studied, the rifampicin molecule was found to exist as a zwitterion, resulting from proton transfer from a hydroxyl group on the chromophore to nitrogen atom N4 of the piperazinyl ring. Since the packing modes of the four solvates are almost identical and the distributions of the alcohol and water molecules are similar, the host-host O···O, N···N, C···O, C···N intramolecular and intermolecular hydrogen bonds involve analogous hydrogen bond donors and acceptors. Furthermore, the average interatomic O···O distance is very similar in each solvate. The same applies to N···N, C···O and C···N distances. It is noteworthy that no π-π interactions are found in the solvates. Such interactions are potentially possible through stacking of the chromophore units of adjacent molecules.

Guest-host Hydrogen Bond Interactions

Six atoms in the rifampicin host molecule are involved in the guest-host intermolecular hydrogen bond motif, namely O2, O4, O10, O6, O11 and N4. This applies to each

solvate due to the almost identical packing arrangements and similar distribution mode of the alcohol and water molecules. However, O2GA in P3 is located in a unique position and O3W in P4 has only one hydrogen bond acceptor (O11).

Guest-guest Hydrogen Bond Interactions

The water and alcohol molecules are generally described as guest molecules in all four solvates. They display a variety of disordered arrangements. Specifically, one molecule is disordered over two positions (O3WA and O3WB in P1 as well as O1WA and O1WB in P4); one molecule is disordered over three positions (O2GA-C3GA-C4GA, O2GB-C3GB-C4GB, O2GC-C3GC-C4GC in P3) and in P4, three solvent molecules O1GA-C1GA-C2GA , O4WB and O5WB are not present with full site-occupancy.

In the structures of P1 and P3, whose data were collected immediately following their removal from mother liquor, the guest molecules (except the methanol molecules O1G-C1G which are hydrogen bonded to O11 in the host molecule) assemble to form an isolated solvent cluster that is closely associated with five neighbouring rifampicin molecules. In the structures of P2 and P4, which resulted from exposure of P1 and P3 to the atmosphere for a period of 10 hours, the guest molecules (except those which are hydrogen bonded to O11 of the host molecule) assemble into a solvent cluster which extends infinitely through the channel created by five rifampicin molecules. Notably, in all four solvates a hydrogen bond donor can always be found adjacent to atom O11 which acts as a hydrogen bond acceptor. In addition, there is no other hydrogen bond acceptor in the vicinity of this particular donor in each solvate.

Crystal Packing

Despite the subtle differences in the conformations of the host molecules and the different content of guest molecules in each solvate, solvates P1, P2, P3 and P4 crystallise in the same space group $P2_12_12_1$ and pack in almost identical modes. For the four solvates, solvent molecules are located in the tunnel parallel to the *a*-axis in-between the layers of rifampicin molecules. The tunnel provides access to atmospheric water

molecules which can enter the crystal, changing the compositions of the entrapped solvent mixtures. After sufficient time, all four solvates transform into the pentahydrate.

In the following part of this chapter, we report three other isostructural rifampicin solvates which belong to a different isostructural series from that exemplified by solvates P1-P4.

Part Two

Crystal Preparation

The abbreviations for the discrete rifampicin solvates in this chapter are as follows:

Rifampicin • 2.50(1-propanol) • 4.30H_2O: P5

Rifampicin • 1.58(1-propanol) • 8.41H_2O: P6

Rifampicin • 0.60(iso-propanol) • 8.09H_2O: P7

Suitable crystals of P5 and P7 were obtained by dissolving 0.020 g (0.024 mmol) of the host drug (rifampicin) in 2 ml of 1-propanol-water mixture (9:1 v/v) and iso-propanol-acetone-water mixture (3:14:3 v/v) at 25 ^{o}C, respectively. Neither solution was filtered. Crystals of suitable quality appeared by slow solvent evaporation at 4 ^{o}C over a period of two weeks.

Crystals of P5 were allowed to stand on an open bench at 25 ^{o}C. After equilibrating with the atmosphere for a period of 10 h, crystals of P5 were found to have transformed to phase P6, with a different solvent composition from P5.

The host and guest numbering schemes are given in Figure 19.

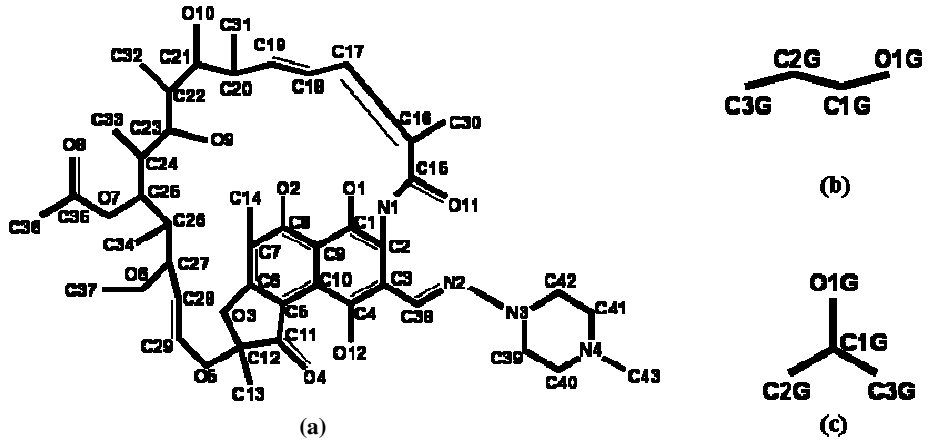

Figure 19 Host and guest numbering schemes: (a) rifampicin, (b) 1-propanol, (c) iso-propanol. Hydrogen atoms have been omitted for clarity.

Single crystal X-Ray Diffraction

Data-collection and Space Group Determination

A crystal of P5 was removed from its mother liquor and was covered in paratone N oil without delay in order to prevent the loss of solvent molecules. The crystals of P5 and P7 were handled in the same way. The X-ray intensity data for P5, P6 and P7 were collected on a Bruker Apex Duo diffractometer at 100 K.

The unit cell parameters, crystal systems and space groups were determined from the X-ray diffraction data which revealed Laue *mmm* symmetry for all three solvates. Therefore, these solvates belong to the orthorhombic system; the space group was determined as $P2_12_12_1$ from the systematic absences: *hkl*: *none*; *h00*: $h = 2n+1$; *0k0*: $k = 2n+1$; *00l*: $l = 2n+1$.

Structure Solution and Refinement

For all three crystals, program SHEXLD[1] was used to solve the structures by *ab initio* methods, which revealed the positions of all the non-hydrogen atoms of the rifampicin molecule (host) in each structure. In each case, the value of $Z = 4$ indicated that the asymmetric unit comprised one drug molecule and its complement of solvent molecules. Full-matrix least-squares refinements were performed with SHELXH-97.[2] Difference Fourier maps revealed the positions of the oxygen and carbon atoms of the water and solvent molecules (guest). Some of these atoms were found to have full site-occupancy while the others were generally disordered over two or even three positions. The host and guest molecules having full s.o.f. were then refined isotropically. Atom C37 in phase P7 is disordered over two positions (C37A and C37B). C37A, the major component, was assigned a value of x for its s.o.f. while the minor component C37B was allocated the value 1-x. The s.o.f.s refined to 0.71(4) and 0.29(4) respectively while their U_{iso} values refined to 0.060(3) $Å^2$ and 0.030(6) $Å^2$, respectively.

For the disordered solvent molecules, a fixed U_{iso} (the mean of U_{eq} for the chemically equivalent ordered atoms) was assigned to each molecule and these atoms were allowed to refine with site-occupancies x and 1-x, with x variable. For some molecules, the s.o.f.s were then assigned as fixed values, allowing the U_{iso} parameters to refine freely. For some of the other molecules, both the U_{iso} values and s.o.f.s refined freely. The details of the U_{iso} parameters and s.o.f.s of the guest molecules in each solvate are listed in Tables 23, 24 and 25.

Table 23 Isotropic thermal parameters and site-occupancy factors for the guest molecules of the solvate P5

Guest molecule	U_{iso} (Å^2)	s.o.f.
O1W	0.04	1.00
O2WA	0.03	0.49
O2WB	0.03	0.42
O3WA	0.09	0.63
O3WB	0.06	0.37
O4W	0.03	1.00
O5WB	0.08	0.37
O1GA/O1GB-C1G-C2G-C3G	0.06/0.03-0.06-0.06-0.08	1.00 (O1GA-0.63;O1GB-0.37)
O2GA-C4GA-C5GA-C6GA	0.12 (global U_{iso})	0.71
O3GA-C7GA-C8GA-C9GA	0.09 (global U_{iso})	0.41
O3GB-C7GB-C8GB-C9GB	0.09 (global U_{iso})	0.38

Table 24 Isotropic thermal parameters and site-occupancy factors for the guest molecules of the solvate P6

Guest molecule	U_{iso} (Å^2)	s.o.f.
O1W	0.04	1.00
O2WA	0.03	0.56
O2WB	0.03	0.44
O3W	0.05	1.00
O4WA	0.05	0.56
O4WB	0.03	0.44
O5W	0.02	1.00
O6W	0.04	1.00
O7W	0.03	1.00
O8WB	0.06	0.44
O9WA	0.07	0.41
O10W	0.09	0.41
O11W	0.05	0.16
O1GA-C1GA-C2GA-C3GA	0.03-0.03-0.03-0.05	0.84
O2GB-C4GB-C5GB-C6GB	0.07-0.04-0.06-0.07	0.44
O3GA-C7GA-C8GA-C9GA	0.12 (global U_{iso})	0.30

Table 25 Isotropic thermal parameters and site-occupancy factors for the guest molecules of the solvate P7

Guest molecule	U_{iso} (Å^2)	s.o.f.
O1W	0.07	0.65
O2WA	0.04	0.70
O2WB	0.05	0.25
O3W	0.07	1.00
O4W	0.03	0.56
O5W	0.03	1.00
O6W	0.06	1.00
O7W	0.07	1.00
O8W	0.06	0.56
O9W	0.07	0.21
O10W	0.06	0.49
O11W	0.06	0.10
O12W	0.05	0.14
O13W	0.06	0.23
O14W	0.07	0.19
O1G-C1G-C2G-C3G	0.02-0.03-0.05-0.04	0.60

In general, location of all the hydrogen atoms in each solvate from difference Fourier maps was attempted. When geometrically reasonable Δρ peaks indicating hydrogen atom presence were found, the hydrogen atoms were placed in idealised postions in a riding model. For water molecules, models were generated so as to satisfy hydrogen bonding requirements. All the methyl hydrogen atoms were refined with isotropic temperature factors 1.5 times those of their parent atoms while all the other hydrogen atoms were assigned temperature factors 1.2 times those of their parent atoms.

For the 1-propanol and iso-propanol molecules as well as the hydrogen atoms of water molecules, distance restraints were employed to ensure reasonable molecular geometries. For the 1-propanol molecules, the bond lengths O1G-C1G, C1G-C2G and C2G-C3G were set at 1.43, 1.52 and 1.51 Å, respectively. For the iso-propanol molecules, the bond lengths O1G-C1G, C1G-C2G and C1G-C3G were set at 1.43, 1.52 and 1.52 Å, respectively. The standard deviation σ for these bonds in both molecules was set between 0.001 and 0.008 Å. The O-H bond length of water molecules was fixed at 0.84 Å with the H-O-H angle set at 104.5^o. The standard deviations σ were set between 0.001 and 0.008 Å.

Crystal and refinement parameters for each solvate are presented in Table 26.

Table 26 Crystal and refinement data for P5, P6 and P7.

Parameter	P5	P6	P7
Formula unit	Rifampicin · 2.50(1-propanol) · 4.30H_2O	Rifampicin · 1.58(1-propanol) · 8.41H_2O	Rifampicin · 0.60(isopropanol) · 8.09H_2O
Formula Weight / g mol^{-1}	1050.13	1069.59	1004.90
Crystal system	orthorhombic	orthorhombic	orthorhombic
Space group	$P2_12_12_1$	$P2_12_12_1$	$P2_12_12_1$
a / Å	13.4396(2)	13.1941(4)	13.4525(8)
b / Å	16.869(2)	16.3019(5)	17.0141(10)
c / Å	25.962(3)	26.5732(9)	25.9219(16)
α / ^{o}	90.00	90.00	90.00
β / ^{o}	90.00	90.00	90.00
γ / ^{o}	90.00	90.00	90.00
Volume / Å^3	5886.0(13)	5715.6(3)	5933.1(6)
Z	4	4	4
Density$_{calc}$ / g cm^{-3}	1.1849	1.2428	1.1249
μ (MoK$_α$) /mm^{-1}	0.090	0.098	0.089
F (000)	2271	2312	2166
Crystal size /mm^3	0.09x0.12x0.23	0.06x0.13x0.07	0.20x0.25x0.47
Temperature / K	100(2)	100(2)	100(2)
Range scanned θ / ^{o}	$2.18 \leq \theta \leq 25.03$	$1.98 \leq \theta \leq 28.42$	$2.18 \leq \theta \leq 27.11$
Index ranges	h: -14, 15	h: -17, 17	h: -17, 17
	k: -14, 20	k: -20, 21	k: -21, 21
	l: -30, 17	l: -35, 35	l: -33, 12
φ scan angle / ^{o}	0.5	0.5	0.5
ω scan angle / ^{o}	0.5	0.5	0.5
Dx / mm	48	40	50
No. of measured reflections	16658	48858	43643
No. of unique reflections	5653	7785	7128
No. of reflections with I > 2σ(I)	4804	6726	6062
No. of L.S. parameters	691	738	710
R_{int}, $R_σ$	0.0392, 0.0464	0.0396, 0.0265	0.0294, 0.0224
S	1.046	1.054	1.059
R_1 ($F_o > 4σ(F_o)$)	0.0844	0.0521	0.0729
No. of reflections omitted	26	19	44
wR2 (all reflections)	0.2409	0.1421	0.2289
Weighting scheme	a = 0.1524	a = 0.0642	a = 0.1562
	b = 9.1387	b = 4.9277	b = 3.5628
$(Δ / σ)_{mean}$	< 0.001	< 0.001	< 0.001
Δρ excursions / eÅ^{-3}	-0.496, 0.916	-0.314, 0.672	-0.589, 0.775

Structural Description

Rifampicin Molecule Conformation and Antibiotic Activity

Similar to the rifampicin host molecules in solvates P1, P2, P3 and P4, the host molecules in solvates P5, P6 and P7 were also investigated with regard to their solid-state conformations. The antibiotic activity of the host molecules has been correlated with the conformation of the ansa chain, as determined from single crystal X-ray diffraction.[3] Figure 20 shows the overlay of the rifampicin host molecule skeletons in the three solvates.

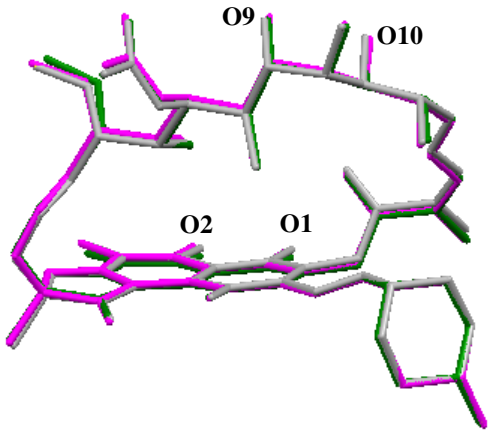

Figure 20 An overlay of the host molecules in solvates P5 (green), P6 (pink) and P7 (gray). Guest molecules and hydrogen atoms are omitted for clarity.

These host molecules are found to adopt a remarkably similar conformation. However, the dihedral angles between planes A (ansa chain) and B (chromophore) as well as those between planes B and C (piperazinyl substituent) are slightly different in each case. The relevant data for each solvate are listed in Table 27. The fact that the dihedral angles between planes A and B are similar in the three cases while the angles between planes B and C are also similar further supports the conclusion of an essentially constant conformation.

Table 27 The dihedral angles between planes A and B as well as those between planes B and C of the host molecule in each solvate.

solvates	**P5**	**P6**	**P7**
Angle between A and B(°)	56.98(5)	61.34(2)	57.94(3)
Angle between B and C(°)	73.47(9)	66.9(2)	72.2(3)

It is noteworthy that the average dihedral angle between planes A and B as well as that between planes B and C in the host molecules of P5, P6 and P7 are very different from their counterparts in P1, P2, P3 and P4 (Table 26 in Part One). This indicates the existence of a solvatomorphic phase of rifampicin which has not been observed previously. This feature is discussed in detail in the conclusion section.

Figure 21 shows the crystal structure of the rifampicin molecule in solvate P5 and the torsion angle labelling along the ansa chain backbone.

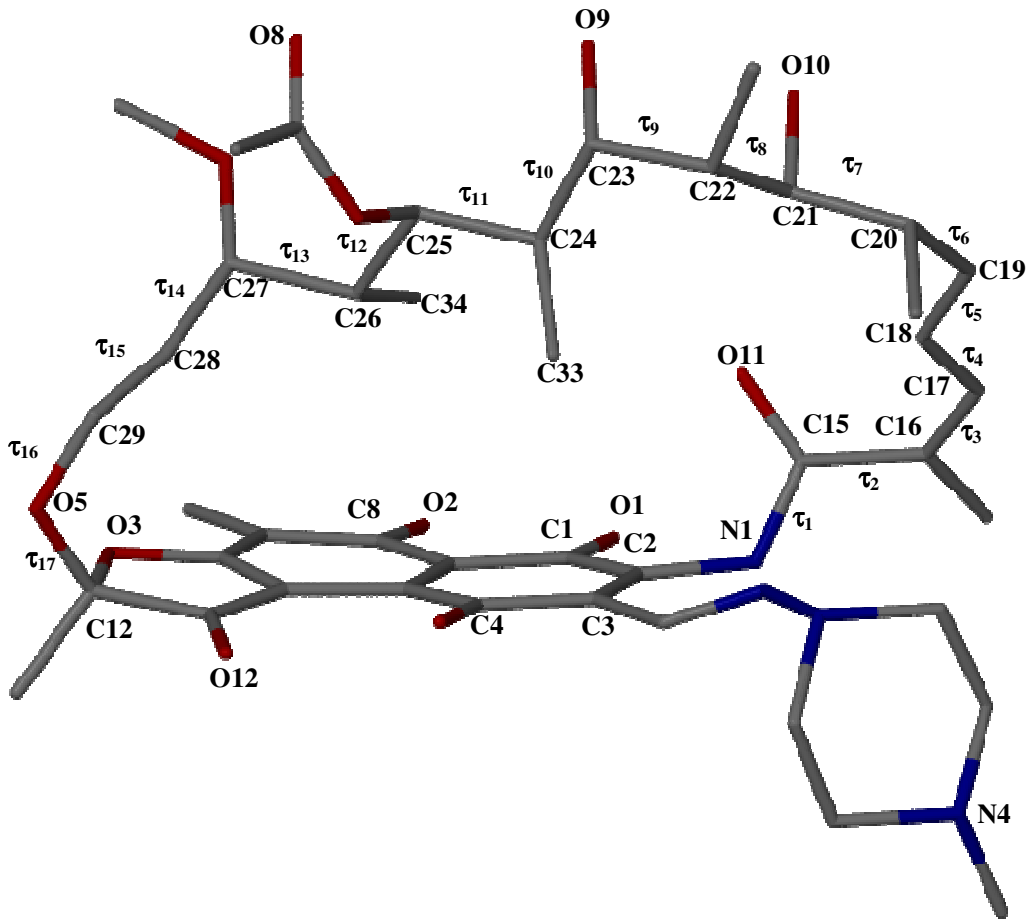

Figure 21 The molecular structure and torsion angle scheme along the ansa chain in the rifampicin molecule.

Table 28 lists the torsion angles τ_1-τ_{17} along the ansa chain backbone of the rifampicin host in solvates P5, P6 and P7. The chromophore plane adopts a *trans* conformation (τ_1) with respect to the plane of the ansa chain. This corresponds to the situation in the rifampicin host molecules in solvates P1, P2, P3 and P4. Furthermore, it is known that the torsion angles τ_9 and τ_{17} in the host molecules fall within the respective preferred ranges 59 ± 6° and -65 ± 13° for active rifamycins.[9, 17] This also serves as evidence for the conclusion that the crystals (P5, P6 and P7) contain the rifampicin molecule in the biologically relevant conformation.

Table 28 The torsion angles along the ansa chain in the rifampicin host molecule of each solvate

Torsion angles (°)	**P5**	**P6**	**P7**
C2-N1-C15-C16 (τ_1)	172.6(5)	170.1(3)	172.2(4)
N1-C15-C16-C17 (τ_2)	-126.3(6)	-123.4(3)	-125.6(5)
C15-C16-C17-C18 (τ_3)	8.5(9)	8.1(4)	8.9(7)
C16-C17-C18-C19 (τ_4)	-177.6(6)	-175.6(3)	-175.4(5)
C17-C18-C19-C20 (τ_5)	-174.3(6)	-175.6(3)	-176.5(4)
C18-C19-C20-C21 (τ_6)	-40.4(9)	-44.1(4)	-43.4(6)
C19-C20-C21-C22 (τ_7)	168.6(6)	170.5(3)	169.4(4)
C20-C21-C22-C23 (τ_8)	-175.3(6)	-173.1(3)	-173.5(4)
C21-C22-C23-C24 (τ_9)	55.4(7)	59.0(4)	59.6(5)
C22-C23-C24-C25 (τ_{10})	173.6(5)	169.3(3)	171.8(4)
C23-C24-C25-C26 (τ_{11})	173.6(5)	173.8(2)	172.6(4)
C24-C25-C26-C27 (τ_{12})	176.7(5)	170.5(3)	171.6(4)
C25-C26-C27-C28 (τ_{13})	-166.0(5)	-167.4(3)	-170.2(4)
C26-C27-C28-C29 (τ_{14})	109.5(8)	108.3(3)	111.7(5)
C27-C28-C29-O5 (τ_{15})	-173.8(7)	-174.3(3)	-174.4(4)
C12-O5-C29-C28 (τ_{16})	43.9(10)	46.3(4)	47.2(7)
C29-O5-C12-O3 (τ_{17})	-76.6(7)	-72.4(3)	-78.3(5)

Figure 22 shows the rifampicin host molecule in P5 viewed side-on to the ansa chain backbone. As explained in the former chapter, again, the four oxygen atoms (O9, O10, O1 and O2) protrude from the cavity of the ansa chain and the chromophore face while being roughly perpendicular to the average plane of the ansa chain. Although the bonds C21-O10 and C23-O9 are not exactly parallel to the aromatic plane, all four of the oxygen atoms are disposed in the opposite direction from the piperazinyl subsitituent. Furthermore, the intramolecular distances among the four oxygen atoms O1, O2, O9 and O10 (listed in Table 29) fall in the range (~5.41 to 9.58 Å) which is favourable for active rifamycin derivatives.[4] This also allows these host molecules to adopt an open

conformation, which once more gives rise to the conclusion that the host molecules adopt the antibiotically active conformation in the solid state.[10]

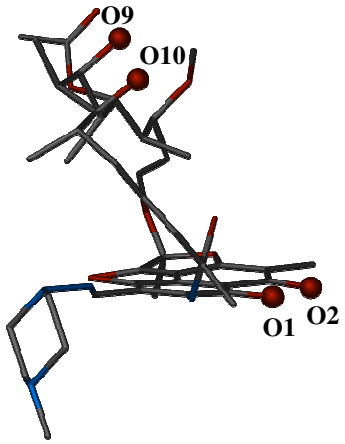

Figure 22 Diagram of the rifampicin host molecule in P1 viewed side-on with respect to the ansa chain. The relevant oxygen atoms are shown as spheres.

Table 29 The intramolecular distances involving O1, O2, O9 and O10 atoms in the host molecules in the three solvates[a]

Distance (Å)	**P5**	**P6**	**P7**
O1-----O9	8.237	8.017	8.138
O1-----O10	7.567	7.511	7.562
O2-----O9	9.032	8.709	8.910
O2-----O10	8.995	8.887	8.993

[a] Average e.s.d. 0.004 Å.

In conclusion, the conformational parameters for the rifampicin molecules in the three solvated crystals generally span quite narrow ranges. Furthermore, the values of these parameters (interplanar angles between planes A and B and between planes B and C, dihedral angles, τ_1 - τ_{17}, spatial arrangement of O1, O2, O9 and O10 and their interatomic distances) fall within the ranges previously established as prerequisites for rifamycin antibiotic activity.[4]

Intra- and Intermolecular Interactions

Host Intramolecular Interactions

As discussed in the previous part, rifampicin is known to exist as a zwitterion in the solid state.[12] Again, a noteworthy observation is that the bond length C8-O2 is significantly shorter than those of the other C-O bonds which are in a similar chemical environment (distances listed in Table 30). Based on the data listed in the International Tables for Crystallography,[11] the typical distance for the C-O bond in the above chemical environment is 1.333 Å. Therefore, although bonds C14-O12, C1-O1 and C8-O2 are all represented as single bonds in Figure 19, the former two bonds can be confirmed as being single whilst C8-O2 has significant double bond character.

Table 30 Bond lengths C4-O12, C1-O1 and C8-O2 in the host molecule of each solvate.

Bond length (Å)	**P5**	**P6**	**P7**
C4-O12	1.360(7)	1.363(4)	1.364(4)
C1-O1	1.341(7)	1.351(4)	1.357(5)
C8-O2	1.280(8)	1.285(4)	1.280(5)

Furthermore, during the structural refinements of all four solvates, geometrically sensible electron density peaks, that qualified as potential H atoms, were found around all the hydroxyl oxygen atoms (O1, O9, O10, O12) except atom O2. At the same time, an extra peak was found around the N4 atom having an electron density value similar to the other peaks which had been assigned as hydrogen atoms. Also, between N4 and oxygen atoms of disordered water molecules, this specific peak was ideally located, accounting for the formation of a N^{+}-H···O hydrogen bond with very favourable geometry. Therefore, it can again be assumed that the proton transferred from the hydroxyl group on C8 to the nitrogen atom N4, forming a zwitterion as was found in the series of rifampicin solvates P1 – P4.

Three analogous intramolecular O-H···O hydrogen bond (H-bond) interactions were found in the host molecules of P5, P6 and P7, as listed in Table 31.

Table 31 Intramolecular O1-H1···O2, O10-H10···O9 and O12-H12···O4 H-bond interactions in the host molecules of the three solvates[a]

Hydrogen bond	O···O Distance (Å)	Angle (°)
P5		
O1-H1···O2	2.467(6)	149
O10-H10···O9	2.649(7)	147
O12-H12···O4	2.606(6)	168
P6		
O1-H1···O2	2.474(3)	149
O10-H10···O9	2.662(3)	148
O12-H12···O4	2.617(3)	166
P7		
O1-H1···O2	2.478(5)	148
O10-H10···O9	2.671(5)	147
O12-H12···O4	2.605(5)	169

[a] Where no e.s.d. is reported for the angle, H atoms involved were added in idealised positions in a riding model.

The distance between the hydrogen bond acceptor and donor, the hydrogen bond angles, the distance ranges and the angle ranges for the O-H···O interactions in the host molecules of each solvate are summarised in Table 32. The average distances for the O-H···O interactions are quite uniform.

Table 32 The mean distances and angles as well as their ranges for the O-H···O interactions in the host molecules of each solvate

O···O	**P5**	**P6**	**P7**
Average distance (Å)	2.57	2.58	2.59
Distance range (Å)	2.47 – 2.65	2.47-2.66	2.48 – 2.67
Average angle (°)	154.67	154.3	162.0
angle range (°)	147 – 168	148 – 166	148-169

Figure 23 shows the zwitterionic structure and the intramolecular O-H···O interactions for each rifampicin host molecule. The host molecules in each solvate adopt the same motif of intramolecular O-H···O interactions.

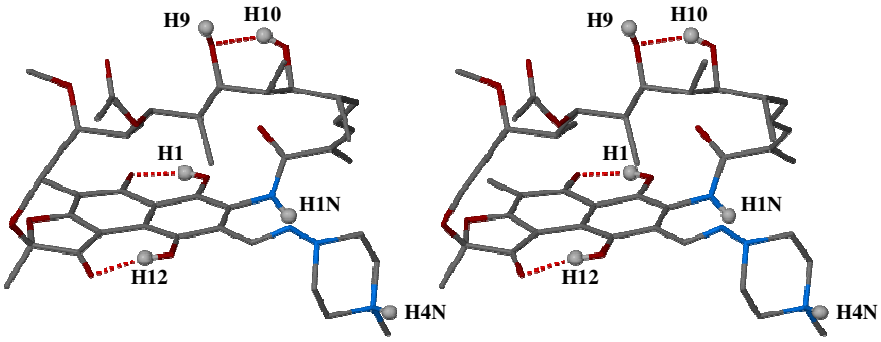

(a) P5

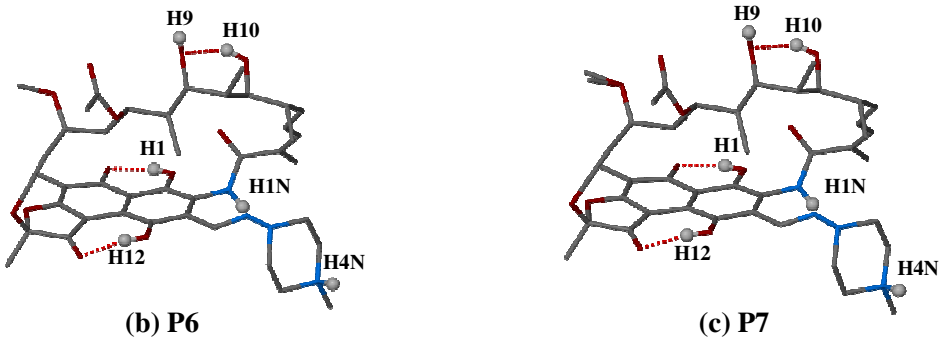

(b) P6 **(c) P7**

Figure 23 The zwitterionic structures and the intramolecular O-H···O interactions for each rifampicin host molecule. The relevant hydrogen atoms are shown as spheres. The other hydrogen atoms and the guest molecules are omitted for clarity. The host molecule in P5 is shown as a stereoview.

Several intramolecular C-H···O interactions (Table 33) were found to be associated with the rifampicin conformations in P5, P6 and P7. Identical hydrogen bond interactions are found to exist in the host molecule for each solvate.

.

Table 33 Intramolecular C-H···O interactions in the host molecules of the three solvates[a]

Hydrogen bond	C···O Distance (Å)	Angle (°)
P5		
C14-H14A···O3	2.905(8)	107
C18-H18···O11	2.999(8)	114
C23-H23···O7	2.940(9)	104
C25-H25···O8	2.726(8)	106
C25-H25···O9	2.886(7)	104
C27-H27···O7	2.872(8)	107
C28-H28···O3	3.105(8)	119
P6		
C14-H14A···O3	2.895(4)	107
C18-H18···O11	3.051(4)	113
C23- H23···O7	2.913(4)	106
C25-H25···O8	2.731(4)	105
C25-H25···O9	2.929(4)	104
C27-H27···O7	2.844(4)	107
C28-H28···O3	3.046(4)	118
P7		
C14-H14A···O3	2.885(6)	107
C18-H18···O11	3.020(6)	113
C23-H23···O7	2.923(5)	105
C25-H25···O8	2.734(7)	106
C25-H25···O9	2.886(5)	105
C27-H27···O7	2.830(6)	106
C28-H28···O3	3.116(6)	118

[a] Where no e.s.d. is reported for the angle, H atoms involved were added in idealised positions in a riding model.

The average distances, angles and their ranges for the intramolecular C-H···O interactions of each solvate are summarised in Table 34. The average distances are very similar in each host molecule, as are the average angles. This is consistent with the previous observations that indicated a high level of conformational similarity among the three independent rifampicin molecules.

Table 34 The average distances and angles as well as their ranges for the intramolecular C-H···O interactions in the host molecules of each solvate

C···O	**P5**	**P6**	**P7**
Average distance (Å)	2.92	2.92	2.91
Distance range (Å)	2.73 – 3.11	2.73-3.05	2.74 – 3.12
Average angle (°)	109	109	109
angle range (°)	104 – 119	104 – 118	105-118

In addition, these intramolecular O-H···O and C-H···O hydrogen bond interactions stabilise the conformations of the host molecules in P5, P6 and P7.

Host-host Interactions

No host-host intermolecular O-H···O interaction is observed in any of the structures. However, three common host-host intermolecular C-H···O interactions are found in P5, P6 and P7. The geometrical details of these interactions in the three solvates are listed in Table 35.

Table 35 Intermolecular C-H···O interactions between the rifampicin molecules[a]

Hydrogen bond	C···O Distance (Å)	Angle (°)	Symmetry operator[b]
P5			
C40-H40B···O8	3.336(10)	146	3/2-x, 2-y, 1/2+z
C41-H41A···O11	3.366(10)	136	-1/2+x, 3/2-y, 1-z
C43-H43A···O11	3.387(11)	138	-1/2+x, 3/2-y, 1-z
P6			
C40-H40B···O8	3.247(5)	143	3/2-x, 2-y, 1/2+z
C41-H41B···O11	3.429(4)	145	-1/2+x, 3/2-y, 1-z
C43-H43B···O11	3.437(6)	146	-1/2+x, 3/2-y, 1-z
P7			
C40-H40B···O8	3.348(7)	139	3/2-x, 2-y, 1/2+z
C41-H41B···O11	3.415(6)	140	-1/2+x, 3/2-y, 1-z
C43-H43C···O11	3.334(6)	149	-1/2+x, 3/2-y, 1-z

[a] Where no e.s.d. is reported for the angle, H atoms involved were added in idealised positions in a riding model.
[b] Symmetry operator only applies to hydrogen bond acceptors.

The mean distances and angles, and the ranges for the host-host intermolecular C-H···O interactions in each solvate are summarised in Table 36. The average C···O distances are very close in each solvate.

Table 36 The average distances and angles as well as their ranges for the host-host intermolecular C-H···O interactions in the host molecules of each solvate

C···O	**P5**	**P6**	**P7**
Average distance (Å)	3.36	3.37	3.36
Distance range (Å)	3.34 – 3.39	3.25 – 3.44	3.34 – 3.41
Average angle (°)	140	145	143
angle range (°)	136 – 146	143 – 146	139-150

These interactions stabilise two rifampicin molecules when they assemble. Furthermore, the existence of the common host-host intermolecular C-H···O interactions in the crystals of P5, P6 and P7 not only provides proof for the remarkable similarity in the conformations of the host molecules, but also indicates a high similarity of the molecular packing in each solvate.

Host-guest Interactions

The host-guest intermolecular O-H···O and N-H···O interactions in solvates P5, P6 and P7 are shown in Figure 24. Analogous interactions are found in each solvate.

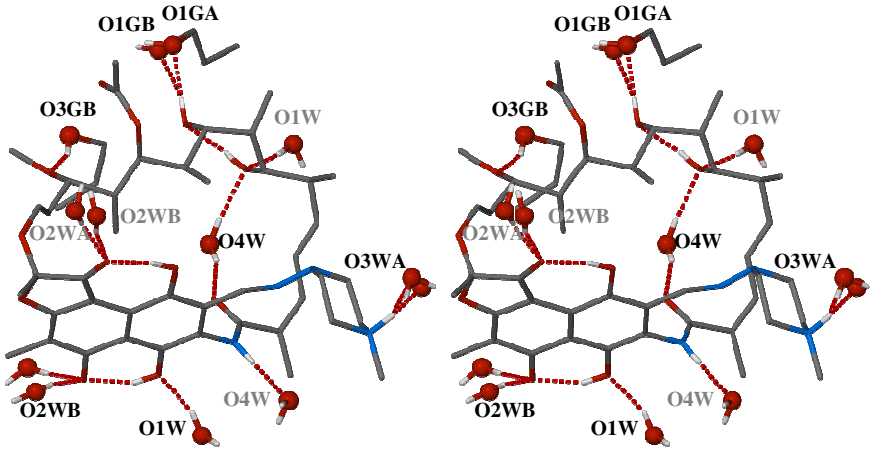

(a) P5

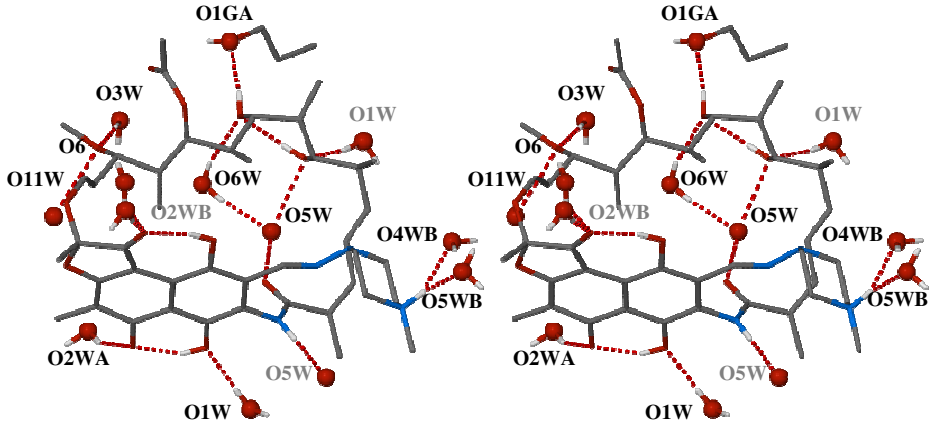

(b) P6

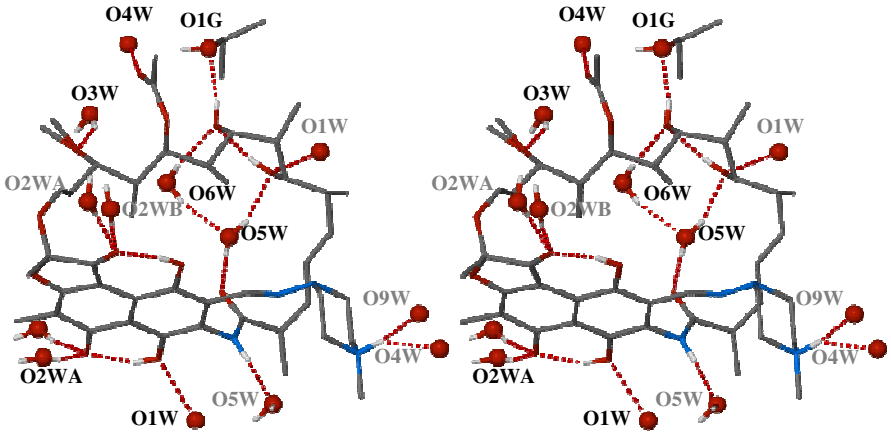

(c) P7

Figure 24 Stereoviews of the intermolecular O-H···O and N-H···O hydrogen bonds between the host and guest molecules in the solvates P5, P6 and P7. The oxygen atoms in the guest molecules are shown as spheres. The other hydrogen atoms and guest molecules are omitted for clarity. Atoms with gray labels have been symmetry-generated from their asymmetric unit counterparts.

For all the solvates, atoms N1 serve as hydrogen bond donor to a water molecule (O4W in P5, O5W in both P6 and P7), thus linking the water molecules to the ansa bridge of each rifampicin host molecule via the hydrogen bond N1-H1N···O_{water}. Atoms $N4^+$ also serve as hydrogen bond donor to water molecules which are disordered over two positions in all three cases. The hydrogen bonds $N4^+$-H4N···O_{water} connect the water molecules to the piperazinyl substituent of each host molecule. Table 37 lists the distances between hydrogen bond donors (N1 and N4) and acceptor (water molecules) as well as the angles subtended at the hydrogen atom in the three solvates.

Table 37 Intermolecular N1-H1N···O_{water} and $N4^+$-H4N···O_{water} H-bond interactions in the three solvates[a]

Hydrogen bond	N···O Distance (Å)	Angle (°)	Symmetry operator[b]
P5			
N1-H1N···O4W	2.878(6)	166	-1/2+x, 3/2-y, 1-z
N4-H4N···O3WA	3.103(17)	139	x, y, z
N4-H4N···O3WB	2.62(2)	157	x, y, z
P6			
N1-H1N···O5W	2.921(3)	169	-1/2+x, 3/2-y, 1-z
N4-H4N···O4WA	2.585(6)	163	x, y, z
N4-H4N···O4WB	2.914(6)	158	x, y, z
P7			
N1-H1N···O5W	2.906(4)	164	-1/2+x, 3/2-y, 1-z
N4-H4N···O9W	2.78(2)	163	3/2-x, 2-y, 1/2+z
N4-H4N···O4W	2.799(7)	143	3/2-x, 2-y, 1/2+z

[a] Where no e.s.d. is reported for the angle, H atoms involved were added in idealised positions in a riding model.
[b] Symmetry operator only applies to hydrogen bond acceptors.

The average distances and angles for the host-guest intermolecular N-H···O interactions for the three solvate molecules are summarised in Table 38. The mean distances are very close (~ 2.8 Å) in all cases.

Table 38 The average distances and angles for the host-guest intermolecular N-H···O interactions in all solvate molecules

N···O	**P5**	**P6**	**P7**
Average distance (Å)	2.87	2.81	2.83
Average angle (°)	154	164	157

For host-guest intermolecular O-H···O interactions, very similar but not identical H-bond interactions can be found among the three cases. For all the solvates, the hydroxyl

groups O9-H serve as H-bond donors and function as bridges which stabilise the ansa chain in one host molecule with an alcohol molecule. This is the only hydroxyl oxygen which functions as a donor in host-guest H-bond intermolecular interaction. Furthermore, O9 atoms also serve as H-bond acceptor to water molecules; however, this occurs only in P6 and P7, not in P5 (Figure 24).

Atoms O1, O2, O4, O6, O10 and O11 serve as H-bond acceptors to water molecules (except O6 H-bonded to an alcohol molecule in P5), thus associating host with water molecules. Furthermore, O6 functions as acceptor to two distinct water molecules simultaneously only in P6 while O10 serves as acceptor to two distinct water molecules in all three cases. Notably, hydroxyl oxygen O12 is not involved in guest-host intermolecular interactions in any solvate.

Water molecules O4W in P5 as well as O5W in P6 and P7 stabilise each independent host molecule by serving as H-bond donors to O11 and O10 on the ansa chain simultaneously. Atoms O1W and O2WB in P5, P6 and P7 as well as atoms O2WA in P5 and P7 form a long hydrogen bonded chain O9···O10···O1W···O1···O2···O2WB(O2WA)···O4···O12, which connects the ansa bridge (O9 and O10) in one host molecule with the chromophore plane (O1 and O2) in a second host molecule through O1W; the latter is then associated with the chromophore plane (O4 and O12) of a third host molecule through O2WB (O2WA), as shown in Figure 25.

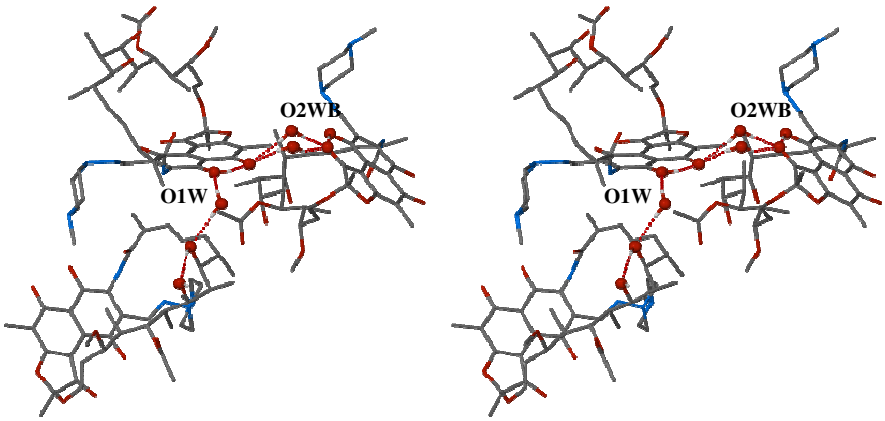

Figure 25 Representative stereoview of the long hydrogen bonded chain O9···O10···O1W···O1···O2···O2WB (O2WA)···O4···O12 in P5. The relevant oxygen atoms are shown as spheres.

The geometrical details of the above hydrogen bonds are listed in Table 39. Due to the low site-occupancy of some water molecules, their hydrogen atoms could not be located. In P5, the distance between the hydrogen bond donor (O2WA) and the acceptor (O2) is very short, implying strong hydrogen bonding.

Table 39 Host-guest intermolecular O-H···O interactions in three solvates[a]

Hydrogen bond	O···O Distance (Å)	Angle (°)	Symmetry operator[b]
P5			
O9-H9···O1GA	2.696(11)	175	x, y, z
O9-H9···O1GB	2.847(13)	155	x, y, z
O1W-H1W1···O1	2.782(6)	159(1)	x, y, z
O2WA-H2W1···O2	2.594(12)	169(5)	x, y, z
O2WB-H2W3···O2	2.898(13)	168(6)	x, y, z
O2WA-H2W2···O4	2.688(12)	159(15)	1-x, 1/2+y, 1/2-z
O2WB-H2W4···O4	2.786(13)	167(13)	1-x, 1/2+y, 1/2-z
O3GB-H3GB···O6	3.135(17)	150	x, y, z
O1W-H1W2···O10	2.802(7)	174(6)	1/2+x, 3/2-y, 1-z
O4W-H4W2···O10	2.840(7)	173(5)	x, y, z
O4W-H4W1···O11	2.743(6)	163(5)	x, y, z
P6			
O9-H9···O1GA	2.744(4)	172	x, y, z
O6W-H6W2···O9	3.016(3)	168(2)	x, y, z
O1W-H1W1···O1	2.815(3)	174(2)	x, y, z
O2WA-H2W1···O2	2.805(5)	157(2)	x, y, z
O2WA-H2W2···O4	2.674(5)	146(2)	1-x, 1/2+y, 1/2-z
O2WB-H2W3···O4	2.865(6)	167(5)	1-x, 1/2+y, 1/2-z
O3W-H3W2···O6	2.918(6)	168(3)	x, y, z
O11W···O6	2.88(2)	--------	x, y, z
O1W-H1W2···O10	2.819(4)	163(2)	1/2+x, 3/2-y, 1-z
O5W···O10	2.776(3)	--------	x, y, z
O5W···O11	2.685(3)	--------	x, y, z
P7			
O9-H9···O1G	2.715(5)	168	x, y, z
O6W-H6W2···O9	3.042(6)	172(4)	x, y, z
O1W···O1	2.791(8)	--------	x, y, z
O2WA-H2W2···O2	2.654(6)	170(3)	x, y, z
O2WB-H2W3···O2	2.955(12)	166(5)	x, y, z
O2WA-H2W1···O4	2.720(6)	169(4)	1-x, 1/2+y, 1/2-z
O2WB-H2W4···O4	2.843(13)	164(7)	1-x, 1/2+y, 1/2-z
O3W-H3W2···O6	2.828(7)	151(3)	x, y, z
O5W-H5W1···O10	2.774(5)	161(2)	x, y, z
O1W···O10	2.742(8)	--------	1/2+x, 3/2-y, 1-z
O5W-H5W2···O11	2.719(4)	178(8)	x, y, z

[a] Where no e.s.d. is reported for the angle, H atoms involved were added in idealised positions in a riding model.

[b] Symmetry operator only applies to hydrogen bond acceptors.

The mean distances and angles as well as ranges for the host-guest intermolecular O-H···O interactions in each solvate are summarised in Table 40. The mean distances are very close in each solvate.

Table 40 The average distances and angles as well as their ranges for the host-guest intermolecular O-H···O interactions in the three solvates.

O···O	**P5**	**P6**	**P7**
Average distance (Å)	2.80	2.82	2.80
Distance range (Å)	2.594 – 3.135	2.67 – 3.02	2.65 – 3.04
Average angle (°)	164.7	164.4	166.6
angle range (°)	150 – 175	146 – 172	151 – 178

Several host-guest intermolecular C-H···O interactions are found in the structures of P5, P6 and P7. Geometrical details are listed in Table 41.

Table 41 Intermolecular C-H···O interactions between the rifampicin and guest molecules[a]

Hydrogen bond	C···O Distance (Å)	Angle (°)	Symmetry operator[b]
P5			
C40-H40···O4W	3.421(10)	159	-1/2+x, 3/2-y, 1-z
C42-H42B···O3WA	3.310(17)	130	x, y, z
P6			
C14-H14C··· O2WA	3.397(6)	139	x, y, z
C40-H40A···O5W	3.416(4)	164	-1/2+x, 3/2-y, 1-z
C41-H41A···O1W	3.275(5)	130	-1/2+x, 3/2-y, 1-z
P7			
C37A-H37D···O3W	3.103(13)	113	x, y, z
C40-H40A···O5W	3.409(6)	160	-1/2+x, 3/2-y, 1-z

[a] Where no e.s.d. is reported for the angle, H atoms involved were added in idealised positions in a riding model.
[b] Symmetry operator only applies to hydrogen bond acceptors.

The average distances and angles for the host-guest intermolecular C-H···O interactions for each solvate are summarised in Table 42. The mean distances are close (~ 3.3 Å) in all cases.

Table 42 The average distances and angles for the host-guest intermolecular C-H···O interactions in the three solvates.

C···O	**P5**	**P6**	**P7**
Average distance (Å)	3.37	3.36	3.26
Average angle (°)	144.5	144.3	136.5

Guest-guest Interactions

For the three solvates, guest molecules (water and 1-propanol/iso-propanol molecules) display a variety of disordered arrangements. Furthermore, the 1-propanol molecule can be disordered in many different ways. Figure 26 illustrates the different disordered motifs of 1-propanol molecules in P5 and P6.

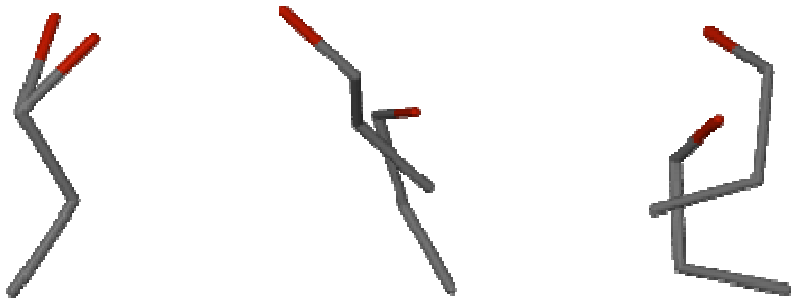

(a) **(b)** **(c)**

Figure 26 Disordered 1-propanol molecules (a) O1GA/O1GB-C1GA-C2GA-C3GA in P5, (b) O3GA-C7GA-C8GA-C9GA and O3GB-C7GB-C8GB-C9GB in P5, (c) O2GB-C4GB-C5GB-C6GB and O3GA-C7GA-C8GA-C9GA in P6.

In the structures of P5, P6 and P7, guest clusters are formed by the alcohol and water molecules, as shown in Figure 27.

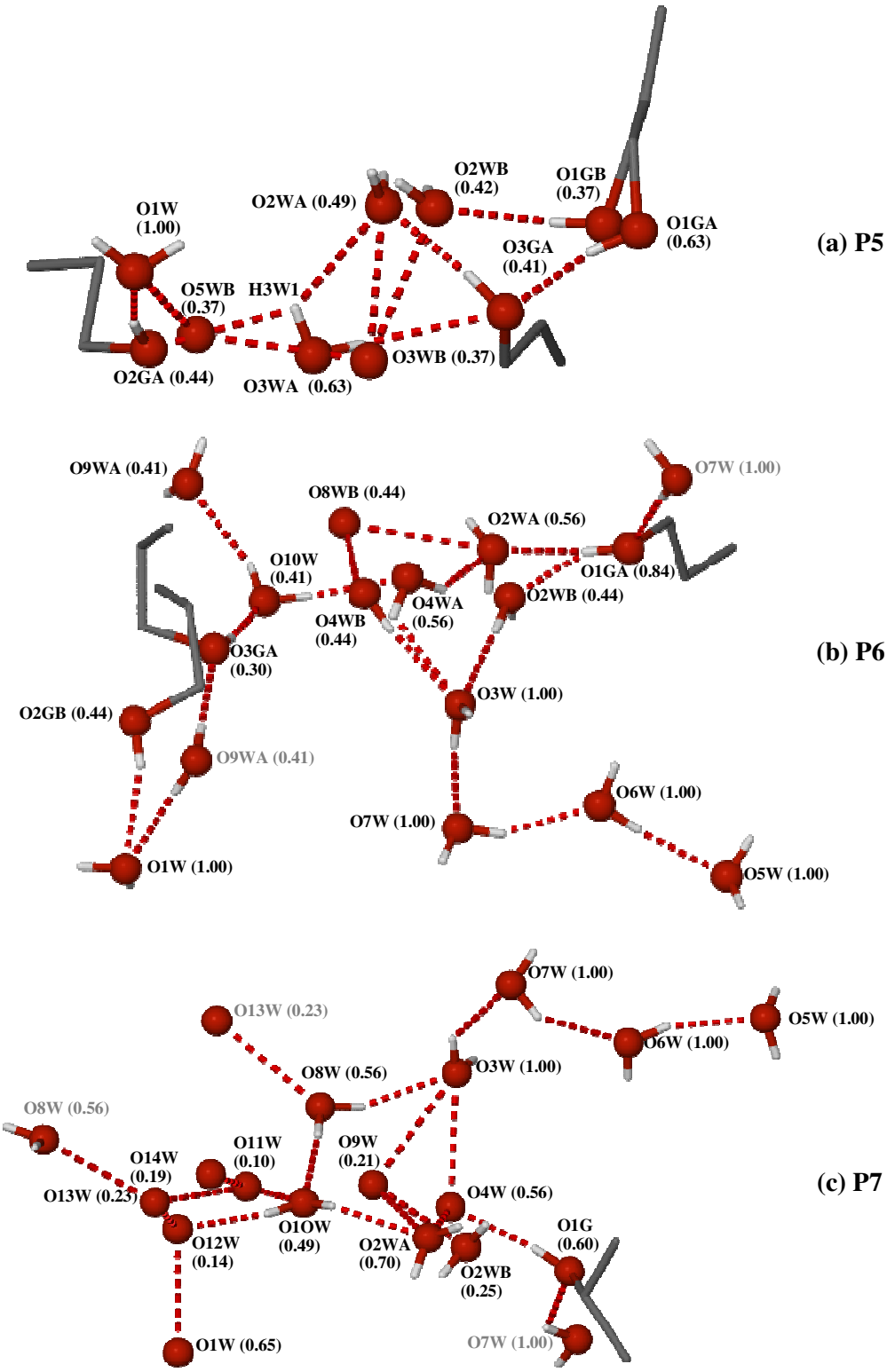

Figure 27 The guest-guest intermolecular O-H···O interactions among the water and alcohol molecules in (a) P5, (b) P6 and (c) P7. Atoms with gray labels have been symmetry-generated from their asymmetric unit counterparts. The disordered atoms are labelled with their site-occupancies.

In P5, the guest cluster is completely isolated. Water molecule O4W and the 1-propanol molecule O3GB-C7GB-C8GB-C9GB are two isolated guest molecules. The former occupies the cavity of the ansa chain while the latter is linked to atom O6 in the host molecule (shown in Figure 24). In the guest cluster, water molecule O5W is located very close to the hydrogen bond O3WA-H3W1···O2GA. Furthermore, three solvent sites (O5W, O2GA-C4GA-C5GA-C6GA and O3WA) are not fully-occupied. In addition, O5W is hydrogen bonded to O3WB which is then hydrogen bonded to disordered water molecules O2WA and O2WB. Also, O3WA is situated very close to the hydrogen bond O5W···O3WB. A noteworthy observation is that the hydrogen H3W1 in O3WA is involved in a bifurcated hydrogen bond with O2GA and O2WA.

In P6, an infinitely extended guest cluster and an isolated water molecule O11W can be observed. Atom O4WB is located very close to the hydrogen bond O10W-H101···O4WA and both O4WA and O4WB function as H-bond donors to O3W. O11W is only hydrogen bonded to O6 in the host molecule (Figure 24). In addition, O11W occupies a unique position compared with the situation in the other two solvates.

In P7, all the guest molecules assemble in a cluster which extends infinitely. A variety of disordered arrangements involving water molecules occurs.

The geometrical details of the guest-guest intermolecular O-H···O hydrogen bond interactions in the three solvates are listed in Tables 43, 44 and 45.

Table 43 Guest-guest intermolecular H-bond interactions in solvate P5[a]

Hydrogen bond	O···O Distance (Å)	Angle (°)	Symmetry operator[b]
O2GA-H2GA···O1W	2.66(2)	163.0	x, y, z
O5WB···O1W	2.96(2)	------	x, y, z
O5WB···O3WB	2.81(3)	------	1/2+x, 3/2-y, 1-z
O3WB···O2WA	2.648	------	x-1/2, 3/2-y, 1-z
O3WB···O2WB	2.754	------	x-1/2, 3/2-y, 1-z
O3WA-H3W1···O2GA	2.716	98.5	x-1/2, 3/2-y, 1-z
O3WA-H3W1···O2WA	2.756	105.7	x-1/2, 3/2-y, 1-z
O3WA-H3W2···O3GA	3.160	153.9	3/2-x, 2-y, 1/2+z
O3GA-H3GA···O2WA	2.656	168.2	2-x,1/2+y, 1/2-z
O1GA-H1GA···O3GA	2.697	154.3	x, y, z
O1GB-H1GB···O2WB	2.873	174.7	2-x, 1/2+y, 1/2-z

[a] Average e.s.d.s 0.009 Å for distance and 0.3° for angle
[b] Symmetry operator only applies to hydrogen bond acceptors.

Table 44 Guest-guest intermolecular H-bond interactions in solvate P6[a]

Hydrogen bond	O···O Distance (Å)	Angle (°)	Symmetry operator[b]
O2GB-H2GB···O1W	2.805(7)	157.0	x, y, z
O3GA-H3GA···O10W	2.793	171.7	x, y-1, z
O10W-H102···O9WA	2.85(2)	160.4	x-1/2, 3/2-y, 1-z
O10W-H101···O4WA	2.76(1)	174.0	x, y, z
O4WA-H4W1···O2WA	2.714(7)	139.0	-1/2+x, 3/2-y,1-z
O4WA-H4W2···O3W	2.653(6)	123.4	3/2-x, 2-y, 1/2+z
O4WB-H4W3···O8WB	2.75(1)	150.7	x, y, z
O8WB···O2WA	2.877	------	x-1/2, 3/2-y, 1-z
O4WB-H4W4···O3W	2.771	168.5	3/2-x, 2-y, 1/2+z
O3W-H3W1···O7W	2.753	168.5	x, y, z
O7W-H7W1···O6W	2.739	156.7	x, y, z
O6W-H6W1···O5W	2.813	173.0	x, y, z
O2WB-H2W4···O3W	2.974	173.7	2-x, y-1/2, 1/2-z
O1GA-H1GA···O2WA	2.931	160.9	2-x, 1/2+y, 1/2-z
O1GA-H1GA···O2WB	2.531	154.4	2-x, 1/2+y, 1/2-z
O7W-H7W2···O1GA	2.837	174.5	2-x, y-1/2, 1/2-z
O9WA-H9W2···O3GA	2.736	178.2	x, y, z
O9WA-H9W1···O1W	2.739	172.9	x, y, z

[a] Average e.s.d.s 0.005 Å for distance and 0.8° for angle
[b] Symmetry operator only applies to hydrogen bond acceptors.

Table 45 Guest-guest intermolecular H-bond interactions in solvate P7[a]

Hydrogen bond	O···O Distance (Å)	Angle (°)	Symmetry operator[b]
O8W···O3W	2.823	------	2-x, y-1/2, 1/2-z
O13W···O11W	3.090	------	1-x, 1/2+y, 1/2-z
O11W···O14W	3.045	------	1-x, y-1/2, 1/2-z
O13W···O12W	2.879	------	1-x, 1/2+y, 1/2-z
O12W···O1W	2.59(3)	------	x, y, z
O10W-H102···O12W	2.699	165.2	x, y, z
O10W-H101···O2WA	2.749	139.6	x, y, z
O8W-H8W2···O10W	2.768	173.0	x, y, z
O8W-H8W1···O3W	2.824(9)	151.7	2-x, y-1/2, 1/2-z
O3W···O9W	2.90(2)	------	x, y, z
O9W···O2WA	2.59(3)	------	2-x, 1/2+y, 1/2-z
O9W···O2WB	2.724	------	2-x, 1/2+y, 1/2-z
O2WA···O4W	2.642	------	2-x, y-1/2, 1/2-z
O4W···O3W	2.725(7)	------	x, y, z
O3W-H3W1···O7W	2.842(7)	138.4	x, y, z
O7W-H7W1···O6W	2.806(7)	136.2	x, y, z
O6W-H6W1···O5W	2.802(6)	158.4	x, y, z
O1G-H1G···O4W	2.745	169.1	x, y, z
O7W-H7W2···O1G	2.887(6)	121.6	2-x, y-1/2, 1/2-z
O8W···O13W	2.712	------	3/2-x, 1-y, 1/2+z

[a] Average e.s.d.s 0.004 Å for distance and 0.7° for angle
[b] Symmetry operator applies to hydrogen bond acceptor atoms.

The average distances, average angles, the distance ranges and the angle ranges for the guest-guest intermolecular O-H···O interactions for the three solvates are summarised in Table 46 (bifurcated hydrogen bonds O3WA-H3W1···O2GA and O3WA-H3W1···O2WA in P5 are not considered). The mean distances for the intermolecular guest-guest O···O interactions in P5, P6 and P7 are very close (~ 2.8 Å).

Table 46 The average distances and angles as well as their ranges for the guest-guest intermolecular O-H···O interactions in all three solvates.

O···O	**P5**	**P6**	**P7**
Average distance (Å)	2.79	2.78	2.79
Distance range (Å)	2.66 – 3.66	2.53 – 2.97	2.59 – 3.09
Average angle (°)	163	162	150
angle range (°)	153.9 – 168.2	123.0 – 178.2	121.3 – 173.0

No significant intermolecular guest-guest C-H···O interactions occur in the structures of P5 – P7.

Overall Intramolecular and Intermolecular Interactions in P5, P6 and P7

Figure 28 shows the overall hydrogen bond interactions in solvates P5, P6 and P7. A common assembly of five rifampicin molecules around the solvent cluster is observed in each solvate structure. The same set of oxygen and nitrogen atoms in the five symmetry-related rifampicin molecules of solvates P5 – P7 is involved in hydrogen bonding with guest molecules. In other words, although the content of the solvent cluster is different in each solvate, the hydrogen bonding environments provided by the rifampicin molecules are identical in P5, P6 and P7.

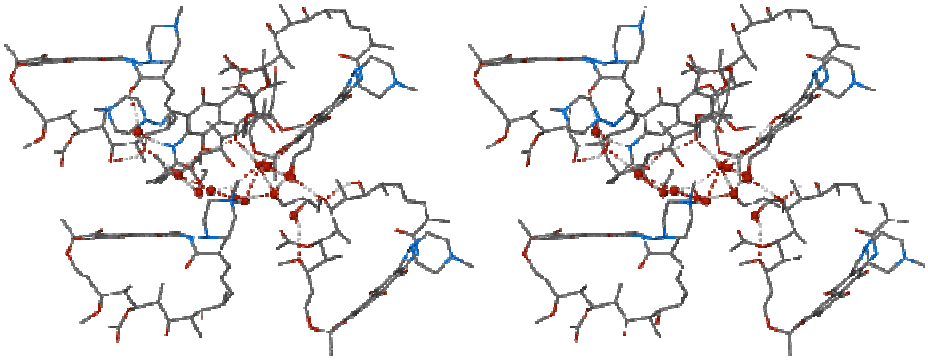

(a) P5

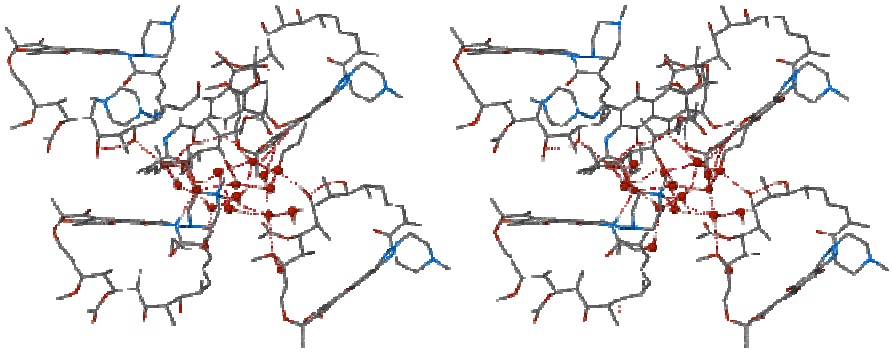

(b) P6

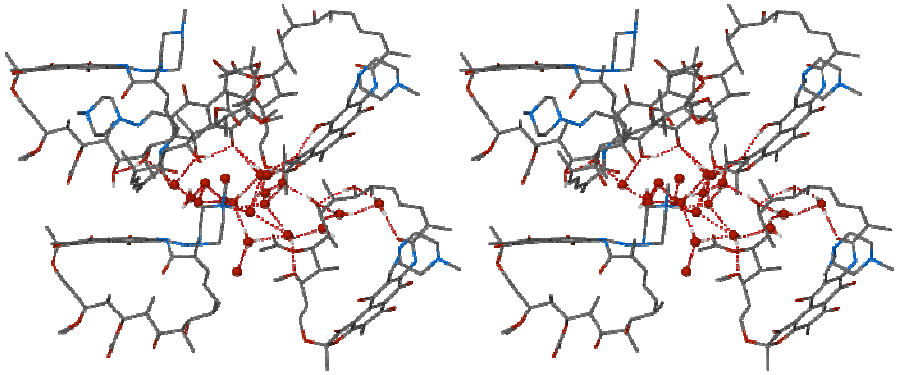

(c) P7

Figure 28 Stereoviews of the overall hydrogen bond interactions in (a) P5, (b) P6 and (c) P7. The oxygen atoms in the guest molecules are shown as spheres.

Crystal Packing

The packing arrangements for solvates P5, P6 and P7 [Figures 29 (a), (b) and (c)] are identical. This arrangement gives rise to solvent tunnels [Figure 29 (d)] along the *a*-axis, which provide the possibility of facile replacement of solvent molecules in the crystals with water molecules in the atmosphere.

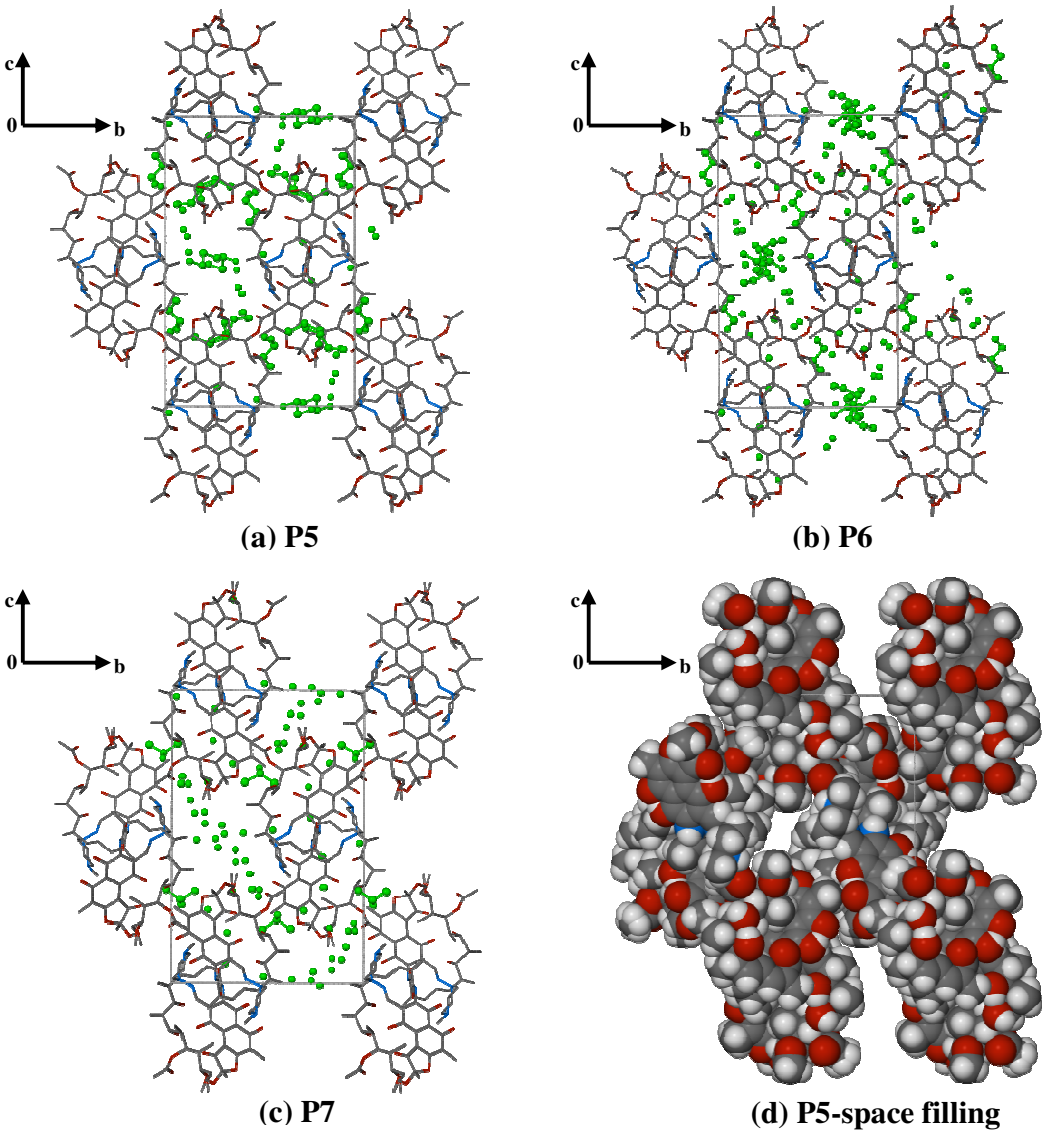

Figure 29 Crystal packing diagrams for (a) P5, (b) P6 and (c) P7 viewed along [100]; solvent molecules are shown as green spheres for clarity. (d) Solvents channels viewed along [100]. Rifampicin host molecules are drawn in space-filling mode and guest molecules are omitted.

The solvent channels for P5, P6 and P7 were examined using the program SECTION[14], which was used to view planes through the unit cells along the *a*-axis. The sections for P6 are shown in Figure 30 as representatives of those for P5, P6 and P7. A series of views taken at regular intervals along the *a*-axis clearly illustrates the continuous channels in which the guest molecules are accommodated.

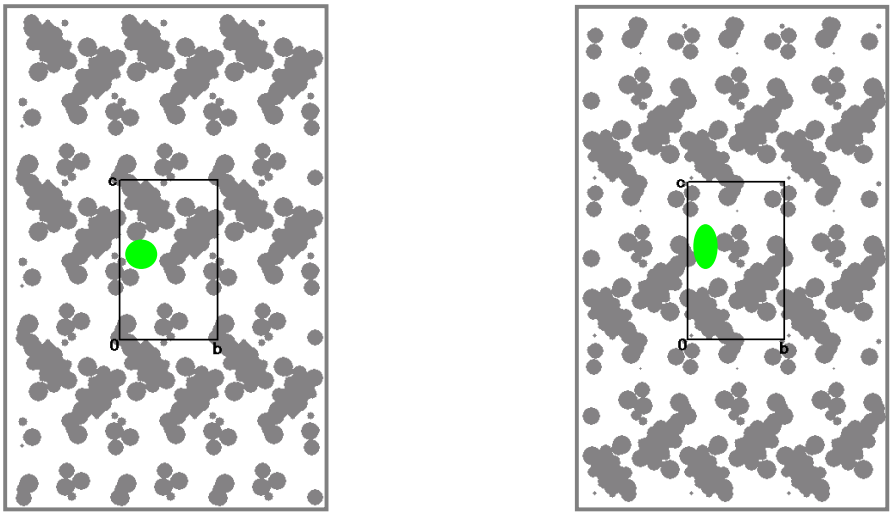

(a) 0 Å **(b) 6.5 Å**

Figure 30 Sections of P6 with guest molecules omitted and host molecules represented by gray areas, viewed along [100] with the unit cell sectioned at (a) 0 Å (b) 6.5 Å from the origin 0,0,0. A representative channel location is shown in green.

Comparative PXRD

The calculated and experimental PXRD traces for solvates P5, P6 and P7 are shown in Figure 31. For all three solvates, the experimental PXRD traces are in reasonable agreement with the calculated ones, confirming that each prepared sample was homogeneous. Corresponding PXRD peaks for the solvates P5 – P7 generally have different intensities. This is expected since their solvent contents differ. Preferred orientation in experimental samples is another factor that contributes to the differences.

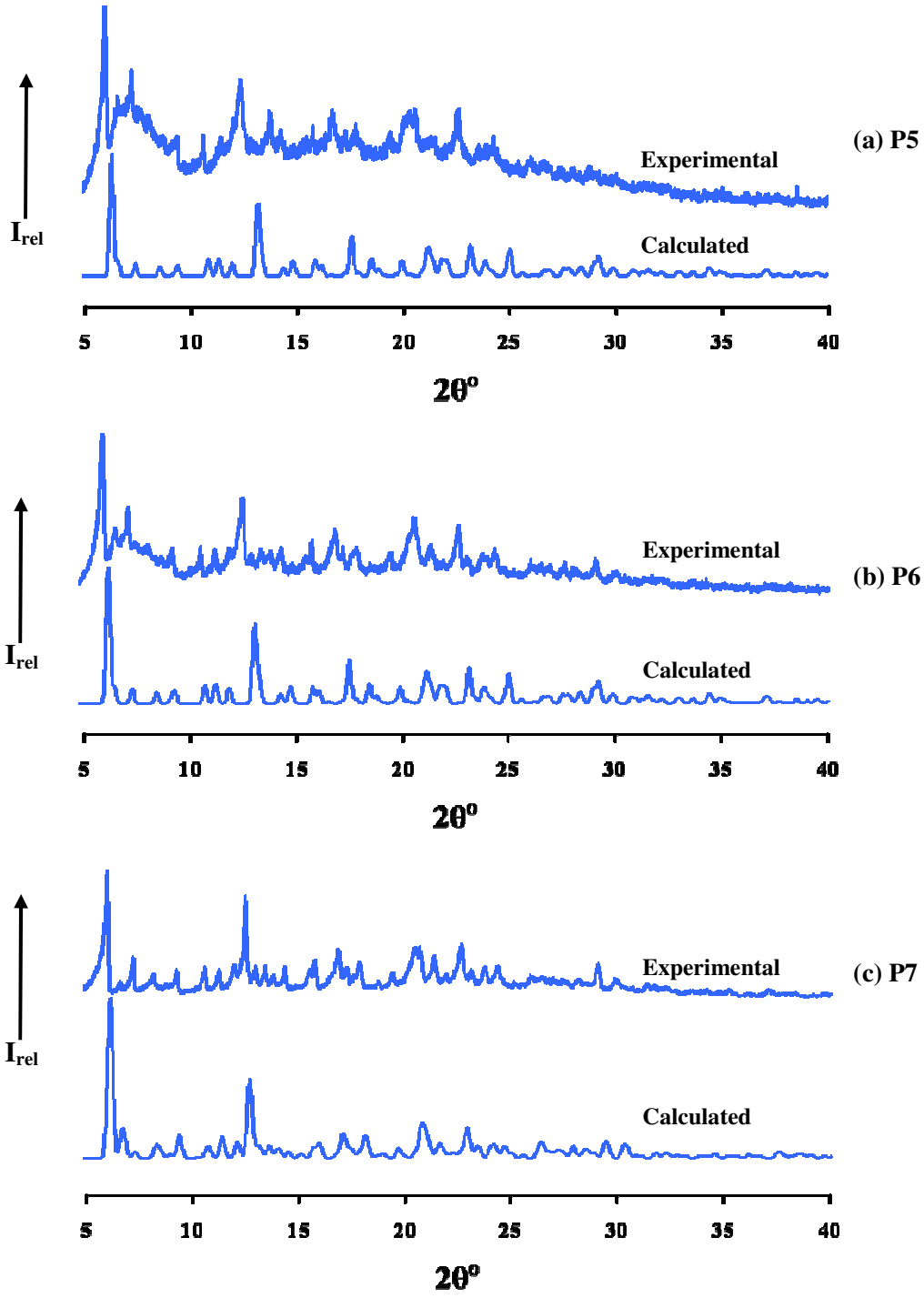

Figure 31 Calculated and experimental PXRD traces for (a) P5, (b) P6 and (c) P7.

Conclusion

Isostructurality

The solvates P5, P6 and P7 display similar unit cell dimensions (a = ~13, b = ~17, c = ~26 Å, $\alpha = \beta = \gamma = 90°$), and crystallise in the same space group $P2_12_12_1$. Their calculated PXRD traces are stacked here for comparison as presented in Figure 32. A remarkable similarity can be found among the three traces. In addition, the three – dimensional packing arrangements of the drug molecules in each solvate are the same (Figure 29). Furthermore, the host molecules in the three solvates adopt similar conformations evidenced by the fact they are superimposable (Figure 20). Consequently, P5, P6 and P7 are identified as isostructural compounds with regard to the uniform host rifampicin molecular assemblies. Also, any of the calculated PXRD patterns in Figure 32 could serve as a reference for the identification of future crystalline forms belonging to this isostructural series. [15]

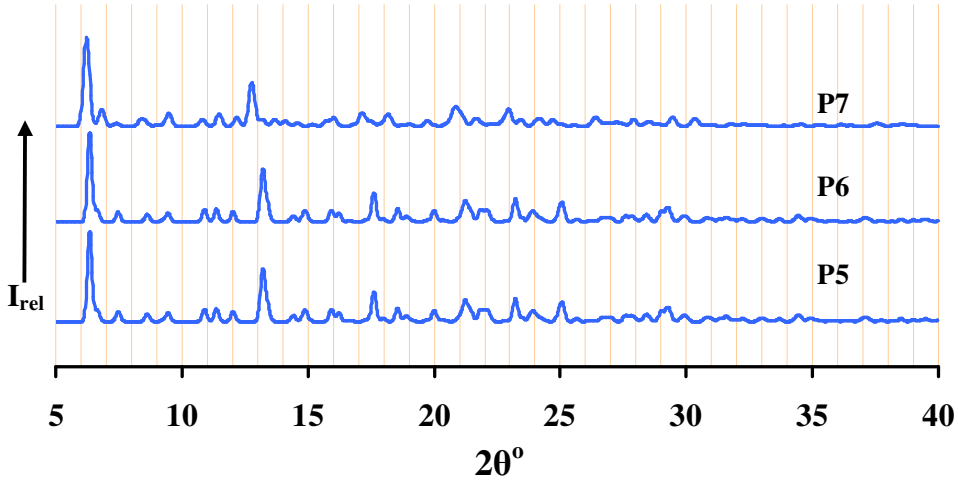

Figure 32 Calculated PXRD traces for solvates P5, P6 and P7.

Guest Exchange

Crystals of P5 were converted to a solvate with a different solvent composition after equilibrating with the atmosphere for a certain period. This can be explained as spontaneous guest exchange from alcohol molecules to atmospheric water molecules. For the crystals which had experienced a one-week exposure to the atmosphere, single crystal X-ray structure determination was attempted to examine the structural change, if

any. However, the attempt failed since the crystals cracked during the guest exchange process. TGA and PXRD analyses were then carried out to characterise the nature of these crystals. The PXRD pattern revealed that a phase change had occurred during the equilibration. The TGA result showed a mass loss during the heating process. However, the exact composition of the solvent content in the phase could not be determined from the above data.

Conformation of the Rifampicin Host Molecules

The similarity of the hosts of P5, P6 and P7 was demonstrated in the overlay diagram (Figure 20) and reflected in the parameters that described the similar dihedral angles among the three principal planes (Table 27) and similar torsion angles along the ansa chain (Table 28). A considerable difference can be observed between the conformations of the rifampicin molecule in the two isostructural series 1 (P1 – P4) and 2 (P5 – P7), as shown in Figure 33. In the former series, the piperazinyl moiety is linked to the rest of the molecule through an equatorial N3-N2 bond, whereas in the latter, this bond is axial. Furthermore, the O11 atom in the former points away from the ansa chain while that in the latter points towards the ansa chain. In other words, atoms O11 point in different directions in the host molecules in series 1 and 2. Therefore, the structures of host molecules in series 1 and those in series 2 can be identified as two significantly different conformations of the rifampicin molecules.

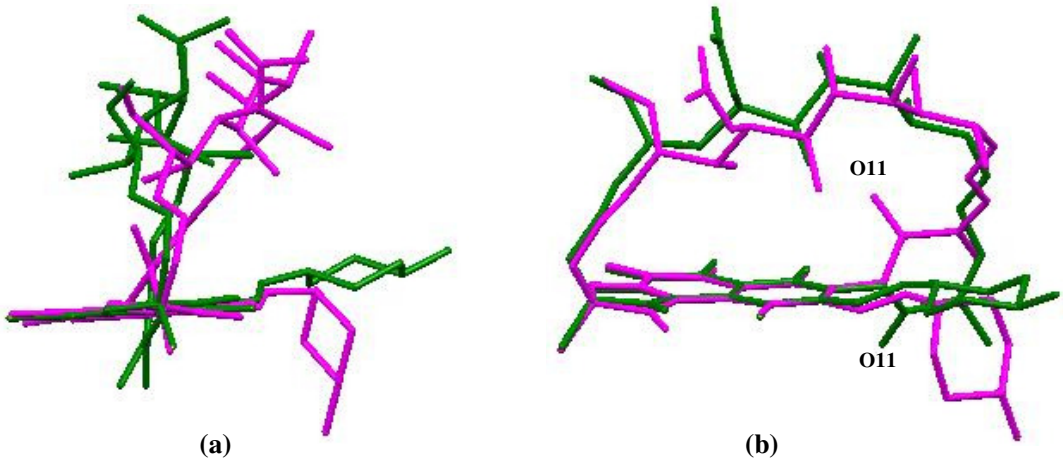

Figure 33 An overlay diagram of the rifampicin molecules in P1 (green) and P5 (red). Guest molecules and hydrogen atoms are omitted for clarity. (a) View side-on with respect to the ansa chain, (b) view normal to the ansa chain backbone.

A common feature in all of the rifampicin molecules in solvates P1 – P7 is their zwitterionic nature, resulting from proton transfer from a hydroxyl group on the chromophore to nitrogen atom N4 of the piperazinyl ring.

However, in both series 1 and 2, these host molecules all adopt an open conformation, which leads to the conclusion that the two conformationally different rifampicin molecules both adopt antibiotically active conformations in the solid state, i.e. their conformational parameters fall within the ranges associated with biological activity.[4]

Host-host Intramolecular and Intermolecular Hydrogen Bond Interactions

Since the packing modes of the three solvates P5 – P7 are almost identical, the host-host O-H···O and C-H···O intramolecular hydrogen bonds have identical hydrogen bond donors and acceptors. Furthermore, the average interatomic O···O distance is very similar in each solvate. This also applies to C···O distances. It is noteworthy that no host-host O···O intermolecular hydrogen bonds or π-π interactions are found in the solvates.

In addition, the hydrogen bond donors and acceptors of host-host O···O intramolecular interactions in series 2 are identical with those in series 1 except that hydrogen bond N1-H1N···N2 occurs in the latter. This is associated with the equatorial configuration of the piperazinyl substituent in series 1.

Guest-host Hydrogen Bond Interactions

Atoms O1, O2, O4, O6, O10, O11, N1 and $N4^+$ in the rifampicin host molecule are involved in the guest-host intermolecular hydrogen bond motif. This applies to each solvate due to the almost identical common crystal packing arrangement. However, O6 functions as acceptor to two distinct water molecules simultaneously only in P6 while O9 serves as H-bond acceptor to water molecules only in P6 and P7. Furthermore, both N1 and $N4^+$ atoms function as hydrogen bond donors to water molecules in all three cases.

The fact that the piperazinyl substituent adopts an axial configuration in isostructural series 2 gives rise to the interaction N1···O_{water} which cannot be observed in the structures of series 1.

Guest-guest Hydrogen Bond Interactions

The water and alcohol molecules are generally described as guest molecules in all three solvates. They display a variety of disordered arrangements. For example, most of the water molecule sites are partially occupied. Therefore, the hydrogen bond networks are very complicated in all three cases. In the structure of the crystal of P5, whose data were collected immediately following its removal from the mother liquor, the guest molecules (except the water molecule O4W and 1-propanol molecule O3GB-C7GB-C8GB-C9GB) assemble to form an isolated solvent cluster that is closely associated with five neighbouring rifampicin molecules. In the structure of P6, which resulted from exposure of P5 to the atmosphere for a period of 10 hours, an infinitely extended guest cluster and an isolated water molecule O11W can be observed. However, although the data for the crystals of P7 were collected immediately following their removal from mother liquor, all the guest molecules in the structure of P7 assemble into a guest cluster which extends infinitely. The average O···O distance of guest-guest O-H···O interactions in series 2 is very close to that in series 1 (~2.8 Å).

Crystal Packing

Despite the subtle differences in the conformations of the host molecules and the different content of guest molecules in each crystal, solvates P5, P6 and P7 pack in almost identical modes. Solvent molecules are located in the continuous channel parallel to the *a*-axis. This channel provides access to atmospheric water molecules which can enter the crystal, changing the compositions of the entrapped solvent mixtures. Infinite solvent channels which allow easy guest exchange can be found in both solvate series 1 and 2. The difference between the packing arrangements of series 1 and 2 will be discussed further in Part Three, where we also report a series of four distinct rifampicin solvates with different unit cell dimensions and packing arrangements.

Part Three

Here we report the isolation and characterisation of four distinct rifampicin solvates that contain water and one of each of the solvents iso-propanol, 1-butanol, ethylene glycol and 1,4-dioxane. The host conformation and PXRD patterns of each solvate will be discussed together; however, the intra- and intermolecular interactions as well as packing arrangements in each solvate will be discussed separately.

Crystal Preparation

The abbreviations for the discrete rifampicin solvates in this chapter are as follows:

2rifampicin • 4.30iso-propanol • 14.7H_2O:	P8
2rifampicin • 5.53(1-butanol) • 1.40H_2O:	P9
2rifampicin • 5.75ethylene glycol • 5.59H_2O:	P10
2rifampicin • 6(1, 4-dioxane) • 3H_2O:	P11

Suitable crystals of P8 were obtained by dissolving 0.020 g (0.024 mmol) of the host drug (rifampicin) in 2 ml of (iso-propanol)-acetone-water mixture (3:14:3 v /v /v) at 25 ^oC. The solution was then filtered. Crystals of suitable quality appeared by slow evaporation at 4 ^oC over a period of two weeks. It is noteworthy that the only difference between the crystal preparation methods of P7 (also containing isopropanol and water) and P8 is that the solution was not filtered in the former but was filtered in the latter.

Suitable crystals of P9 and P10 were obtained by dissolving 0.020 g (0.024 mmol) of the host drug (rifampicin) in 2 ml of 1-butanol-water mixture (9:1 v/v) and ethylene glycol-ethanol-water mixture (3:15:2 v/v/v) at 25 ^oC, respectively. The solutions were then filtered. Crystals of suitable quality appeared by slow evaporation at 4 ^oC over a period of two weeks.

Suitable crystals of P11 were obtained by dissolving 0.020 g (0.024 mmol) of the host drug (rifampicin) in 2 ml of 1, 4-dioxane-water mixture (19:1 v/v) at 25 ^oC. The solution

was not filtered. Crystals of suitable quality appeared by slow evaporation at 25 ^{o}C over a period of three weeks.

The host and guest numbering schemes are given in Figure 34.

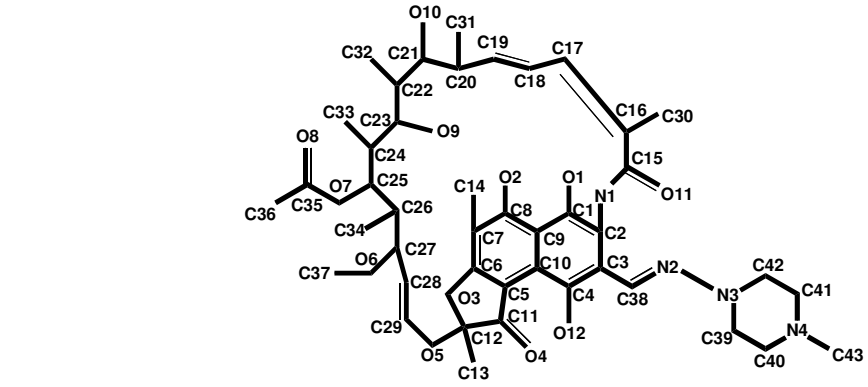

(a) rifampicin

(b) iso-propanol **(c) 1-butanol** **(d) ethylene glycol** **(e) 1, 4-dioxane**

Figure 34 Host and guest numbering schemes: (a) rifampicin, (b) iso-propanol, (c) 1-butanol, (d) ethylene glycol and (e) 1, 4-dioxane. Hydrogen atoms have been omitted for clarity.

Single crystal X-Ray Diffraction

Data-collection and Space Group Determination

A crystal of P8 was moved from its mother liquor and was covered in paratone N oil without delay in order to prevent the loss of solvent molecules. The crystals of P9, P10 and P11 were handled in the same way. A Nonius Kappa CCD four-circle diffractometer was employed to collect the data for all four solvates at 100 K.

The unit cell parameters, crystal systems and space groups were determined from the X-ray diffraction data which revealed Laue 2*/m* symmetry for all four solvates. Therefore, these solvates belong to the monoclinic system. The reflection conditions were: *hkl*:

none; *h0l*: *none*; *0k0*: *k* = *2n*. The two space group choices were $P2_1$ and $P2_1/m$. The former was chosen due to the chirality of the rifampicin host molecules.

Structure Solution and Refinement

From unit cell data and density considerations, each of the solvates was found to contain a total of four rifampicin molecules (plus complementary solvent molecules) per unit cell. Since the number of equivalent positions in the space group $P2_1$ is two, it follows that the asymmetric unit comprises two independent rifampicin molecules (plus solvent complement) in each case.

For all four solvates, program SHEXLD[1] was used to solve the structures by *ab initio* methods, which revealed the positions of all the non-hydrogen atoms of the two independent rifampicin molecules (host) in each structure. Full-matrix least-squares refinements were performed with SHELXH-97.[2] Difference Fourier maps yielded the positions of the oxygen and carbon atoms of the water and organic solvent molecules (guest). Some of these atoms were found to have full site-occupancy while the others were disordered over two or even three positions. The host and guest molecules having full s.o.f. were then refined isotropically.

A few atoms in the host molecules were found to be disordered over two positions in all four solvates except P10. In P8, atoms C41 and C42 in the host molecule A are disordered over two positions (C41A and C41C as well as C42A and C42 C). C41C and C42C, the major components, were assigned a value of x for their s.o.f.s while the minor components C41A and C42A were allocated the value 1-x. The s.o.f.s refined to 0.63(2) and 0.37(2) respectively while the U_{iso} values of C41C, C41A, C42C and C42A refined to 0.051(3), 0.014(3), 0.041(3) and 0.021(3) $Å^2$, respectively. In P9, atom C36 in the host molecule A is disordered over two positions (C36A and C36C). Their s.o.f.s refined to 0.67(3) and 0.33(3) respectively while their U_{iso} values refined to 0.072(3) and 0.022(4) $Å^2$, respectively. In P11, atoms C18 and O11 in the host molecule B are disordered over two positions (C18B and C18E as well as O11B and O11E). The s.o.f.s of C18B and C18E refined to 0.80(2) and 0.20(2) respectively while their U_{iso} values refined to

0.039(3) and 0.034(7) $Å^2$, respectively. The s.o.f.s of O11B and O11E refined to 0.78(1) and 0.22(1) respectively while their U_{iso} values refined to 0.029(2) and 0.045(6) $Å^2$, respectively

For the disordered solvent molecules, a fixed U_{iso} (the mean of U_{eq} for the chemically equivalent ordered atoms) was assigned to each molecule and these atoms were allowed to refine with site-occupancies x and 1-x, with x variable. For some molecules, the s.o.f.s were then assigned as fixed values, allowing the U_{iso} parameters to refine freely. For some of the other molecules, both the U_{iso} values and s.o.f.s refined freely. The details of the U_{iso} parameters and s.o.f.s of the guest molecules in each solvate are listed in Tables 47, 48, 49 and 50.

Table 47 Isotropic thermal parameters and site-occupancy factors for the guest molecules of P8

Guest molecule	U_{iso} ($Å^2$)	s.o.f.
O1W	0.04	1.00
O2W	0.04	1.00
O3W	0.03	1.00
O4W	0.05	0.70
O5W	0.03	1.00
O6W	0.05	1.00
O7W	0.04	1.00
O8W	0.05	1.00
O9W	0.04	1.00
O10W	0.06	1.00
O11W	0.05	0.50
O12W	0.06	0.85
O13W	0.05	0.28
O14W	0.06	0.30
O15W	0.04	0.50
O16W	0.05	0.50
O17W	0.05	0.38
O18W	0.06	0.70
O19W	0.06	0.60
O20W	0.06	0.20
O21W	0.07	0.21
O1G-C1G-C2G-C3G	0.07-0.06-0.09-0.07	1.00
O2G-C4G-C5G-C6G	0.08-0.05-0.04-0.05	0.50
O3G-C7G-C8G-C9G	0.04-0.03-0.07-0.05	0.70
O4G-C10G-C11G-C12G	0.07-0.05-0.06-0.07	1.00
O5GA-C13G-C14G-C15G	0.02 (global U_{iso})	0.34
O6GA-C16G-C17G-C18G	0.02 (global U_{iso})	0.34
O6GB-C19G-C21G-C20G	0.06 (global U_{iso})	0.42

Table 48 Isotropic thermal parameters and site-occupancy factors for the guest molecules of P9

Guest molecule	U_{iso} (Å^2)	s.o.f.
O1W	0.07	1.00
O2W	0.03	0.40
O1G-C1G-C2GA/C2GB-C3G-C4GA/C4GB	0.13-0.11-0.05/0.14-0.14-0.07/0.16	1.00-1.00-0.50/0.50-1.00-0.50/0.50
O2G-C5G-C6G-C7G-C8G	0.03-0.03-0.03-0.04-0.04	1.00
O3G-C9G-C10G-C11G-C12G	0.06-0.08-0.08-0.07-0.10	0.94
O4G-C13G-C14G-C15G-C16G	0.11-0.08-0.08-0.04-0.04	0.60
O5GA-C17C-C18C-C19C-C20C	0.07-0.05-0.06-0.05-0.04	0.46
O5GB-C17D-C18D-C19D-C20D	0.05-0.08-0.07-0.09-0.11	0.54
O6G-C21G-C22C/C22D-C23G-C24G	0.06-0.09-0.06/0.05-0.09-0.10	1.00

Table 49 Isotropic thermal parameters and site-occupancy factors for the guest molecules of P10

Guest molecule	U_{iso} (Å^2)	s.o.f.
O1W	0.07	1.00
O2W	0.08	1.00
O3W	0.06	0.15
O4W	0.08	1.00
O5W	0.07	0.61
O6W	0.07	0.50
O7W	0.06	0.20
O8W	0.06	0.32
O9W	0.07	0.46
O10W	0.06	0.15
O11W	0.07	0.20
O1G-C1G-C2G-O2G	0.09 (global U_{iso})	0.73
O3G-C3G-C4G-O4G	0.08 (global U_{iso})	0.63
O5G-C5G-C6G-O6G	0.07 (global U_{iso})	0.67
O7G-C7G-C8G-O8G	0.08 (global U_{iso})	0.70
O9G-C9G-C10G-O10G	0.09 (global U_{iso})	0.61
O11G-C11G-C12G-O12G	0.09-0.09-0.09-0.10	1.00
O13G-C13G-C14G-O14G	0.09 (global U_{iso})	0.73
O15G-C15G-C16G-O16G	0.09 (global U_{iso})	0.67

Table 50 Isotropic thermal parameters and site-occupancy factors for the guest molecules of P11

Guest molecule	U_{iso} (Å^2)	s.o.f.
O1W	0.04	1.00
O2W	0.04	1.00
O3W	0.06	1.00
O1C-C1C-C2C-O2C-C3C-C4C	0.05-0.06-0.08-0.06-0.05-0.05	0.65
O1D-C1D-C2D-O2D-C3D-C4D	0.06-0.06-0.03-0.09-0.07-0.06	0.35
O3C-C5C-C6C-O4C-C7C-C8C	0.03-0.03-0.03-0.04-0.04-0.04	0.66
O3D-C5D-C6D-O4D-C7D-C8D	0.05 (global U_{iso})	0.44
O5G-C9G-C10G-O6G-C11G-C12G	0.03-0.03-0.03-0.04-0.03-0.03	1.00
O7G-C13G-C14G-O8G-C15G-C16G	0.04-0.05-0.07-0.09-0.05-0.03	1.00
O9G-C17G-C18G-O10G-C19G-C20G	0.06-0.05-0.05-0.06-0.05-0.06	1.00
O11C-C21C-C22C-O12C-C23C-C24C	0.06-0.02-0.04-0.07-0.04-0.06	0.62
O11D-C21D-C22D-O12D-C23D-C24D	0.09 (global U_{iso})	0.38

Hydrogen atoms were identified in successive difference electron-density maps. Based on the positions of the peaks found, a riding model was employed to place hydrogen atoms for the rifampicin and solvent molecules in idealised positions except for the water hydrogen atoms which were positioned based on reasonable locations of suitable electron-density peaks and appropriate hydrogen bond geometry. All the methyl hydrogen atoms were refined with isotropic temperature factors equal to 1.5 times those of their parent atoms while all the other hydrogen atoms were assigned temperature factors 1.2 times those of their parent atoms.

For the iso-propanol, 1-butanol, ethylene glycol and 1, 4-dioxane molecules as well as the hydrogen atoms of water molecules, distance restraints were employed to ensure reasonable molecular geometries. For the iso-propanol molecules, the bond lengths O1G-C1G, C1G-C2G and C1G-C3G were set at 1.43, 1.52 and 1.52 Å, respectively. The standard deviation σ for these bonds was set between 0.001 and 0.01 Å. For the 1-butanol molecules, the bond lengths O1G-C1G, C1G-C2G, C2G-C3G and C3G-C4G were set at 1.53, 1.52, 1.52 and 1.51 Å, respectively. The standard deviation σ for these bonds was set between 0.001 and 0.004 Å. For the ethylene glycol molecule, the bond lengths O1G-C1G, C1G-C2G and C2G-O2G were set at 1.40, 1.52 and 1.53 Å, respectively. The standard deviation σ for these bonds was set at 0.01 Å. For the 1,4-dioxane molecules, the bond lengths O1G-C1G, C1G-C2G, C2G-O2G, O2G-C3G, C3G-C4G and C4G-O1G were set at 1.52, 1.42, 1.52, 1.52, 1.42 and 1.52 Å, respectively.

The standard deviation σ for these bonds was set between 0.004 and 0.008 Å. The O-H bond length of water molecules was fixed at 0.84 Å with the H-O-H angle set at 104.5°. The standard deviations σ were set between 0.001 and 0.008 Å.

Crystal and refinement parameters for each solvate are presented in Tables 51 and 52. A variety of disordered arrangements is observed in each case. Large fractions of solvent disorders (30, 40, 49 and 32 %) are observed in the structures of solvates P8, P9, P10 and P11, respectively. This gives rise to the difficulty in achieving low final residual factors (R_1, wR2).

This was especially the case for solvate P10, whose crystals diffracted poorly. It should be noted here that for each solvate, at least two, and in some cases, three full intensity data-collections and subsequent refinements were performed in an effort to obtain the highest quality data. Despite all data-collections being carried out at low temperature (typically 100 K), solvent disorder persisted and presented formidable challenges in modelling the guest molecules satisfactorily.

Table 51 Crystal and refinement data for P8 and P9

Parameter	**P8**	**P9**
Formula unit	2rifampicin · 4.30iso-propanol · 14.7H_2O	2rifampicin · 5.53(1-butanol) · 1.40H_2O
Formula Weight / g mol^{-1}	2169.58	2081.14
Crystal system	Monoclinic	Monoclinic
Space group	$P2_1$	$P2_1$
a / Å	13.9354(7)	14.0774(13)
b / Å	17.6109(8)	23.401(2)
c / Å	25.4284(12)	17.4839(16)
α / ^{o}	90.00	90.00
β / ^{o}	94.2140(10)	90.689(2)
γ / ^{o}	90.00	90.00
Volume / Å^3	6223.6(5)	5759.3(9)
Z	2	2
Density$_{calc}$ / g cm^{-3}	1.158	1.200
μ (MoK$_\alpha$) /mm^{-1}	0.090	0.087
F (000)	2347	2253
Crystal size /mm^3	0.25x0.22x0.06	0.18x0.34x0.41
Temperature / K	100(2)	100(2)
Range scanned θ / ^{o}	$1.99 \leq \theta \leq 27.88$	$1.85 \leq \theta \leq 28.44$
Index ranges	h: -18, 18	h: -18, 18
	k: -23, 23	k: -31, 31
	l: -33, 33	l: -23, 23
φ scan angle / ^{o}	0.5	0.5
ω scan angle / ^{o}	0.5	0.5
Dx / mm	42	40
No. of measured reflections	85745	60374
No. of unique reflections	15309	14710
No. of reflections with I > 2σ(I)	11589	12138
No. of L.S. parameters	1414	1375
R_{int}, R_σ	0.0336, 0.0276	0.0426, 0.0406
S	1.025	1.027
R_1 ($F_o > 4\sigma(F_o)$)	0.0881	0.0598
No. of reflections omitted	31	37
wR2 (all reflections)	0.2709	0.1738
Weighting scheme	0.1701	0.1142
	6.6353	1.9393
$(\Delta / \sigma)_{mean}$	< 0.001	< 0.001
Δρ excursions / eÅ^{-3}	-0.566, 0.991	-0.772, 0.897

Table 52 Crystal and refinement data for P10 and P11

Parameter	**P10**	**P11**
Formula unit	2rifampicin · 5.75ethylene glycol · 5.59H_2O	2rifampicin · 6(1,4-dioxane) · 3H_2O
Formula Weight / g mol^{-1}	2103.36	2228.56
Crystal system	Monoclinic	Monoclinic
Space group	$P2_1$	$P2_1$
a / Å	13.802(4)	12.1131(14)
b / Å	17.517(5)	20.515(2)
c / Å	24.848(8)	23.438(3)
α / °	90.00	90.00
β / °	105.803(6)	98.020(2)
γ / °	90.00	90.00
Volume / Å^3	5781(3)	5767.4(11)
Z	2	2
Density$_{calc}$ /g cm^{-3}	1.208	1.283
μ (MoK$_α$) /mm^{-1}	0.094	0.097
F (000)	2263	2396
Crystal size /mm^3	0.02x0.17x0.28	0.20x0.31x0.42
Temperature / K	100(2)	100(2)
Range scanned θ / °	2.28 ≤ θ ≤ 24.98	2.17 ≤ θ ≤ 27.54
Index ranges	h: -16, 13	h: -15, 15
	k: -20, 20	k: -26, 26
	l: -29, 28	l: -30, 30
φ scan angle / °	0.5	0.5
ω scan angle / °	0.5	0.5
Dx / mm	65	50
No. of measured reflections	32578	48483
No. of unique reflections	10456	13629
No. of reflections with I > 2σ(I)	6192	12331
No. of L.S. parameters	1151	1436
R_{int}, $R_σ$	0.1040, 0.1318	0.0300, 0.0294
S	1.310	1.057
R_1 ($F_o > 4σ(F_o)$)	0.1367	0.0625
No. of reflections omitted	8	12
wR2 (all reflections)	0.3769	0.1745
Weighting scheme	0.2000	0.1046
	0.0000	4.5133
$(Δ / σ)_{mean}$	< 0.001	< 0.001
Δρ excursions / eÅ^{-3}	-0.685, 0.910	-0.549, 0.715

Structural Description

Rifampicin Molecule Conformation and Antibiotic Activity

Similar to the rifampicin host molecules in series 1 (solvates P1 - P4) and 2 (P5 - P7), the host molecules in solvates P8, P9, P10 and P11 were also investigated with regard to their solid-state conformations. The antibiotic activity of the host molecules has been correlated with the conformation of the ansa chain, as determined from single crystal X-ray diffraction.[3]

In each case, the value of $Z = 4$ indicated that the asymmetric unit comprised two crystallographically independent drug molecules (A and B) and their complements of solvent molecules. The two independent host molecules A and B in each solvate are overlayed in Figure 35. For P8, a remarkable similarity is found in the conformations of the molecules A and B. However, small but significant differences between the conformations of the host molecules can be observed, which confirms the presence of two symmetry-independent host molecules in the asymmetric unit. This also applies to solvates P9 and P10. In the molecule B of solvate P11, atom C18 is disordered over two positions where C18B has the major site-occupancy [0.80(1)]. It is important to note that C18B in molecule B points towards the ansa chain while C18A in molecule A points away from the ansa chain. This strongly indicates that host molecules A and B are two symmetry-independent molecules in the asymmetric unit of P11.

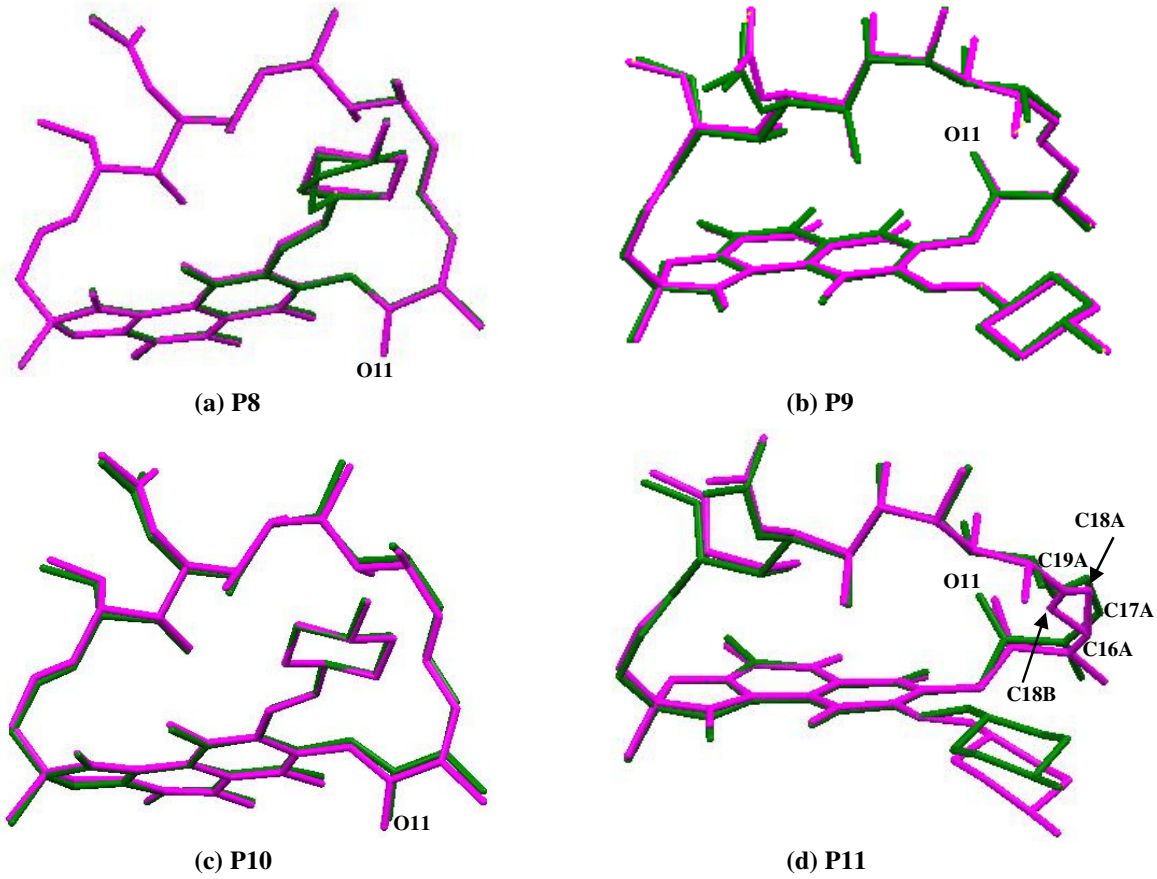

Figure 35 Overlay diagrams of the crystallographically independent host molecules A (green) and B (pink) in solvates (a) P8, (b) P9, (c) P10 and (d) P11. Guest molecules and hydrogen atoms are omitted for clarity.

A noteworthy observation is that atom O11 points away from the ansa chain in the host molecules of solvates P8 and P10 while it points towards the ansa chain in solvates P9 and P11, as shown in Figure 36. This indicates the existence of two distinct conformations of the rifampicin molecules.

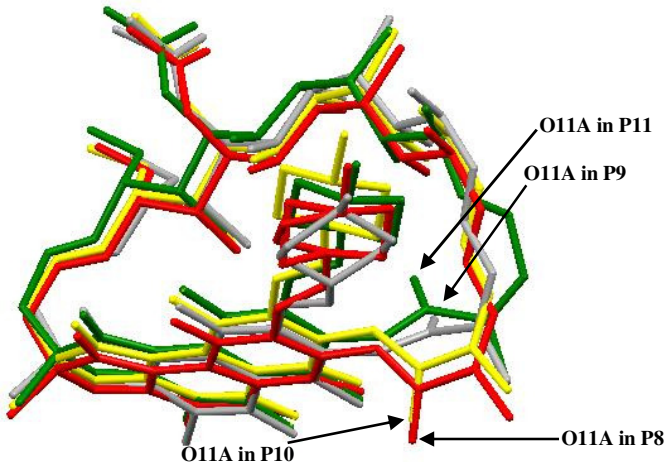

Figure 36 An overlay of the host molecules A in solvates P8 (red), P9 (gray), P10 (yellow) and P11 (green). Hydrogen atoms are omitted for clarity.

Table 53 lists the dihedral angles between planes A (ansa chain) and B (chromophore) as well as those between planes B and C (piperazinyl substituent) in the two independent host molecules (A and B) in each solvate. For each solvate, the difference between the chemically equivalent dihedral angles in molecules A and B provides firm evidence for the existence of two independent host molecules in the asymmetric unit. Furthermore, since dihedral angles between planes A and B lie within the range 64 to 124° (established as critical for antibiotic activity),[4, 5, 6, 7] we conclude that the crystals in the four solvates contain the rifampicin molecule in biologically relevant conformations. Also, for the molecules A and B in P11, the difference between the dihedral angles of planes B and C is much more significant than those of others.

Table 53 The dihedral angles (°) between planes A and B as well as those between planes B and C of the host molecules (A and B) in each solvate.

Angles between planes	**P8**		**P9**		**P10**		**P11**	
	A	B	A	B	A	B	A	B
A and B(°)	72.58(4)	71.24(4)	62.02(3)	58.52(3)	73.0(1)	70.3(2)	56.02(4)	49.66(4)
B and C(°)	12.9(2)	7.7(1)	15.8(1)	15.82(9)	8.9(3)	7.9(3)	3.81(8)	16.96(7)

Tables 54 and 55 list the torsion angles τ_1-τ_{17} along the ansa chain backbone of the rifampicin host molecules (the scheme was shown in earlier parts of this chapter). Among these angles, τ_1 defines the junction between the chromophore and the ansa chain, indicating a *trans* conformation in the rifampicin molecules of all four solvates.

The torsion angle τ_{17} indicates a *gauche* conformation of the etheric junction in the rifampicin molecule in each case. These are similar to the conformations of the host molecules in series 1 and 2. Furthermore, it is known that the torsion angles τ_9 and τ_{17} in the host molecules fall within the preferred range 59 ± 6° and -65 ± 13° respectively for active rifamycins.[9, 17] This also serves as evidence for the conclusion that the crystals of P8, P9, P10 and P11 contain the rifampicin molecule in biologically relevant conformations.

Table 54 The torsion angles along the ansa chain in the rifampicin host molecules A and B in solvates P8 and P9, respectively.

Torsion angles (°)	**P8**		**P9**	
	A	B	A	B
C2-N1-C15-C16 (τ_1)	179.7(4)	-179.6(4)	169.6(3)	169.2(3)
N1-C15-C16-C17 (τ_2)	-24.4(7)	-23.5(7)	-105.3(4)	-96.8(4)
C15-C16-C17-C18 (τ_3)	-1.4(9)	-0.7(9)	0.5(6)	-1.3(6)
C16-C17-C18-C19 (τ_4)	158.1(6)	157.0(6)	174.3(4)	172.6(4)
C17-C18-C19-C20 (τ_5)	-169.8(5)	-167.9(5)	-173.7(4)	-174.6(4)
C18-C19-C20-C21 (τ_6)	-5.6(7)	-5.9(7)	-8.0(6)	-16.8(6)
C19-C20-C21-C22 (τ_7)	169.6(4)	169.2(4)	171.9(3)	171.3(3)
C20-C21-C22-C23 (τ_8)	179.0(4)	179.3(4)	-178.6(3)	-171.9(3)
C21-C22-C23-C24 (τ_9)	55.2(6)	56.6(6)	54.5(4)	61.4(4)
C22-C23-C24-C25 (τ_{10})	173.8(4)	173.6(4)	170.8(3)	164.6(3)
C23-C24-C25-C26 (τ_{11})	160.7(4)	160.1(4)	159.4(3)	163.2(3)
C24-C25-C26-C27 (τ_{12})	161.2(4)	161.5(4)	174.3(3)	169.0(3)
C25-C26-C27-C28 (τ_{13})	-175.2(4)	-176.9(4)	-169.5(3)	-171.0(3)
C26-C27-C28-C29 (τ_{14})	112.8(5)	112.9(5)	106.4(4)	104.8(4)
C27-C28-C29-O5 (τ_{15})	-173.6(4)	-173.4(4)	-171.3(3)	-172.5(3)
C12-O5-C29-C28 (τ_{16})	58.4(6)	58.0(6)	52.6(4)	57.7(4)
C29-O5-C12-O3 (τ_{17})	-77.8(5)	-77.2(5)	-80.1(3)	-79.8(3)

Table 55 The torsion angles along the ansa chain in the rifampicin host molecules A and B in solvates P10 and P11, respectively.

Torsion angles (°)	**P10**		**P11**	
	A	B	A	B
C2-N1-C15-C16 (τ_1)	180(1)	176(1)	-168.7(4)	172.5(4)
N1-C15-C16-C17 (τ_2)	-34(2)	-25(2)	-127.5(4)	-86.6(5)
C15-C16-C17-C18 (τ_3)	6(3)	2(2)	6.8(7)	1.8(8)
C16-C17-C18-C19 (τ_4)	158(2)	153(2)	43.2(7)	177.2(6)
C17-C18-C19-C20 (τ_5)	-164(2)	-167(1)	-170.6(4)	178.9(5)
C18-C19-C20-C21 (τ_6)	-18(2)	-8(2)	109.2(5)	-9.1(8)
C19-C20-C21-C22 (τ_7)	172(1)	173(1)	175.2(3)	-179.4(4)
C20-C21-C22-C23 (τ_8)	-178(1)	-180(1)	173.1(3)	179.2(3)
C21-C22-C23-C24 (τ_9)	59(2)	52(2)	51.4(4)	54.9(4)
C22-C23-C24-C25 (τ_{10})	168(1)	174(1)	178.8(3)	176.6(3)
C23-C24-C25-C26 (τ_{11})	160(1)	163(1)	156.9(3)	159.8(3)
C24-C25-C26-C27 (τ_{12})	161(1)	159(1)	167.2(3)	166.7(3)
C25-C26-C27-C28 (τ_{13})	-173(1)	-179(1)	-179.3(3)	-174.1(3)
C26-C27-C28-C29 (τ_{14})	113(2)	116(2)	104.5(4)	107.2(4)
C27-C28-C29-O5 (τ_{15})	-177(1)	-175(1)	-168.7(3)	-168.1(4)
C12-O5-C29-C28 (τ_{16})	60(2)	63(2)	57.1(5)	51.9(6)
C29-O5-C12-O3 (τ_{17})	-77(1)	-82(1)	-80.6(4)	-82.5(5)

Interestingly, τ_4 in the molecule A in solvate P11 indicates a *gauche* conformation while that in all the other solvates indicates a *trans* conformation. This indicates the existence of yet another conformation of the rifampicin molecule. In addition, τ_4 in the molecule B in solvate P11 indicates a *trans* conformation, showing clearly that the two crystallographically independent rifampicin molecules in P11 adopt different conformations.

Figure 37 shows the rifampicin host molecules A viewed side-on to the ansa chain backbone in P8, P9, P10 and P11, respectively. Similarly to the rifampicin molecules in series 1 and 2, the four oxygen atoms (O9, O10, O1 and O2) are approximately perpendicular to the average plane of the ansa chain and roughly parallel to the aromatic plane. Furthermore, all four oxygen atoms protrude from the cavity of the ansa chain and the chromophore face, their C-O vectors pointing away from the piperazinyl subsitituent. In addition, the intramolecular distances among the four oxygen atoms O1, O2, O9 and O10 (listed in Table 56) fall in the range (~5.41 to 9.58 Å) which is favourable for active rifamycin derivatives.[4] This also allows these host molecules to adopt an open

conformation, which again leads to the conclusion that the host molecules adopt antibiotically active conformations in the solid state.[10]

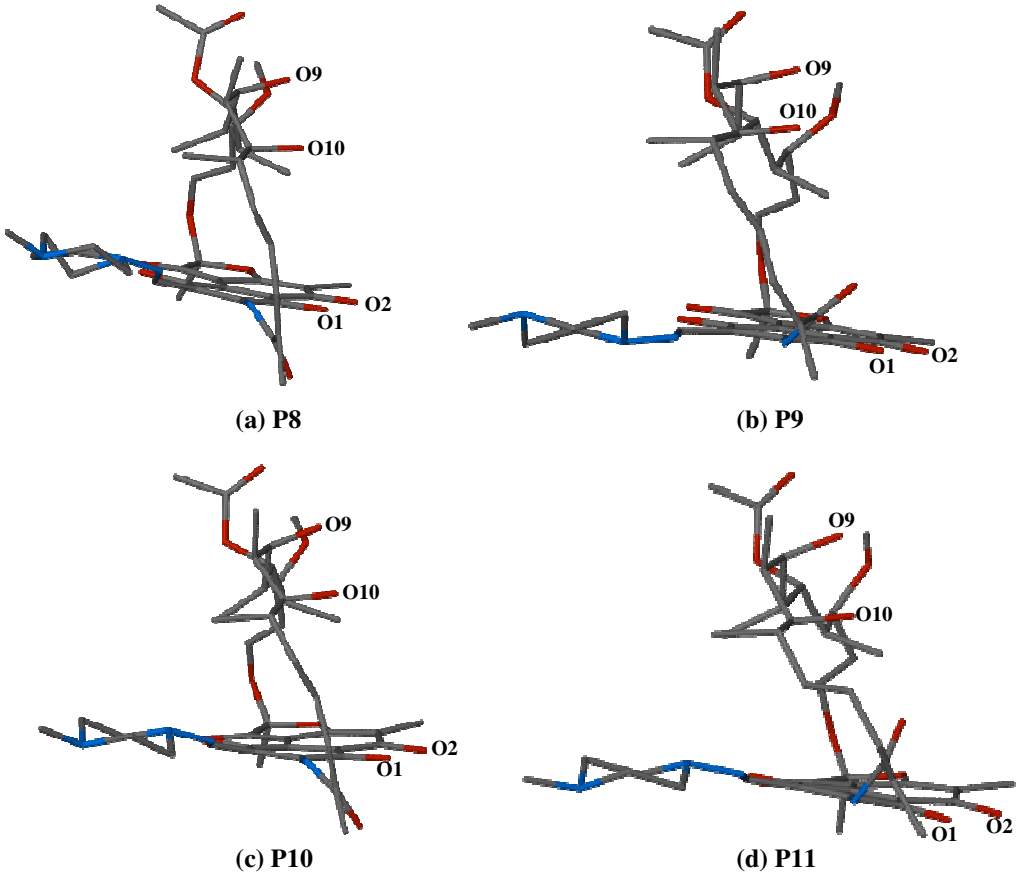

Figure 37 Diagrams of the rifampicin host molecule A viewed side-on with respect to the ansa chain in solvates (a) P8, (b) P9, (c) P10 and (d) P11.

Table 56 Interatomic distances involving O1, O2, O9 and O10 atoms in the host molecules in the four solvates[a]

Distance (Å)	**P8**		**P9**		**P10**		**P11**	
	A	B	A	B	A	B	A	B
O1···O9	6.592	6.618	7.163	7.351	6.627	6.813	7.320	7.610
O1···O10	5.357	5.432	6.291	6.793	5.459	5.563	5.661	6.412
O2···O9	7.287	7.312	7.912	8.121	7.398	7.544	7.965	8.216
O2···O10	6.871	6.940	7.795	8.290	7.015	7.073	7.045	7.759

[a] Average e.s.d. 0.008 Å.

In conclusion, indications of different conformations for the rifampicin molecule are observed. However, all the rifampicin host molecules in the solvates P8 – P11 were

confirmed to adopt conformations whose parameters fall within the range identified with antibiotic activity.[4, 5, 6, 7, 10]

As discussed in the previous parts of this chapter, rifampicin is known to exist as a zwitterion in the solid state.[12] For all the host molecules in solvates P8 - P11, the bond length C8-O2 is significantly shorter than those of the other C-O bonds which are in a similar chemical space environment except in the case of molecule A in P10 (listed in Table 57). Based on the lists of standard bond distances in International Tables for Crystallography,[11] the typical distance for the C-O bond in the above chemical environment is 1.333 Å. Therefore, although bonds C14-O12, C1-O1 and C8-O2 are all represented as single bonds in Figure 34, the former two bonds can be confirmed as being single whilst C8-O2 has significant double bond character. However, in the molecule A in P10, the bond C8-O2 cannot be confirmed as having a double bond character as its length is not significantly different from that of C1-O1.

Table 57 Bond lengths of C4-O12, C1-O1 and C8-O2 in the host molecule of each solvate.

Bond length (Å)	**P8**		**P9**		**P10**		**P11**	
	A	B	A	B	A	B	A	B
C4-O12	1.366(7)	1.370(6)	1.354(4)	1.354(4)	1.35(2)	1.36(2)	1.368(4)	1.352(5)
C1-O1	1.363(6)	1.357(5)	1.356(4)	1.358(4)	1.34(2)	1.36(1)	1.363(4)	1.359(5)
C8-O2	1.289(6)	1.285(6)	1.286(4)	1.274(4)	1.32(2)	1.25(2)	1.268(5)	1.254(5)

Furthermore, during the structural refinements of all four solvates, geometrically sensible electron density peaks, that qualified as potential H atoms, were found at ~ 1 Å from the hydroxyl oxygen atoms (O1, O9, O10 and O12) but not near the atom O2. At the same time, a peak was found around the N4 atom having an electron density value similar to the other peaks which had been assigned as hydrogen atoms. Also, between N4 and oxygen atoms of other molecules, this specific peak was ideally located, accounting for the formation of a N^{+}-H···O hydrogen bond with very favourable geometry. Consequently, it can be assumed that the proton transferred from the hydroxyl group on C8 to the nitrogen atom N4, forming a zwitterion. This phenomenon occurs in both host molecules A and B in solvates P8, P9 and P11 as well as in the host molecule B in P10; however, for the host molecule A in P10, the situation is not definitive (i.e. zwitterionic character could not be confirmed).

Intra- and Intermolecular Interactions

Solvate P8 – 2rifampicin • 4.30iso-propanol • 14.7H_2O

Host Intramolecular Interactions

Three analogous intramolecular O-H···O hydrogen bonds and one N-H···N hydrogen bond are found in the host molecules A and B of P8 as presented in Figure 38.

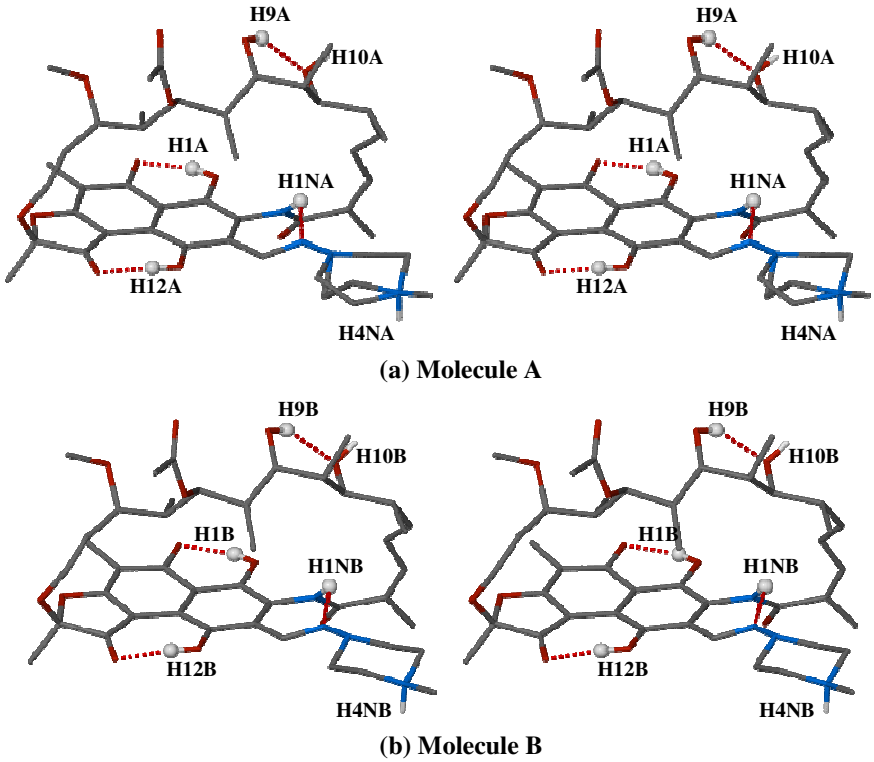

Figure 38 The zwitterionic structures and the stereoviews of intramolecular O-H···O and N-H···N interactions for host molecules A and B in P8. The relevant hydrogen atoms are shown as spheres. The other hydrogen atoms and the guest molecules are omitted for clarity.

The geometrical details of these O-H···O and N-H···N hydrogen bond interactions are listed in Table 58. For P8, the O···O distances range from 2.49 to 2.70 Å with a mean value of 2.59 Å while the O-H···O angles range from 142 to 176° with a mean value of 156°.

Table 58 Intramolecular O-H···O and N-H···N interactions in the host molecules A and B of solvate P8[a]

Hydrogen bond	O···O or N···N Distance (Å)	Angle (°)
O1A-H1A···O2A	2.489(5)	149
O9A-H9A···O10A	2.704(4)	142
O12A-H12A···O4A	2.575(6)	176
O1B-H1B···O2B	2.495(5)	147
O9B-H9B···O10B	2.689(5)	145
O12B-H12B···O4B	2.573(5)	174
N1A-H1NA···N2A	2.704(6)	113
N1B-H1NB···N2B	2.696(5)	113

[a] Where no e.s.d. is reported for the angle, H atoms involved were added in idealised positions in a riding model.

Several intramolecular C-H···O and C-H···N interactions (Table 59) are found to be associated with the host rifampicin conformations in P8. The hydrogen bonds C14-H···O2, C18-H···N1, C25-H···O8, C25-H···O9, C27-H···O7 and C28-H···O3 are found to exist in the both host molecules A and B. The C···O distances range from 2.66 to 3.11 Å with a mean value of 2.87 Å. The C-H···O angles range from 100 to 116° with a mean value of 107°.

Table 59 Intramolecular C-H···O and C-H···N interactions in the host molecules A and B of P8[a]

Hydrogen bond	C···O or C···N Distance (Å)	Angle (°)
C14A-H14B···O2A	2.816(7)	100
C14B-H14D···O2B	2.836(6)	107
C18A-H18A···N1A	2.893(6)	107
C18B-H18B···O10B	3.110(5)	116
C18B-H18B···N1B	2.905(6)	107
C25A-H25A···O8A	2.747(6)	106
C25A-H25A···O9A	2.871(5)	109
C25B-H25B···O8B	2.761(6)	106
C25B-H25B···O9B	2.869(6)	109
C27A-H27A···O7A	2.780(6)	102
C27B-H27B···O7B	2.769(6)	101
C28A-H28A···O3A	3.085(6)	114
C28B-H28B···O3B	3.088(6)	114
C38B-H38B···O12B	2.658(7)	101

[a] Where no e.s.d. is reported for the angle, H atoms involved were added in idealised positions in a riding model.

The intramolecular hydrogen bonds O-H···O, N-H···N, C-H···O and C-H···N stabilise the conformations of the host molecules A and B in P8.

Host-host Interactions

No host-host intermolecular O-H···O interaction are observed in solvate P8. However, three host-host intermolecular C-H···O interactions occur. The geometrical details of these C-H···O interactions are listed in Table 60. The C···O distances range from 3.33 to 3.43 Å with a mean value of 3.38 Å. The C-H···O angles range from 147 to 168° with a mean value of 161°.

Table 60 Intermolecular C-H···O interactions between the rifampicin molecules A and B in P8[a]

Hydrogen bond	C···O Distance (Å)	Angle (°)	Symmetry operator[b]
C29A-H29A···O2A	3.396(6)	167	1-x, -1/2+y, -z
C29B-H29B···O2B	3.331(6)	168	3-x, -1/2+y, 1-z
C40A-H40B···O1A	3.427(6)	147	2-x, -1/2+y, -z

[a] Where no e.s.d. is reported for the angle, H atoms involved were added in idealised positions in a riding model.
[b] Symmetry operator applies to hydrogen bond acceptor atoms.

Host-guest Interactions

The host-guest intermolecular O-H···O and N-H···O interactions in P8 are shown in Figure 39.

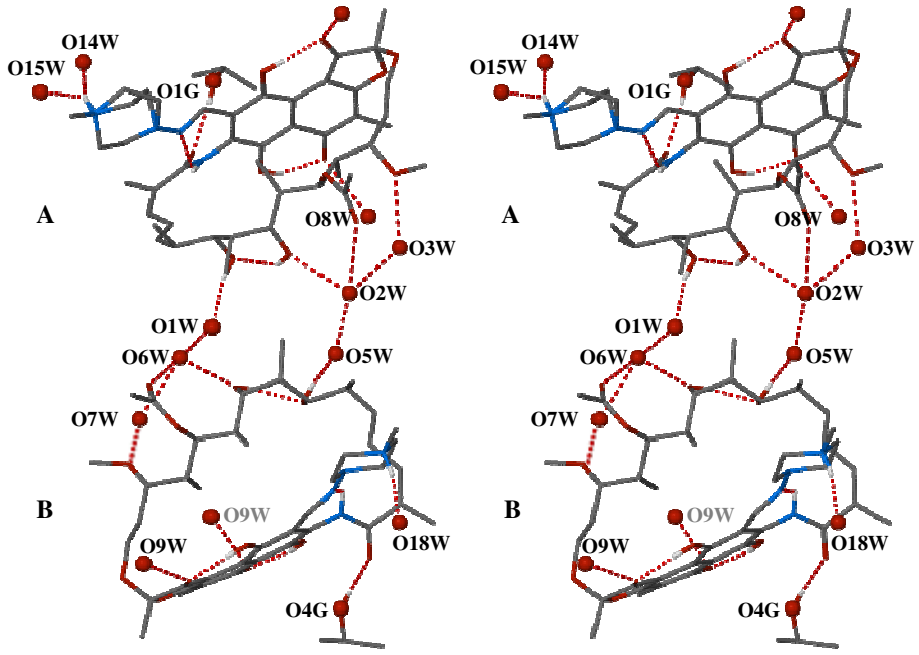

Figure 39 Stereoviews of the intermolecular O-H···O and N-H···O hydrogen bonds between the host and guest molecules in P8. The relevant oxygen atoms in the guest molecules are shown as spheres. The other hydrogen atoms and guest molecules are omitted for clarity. Atoms with gray labels have been symmetry-generated from their asymmetric unit counterparts.

The same atoms (O2, O4, O6, O8, O10, O11 and N4) are involved in the host-guest intermolecular interactions in the molecules A and B. Specifically, atoms O2, O4, O6 and O8 serve as H-bond donors to the water molecules. O11 atoms function as H-bond donors to the iso-propanol molecules in both molecules A and B. O10 and $(N4)^+$ atoms serve as H-bond acceptors for water molecules.

Water molecule O6W serves as hydrogen bond donor to O8B and O9B simultaneously (Figure 39). This also applies to water molecule O8W which functions as H-bond donor linking O2A and O4A of different A molecules (Figure 40). Water molecules O8W function as bridges to associate one host molecule A with a symmetry-generated host molecule A while O9W connects two host molecules B, as shown in Figure 40. The identical hydrogen bond chains (O12-H12···O4···O8W/O9W···O2···H1-O1) can be found between two molecules A and between two molecules B.

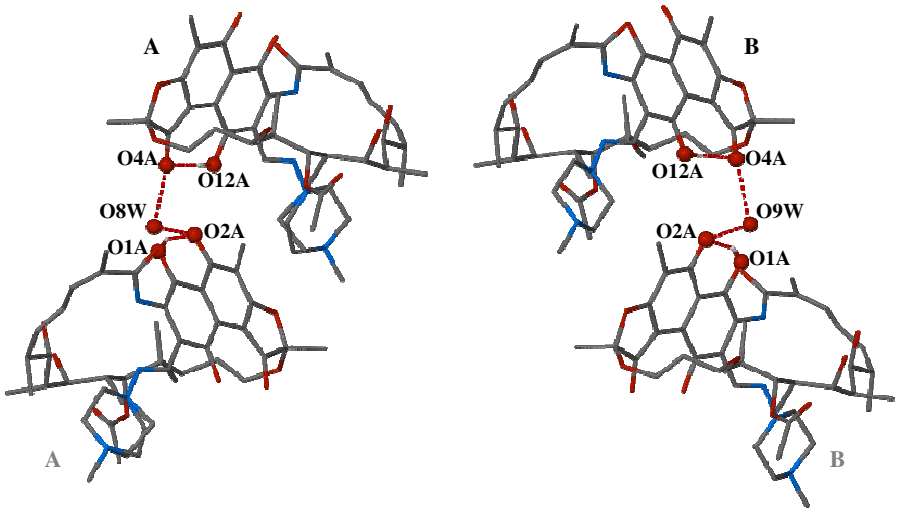

Figure 40 Water molecules O8W associating two host molecules A while O9W associates two host molecules B. The relevant oxygen atoms are shown as spheres. Atoms with gray labels have been symmetry-generated from their asymmetric unit counterparts.

Table 61 lists the distances and angles for host-guest intermolecular O-H···O and N-H···O interactions. The O···O distances range from 2.72 to 3.06 Å with a mean value of 2.84 Å. The O-H···O angles range from 137 to 174° with a mean value of 163°.

Table 61 Host-guest intermolecular O-H···O and N-H···O interactions for P8.[a]

Hydrogen bond	O···O or N···O Distance (Å)	Angle (°)	Symmetry operator[b]
O1G-H1G···O11A	2.843(6)	172	x, y, z
N4A-H4NA···O15W	2.814(9)	137	x, y, z
O4G-H4G···O11B	2.846(6)	174	x, y, z
N4B-H4NB···O18W	2.762(9)	167	x, y, z
O10A-H10A···O1W	2.756(5)	163	x, y, z
O10B-H10B···O5W	2.719(5)	164	x, y, z
O4A···O8W	2.804(6)	-------	x, y, z
O2A···O8W	2.858(6)	-------	1-x, 1/2+y, -z
O6A···O3W	2.888(5)	-------	x, y, z
O9A···O2W	2.752(5)	-------	x, y, z
O8B···O6W	3.059(7)	-------	x, y, z
O6B···O7W	2.837(5)	-------	x, y, z
O4B···O9W	2.789(6)	-------	x, y, z
O2B···O9W	2.893(6)	-------	3-x, 1/2+y, 1-z

[a] Where no e.s.d. is reported for the angle, H atoms involved were added in idealised positions in a riding model.
[b] Symmetry operator applies to hydrogen bond acceptor atoms.

Two host-guest intermolecular C-H···O interactions are found in the structure of P8 (Table 62). The mean value of the O···O distances is 3.418 Å with a mean angle of 150°.

Table 62 Intermolecular C-H···O interactions between the rifampicin and guest molecules[a]

Hydrogen bond	C···O Distance (Å)	Angle (°)	Symmetry operator[b]
C40A-H40A···O8W	3.457(8)	146	1+x, y, z
C43A-H43B···O8W	3.379(8)	154	1+x, y, z

[a] Where no e.s.d. is reported for the angle, H atoms involved were added in idealised positions in a riding model.
[b] Symmetry operator applies to hydrogen bond acceptor atoms.

Guest-guest Interactions

For P8, the water molecules display a variety of disordered arrangements. All the guest molecules assemble into a guest cluster which extends infinitely (Figure 41).

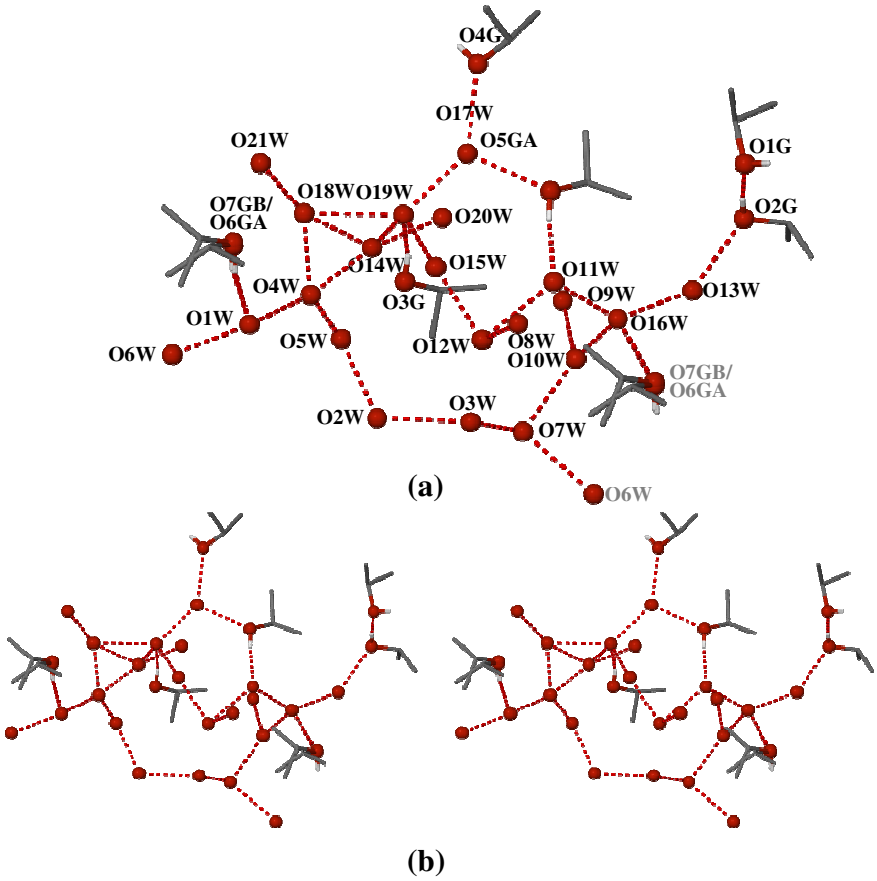

Figure 41 The guest-guest intermolecular O-H···O interactions among the water and iso-propanol molecules in P8. (a) Numbering scheme of these interactions; (b) Stereoview of these interactions. Atoms with gray labels have been symmetry-generated from their asymmetric unit counterparts.

The geometrical details of the guest-guest intermolecular O-H···O interactions in P8 are listed in Table 63. Due to low site-occupancy of the water molecules, the hydrogen atoms of these water molecules cannot be located. The O···O distances range from 2.52 to 3.02 Å with a mean value of 2.75 Å. The O-H···O angles range from 152.8 to 174.0° with a mean value of 166°.

Table 63 Guest-guest intermolecular H-bonds interactions in solvates P8[a]

Hydrogen bond	O···O Distance (Å)	Angle (°)	Symmetry operator[b]
O2W···O5W	2.660(7)	---------	x, y, z
O6W···O1W	2.691(7)	---------	x, y, z
O1W···O4W	2.775(7)	---------	x, y, z
O4W···O5W	2.766(7)	---------	x, y, z
O2W···O3W	2.870(6)	---------	x, y, z
O3W···O7W	2.785(6)	---------	x-1, y, z
O6W···O7W	2.855(6)	---------	x, y, z
O4W···O18W	2.597(11)	---------	2-x, 1/2+y, 1-z
O7GB-H7GB···O1W	2.81(2)	162.0	x, y, z
O6GA-H6GA···O1W	2.719(17)	167.0	x, y, z
O18W···O21W	3.00(3)	---------	x, y, 1+z
O18W···O14W	2.906	---------	2-x, y-1/2, 1-z
O18W···O19W	3.021	---------	2-x, y-1/2, 1-z
O19W···O14W	2.64(2)	---------	x, y, z
O14W···O20W	2.899	---------	x, y, z
O19W···O15W	2.707	---------	2-x, 1/2+y, -z
O15W···O12W	2.645	---------	1+x, y, z
O12W···O8W	2.741(9)	---------	x, y, z
O12W···O11W	2.850	---------	x-1, y, z-1
O5GA···O17W	2.748	---------	x, y, z
O11W···O16W	2.931	---------	3-x, y-1/2,1-z
O16W···O10W	2.621	---------	3-x, 1/2+y, 1-z
O16W···O7GB	2.662	---------	x, y, z
O16W···O6GA	2.706	---------	x, y, z
O16W···O13W	2.703	---------	2-x, 1/2+y, -z
O13W···O2G	2.71(2)	---------	x, y, z
O2G-H2G···O1G	2.634(14)	173.0	x, y, z
O5GA-H5GA···O11W	2.793(13)	174.0	x, y, z
O4W···O14W	2.158	---------	x, y, z
O3G-H3G···O19W	2.747	152.8	x, y, z
O19W···O17W	2.673(16)	---------	2-x, 1/2+y, 1-z
O17W···O14G	2.730	---------	x, y, z
O7W···O10W	2.846(8)	---------	3-x, 1/2+y, 1-z
O10W···O9W	2.750(7)	---------	x, y, z

[a] Average e.s.d.s 0.004 Å for distance and 0.7° for angle
[b] Symmetry operator applies to hydrogen bond acceptor atoms.

Overall Intramolecular and Intermolecular Interactions in P8

Figure 42 shows the overall hydrogen bond interactions in solvate P8. Six rifampicin molecules form two layers which consist of the molecules A (the top layer) and the molecules B (the bottom layer), respectively. The guest cluster is located in-between the two layers.

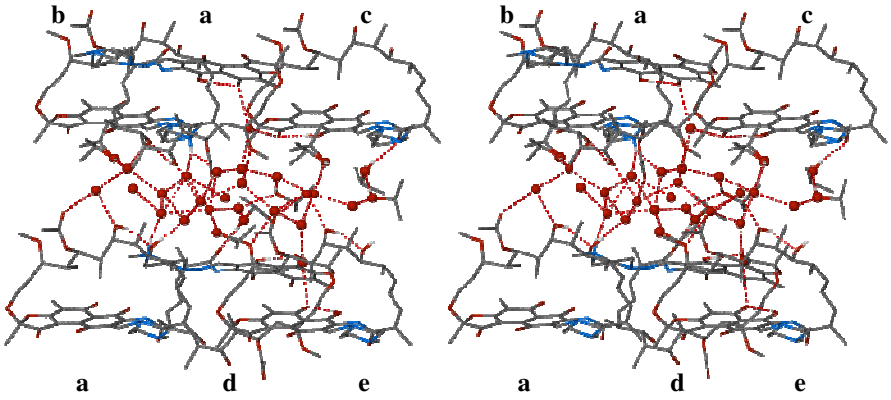

Figure 42 Stereoviews of the overall hydrogen bond interactions in P8. The oxygen atoms in the guest molecules are shown as spheres. The code letter for the symmetry operator of each rifampicin molecule is labelled. (a = x, y, z; b = 2-x, 1/2+y, -z; c = 1-x, 1/2+y, -z; d = 2-x, 1/2+y, 1-z; e = x-1, y, z).

Crystal Packing

The packing arrangement for P8 is shown in Figure 43. Host molecules A and B are related by a pseudo 2-fold rotation axis parallel to the *b*-axis, leading to the formation of alternating layers (A, B) along the *c*-axis, interleaved by layers of guest molecules. In each layer parallel to the *b*-axis, the host molecules pack in a head-to-tail mode, associating through mediation of water molecules.

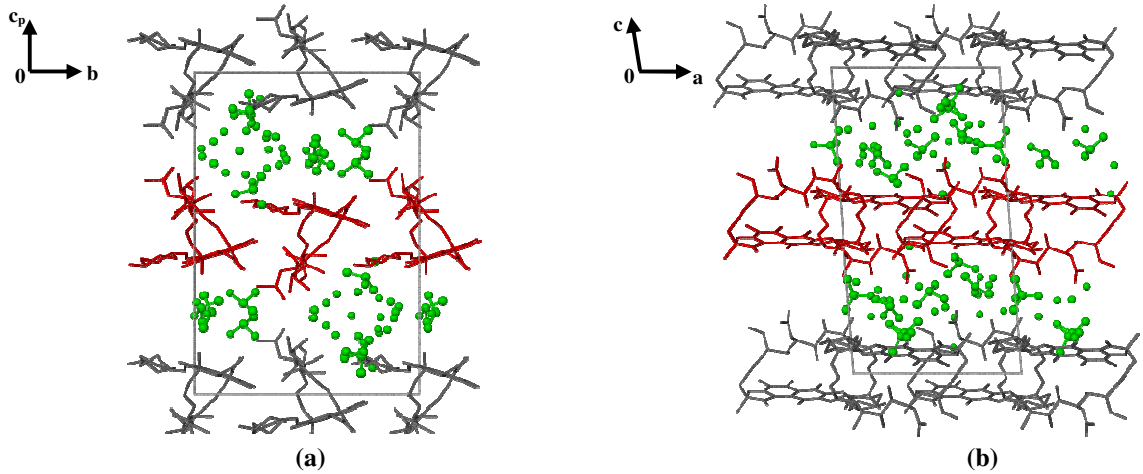

Figure 43 Crystal packing diagrams for P8 viewed along (a) [100] and (b) [010]. Solvent molecules are shown as green spheres for clarity. Host molecules A and B are shown in gray and red, respectively.

The program SECTION[14] was employed to examine the solvent channels for P8. The section views are taken at regular intervals through the unit cell along the *a*-axis. Figure 44 shows two representative views, illustrating the 'endless' channels in which the guest molecules are accommodated.

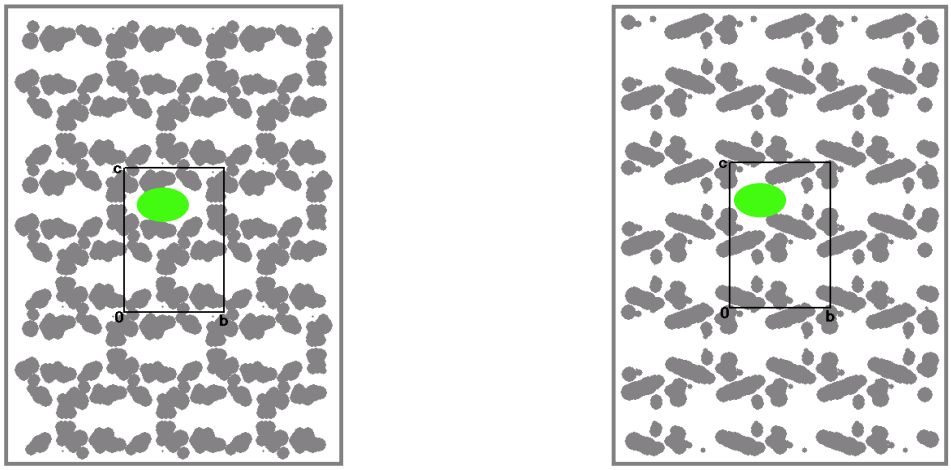

(a) 0 Å **(b) 7 Å**

Figure 44 Sections of P8 with guest molecules omitted and host molecules represented by gray areas, viewed along [100] with the unit cell sectioned at (a) 0 Å (b) 7 Å from the origin 0,0,0. A representative channel location is shown in green.

Solvate P9 – 2rifampicin • 5.53(1-butanol) • 1.40H_2O

Host Intramolecular Interactions

In the structure of P9, three analogous intramolecular O-H···O H-bonds and one N-H···N H-bond are found in the host molecules A and B as presented in Figure 45.

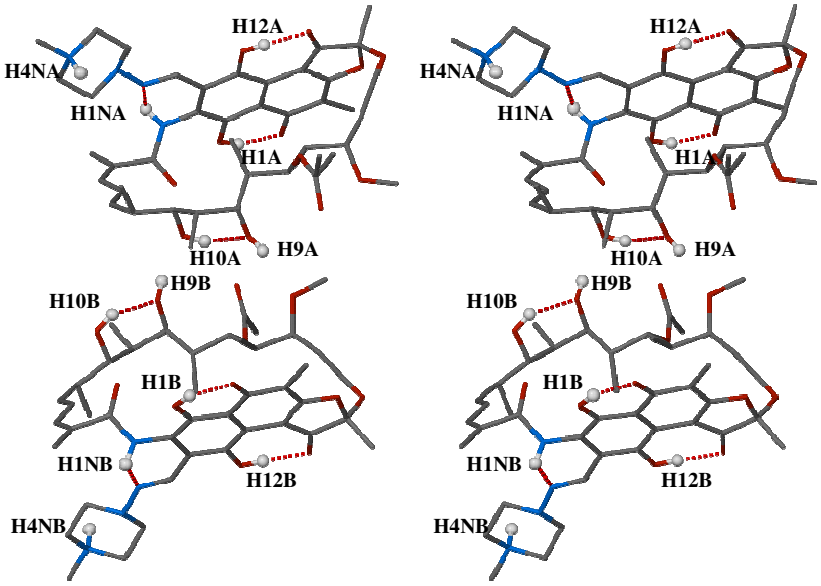

Figure 45 Stereoview of the zwitterionic structures and the intramolecular O-H···O and N-H···N interactions for host molecules A and B in P9. The relevant hydrogen atoms are shown as spheres. The other hydrogen atoms and the guest molecules are omitted for clarity.

The geometrical details of these O-H···O and N-H···N interactions are listed in Table 64. For P9, the O···O distances range from 2.429 to 2.706 Å with a mean value of 2.57 Å. The O-H···O angles range from 146 to 178° with a mean value of 158°.

Table 64 Intramolecular O-H···O and N-H···N interactions in the host molecules A and B of P9[a]

Hydrogen bond	O···O or N···N Distance (Å)	Angle (°)
N1B-H1NB···N2B	2.681(4)	111
O1A-H1A···O2A	2.429(3)	151
O1B-H1B···O2B	2.453(3)	150
N1A-H1NA···N2A	2.683(4)	108
O10A-H10A···O9A	2.706(4)	148
O10B-H10B···O9B	2.646(4)	146
O12A-H12A···O4A	2.575(3)	176
O12B-H12B···O4B	2.587(3)	178

[a] Where no e.s.d. is reported for the angle, H atoms involved were added in idealised positions in a riding model.

Several intramolecular C-H···O interactions (Table 65) were found to be associated with the rifampicin conformations in both molecules A and B of P9. The hydrogen bonds C25-H···O8, C25-H···O9, C27-H···O7, C28-H···O3 and C38-H38···O12 are found to exist in both molecules A and B. The C···O distances range from 2.67 to 3.35 Å with a mean value of 2.93 Å. The C-H···O angles range from 102 to 135° with a mean value of 110°.

Table 65 Intramolecular C-H···O interactions in the host molecules A and B of P9[a]

Hydrogen bond	C···O Distance (Å)	Angle (°)
C14B-H14F···O3B	2.923(4)	104
C18A-H18A···O10A	3.023(5)	113
C18A-H18A···O11A	3.141(5)	119
C23B-H23B···O8B	3.346(4)	135
C25A-H25A···O8A	2.743(5)	103
C25A-H25A···O9A	2.870(5)	107
C25B-H25B···O8B	2.788(5)	103
C25B-H25B···O9B	2.983(4)	104
C27A-H27A···O7A	2.833(4)	106
C27B-H27B···O7B	2.835(4)	105
C28A-H28A···O3A	3.097(4)	116
C28B-H28B···O3B	3.105(5)	114
C38A-H38A···O12A	2.668(4)	102
C38B-H38B···O12B	2.672(4)	102

[a] Where no e.s.d. is reported for the angle, H atoms involved were added in idealised positions in a riding model.

The intramolecular hydrogen bonds O-H···O, N-H···N and C-H···O stabilise the conformations of the host molecules in P9.

Host-host Interactions

Two host molecules A and two host molecules B are associated by the intermolecular O-H···O and N-H···O interactions which include three bifurcated hydrogen bonds (Figure 46). Specifically, the hydrogen H4NA in host molecule A forms two hydrogen bonds with two distinct acceptors simultaneously, namely O1B and O11B. Similarly, the hydrogen H4NB in the host molecule B forms a bifurcated hydrogen bond with O1A and O11A, associating host B with a symmetry-generated host A. Between the host molecules A and B of the original asymmetric unit, H10A forms an intramolecular hydrogen bond with O9A and an intermolecular hydrogen bond with O8B simultaneously.

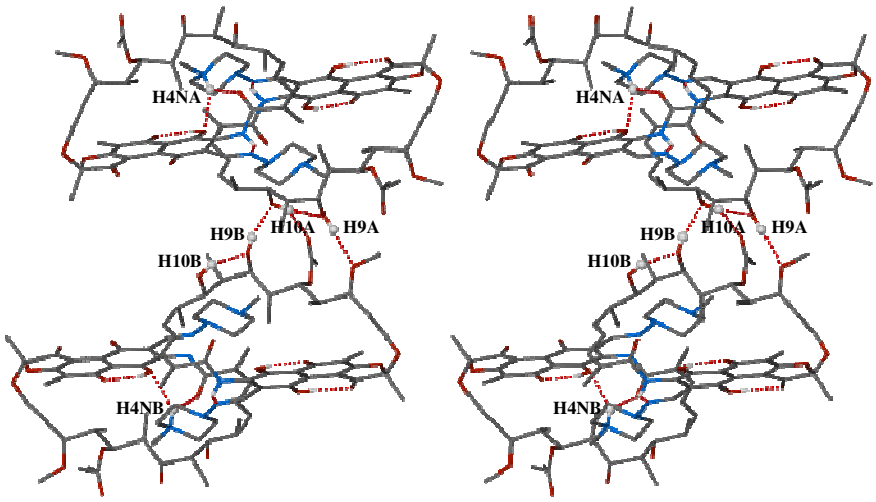

Figure 46 Stereoview of host-host intermolecular O-H···O and N-H···O interactions in P9. The relevant hydrogen atoms are shown as spheres while the other H atoms and the guest molecules are omitted for clarity.

The geometrical details of the O-H···O and N-H···O hydrogen bond interactions are listed in Table 66. For P9, the O···O distances range from 2.66 to 3.08 Å with a mean value of 2.85 Å. The O-H···O angles range from 124 to 154° with a mean value of 143°. For N···O distances, the range is 2.67 to 2.91 (mean 2.8 Å).

Table 66 Intermolecular O-H···O and N-H···O interactions between the rifampicin molecules A and B in P9[a]

Hydrogen bond	O···O or N···O Distance (Å)	Angle (°)	Symmetry operator[b]
N4B-H4NB···O1A	2.912(4)	142	1-x, 1/2+y, 1-z
N4B-H4NB···O11A	2.663(4)	131	1-x, 1/2+y, 1-z
N4A-H4NA···O1B	2.902(4)	145	1-x, -1/2+y, -z
N4A-H4NA···O11B	2.723(4)	129	1-x, -1/2+y, -z
O9A-H9A···O6B	2.816(4)	152	x, y, z
O9B-H9B···O10A	2.656(4)	154	x, y, z
O10A-H10A···O8B	3.079(4)	124	x, y, z

[a] Where no e.s.d. is reported for the angle, H atoms involved were added in idealised positions in a riding model.
[b] Symmetry operator applies to hydrogen bond acceptor atoms.

Furthermore, two analogous close contacts (C41A···O11B and C41B···O11A) are found between host molecules A and B when they assemble (Figure 47). The distances C41A···O11B and C41B···O11A are 2.905(5) and 2.878(5) Å, respectively. Considering the interactions described in Figures 46 and 47, the N-H···O, O-H···O and C-H···O

interactions stabilise the four host molecules (two A and two B molecules) when they assemble.

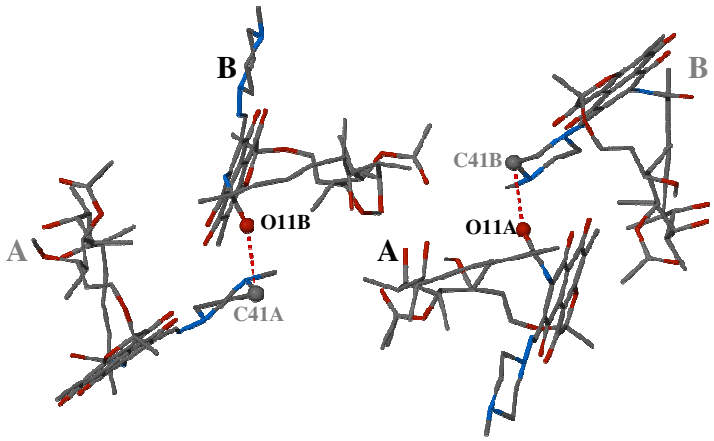

Figure 47 The close contacts C41A···O11B and C41B···O11A between host molecules A and B

Several host-host intermolecular C-H···O interactions are found in P9. The geometrical details are listed in Table 67. The C···O distances range from 2.91 to 3.54 Å with a mean value of 3.23 Å. The C-H···O angles range from 102 to 172° with a mean value of 140 °.

Table 67 Intermolecular C-H···O interactions between the rifampicin molecules in P9[a]

Hydrogen bond	C···O Distance (Å)	Angle (°)	Symmetry operator[b]
C14A-H14A···O7B	3.544(4)	172	2-x, -1/2+y, 1-z
C29A-H29A···O2B	3.341(4)	153	2-x, -1/2+y, -z
C29B-H29B···O2A	3.222(4)	154	2-x, 1/2+y, 1-z
C31B-H31D···O1A	3.187(5)	140	1-x, 1/2+y, 1-z
C40A-H40B···O2B	3.407(4)	149	1-x, -1/2+y, -z
C41A-H41A···O11B	2.905(5)	105	1-x, -1/2+y, -z
C41B-H41C···O11A	2.878(5)	102	1-x, 1/2+y, 1-z
C37B-H37E···O8A	3.319(7)	145	x, y, z

[a] Where no e.s.d. is reported for the angle, H atoms involved were added in idealised positions in a riding model.
[b] Symmetry operator applies to hydrogen bond acceptor atoms.

Host-guest Interactions

The host-guest O-H···O interactions in solvate P9 are shown in Figure 48. The host oxygen atoms which are involved in these interactions are different for host molecules A and B.

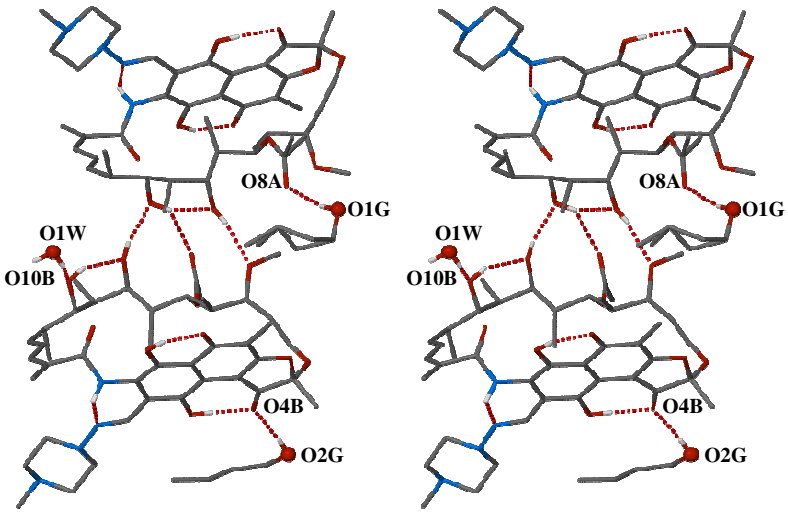

Figure 48 Stereoview of the O-H···O hydrogen bonds between the host and guest molecules in P9. The relevant oxygen atoms are shown as spheres. The other hydrogen atoms and guest molecules are omitted for clarity.

The geometrical details of these O-H···O hydrogen bond interactions are listed in Table 68. For P9, the O···O distances range from 2.77 to 2.84 Å with a mean value of 2.80 Å. The O-H···O angles range from 139.4 to 173° with a mean value of 159°.

Table 68 O-H···O interactions between the host and guest molecules in P9[a]

Hydrogen bond	O···O Distance (Å)	Angle (°)
O1G-H1G···O8A	2.835(9)	165(3)
O2G-H2G···O4B	2.768(4)	173(2)
O1W-H1W1···O8B	2.802(5)	139(2)

[a] Where no e.s.d. is reported for the angle, H atoms involved were added in idealised positions in a riding model.

Two host-guest C-H···O interactions are found in P9. The geometrical details are listed in Table 69. The mean C-H···O distance is 3.46 Å with a mean angle of 155°.

Table 69 Intermolecular C-H···O interactions between the rifampicin molecules in P9[a]

Hydrogen bond	C···O Distance (Å)	Angle (°)	Symmetry operator[b]
C40A-H40A···O5GB	3.461(8)	154	-1+x,y,z
C41A-H41A···O1W	3.453(5)	155	1-x,-1/2+y,-z

[a] Where no e.s.d. is reported for the angle, H atoms involved were added in idealised positions in a riding model.
[b] Symmetry operator applies to hydrogen bond acceptor atoms.

Guest-guest Interactions

For P9, two isolated clusters are formed by the guest molecules (Figure 49). One guest cluster consists of the 1-butanol molecules, indicated by their oxygen atoms O1G, O6G and O5GB. Water molecules O1W and O2W, whose hydrogen atoms cannot be located due to their low site-occupancy, are also involved in this guest cluster. The other guest cluster is composed of 1-propanol molecules, indicated by their oxygen atoms O4G, O3G and O2G. In more detail, a 1-butanol molecule is disordered over two positions O5GB-C17D-C18D-C19D-C20D and O5GA-C17C-C18C-C19C-C20C. The former is hydrogen bonded to O2W while the latter functions as H-bond donor to O4G. Furthermore, O2W and the molecule O4G-C13G-C14G-C15G-C16G are two disordered components.

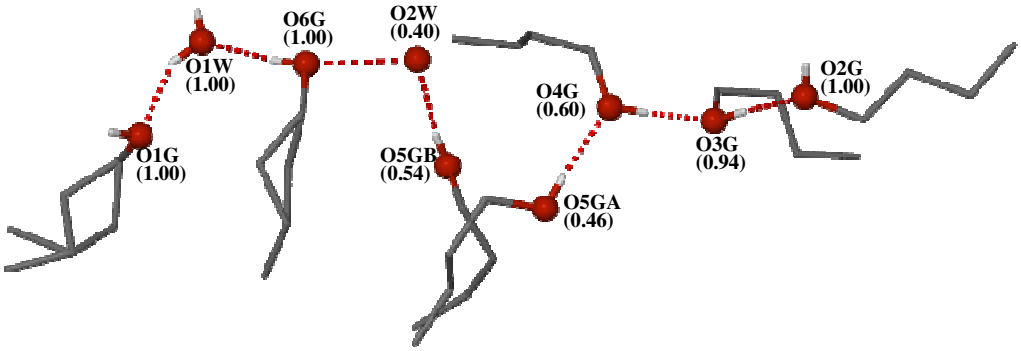

Figure 49 The guest-guest intermolecular O-H···O interactions among the water and 1-butanol molecules in P9. The disordered atoms are labelled with their site-occupancies.

In addition, 1-butanol molecules display a variety of disordered arrangements. As shown in Figure 49, both the second and fourth carbon atoms are disordered over two positions in molecule O1G-C1G-C2GA/C2GB-C3G-C4GA/C4GA while only the second carbon atom is disordered over two positions in the molecule O6G-C21G-C22C/C22D-C23G-C24G. Also, the entire 1-butanol molecule can be disordered over two positions as illustrated by the molecules O5GA-C17C-C18C-C19C-C20C and O5GB-C17D-C18D-C19D-C20D.

Details of guest-guest intermolecular O-H···O hydrogen bond interactions are listed in Table 70. The O···O distances range from 2.42 to 2.73 Å with a mean value of 2.66 Å. The O-H···O angles range from 146.0 to 175.0^{o} with a mean value of 168^{o}.

Table 70 The details of guest-guest intermolecular hydrogen bond interactions in solvate P9[a]

Hydrogen bond	O···O Distance (Å)	Angle (°)	Symmetry operator[b]
O1W-H1W2···O1G	2.575(10)	146(5)	x-1, y, z
O6G-H6G···O1W	2.725(7)	173.0	1+x, y, z
O2W···O6G	2.639(9)	-------	3-x, 1/2+y, -z
O5GB-H5GB···O2W	2.760(10)	173.0	x, y, z
O5GA-H5GA···O4G	2.751	175.0	x, y, z
O4G-H4G···O3G	2.424	167.3	x, y, z
O3G-H3G···O2G	2.731(5)	173.0	x, y, z

[a] Where no e.s.d. is reported, the average values are 0.01 Å for distances and 0.4° for angles.
[b] Symmetry operator applies to hydrogen bond acceptor atoms.

One guest-guest C···O interaction (C15G-H15G···O4G) occurs in the structure of P9. The hydrogen bond angle and distance C···O are 104° and 2.90(1) Å, respectively.

Overall Intramolecular and Intermolecular Interactions in P9

Figure 50 shows the overall hydrogen bond interactions in solvate P9. Three host molecules A and three host molecules B are associated by the overall intermolecular interactions. The two disordered guest clusters are both intimately associated with the rifampicin molecules. A noteworthy observation is that there are only two oxygen atoms (O6G and O5GB) located within hydrogen bonding distance of the water molecule O2W. In addition, O5GB is determined as functioning as hydrogen bond donor to the atom O2W. This implies that O2W serves as hydrogen bond donor to only one oxygen atom in the structure, in the bond O2W-H···O6G (Table 70).

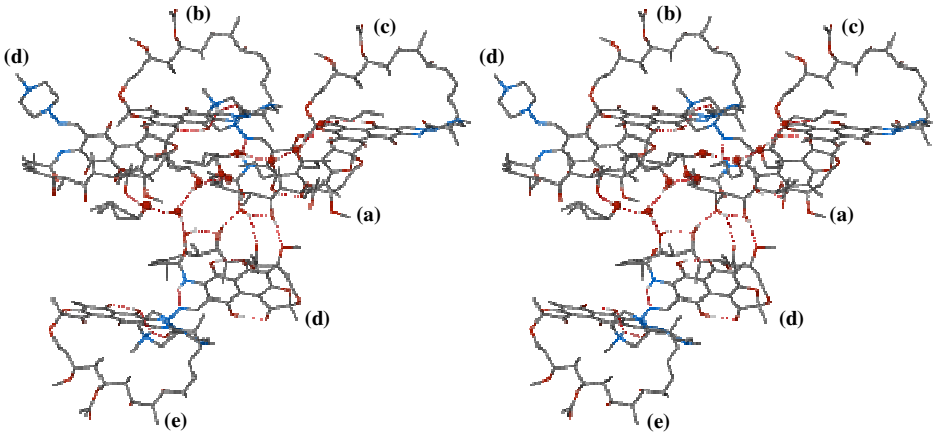

Figure 50 Stereoview of the overall hydrogen bond interactions in P9. The oxygen atoms in the guest molecules are shown as spheres. The code letter for the symmetry operator of each rifampicin molecule is given (a = x, y, z; b = 1-x, y-1/2, -z; c = 2-x, y-1/2, -z; d = x-1, y, z; e = 1-x, 1/2+y, 1-z).

Crystal Packing

The packing diagram for P9 is shown in Figure 51. Host molecules A and B are related by a pseudo 2-fold screw axis parallel to the *a*-axis and are associated by host-host interactions parallel to the *b*-axis, forming layers parallel to *c*. Each layer consists not only of host molecules A but also of B molecules which are linked by other host-host intermolecular and C···O close contact interactions parallel to the *c*-axis. Solvent molecules are intimately associated with the rifampicin molecules, and are located in channels parallel to the *a*-axis. The layers of host molecules parallel to the *c*-axis are connected both directly by hydrogen bonding and indirectly by hydrogen bonding *via* mediation of solvent molecules.

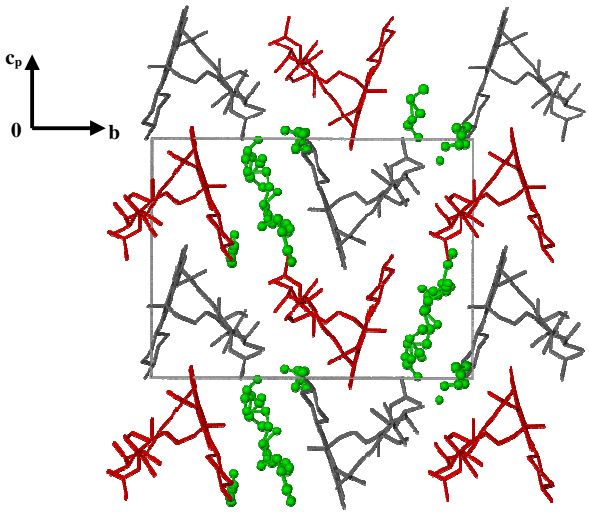

Figure 51 Crystal packing diagram for P9 viewed along [100]; solvent molecules are shown as green spheres for clarity. Host molecules A and B are shown in gray and red, respectively.

The solvent channels for P9 were examined using the program SECTION,[14] as shown in Figure 52. A series of views were taken at regular intervals through the unit cell along the *a*-axis, illustrating the 'endless' channels in which the guest molecules are located.

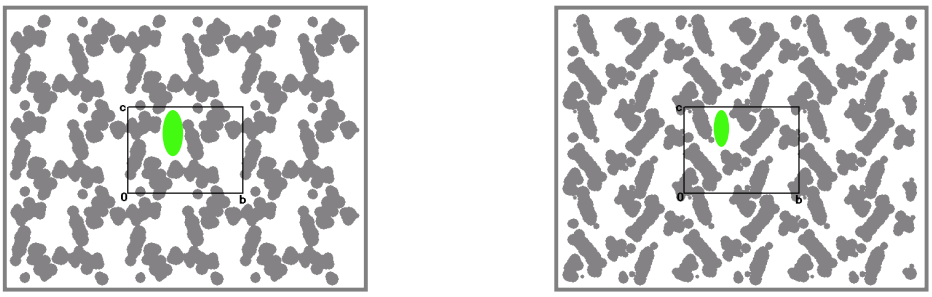

(a) 0 Å **(b) 7 Å**

Figure 52 Sections of P9 with guest molecules omitted and host molecules represented by gray areas, viewed along [100] with the unit cell sectioned at (a) 0 Å (b) 7 Å from the origin 0,0,0. A representative channel location is shown in green.

Solvate P10 – 2rifampicin • 5.75ethylene glycol • 5.59H_2O

Host Intramolecular Interactions

Figure 53 shows the intramolecular interactions for the host molecules A and B and the zwitterionic structure of the molecule B in P10. The appearance of hydrogen atoms H2A in the molecule A and H4NB in the molecule B is attributed to the probable absence of a zwitterion in the fomer and its presence in the latter. Although the geometrical location of H2A is not chemically reasonable, it is positioned based on the location of a peak which appeared at ~1 Å from atom O2A in difference Fourier maps. However, it is more likely that H1A and H2A are disordered and the model (Figure 53) shows a pair with partial site-occupancies (e.g. 0.5 each).

Furthermore, three analogous hydrogen bond interactions occur in host molecules A and B. In addition, the atom O9A serves as H-bond donor and O10A functions as acceptor in the molecule A while the atom O10B serves as H-bond donor and O9B functions as acceptor in the molecule B.

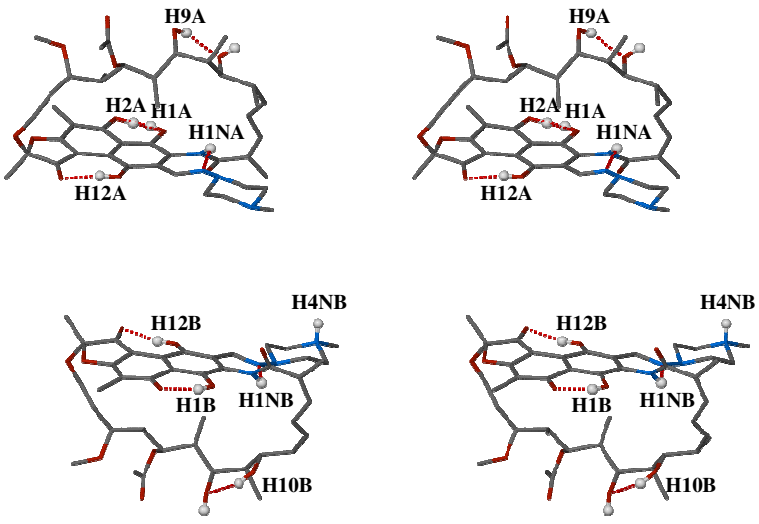

Figure 53 Stereoview of the zwitterionic structure (molecule B) and the intramolecular O-H···O and N-H···N interactions for P10. The relevant hydrogen atoms are shown as spheres. The other hydrogen atoms and the guest molecules are omitted for clarity.

Details of guest-guest intermolecular O-H···O and N-H···O hydrogen bonds are listed in Table 71. The O···O distances range from 2.47 to 2.70 Å with a mean value of 2.60 Å. The O-H···O angles range from 148 to 172^o with a mean value of 157^o.

Table 71 Intramolecular O-H···O and N-H···O hydrogen bond interactions in the host molecules in P10[a]

Hydrogen bond	O···O or N···N Distance (Å)	Angle (°)
N1B-H1NB···N2B	2.656(15)	118
O1B-H1B···O2B	2.466(13)	148
N1A-H1NA···N2A	2.653(15)	119
O9A-H9A···O10A	2.686(14)	142
O10B-H10B···O9B	2.699(14)	152
O12A-H12A···O4A	2.584(15)	172
O12B-H12B···O4B	2.588(15)	169

[a] Where no e.s.d. is reported for the angle, H atoms involved were added in idealised positions in a riding model.

Several intramolecular C-H···O and C-H···N interactions (Table 72) are found to be associated with the rifampicin conformations in P10. The hydrogen bonds C18-H18···N1, C25-H···O8, C25-H···O9, C27-H···O7, C28-H···O3 and C38-H18···O12 are found to exist in both molecules A and B. The C···O distances range from 2.62 to 3.08 Å with a mean value of 2.86 Å. The C-H···O angles range from 100 to 115° with a mean value of 107°.

Table 72 Intramolecular C-H···O and C-H···N interactions in the host molecules of P10[a]

Hydrogen bond	C···O or C···N Distance (Å)	Angle (°)
C14A-H14A···O3A	2.943(16)	108
C14B-H14F···O2B	2.849(19)	106
C18A-H18A···N1A	2.917(19)	109
C18B-H18B···O10B	3.082(18)	113
C18B-H18B···N1B	2.903(19)	105
C25A-H25A···O8A	2.758(18)	106
C25A-H25A···O9A	2.938(17)	108
C25B-H25B···O8B	2.70(2)	107
C25B-H25B···O9B	2.846(17)	107
C27A-H27A···O7A	2.789(15)	103
C28A-H28A···O3A	3.042(17)	116
C28B-H28B···O3B	3.039(19)	115
C30A-H30A···O11A	2.768(19)	107
C38A-H38A···O12A	2.659(18)	101
C38B-H38B···O12B	2.615(16)	100

[a] Where no e.s.d. is reported for the angle, H atoms involved were added in idealised positions in a riding model.

Host-host Interactions

A host-host hydrogen bond O9B-H9B···O8A is found to associate the host molecule B with a symmetry generated host molecule A, as shown in Figure 54. The distance

between the hydrogen bond donor and acceptor (O9B···O8A) is 2.784(15) Å while the angle of this hydrogen bond is 167°.

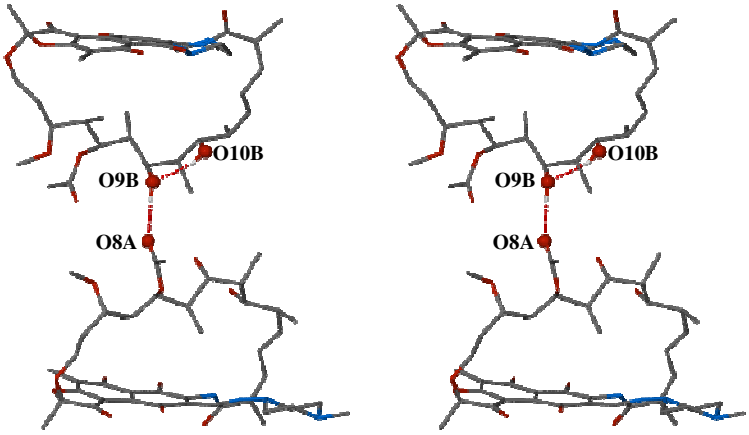

Figure 54 Stereoview of the host-host intermolecular O-H···O interactions in P10. The relevant oxygen atoms are shown as spheres while the remaining H atoms and the guest molecules are omitted for clarity.

Several intermolecular C-H···O and C-H···N interactions (Table 73) are found to be associated with the rifampicin conformations in P10. The C···O distances range from 3.12 to 3.47 Å with a mean value of 3.32 Å. The C-H···O angles range from 120 to 158° with a mean value of 146°.

Table 73 Intermolecular C-H···O interactions in the host molecules of P10[a]

Hydrogen bond	C···O Distance (Å)	Angle (°)	Symmetry operator[b]
C14B-H14D···O7B	3.12(3)	120	x, y, z
C29A-H29A···O2A	3.29(2)	158	-x, -1/2+y, 2-z
C29B-H29B···O2B	3.41(2)	156	-x, 1/2+y, 1-z
C37A-H37A···O8B	3.23(2)	137	x, y, 1+z
C40A-H40B···O1A	3.47(2)	148	1-x, -1/2+y, 2-z
C43A-H43C···O1A	3.40(2)	154	1-x, -1/2+y, 2-z

[a] Where no e.s.d. is reported for the angle, H atoms involved were added in idealised positions in a riding model.
[b] Symmetry operator applies to hydrogen bond acceptor atoms.

Host-guest Interactions

The host-guest O-H···O and N-H···O interactions in P10 are shown in Figure 55. Atoms O4, O6, O10, O11 and N4 are involved in the interactions in both molecules A and B. In more detail, the atom O10A serves as H-bond donor in the molecule A while O10B functions as acceptor for two disordered guest molecules in the molecule B. Both O11A

and O11B function as hydrogen bond acceptor; however, O11A is associated with one ethylene glycol molecule while O11B connects with one ethylene glycol molecule and one water molecule simultaneously. Due to the zwitterionic structure of the molecule B, $(N4B)^+$ functions as hydrogen bond donor to a water molecule and an ethylene glycol molecule while N4A serves as H-bond acceptor for an ethylene glycol molecule.

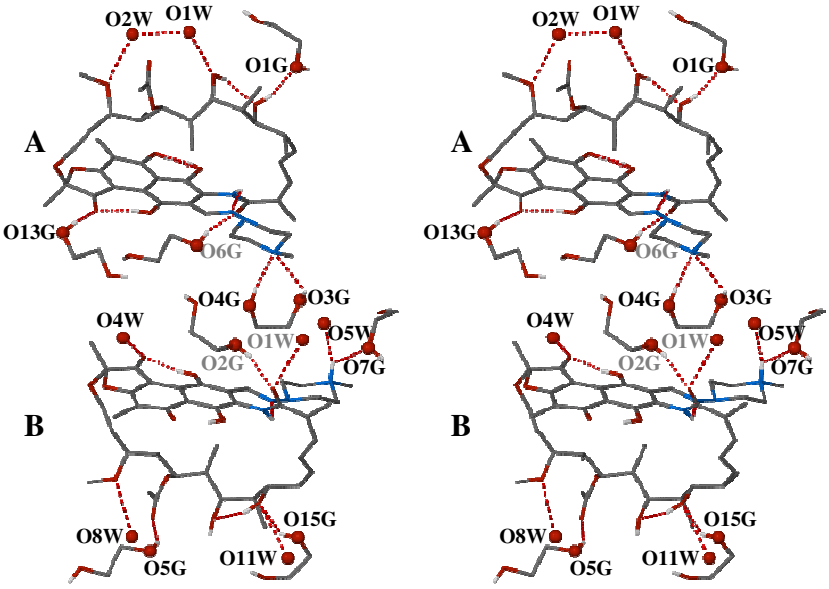

Figure 55 The stereoview of the intermolecular O-H···O and N-H···O hydrogen bonds between the host and guest molecules in P10. The relevant oxygen atoms are shown as spheres. The other hydrogen atoms and guest molecules are omitted for clarity. Atoms with gray labels have been symmetry-generated from their asymmetric unit counterparts.

Molecules O1G-C1G-C2G-O2G, O1W and O5G-C5G-C6G-O6G all serve as bridges linking host molecules. In Figure 56, molecule A is thus linked to two molecules B which are located at 1-x, 1/2+y, 2-z and –x, 1/2+y, 1-z, respectively.

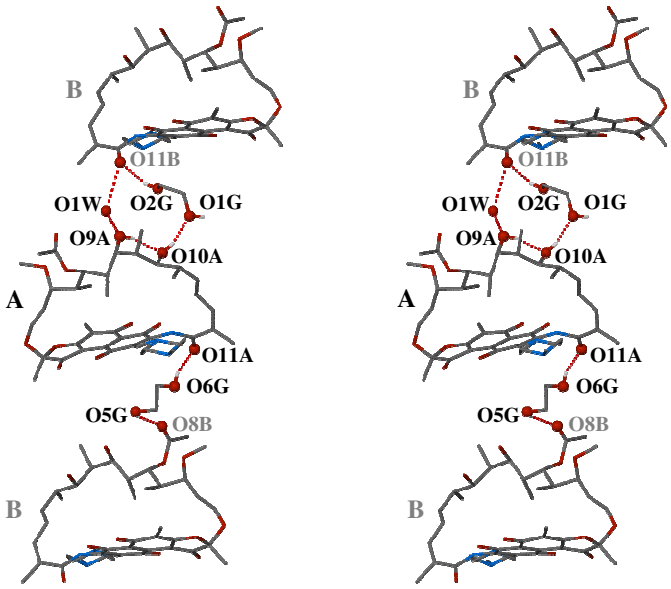

Figure 56 Guest molecules O1G-C1G-C2G-O2G, O1W and O5G-C5G-C6G-O6G serving as bridges to associate host molecules A and B. The relevant oxygen atoms are shown as spheres. The other hydrogen atoms and guest molecules are omitted for clarity. Atoms with gray labels have been symmetry-generated from their asymmetric unit counterparts.

Details of host-guest intermolecular O-H···O and N-H···O hydrogen bond interactions are listed in Table 74. The O···O distances range from 2.64 to 3.14 Å with a mean value of 2.84 Å. The O-H···O angles range from 137 to 160° with a mean value of 152°.

Table 74 Intermolecular $(N4)^+$-H4NB···O and O-H···O interactions in P10[a]

Hydrogen bond	N^+···O or O···O Distance (Å)	Angle (°)	Symmetry operator[b]
O4G-H4G···N4A	2.83(3)	142	x, y, z
O3G-H3G···N4A	3.08(2)	118	x, y, z
O2W···O6A	2.86(2)	--------	x, y, z
O1W···O9A	2.77(2)	--------	x, y, z
O10A-H10A···O1G	2.71(2)	160	x, y, z
O13G-H13G···O4A	2.67(2)	147	x, y, z
O6G-H6G···O11A	2.64(2)	159	-x, 1/2+y, 1-z
O2G-H2G···O11B	2.78(2)	162	1-x, y-1/2, 2-z
O1W···O11B	2.96(2)	--------	1-x, y-1/2, 2-z
$(N4B)^+$-H4B···O5W	2.83(2)	135	x, y, z
$(N4B)^+$-H4B···O7G	2.94(2)	126	x, y, z
O4W···O4B	2.69(2)	--------	x, y, z
O8W···O6B	3.14(4)	--------	x, y, z
O5G-H5G···O8B	2.87(2)	149	x, y, z
O11W···O10B	3.06(7)	--------	x, y, z
O15G-H15G···O10B	2.73(2)	137	x, y, z

[a] Where no e.s.d. is reported for the angle, H atoms involved were added in idealised positions in a riding model.
[b] Symmetry operator only applies to hydrogen bonding donors.

Several host-guest C-H···O interactions are found in the structure of P10. Geometrical details are listed in Table 75. The C···O distances range from 3.02 to 3.34 Å with a mean value of 3.19 Å. The C-H···O angles range from 111 to 146° with a mean value of 128°.

Table 75 Intermolecular C-H···O interactions between the host and guest molecules in P10[a]

Hydrogen bond	C···O Distance (Å)	Angle (°)	Symmetry operator[b]
C5G-H5G1···O8B	3.12(3)	120	x, y, z
C30A-H30A···O16G	3.18(3)	120	1-x, 1/2+y, 1-z
C36A-H36B···O5G	3.34(2)	146	x, y, 1+z
C36A-H36C···O16G	3.26(2)	141	x, y, 1+z
C40B-H40D···O7G	3.02(2)	111	x, y, z
C42B-H42D···O12G	3.20(2)	129	x, y, z

[a] Where no e.s.d. is reported for the angle, H atoms involved were added in idealised positions in a riding model.
[b] Symmetry operator only applies to hydrogen bonding donors.

Guest-guest Interactions

The guest molecules assemble into one extended cluster, as shown in Figure 57. A variety of disordered arrangements occurs in the cluster. For instance, the atom O8G functions as hydrogen bond donor to two disordered molecules (O8W and O5G-C5G-C6G-O6G) simultaneously.

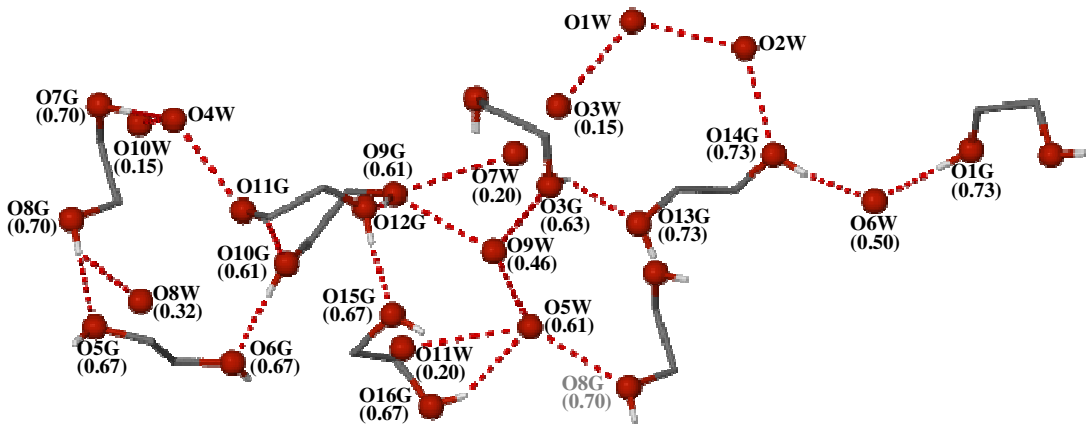

Figure 57 The extended guest cluster in P10. Atoms with gray labels have been symmetry-generated from their asymmetric unit counterparts. The disordered atoms are labelled with their site-occupancies.

Details of guest-guest intermolecular O-H···O and N-H···O hydrogen bond interactions are listed in Table 76. The O···O distances range from 2.59 to 3.08 Å with a mean value of 2.66 Å. The O-H···O angles range from 143.3 to 177.8° with a mean value of 165°.

Table 76 The details of guest-guest intermolecular hydrogen bond interactions in P10[a]

Hydrogen bond	O···O Distance (Å)	Angle (°)	Symmetry operator[b]
O8G-H8G···O5G	2.818	177.8	1-x, 1/2+y, 1-z
O8G-H8G···O8W	2.970	143.3	1-x, 1/2+y, 1-z
O7G-H7G···O4W	2.72(2)	160.0	1+x, y , z
O4W···O10W	2.79(7)	---------	x-1, y, z
O4W···O11G	2.73(2)	---------	x, y, z
O11G-H11G···O10G	2.62(3)	152.0	x, y, z
O10G-H10G···O6G	2.668	176.7	-x, 1/2+y, 1-z
O12G-H12G···O15G	2.60(3)	174.0	1-x, 1/2+y, 1-z
O16G-H16G···O5W	3.023	152.8	1-x, y-1/2, 1-z
O5W···O11W	3.07(6)	---------	1-x, 1/2+y, 1-z
O5W···O8G	2.717	---------	x, y, z
O5W···O9W	2.829	---------	x, y, z
O9W···O9G	2.674	---------	x, y, z
O9G-H9G···O12G	2.64(3)	165.0	x, y, z
O9G···O7W	3.08(6)	---------	x, y, z
O9W···O3G	2.936	---------	x, y, z
O3G-H3G···O13G	2.576	117.5	1+x, y, z
O1W···O3W	2.70(7)	---------	1-x, 1/2+y, 2-z
O1W···O2W	2.73(2)	---------	x, y, z
O2W···O14G	2.67(2)	---------	-x, 1/2+y, 2-z
O14G-H14G···O6W	2.693	170.6	x, y, z
O1G-H1G···O6W	2.590	176.0	1-x, 1/2+y, 2-z

[a] Where no e.s.d. is reported, the average values are 0.01 Å for distances and 0.6° for angles.
[b] Symmetry operator applies to hydrogen bond acceptor atoms.

Overall Intramolecular and Intermolecular Interactions in P10

Figure 58 shows the overall hydrogen bond interactions for the solvate P10. Seven rifampicin molecules are found to assemble around the solvent cluster which forms an extended solvent distribution. The hydrogen H3G in the molecule O3G-C3G-C4G-O4G forms two hydrogen bonds with two distinct acceptors simultaneously, i.e. bifurcated host-guest and guest-guest hydrogen bonds with N4A and O13G, respectively.

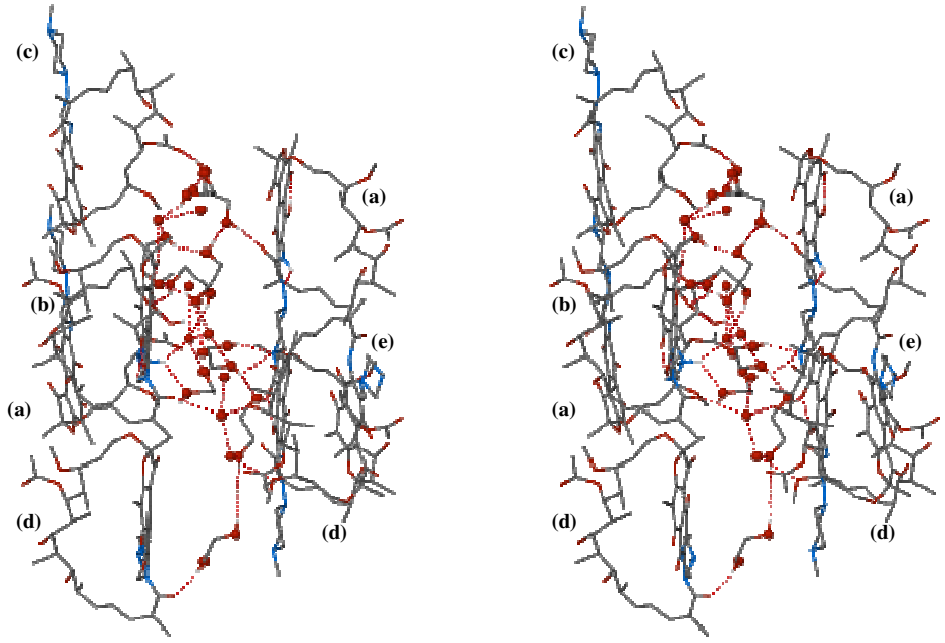

Figure 58 Stereoviews of the overall hydrogen bond interactions in P10. The oxygen atoms in the guest molecules are shown as spheres. The code letter for the symmetry operator of each rifampicin molecule is labelled (a = x, y, z; b = 1-x, 1/2+y, 1-z; c = -x, 1/2+y, 1-z; d = 1+x, y, z; e = 1-x, y-1/2, 2-z).

Crystal Packing

The packing diagram for P10 is shown in Figure 59. Host molecules A and B are related by a pseudo 2-fold screw-axis parallel to the *a*-axis, forming separate layers normal to the *c*-axis which only consist of the molecules A or B. In each layer along the *b*-axis, the molecules pack in a head-to-tail mode. The molecules A and B pack in alternating tail-to-tail and head-to-head modes parallel to the *c*-axis. The solvent molecules are located in channels parallel to the *a*-axis.

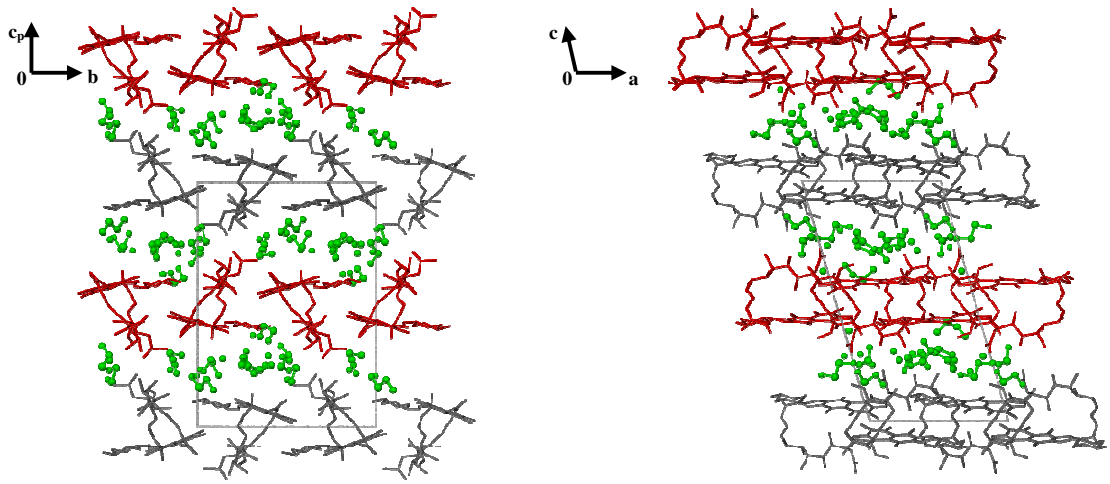

(a) (b)

Figure 59 Crystal packing diagrams for P10 viewed along (a) [100] and (b) [010]. Solvent molecules are shown as green spheres for clarity. Host molecules A and B are shown in gray and red, respectively.

In a more detailed description, the host-host hydrogen bond interactions associate the tail of the molecule A with that of the molecule B along the *c*-axis while the guest-host hydrogen bond interactions connect the molecule A with two adjacent molecules B, as shown in Figure 60. When the molecules A and B assemble in head-to-head mode along the *c*-axis, no interaction is observed to associate the two host molecules. This introduces the voids where the solvent molecules can be accommodated.

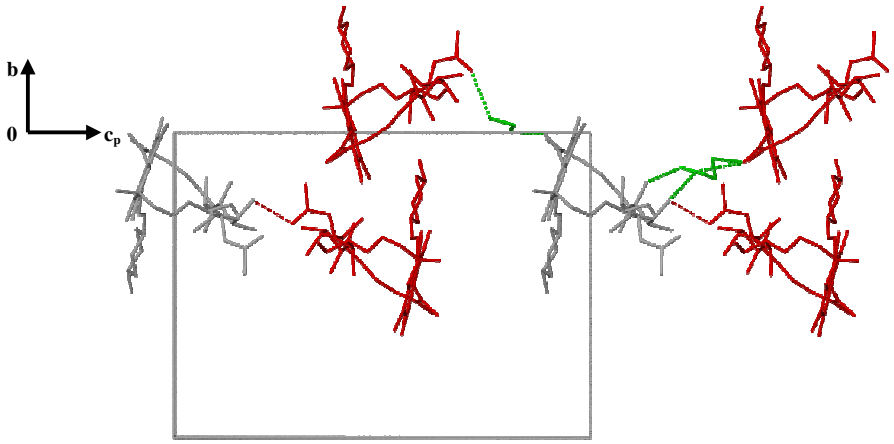

Figure 60 Host-host and guest-host hydrogen bond interactions associating host molecule layers along the *b*-axis. The solvent, A and B molecules are shown in green, gray and red, respectively. The host-host and guest-host intermolecular interactions are shown in red and green dashed lines, respectively.

The program SECTION[14] was used to examine the voids occupied by guest molecules. A series of representative views take at regular intervals along the *a*-axis is shown in Figure 61. This clearly illustrates the 'endless' channels in which the guest molecules are accommodated.

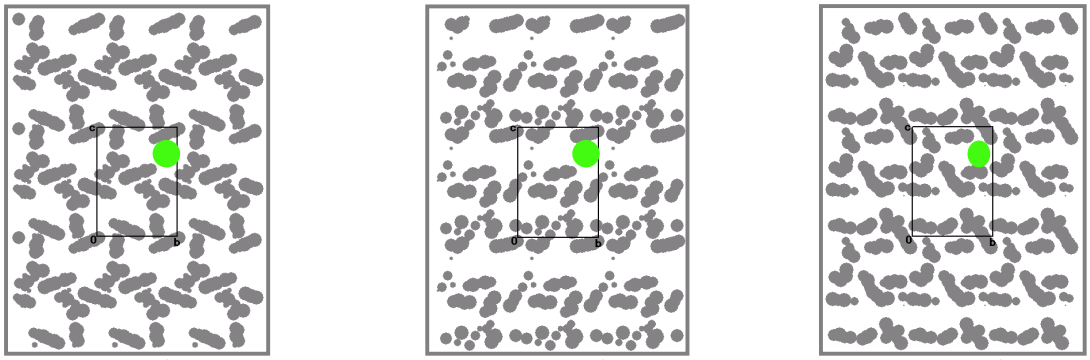

(a) 0 Å **(b) 4 Å** **(c) 8 Å**

Figure 61 Sections through P10 with guest molecules omitted and host molecules represented by gray areas, viewed along [100] with the unit cell sectioned at (a) 0 Å, (b) 4 Å and (c) 8 Å from the origin 0,0,0. A representative channel location is shown in green.

Solvate P11 – 2rifampicin • 6(1, 4-dioxane) • $3H_2O$

Host Intramolecular Interactions

In the structure of P11, three analogous intramolecular O-H···O hydrogen bond interactions (O1-H1···O2, O9-H9···O10, O12-H12···O4) are found in the host molecules A and B, as presented in Figure 62. An additional hydrogen bond N1B-H1NB···N2B is found in the molecule B. This specific hydrogen bond can often be observed in the host molecules of other solvates; however, it does not occur in the host molecule A in P11. This corresponds to the fact that the molecule A adopts a much smaller dihedral angle between the planes of the chromophore (B) and the piperazinyl residue (C) [3.81(8)^o] than that in the molecule B [16.96(7)^o]. Furthermore, this introduces a unique host intramolecular interaction O10A-H10A···O11A which is not found in the host molecules in all the other solvates.

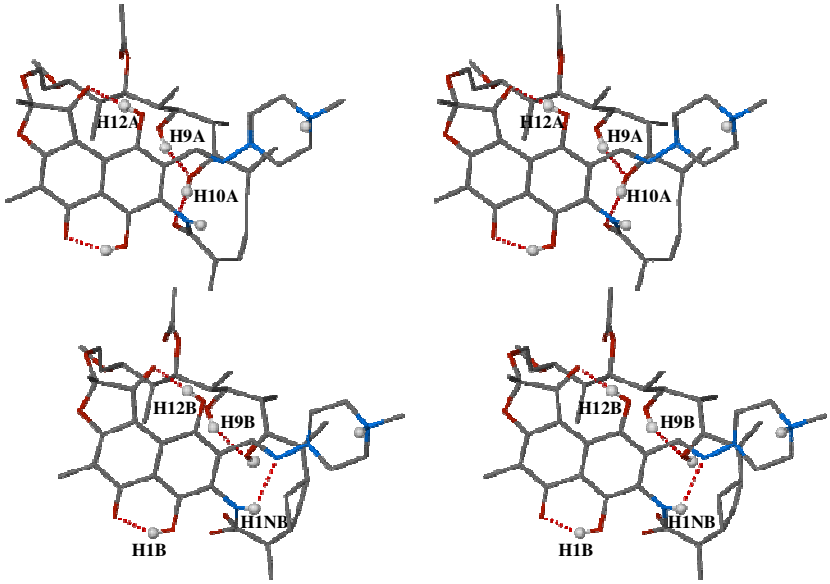

Figure 62 The zwitterionic structures and the intramolecular O-H···O and N-H···N interactions for rifampicin host molecules A and B in P11. The relevant hydrogen atoms are shown as spheres. The other hydrogen atoms and the guest molecules are omitted for clarity.

Details of host intramolecular O-H···O and N-H···N interactions are listed in Table 77. The O···O distances range from 2.48 to 2.83 Å with a mean value of 2.61 Å. The O-H···O angles range from 138 to 179^o with a mean value of 158^o.

Table 77 Intramolecular hydrogen bond interactions in the host molecules A and B in P11[a]

Hydrogen bond	O···O or N···N Distance (Å)	Angle (°)
O1A-H1A···O2A	2.481(4)	148.0
O1B-H1B···O2B	2.469(5)	148.0
O9A-H9A···O10A	2.688(4)	138.0
O9B-H9B···O10B	2.648(4)	143.0
O12A-H12A···O4A	2.593(4)	174.0
O12B-H12B···O4B	2.584(4)	179.0
N1B-H1NB···N2B	2.701(5)	109.0
O10A-H10A···O11A	2.829(4)	175.0

[a] Where no e.s.d. is reported for the angle, H atoms involved were added in idealised positions in a riding model.

Several intramolecular C-H···O interactions (Table 78) were found to be associated with the rifampicin conformations in P11. The hydrogen bonds C14-H···O3, C25-H···O8, C25-H···O9, C27-H···O7 and C38-H···O12 are found to exist in both molecules A and B. The C···O distances range from 2.65 to 3.11 Å with a mean value of 2.83 Å. The C-H···O angles range from 102 to 115° with a mean value of 107°.

Table 78 Intramolecular C-H···O interactions in the host molecules of P11[a]

Hydrogen bond	C···O or C···N Distance (Å)	Angle (°)
C14A-H14A···O3A	2.944(5)	106.0
C14B-H14D···O3B	2.922(6)	105.0
C18B-H18B···O10B	2.957(6)	112.0
C25A-H25A···O8A	2.739(5)	105.0
C25A-H25A···O9A	2.828(4)	110.0
C25B-H25B···O8B	2.723(5)	106.0
C25B-H25B···O9B	2.865(5)	110.0
C27A-H27A···O7A	2.757(4)	100.0
C27B-H27B···O7B	2.787(4)	103.0
C28B-H28B···O3B	3.107(5)	115.0
C38A-H38A···O12A	2.671(4)	103.0
C38B-H38B···O12B	2.648(5)	102.0

[a] Where no e.s.d. is reported for the angle, H atoms involved were added in idealised positions in a riding model.

Host-host Interactions

Host-host hydrogen bond interactions $(N4A)^+$-H···O8A and $(N4A)^+$-H···O9A and two close contacts O9A···C41A [2.978(5) Å] and O8A···C40A [3.130(5) Å] are observed between the host molecule A and a symmetry transformed molecule A, as shown in Figure 63. Analogous interactions are associated with the B molecules.

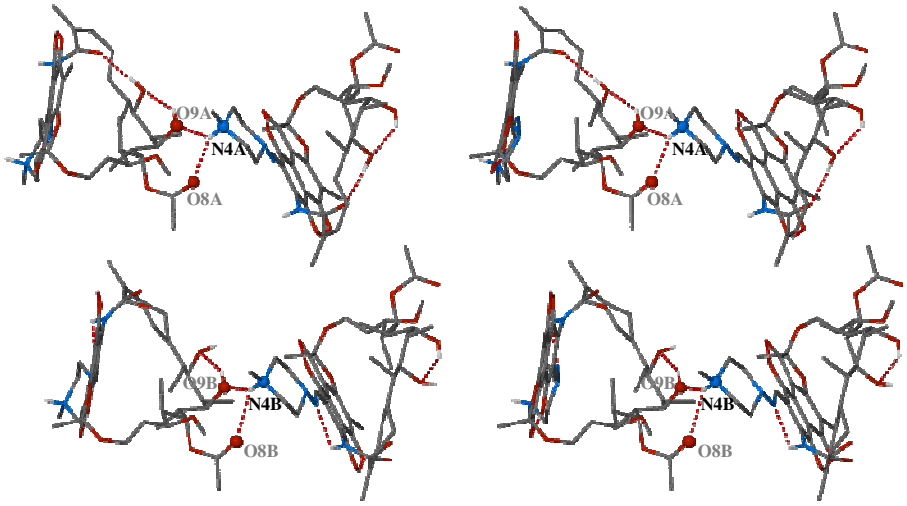

Figure 63 Stereoview of host-host intermolecular N-H···O interactions in P11. The relevant oxygen and nitrogen atoms are shown as spheres, while the other H atoms and the guest molecules are omitted for clarity. Atoms with gray labels have been symmetry-generated from their asymmetric unit counterparts.

A detailed description of these interactions is as follows: H4NA in the host molecule A forms bifurcated hydrogen bonds with O9A and O8A of a symmetry-transformed host molecule A. Analogous interactions occur for the pair of B molecules. In addition, close contacts O9B···C41B [3.143(5) Å] and O8B···C40B [3.053(5) Å] are found between two B molecules.

Details of host intermolecular N-H···O hydrogen bond interactions are listed in Table 79. The bifurcated N···O distances range from 2.84 to 3.17 Å with a mean value of 2.98 Å. The N-H···O angles range from 121 to 148° with a mean value of 133°.

Table 79 Intermolecular H-bond interactions in the host molecules A and B in P11[a]

Hydrogen bond	N···O Distance (Å)	Angle (°)	Symmetry operator[b]
N4A-H4NA···O8A	3.026(5)	134.0	-x,-1/2+y, -z
N4A-H4NA···O9A	2.862(4)	130.0	-x,-1/2+y, -z
N4B-H4NB···O8B	3.165(5)	121.0	1-x, y-1/2, 1-z
N4B-H4NB···O9B	2.842(5)	148.0	1-x, y-1/2, 1-z

[a] Where no e.s.d. is reported for the angle, H atoms involved were added in idealised positions in a riding model.
[b] Symmetry operator applies to hydrogen bond acceptor atoms.

Several host-host intermolecular C-H···O interactions are found in P11. The details of all C-H···O interactions are listed in Table 80. The C···O distances range from 2.97 to 3.25Å with a mean value of 3.18 Å. The C-H···O angles range from 104 to 163° with a mean value of 130°.

Table 80 Intermolecular C-H···O interactions between the rifampicin molecules[a]

Hydrogen bond	C···O Distance (Å)	Angle (°)	Symmetry operator[b]
C39A-H39B···O8A	3.249(5)	129.0	-x, -1/2+y, -z
C41A-H41B···O9A	2.978(5)	104.0	-x, -1/2+y, -z
C41B-H41C···O2B	3.251(5)	163.0	1+x, y, z
C42A-H42A···O9A	3.233(5)	122.0	-x, -1/2+y, -z

[a] Where no e.s.d. is reported for the angle, H atoms involved were added in idealised positions in a riding model.
[b] Symmetry operator applies to hydrogen bond acceptor atoms.

Host-guest Interactions

The host-guest O-H···O and N-H···O interactions in P11 are shown in Figure 64. Two bifurcated hydrogen bonds are found among the host-guest interactions. H1NA in the host molecule A forms hydrogen bonds with two acceptors O3D and O3C which belong to two disordered 1,4-dioxane molecules. H10B in the molecule B forms bifurcated hydrogen bonds with O1D and O1C which belong to the disordered 1,4-dioxane molecule. The water molecule O1W serves as a bridge linking two host molecules A and B in the asymmetric unit.

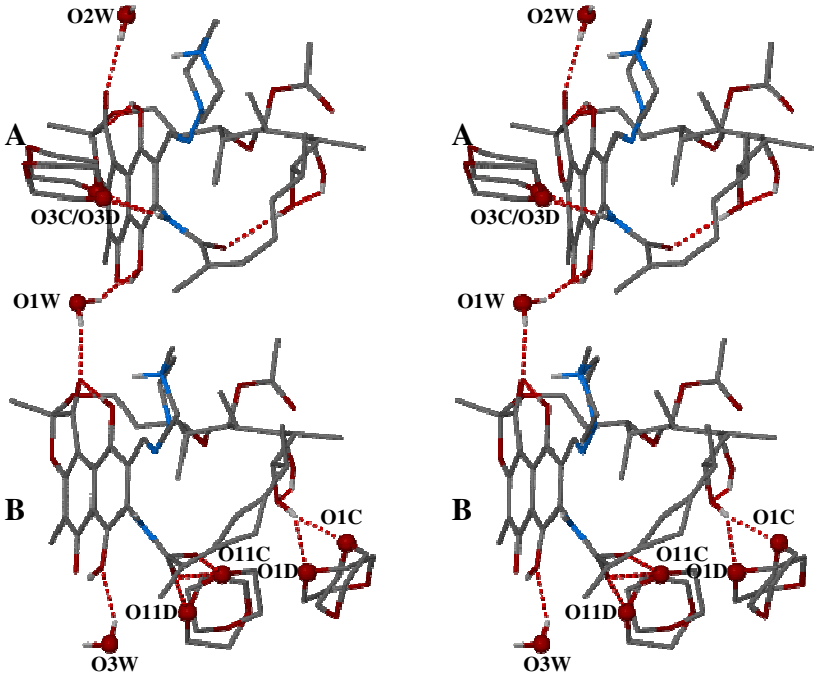

Figure 64 Stereoviews of the intermolecular O-H···O and N-H···O hydrogen bonds between the host and guest molecules in the P11. The relevant oxygen atoms are shown as spheres. The other hydrogen atoms and guest molecules are omitted for clarity.

Details of host intermolecular O-H···O and N-H···O hydrogen bonds are listed in Table 81. The O···O distances range from 2.82 to 3.13 Å with a mean value of 2.95 Å. The O-H···O angles range from 140 to 169° with a mean value of 154°.

Table 81 Host-guest O-H···O or N-H···O interactions and O···O short contacts in the structure of P11[a]

Hydrogen bond	O···O or N···O Distance (Å)	Angle (°)
O3W-H3W1···O1B	2.895(6)	153(4)
O11B···O11D	3.060	----------
O11B···O11C	3.043	----------
O11E···O11C	2.967	----------
O10B-H10B···O2D	2.96(2)	145.0
O10B-H10B···O1C	2.739(7)	147.0
O1W-H1W2···O4B	2.928(4)	168(2)
O1W-H1W1···O1A	3.126(4)	154(2)
N1A-H1NA···O3D	3.08(2)	153.0
N1A-H1NA···O3C	3.036(5)	140.0
O2W-H2W1···O4A	2.815(4)	169(6)

[a] Where no e.s.d. is reported for the angle, H atoms involved were added in idealised positions in a riding model. Where no e.s.d. is reported, the average value is 0.004 Å for distances.

Several host-guest C-H···O interactions are found in the structure of P11. Geometrical details are listed in Table 82. The C···O distances range from 3.31 to 3.46 Å (mean 3.40 Å) while the C-H···O angles range from 146 to 165° (mean 156°).

Table 82 C-H···O interactions between the rifampicin and guest molecules[a]

Hydrogen bond	C···O Distance (Å)	Angle (°)	Symmetry operator[b]
C9G-H9D···O12A	3.424(5)	146.0	x, y, z
C11G-H11D···O10A	3.361(5)	156.0	-x, -1/2+y, -z
C29A-H29A···O3W	3.462(6)	165.0	-1+x, y, -1+z
C37B-H3C···O8G	3.425(8)	151.0	x, y, z
C43A-H43C···O7G	3.306(5)	163.0	-x, -1/2+y, -z

[a] Where no e.s.d. is reported for the angle, H atoms involved were added in idealised positions in a riding model.
[b] Symmetry operator applies to hydrogen bond acceptor atoms.

Guest-guest Interactions

A variety of disordered arrangements occur in the 1,4-dioxane molecules, as shown in Figure 65. Three 1,4-dioxane molecules are disordered over two positions. However, the geometrical distributions of the two disordered components are different in each case. The solvent molecules retain a chair-conformation throughout.

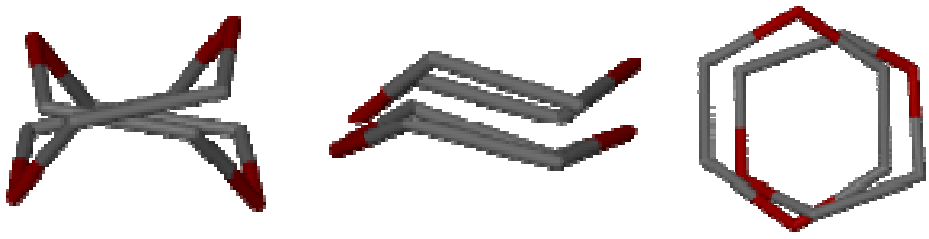

(a) **(b)** **(c)**

Figure 65 Three 1,4-dioxane molecules disordered over two positions. (a) O1C-C1C-C2C-O2C-C3C-C4C and O1D-C1D-C2D-O2D-C3D-C4D; (b) O3C-C5C-C6C-O4C-C7C-C8C and O3D-C5D-C6D-O4D-C7D-C8D; (c) O11C-C21C-C22C-O12C-23C-24D and O11D-C21D-C22D-O12D-C23D-C24D.

Two water molecules O3W and O2W as well as a 1,4-dioxane molecule O5G-C9G-C10G-O6G-C11G-C12G are connected by a hydrogen bond chain: O3W-H3W2···O2W-H2W2···O5G (shown in Figure 66).

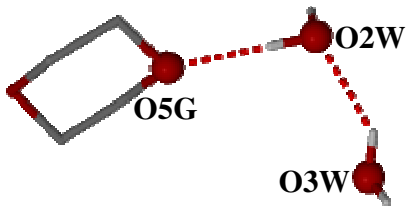

Figure 66 The guest-guest intermolecular O-H···O interactions among the water and 1, 4-dioxane molecules.

Details of host intermolecular O-H···O interactions are listed in Table 83. The O···O distances range from 2.76 to 2.91 Å (mean value 2.84 Å). The average value of O-H···O angles is 161°.

Table 83 Guest-guest intermolecular O-H···O interactions and O···O short contacts among guest molecules

Hydrogen bond	O···O Distance (Å)	Angle (°)	Symmetry operator[b]
O2W-H2W2···O5G	2.865(4)	177(4)	x, y, z
O3W-H3W2···O2W	2.906(7)	145(2)	1+x, y, 1+z
O3D···O2C	2.76(2)	--------	1-x, y-1/2, 1-z

[b] Symmetry operator applies to hydrogen bond acceptor atoms.

Overall Intramolcular and Intermolecular Interactions in P11

The overall hydrogen bond interactions of P11 are shown in Figure 67. Five rifampicin host molecules (including three host molecules A and two host molecules B) assemble through these interactions.

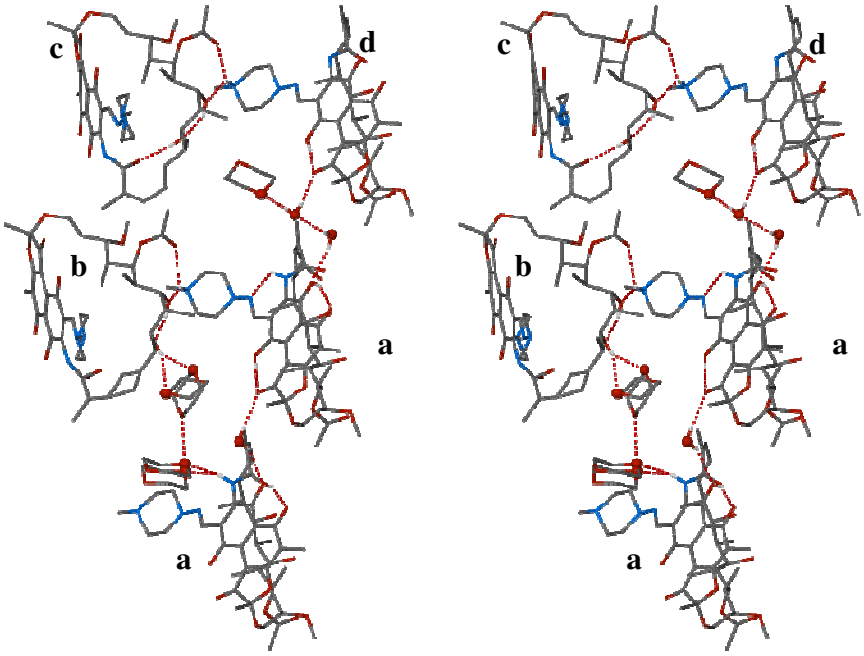

Figure 67 Stereoview of the overall hydrogen bond interactions in P11. The oxygen atoms in solvent molecules are shown as spheres. The code letter for the symmetry operator of each rifampicin molecule is labelled. (a = x, y, z; b = 1-x, y-1/2, 1-z; c = 1-x, y-1/2, 1-z; d = 1+x, y, 1+z).

A noteworthy observation is that the oxygen atoms in the 1,4-dioxane molecules O7G-C13G-C14G-O8G-C16G-C17G and O9G-C18G-C19G-O10G-C20G-C21G are not hydrogen bonded to other oxygen atoms. However, C16G in the former molecule is within C-H···O H-bonding distance of atom O11A [3.064(4) Å]. Initially it was thought that the atoms C16G may have been misassigned as carbon and should instead have been treated as oxygen. However, the original atom assigned as oxygen had a significantly higher electron-density than those atoms assigned as carbons in the 1,4-dioxane molecules. The rather short C16G···O11A distance was finally accepted as a real feature. Thus, the molecule of 1,4-dioxane labelled O7G-C13G-C14G-O8G-C16G-C17G is in close contact with host molecule A while the 1,4-dioxane molecule O9G-C18G-C19G-O10G-C20G-C21G is isolated.

Crystal Packing

The packing diagrams of P11 are shown in Figure 68. Host molecules A and B are related by a pseudo *B*-centering translation. Host molecules A form columns parallel to

the *b*-axis, as do the B molecules. Layers, assembled from interlocking lattices of A and B molecules, lie perpendicular to the *b*-axis. Analogous host-host interactions and C···O close contacts are found to associate host molecules A to A and B to B parallel to the *b*-axis while the host-guest intermolecular interactions are found to associate the host molecules A and B along the *c*-axis. This arrangement results in the formation of isolated solvent cluster.

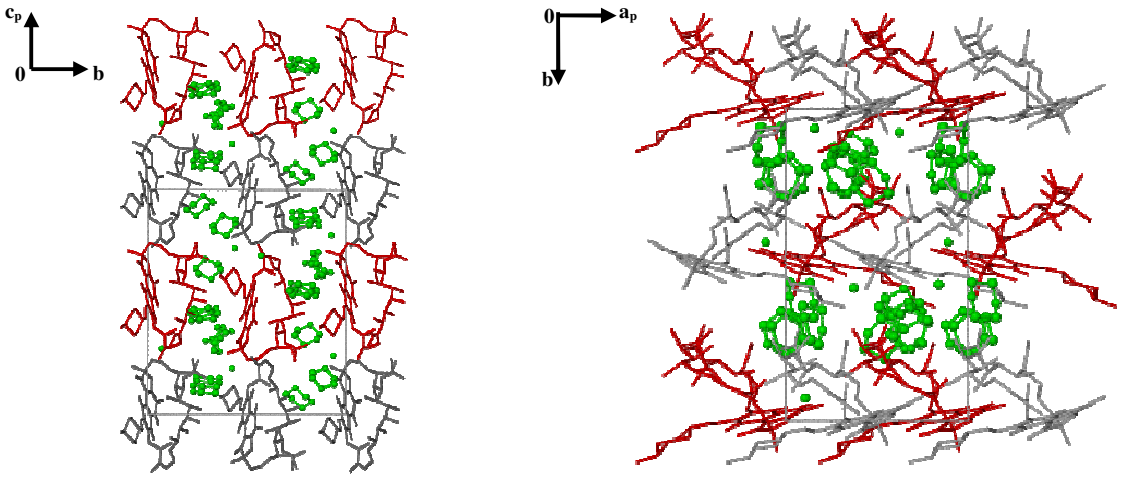

Figure 68 Crystal packing diagram for P11 viewed along (a) [100] and (b) [001]. Solvent molecules are shown in green and spheres for clarity. Host molecules A and B are shown in gray and red, respectively.

The program SECTION[14] was used to view planes at x = 0 and x = 7.7 through the unit cell along the *a*-axis (Figure 69). The isolated sets of 1,4-dioxane molecules are evident.

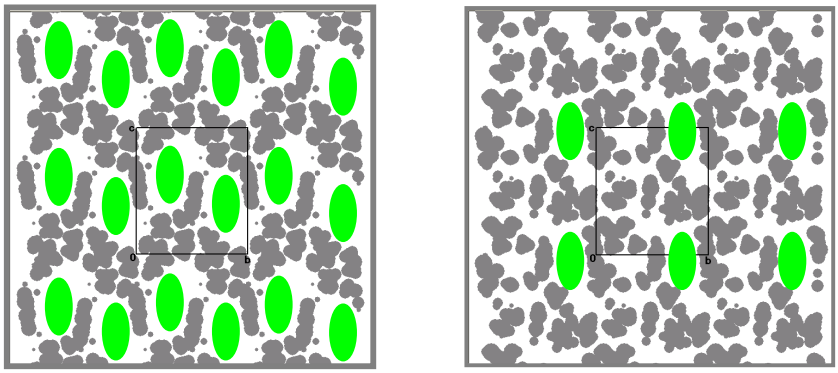

Figure 69 Sections through P11 with guest molecules and host molecules represented by green and gray areas, respectively; viewed along [100] with the unit cell sectioned at (a) 0 Å and (b) 7.7 Å from 0,0,0.

Comparative PXRD

The PXRD traces for solvates P8 - P11 generated from their single crystal X-ray structures are shown in Figure 70. These traces are all significantly different, excluding the possibility of isostructurality in this solvate series.

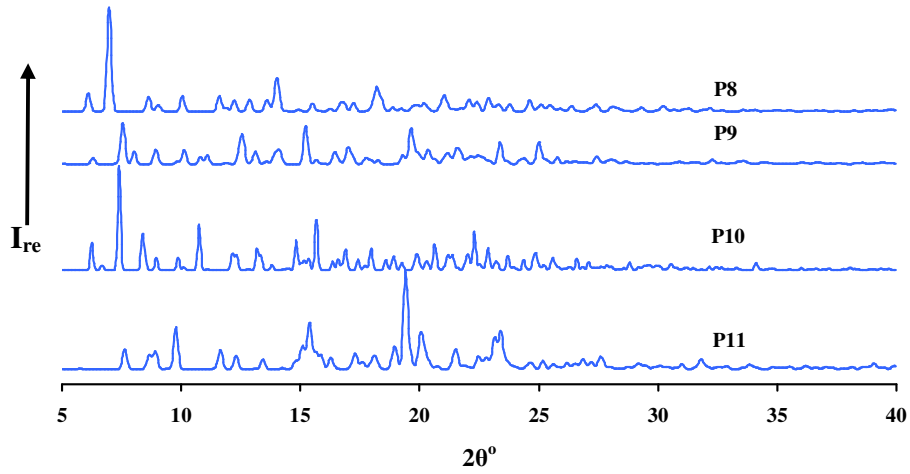

Figure 70 Calculated PXRD traces for P8, P9, P10 and P11.

Conclusion

Concluding remarks, based on the data discussed above for all the rifampicin solvates (isostructural series 1 and 2, P8, P9, P10 and P11) are presented here.

Crystal Preparation

For the preparation of the crystals of all the solvates, certain amounts of water were required in the mother liquors to dissolve the raw material at 25 °C. Furthermore, all the crystals grew at 4 °C except those of P11 which grew at 25 °C. In addition, the only difference between the preparative methods for P7 and P8 is that the recrystallisation solution of the former was not filtered while that of the latter was filtered. The above is merely a summary of crystallisation procedures employed. No particular correlation between e.g. temperature of crystallisation and drug conformation in the resulting crystal structure was observed.

Powder X-ray Diffraction

The experimental PXRD traces for isostructural series 1 and 2 were in reasonable agreement with their respective calculated traces which were based on single crystal X-ray data. The latter are included in Figure 71. In general, the dissimilarity among these traces is sufficiently marked to identify and distinguish the six distinct solvatomorphic phases of rifampicin identified and characterised in this study.

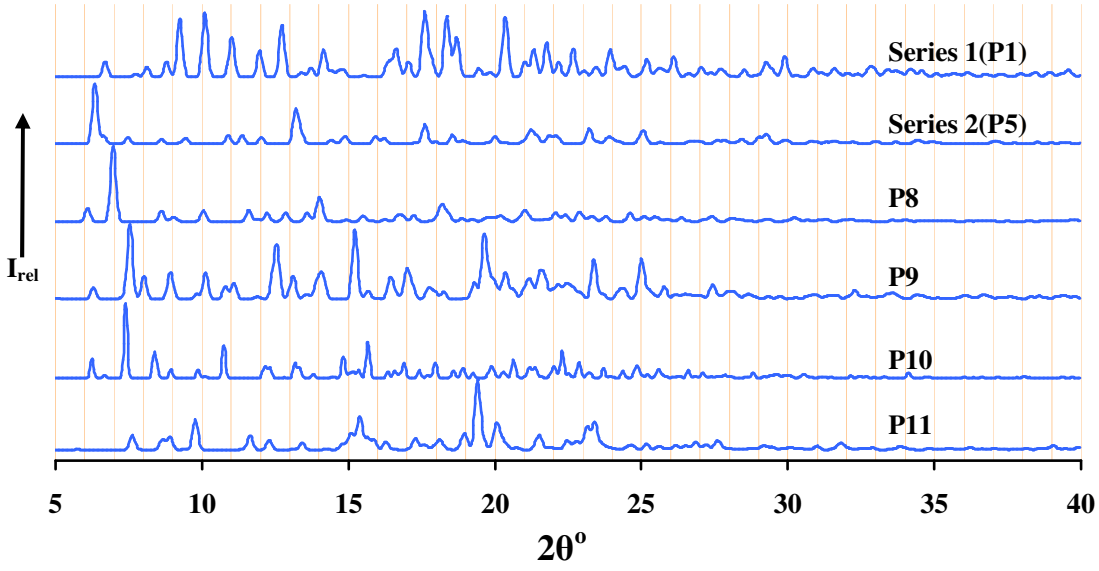

Figure 71 Calculated PXRD traces of isostructural series 1 (P1 as representative) and 2 (P5 as representative), P8, P9, P10 and P11.

Conformation of the Rifampicin Host Molecules

Rifampicin molecules in the isostructural series 1 adopt a similar conformation to those in P8 and P10 of series 2, as presented in Figure 72. The host molecule in P1 is chosen as a representative for the host molecules in series 1 while the host molecules A in P8 and P9 are selected for comparison. Although subtle differences exist among these molecules, the overall conformations are very similar.

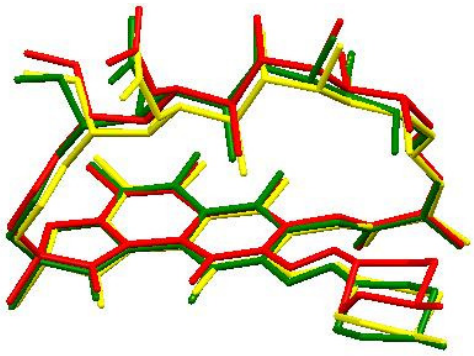

Figure 72 An overlay of host molecules in P1 (green), A in P8 (red) and A in P10 (yellow).

As discussed previously, two distinct conformations of rifampicin molecules are found to co-exist in the structure of P11. The rifampicin molecule A in P9 is overlayed with the molecule B in P11 (Figure 73). In the latter, the atom C18 is disordered over two positions where C18B is the major component [s.o.f. 0.78(1)]. The major conformational difference is in the orientation of the piperazinyl moiety in the two molecules.

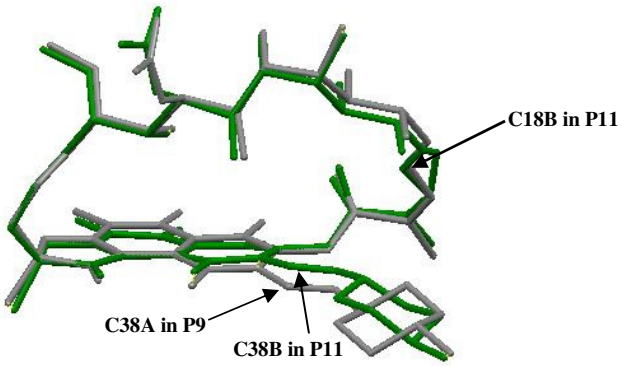

Figure 73 An overlay of the host molecule A in P9 (gray) and B in P11 (green).

Indications of four distinct conformations of the rifampicin molecules were found during the investigation of the rifampicin solvates. The host molecule in P1 is employed as a representative for those in series 1, P8 and P10 while that in P5 is selected as a representative for those in series 2. The conformational differences among these rifampicin molecules are reflected in the values of all the torsion angles along the ansa chain, as listed in Table 84. The main differences are reflected in the torsion angles τ_2, τ_4 and τ_6.

Table 84 The conformations reflected by the torsion angles along the ansa chain in the host molecules of series 1, series 2, A in P9 and A in P11, respectively.

Torsion angles (°)	**Series 1**	**Series 2**	**P9 (A)**	**P11 (A)**
C2-N1-C15-C16 (τ_1)	*trans*	*trans*	*trans*	*trans*
N1-C15-C16-C17 (τ_2)	*cis*	*anticlinal*	*anticlinal*	*anticlinal*
C15-C16-C17-C18 (τ_3)	*cis*	*cis*	*cis*	*cis*
C16-C17-C18-C19 (τ_4)	*trans*	*trans*	*trans*	*gauche*
C17-C18-C19-C20 (τ_5)	*trans*	*trans*	*trans*	*trans*
C18-C19-C20-C21 (τ_6)	*cis*	*gauche*	*cis*	*anticlinal*
C19-C20-C21-C22 (τ_7)	*trans*	*trans*	*trans*	*trans*
C20-C21-C22-C23 (τ_8)	*trans*	*trans*	*trans*	*trans*
C21-C22-C23-C24 (τ_9)	*gauche*	*gauche*	*gauche*	*gauche*
C22-C23-C24-C25 (τ_{10})	*trans*	*trans*	*trans*	*trans*
C23-C24-C25-C26 (τ_{11})	*trans*	*trans*	*trans*	*trans*
C24-C25-C26-C27 (τ_{12})	*trans*	*trans*	*trans*	*trans*
C25-C26-C27-C28 (τ_{13})	*trans*	*trans*	*trans*	*trans*
C26-C27-C28-C29 (τ_{14})	*anticlinal*	*anticlinal*	*anticlinal*	*anticlinal*
C27-C28-C29-O5 (τ_{15})	*trans*	*trans*	*trans*	*trans*
C12-O5-C29-C28 (τ_{16})	*gauche*	*gauche*	*gauche*	*gauche*
C29-O5-C12-O3 (τ_{17})	*gauche*	*gauche*	*gauche*	*gauche*

The torsion angle τ_2 in the host molecules of series 1 [Figure 74 (a)] is distinctly different from the τ_2 values for the other molecules in Figure 74. This corresponds to the fact that the C15=O11 bond in series 1 points away from the ansa chain while it points towards the chain in the others. The torsion angle τ_4 in the host molecule A of P11 [Figure 74 (d)] is distinct. Accompanying this, τ_6 in this molecule is distinctive. Finally, we note that for P5, the piperazinyl substituent ('plane' C) is unique in linking to the imine group *via* an axial N-N bond [Figure 74 (b)] whereas in the other molecules shown, the N-N bond is equatorial. For the latter cases, plane C is located above, parallel to, and below the chromophore (plane B) in series 1, P9 and P11, respectively. This is one of the several novel features established for rifampicin in this study.

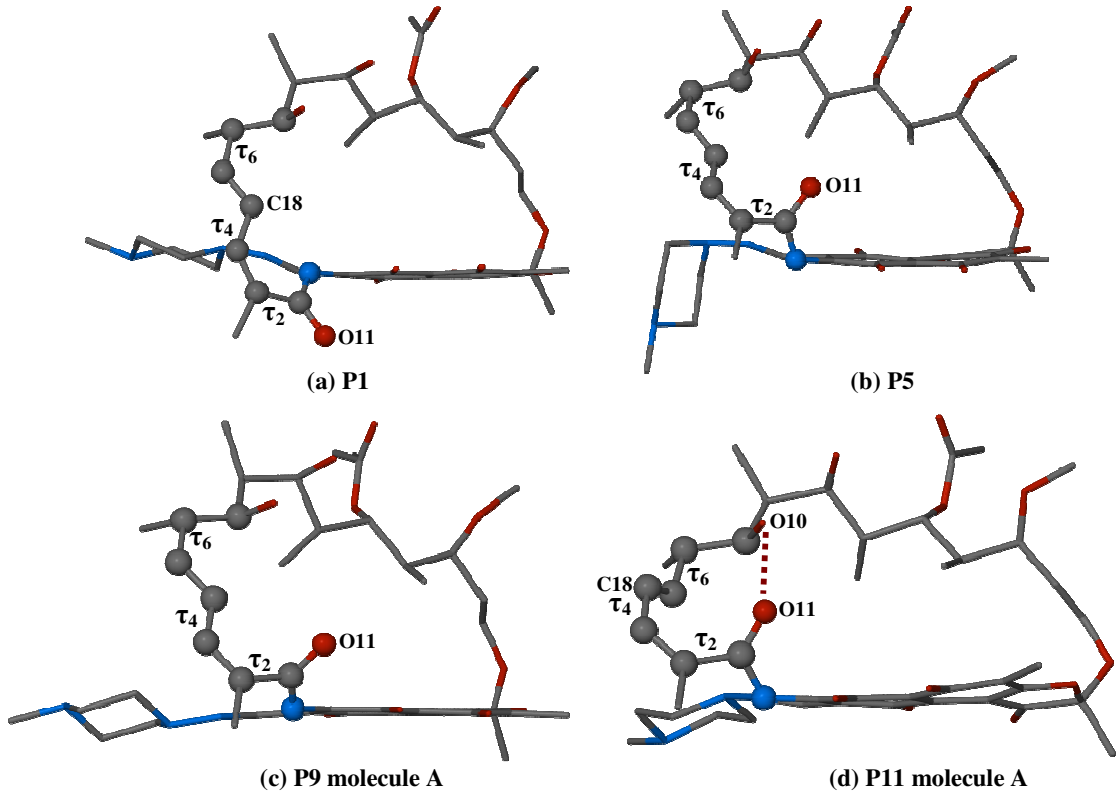

Figure 74 Conformational differences among rifampicin host molecules in (a) P1, (b) P5, (c) molecules A in P9 and (d) molecule A in P11. O11 atoms in each molecule are shown as spheres for clarity.

Figure 75 illustrates the overlay diagram of these four molecules for comparison. The unique configuration of the piperazinyl moiety (in blue) is quite evident.

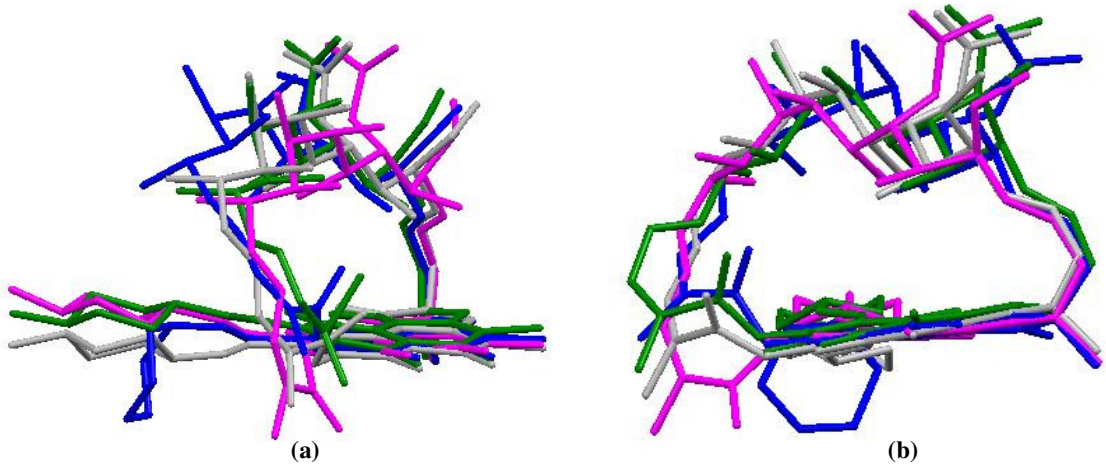

Figure 75 An overlay of the host molecules in solvates P1 (pink), P5 (blue), A in P9 (gray) and A in P11 (green). Guest molecules and hydrogen atoms are omitted for clarity. (a): view roughly side-on with respect to the ansa chain; (b): view normal to the ansa chain backbone.

In addition, the dihedral angles between the plane of the ansa chain (plane A) and the chromophore (plane B) differ significantly among the host conformations of the four solvatomorphic phases. This also applies to the dihedral angles between the planes B and C (piperazinyl residue), as listed in Table 85. In more detail, the angles for the series 1 and series 2 are the average values of those in P1, P2, P3, P4, P8 and P10 as well as P5, P6 and P7, respectively. The angles listed for P9 are the average values of those in the molecules A and B in P9 and in the molecule B in P11, while the angle for P11 is the angle for the molecule A in P11.

Table 85 The dihedral angles between planes A and B as well as those between planes B and C of the rifampicin molecule in the series 1, series 2, P9 and P11.

solvates	**Series 1**	**Series 2**	**P9**	**P11**
Angle between A and B(°)	76.37(2)	58.76(3)	56.73(3)	56.02(4)
Angle between B and C(°)	10.15(8)	70.86(6)	16.2(5)	3.81(8)

Thus, the existence of four distinct conformations of the rifampicin molecule can be confirmed. Three main indicators can be applied to determine the different conformations, as shown in Table 86 and evident from Figure 74.

Table 86 Directional indicators for different conformations of the rifampicin molecule*

Indicators	**Series 1**	**Series 2**	**P9 (A)**	**P11 (A)**
C15=O11 bond and ansa chain	away	towards	towards	towards
C18 and ansa chain	towards	towards	towards	away
piperazinyl substituent	equatorial	axial	equatorial	equatorial

* 'away' meaning pointing away from each other, 'towards' meaning the opposite.

Furthermore, as previously discussed, all the rifampicin molecules in the solvate P1 – P11 adopt antibiotically active conformations in the solid state. In other words, the parameters defining the four distinct conformations lie within the ranges associated with biological relevance.

In addition, zwitterionic nature is a common feature in all of the rifampicin molecules in solvates P1 – P11, with the possible exception of the molecule A in P10. Moreover, a consequence of the zwitterionic nature that is common to all the rifampicin molecules is the formation of one or more N^+-H···O hydrogen bonds to neighbouring donor atoms.

It is relevant to mention that the X-ray structure of a phase described as rifampicin pentahydrate was reported by Gadret et al. in 1975.[16] (This is the only crystal structure of rifampicin hitherto published).[18] The host molecule in the pentahydrate adopts a similar conformation to those in series 1 reported here. Furthermore, the pentahydrate has similar unit cell dimensions and calculated PXRD patterns to those of series 1. In addition, the atomic co-ordinates of the water molecules in the hydrate are found to correspond closely to the co-ordinates of the oxygen atoms in the guest molecules in each solvate of series 1. It can thus be confirmed that rifampicin pentahydrate belongs to the isostructural series 1. However, there are shortcomings in the structural report for the pentahydrate, namely omission of H atoms on the water molecules in the crystallographic modelling and no definitive statement as regards the possibility of a zwitterionic structure for the rifampicin molecules.[16] In this study, a significantly more detailed and systematic investigation of the solvatomorphism of rifampicin has been undertaken.

Host Intramolecular Hydrogen Bond Interactions

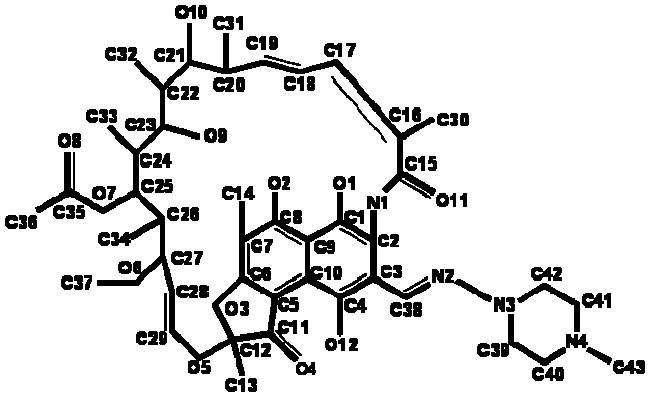

A common intramolecular hydrogen bond O12-H12···O4 is found in the host molecules in all the solvates. Hydrogen bond O1-H1···O2 can be found in all of the host molecules expect the molecule A in P10 due to its apparent non-zwitterionic nature. The hydrogen bond N1-H1N···O2N can be found in the host molecules of series 1, P8, P9, P10 and B in P11 but not in series 2 and the molecule A in P11. These can be attributed to the axial configuration of the host molecules of series 2 and the very small dihedral angles between planes B and C [3.81(8)^{o}] in the host molecule A of P11. The hydrogen bond O10-H10···O9 is observed in the host molecules of series 1, series 2 and P9 while O9-

H9···O10 is found in those of P8, P10 and P11. This indicates that the existence of a hydrogen bond interaction between O10 and O9 is indispensable for the host molecules in all the solvates. However, the geometrical orientation of this hydrogen bond depends on other conditions, for instance, the positions of the oxygen atoms in the neighbouring guest or host molecules. Furthermore, the unique hydrogen bond O10A-H10A···O11A is only found in the host molecule A of P11. The formation of this H-bond is facilitated by the distinct combination of torsion angles τ_4 and τ_6 [Figure 74 (d)] which enable the donor and acceptor atoms to approach one another sufficiently closely. In all of the solvates, the O···O distances of host O-H···O intramolecular hydrogen bonds are short (~2.6 Å) and span a narrow range.

Host-host Hydrogen Bond Interactions

No common host-host intermolecular interactions and C···O close contacts are found in the structures of series 1, series 2 and solvates P8 - P11 since each solvatomorphic form adopts a unique packing motif. Furthermore, no O-H···O and C-H···O interactions exist between the host molecules in series 2 and P8. Figure 76 illustrates the host-host interactions for the structures of series 1, P9, P10 and P11.

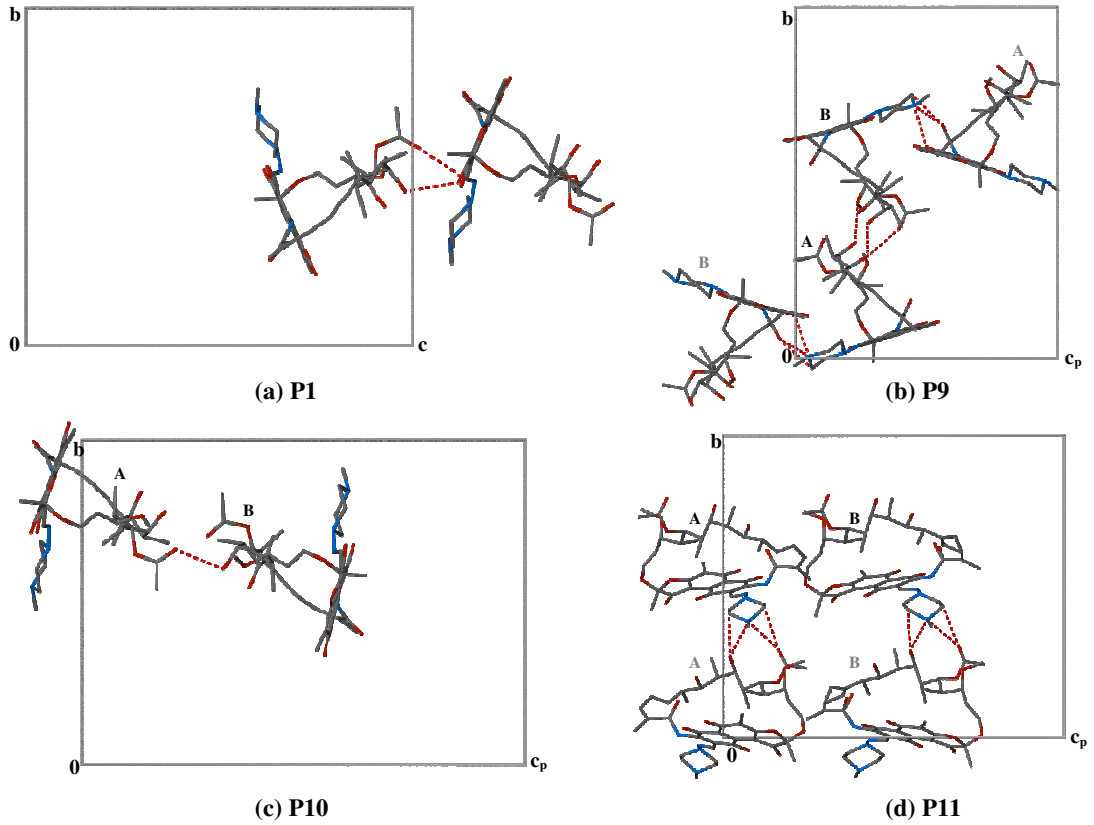

Figure 76 The host-host interaction and C···O close contacts viewed down the *a*-axis in (a) P1, (b) P9, (c) P10 and (d) P11. Atoms with gray labels have been symmetry- generated from their asymmetric unit counterparts

In the structure of P9, similar atoms function as acceptors and donors in the molecules A and B. For example, both of the hydrogen bonds N4A-H4NA···O1B/O11B have counterparts N4B-H4NB···O1A/O11A. In the structure of P11, the host A···A and B···B molecular interactions are common. For example, the N4A-H4NA···O8A/O9A hydrogen bonds have counterparts N4B-H4NB···O8B/O9B

Furthermore, the average O···O distances for the host-host O-H···O interactions (~2.9 Å) are very similar in all the solvates. This also applies to those of C···O close contacts (~3.0 Å).

Host-guest Hydrogen Bond Interactions

In the host molecules of each solvatomorphic form, not all oxygen and nitrogen atoms participate in host-guest intermolecular hydrogen bond interactions. Furthermore, the

specific N and O atoms which are involved in the interactions are different in each solvatomorphic form.

For the rifampicin molecules in series 1, the oxygen and nitrogen atoms which are involved in the hydrogen bond interactions with the guest molecules are identical in P1, P2, P3 and P4. In other words, although the content of the solvent cluster is different in each solvate, the hydrogen bonding environments provided by the rifampicin molecules are identical. This also applies to the rifampicin molecules in series 2.

Table 87 indicates which, if any, of the host N and O atoms is involved in hydrogen bonding with guest molecules. Notably, the atom N1 is only involved in the host-guest interactions in the structures of series 2 and the molecules A in P11; this may attributed to the fact that atom N1 in all the other solvates participates in the common N1-H1N···O2N intramolecular hydrogen bond, thereby precluding intermolecular H-bonding. Again, the average O···O distances for host-guest interactions (~2.9 Å) are very similar in all the solvatomorphic forms.

Table 87 Involvement of the nitrogen and oxygen atoms in the host-guest H-bond interactions in each solvatomorphic form of rifampicin.

Atom	**Series 1**	**Series 2**	**P8**		**P9**		**P10**		**P11**	
			A	B	A	B	A	B	A	B
N1	-------	yes	-------	-------	-------	-------	-------	-------	yes	------
$N4^+$	yes	yes	yes	yes	-------	-------	yes	yes	-------	------
O1	-------	yes	-------	-------	-------	-------	-------	-------	yes	yes
O2	yes	yes	yes	yes	-------	-------	-------	-------	-------	------
O4	yes	yes	yes	yes	-------	yes	yes	yes	yes	yes
O6	yes	yes	yes	yes	-------	-------	yes	yes	-------	------
O8	-------	-------	-------	yes	yes	yes	-------	yes	-------	-------
O9	-------	-------	yes	-------	-------	-------	yes	-------	-------	-------
O10	yes	yes	yes	yes	-------	-------	yes	yes	-------	yes
O11	yes	yes	yes	yes	-------	-------	yes	yes	-------	yes

Finally, a guest-host C···O close contact C16G···O11A is found only in the structure of the solvate P11.

Guest-guest Hydrogen Bond Interactions

For all the solvates, the guest molecules display a variety of disordered arrangements. For instance, one molecule may be completely or partially disordered over two positions in different ways [Figure 77 (a) and (b)]. Furthermore, one ethanol molecule can be disordered over three different positions as in P3 [Figure 77 (c)]. Also, two solvent sites (for a water molecule and a methanol molecule) are not fully-occupied [Figure 77 (d)]. Furthermore, a large number of water molecules which are partially occupied can be located very close to one another.

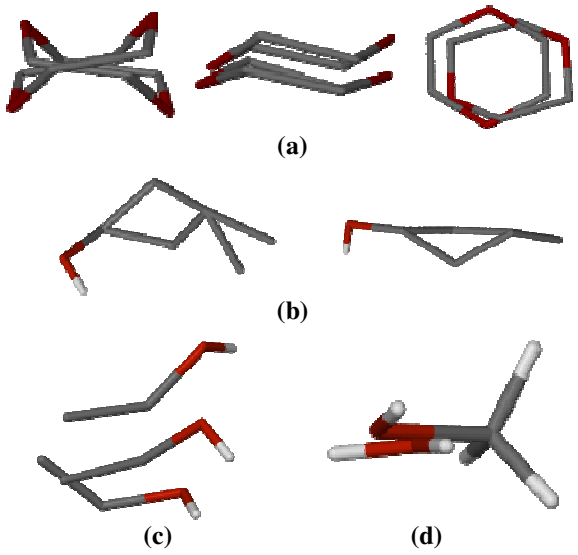

Figure 77 A variety of disordered arrangements displayed by guest molecules.

In each solvate, guest molecules form clusters. For solvates P7 and P8, all the guest molecules assemble into a complete cluster. For the other solvates, some guest molecules are found to be involved only in the host-guest interactions.

Some of the guest clusters are intimately associated with the rifampicin molecules (P1, P3, P5, P9 and P11) while others form a more continuous solvent distribution, extending indefinitely through the crystal (P2, P4, P6, P7, P8 and P10). Interestingly, the higher the water content in the structure of the solvate, the more chance there is that the guest cluster will extend indefinitely. This may be associated with the fact that the crystals of rifampicin solvates easily tend to absorb atmospheric water molecules, changing the compositions of the entrapped solvent. It can be assumed that the crystals of each solvate

have a saturated solvent molecule condition where the guest clusters are intimately associated with the rifampicin molecules. After equilibrating with the atmosphere for a certain period, atmospheric water molecules enter the crystals while solvent molecules diffuse out of the crystals, resulting in the formation of water-rich guest clusters which extend indefinitely through the solvent channel.

Crystal Packing

Both isostructural series 1 and 2 crystallise in the same space group $P2_12_12_1$ while solvates P8, P9, P10 and P11 all crystallise in the space group $P2_1$. In the structures of series 1, P8, P9, P10 and P11, host molecules form layers, interleaved by layers of guest molecules parallel to the *a*- or the *c*-axis. However, extensive hydrogen bonding links the respective layers in each case. In the structures of series 2, no host or guest molecule layers are formed. Nevertheless, using program SECTION[14] to examine crystal voids, infinite guest channels can be found in all the solvates except P11. The shapes and positions of the solvent channels were clearly visualised.

The packing diagrams in the structures of series 1, P8, P10 and P11 are comparable, as shown in Figure 78. There is one symmetry-independent host molecule in the structures of series 1 (P1 is shown as representative) while two (A and B) occur in the structures of P8, P10 and P11. In all four cases, the molecules repeat themselves in the same way, being generated by a 2-fold screw-axis running parallel to [010]. Series 1 forms layers A and A′ parallel to the *b*-axis. P8, P10 and P11 also form layers A and B parallel to the *b*-axis. However, layers A contain only molecules A while layers B contain only B. Furthermore, in the structure of P8, molecules A and B are related by a pseudo 2-fold symmetry parallel to the *b*-axis. In the structure of P10, molecules A and B are related by a pseudo 2-fold screw axis parallel to the *a*-axis. In the structure of P11, molecules A and B are related by a pseudo *B*-centering translation.

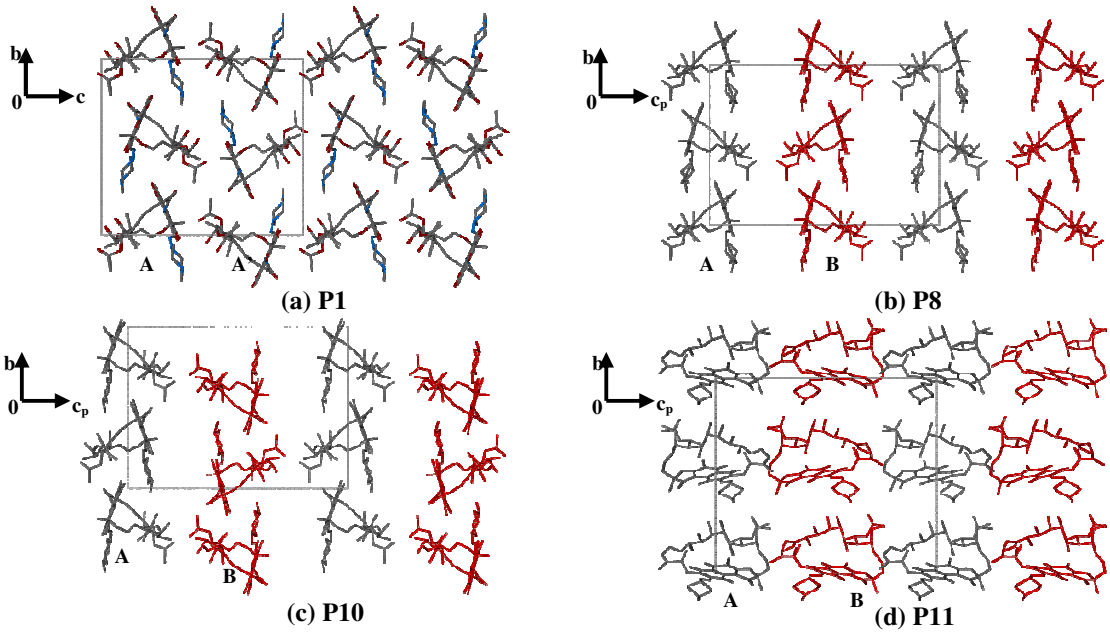

Figure 78 The similarities and differences among the packing diagrams of (a) P1, (b) P8, (c) P10 and (d) P11. The guest molecules and hydrogen atoms are omitted for clarity. The symmetry-independent molecules A and B are shown in gray and red, respectively.

Molecular packing in the crystals of series 2 and P9 are significantly different from each other and from those in series 1, P8, P10 and P11, as shown in Figure 79. There is one symmetry-independent host molecule in the structures of series 2 (P5 is shown as representative) while there are two (A and B) in the structure of P8. For P5, host molecules formed layers parallel to the unit cell *bc*-diagonal. For P9, host molecules form layers which consist of both molecules A and B parallel to the *b*- or the *c*-axis.

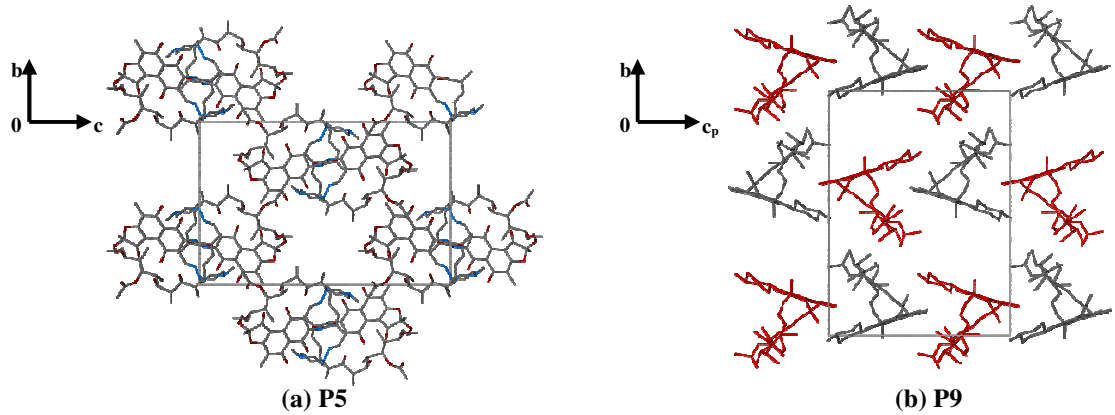

Figure 79 The packing diagrams of (a) P5 and (b) P9. The guest molecules and hydrogen atoms are omitted for clarity. The symmetry-independent molecules A and B are shown in gray and red, respectively.

References:

1. Sheldrick, G. M., In: *Direct Methods for Solving Macromolecular Structures*, Fortier, S. (eds.), Kluwer Academic Publishers: Dordrecht, **1998**, 401-411.
2. Sheldrick, G. M., SHELXH, *Acta Crystallogr.*, **2008**, A64, 112-122.
3. Bacchi, A. and Pelizzi, G., *J. Comput.-Aided Mol. Des*., **1999**, 13, 385-396.
4. Bacchi, A. and Pelizzi, G., *J. Med. Chem*., **1998**, 41, 2319-2332.
5. Bartolucci, C., Cellai, L., Cerrini, S., Lamba, D., Segre, A. L., Brizzi, V., Brufani, M., *Helv. Chim. Acta*, **1990**, 73, 185-198.
6. Arora, S. K. and Main, P., *J. Antibiot*., **1984**, 37, 178-181.
7. Arora, S. K., *Acta Crystallogr.*, **1981**, B37, 152-157.
8. Brufani, M., Cerrini, S., Fedeli, W. and Vaciago, A., *J. Mol. Biol*., **1974**, 87, 409-435.
9. Arora, S. K. and Arjunan, P., *J. Antibiot*., **1992**, 45, 428-431.
10. Bacchi, A., Carcelli, M. and Pelizzi, G., *New J. Chem.*, **2008**, 32, 1725-1735.
11. Allen, F. H., Watson, D. G., Brammer, L., Orpen A. G. and Taylor R. In: *International Tables for Crystallography, Vol. C*, Prince, E. (eds.), © International Union of Crystallography **2006**, Ch 9.5, 790–811.
12. Gallo, G. G. and Radaelli, P., In: *Analytical Profiles of Drug Substances*, Florey, K. (eds.), New York, NY: Academic Press, **1976**, 468-513.
13. Caira, M. R., Griffith, V. J., Nassimbeni, L. R. and van Oudtshoorn, B., *J. Inclusion Phenom. Mol. Recognit. Chem.*, **1995**, 20, 277-290.
14. Barbour, L. J., SECTION - a computer program for the graphic display of cross sections through a unit cell, *J. Appl. Cryst.* **1999**, 32, 353.
15. Caira, M. R., In: *Encyclopaedia of Supramolecular Chemistry* (Vol. 1), Atwood, J. L. and Steed, J. W. (eds.), Marcel Dekker, Inc., **2004**, 767.
16. Gadret, M., Goursolle, M., Leger, J. M. and Colleter, J. C., *Acta Crystallogr.*, **1975**, B31, 1454-1462.
17. Arora, S. K., *J. Med. Chem.*, **1985**, 28, 1099-1102.
18. Cambridge Structural Database and Cambridge Structural Database system, Version 5.31, November **2009** (updates Feb 2010), Cambridge Crystallographic Data Centre, University Chemical Laboratory, Cambridge, England.

Chapter 5

Rifaximin Solvates

We report here the isolation of two rifaximin solvates (a rifaximin hydrate and a rifaximin solvate containing ethylene glycol and water molecules) and we investigate the solid-state features of these two modifications using single crystal and powder X-ray diffraction.

Crystal Preparation

The abbreviations for the discrete rifaximin hydrate and rifaximin solvate in this chapter are as follows:

2Rifaximin • 7.4H_2O: F1

4Rifaximin • 7.72ethylene glycol • 6.83H_2O: F2

Suitable crystals of F1 were obtained by dissolving 20 mg (0.025 mmol) of the host drug (rifaximin) in 2 ml of acetone-water mixture (2:3 v/v) at 25 ^oC. The solution was stirred for 20 min and filtered (0.45 μm nylon filter) while hot. The clear solution was then left on the bench at 25 ^oC. Crystals of suitable quality were obtained over a period of one week. Suitable crystals of F2 were obtained by dissolving 20 mg (0.025 mmol) of the host drug (rifaximin) in 2 ml of ethylene glycol–water mixture (95:5 v/v) at 54 ^oC. The solution was stirred until clear and not filtered. The clear solution was then left on the hotplate at 54 ^oC in a sealed vial. Crystals of suitable quality grew over a period of three weeks.

The host and guest numbering schemes are given in Figure 1.

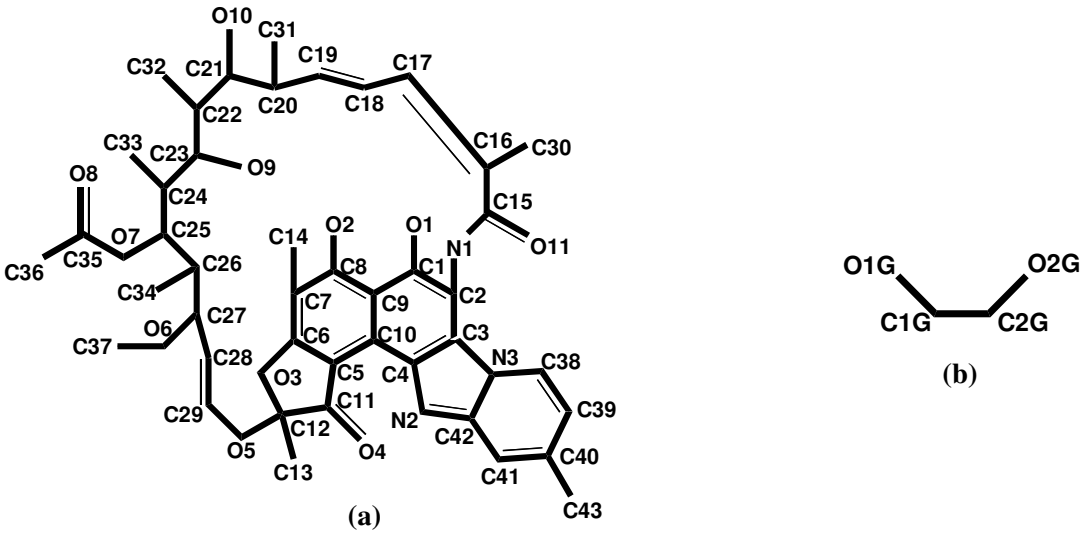

Figure 1 Host and guest numbering schemes: (a) rifaximin, (b) ethylene glycol. Hydrogen atoms have been omitted for clarity.

Single crystal X-Ray Diffraction

Data-collection and Space Group Determination

A crystal of F1 removed from the mother liquor was rapidly covered in paratone N oil in order to reduce solvent loss to a minimum. The crystals of F2 were handled in the same way. A Nonius Kappa CCD four-circle diffractometer was employed to collect X-ray intensity data for F1 and F2 at 173 K.

The unit cell parameters, crystal systems and space groups were determined from the X-ray diffraction data which revealed Laue 2/*m* symmetry for both F1 and F2. Therefore, they belong to the monoclinic system. Reflection conditions were *hkl*: *none*; *h0l*: *none*; *0k0*: $k = 2n$, indicating the space groups $P2_1$ or $P2_1/m$. Given that the rifaximin molecule is chiral, the former space group was selected for the analysis. The program XPREP[1] was used to confirm the choice of the space group in both cases.

Structure Solution and Refinement

For both F1 and F2, program SHEXLD[2] was used to solve the structures by *ab initio* methods, which revealed the positions of all the non-hydrogen atoms of the rifaximin molecule (host) in each structure. In F1, the value of $Z = 4$ indicated that there are two crystallographically independent rifaximin molecules (A and B) with their complement of water molecules in the asymmetric unit. In F2, there are four symmetry-independent rifaximin molecules (A, B, C, D) in the asymmetric unit. Full-matrix least-squares refinements were performed with SHELXH-97.[3] Difference Fourier maps revealed the positions of oxygen and carbon atoms of the water and ethylene glycol molecules (guest). Some of these atoms were found to have full site-occupancy while the others were generally disordered over two positions.

For F1, the host and guest molecules having full s.o.f. were then refined isotropically. For the disordered water molecules, a fixed U_{iso} (the mean of U_{eq} for the chemically equivalent ordered atoms) was assigned to each molecule and these atoms were allowed

to refine with s.o.f.s x and 1-x, with x variable. The details of the U_{iso} values and s.o.f.s of the water molecules in F1 are listed in Table 1.

Table 1 Isotropic thermal parameters and site-occupancy factors for the water molecules of F1

Water molecules	U_{iso} (Å^2)	s.o.f
O1W	0.08	0.36
O2W	0.07	0.70
O3W	0.07	0.60
O4W	0.06	1.00
O5W	0.07	1.00
O6W	0.08	1.00
O7W	0.07	0.74
O8W	0.07	1.00
O9W	0.08	1.00

For F2, the host molecules were refined isotropically, with the exception of atoms C5A, C9A, C34A, O6C, C4C, C37C, O8D, C2D, C7D, C13D, C14D, C20D, C28D and C29D, which were refined anisotropically. (This was necessitated by the very large number of atoms in the crystal asymmetric unit. Even with these limitations to the model, the number of least-squares variables exceeded 2000). Distance restraints were employed to ensure reasonable molecular geometries. The single and double C-C bond lengths were set at ~ 1.5 Å with a standard deviation σ = 0.004 Å and ~ 1.3 Å with σ = 0.004 Å, respectively. For ethylene glycol molecules, distance restraints were similarly employed to ensure reasonable molecular geometries. The C-O and C-C bond lengths in the ethylene glycol molecule were set at 1.40 Å with a standard deviation σ = 0.004 Å and 1.53 Å with σ = 0.001 Å, respectively. For all the guest molecules (water and ethylene glycol), only those with full site-occupancy were refined anisotropically. The details of the U_{iso} values and s.o.f.s of the guest molecules in F2 are listed in Table 2.

Table 2 Isotropic thermal parameters and site-occupancy factors for the guest molecules of F2

Water and ethylene glycol molecules	U_{iso} (Å^2)	s.o.f
O1W	0.08	0.45
O2WA	0.08	0.36
O2WB	0.08	0.26
O3W	0.09	1.00
O4WA	0.08	0.32
O4WB	0.08	0.28
O5W	0.06	1.00
O6W	0.08	0.22
O7W	0.11	1.00
O8WA	0.08	0.19
O8WB	0.08	0.20
O9WA	0.08	0.28
O9WB	0.08	0.23
O9WC	0.09	0.16
O10W	0.08	0.29
O11W	0.08	0.35
O12W	0.08	0.24
O1G-C1G-C2G-O2G	0.12-0.12-0.08-0.08	1.00
O3G-C3G-C4G-O4G	0.07-0.08-0.08-0.09	1.00
O5G-C5G-C6G-O6G	0.09	0.39
O7G-C7G-C8G-O8G	0.09	0.40
O9G-C9G-C10G-O10G	0.07	0.43
O11G-C11G-C12G-O12G	0.09	0.59
O13G-C13G-C14G-O14G	0.09	0.39
O15G-C15G-C16G-O16G	0.10	0.41
O17G-C17G-C18G-O18G	0.09	0.32
O19G-C19G-C20G-O20G	0.11-0.12-0.10-0.10	1.00
O21G-C21G-C22G-O22G	0.10	0.71
O23G-C23G-C24G-O24G	0.09	0.40
O25G-C25G-C26G-O26G	0.09	0.31
O27G-C27G-C28G-O28G	0.09	0.37

Following refinement of the non-H atoms, efforts were made to identify all H atoms in difference Fourier syntheses. Based on the positions of the peaks found, a riding model was employed to place hydrogen atoms for rifaximin and ethylene glycol molecules in idealised positions. The hydrogen atoms of the water molecules in F1 were positioned based on reasonable locations of suitable electron density peaks and their reasonable hydrogen bonding geometry. Furthermore, distance restraints were employed to ensure reasonable water molecular geometries. The O-H bond length was fixed at 0.84 Å with the H-O-H angle restrained to 104.5^o. The standard deviations (σ) for distance restraints were set between 0.004 and 0.01 Å. Hydrogen atoms of the water molecules in F2 could

not be located due to the very low site-occupancies of the water molecules. All the methyl hydrogen atoms in F1 and F2 were refined with isotropic temperature factors 1.5 times those of their parent atoms while all the other hydrogen atoms were assigned temperature factors 1.2 times those of their parent atoms. Crystal and refinement parameters for F1 and F2 are presented in Table 3.

Table 3 Crystal and refinement data for F1 and F2

Parameter	**F1**	**F2**
Formula unit	2rifaximin · 7.4H_2O	4rifaximin· 7.72ethylene glycol · 6.83H_2O
Formula Weight / g mol^{-1}	1697.84	3794.56
Crystal system	Monoclinic	Monoclinic
Space group	$P2_1$	$P2_1$
a / Å	13.7912(3)	14.4931(2)
b / Å	19.8434(3)	36.2486(4)
c / Å	16.4341(4)	21.2664(3)
α / ^{o}	90.000	90.000
β / ^{o}	92.351(1)	90.183(1)
γ / ^{o}	90.000	90.000
Volume / Å^3	4493.6(2)	11172.3(3)
Z	2	2
Density$_{calc}$ / g cm^{-3}	1.255	1.128
μ (MoK$_α$) /mm^{-1}	0.094	0.086
F (000)	1812	4059
Crystal size /mm^3	0.09x0.15x0.18	0.09x0.12x0.19
Temperature / K	173(2)	173(2)
Range scanned θ / ^{o}	1.00≤ θ ≤ 25.35	1.79 ≤ θ ≤ 24.71
Index ranges	h: -16, 16	h: -17, 17
	k: -23, 23	k: -42, 42
	l: -19, 19	l: -25, 25
φ scan angle / ^{o}	1.0	0.5
ω scan angle / ^{o}	1.0	0.5
Dx / mm	32	45
No. of measured reflections	16385	37600
No. of unique reflections	16385	19315
No. of reflections with I > 2σ(I)	12355	9358
No. of L.S. parameters	1144	2299
R_{int}, $R_σ$	0.0000, 0.0516	0.1133, 0.1573
S	1.049	1.070
R_1 (F_o > 4σ(F_o))	0.0661	0.1149
No. of reflections omitted	36	55
wR2 (all reflections)	0.1903	0.3386
Weighting scheme	a = 0.1136	a = 0.2000
	b = 1.7790	b = 0.0000
(Δ / σ)$_{mean}$	< 0.001	< 0.001
Δρ excursions / eÅ^{-3}	-0.28, 0.85	-0.49,0.79

Structural Description

Rifaximin Molecule Conformation and Antibiotic Activity (F1 and F2)

As explained in the introductory section, rifaximin belongs to the rifamycin derivatives. Similarly to rifampicin in Chapter 4, rifaximin was also investigated with regard to its solid-state conformations which can be correlated with antibiotic activity in this study.

Again, similarly to the rifampicin molecule, the rifaximin molecule (Figure 1) can be described in terms of the ansa chain, comprising atoms from C15 to C29, N1 and O5; the chromophore system, comprising atoms from C1 to C12, from O1 to O4, and O11; and finally the benzimidazole ring system at C3, formed by carbon atoms from C38 to C43, and nitrogen atoms from N2 and N3.[4] Based on this structure, planes A, B, C are introduced to describe the average planes of the ansa chain backbone, the naphthoquinonic chromophore and the fused benzimidazole system, respectively.

The rationale for this division is as follows. In the rifamycin series, biologically relevant parameters included the dihedral angle between the ansa chain and the chromophore (A and B respectively) and the dihedral angle between plane B and a substituent bonded to the chromophore (e.g. piperazinyl in the case of rifampicin). In rifaximin, the benzimidazole residue is fused to the chromophore, rendering the entire 4-ring fused system planar, in theory. However, since we observed some degree of non-planarity between the chromophore moiety and the benzimidazole system, it was decided to treat as separate 'planes' B and C, and to calculate all relevant dihedral angles involving planes A, B and C.

The rifaximin host molecule skeletons in F1 and F2 are overlaid in Figure 2. A remarkable similarity is found in the conformations of the host molecule A in F1 and the host molecules A, B, C and D in F2. However, a significantly different structural conformation can be observed in the host molecule B in F1, reflected in the orientation of the C15B=O11B bond. Specifically, the bond C15B=O11B points towards the ansa chain in the host molecule B of F1 while it points away from the ansa chain in the others.

For the host molecule A in F1 as well as the host molecules A, B, C and D in F2, the dihedral angles between planes A and B as well as those between planes B and C are slightly different in each molecule (Table 4). The fact that the dihedral angles between planes A and B are similar while the angles between planes B and C are also similar represents quantitative evidence for the overall similarity of the host conformations in F2. This also applies to the host molecule A in F1 when compared with the host molecules in F2. However, the host molecule B in F1 adopts a very different dihedral angle between planes A and B as well as that between planes B and C. This is associated with the unusual orientation of the C15B=O11B bond in F1, as shown in Figure 2.

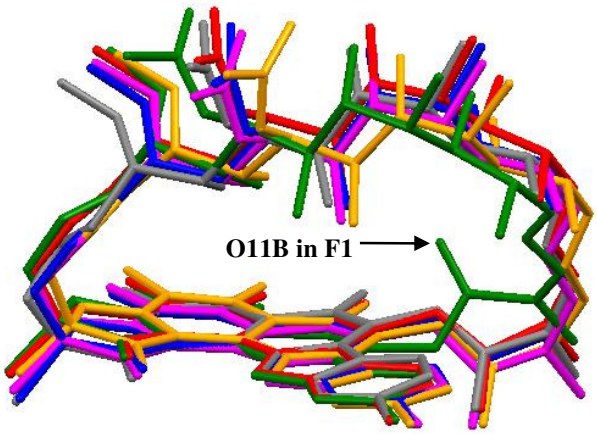

Figure 2 An overlay of the host molecules A (red), B (green) in F1 and A (orange), B (pink), C (blue) and D (gray) in F2. Guest molecules and hydrogen atoms are omitted for clarity.

Table 4 The dihedral angles between planes A and B as well as those between planes B and C of the host molecules A and B in F1 and molecules A, B, C and D in F2.

Angles between	**F1**		**F2**			
	A	B	A	B	C	D
A and B(°)	67.9(4)	49.8(4)	64.7(2)	67.4(2)	67.4(1)	72.4(2)
B and C(°)	6.6(1)	9.6(1)	7.2(3)	7.5(3)	6.3(3)	6.0(4)

The structure of the rifaximin molecule and the torsion angle labelling along the ansa chain backbone are shown in Figure 3.

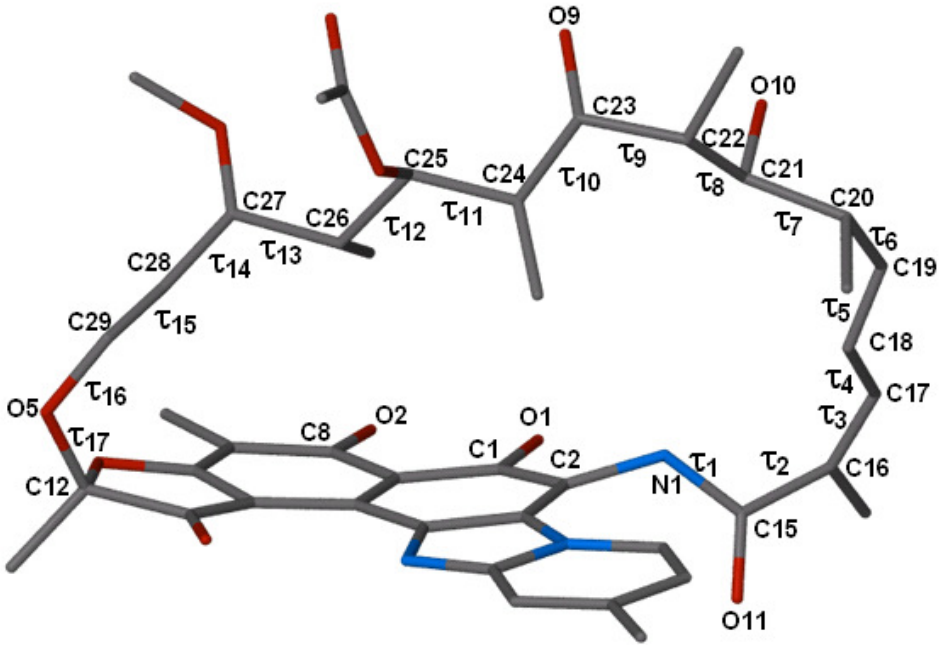

Figure 3 The molecular structure and torsion angle scheme along the ansa chain.

Table 5 lists the torsion angles τ_1-τ_{17} along the ansa chain backbone of the rifaximin host molecule. The torsion angle τ_1 defines the junction between the chromophore and the ansa chain. A *trans* conformation at this junction is indicated for all the host molecules in F1 and F2. However, the torsion angle τ_2 in the host molecule A in F1 and A, B, C and D in F2 indicates a *gauche* conformation while an *anticlinal* conformation is found in the host molecule B in F1. This again can be associated with the unique orientation of the C15B=O11B bond in F1.

Table 5 The torsion angles along the ansa chain in each rifaximin host molecule of F1 and F2

Torsion angles (°)	F1		F2			
	A	B	A	B	C	D
C2-N1-C15-C16 (τ_1)	162.4(4)	165.6(3)	165(1)	177(1)	167(1)	166(1)
N1-C15-C16-C17 (τ_2)	57.3(6)	-128.3(4)	65(2)	53(2)	55(2)	50(2)
C15-C16-C17-C18 (τ_3)	1.6(7)	4.6(6)	-2(2)	-3(2)	3(2)	12(2)
C16-C17-C18-C19 (τ_4)	-166.9(4)	178.9(4)	-167(2)	177(2)	-168(2)	-170(2)
C17-C18-C19-C20 (τ_5)	175.6(4)	-172.2(4)	-178(1)	-172(1)	177(1)	176(2)
C18-C19-C20-C21 (τ_6)	-73.8(6)	-37.3(6)	-62(2)	-42(2)	-65(2)	-64(2)
C19-C20-C21-C22 (τ_7)	170.1(4)	171.8(3)	176(1)	175(1)	-178(1)	-171(1)
C20-C21-C22-C23 (τ_8)	-168.9(4)	-171.5(3)	178(1)	178(1)	-175(1)	-180(1)
C21-C22-C23-C24 (τ_9)	55.6(5)	59.3(4)	51(2)	51(2)	55(2)	55(2)
C22-C23-C24-C25 (τ_{10})	170.5(3)	-177.3(3)	-179(1)	178(1)	170(1)	171(1)
C23-C24-C25-C26 (τ_{11})	171.6(3)	172.3(3)	167(1)	164(1)	160(1)	163(1)
C24-C25-C26-C27 (τ_{12})	175.8(3)	174.4(3)	170(1)	172(1)	173(1)	169(1)
C25-C26-C27-C28 (τ_{13})	-173.9(4)	-167.8(3)	-175(1)	-169(1)	-175(1)	-157(1)
C26-C27-C28-C29 (τ_{14})	110.5(5)	110.0(5)	102(2)	97(2)	113(2)	-99(2)
C27-C28-C29-O5 (τ_{15})	-175.5(4)	-172.5(4)	-177(1)	-178(1)	-173(2)	176(2)
C12-O5-C29-C28 (τ_{16})	55.4(7)	31.8(7)	70(2)	69(2)	57(2)	-102(2)
C29-O5-C12-O3 (τ_{17})	-79.3(5)	-75.5(5)	-82(1)	-80(1)	-84(1)	-58(2)

Figure 4 shows the rifaximin host molecules A and B in F1 and host molecule A (as representative for the host molecules B, C and D) in F2 viewed side-on to the ansa chain backbone.

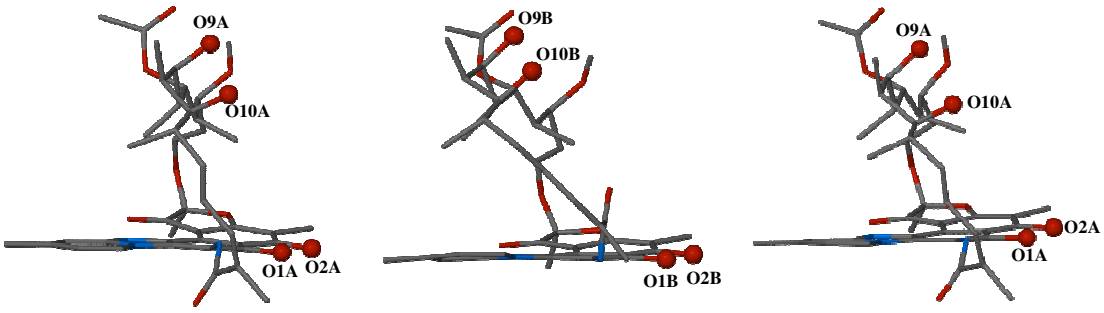

Figure 4 Diagram of the rifampicin host molecule in F1 viewed side-on with respect to the ansa chain. (a) The molecule A in F1, (b) The molecule B in F1, (c) The molecule A in F2.

Four oxygen atoms (O9, O10, O1 and O2) protrude from the cavity of the ansa chain and the chromophore face while being nearly perpendicular to the ansa chain. Furthermore, all four oxygen atoms are disposed in the opposite direction from the cyclic ring subsitituent. In addition, the intramolecular distances among the four oxygen atoms O1, O2, O9 and O10 (listed in Table 6) fall in the range (~5.41 to 9.58 Å) which is favourable

for active rifamycin derivatives.[4] Based on these structural features, these rifaximin host molecules are seen to retain an open conformation which is the characteristic arrangement of the four oxygen atoms necessary for antibiotic action through the postulated drug-enzyme interaction.[5 – 7]

Table 6 Interatomic distances involving atoms O1, O2, O9 and O10 in each host molecule in F1 and F2[a]

Distance (Å)	**F1**		**F2**			
	A	B	A	B	C	D
O1···O9	7.365	8.628	7.438	7.297	6.968	6.722
O1···O10	6.641	7.906	6.065	6.037	5.923	5.555
O2···O9	8.307	9.424	8.372	8.171	7.942	7.662
O2···O10	8.330	9.335	7.645	7.621	7.609	7.241

[a] Average e.s.d. 0.009 Å.

From the above data, the four symmetry-independent host molecules in F2 adopt a similar conformation to that of the host molecule A in F1, the other symmetry-independent host molecule B in F1 presenting a distinctly different conformation of the rifaximin molecule. Furthermore, all these molecules can be confirmed as being in biologically relevant conformations.

Similar to the structure of rifampicin molecules, a noteworthy observation is that the bond length C8-O2 is significantly shorter than C1-O1, which is in a similar chemical environment (Table 7). Based on the values for interatomic distances listed in International Tables for Crystallography[8], the typical distance for the C-O bond in the above environment is 1.333 Å. Therefore, although bonds C1-O1 and C8-O2 are all represented as single bonds in Figure 1, the former bond can be confirmed as being single whilst C8-O2 tends to display some double bond character. A significance test shows that the C1-O1 and C8-O2 bonds are significantly different except in entries C and D in Table 7, where C8-O2 is only nominally shorter than C1-O1.

Table 7 Bond lengths C1-O1 and C8-O2 in each host molecule of F1 and F2.

Bond length (Å)	**F1**		**F2**			
	A	B	A	B	C	D
C1-O1	1.360(5)	1.342(5)	1.38(1)	1.37(2)	1.33(1)	1.32(2)
C8-O2	1.294(5)	1.301(5)	1.33(1)	1.30(2)	1.32(2)	1.31(2)

This trend is consistent with the known zwitterionic nature of rifaximin in the solid-state.[9, 10] Furthermore, during the structural refinements of both F1 and F2, geometrically reasonable electron density peaks, that qualified as potential H atoms, were found at ~1 Å from all the hydroxyl oxygen atoms (O1, O9 and O10) but not in the vicinity of O2. At the same time, an extra peak, with electron density value similar to that of the previously located H atoms, was found at ~1 Å from the imidazole nitrogen atom N2. Also, between N2 and an oxygen atom of another molecule, this specific peak was ideally located, accounting for the formation of a N^+-H···O hydrogen bond with very favourable geometry. Therefore, it can be assumed that a zwitterion is formed in each host molecule, as a result of proton transfer from the hydroxyl group at C8 to the atom N2.

Intra- and Intermolecular Interactions

F1 – 2Rifaximin • 7.4H2O

Host-host Intra- and Intermolecular Hydrogen Bond Interactions

Figure 5 illustrates the zwitterionic structure, the host intramolecular interactions and a host-host intermolecular hydrogen bond N1B-H1NB···O11A for F1. The hydrogen bonds O1-H1···O2 and $N2^{+}$-H2N···O4 are common intramolecular interactions in the host molecules A and B. As regards the O9···O10 interaction on the ansa chain, in the molecule A, the atom O10A serves as a hydrogen bond donor while O9A serves as an acceptor. On the other hand, in the molecule B, O9B serves as hydrogen bond donor while O10 B acts as acceptor. Finally, the intermolecular hydrogen bond N1B-H1NB···O11A links the two symmetry-independent molecules A and B in the asymmetric unit.

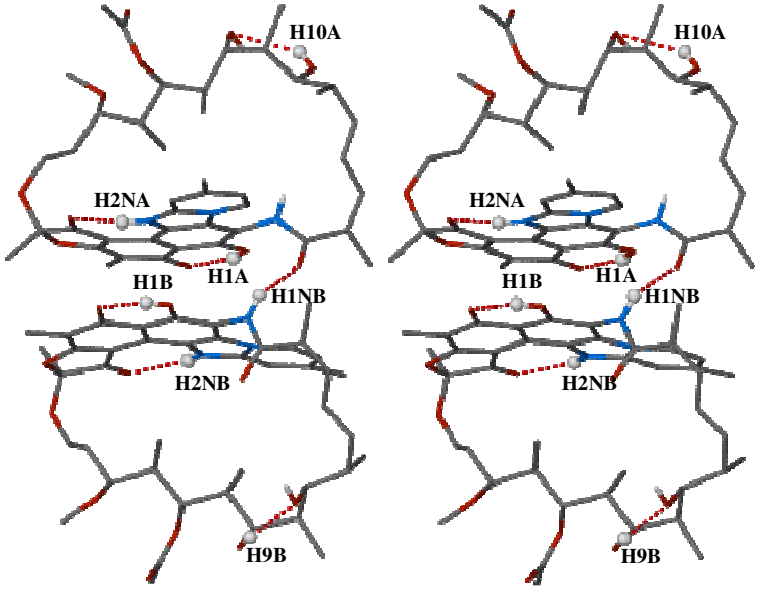

Figure 5 The zwitterionic structures, the host intramolecular O-H···O interactions and one host-host intermolecular hydrogen bond N1B-H1NB···O11A for F1. The relevant hydrogen atoms are shown as spheres. The other hydrogen atoms and the guest molecules are omitted for clarity.

Figure 6 illustrates additional host-host hydrogen bond interactions for F1. Three intermolecular interactions are thus found between molecule A and a symmetry-generated molecule B located at 2-x, -1/2+y, 1-z.

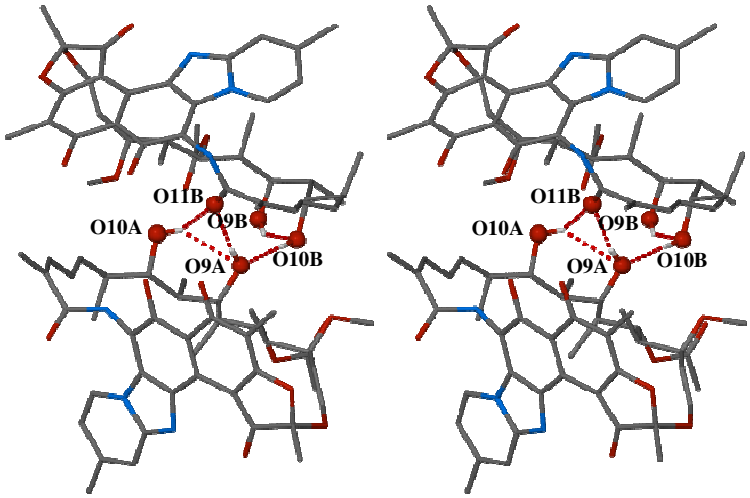

Figure 6 Additional host-host intermolecular O-H···O interactions in F1. The relevant oxygen atoms are shown as spheres, while the remaining H atoms are omitted for clarity.

Geometrical details of these hydrogen bonds are listed in Table 8. For the intramolecular interactions, the average O···O distance for the O-H···O interactions is 2.68 Å while the mean angle is 146°. Furthermore, the average N···O distance for the N-H···O interactions is 2.78 Å with the average angle is 141°. For the intermolecular O-H···O interactions, the mean distance is 2.77 Å while the mean angle is 149°.

Table 8 The details of host intramolecular interactions and host-host interactions in hydrate F1.[a]

Hydrogen bond	O···O or N···O Distance (Å)	Angle (°)	Symmetry operator[b]
Intramolecular			
O1A-H1A···O2A	2.474(4)	150.0	x, y, z
O1B-H1B···O2B	2.428(4)	150.0	x, y, z
$N2A^{+}$-H2NA···O4A	2.759(4)	141.0	x, y, z
$N2B^{+}$-H2NB···O4B	2.811(4)	140.0	x, y, z
O10A-H10A···O9A	3.065(5)	138.0	x, y, z
O9B-H9B···O10B	2.730(4)	144.0	x, y, z
Intermolecular			
N1B-H1NB···O11A	2.830(4)	131.0	x, y, z
O9A-H9A···O11B	2.861(4)	166.0	2-x, -1/2+y, 1-z
O10A-H10A···O11B	2.722(5)	111.0	2-x, -1/2+y, 1-z
O10B-H10B···O9A	2.727(4)	169.0	2-x, 1/2+y, 1-z

[a] Where no e.s.d. is reported for the angle, H atoms involved were added in idealised positions in a riding model.
[b] Symmetry operator applies to hydrogen bond acceptor atoms.

Several intramolecular and intermolecular C-H···O and C-H···N interactions are found in the structure of F1. Figure 7 shows the intramolecular C-H···O interactions and one intermolecular C-H···O interaction for F1. Similar intramolecular hydrogen bond interactions can be found in the molecules A and B. The difference between the torsion angles τ_{2A} and τ_{2B} gives rise to the distinct interactions C38A-H38A···O11A, C38B-H38B···O11A, C38B-H38B···N1B and C18B-H18B···O11B. The appearance of the interaction C38A-H38A···O11A is due to the fact that the atom O11A points away from the ansa chain in the molecule A. Furthermore, the appearance of the interaction C18B-H18B···O11B is associated with the bond C11B=O11B that points towards the ansa chain in the molecule B. In addition, the intermolecular interaction C38B-H38B···O11A links the two symmetry-independent rifaximin molecules A and B in the asymmetric unit.

Table 9 lists the geometrical details of all the intramolecular and intermolecular C-H···O and C-H···N hydrogen bonds. For the intramolecular C···O interactions, the mean distance is 2.91 Å while the mean angle is 108°. For the intermolecular C···O interactions, the mean distance is 3.15 Å while the mean angle is 129°.

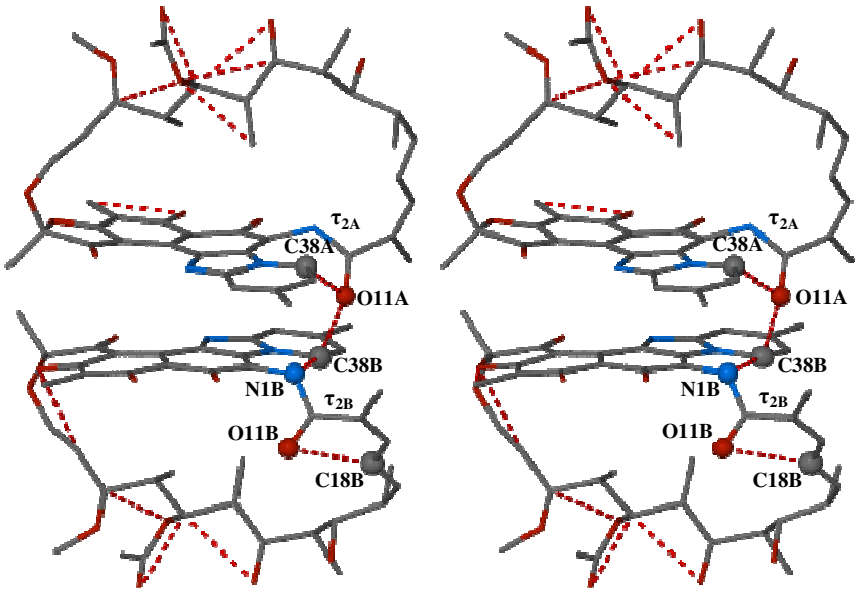

Figure 7 Stereoview of the intramolecular and intermolecular C-H···O and C-H···N interactions in F1. The relevant O, N and C atoms are shown as spheres, while the H atoms and the guest molecules are omitted for clarity.

Table 9 Intramolecular and intermolecular C-H···O and C-H···N interactions in the rifaximin molecules[a]

Hydrogen bond	C···O or C···N Distance (Å)	Angle (°)	Symmetry operator[b]
Intramolecular			
C14A-H14B···O2A	2.824(6)	107.0	x, y, z
C14B-H14F···O3B	2.935(5)	103.0	x, y, z
C18B-H18B···O11B	2.982(5)	118.0	x, y, z
C23A-H23A···O7A	2.950(5)	106.0	x, y, z
C25A-H25A···O8A	2.726(6)	105.0	x, y, z
C25A-H25A···O9A	2.903(5)	105.0	x, y, z
C25B-H25B···O8B	2.743(5)	105.0	x, y, z
C25B-H25B···O9B	2.855(5)	104.0	x, y, z
C27A-H27A···O7A	2.886(5)	104.0	x, y, z
C27B-H27B···O7B	2.897(5)	105.0	x, y, z
C28B-H28B···O3B	3.118(6)	120.0	x, y, z
C33A-H33C···O7A	2.867(5)	100.0	x, y, z
C38A-H38A···O11A	3.172(6)	125.0	x, y, z
C38B-H38B···N1B	3.094(5)	120.0	x, y, z
Intermolecular			
C38B-H38B···O11A	2.970(6)	107.0	x, y, z
C34B-H34E···O10A	3.107(7)	117.7	2-x, 1/2+y, 1-z
C43A-H43A···O9B	3.373(6)	163.0	x, y, -1+z

[a] Where no e.s.d. is reported for the angle, H atoms involved were added in idealised positions in a riding model.
[b] Symmetry operator applies to hydrogen bond acceptor atoms.

Three π-π interactions are found between the rifaximin molecules (Figure 8).

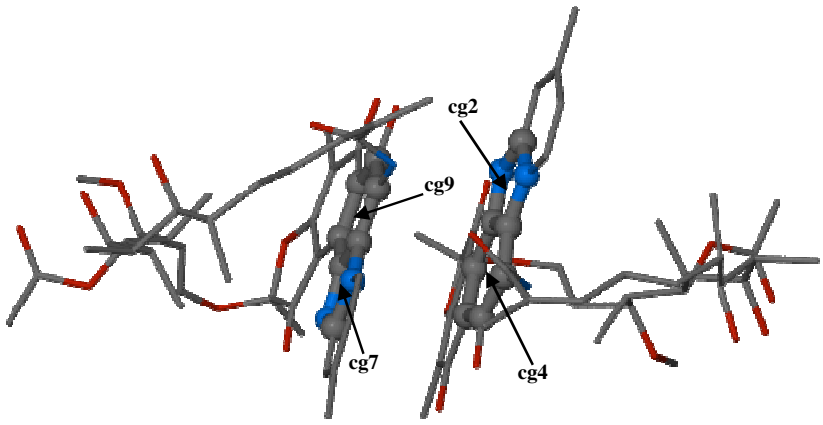

Figure 8 Aromatic rings involved in π-π interactions between the rifaximin molecules A and B in the asymmetric unit. (Cg2 represents the centroid of the imidazole ring N2A-C4A-C3A-N3A-C42A; Cg4 is C centroid of the phenyl ring C1A-C2A-C3A-C4A-C10A-C9A; Cg7 is the centroid of imidazole ring N2B-C4B-C3B-N3B-C42B; Cg9 is the centroid of phenyl ring C1B-C2B-C3B-C4B-C10B-C9B)

A summary of the π-π and C-H···π interactions are given in Table 10. The average distance for the π-π interactions is 3.74 Å. The mean distance for the C-H···π interactions is 3.31 Å with a mean angle of 128°.

Table 10 All possible π-π interactions with cg···cg < 4 Å and C-H···π interactions between the rifaximin molecules[a]

Interactions	cg···cg or C···cg Distance (Å)	Angle (°)
π-π interaction		
cg2···cg9	3.824(2)	--------
cg4···cg7	3.880(2)	--------
cg4···cg9	3.518(2)	--------
C-H···π interactions		
C28A-H28A···cg1(O3A-C6B-C5A-C11A-C12A)	3.000(6)	99.0
C28B-H28B···cg6(O3B-C6B-C5B-C11B-C12B)	2.947(5)	112 .0
C33A-H33B···cg2(N2A-C4A-C3A-N3A-C42A)	3.758(5)	149.0
C34A-H34C···cg5(C5A-C6A-C7A-C8A-C9A-C10A)	3.526(5)	151.0

[a] Where no e.s.d. is reported for the angle, H atoms involved were added in idealised positions in a riding model.

Host-guest Interactions

Figure 9 shows the host-guest hydrogen bond interactions among the host and the water molecules. The O8A and O8B atoms in the molecules A and B are hydrogen bonded to the water molecules O9W and O6W, respectively. The water molecules O5W and O9W both serve as bridges in associating the rifaximin molecules A with a symmetry-generated host molecule B. Similar to the host-host intermolecular interaction N1B···O11A, the water molecule O8W also assists in stabilising the two symmetry-independent rifaximin molecules A and B in the asymmetric unit of F1.

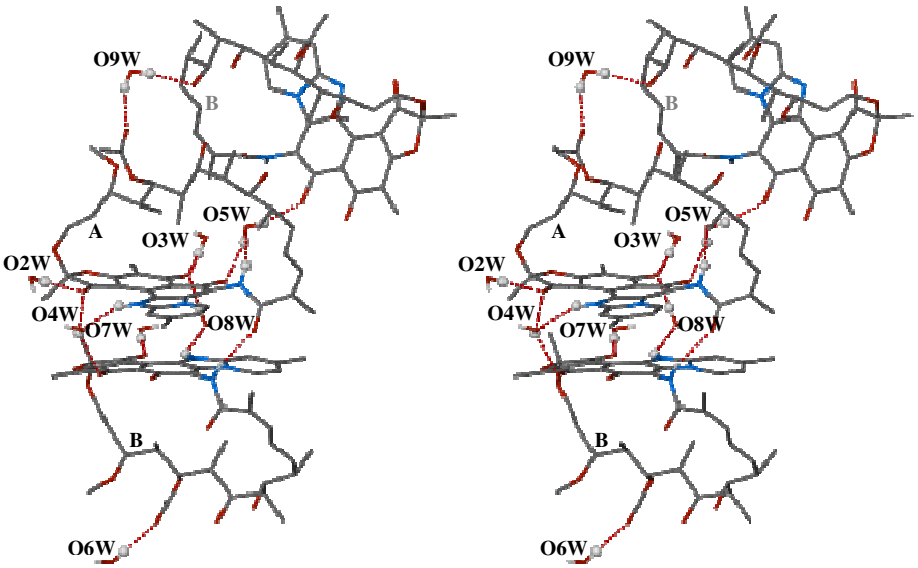

Figure 9 Stereoview of the intermolecular O-H···O and N-H···O hydrogen bonds among the host and guest molecules in F1. The relevant hydrogen atoms are shown as spheres. The other hydrogen atoms and guest molecules are omitted for clarity.

The distances O4A···O4W and O2B···O4W are 2.945(6) and 2.799(6) Å, respectively. Therefore, both O4A and O2B are located within hydrogen bonding distance of O4W. During the structure refinement, a geometrically sensible electron density peak located in the difference Fourier maps, was assigned as the hydrogen atom H4W2 (Figure 10). The angles of the H-bond interactions O4W-H4W2···O4A and O4W-H4W2···O2B are 118.4(6)^{o} and 116.6(9)^{o}, respectively (Figure 10). In other words, the hydrogen H4W2 is involved in a bifurcated hydrogen bond to acceptor atoms O4A and O2B.

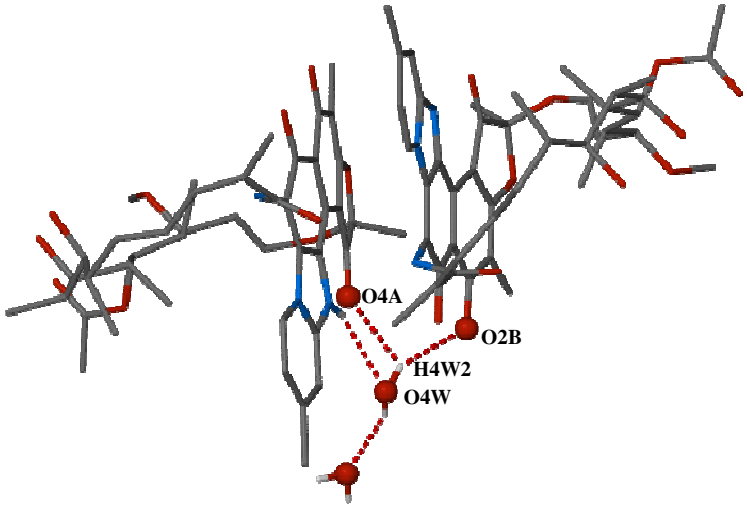

Figure 10 The hydrogen bond environment of the water molecule O4W. The relevant oxygen atoms are shown as spheres. The hydrogen atoms in the rifaximin molecules are omitted for clarity.

The geometrical details for the host-guest intermolecular N-H···O and O-H···O interactions are listed in Table 11. The mean N···O distance is 2.93 Å while the mean angle is 134°. The average O···O distance is 2.86 Å while the average angle is 160°.

Table 11 Host-guest intermolecular N-H···O and O-H···O interactions in F1[a]

Hydrogen bond	O···O or N···O Distance (Å)	Angle (°)	Symmetry operator[b]
N1A-H1NA···O5W	2.845(5)	140.0	x, y, z
N2A-H2NA···O4W	3.049(6)	135.0	x, y, z
N2B-H2NB···O8W	2.907(5)	128.0	x, y, z
O2W-H2W1···O4A	2.843(6)	169(4)	x, y, z
O5W-H5W1···O1B	2.775(5)	163(2)	2-x, -1/2+y, 1-z
O9W-H9W1···O10B	2.864(6)	167.0(4)	2-x, -1/2+y, 2-z
O5W-H5W2···O1A	2.938(6)	161.0(5)	x, y, z
O6W-H6W1···O8B	2.861(5)	169(5)	1-x, 1/2+y, 2-z
O7W-H7W2···O4B	2.873(6)	170.0(6)	x, y, z
O9W-H9W2···O8A	2.757(6)	155.0(4)	x, y, 1+z
O3W-H3W1···O2A	2.908(7)	138.0(3)	1-x, 1/2+y, 1-z
O8W-H8W1···O2A	2.926(6)	146.0(5)	x, y, z

[a] Where no e.s.d. is reported for the angle, H atoms involved were added in idealised positions in a riding model.
[b] Symmetry operator applies to hydrogen bond acceptor atoms.

There are three intermolecular C-H···O interactions between the rifaximin and water molecules (Table 12). The mean C···O distance is 3.20 Å with a mean angle of 140°.

Table 12 Host-guest intermolecular C-H···O and N-H···O interactions in F1[a]

Hydrogen bond	C···O or N···O Distance (Å)	Angle (°)	Symmetry operator[b]
C39A-H39A···O3W	3.365(7)	162.0	1+x, y, z
C41A-H41A···O4W	3.189(8)	131.0	x, y, z
N41B-H41B···O8W	3.035(6)	128.0	x, y, z

[a] Where no e.s.d. is reported for the angle, H atoms involved were added in idealised positions in a riding model.
[b] Symmetry operator applies to hydrogen bond acceptor atoms.

Water-water Interactions

Figure 11 illustrates the water-water interactions in F1. Water molecules form a cluster, except for O5W which is isolated by forming hydrogen bond interactions with two distinct rifaximin molecules. The hydrogen atoms of O1W could not be located due to its very low site-occupancy (0.36).

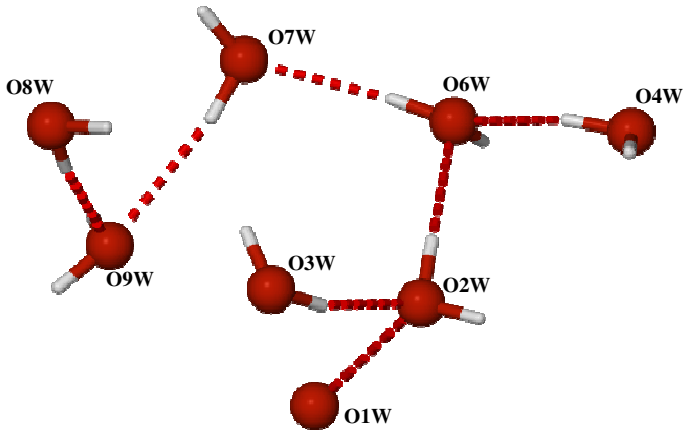

Figure 11 The water-water intermolecular O-H···O interactions among the water molecules in F1.

The details of the water-water intermolecular hydrogen bond interactions are listed in Table 13. The mean O···O distances for these interactions is 2.85 Å while the mean O-H···O angle is 160°.

Table 13 The details of water-water hydrogen bond interactions in hydrate F1[a]

Hydrogen bond	O···O Distance (Å)	Angle (°)	Symmetry operator[b]
O4W-H4W1···O6W	2.765(6)	146.0	1-x, 1/2+y, 1-z
O7W-H7W1···O9W	2.859(7)	163.0	x, y, z
O2W-H2W2···O6W	2.975(7)	154.0	1-x, 1/2+y, 1-z
O6W-H6W2···O7W	2.759(7)	167.0	x, y, z
O8W-H8W2···O9W	2.889(7)	169.0	x, y, z

[a] Where no e.s.d. is reported for the angle, H atoms involved were added in idealised positions in a riding model.
[b] Symmetry operator applies to hydrogen bond acceptor atoms.

Overall Intramolecular and Intermolecular Interactions in F1

The overall hydrogen bond interactions of F1 are shown in Figure 12. The water cluster is found to be intimately associated with seven rifaximin molecules. The water molecule O2W functions as hydrogen bond donor to two molecules and serves as a hydrogen bond acceptor to two other molecules simultaneously. This also applies to water molecules O6W and O9W. The water molecule O7W functions as a hydrogen bond donor to two different molecules while simultaneously serves as a hydrogen bond acceptor to another molecule. This also applies to the water molecule O8W. Due to the bifurcated hydrogen bonds formed by H4W2 of O4W, O4W servers as a hydrogen bond donor to three different molecules while it functions as a hydrogen bond acceptor to another molecule. The water molecule O3W functions as hydrogen bond donor to two different molecules but is not an acceptor of hydrogen bonds.

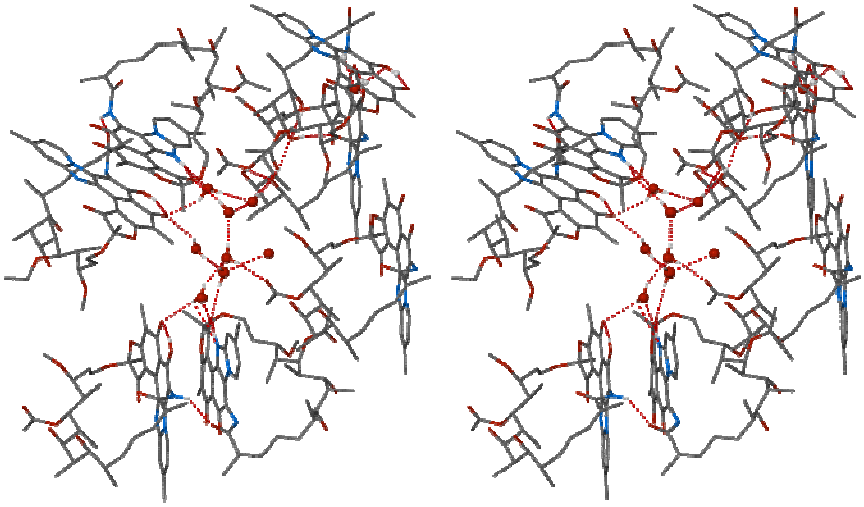

Figure 12 Stereoview of the overall hydrogen bond interactions in F1. The oxygen atoms in water molecules are shown as spheres.

A noteworthy observation is that the water molecule O5W is isolated from the water cluster described above. O5W associates one host molecule A with a symmetry-generated host molecule B by serving as hydrogen bond donor to O1A and O1B while functioning as hydrogen bond acceptor to N1A (Figure 13).

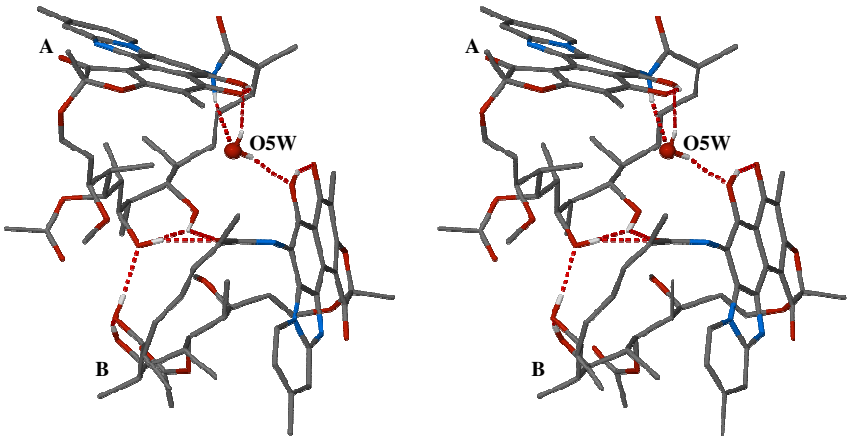

Figure 13 The hydrogen bond environment of the water molecule O5W, whose oxygen atom is shown as a sphere. Molecule B is located at the position 2-x, -1/2+y, 1-z.

The schematic diagram illustrating the overall hydrogen bond interactions for F1 are presented in Figure 14. Notably, not only the hydrogen atom H4W2 of O4W forms bifurcated hydrogen bonds; this also applies to H10A (with O9A and O11B), H2NA (with O4W and O4A) as well as H2NB (with O8W and O4B).

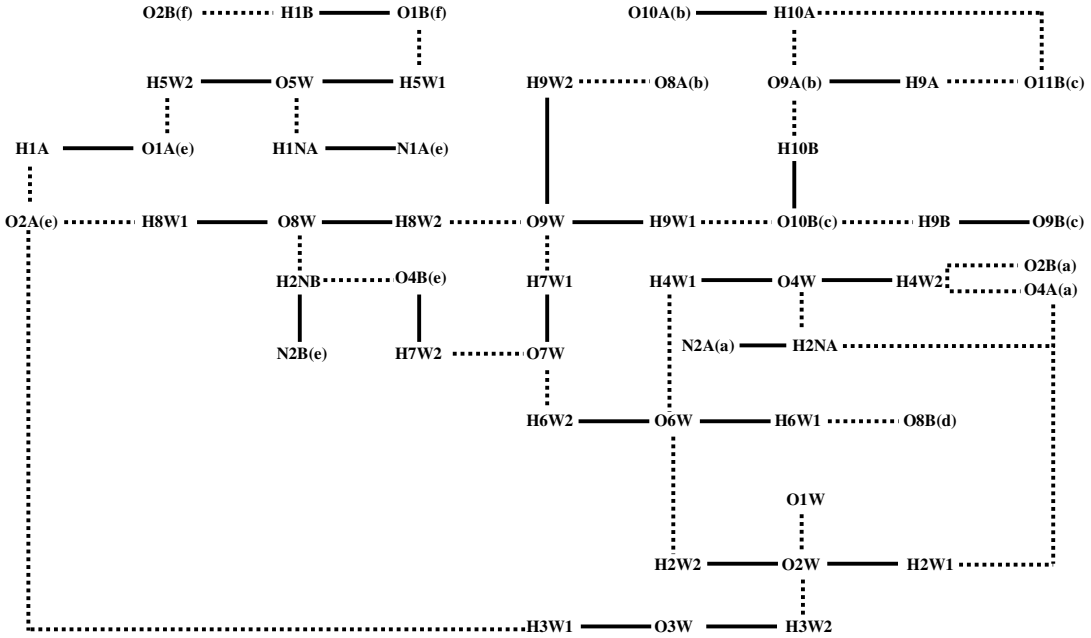

Figure 14 The schematic diagram for the overall hydrogen bond interactions in hydrate F1. The code letter for the symmetry operator of each rifaximin molecule is given as a suffix in the atom label (a = x, y, z; b = 1-x, 1/2+y, -z; c= x-1, y, z-1; d = x, y, z-1; e = 1-x, 1/2+y, 1-z; f = x-1,y, z).

Crystal Packing

F1 packs in a layer arrangement, as shown in Figure 15. Host molecules A and B are related by a pseudo 2-fold rotation parallel to the *a*-axis, forming layers which consist of both molecules A and B parallel to the *c*-axis. In each layer, the host molecules are associated by π-π interactions when they pack in head-to-head mode and associated by water molecules when they pack in tail-to-tail mode. Furthermore, the host molecules are connected by intermolecular interactions, some mediated by water molecules, when they pack along the *b*-axis. This arrangement introduces isolated sites where guest molecules are accommodated.

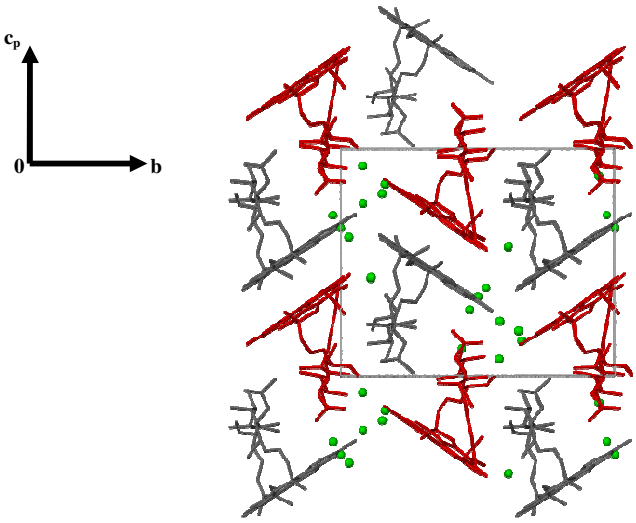

Figure 15 Crystal packing diagram of F1 viewed along [100]; water molecules are shown as green spheres for clarity. Host molecules A and B are shown in gray and red, respectively.

F2 – 4Rifaximin • 7.72ethylene glycol • 6.83H_2O

As indicated above, the crystal of F2 has a formula unit consisting of four independent rifaximin molecules as well as approximately eight ethylene glycol molecules and seven water molecules. As such, its structural refinement presented a considerable challenge. A detailed account of the crystal structure follows.

Host-host Intra- and Intermolecular Hydrogen Bond Interactions

Figure 16 shows the zwitterionic structures as well as the host-host intra- and intermolecular hydrogen bond interactions in the asymmetric unit of F2. Each host molecule adopts a similar motif of intra- and intermolecular hydrogen bond interactions. A unique interaction occurs in the molecule A in which the hydrogen bond O9A-H9A···O8A is formed. In each molecule, the hydrogen atom H2N simultaneously forms an intramolecular hydrogen bond with O4 and an intermolecular hydrogen bond with O11 of the neighbouring rifaximin molecule. In other words, H2NA, H2NB, H2NC and H2ND all form bifurcated hydrogen bonds. Hydrogen bonds $N2A^+$-H2NA···O11C and $N2C^+$-H2NC···O11A act as tethers, stabilising the formation of the dimeric unit A···C. The dimeric unit B···D is stabilised in an analogous fashion. However, there is no O-H···O or N^+-H···O intermolecular hydrogen bond between the host molecules A and B.

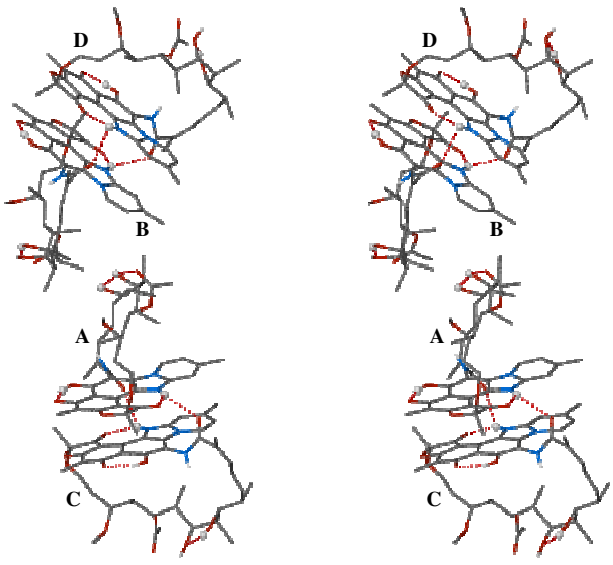

Figure 16 The zwitterionic structures, and the host-host intra- and intermolecular hydrogen bond interactions for solvate F2. The relevant hydrogen atoms are shown as spheres. The other hydrogen atoms and the guest molecules are omitted for clarity.

Table 14 lists the geometrical details of the hydrogen bond interactions. For the intramolecular interactions, the average O···O distance is 2.62 Å with a mean angle of 149°. Furthermore, the mean N···O distance is 2.74 Å and the average angle is 146°. For the O-H···O intermolecular interactions, the mean hydrogen bonding distance is 3.04 Å while the mean angle is 124°.

Table 14 Intra- and intermolecular hydrogen bond interactions in the host molecules of solvate F2[a]

Hydrogen bond	O···O or N···O Distance (Å)	Angle (°)
Intramolecular		
O1A-H1A···O2A	2.403(12)	151.0
O1B-H1B···O2B	2.453(13)	150.0
O1C-H1C···O2C	2.455(11)	151.0
O1D-H1D···O2D	2.483(14)	150.0
$N2A^{+}$-H2NA···O4A	2.756(11)	146.0
$N2B^{+}$-H2NB···O4B	2.780(13)	143.0
$N2C^{+}$-H2NC···O4C	2.722(12)	146.0
$N2D^{+}$-H2ND···O4D	2.715(13)	148.0
O10A-H10A···O9A	2.775(14)	143.0
O10B-H10B···O9B	2.743(15)	152.0
O10C-H10C···O9C	2.732(14)	149.0
O10D-H10D···O9D	2.705(4)	152.0
O9A-H9A···O8A	2.819(14)	142.0
Intermolecular		
$N2A^{+}$-H2NA···O11C	3.040(13)	122.0
$N2C^{+}$-H2NC···O11A	3.043(14)	127.0
$N2B^{+}$-H2NB···O11D	2.925(14)	126.0
$N2D^{+}$-H2ND···O11B	3.147(15)	119.0

[a] Where no e.s.d. is reported for the angle, H atoms involved were added in idealised positions in a riding model.

Numerous intramolecular C-H···O and C-H···N interactions (Table 15) are associated with the rifaximin conformations in F2. For the intramolecular interactions, the average C···O distance is 2.87 Å while the average angle is 107°. Also, the mean C···N distance is 3.03 Å and mean angle 112°. For the intermolecular interactions, the mean C···O distance is 3.36 Å while the average angle is 148°. Notably, a C···O close contact C31B···O8A [3.24(2) Å] is found; this is the only significant observable interaction between the host molecules A and B.

Table 15 Intra- and intermolecular C-H···O and C-H···N interactions in the host molecules of F2[a]

Hydrogen bond	C···O or C···N Distance (Å)	Angle (°)	Symmetry operator[b]
Intramolecular			
C14A-H14B···O3A	2.90(2)	105.0	x, y, z
C14B-H14E···O2B	2.88(2)	106.0	x, y, z
C14C-H14I···O2C	2.83(2)	108.0	x, y, z
C14D-H14K···O3D	2.88(2)	106.0	x, y, z
C18B-H18B···N1B	3.09(2)	118.0	x, y, z
C18D-H18D···N1D	2.97(2)	106.0	x, y, z
C25A-H25A···O8A	2.77(2)	104.0	x, y, z
C25A-H25A···O9A	2.91(2)	108.0	x, y, z
C25B-H25B···O8B	2.78(2)	102.0	x, y, z
C25B-H25B···O9B	2.85(2)	108.0	x, y, z
C25C-H25C···O8C	2.74(2)	106.0	x, y, z
C25C-H25C···O9C	2.93(2)	107.0	x, y, z
C25D-H25D···O8D	2.73(2)	103.0	x, y, z
C25D-H25D···O9D	2.92(2)	107.0	x, y, z
C27A-H27A···O7A	2.82(2)	104.0	x, y, z
C27B-H27B···O7B	2.84(2)	108.0	x, y, z
C27C-H27C···O7C	2.85(2)	104.0	x, y, z
C27D-H27D···O7D	2.87(2)	111.0	x, y, z
C28C-H28C···O3C	3.09(2)	115.0	x, y, z
C30D-H30J···O11D	2.91(2)	102.0	x, y, z
C32A-H32C···O9A	2.80(2)	101.0	x, y, z
C33D-H33B···O7D	2.75(2)	100.0	x, y, z
C33A-H33L···O7A	2.83(2)	101.0	x, y, z
C33C-H33M···O7C	2.69(2)	100.0	x, y, z
C36A-H38A···O11A	3.11(2)	123.0	x, y, z
C38B-H38B···O11B	3.05(2)	112.0	x, y, z
C38D-H38D···O11D	3.09(2)	113.0	x, y, z
Intermolecular			
C13B-H13F···O1D	3.31(2)	142.0	x, y, z
C13D-H13J···O1B	3.42(2)	152.0	x, y, z
C13C-H13M···O1A	3.43(2)	162.0	x, y, z
C41A-H41A···O11C	3.16(2)	120.0	x, y, z
C31C-H31H···O2A	3.39(2)	153.0	1+x, y, z
C36B-H36F···O8C	3.47(2)	158.0	1-x, 1/2+y, 1-z

[a] Where no e.s.d. is reported for the angle, H atoms involved were added in idealised positions in a riding model.
[b] Symmetry operator applies to hydrogen bond acceptor atoms.

Figure 17 shows the π-π interactions between the host molecules D and B as well as those between the molecules A and C in the asymmetric unit. Table 16 lists the details of the π-π and C-H···π interactions. The average distance for the π-π interactions is 3.70 Å (range 3.374 to 3.992 Å). The mean distance for the C-H···π interactions is 3.39 Å with a mean angle of 124°.

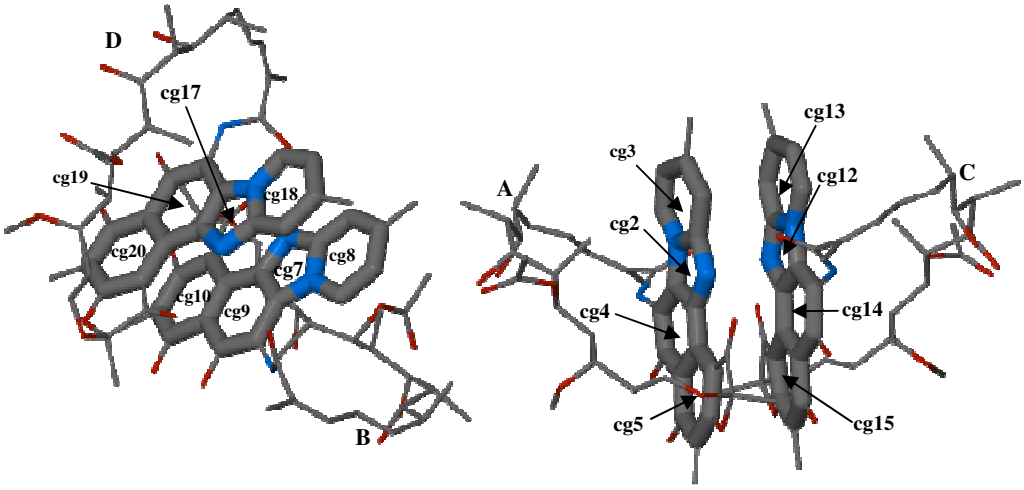

Figure 17 Aromatic rings involved in π-π interactions between rifaximin molecules B and D, and between A and C in the asymmetric unit. The labelling of the centroids is analogous to that shown in the caption of Figure 8.

Table 16 All possible π-π interactions with cg···cg < 4 Å and C-H···π interactions among the rifaximin molecules in F2[a]

Interactions	cg···cg or C···cg Distance (Å)	Angle (°)
π-π interaction		
cg2···cg12	3.387(7)	--------
cg2···cg14	3.742(7)	--------
cg3···cg12	3.849(7)	--------
cg3···cg13	3.508(8)	--------
cg4···cg14	3.855(7)	--------
cg4···cg15	3.910(7)	--------
cg5···cg15	3.707(7)	--------
cg7···cg17	3.374(8)	--------
cg7···cg19	3.962(8)	--------
cg8···cg18	3.530(8)	--------
cg9···cg19	3.992(8)	--------
cg10···cg20	3.641(8)	--------
C-H···π interactions		
C28A-H28A···cg1(O3A-C6A-C5A-C11A-C12A)	3.08(2)	89.0
C28B-H28B···cg6(O3B-C6B-C5B-C11B-C12B)	3.03(2)	91.0
C28C-H28C···cg11(O3C-C6C-C5C-C11C-C12C)	2.94(2)	98.0
C29D-H29D···cg16(O3D-C6D-C5D-C11D-C12D)	2.65(2)	66.0
C33B-H33E···cg7(N2B-C4B-C3B-N3B-C42B)	3.67(2)	149.0
C33C-H33H···cg12(N2C-C4C-C3C-N3C-C42C)	3.82(2)	145.0
C33A-H33K···cg2(N2A-C4A-C3A-N3A-C42A)	3.69(2)	145.0
C34A-H34A···cg5(C5A-C6A-C7A-C8A-C9A-C10A)	3.56(2)	144.0
C34B-H34E···cg10(C5B-C6B-C7B-C8B-C9B-C10B)	3.55(2)	148.0
C34D-H34K···cg19(C1D-C2D-C3D-C4D-C10D-C9D)	3.64(2)	125.0
C34D-H34L···cg20(C5D-C6D-C7D-C8D-C9D-C10D)	3.44(2)	140.0
C34C-H34M···cg15(C5C-C6C-C7C-C8C-C9C-C10C)	3.56(2)	149.0

[a] Where no e.s.d. is reported for the angle, H atoms involved were added in idealised positions in a riding model.

Host-guest Interactions

The host-guest hydrogen bond interactions are shown in Figure 18. Atoms O2, O10, O11 and N1 are involved in the hydrogen bond interactions in all four symmetry-independent host molecules. A noteworthy observation is that no guest molecule serves as a bridge to associate the molecules B and A. Furthermore, the overall hydrogen bond pattern is very complicated; therefore, the hydrogen bonds relating to molecules A and C, as well as those relating to molecules B and D, are discussed separately.

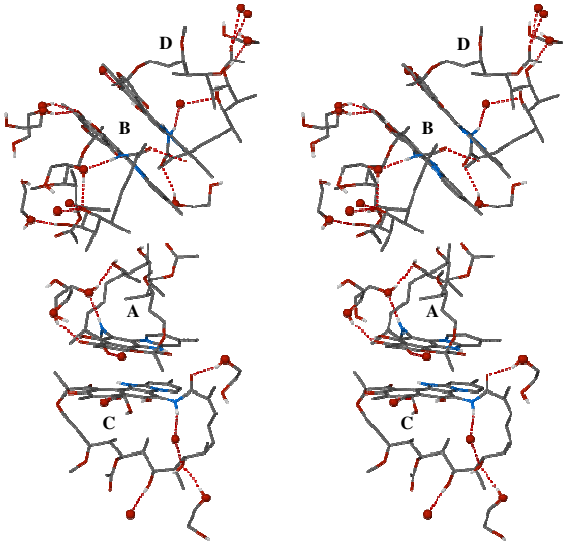

Figure 18 Stereoview of the intermolecular O-H···O and N-H···O hydrogen bonds between the host and guest molecules in solvate F2. The relevant oxygen atoms in the guest molecules are shown as spheres. The hydrogen atoms are omitted for clarity.

The O-H···O and N-H···O hydrogen bonds between the hosts (rifaximin molecules A and C) and the guests (ethylene glycol and water molecules) are shown in Figure 19. No guest molecule is found to serve as a bridge to associate two rifaximin molecules A and C. However, the ethylene glycol molecule (O3G-C3G-C4G-O4G) is found to associate molecule A and a symmetry-generated host molecule C by forming a hydrogen bond chain O1A···O2A···O3G-C3G-C4G-O4G···O11C (Figure 20).

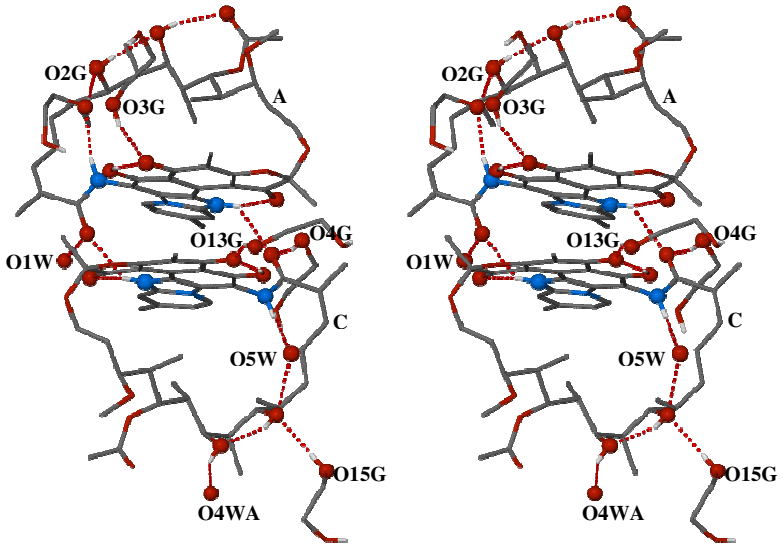

Figure 19 Stereoview of the O-H···O and N-H···O hydrogen bonds between the host (A and C) and guest molecules in F2. The relevant oxygen and nitrogen atoms in the guest molecules are shown as spheres. The other hydrogen atoms and guest molecules are omitted for clarity.

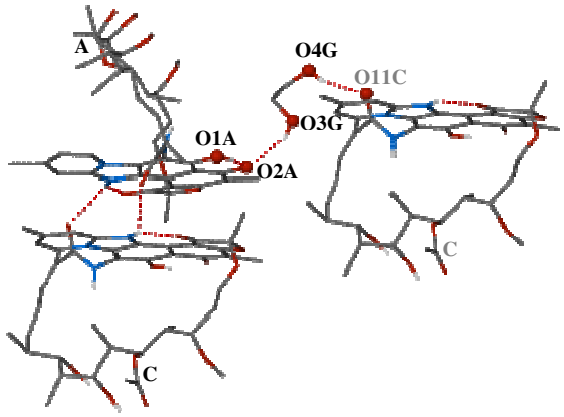

Figure 20 The long hydrogen bonded chain O1A···O2A···O3G-C3G-C4G-O4G···O11C in F2. The relevant oxygen atoms are shown as spheres. Atoms with gray labels have been symmetry-generated from their asymmetric unit counterparts.

The O-H···O and N-H···O hydrogen bonds between the host (rifaximin molecules B and D) and the guest (the ethylene glycol and water molecules) are shown in Figure 21. Molecules B and D are not bridged *via* any solvent molecules. However, the ethylene glycol molecule (O7G-C7G-C8G-O8G) and the disordered water molecules O2WA and O2WB associate the molecule B and two symmetry-generated molecules D by forming two hydrogen bond chains O1B···O2B···O7G-C7G-C8G-O8G···O11D and O9B···O10B···O2WA/O2WB···O8D, respectively (Figure 22).

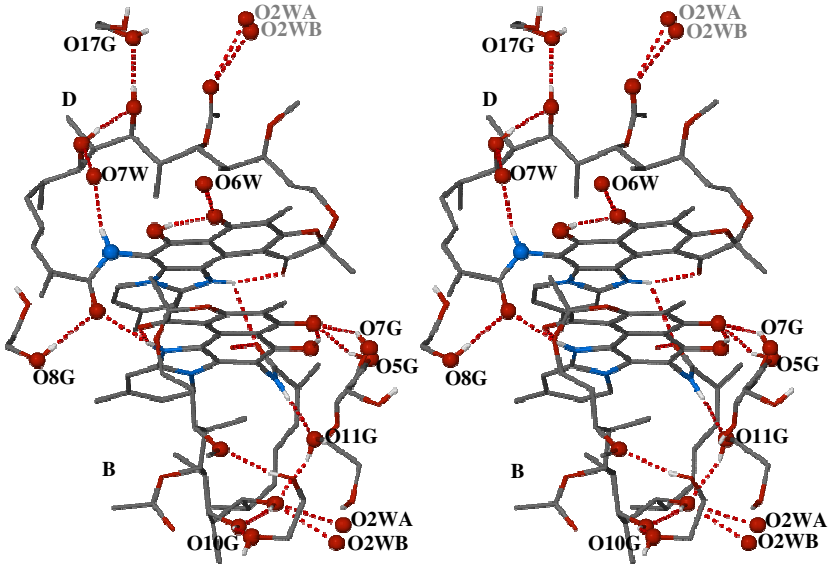

Figure 21 Stereoview of the O-H···O and N-H···O hydrogen bonds between the hosts (B and D) and guest molecules in F2. The relevant oxygen atoms are shown as spheres. The other hydrogen atoms and guest molecules are omitted for clarity. Atoms with gray labels have been symmetry-generated from their asymmetric unit counterparts.

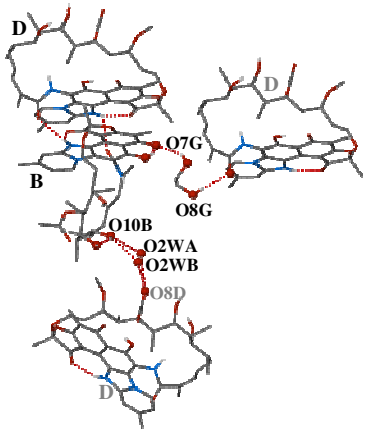

Figure 22 The long hydrogen bonded chains O1B···O2B···O7G-C7G-C8G-O8G···O11D and O9B···O10B···O2WA/O2WB···O8D in F2. The relevant oxygen atoms are shown as spheres. Atoms with gray labels have been symmetry-generated from their asymmetric unit counterparts.

The details of these hydrogen bond interactions are listed in Table 17. The average O···O distance for O-H···O interactions is 2.81 Å (range 2.699 to 3.022 Å). The mean N···O distance for N-H···O interactions is 2.973 Å (range 2.93-3.03 Å) with a mean angle of 161^{o} (range 158.0 -163.0^{o}).

Table 17 Host-guest intermolecular hydrogen bond interactions in solvate F2[a]

Hydrogen bond	O···O and N···O Distances (Å)	Angle (°)	Symmetry operator[b]
O9D-H9D···O17G	2.73(4)	165	x, y, z
O2WB···O8D	2.95(4)	-----	-x, y-1/2, 2-z
O2WA···O8D	2.90(3)	-----	-x, y-1/2, 2-z
O6W···O2D	2.79(5)	-----	x, y, z
O7W···O10D	2.77(2)	----	x, y, z
O8G-H8G···O11D	3.02(3)	150	x-1, y, z
O3W···O11B	2.82(2)	-----	x, y, z
O7G-H7G···O2B	2.70(3)	147	x, y, z
O5G-H5G···O2B	2.74(4)	158	x, y, z
O10B···O2WB	2.73(4)	-----	x, y, z
O10B···O2WA	2.82(3)	-----	x, y, z
O9B-H9B···O10G	2.70(2)	148	x, y, z
O9G-H9G···O6B	2.91(2)	162	x, y, z
O2G-H2G···O10A	2.85(2)	163	x, y, z
O1G-H1G···O1A	2.79(2)	152	x, y, z
O3G-H3G···O2A	2.87(1)	155	x, y, z
O1W···O11A	2.77(2)	-----	x, y, z
O4G-H4G···O11C	2.83(2)	155	x-1, y, z
O5W···O10C	2.74(1)	-----	x, y, z
O13G-H13G···O2C	2.72(3)	154	x, y, z
O9C-H9C···O4WA	2.85(3)	139	x, y, z
O15G-H15G···O10C	2.93(3)	171	x, y, z
O11G-H11G···O10B	2.83(2)	156	x, y, z
N1D-H1ND···O7W	3.03(2)	158	x, y, z
N1B-H1NB···O11G	2.98(2)	161	x, y, z
N1A-H1NA···O2G	2.96(1)	163	x, y, z
N1C-H1NC···O5W	2.92(2)	161	x, y, z

[a] Where no e.s.d. is reported for the angle, H atoms involved were added in idealised positions in a riding model.
[b] Symmetry operator applies to hydrogen bond acceptor atoms.

In addition, a host guest C-H···O hydrogen bond (C41D-H41D···O3W) is observed. [C···O 3.29(2) Å, C-H···O angle 155°]

Guest-guest Interactions

In the structure of F2, two different guest clusters are formed by the ethylene glycol and water molecules. One of the clusters (namely cluster 1) is shown in Figure 23. It is extended and a variety of disordered arrangements involving guest molecules occurs.

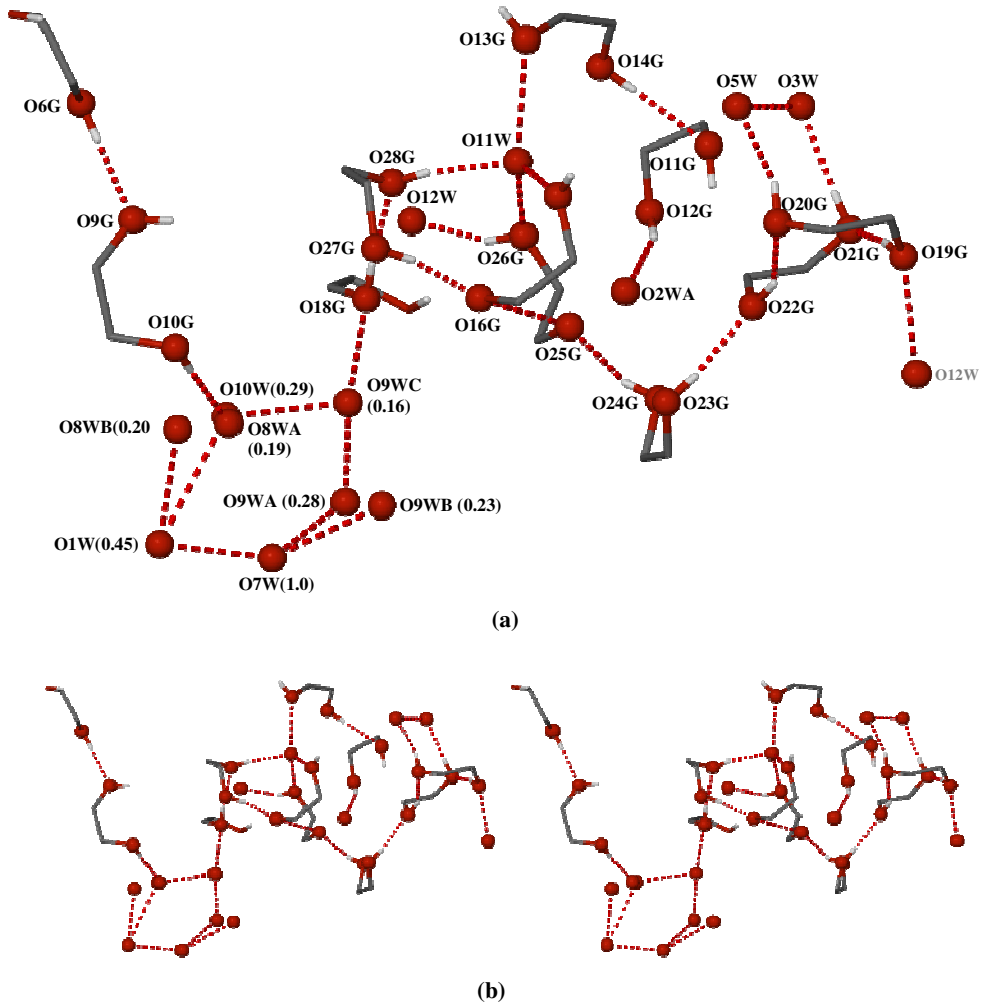

Figure 23 The guest-guest intermolecular O-H···O interactions among the water and ethylene glycol molecules in F2. (a) The labelling scheme of the cluster 1. Atoms with gray labels have been symmetry-generated from their asymmetric unit counterparts. The disordered atoms are labelled with their site-occupancies. (b) Stereoview of the cluster 1.

Figure 24 presents the second guest cluster (cluster 2) which is intimately associated with two symmetry-independent host molecules A and D. This cluster, which is relatively uncomplicated, also serves as a bridge associating these two host molecules.

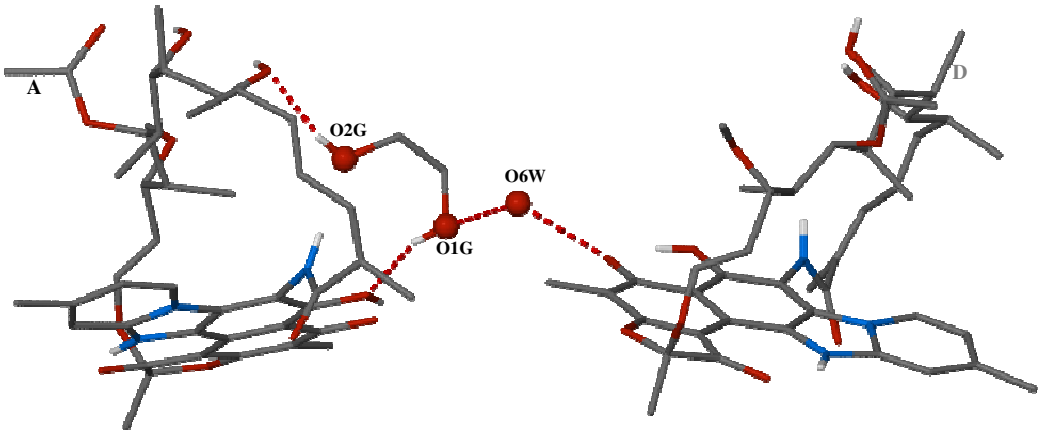

Figure 24 The hydrogen bond interactions in the cluster 2. The host molecule D with gray label has been symmetry-generated from its asymmetric unit counterparts.

The water molecules O2WB, O4WA and O4WB as well as the ethylene glycol molecules O3G-C3G-C4G-O4G and O7G-C7G-C8G-O8G are not hydrogen bonded to any other guest molecules. Specifically, the molecule O3G-C3G-C4G-O4G associates the rifaximin molecules A and C while the molecule O7G-C7G-C8G-O8G connects rifaximin molecules B and D.

The details of the guest-guest intermolecular O-H···O interactions are listed in Table 18. The average O···O distance is 2.78 Å with a mean angle of 163°.

Table 18 The details of the guest-guest intermolecular hydrogen bond interactions in solvate F2[a]

Hydrogen bond	O···O Distance (Å)	Angle (°)	Symmetry operator[b]
O10G-H10G···O10W	3.152	175.2	x-1, y, z
O6G-H6G···O9G	2.731	168.8	x, y, z
O10W··O8WA	3.077	-----	x, y, z
O8WA···O1W	3.049	-----	x, y, z
O1W···O8WB	2.643	-----	x, y, z
O8WA···O9WC	2.770	-----	1-x, y-1/2, 1-z
O1W···O7W	2.603	-----	1-x, y-1/2, 1-z
O7W···O9WA	2.643	-----	x, y, z
O9WC···O9WA	2.690	-----	x, y, z
O7W···O9WB	2.725	-----	x, y, z
O18G···O9WC	2.599	-----	x, y, z
O23G-H23G···O22G	2.726	161.4	x, y, z
O22G-H22G···O20G	2.820	149.6	x, y, z
O24G-H24G···O25G	2.844	159.4	x, y, z
O21G-H21G···O3W	2.794	171.4	x, y, z
O20G-H20G···O5W	2.739	159.1	1-x, 1/2+y, 2-z
O5W···O3W	2.773	-----	1-x, y-1/2, 2-z
O21G···O19G	2.673	-----	x, y, z
O19G···O12W	2.717	-----	1-x, y-1/2, 2-z
O25G···O16G	3.050	-----	1-x, 1/2+y, 2-z
O26G-H26G···O12W	2.537	157.6	-x, y-1/2, 2-z
O27G-H27G···O16G	2.511	166.8	x, y, z
O28G-H28G···O11W	2.708	150.7	1+x, y, z
O11W···O13G	2.857	-----	x, y, z
O15G···O11W	2.672	-----	1+x, y, z
O11W···O26G	2.933	-----	-x, y-1/2, 2-z
O14G-H14G···O11G	2.851	167.2	-x, y-1/2, 2-z
O12G-H12G···O2WA	2.758	156.6	x, y, z
O18G-H18G···O28G	2.826	173.4	x-1, 1+y, z
O1G···O6W	2.872	-----	-x, y-1/2, 1-z

[a] Average e.s.d.s 0.008 Å for distance and 0.9° for angle

[b] Symmetry operator applies to hydrogen bond acceptor atoms.

Overall Intramolecular and Intermolecular Interactions in F2

Figure 25 shows the overall hydrogen bond interactions in solvate F2. The hydrogen bond network is fairly complicated; therefore, a schematic diagram illustrating the network for F2 is presented in Figure 26.

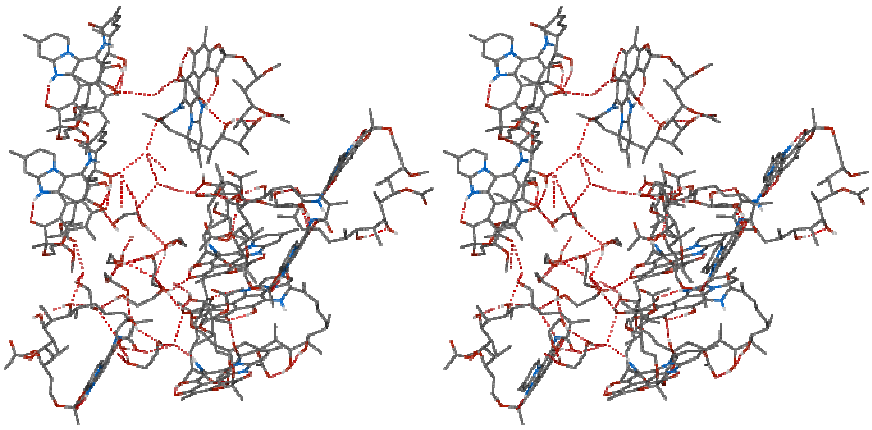

Figure 25 Stereoview of the overall hydrogen bond interactions in F2.

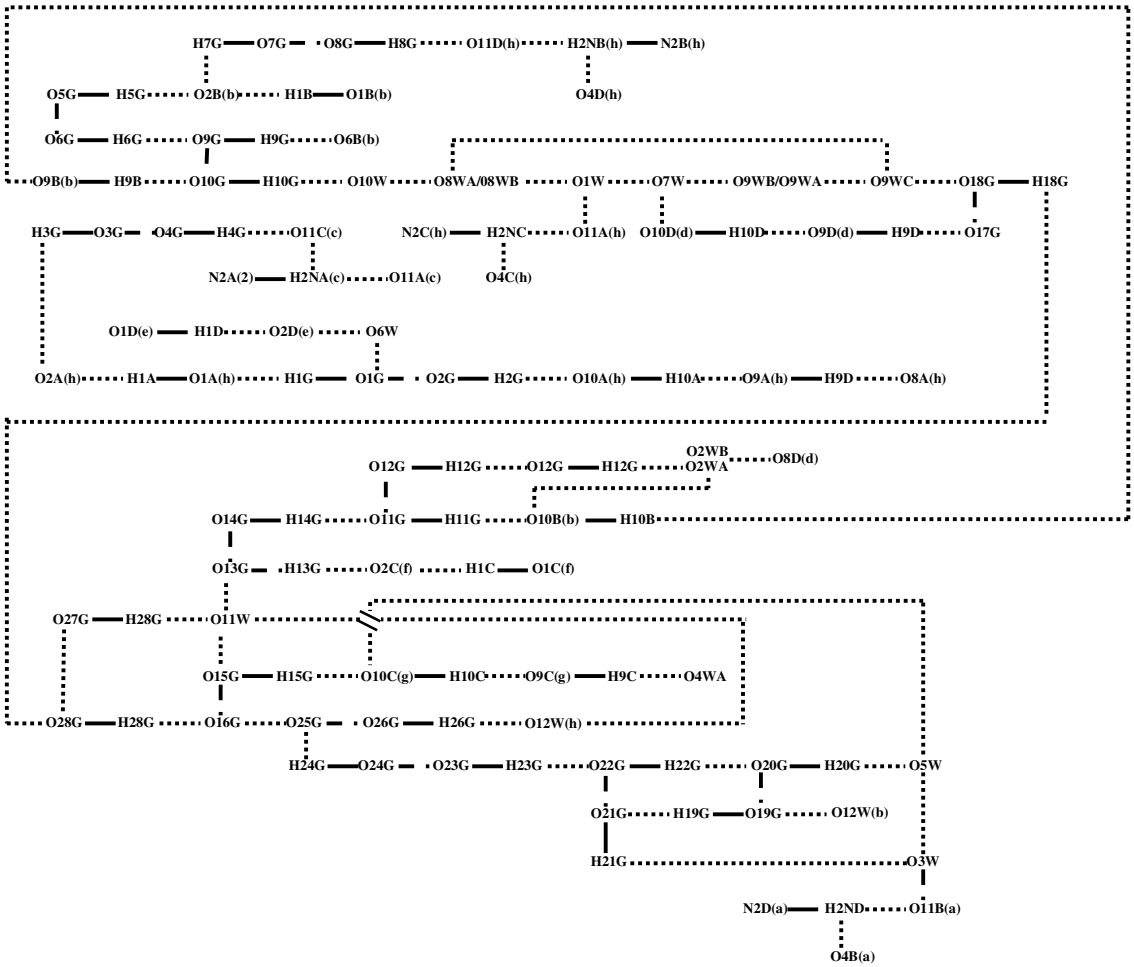

Figure 26 Schematic diagram of the overall hydrogen bond interactions in F2. The code letter for the symmetry operator of each rifaximin molecule is given as a suffix in the atom label. (a = x, y, z; b = x, y, 1+z; c = x-2, y, 1+z; d = -x, y-1/2, 2-z; e = -x-1, y-1/2, 2-z; f = -x, 1/2+y, 2-z; g = 1-x, 1/2+y, 2-z and h = x-1, y, 1+z.)

Crystal Packing

The host molecules A and C in F2 are related by a pseudo 2-fold rotation axis, as are molecules B and D (Figure 27). In addition, the host molecules A and B are also related by pseudosymmetry.

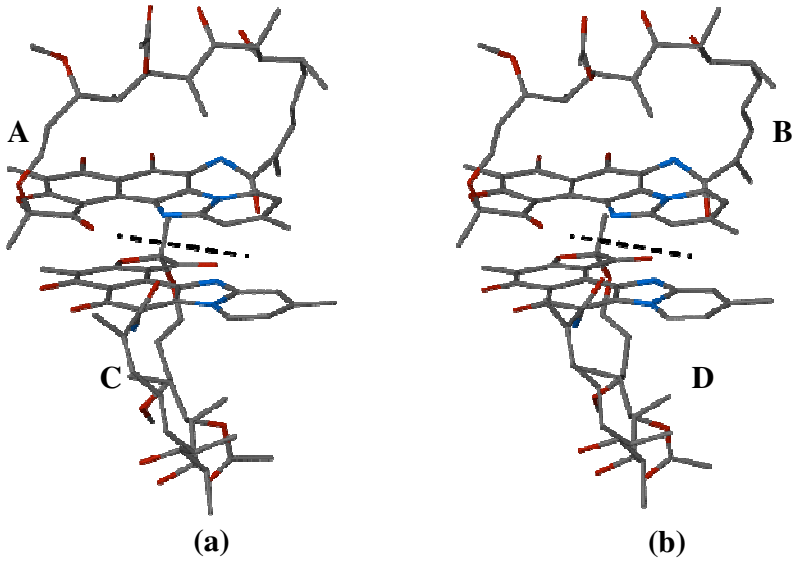

Figure 27 (a) A pseudo 2-fold rotation axis relating molecules A and C. (b) A pseudo 2-fold rotation axis relating molecules B and D.

The packing arrangement for F2 is shown in Figure 28. Notably, no host-host intermolecular or host-guest intermolecular interactions are found involving the host molecules A and B. The only interaction between them is the close contact C31B···O8A. Host-host interactions associate the host molecules parallel to the *b*-axis. This arrangement introduces isolated sites which extend parallel to the *a*-axis and accommodate solvent molecules.

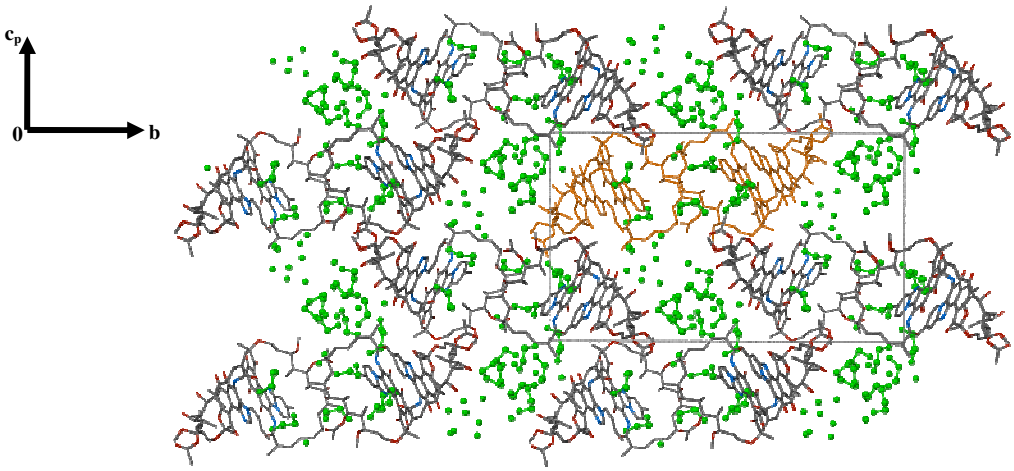

Figure 28 Crystal packing diagram for F2 viewed along [100]; solvent molecules are shown as green spheres for clarity. Host molecules A, B, C and D in the asymmetric unit are shown in brown.

Comparative PXRD

The calculated and experimental PXRD traces for the tetrahydrate F1 and the ethylene glycol-water solvate F2 are shown in Figure 29. In both cases, a slight shift in the computed trace to higher 2θ angles can be observed; this is due to the temperature difference at which the data were collected (experimental trace at 298 K, calculated trace at 173 K). Furthermore, differences in intensities between corresponding PXRD peaks can be attributed to preferred orientation effects in samples of both F1 and F2. However, the agreement between the experimental and calculated traces is generally convincing, indicating that each prepared sample was homogeneous.

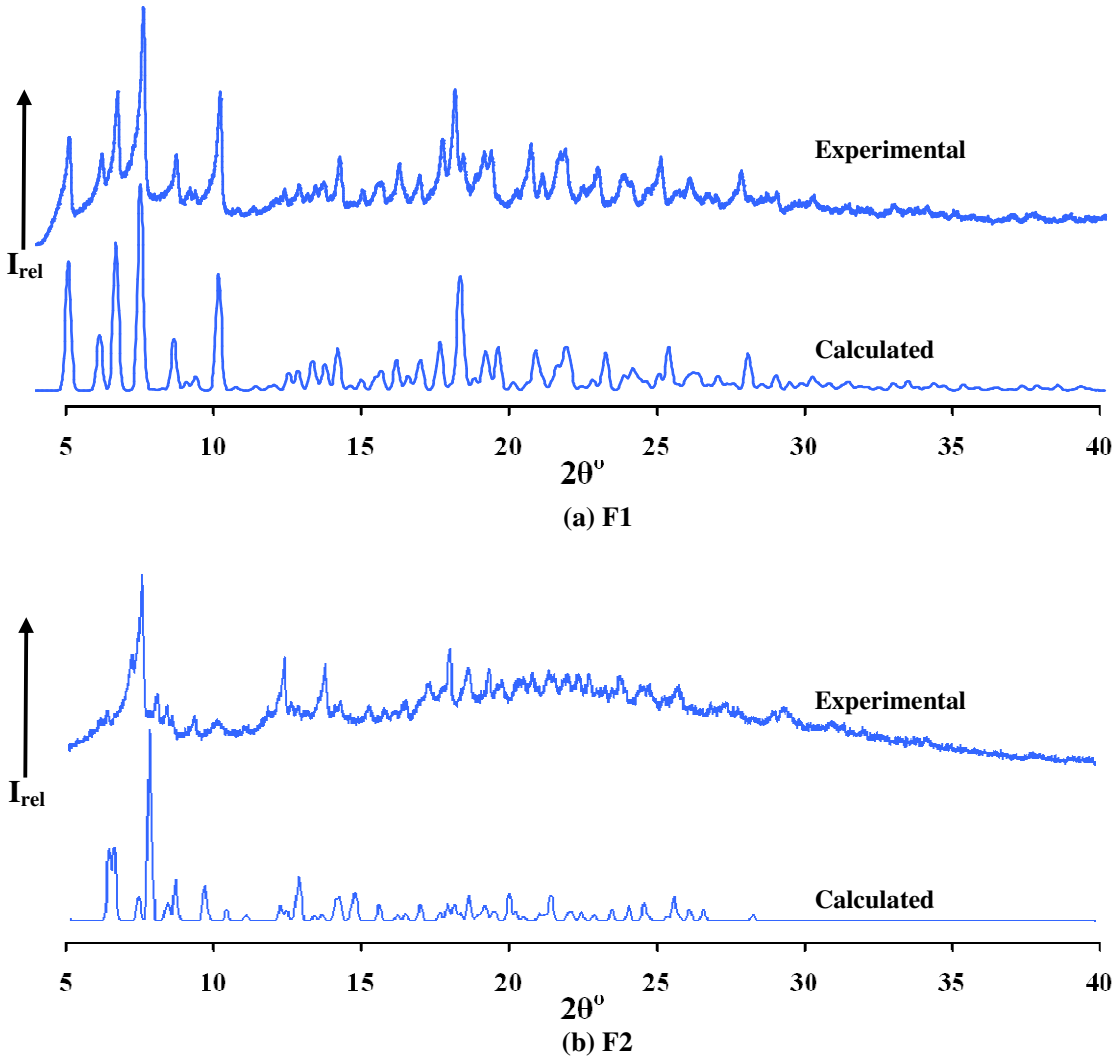

Figure 29 Calculated and experimental PXRD traces for (a) F1 and (b) F2.

Conclusion

A hydrate F1 of rifaximin and an ethylene glycol-water solvate F2 were isolated by recrystallisation and characterised by X-ray diffraction methods.

Conformation of the Rifaximin Host Molecules

The similarity between the host molecule A of F1 and the hosts of F2 was demonstrated in the overlay diagram (Figure 2) and reflected in the parameters that described the relevant dihedral angles involving the three principal planes (Table 4) and relevant torsion angles along the ansa chain (Table 5).

A considerable difference can be observed between the conformations of the rifaximin molecule B in F1 and those of the other host molecules (shown in Figure 2). The main difference is reflected in the orientation of the bond C15=O11. Specifically, this bond points away from the ansa chain in the host molecule B of F1 while pointing towards the ansa chain in the other host molecules. This indicates the existence of two quite distinct conformations of the rifaximin molecule. The ability of different included solvents to induce subtle variations in rifaximin molecular conformations is nicely illustrated in the solvate F2, with $Z' = 4$ (Figure 2 and Table 4).

Zwitterionic structure is a common feature associated with these distinct rifaximin conformations. It results from proton transfer from a hydroxyl group on the chromophore to nitrogen atom N2 of the imidazole ring.

The host molecules all adopt an open conformation. Each of the distinct conformations of rifaximin observed in this study has geometrical parameters that fall within the range required for antibiotic activity.

Hydrogen Bond Interactions

Identical intramolecular hydrogen bond interactions O1-H1···O2 and N2-H2··O4 are found in all the rifaximin molecules in F1 and F2. Furthermore, the average distance between O1 and O2 is 2.45 Å (range 2.40 – 2.48 Å) with an average angle of 150^{o}. The

mean N2···O4 distance is 2.76 Å (range 2.72 – 2.81 Å) with a mean angle of 144^{o} (range 140.0 – 148.0^{o}). The intramolecular hydrogen bond interaction O10-H10···O9 is found in the molecule A in F1 and in the molecules A, B, C and D in F2; however, host molecule B in F1 does not display this feature. A unique intramolecular hydrogen bond O9B-H9B···O10B exists in the molecule B in F1 while a unique hydrogen bond O9A-H9A···O8A is present in the molecule A in F2.

The motif of host-host intermolecular hydrogen bonds in F1 is completely different from that in F2. In F1, the hydrogen bond O1B-H1NB···O11A stabilises the two symmetry-independent rifaximin molecules in the asymmetric unit while another three host-host intermolecular hydrogen bonds associate the host molecules along the *b*-axis (Table 8 and Figure 15). In F2, all the host-host interactions among the rifaximin molecules occur only within the asymmetric unit. In more detail, similar hydrogen bonds ($N2^{+}$-H2N···O11) associate the molecules A and C, and a similar pattern is found for molecules B and D. However, no such host-host hydrogen bond can be observed between host molecules A and B. In fact, only a close contact O8A···C31B serves to associate these two symmetry-independent host molecules.

Pseudosymmetry, in the form of pseudo 2-fold rotation axes, was found to exist in the packing arrangements of the crystals of F1 and F2. Thus, host molecules A and B in F1 are related a pseudo 2-fold axis, as are molecules A and C as well as molecules B and D in F2. (A more complex pseudosymmetry relates molecules A and B in solvate F2). Furthermore, the pseudo torsion angles C43A···C7A···C7B···C43B in F1, C43A···C7A···C7C···C43C in F2 and C43B···C7B···C7D···C43D in F2 are -78.3(2), -6.5(8) and -8.7(9)^{o}, respectively (Figure 30). Corresponding to these three torsional relationships, there are three, seven and five π-π interactions respectively, the smallest torsion angle coinciding with the largest extent of π-π interaction, as expected.

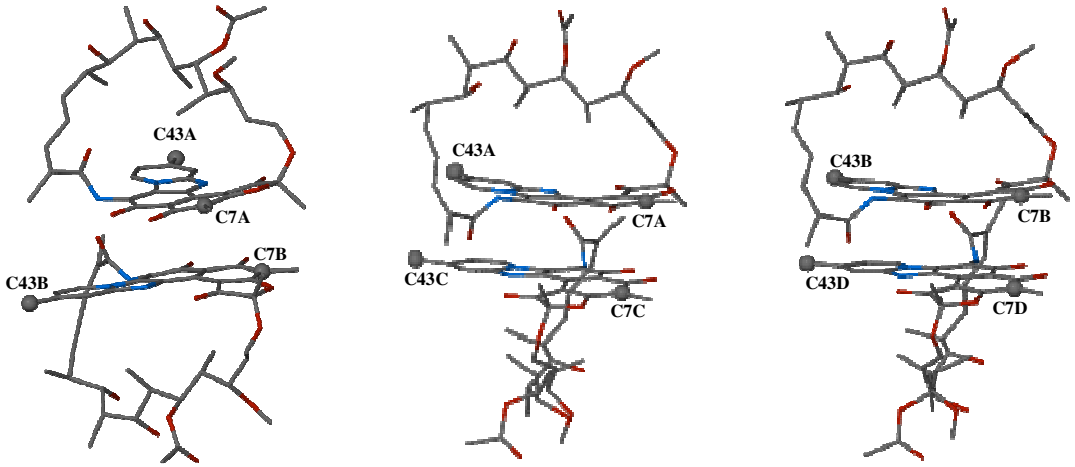

(a) Molecules A and B in F1 **(b) Molecules A and C in F2** **(c) Molecules B and D in F2**

Figure 30 Atoms defining the pseudo torsion angles (a) C43A···C7A···C7B···C43B in the molecules A and B in F1, (b) C43A···C7A···C7C···C43C in the molecules A and C in F2 and (c) C43B···C7B···C7D···C43D in the molecules B and D in F2.

The host-guest intermolecular hydrogen bond interactions in F1 are compared with those in F2. Whether the hydroxyl oxygen atoms and the nitrogen atoms in the host molecules are involved in the hydrogen bonds with the guest molecules are shown individually in Table 19. In each molecule, both the O2 and O10 atoms are involved in the host-guest interactions. Furthermore, the N and O atoms which are involved in the interactions are different between the crystallographically independent host molecule in the same hydrate or solvate.

Table 19 Shows whether the nitrogen and oxygen atoms in the host molecules are involved in the host-guest H-bond interactions in F1 and F2.

molecule		O1	O2	O4	O6	O8	O9	O10	O11	N1	N2
F1	A	Yes	Yes	Yes	-----	Yes	-----	Yes	-----	Yes	Yes
	B	Yes	Yes	Yes	-----	Yes	-----	Yes	-----	-----	Yes
F2	A	Yes	Yes	-----	-----	-----	-----	Yes	Yes	Yes	-----
	B	-----	Yes	-----	Yes	-----	Yes	Yes	Yes	Yes	-----
	C	-----	Yes	-----	-----	-----	Yes	Yes	Yes	Yes	-----
	D	-----	Yes	-----	-----	Yes	Yes	Yes	-----	Yes	-----

The packing diagrams of F1 are completely different from those of F2. However, isolated sites for the included solvent molecules, located parallel to the *a*-axis, are found in both cases.

Closing Remarks – Status of Rifaximin Species

It is very relevant to note here that the author first isolated single crystals of solvate F1 in 2007, subsequently solving and refining the crystal structure by the end of that year. In 2008, the crystal structure of a solvate described as rifaximin tetrahydrate was reported by Bacchi et al.[7] Exhaustive comparison of the crystal structure of F1 (TGA-derived formula rifaximin·3.7H_2O) with the published structure of the tetrahydrate confirmed that they were indeed the same phase, the latter crystal evidently containing ~8% more water of crystallization. Bacchi et al. collected their X-ray data at 293 K. Interestingly, the lower temperature of the author's data-collection (173 K) did not yield significantly more accurate molecular and crystal packing parameters. An overlay of the two crystal asymmetric units, presented in Figure 32, reveals only small host conformational differences and the subtle effects of temperature on solvent molecule locations.

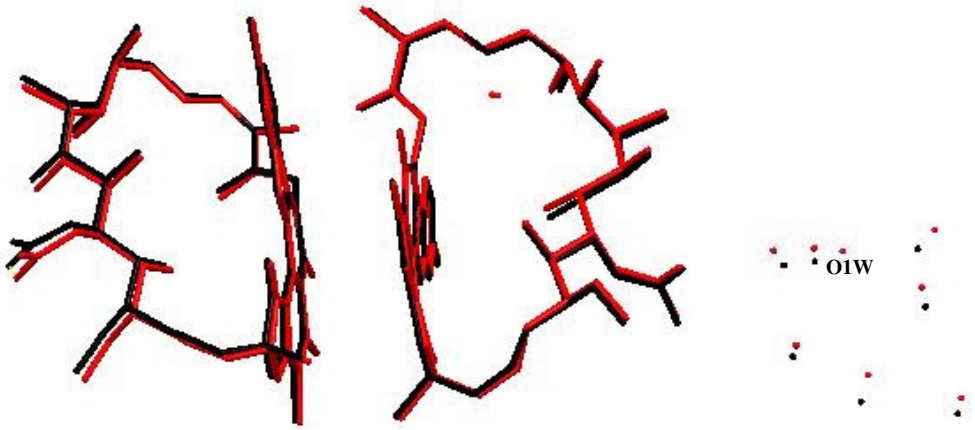

Figure 32 An overlay diagram of the tetrahydrate[7] (black) and F1 (red). Hydrogen atoms are omitted for clarity.

The zwitterionic structure of rifaximin was established in both crystal structure determinations. One minor difference is that water molecule O1W (with s.o.f. 0.36) in F1 adopts a unique position, not matched by a counterpart in the tetrahydrate.

Despite the unforeseen duplication described above for F1 and the subsequently published tetrahydrate structure,[7] the author pursued the search for other solid phases of rifaximin, successfully isolating solvate F2, which turned out to be a much more challenging structural problem. For this phase, a satisfactorily refined structural model

was eventually obtained only after much effort to optimise the crystal quality and several X-ray data-collections to achieve the required resolution.

To the author's knowledge, the structures of the phases F1 and F2 are the only ones known for the drug rifaximin. Given the fact that they are not isostructural, a comparison of their similarities and differences was considered a worthy goal of this study. In particular, the high Z' value for the solvate F2 (viz. 4) presented the opportunity for observing for the first time a potentially wider range of rifaximin conformations in the solid state than those afforded by solvate F1 ($Z' = 2$), as well as novel crystal packing features.

References:

1. XPREP, *Data Preparation and Reciprocal Space Exploration*, Version 5.1, © Bruker Analytical X-ray Systems, **1997**.
2. Sheldrick, G. M., In: *Direct Methods for Solving Macromolecular Structures*, Fortier, S. (eds.), Kluwer Academic Publishers: Dordrecht, **1998**, 401-411.
3. Sheldrick, G. M. SHELXH, *Acta Crystallogr.*, **2008**, A64, 112-122.
4. Bacchi, A. and Pelizzi, G., *J. Med. Chem.*, **1998**, 41, 2319-2332.
5. Brufani, M., Cerrini, S., Fedeli, W. and Vaciago, A., *J. Mol. Biol.*, **1974**, 87, 409-435.
6. Arora, S. K. and Arjunan, P., *J. Antibiot.*, **1992**, 45, 428-431.
7. Bacchi, A., Carcelli, M. and Pelizzi, G., *New J. Chem.*, **2008**, 32, 1725-1735.
8. Allen, F. H., Watson, D. G., Brammer, L., Orpen A. G. and Taylor R. In: *International Tables for Crystallography, Vol. C*, Prince, E. (eds.), © International Union of Crystallography **2006**, Ch 9.5, 790–811.
9. Howes, B. D., Scatragli, S., Marzocchi, M. P. and Smulevich, G., *J. Raman Spectrosc.*, **2006**, 37, 900-909.
10. Marchi, E., Montecchi, L., Venturini, A. P., Mascellani, G., Brufani, M., and Cellai, L., *J. Med. Chem.,* **1985**, 28, 960-963.

Chapter 6

Thermal Analysis

In this chapter, we describe the thermal behaviours of the rifampicin and rifaximin solvates and attempt to reconcile them with their respective crystal structures.

As explained in chapters 4 and 5, the derivation of molecular formulae for the solvates was achieved by combining data obtained from multiple Thermogravimetric Analysis (TGA) measurements with data from X-ray structural refinements. In this chapter, the experimental mass loss (average data of multiple TGA measurements) for each solvate is compared with the respective calculated mass loss, implied by the derived solvate formula.

Rifampicin Isostructural Series 1 (P1, P2, P3 and P4)

P1: rifampicin • 1.57methanol • $3H_2O$,

P2: rifampicin • 0.39methanol • $4.17H_2O$,

P3: rifampicin • 2ethanol •$2H_2O$,

P4: rifampicin • 0.54ethanol • $3.92H_2O$

Hot Stage Microscopy (HSM)

The crystals of solvates P1 and P2 were placed on the same slide under silicone oil (Figure 1). The colour of the crystal P2 was lighter than that of P1 at 30 ^oC. This is probably due to the different compositions of P1 and P2. The water and methanol molecules of P1 started to escape at ~70 ^oC resulting in bubbles forming on the surface of the crystal while no obvious appearance of bubbles was observed around the crystal P2. At 200 ^oC, both crystals began to decompose and turned dark brown in colour.

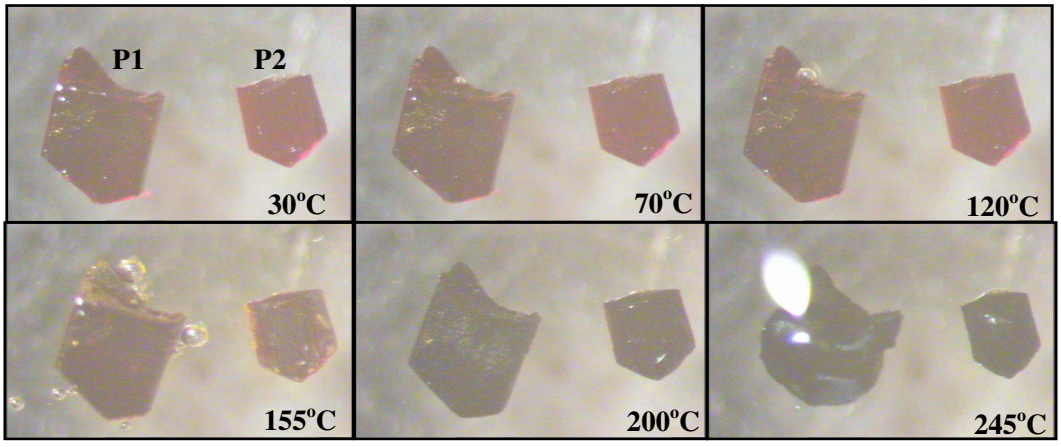

Figure 1 Thermal decay for solvates P1 and P2

The crystals of P3 and P4 were treated in the same way and the corresponding HSM photographs are shown in Figure 2. Similarly to the crystals of P1 and P2, the colour of crystal P3 was darker than that of P4 at 30 °C. No appearance of bubbles was observed during the heating of P3 and P4. However, both crystals were gradually surrounded by a yellow solution, resulting from re-dissolution of partially desolvated drug in ethanol liberated from the solvates.

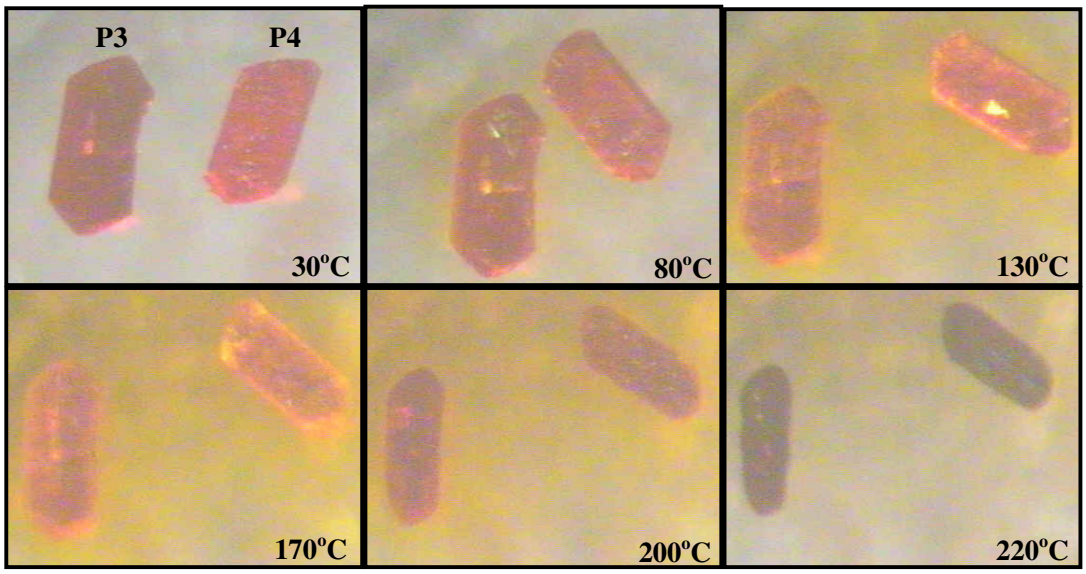

Figure 2 Thermal decay for the crystals of P3 and P4.

All four crystals shown in Figures 1 and 2 started to show signs of decomposition at ~200 °C and totally decomposed at ~220 °C. This provides visual evidence that the crystals of P1, P2, P3 and P4 apparently changed into the same species after desolvation. It should be noted that for this solvate series as well as all the other series, variable temperature PXRD was employed in an attempt to characterise the desolvated material. (The likelihood of different amorphous forms of a given drug arising from different isostructural solvate series is mooted in the Discussion Section).

TGA

The TGA traces for P1 and P2 are shown in Figure 3. The crystals of P1 lose mass immediately above 30 °C while those of P2 only start to lose mass at approximately 42 °C. This corresponds to the observation that crystals of P1 desolvate instantly when exposed to the atmosphere and this is represented by A in the Figure. Based on the first

derivative curves (DTG curves) of P1 and P2 (not shown), both solvates showed multiple-step mass loss indicating that they lost methanol and water molecules simultaneously during the heating process (given as B in Figure 3). Point C indicates the decomposition of both samples with an onset temperature of ~180 °C. The calculated mass loss is comparable to the experimental mass loss for P1 in the temperature range of 30 °C to 134.2 °C; these losses are 12.5% and 12.4 ± 0.5% (n = 3), respectively. The experimental mass loss for P2 is 9.7 ± 0.3% (n = 3) in the temperature range of 42.1 °C to 133.2 °C; this is consistent with its calculated mass loss 9.6%.

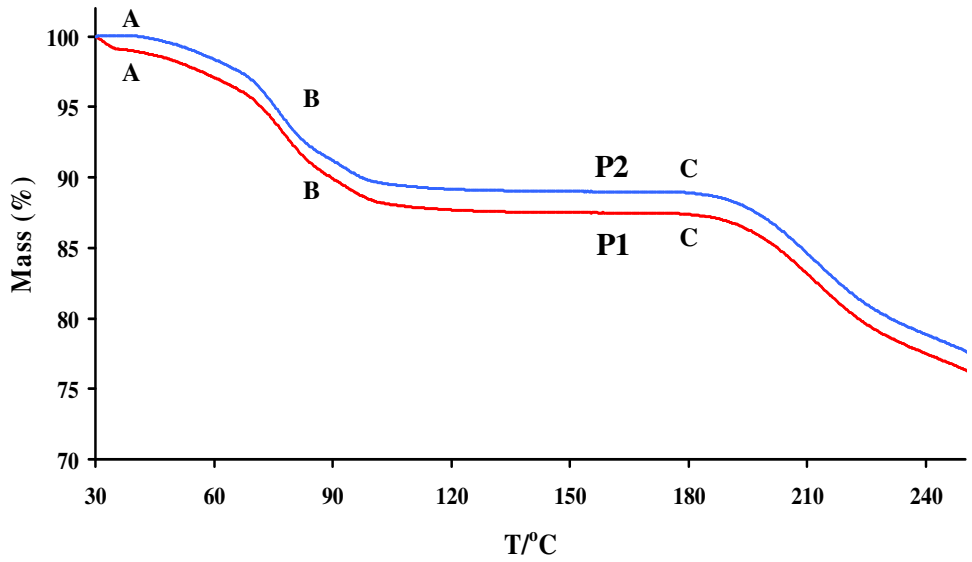

Figure 3 TGA traces for rifampicin solvates P1 (red) and P2 (blue)

Similarly to P1 and P2, crystals of P3 (Figure 4, red) exhibited an instantaneous mass loss above 30 °C whilst those of P4 (Figure 4, blue) only lost mass at ~37 °C. This result is consistent with the fact that P3 desolvates immediately after being removed from the crystallising solvent (indicated by point A in Figure 3). Both curves exhibited multiple-step mass loss, none of which corresponded convincingly to that of only ethanol or water molecules in the stated solvate formula. This provides proof that both solvates lose the ethanol and water molecules concurrently during the heating process (represented by B in Figure 4). The decomposition of the desolvated crystals occurred at ~180 °C, shown by C in the Figure. The calculated mass loss is comparable to the experimental mass loss for P3 in the temperature range of 30 °C to 150.0 °C; these are 13.5% and 12.6 ± 0.9 % (n = 3), respectively. The experimental mass loss for P2 is 10.3 ± 0.8% (n = 4) in the

temperature range of 37.2 °C to 168.5 °C, and this is consistent with its calculated mass loss of 10.3%.

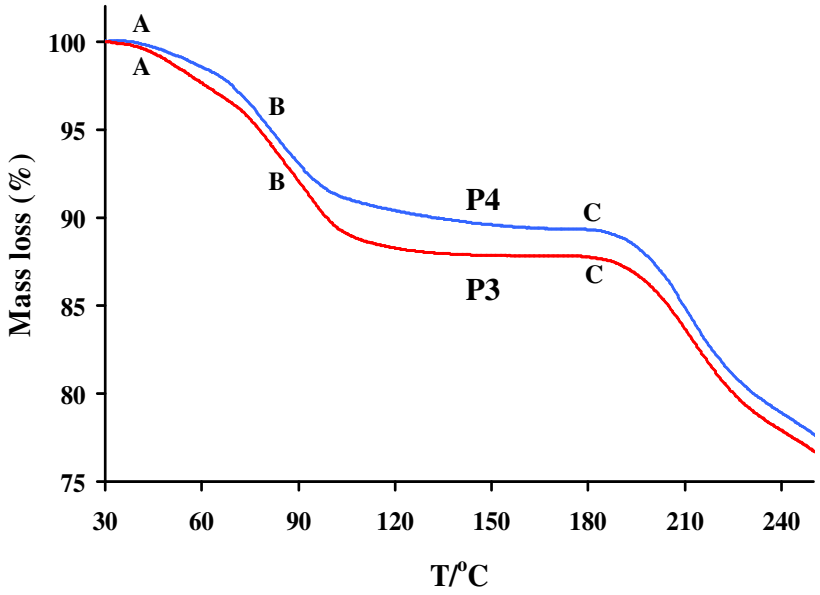

Figure 4 TGA traces for rifampicin solvates P3 (red) and P4 (blue)

For all four solvates P1, P2, P3 and P4, the experimental mass loss matches the respective calculated mass loss within the quoted experimental errors. The consistency of the decomposition temperature (~180 °C) in these TGA traces strongly suggests that all the four solvates were converted into the same product after desolvation.

Differential Scanning Calorimetry (DSC)

The DSC traces of the four solvates are very similar (Figure 5). They all exhibited one broad desolvation endotherm D, comprising two overlapping peaks. This indicates the possibility of the presence of a solvent mixture (methanol/water, ethanol/water), which is consistent with the multiple-step mass loss B in the TGA traces for all four solvates in Figures 3 and 4.

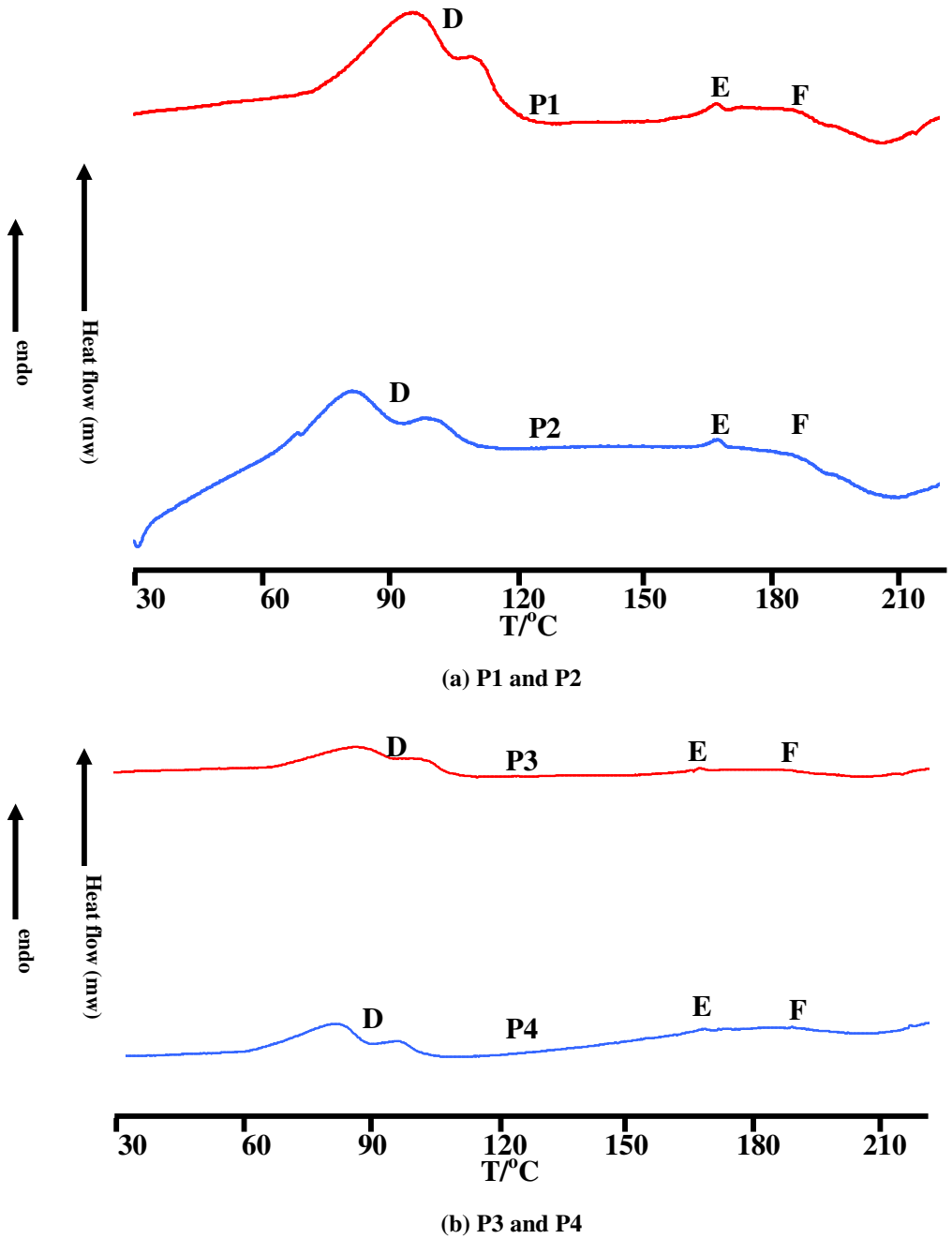

Figure 5 DSC traces for P1 and P2 (a); P3 and P4 (b)

For all four traces, a small endotherm E, interpreted as initial uptake of heat by the amorphous form of rifampicin, was observed and it is directly followed by an exotherm F indicating decomposition. Furthermore, the onset temperatures of F in the four solvates are very similar (~187 ^{o}C). This temperature is also consistent with the onset temperature of event C in the TGA traces for the four solvates in Figures 3 and 4. The temperatures

of decomposition using DSC (~187 °C) and HSM (~220 °C) differ due to differences in crystal sizes and experimental conditions.

Rifampicin Isostructural Series 2 (P5, P6 and P7)

P5: rifampicin • 2.5(1-propanol) • 4.3H_2O

P6: rifampicin • 1.58(1-propanol) • 8.41H_2O

P7: rifampicin • 0.6(iso-propanol) • 8.09H_2O

HSM

Crystals of solvates P5 and P6 were immersed in silicone oil and placed side by side on a microscope slide (Figure 6). For the crystal of solvate P5, the bubbling phenomenon appeared twice during the heating process. The first appearance was observed between ~91 °C and ~104 °C. The second appearance was observed between ~121 °C and ~163 °C. Meanwhile, the crystal P6 experienced no obvious optical change until decomposition. Both crystals decomposed at ~200 °C.

Figure 6 HSM micrographs of solvates P5 and P6 recorded at various temperatures.

Similarly to the crystal of P5, a crystal of solvate P7 (Figure 7) also experienced the bubbling phenomenon twice during the heating process. The first bubbles formed at ~83 °C, and continued until 114 °C. The second bubbling phenomenon occurred in the range ~142 – 171 °C. The crystal completely decomposed at ~200 °C.

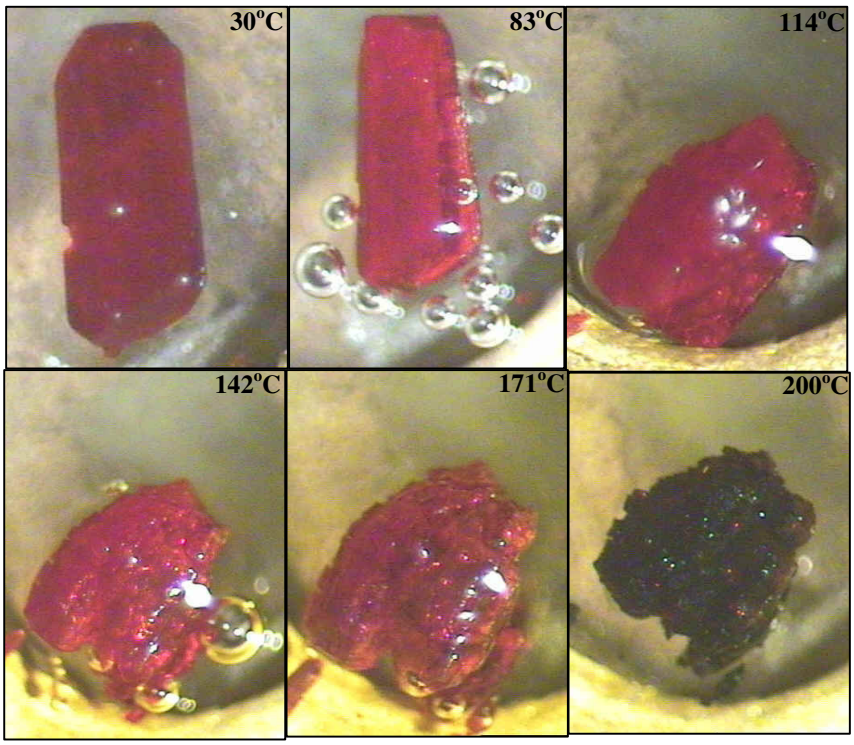

Figure 7 HSM micrographs of solvate P7 recorded at various temperatures.

The bubbling phenomenon indicates simultaneous loss of water and the included alcohol from the crystals. Furthermore, the decomposition temperatures were almost identical in the cases of P5, P6 and P7.

TGA

The TGA traces for solvates P5, P6 and P7 are very similar (Figure 8). They each displayed three thermal events A, B and C. For P5 and P7, event A showed that the crystals lost mass instantly above 30 °C while the crystals of P6 only started to lose mass after ~37 °C. These results are consistent with the fact that the crystals of P6 were obtained by leaving those of P5 on an open bench. In each case, B indicates further simultaneous loss of water and alcohol while C indicates the onset of decomposition of the material.

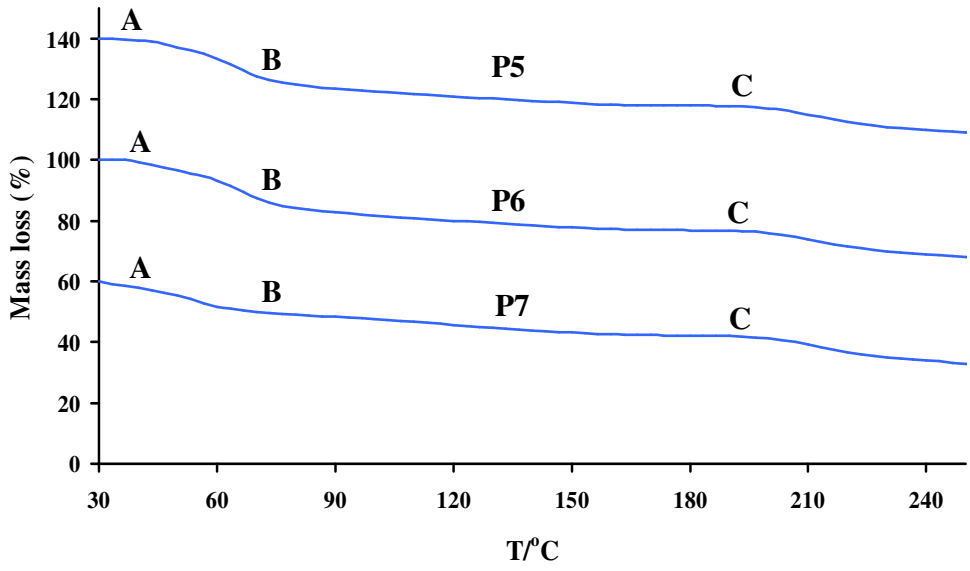

Figure 8 TGA traces for rifampicin solvates P5 (top), P6 (middle) and P4 (bottom)

The experimental mass loss for P5 is 22.1 ± 0.8% (n = 3) in the temperature range 30 °C to 170.0 °C while its calculated mass loss is 21.6%. The experimental traces for P6 showed a mass loss of 23.0 ± 0.4 % (n = 3) in the temperature range of 36.7 °C to 166.7 °C while the calculated mass loss is 23.1%. The experimental mass loss for P7 is17.4 ± 0.8% (n = 3) in the temperature range of 30.0 °C to 160.0 °C while the calculated mass loss is 18.1%. Hence, the total experimental mass loss for each solvate correlates well with the calculated mass loss. The fact that the decomposition temperature in each TGA trace is very close (~189 °C) indicates that all the three solvates had transformed into the same species after desolvation.

DSC

The DSC trace for each of the solvates P5, P6 and P7 (Figure 9) showed three thermal events namely D, E and F. Events D and E indicate the simultaneous desolvation followed by the decomposition of the material indicated by F. Events D and E are attributed to desolvation since stepwise mass losses in TGA did not yield separate solvent contents in close accord with the stoichiometric formulae of the solvates. Simultaneous loss of water and alcohol is presumably occurring. However, the appearance of well-separated peaks D, E possibly indicates some degree of solvent differentiation with temperature. The structural analysis indicated that P5 and P6 possess an isolated and

infinite guest cluster, respectively. This possibly gives rise to the wider desolvation temperature range of D in P5 compared with that in P6.

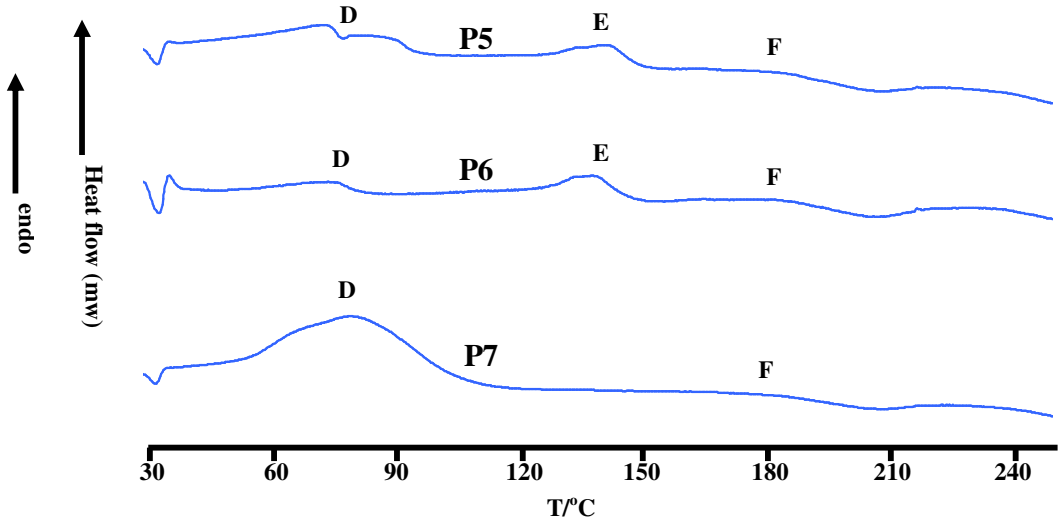

Figure 9 DSC traces for solvates P5 (top), P6 (middle) and P7 (bottom)

In all three DSC traces, rifampicin decomposition commenced at ~186 °C. The corresponding exotherm F correlates very well with the onset of decomposition shown in the TGA traces in Figure 8. Again, it strongly suggested that all three solvates had been converted into the same species after desolvation.

The following solvates (P8 - P11) do not belong to either of the previous isostructural series. Each of them belongs to a unique solvate category.

Solvate P8

2rifampicin • 4.30iso-propanol • 14.7H_2O

HSM

The crystal of P8 showed a colour change in the temperature range 30 °C to 190 °C, indicating the desolvation process (Figure 10). The crystal showed signs of decomposition at ~190 °C.

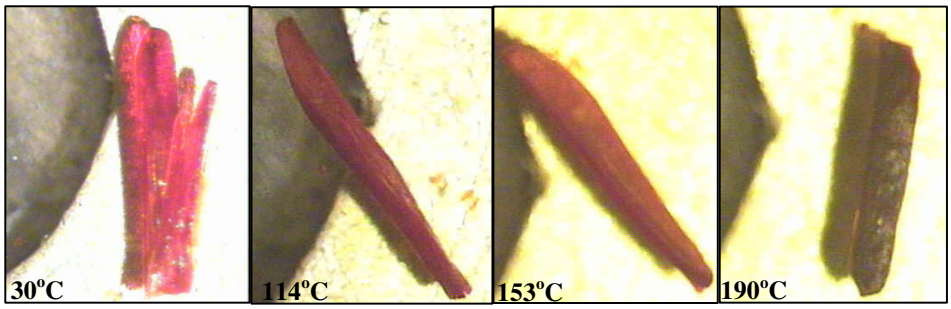

Figure 10 HSM micrographs of solvate P8 recorded at various temperatures.

TGA

The TGA trace for P8 exhibited two thermal events, A and B (Figure 11). The desolvation occurred over a wide temperature range (30 °C to 172.0 °C) and in what appear to be three steps, indicating the concurrent release of iso-propanol and water molecules from the solvate crystal. Event B indicated the decomposition onset of P8 at 187.9 °C.

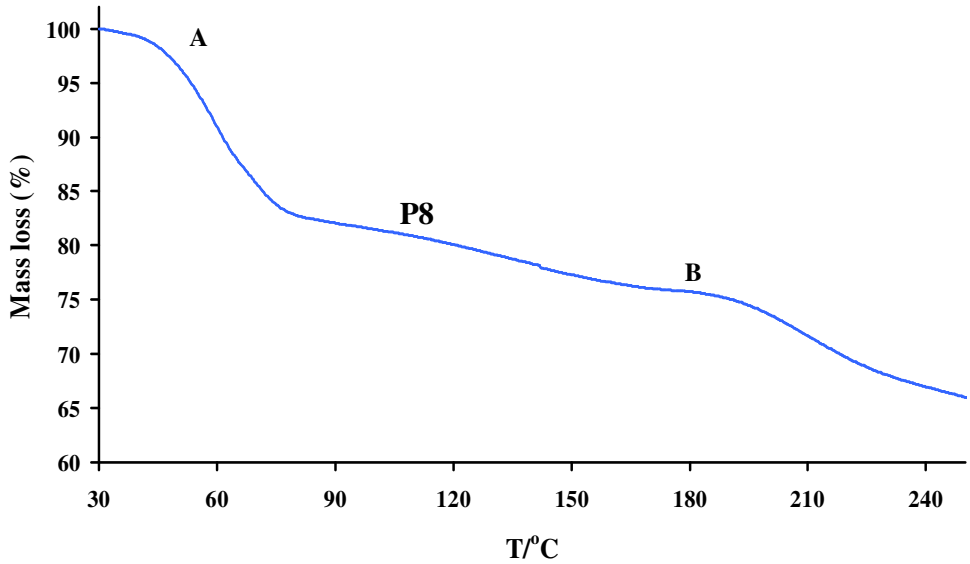

Figure 11 TGA trace for rifampicin solvate P8

DSC

The DSC trace for solvate P8 (Figure 12) showed a broad endotherm labelled C, indicating loss of included solvent between the temperatures of 37.6 °C and 133.3 °C. A small endotherm D with onset temperature 175.3 °C represented initial uptake of heat by the compound and this was followed by a decomposition exotherm E at 187.1 °C.

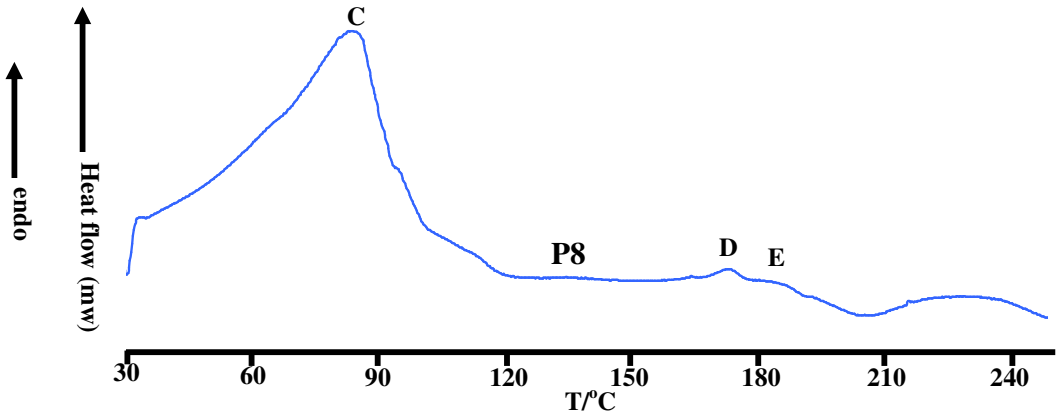

Figure 12 DSC trace for rifampicin solvate P8

For solvate P8, the onset temperatures of the thermal events that occurred in both TGA and DSC analysis correlated well with those shown in hot stage analysis.

Solvate P9

2rifampicin • 5.53(1-butanol) • 1.40H_2O

HSM

The crystal of solvate P9 was clear at room temperature (Figure 13, 30 °C). Micro-fissures gradually appeared in the crystal during the heating process, indicating desolvation of the crystal. Obvious bubbles started to appear at ~112 °C and stopped forming at ~146 °C, which again provides evidence of desolvation of the solvate crystal. The crystal then completely decomposed at ~188 °C, changing colour to dark brown.

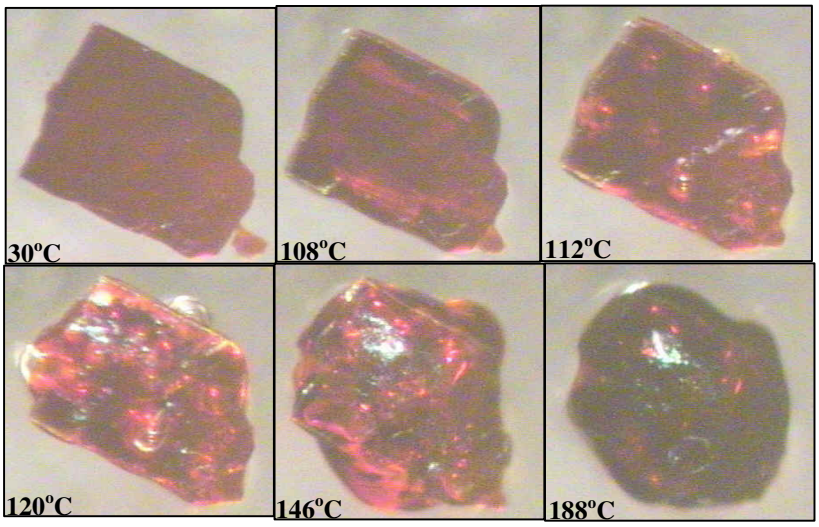

Figure 13 HSM micrographs of solvate P9 recorded at various temperatures.

TGA

The TGA trace for solvate P9 showed a significant mass loss of 20.3 ± 0.7% (n = 3) in the temperature range 30.0 °C to 171.7 °C (represented by A in Figure 14). This experimental mass loss is very close to the calculated mass loss (20.9%). Event A shows essentially a two-step mass loss. However, neither mass loss correlates well with that predicted from the derived stoichiometric formula. This implies that there is simultaneous loss of water and 1-butanol. Event B indicates the onset of decomposition of the desolvated compound at 191.5 °C.

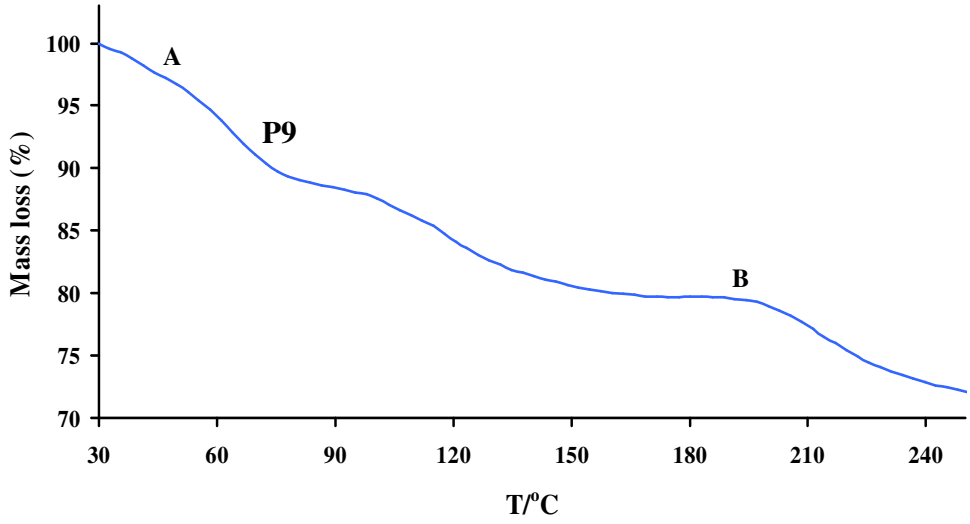

Figure 14 TGA trace for rifampicin solvate P9

DSC

The DSC trace for solvate P9 exhibited two endotherms D and E due to 1-butanol and water loss, followed by a decomposition exotherm F with the onset temperature of 188.3 °C (Figure 15). The onset of decomposition in DSC analysis corresponds well with that observed on TGA analysis.

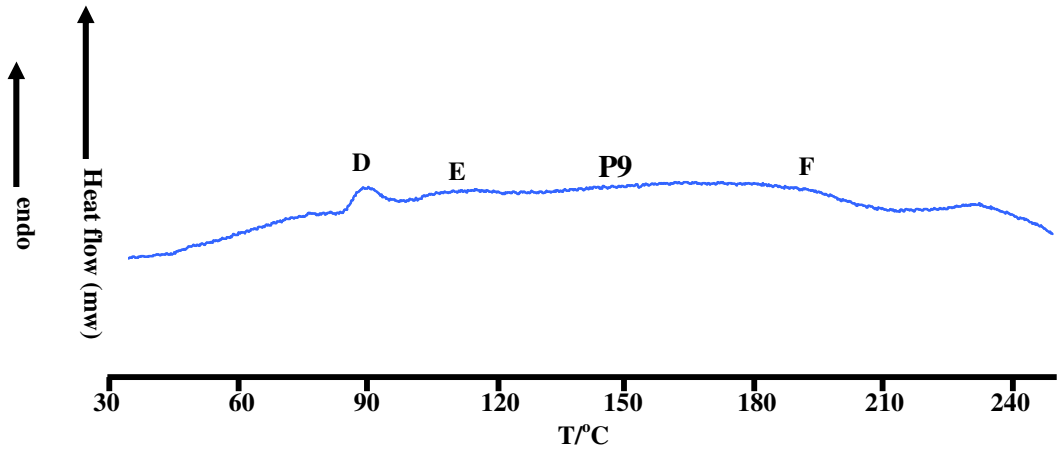

Figure 15 DSC trace for rifampicin solvate P9

Solvate P10

2rifampicin • 5.75ethylene glycol • 5.59H_2O

HSM

Formation of micro-fissures in the crystal of solvate P10 was observed during the heating process (Figure 16). These were attributed to the dehydration and loss of ethylene glycol from the crystal although no obvious bubbles appeared. The crystal underwent a colour change (red to dark brown) at ~189 °C, suggesting the onset of decomposition.

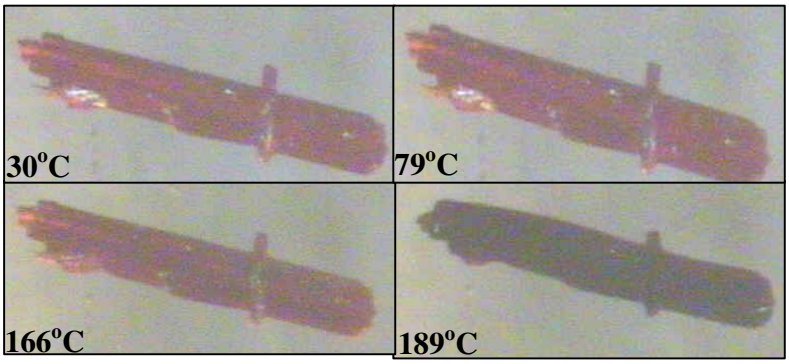

Figure 16 HSM micrographs of solvate P10 recorded at various temperatures.

TGA

The TGA traces for solvate P10 showed a total mass loss of 21.0 ± 0.9% (n = 3) in the range from 30.0 °C to 164.2.0 °C (Figure 17). The calculated mass loss is 21.8%. Event A represents multiple-step mass loss which indicates simultaneous loss of water and ethylene glycol. The desolvated form then decomposed at ~191 °C, shown by B.

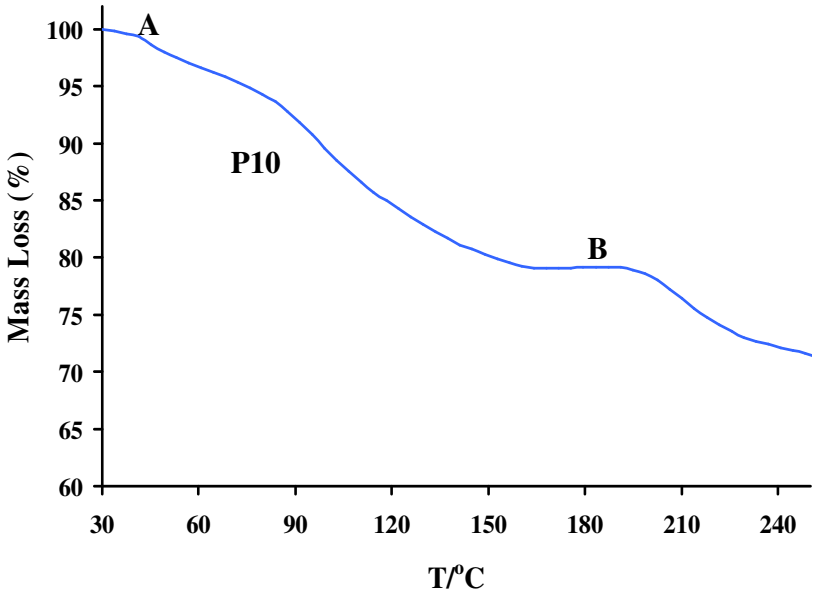

Figure 17 TGA trace for rifampicin solvate P10

DSC

The DSC trace of solvate P10 (Figure 18) exhibited two broad endotherms D and E which are due to the loss of ethylene glycol and water molecules in the crystal, followed by a tiny decomposition exotherm F with the onset temperature of 188 °C.

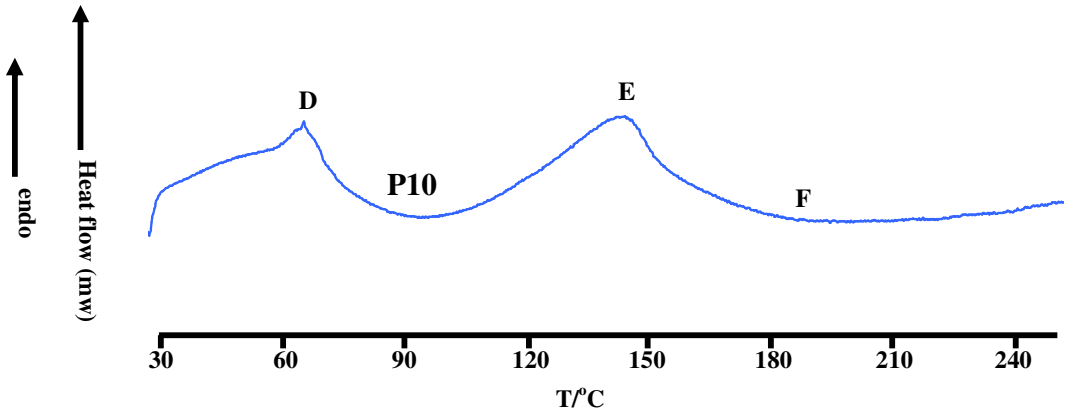

Figure 18 DSC trace for rifampicin solvate P10

Solvate P11

2rifampicin • 6(1,4-dioxane) • $3H_2O$

HSM

The water and 1,4-dioxane molecules were released at ~53 °C, evidenced by the formation of bubbles from the crystal of solvate P11 (Figure 19). The dehydration and desolvation continued until 154 °C during the heating process. The crystal decomposed at ~201 °C evidenced by an obvious colour change to dark brown.

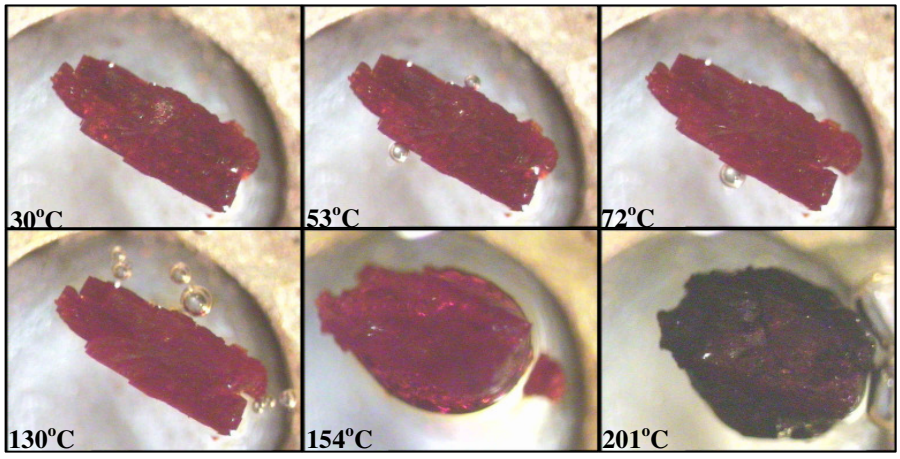

Figure 19 HSM micrographs of solvate P11 recorded at various temperatures.

TGA

The TGA trace for P11 (Figure 20) showed multiple-step mass loss A, which is attributed to the simultaneous release of 1,4-dioxane and water molecules between the temperature

30.0 °C and 171.7 °C with the experimental mass loss of 25.3 ± 0.9% (n = 3). This correlates well with the calculated mass loss 26.1%. Event B corresponded to the decomposition of the desolvated form. The onset of this event occurred at ~192 °C.

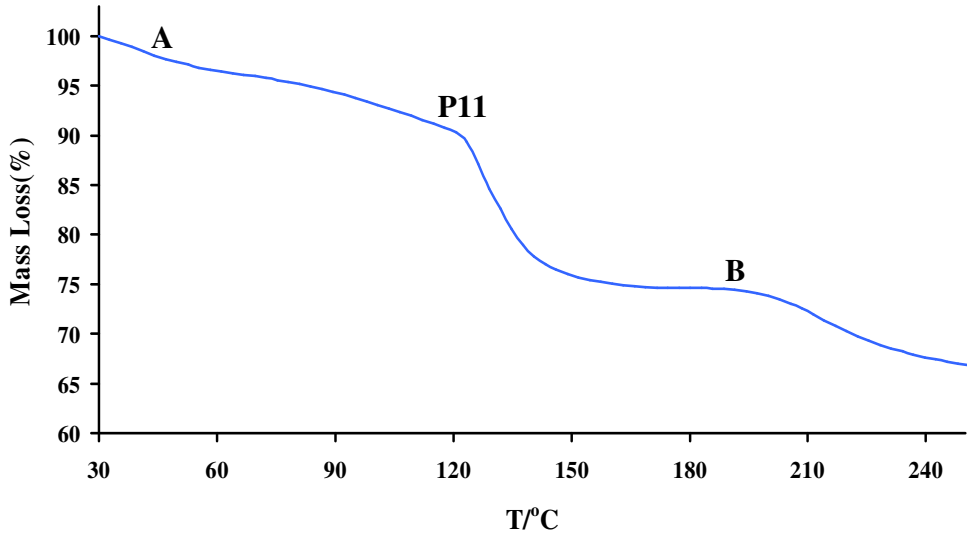

Figure 20 TGA trace for rifampicin solvate P11

DSC

A broad endotherm C and a distinct exotherm D were evident in the DSC trace for solvate P11 (Figure 21). The former was due to the simultaneous loss of water and 1,4-dioxane while the latter was due to the decomposition of the desolvated compound with the onset temperature of 188.5 °C.

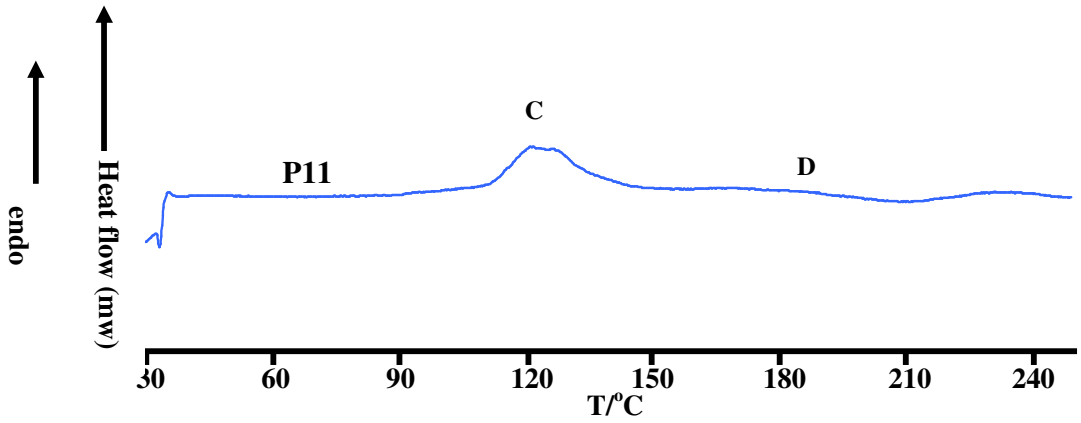

Figure 21 DSC trace for rifampicin solvate P11

Rifaximin Hydrate F1

F1: 2rifaximin • 7.4H_2O

HSM

The crystal of hydrate F1 was clear and transparent at 30 °C (Figure 22). The crystal colour gradually became more intense as a result of dehydration upon heating. Further evidence of escaping water molecules was observed by the appearance of bubbles at ~93 °C. Crystal fragmentation also occurred during heating, indicating further dehydration and signs of decomposition (~226 °C). The crystal completely decomposed at ~235 °C, shown by a colour change to dark brown.

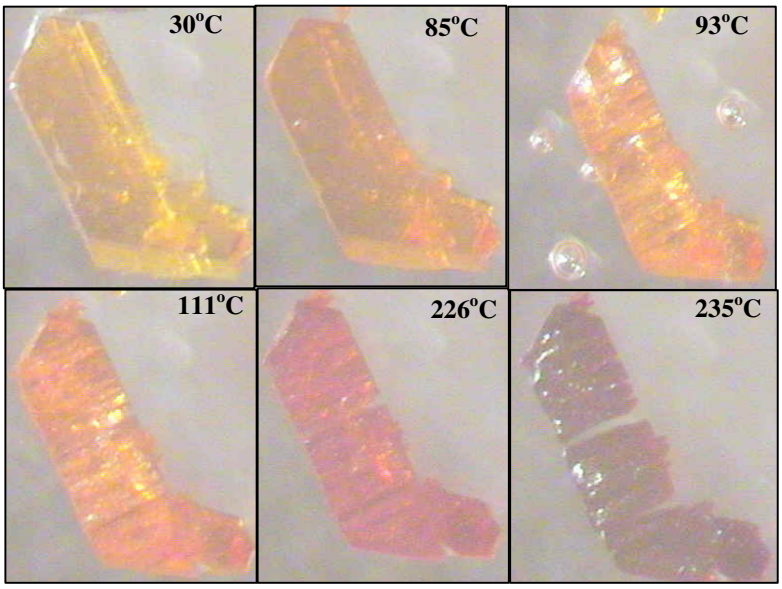

Figure 22 HSM micrographs of hydrate F1 recorded at various temperatures.

TGA

The TGA trace for hydrate F1 showed a two-step mass loss, labelled as A and B, respectively (Figure 23). The first step, A, is attributed to the release of water molecules, occurring over a temperature range from 36.7 °C to 83.3 °C with a mass loss of 7.0 ± 0.8% (n = 3). The calculated mass loss is 7.8% and agrees well with the experimental mass loss. The dehydrated compound then decomposed at ~231 °C.

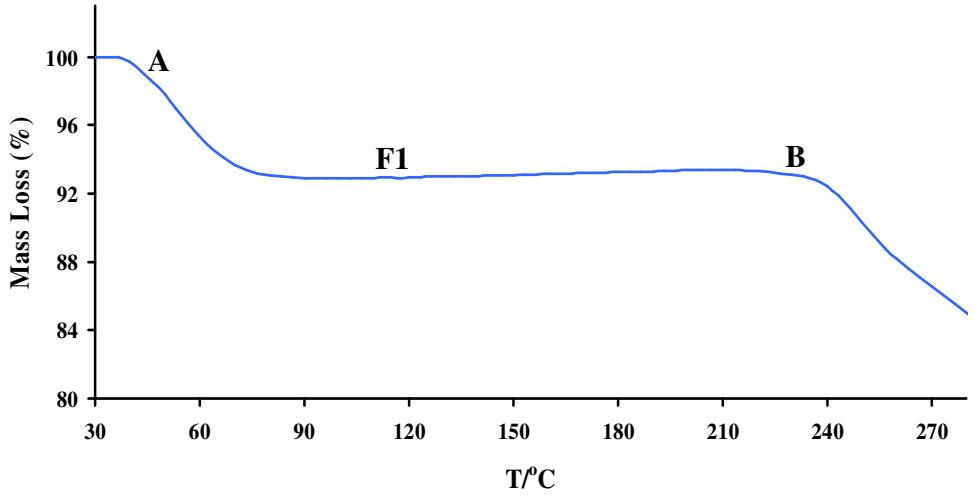

Figure 23 TGA trace for rifaximin hydrate F1

DSC

The DSC trace for hydrate F1 showed three independent thermal events C, D and E (Figure 24). A broad endotherm C was attributed to the water release from 35.1 °C to 134.6 °C. This corresponds to the observation from HSM analysis. A relatively sharp endotherm D represents the melting of the desolvated material followed by the decomposition and this stage can be observed clearly in HSM (colour change to red at 226°C). Exothermic peak E continues into the decomposition stage and appears at ~230 °C. Furthermore, the onset of decomposition determined by DSC corresponds with that obtained by TGA analysis.

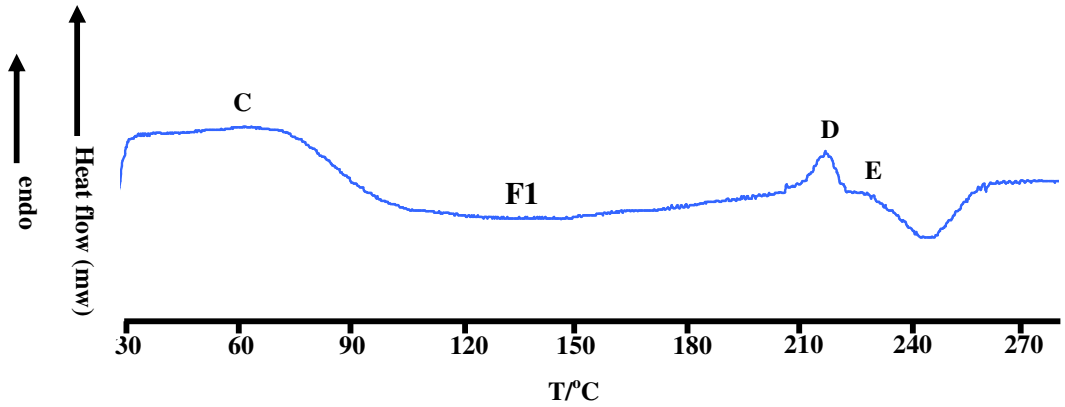

Figure 24 DSC trace for rifaximin hydrate F1

Solvate F2

F2: 4rifampicin • 7.72ethylene glycol • 6.83H_2O

HSM

The colour of the crystal of solvate F2 gradually became more intense with increasing temperature; this strongly suggests that the crystal experienced loss of ethylene glycol and water molecules during the heating process (Figure 25). The crystal finally changed colour to brown and completely decomposed at ~234 °C.

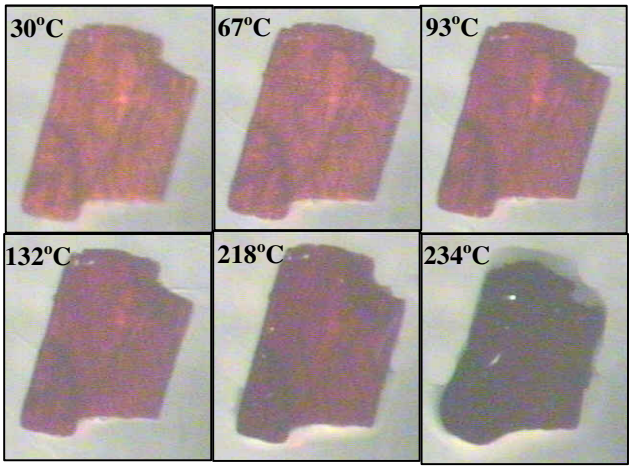

Figure 25 HSM micrographs of solvate F2 recorded at various temperatures.

TGA

Multiple-step mass loss A was evident from 30.0 °C to 206.0 °C (Figure 26). This is attributed to the simultaneous release of ethylene glycol and water molecules from the solvate crystal. The wide temperature range of the mass loss is due to the fact that a large amount of disordered ethylene glycol and water molecules formed a tight guest cluster in the structure of F2. Furthermore, the X-ray analysis revealed that these guest clusters are isolated by intervening host molecules, which therefore impede their escape. The experimental mass loss is 17.4 ± 1.2% (n = 5) while the calculated loss is 16.1%. Thermal event B indicates the onset of decomposition (230 °C) of the desolvated compound.

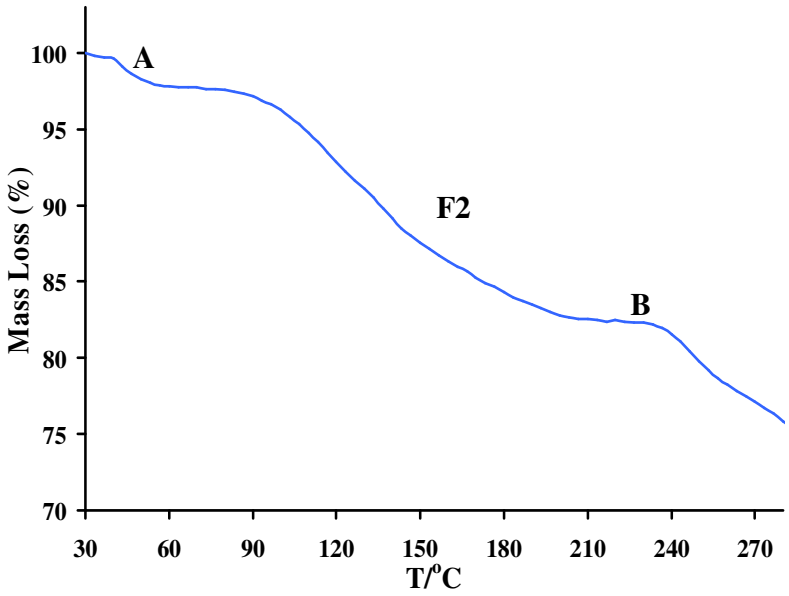

Figure 26 TGA trace for rifaximin solvate F2

DSC

The DSC trace in Figure 27 showed endothermic peaks labelled C and D, which are located in the temperature ranges of 35.1 – 92.0 °C and 94.5 – 138.8 °C respectively. Considering the fact that the dehydration of the hydrate F1 occurs within the temperature range 35.8 to 126.7 °C, one cannot simply assign peaks C and D as the dehydration and desolvation (ethylene glycol loss) peak, respectively. In other words, both endotherm C and D represent the simultaneous loss of ethylene glycol and water molecules. The exotherm E occurs at ~232 °C, demonstrating the decomposition of the desolvated form. Furthermore, this onset temperature determined from DSC analysis is in agreement with that obtained by TGA analysis.

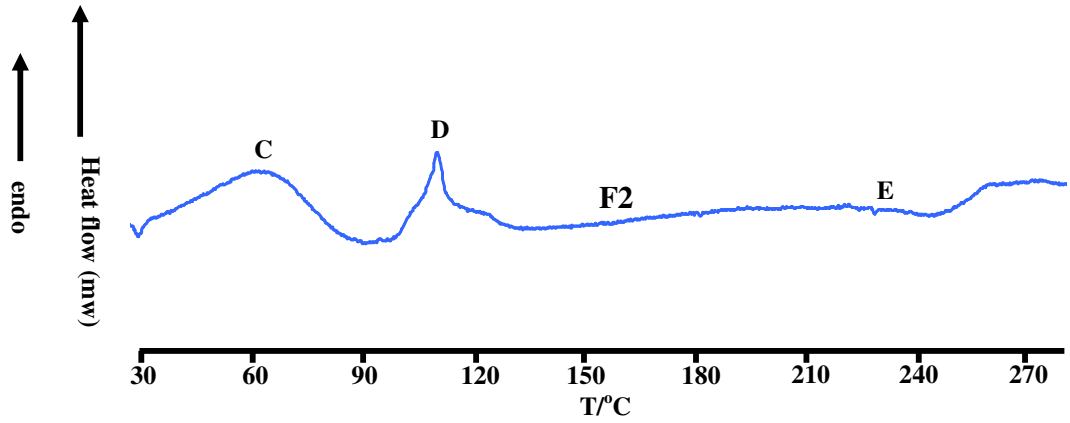

Figure 27 DSC trace for rifaximin solvate F2

Discussion

Generally, the thermal behaviour of rifampicin solvates and rifaximin solvates can be divided into two parts: (a) simultaneous dehydration and loss of included organic solvent and (b) decomposition of the desolvated compound. The temperature range of the event for each solvate determined based on TGA data (Table 1) correlates reasonably well with that obtained from DSC data (Table 2).

Table 1 TGA results for the rifampicin solvates and rifaximin solvates

Solvate	Mass loss range (°C)	Experimental mass loss (%)	Calculated mass loss (%)	Decomposition onset (°C)
P1	30.0 – 134.2	12.4 ± 0.5% (n = 3)	12.5	184.3
P2	42.1 – 133.2	9.7 ± 0.3% (n = 3)	9.6	182.7
P3	30.0 – 150.0	12.6 ± 0.9%(n = 3)	13.5	182.3
P4	37.2 – 168.5	10.3 ± 0.8% (n = 4)	10.3	182.4
P5	30.0 – 170.0	22.1 ± 0.8% (n = 3)	21.6	189.0
P6	36.7 – 166.7	23.0 ± 0.4% (n = 3)	23.1	189.0
P7	30.0 – 160.0	17.4 ± 0.8% (n = 3)	18.1	189.0
P8	30.0 – 172.0	24.0 ± 0.4% (n = 3)	24.1	187.9
P9	30.0 – 171.7	20.3 ± 0.7% (n = 3)	20.9	191.5
P10	30.0 – 164.2	21.0 ± 0.9% (n = 3)	21.8	191.0
P11	30.0 – 171.7	25.3 ± 0.9% (n = 3)	26.1	191.5
F1	36.7 – 83.3	7.0 ± 0.8% (n = 3)	7.8	230.9
F2	30.0 – 206.0	17.4 ± 1.2% (n = 5)	16.1	230.0

Table 2 DSC results for the rifampicin and rifaximin solvates

Solvate	Desolvation			Decomposition onset (^{o}C)
	Range (^{o}C)	Onset (^{o}C)	Peak (^{o}C)	
P1	57.5 – 130.0	75.7	95.5	186.9
P2	60.6 – 118.4	63.7	81.3	186.7
P3	42.7 – 114.5	42.8	85.3	187.5
P4	60.3 – 107.0	63.8	81.2	187.2
P5	39.3 – 105.0	53.3	74.0	186.9
	129.6 – 157.4	130.6	142.5	
P6	47.2 – 90.3	55.6	74.8	186.3
	98.3 – 154.5	125.5	138.5	
P7	38.0 – 127.0	51.9	80.3	186.9
P8	37.6 – 133.3	61.3	85.8	187.1
P9	85.0 – 124.9	85.8	90.8	188.3
P10	32.9 – 94.1	61.3	67.3	188.3
	94.5 – 195.4	112.6	142.7	
P11	70.0 – 151.0	111.46	118.7	188.5
F1	35.1 – 134.6	35.5	73.6	229.7
F2	35.5 – 92.0	39.1	63.8	230.2
	94.5 – 138.8	107.0	112.1	

For rifampicin solvates, the TGA mass loss range and DSC desolvation temperature range in isostructural series 1(P1 – P4) are narrower than those in series 2 (P5 – P7). This may due to the fact that the host molecule framework in the crystal structure of series 1 adopts a layered structure while that in series 2 adopts a clathrate-like structure. Therefore, solvent molecules in series 1 would tend to escape more easily than those in the series 2. Furthermore, the difference between host molecule frameworks in the two series can also be related to the fact that the decomposition onset temperature of the desolvated material recorded in TGA of series 1 is lower (mean ~183 ^{o}C) than that of series 2 (mean ~189 ^{o}C).[1] This trend is not, however, followed by the DSC data.

As stated earlier, PXRD was employed in an attempt to characterise the desolvated materials of the six different solvatomorphic phases of rifampicin. Notably, all the solvates were converted into an amorphous state after desolvation. These amorphous phases possibly demonstrate polyamorphism[2] (the ability of a substance to exist in several different amorphous modifications) based on their different TGA decomposition onset temperatures. However, due to the time constraints on the author's Ph.D study, a confirmation of this assumption is lacking. In future work, more characterisation (e.g.

solubility testing) on these amorphous materials should be carried out to verify the existence of polyamorphism. Furthermore, spectroscopic studies (e.g. NMR and IR) should be employed to confirm whether these amorphous phases have the chemical compositions corresponding to rifampicin.

For rifaximin solvates, the decomposition temperatures of F1 and F2 are very close, indicating a possibility that F1 and F2 were converted into the same desolvated phases on heating. However, more characterisation could be carried out to verify this assumption in future work.

References:

1. Hosokawa, T., Datta, S., Sheth, A. R., Brooks, N. R., Young, V. G., Jr. and Grant, D. J. W., *Cryst. Growth Des.*, **2004**, 4, 1195-1201.
2. Hancock, B. C., Shalaev, E. Y. and Shamblin, S. L., *J. Pharm. Pharmacol*., **2002**, 54, 1151 – 1152.

Chapter 7

Conclusion

Conclusion

The initial intention was to attempt preparation of polymorphs, solvates, cyclodextrin complexes and cocrystals of the antitubercular drug isoxyl as well as to isolate and characterise a range of solvated forms of the antitubercular drugs rifampicin and rifaximin. Achieving this goal would represent a contribution towards systematising the solid-state chemistry of these three drugs.

Isoxyl

The drug isoxyl has been employed as a useful antitubercular since the 1960s. Its polymorphism was investigated in 1971[1] when the unit cell dimensions of low precision and space group assignments for two polymorphic phases α and β were determined from X-ray diffraction photographs, and crude structural arrangements were postulated on the basis of these data. However, no accurate molecular and crystal structures for these phases were subsequently published. Mechanistic aspects of the mode of action of isoxyl were elucidated in 2003 and 2007.[2, 3] New derivatives of isoxyl were synthesised in 2006 and 2008,[4, 5] and a new dosage form of the drug was developed in 2010.[6] These developments indicate an on-going commercial interest in isoxyl and motivated our revisiting the drug in this study.

Polymorphism

In this study, accurate molecular and crystal structures of two polymorphs (designated **1** and **2**) were determined for the first time by X-ray diffraction methods. These two phases are conformational polymorphs. A combination of thermal, X-ray diffraction and solubility data allowed the construction of a schematic Energy-Temperature diagram for this dimorphic system. **Forms 1** and **2** were established as being enantiotropically related, **Form 2** being the metastable phase at room temperature.

Solubility measurements at 25 ^{o}C revealed that **Form 2** dissolved at a faster rate than **Form 1** within the intial 12 h period. This is the expected behaviour since **Form 2** is the metastable form at room temperature. However, a significant portion of **Form 2**

transformed into **Form 1** during the solubility analysis. This results in the solubility of **Form 1** and **Form 2** reaching the same level after 25 h. If the same transition were to occur *in vivo*, then these results indicate that polymorphic control may not be crucial for oral dosage formulation (tablet/capsule) of isoxyl.

Evidence for a third polymorph of isoxyl (designated **Form 3**) has been reported.[7] During the present study, much effort was invested into isolating this form in order to characterise it completely. However, it has to date remained elusive. It is possible that this particular form may have a significantly higher solubility relative to **Forms 1** and **2** since the difficulty experienced in isolating **Form 3** strongly suggests that it is a metastable polymorph. Therefore, the appearance of this 'missing' form could eventually have significance in the pharmaceutical production of the drug isoxyl.

Solvate of Isoxyl

A solvate of isoxyl with 1,4-dioxane (S1) was isolated and characterised successfully by X-ray and thermal methods. The solvate S1 desolvates to yield metastable polymorphic **Form 2** of isoxyl, either following controlled heating or by spontaneous desolvation at ambient temperature during exposure to the atmosphere. We assume that the transformation of S1 to polymorphic **Form 2** (rather than **Form 1**) is facilitated by the presence of similar structural features in the crystals of S1 and **Form 2** and the existence of a common 'tape' motif in their respective packing arrangements.

Cyclodextrin (CD) Complexes

The formation of a genuine β-CD-isoxyl inclusion complex was confirmed by finding that its experimental PXRD pattern matched a reference trace for a specific isostructural series of known β-CD inclusion complexes. A genuine γ-CD-isoxyl inclusion complex was identified in the same manner. Unequivocal identification yielded space group information for each complex and allowed deduction of approximate unit cell dimensions as well as the CD frameworks in the respective inclusion complexes.

For isoxyl, solubility enhancement measurements using β- and γ-CD solutions revealed that the aqueous solubility of the drug in these media increased by at least a factor of two in the former case, and three in the latter case, relative to its concentration in pure water. There is scope for enhancing the solubility of isoxyl more significantly by employing derivatised CDs (e.g. hydroxypropylated β-CD), though this was not a priority of this study.

Cocrystal Formation

A large number of experiments was performed in attempts to isolate cocrystals of isoxyl with over 10 different cocrystal formers. However, little or no indication of cocrystal formation was observed under the conditions employed. Most often, the choice of solvent is crucial and failure to choose the correct solvent or solvent mixture may have been responsible for the lack of success. The negative results from this study could nevertheless serve as useful information for those engaged in screening for cocrystal formation of isoxyl.

It is known that a new polymorph of either or both of the cocrystal partners can accidentally result during the attempted preparation of a cocrystal.[8] In this study, serendipitous precipitations of new polymorphs of two important and widely-used co-formers isonicotinamide and nicotinamide occurred during the attempt to prepare cocrystals of isoxyl. From a practical viewpoint, an important result emerged: under the conditions employed in this study, the appearance of the new polymorph of isonicotinamide does not depend on the presence of isoxyl, while that of the new polymorph of nicotinamide does.

For isonicotinamide, two polymorphs had been isolated earlier and their crystal structures were reported in 2003;[9,10] however, their thermal relationship was hitherto unknown. These two forms, designated **Forms 1** and **2** in this study, were evidently the only known polymorphs of isonicotinamide, despite its successful use as a cocrystal former in 56 different single crystal structures reported for the period 1999 – 2010, based on a CSD[11] search. The new form isolated in this study has been designated **Form 3**. Its crystal

structure was determined and carefully compared with the known structures of **Forms 1** and **2**. The precise differences at the conformational and crystal packing levels have been described in detail in this work. An exhaustive exploration of the thermal behaviours of the three polymorphs of isonicotinamide, coupled with other experimental evidence, led to the conclusions that **Form 1** is enantiotropically related to **Forms 2** and **3**, while **Forms 2** and **3** are monotropically related.

The single crystal structure of nicotinamide (**Form 1**) was determined in 1953[12] while the polymorphism of nicotinamide was first discussed in 2001.[13] During the period 1950 – 2010, although the structures of 18 cocrystals containing nicotinamide were determined successfully based on a CSD[11] survey, the structure of only one nicotinamide polymorph was determined. The new polymorph of nicotinamide characterised in this study has been designated **Form 2**. The two forms may be described as conformational polymorphs. Furthermore, the two forms were established as being monotropically related, Form 1 being the more stable phase.

Schematic Energy-Temperature diagrams for the trimorphic isonicotinamide system and the dimorphic nicotinamide system were constructed in this study. Notably, in both cases, the density order of the polymorphs deduced from the E/T diagrams agrees with their calculated densities at 173 K.

Rifamycins

Rifampicin and rifaximin, two rifamycin derivatives, were investigated with respect to their solvatomorphism in this study. The two compounds were found to crystallise as solvates with various organic solvents, water almost invariably being present in the crystal as well.

The molecules of rifampicin and rifaximin tend to exist as zwitterions in the solid state. For rifampicin, this applies to all the host molecules in solvates P1 – P11 investigated in this study, except molecule A (one of two crystallographically independent host molecules A and B) in the structure of solvate P10. For rifaximin, this applies to all the

host molecules in solvates F1 and F2. Furthermore, the zwitterionic form is invariable, the common N^+-H function being derived by proton transfer from the hydroxyl group on C8 to a nitrogen atom (piperazinyl atom N4 in the rifampicin molecule, and imidazole atom N2 in the rifaximin molecule).

Rifampicin

Administration of rifampicin, a semisynthetic derivative of rifamycin, is part of the standard therapy to treat tuberculosis. It shows excellent oral bioavailability. Although nine solvates of rifampicin have been reported since 1975, only one crystal structure was published, namely that of rifampicin pentahydrate.[14] In the present study, the author successfully isolated and characterized a total of 11 solvated forms of rifampicin. These solvates were classified into six isostructural series and the PXRD patterns computed from their accurately-determined crystal structures will in the future serve as useful references for the identification of new rifampicin solvates (just as the reference patterns for CD inclusion complexes used by the author were employed for the identification of newly prepared inclusion complexes).

Isostructural series 1 comprises four different solvates: Rifampicin • 1.57methanol • 3H_2O (P1), Rifampicin • 0.39methanol • 4.17H_2O (P2), Rifampicin • 2ethanol • 2H_2O (P3) and Rifampicin • 0.54ethanol • 3.92H_2O (P4). Crystals of P2 and P4 may be obtained from the crystals of P1 and P3, respectively, when the latter are exposed to atmospheric humidity. Isostructural series 2 comprises Rifampicin • 2.5(1-propanol) • 4.3water (P5), Rifampicin • 1.58(1-propanol) • 8.41water (P6) and Rifampicin • 0.6iso-propanol • 8.09water (P7). Crystals of P7 result from exposure of crystals of P6 to the atmosphere. Thus, solvent guest exchange with water in the atmosphere, a feature of the solvate crystals P1 – P7, was demonstrated and shown to leave the Rifampicin host frameworks intact. These results indicate that control of humidity is very necessary to ensure constancy and reproducibility in the preparation of particular solvates of Rifampicin.

The rifampicin molecules in solvates P1 – P4 (series 1), P8 and P10 display very similar structural features. The hosts in solvate P9 possess different structural features from those in other solvates, reflected in the spatial arrangements of atoms O11 and C18. This also applies to the rifampicin molecules in solvate P11. All the host molecules in solvates P1 – P4 and P8 – P11 display an equatorial configuration of the piperazinyl ring. However, the rifampicin molecules in solvates P5 – P7 (series 2) show a larger variation in their structural features, including an axial configuration for the piperazinyl residue.

A noteworthy observation is that crystals of P7 and crystals of P8 grew from the identical solvent mixture and crystallised at the same temperature, the only difference in their preparations being the lack of solution filtration in the former case and the need for filtration in the latter. This resulted in crystals with completely different morphology and properties. Once again, this indicates that the need for strict control of preparative methods is essential to ensure constancy and reproducibility in the preparation of a given solvate.

Rifaximin

Rifaximin is a promising new oral drug in the treatment of tuberculosis.[15] It is characterised by a wide spectrum of antibacterial action, however showing less than 1% gastrointestinal absorption. In this study, rifaximin was found to be considerably less prone to solvatomorphism than rifampicin.

The X-ray structure of rifaximin tetrahydrate was published by Bacchi et al.[16] some months after the author had determined essentially the same structure. There are two symmetry-independent host molecules A and B in the crystallographic asymmetric unit. Furthermore, the two molecules adopt significantly different conformations, reflected in two distinct orientations of the C15=O11 bond and consequent changes in proximal torsion angles. The author's investigation of this phase extended to additional characterisation by thermal methods (TGA, DSC and HSM). To the extent that it was possible, the thermal data were reconciled with crystal structural features (in particular the topology of guest solvent molecule inclusion).

A new solvate of rifaximin, F2, containing ethylene glycol and water, was isolated and characterised. The structure of F2 contains four independent host molecules, all of which adopt very similar conformations to that of the host molecule A in the phase F1. However, the unit cell and host molecule framework of F2 are completely different from those of the rifaximin hydrate. Thus, two distinct structural classes of rifaximin solvates have been established in this study.

Regarding the use of ethylene glycol as a solvent in the preparation of solvated phases of the rifamycins, it is important to note here that this was initiated in a systematic study after it was discovered that large crystals of rifampicin, present in compound rifampicin suspensions, contained traces of toxic ethylene glycol, whose source was possibly as a contaminant of other industrial solvents employed in drug processing. This is the subject of a paper by principal author M. M. de Villiers,[17] to which the author of this thesis contributed X-ray crystallographic evidence of the presence of ethylene glycol in solvate P10 as a representative rifampicin solvate.

In summary, the isolation and unequivocal physicochemical characterisation of new solid forms of the antitubercular drugs reported in this thesis provide data that are relevant in the context of their processing, formulation and performance.

Further Work

Specific items that have been identified as meriting further investigation are mentioned here. It is desirable that further efforts to isolate and fully characterise the third polymorphic form of isoxyl (**Form 3**) be carried out.

Another worthy goal is the full X-ray structural elucidation of the β- and γ-CD complexes of isoxyl if single crystals can be grown, and the accurate determination of the stoichiometry and stability constant of each complex in solution using NMR analysis.

A more focused programme utilising commercial screening apparatus should be applied in the search for isoxyl cocrystals, since such cocrystals are likely to have significantly higher aqueous solubilities than that of the untreated drug.

For the rifampicin and rifaximin solvates, the chemical compositions of their desolvated phases, which are produced by controlled heating, could be verified by spectroscopic studies (e.g. NMR and IR). Furthermore, since the variable behaviour of residues resulting from desolvation of rifampicin solvates just prior to their decomposition suggests the possibility of polyamorphism, further characterisation of these phases (e.g. dissolution testing) could be employed to explore this possibility.

Hydrogen bonding networks featured prominently in this work, having been observed and studied in both polymorphs and crystalline solvates. The analyses undertaken were based on X-ray diffraction data, which often limit the location of H atoms, especially those associated with solvent molecules. Future work could include neutron diffraction studies to determine such H atom positions accurately and hence obtain more comprehensive hydrogen bonding schemes. A deeper understanding of the topologies of these networks could lead to their deliberate creation in crystals of new compounds. Other techniques that could be applied to gain more understanding of the hydrogen-bonded networks include density functional theory (DFT) and Natural Bond Orbital (NBO) analysis.

References:

1. Csonka-Horvai, J., David, A., Horvath, G. and Naray-Szabo, G., *Z. Naturforsch., B: Chem. Sci*., **1971**, 26, 21-23.
2. Phetsuksiri, B., Jackson, M., Scherman, H., McNeil, M., Besra, G. S., Baulard, A. R., Slayden, R. A., DeBarber, A. E., Barry, C. E., Baird, M. S., Crick, D. C. and Brennan, P. J., *J. Biol. Chem*., **2003**, 278, 53123-53130.
3. Korduláková, J., Janin, Y. L., Liav, A., Barilone, N., Dos, V. T., Rauzier, J., Brennan, P. J., Gicquel, B. and Jackson, M., *Antimicrob. Agents Chemother*., **2007**, 51, 3824-3829.
4. Bhowruth, V., Brown, A. K., Reynolds, R. C., Coxon, G. D., Mackay, S. P., Minnikin, D. E. and Besra, G. S., *Bioorg. Med. Chem. Lett*., **2006**, 16, 4743-4747.
5. Liav, A., Angala, S. K., Brennan, P. J. and Jackson, M., *Bioorg. Med. Chem. Lett*., **2008**, 18, 2649-2651.
6. Wang, C. and Hickey, A. J., *AAPS PharmSci*, **2010**, 11, 538-549.
7. Buu-Hoi, N. P. and Xuong, N. D., *C.R. Hebd. Seances Acad. Sci*., **1953**, 237, 498-500.
8. Bernstein, J., *Chem. Commun*., **2005**, 40, 5007-5012.
9. Aakeröy, C. B., Beatty, A. M., Helfrich, B. A. and Nieuwenhuyzen M., *Cryst. Growth Des.*, **2003**, 3, 159-165.
10. Vishweshwar, P., Nangia, A. and Lynch, V. M., *Cryst. Growth Des.*, **2003**, 3, 783-790.
11. Cambridge Structural Database and Cambridge Structural Database system, Version 5.31, November **2009** (updates Feb 2010), Cambridge Crystallographic Data Centre, University Chemical Laboratory, Cambridge, England.
12. Wright, W. B. and King, G. S. D., *Acta Crystallogr*., **1954**, 7, 283-288.
13. Hino, T., Ford, J. L. and Powell, M. W., *Thermochim. Acta*, **2001**, 374, 85-92.
14. Gadret, M., Goursolle, M., Leger, J. M. and Colleter, J. C., *Acta Crystallogr.*, **1975**, B31, 1454-1462.
15. Ochoa, T. J., Chen, J., Walker, C. M., Gonzales, E. and Cleary, T. G., *Antimicrob. Agents Chemother*., **2007**, 51, 2837-2841.
16. Bacchi, A., Carcelli, M. and Pelizzi, G., *New J. Chem.*, **2008**, 32, 1725-1735.
17. de Villiers, M. M., Caira, M. R., Strydom, S. J., Bourne, S. A, Li, J. and Liebenberg, W. Crystallization of toxic glycol solvates of rifampin from glycerin and propylene glycol contaminated with ethylene glycol or diethylene glycol. Pharm. Res., for submission, August **2010**.

The folder Appendix on the disk attached to the inside back cover of this thesis contains:

Appendix 1: A full list of the outcomes of recrystallisation of isoxyl from a range of solvents/solvent mixtures, as well as the results from other methods of polymorph preparation.

Appendix 2: A full list of the outcomes of cocrystal formation experiments with isoxyl.

Appendix 3: Supplementary crystallographic information for solved structures in this thesis is saved in a subfolder named according to the designation used in this thesis. The files may be viewed with WORDPAD or NOTEPAD.

Table Results of isoxyl polymorph preparation using various methods

Method	Concentration (mg/ml)	Crystallising form
Crystallisation of raw material from single solvent systems*		
Acetonitrile	**1**	**Form 1**
Methanol	**2**	**Form 1**
Formamide	**1**	**Form 1**
sec-butyl acetate	**2**	**Form 1**
1,3-dioxolane	**1**	**Form 1**
ethyl isobutyrate	**2**	**Form1**
propyl chloride	**2**	**Form 1**
n-propyl acetate	**1**	**Form 1**
ethyl propionate	**2**	**Form 1**
diacetamide	**2**	**Form 1**
m-cresol	**2**	**Form 1**
chloroform	**2**	**Form 1**
bretylium aceticum	**1**	**Form 1**
triethylamine	**1**	**Form 1**
isoamyl Alcohol	**2**	**Form 1**
isopropyl	**2**	**Form 1**
3-nitro toluol	**1**	**Form 1**
1-chloropentane	**2**	**Form 1**
tetrahydropyran	**2**	**Form 1**
dichloromethane	**2**	**Form 1**
2-methylpropan-1-ol	**2**	**Form 1**
2-propanol	**2**	**Form 1**
1-propanol	**2**	**Form 1**
1,2-dimethoxyethane	**2**	**Form 1**
1-octanol	**1**	**Form 1**
toluene	**2**	**Form 1**
2-butanol	**2**	**Form 1**
3-pentanol	**2**	**Form 1**
triophere	**1**	**Form 1**
4-ethylpridine	**1**	**Form 1**
methyl isobutyrate	**1**	**Form 1**
3-pentanone	**1**	**Form 1**
diethylformamide	**1**	**Form 1**
methoxyacetonitrile	**2**	**Form 1**
pinacolone	**1**	**Form 1**
tert-butylacetic acid	**1**	**Form 1**
iso-butyronitrile	**1**	**Form 1**
cyclohexanol	**0.5**	**Form 1**
di-n-butyl ether	**0.5**	**Form 1**
benzol	**0.2**	**Form 1**
n-phenyl acetate	**0.5**	**Form 1**
anylacetate	**0.5**	**Form 1**
dimethyl sulfoxide	**2**	**Form 1**
3-chlorophenol	**2**	**Form 1**
diethyl ether	**2**	**Form 2**

2-nitrotoluol	**2**	**Form 2**
benzotrifluoride	**1**	**Form 2**
formic acid	**1**	**Form 2**
1-chloroheptane	**0.5**	**Form 2**
dimethylformamide	**0.2**	**Form 2**
chlorobenzene	**0.5**	**Form 2**
acetone	**2**	**Form 2**
n-methylformamide	**1**	**Form 2**
1-chlorobutane	**1**	**Form 2**
diatace	**1**	**Form 2**
cyclohexane	**0.1**	**Form 2**
carbon tetrachloride	**0.1**	**Form 2**
3-methyl-1-butanol	**2**	**Form 2**
3,3-dimethyl-2-butanone	**1**	**Form 2**
Crystallisation from binary solvent systems*		
Water:Ethanol (1:9 v/v)	**1**	**Form 1**
Water:Ethanol (2:8 v/v)	**0.5**	**Form 2**
Vapor diffusion		
formamidea:2-propanolb	**1**	**Form 1**
formamidea: Cyclohexanolb	**1**	**Form 1**
formamidea: Ethanol 90%b	**1**	**Form 1**
Solid-state grinding of either Form 1 or Form 2		**No effect**
Sublimation		**Form 1 + Form 2**

* Each solution was prepared at 10 ^{o}C lower than the boiling point of the solvent and filtered. The solution was then allowed to cool to room temperature spontaneously for recystallisation to occur.

[a] solvent, [b] precipitant

Table Results of cocrystal formation experiments with Isoxyl[a]

Co-former	Solvent	Ratio[b]	Result
Isonicotinamide	Ethanol 90%	1:1	Isonicotinamide **Form 1**
		2:1	Isonicotinamide **Form 1**
		1:2	Isonicotinamide **Form 1**
	Acetonitrile	1:1	Isonicotinamide **Form 1**
		2:1	Isonicotinamide **Form 1**
		1:2	Isonicotinamide **Form 1**
	Ethanol 80%	0.75:2	Isoxyl **Form 2**
		1:1	Isonicotinamide **Form 1**
		2:1	Isonicotinamide **Form 1**
		1:2	Isonicotinamide **Form 1**
	Chloroform	4:1	Isonicotinamide Forms **1** and **2**
		6:1	Isonicotinamide Forms **1**, **2**, and **3**
	Ethanol 99.4%	4:1	Isonicotinamide Forms **1** and **2**
		6:1	Isonicotinamide Forms **1** and **2**
	Ethyl acetate	4:1	Isonicotinamide Forms **1** and **2**
		6:1	Isonicotinamide Forms **1** and **2**
	3-methyl-2-butanol	5:1	Isonicotinamide Forms **1** and **2**
	Ethyl isobutyrate	5:1	Isonicotinamide Forms **1** and **2**
	1-butanol	2:1	Isonicotinamide Forms **1**
	1-propanol	1:2	Isonicotinamide Forms **1**
Nicotinamide	Ethanol 90%	1:1	Nicotinamide **Form 1**
		2:1	Nicotinamide **Form 1**
		1:2	Nicotinamide **Form 1**
	Acetonitrile	1:1	Nicotinamide **Form 1**
		2:1	Nicotinamide **Form 1**
		1:2	Nicotinamide **Form 1**
	Ethanol 80%	1:1	Nicotinamide **Form 1**
		2:1	Nicotinamide **Form 1**
		1:2	Nicotinamide **Form 1**
	Ethylene glycol	3:1	Nicotinamide **Form 1**
	Chloroform	6:1	Nicotinamide **Form 1**
	Ethanol 96.4%	6:1	Nicotinamide **Form 1**
	Ethyl acetate	7:1	Nicotinamide **Form 2**
	3-methyl-2-butanol	5:1	Nicotinamide **Form 1**
	Ethyl isobutyrate	5:1	Nicotinamide **Form 1**
	Toluene	6:1	Nicotinamide **Form 1**
	1-butanol	2:1	Nicotinamide **Form 1**
Saccharin	Ethanol 90%	1:1	Saccharin
		2:1	Saccharin
		1:2	Saccharin
	Acetonitrile	1:1	Saccharin
		2:1	Saccharin
		1:2	Saccharin
	Ethanol 80%	1:1	Saccharin
		2:1	Saccharin
		1:2	Saccharin
	Ethanol 99.6%	6:1	Saccharin

Co-former	Solvent	Ratio[b]	Result
Saccharin	Acetone	6:1	Saccharin
	Ethyl acetate	4:1	Saccharin
	3-methyl-2-butanol	5:1	Saccharin
	Ethyl isobutyrate	5:1	Saccharin
	chloroform	4:1	Saccharin
	1,4-dioxane	4:1	Saccharin
	methanol	4:1	Saccharin
	1-butanol	2:1	Saccharin
		4:1	Saccharin
	Toluene	2:1	Saccharin
		6:1	Saccharin
D-(+)-tartaric acid	Acetonitrile	2:1	D-Tartaric acid
	Ethyl acetate	4:1	D-Tartaric acid
		8:1	D-Tartaric acid
	Chloroform	8:1	D-Tartaric acid
	Ethyl isobutyrate	8:1	D-Tartaric acid
	Methanol	4:1	D-Tartaric acid
	Toluene	5:1	D-Tartaric acid
	1-butanol	2:1	D-Tartaric acid
	1-propanol	2:1	D-Tartaric acid
L-(+)-tartaric acid	Acetonitrile	2:1	L+Tartaric acid
		6:1	L+Tartaric acid
	Ethyl acetate	4:1	L+Tartaric acid
		8:1	L+Tartaric acid
	Chloroform	8:1	L+Tartaric acid
	Ethyl isobutyrate	8:1	L+Tartaric acid
	Methanol	4:1	L+Tartaric acid
	1-butanol	2:1	L+Tartaric acid
		5:1	L+Tartaric acid
	1-propanol	1:2	Isoxyl **Form 1**
Succinic acid	1-butanol	3:1	Succinic acid
		2:1	Succinic acid
	Ethanol 96.4%	4:1	Succinic acid
	1-propanol	1:2	Succinic acid
Citric acid	Ethyl acetate	4:1	Citric acid
	Ethanol 96.4%	4:1	Citric acid
	1-butanol	2:1	Citric acid
	1-propanol	1:2	Citric acid
	Methanol	4:1	Citric acid monohydrate
	Ethyl acetate	4:1	Citric acid monohydrate
Salicylic acid	Ethyl acetate	4:1	Salicylic acid
	1-butanol	2:1	Salicylic acid
	Ethanol 96.4%	4:1	Salicylic acid
	1-propanol	1:2	Salicylic acid
Maleic acid	Ethyl acetate	8:1	Maleic acid
	1-butanol	2:1	Maleic acid
	1-propanol	1:2	Maleic acid
Oxalic acid	Ethyl acetate	4:1	Oxalic acid

Co-former	Solvent	Ratio[b]	Result
Oxalic acid	Ethyl acetate	4:1	Oxalic acid
	1-butanol	2:1	Oxalic acid
	Ethanol 96.4	4:1	Oxalic acid
	1-propanol	1:2	Oxalic acid

[a] A physical mixture of 10 mg of isoxyl and the corresponding co-formers was dissolved in 2 ml solution at 10 ^{o}C lower than the boiling point of the solvent and filtered. The solution was stirred for 10 minutes and filtered (0.45 µm nylon filter) while hot. It was then placed in a Dewar flask containing water at the same dissolving temperature to allow for slow cooling to room temperature (spontaneously) for recystallisation to occur.

[b] A molar ratio of cocrystal former: isoxyl is applied.